HydroCen
NORWEGIAN RESEARCH CENTRE FOR HYDROPOWER TECHNOLOGY

CENTRE FOR ENVIRONMENT-FRIENDLY ENERGY RESEARCH

HydroCen Report nr.20

Flexible Sandtraps

Final Report - APPENDIX

Kaspar Vereide, Wolfgang Richter, Ola Haugen Havrevoll, Kiflom Belete, Usha Shrestha, Ushanth Navaratnam, Gasper Mauko and Leif Lia

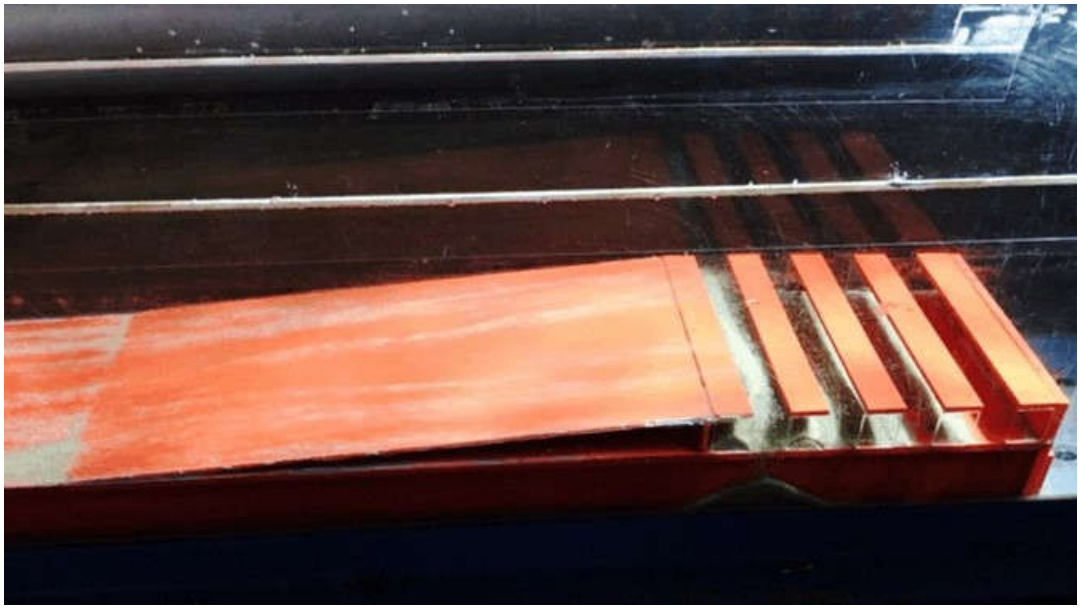

NTNU SINTEF NINA

Appendix

Appendix 1: Report from Physical Model Study of Tonstad Sand Trap (NTNU, 82 pp.)

Appendix 2: Report from PIV-measurement of Ribs in the Tonstad Sandtrap Model (NTNU, 17 pp.)

Appendix 3: Report from Flexible Sandtrap (FlekS) 1.0 (TU Graz, 100 pp.)

Appendix 4: Report from Flexible Sandtrap (FlekS) 2.0 Project Extension (TU Graz, 230 pp.)

Physical Model Study of Tonstad Sand Trap III

ISBN 978-82-8289-018-2(e)
ISBN 978-82-8289-017-5(p)

Trondheim, December 2020

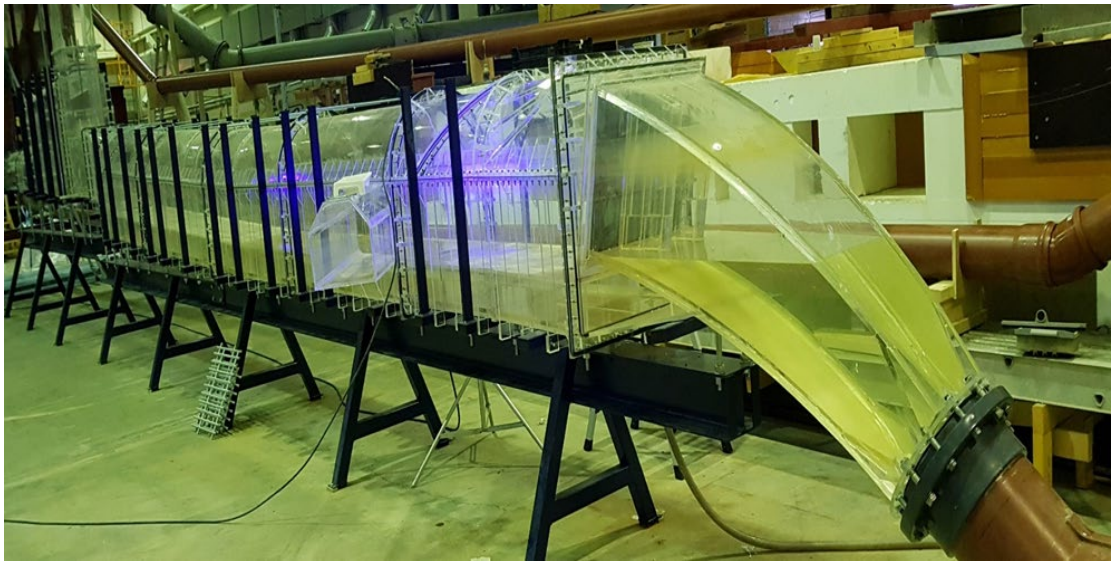

B1-2020

NTNU
Norwegian university of science and Technology
Faculty of engineering
Department of civil and environment

NTNU
Norwegian University of
Science and Technology

Kiflom Belete, Usha Shrestha, Kaspar Vereide

NTNU

Norwegian university of science and technology

Faculty of engineering

Department of civil and environmental engineering

NTNU
Norwegian University of
Science and Technology

Model Study of Tonstad Sand trap III

Employeer/ Client:

Sira-Kvina

Sira-Kvina Kraftselskap,

Postbox 38, 4441 Tonstad

Contact person: Kaspar Vereide

Executed by:

Hydraulic Laboratory

Department of Civil and Environmental Engineering, NTNU

7491 Trondheim

Project leader: Kiflom Belete

Researchers: Usha Shrestha and Kiflom Belete

Executive summary

The Tonstad hydropower plant is the largest power plant in Norway in terms of annual energy production, close to 4 TWh in recent years. The power plant was commissioned the first time in 1968 with two 160 MW units. Two more units were added in 1981, after the completion of the construction of the headrace system increasing the total capacity to 640 MW. The power plant was finally upgraded to a total capacity of 960 MW with the addition of 320 MW unit in 1988. The power plant has a combined design discharge of 250 m^3/s and utilises a gross head of 450 m.

The Tonstad power plant has a highly complex headrace system with unlined tunnels except for smaller sections with poor rock or weakness zones. After construction of the tunnel, sand and gravel were left in the tunnel. To avoid the transport of these rocks and gravels to the turbines, pressurized sand traps were constructed in the downstream end of the headrace. The sand traps are 200 m long with flow area of 110 m^2. The design discharge of the sand traps is 80 m^3/s and the velocity in the sand traps is 0.72 m/s.

After the upgrading of the power plant, due to high head loss and rapid change of peak load or a combination of these, free-surface flow occurred in a sand trap resulting in the flushing of the sand and rocks from the sand trap down to the turbines. This resulted in huge economical loss for the power plant. In this regard, different measures were taken by the owner to avoid problems in operation as well to improve the existing situation of the sand trap. A contract was signed between the Department of Civil and Environmental Engineering (IBM) at NTNU and Sira-Kvina Kraftselskap to conduct a physical model study of the Tonstad sand trap III. The model study was carried out to evaluate the performance of the sand trap III as well as to investigate and test possible modifications that can improve the trapping efficiency of the sand trap.

A 1:20 scale physical model of the Tonstad sand trap III was built to study the flow patterns in the sand trap, assess pressure head losses and evaluate its trap efficiency under steady and unsteady flow conditions. The study also intended to evaluate if the sand trap filling was a likely condition for the transfer of sand and gravels from the sand trap to the turbines downstream. The model was also used to evaluate possible measures to improve the trap efficiency of the sand trap under which the impact of flow calming structures, the lifting of the weir crest level before the trash rack as well as the installation of ribs separating the deposition zone that is intended to avoid the resuspension of the deposited sediments was investigated.

The head loss tests were carried out at four discharges including the design discharge of 80 m^3/s (i.e. 25 %, 50 %, 60 % and 100 % of the design discharge). The trap efficiency tests were carried out at design discharge with sediment having median diameter (d_{50}) equal to 3 mm. The discharge and other dimensions are presented in prototype scale in the report unless specified otherwise.

The model test depicted that, as a general trend pressure head loss measured in the model increased with the increase in discharge. The head loss measured in the model was quite lower which could be due to smooth walls in the model as the surface roughness was not replicated in the model.

The trap efficiency both for the steady state and unsteady state operation of the power plant were found to be about 89 %. Being on conservative side, this test was carried out feeding the sediment from the top. No visible changes in the deposition pattern was observed between the steady and unsteady state tests. However, more erosion occurred in the sand trap transition and more ripples occurred in the sand trap indicating movement of sediment with unsteady test than the steady state test.

Steady state test with sediment feeding from bottom was also carried out during the study to analyse the impact of the sediment feeding mechanism in the model on the trap efficiency of the sand trap. This test showed that the trap efficiency of the sand trap was 5 % higher than the trap efficiency measured in the test by feeding sediment from the top. This indicates that the 89% trap efficiency of the sand trap is more on conservative side and can be expected to be a bit higher in case of the prototype where the sediment approaches the sand trap both as bed load and in suspension.

Filling of the sand trap is assumed to be one of the conditions when free surface flow occurs in the sand trap with the possibility of eroding the deposited sediment into the penstock or turbine downstream. A sand trap filling test was carried out with the surge tank gate opening of about 5 cm. It was observed that the high velocity flow coming through the gate eroded the sediment deposited in about 95 m stretch of the uniform section of the sand trap. However, there was no significant change in the trap efficiency as compared to the steady state operation. This indicated that less or no sediment was eroded from the sand trap and transported downstream of the trash rack during the sand trap filling process except for the displacement of the sand within the sand trap.

In order to tranquilize the high velocity jet coming from the surge tank gate, flow calmers/ tranquilizers were installed in the sand trap transition. With the installation of flow calming structures, the trap efficiency increased by about 4.5 % as the effective length of the sand trap was increased. However, the pressure head loss almost tripled at design discharge. Though incorporation of flow calming structures improved the trap efficiency of the sand trap there was no improvement in the largest grain size that was transported into the penstocks. Thus, the negative effect of the flow calming structures due to higher head loss in the system and the possibility to improve the trap efficiency needs further investigation and optimization.

Another measure adopted to improve the trap efficiency was the lifting of the weir crest at the trash rack. The lifting of the weir crest level by 4.8 m neither improved the trap efficiency nor reduced the largest grain size that can be transported downstream of the sand trap. However, the pressure head loss was slightly less at design discharge after this modification. This modification can be helpful to ensure or reduce the passage of sediment in the penstock downstream during free surface flow in the sand trap.

With the intension to avoid resuspension of sediment deposited in the sand trap, ribs were installed in the sand trap together with diffusers. This improved the trap efficiency of the sand trap only by 0.6 %.

It was also found that particles of about 5 mm size pass through the sand trap for all the tests carried out. However, the volume of this coarse fraction passing through the sand trap to the penstocks was reduced after the modification 1 and 3.

The test results suggest that the trap efficiency of the sand trap could be improved by installing flow calmers in the sand trap. This increased the effective length of the sand trap by improving the hydraulics in initial part of the sand trap. However, possible increase in trap efficiency compared with the associated head loss with this modification needs further investigation and optimisation.

Table of Contents

List of figures

List of tables

1 Introduction

Hydropower plants built-in sediment loaded rivers are exposed to sediment induced wears of their mechanical parts. Although sediment is not a huge problem for hydropower plants in Norway, there are still some rivers with higher sediment concentration. For the Norwegian hydropower plants with sediment problems, a high degree of the sediment load that is transported into the power plants, comes from the brook intakes and muck left in the tunnel during construction. To minimize the transportation of sediment into the turbine, hydropower plants built in sediment loaded rivers consider sand trap as part of the hydraulic structures. The sand trap is a structural component in hydropower plant that limits the amount and size of gravel, sand and fine sediments that can be transported to the turbines and reduce the wear and tear of the electromechanical part of the power plants.

Tonstad hydropower plant (Tonstad HPP) is one of the largest power plants in Norway. The power plant has a highly complex headrace system with long unlined tunnels where part of the blasted material was used to from haul road during the construction period. These materials were left inside the tunnel even after the completion of the construction. Thus, pressurized sand traps are constructed in the downstream end of the headrace to avoid transport of these materials to the turbines. After the upgrading of the power plant and providing frequency restoration reserve (FRR) services, the power plant experienced sediment related problems. This has resulted in the restriction on the operation of the power plant and huge economic loss due to repair and maintenance and ultimately reduced power production revenue [6,8,9,].

Different measures were taken to improve the existing situation of the power plant. As part of these measures, the owner of the power plant decided to build a physical scale model to investigate and understand the hydraulic behaviour of the sand trap and explore possible measures to improve its performance. A 1:20 physical scale model of sand trap III in Tonstad HPP is built at the hydraulic laboratory of NTNU. Model test of the existing and modified design of the sand trap was carried out in the laboratory. This report presents the background of the Tonstad sand trap III model study, main problems in connection to the sand trap performance, procedures followed during the model study at the hydraulic laboratory and the model test results as well as recommendations for further improvement in the performances of the sand trap III.

1.1 Background Tonstad HPP

The Tonstad HPP is located at Tonstad, in the south west part of Norway, in the municipality of Sirdal in Agder county. Figure 1 shows the location map of the Tonstad HPP. It utilizes the water falls of Sira and Kvina river system. The Tonstad HPP is owned by Sira- Kvina Kraftselskap. The Sira- Kvina Kraftselskap was established in 1963 for the development of Sira and Kvina watercourses for power production.

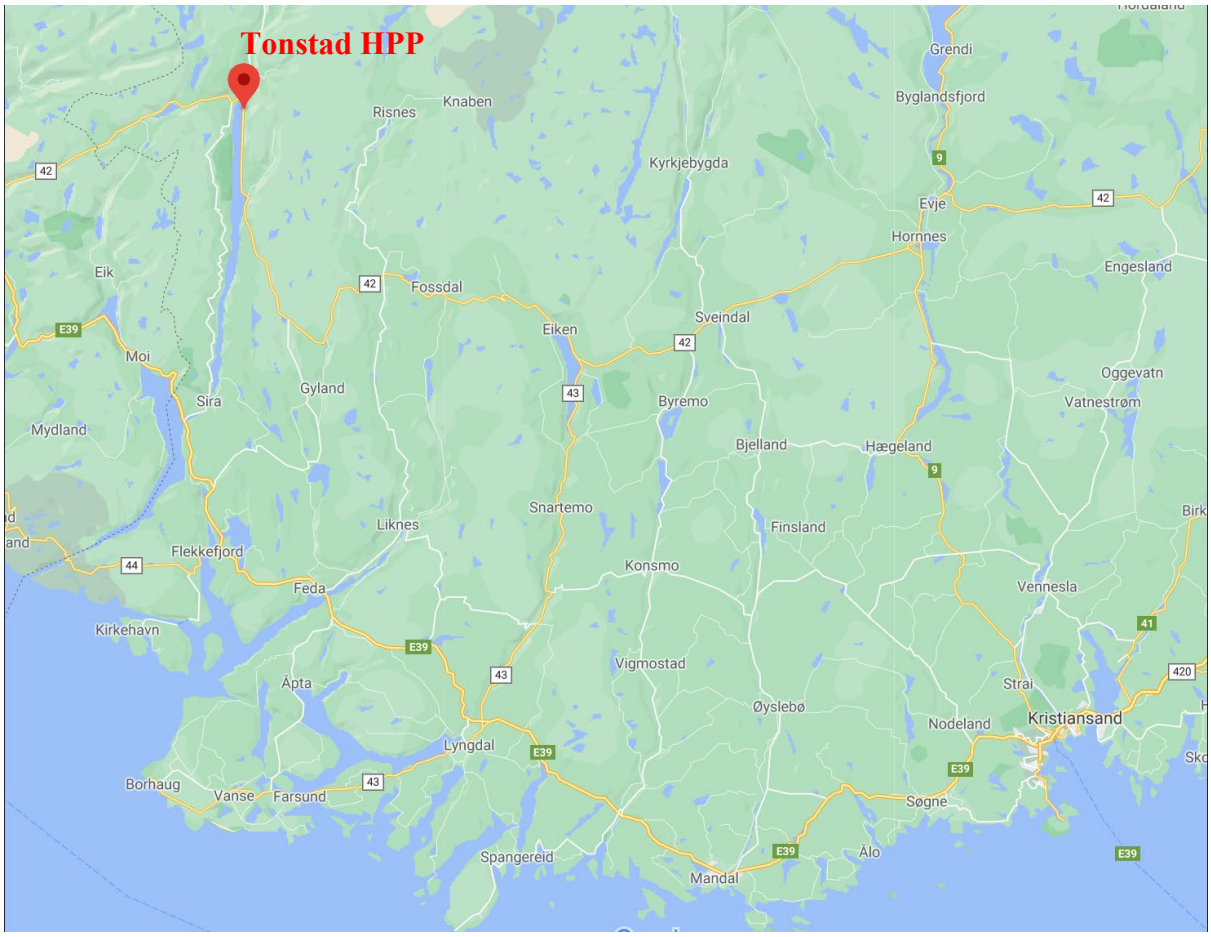

Figure 1: Location map of Tonstad hydropower plant (google)

The Tonstad HPP generates on average, 3800 GWh annually and is the largest hydropower plant in Norway in terms of power production. It has an installed capacity of 960 MW with a design discharge of 250 m^3/s and utilizes a gross head of 450 m. The power plant was constructed in three stages. The first two 160 MW vertical Francis turbines were commissioned in 1968. Two more turbines were added after the completion of the headrace system, such that the total capacity of the plant was 640 MW in 1971. The power plant was upgraded to 960 MW in 1988 by adding a new 320 MW Francis turbine. An addition of a pressure shaft, surge tank

and a sand trap were carried out during the upgrading. However, the headrace system to the reservoir was not upgraded during the process [6,9].

1.2 An overview of Tonstad HPP water flow system

The Tonstad HPP has a complex headrace system with two main reservoirs (Homstøl and Ousdal) and eight brook intakes. Figure 2 shows a schematic overview of the THPP water system. A 16 km long tunnel with 65 m^2 cross-sectional area, transfer water from the river Sira intake at Ousdal reservoir. A 7.5 km long tunnel with 55 m^2 cross-sectional area, transfers water from the river Kvina intake in Homstøl reservoir. These two branches merge into 100 m^2 tunnel continuing about 6 km long until the tunnel splits into three branches each with a surge tank and a sand trap before it continues to the steel-lined penstocks and the turbines. The surge tanks are open to the air and are constructed as a shaft with upper and lower chambers. The power plant finally discharges the water to the Sirdalsvatn reservoir [6,9].

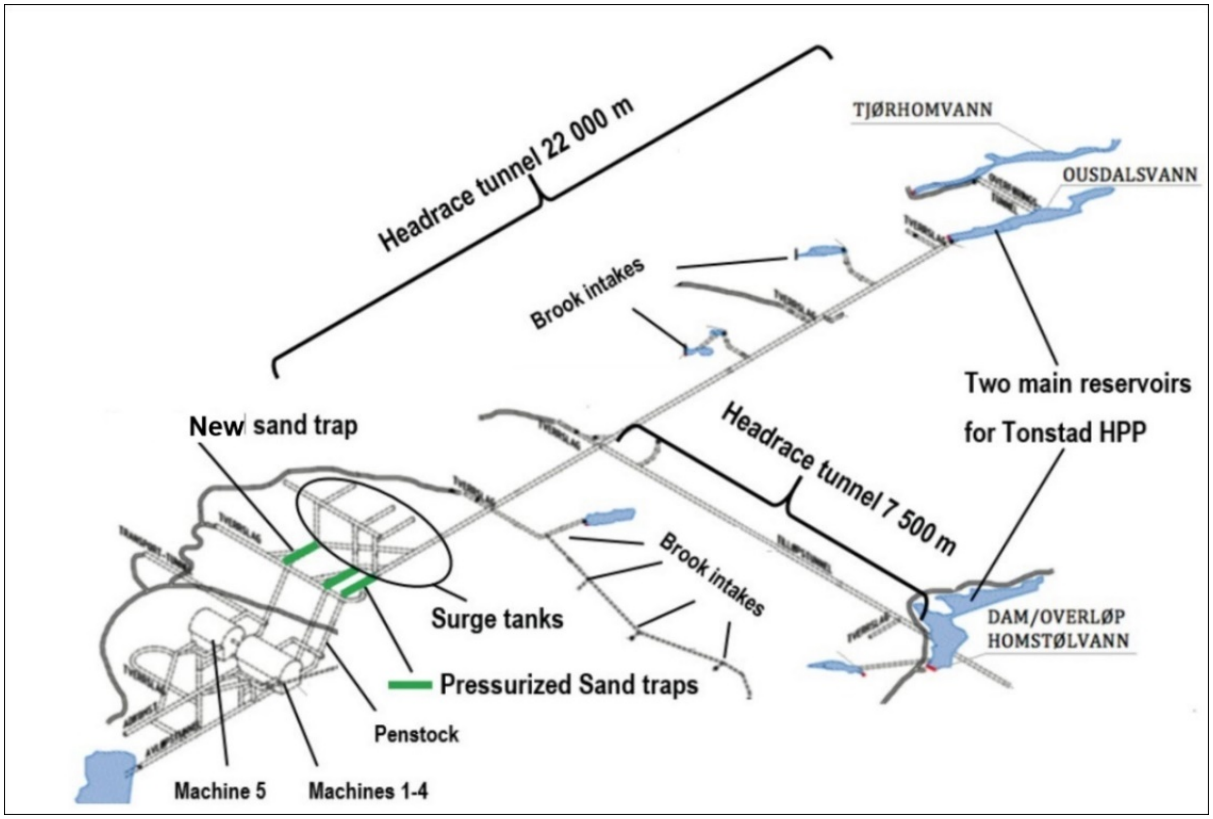

Figure 2: Schematic overview of Tonstad HPP [6] (modified by author)

1.2.1 The sand traps at Tonstad HPP

Due to the large size reservoirs in the upstream water system, one can assume that there is no significant sediment transported from the intakes to the turbine. However, the headrace tunnels

in this power plant are unlined with remains of the blasted material at the invert that was used to form haul roads during construction. Moreover, the power plant has eight brook intakes supplying directly to the headrace tunnel. Large pressurized sand traps are therefore constructed before the penstock and after the surge tanks to trap and avoid these sediments from getting into the turbines. The sand traps are about 200 m long with a cross-sectional area of 110 m^2 maintaining a velocity of about 0.7 m/s at nominal discharge [6,8,9].

As the installed capacity of the power plant was increased, the sediment load to the sand traps increased as a result of increased velocity in the headrace tunnels. It was found that the sand traps work acceptable during steady operation of the power plant. However, this design of the sand trap has not functioned optimally after the power plant started operating with more frequent load changes. Frequent load changes and frequent start and stop operation result in the destabilisation of sediments in the headrace tunnel simultaneously impacting the deposition of sediments in the sand trap[6,9].

The first two sand traps (sand trap 1 and 2) of the power plant were model studied in Trondheim from 1965 to 1966. However, during the upgrading, the Sand Trap III was constructed following the basic principles of the earlier sand traps with no additional model test [6]. An overview of the sand traps in the Tonstad HPP is shown in Figure 3.

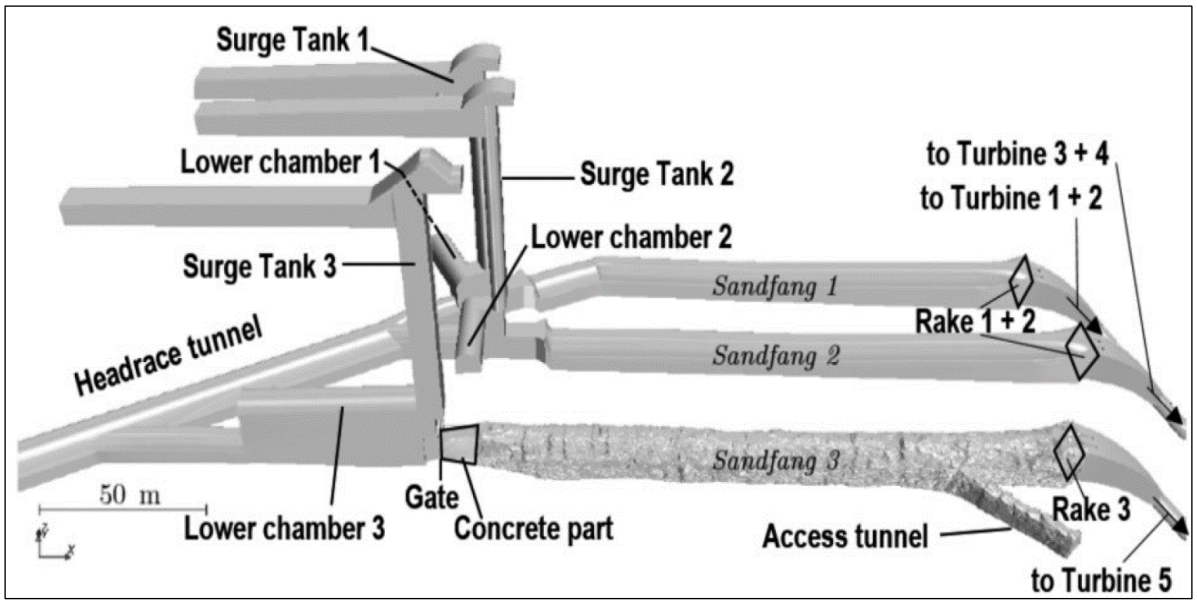

Figure 3: An overview of the surge tanks and the sand traps [6]

1.2.2 An overview of sand trap III

The plan view of the Tonstad HPP sand traps is shown in Figure 4. All the details from the earlier sand trap design, were not incorporated while designing sand trap III. In the new sand

trap (Sand trap III), the lower surge chamber is constructed as an expansion of the main waterway whereas, in case of the sand trap I and II, a separate tunnel is constructed at 90 degrees to the main waterway [7]. This expansion in sand trap III results in deposition of sediments in the lower surge chamber before reaching the sand trap that can be removed only by emptying the whole headrace tunnel. The access tunnel in sand traps (I and II) are closer to the trash racks, this is believed to improve the deposition of sediments in front of the rack. In case of sand trap III, the access tunnel is attached some 30 m upstream from the rakes. The filling valve in the sand trap III does not operate as intended. The filling of this sand trap is carried out by opening the surge tank gate. This operation results in free surface flow in the sand trap with the erosion of sediment deposited inside it [6,9,12].

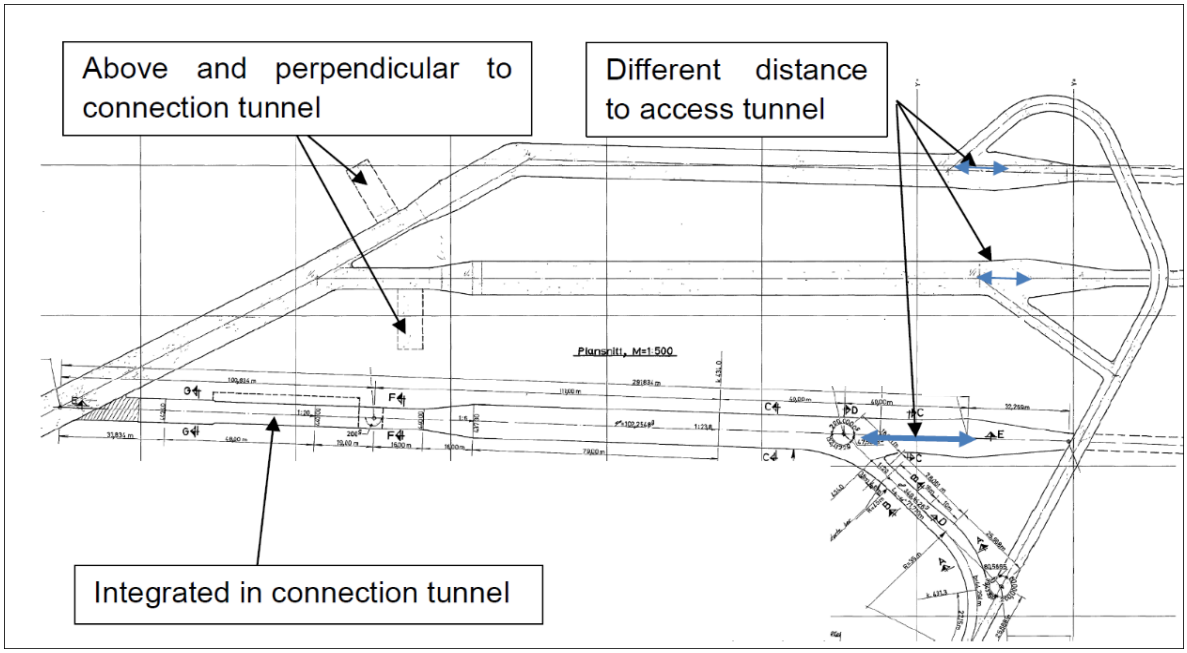

Figure 4: Plan view of sand traps of Tonstad HPP [12]

The performance of the sand trap is mainly affected by the flow velocity and turbulence in it. Thus, to fully understand the flow phenomenon and the sediment deposition in the sand trap, model tests were carried out. Details of the model study are presented in the following chapter.

2 Tonstad sand trap III physical model study

A contract was signed between the department for Civil and Environmental Engineering (IBM) at NTNU and Sira-Kvina Kraftselskap to conduct a physical model study of the Tonstad sand trap III. The model study mainly focused on evaluating the current performance of the sand trap system as well as investigating and testing possible modifications that can improve the performance of the Tonstad sand trap III.

2.1 Function of the sand trap

The function of the sand trap is to trap the sediment brought by the headrace system and deliver relatively clear water to the turbines. The basic principle of the sand trap design is the reduction of the flow velocity with an increase in the cross-sectional area that results in the deposition of the sediment brought by the relatively high-velocity flow in the headrace tunnel. Figure 5 shows the sediment deposit at the Tonstad sand trap III during inspection.

Figure 5: A view inside Tonstad sand trap III during an inspection

In the case of the pressurised sand trap, the water velocity is maximum at the centre and this is not favourable for the deposition of sediments. Moreover, it has more wetted periphery which may induce turbulence in the context of unlined rocks. Thus, positively impacts the dampening of the entrance flow jets and secondary currents [9].

2.2 The problem and need for physical model study

The Tonstad HPP was upgraded from 640 MW to 960 MW in 1988. The headrace system to the reservoirs was not upgraded in the process except, for an additional pressure shaft, surge tank and a sand trap. An increase in sediment transport was recorded with the upgrading of the power plant. Following the upgrading and installation of new turbine governors to meet the fluctuating energy demand, the power plant has experienced sediment related problems. Sediment was reported to have damaged two of the turbines of the power plant. The mass oscillations in the surge tanks due to frequent load changes combined with a high head loss in the headrace tunnel and a free-surface flow is believed to have occurred in the sand trap transporting more sediment particle into the turbine. This has resulted in restrictions on operation, economic loss due to repair and reduced power production revenue. This indicates that in hydropower plants with complex tunnel systems, very detailed studies are necessary to understand the hydraulic behaviour and potential problems in the system[6].

The sand trap III of Tonstad HPP was built without model study, following the basic design principles of the two earlier sand traps. Thus, it has not functioned optimally after the power plant started operating with more frequent load changes [6].

The performance of the sand trap depends on the hydraulic design of the sand trap. The flow condition at the inlet and eddies that may occur at the inlet and outlet transition of the sand trap impacts its trap efficiency. The flow velocity and turbulence are the most important factors affecting the optimal performance of the sand trap. Moreover, frequent start-stop operation also impacts the sedimentation and erosion processes in the sand trap [9].

To fully understand the influence of the different hydraulic parameters on the flow condition and the sediment deposition in the sand trap, both physical model studies and numerical model simulations is beneficial. A combination of both physical and numerical models was implemented to improve the Tonstad sand trap III. The comprehensive 3D- CFD modelling for the Tonstad HPP sand trap III was carried out by the Graz University of Technology and the physical scaled model was carried out by the hydraulic laboratory at the Department of Civil and Environmental Engineering, NTNU.

2.3 Objectives of the physical model study

The main objective of the project was to build a physical scale model of the sand trap III and evaluate the current design as well as explore and test possible design modifications of the sand trap to improve the performance.

In the model study, the basis for evaluation of the performance of the sand trap was the ability of the basin to trap fine sediments so that sediment load to the turbine can be reduced. Equally important was the ability to remove the deposited sediment without interrupting power production or with minimum economic consequences. The model study was also intended to evaluate and improve the operation guidelines of the surge tank gate during filling of the sand trap.

2.3.1 Specific objective of the model study

The specific objective of the model study includes but were not limited to:

I. Building model of the sand trap III and carryout performance test of
    a. The existing design

II. Test the performance of the sand trap with
    a. Inclusion of flow calming structure
    b. Increased downstream weir crest level
    c. Construction of ribs inside the basin of the sand trap

2.4 Related previous studies

The physical model of the first two sand traps (sand trap I and II) of the power plant were built and studied by Sintef from 1965 to 1966. The final design of the sand traps adopted during construction was based on the model test results.

The 3D CFD model study of the Tonstad sand trap III was carried out by Graz University of Technology [12]. The simulations were carried out with a model scale of 1:15 using Froude's model law. The roughness of the sand trap walls was also taken into consideration for the 3D-CFD simulations. In this study, the performance of the existing design of the sand trap was studied together with other possible structural measures to improve its performance. The first promising measure was the inclusion of the flow calming structure in the sand trap transition. This significantly improved the flow condition in the sand trap. The second measure to improve

the trap efficiency involved the increase in cross-section of the sand trap to reduce the flow velocity. In this regard, lowering the bottom of the sand trap was studied. Structures were provided to guide sediment to the trench at the bottom that is expected to be facilitated with automatic sediment sluicing system. The basic finding of the 3D- CFD simulation was that the trap efficiency of the sand trap could be improved by the compact combination of these two measures. Especially, the flow calming structure improved the hydraulics in the sand trap. From the 3D- CFD study, flow calmer with 1 m diameter pipe, covering the cross-section was recommended to be placed around 8 m after the start of the unlined section.

To further investigate measures to improve the sand trap performance, two studies connected to master theses were conducted. The first study was done by Sofie Marie Steinkjer in 2018. This was conducted in a physical model to investigate and propose possible material for sediment modelling [7]. Both sand and PMMA material were tested to represent the smaller fraction of the prototype sediment and were recommended to be used for the model study of the sand trap.

The second study was done by Jana Daxnerová in 2019 [1]. The study was conducted to assess an optimum design of the flow calming structure for the sand trap, using a flume. Different designs of the flow calming structures were tested during the study. A set up of flow calming structure with two flow calmers was recommended for further testing in the physical model of the Tonstad sand trap III.

3 Modelling law and scaling the sand trap model

Turbulent water flow is complicated to be analysed using simple mathematical formulas. Application of such formulas in a turbulent flow condition can only give approximate values with less accuracy and reliability. For optimum structural design and observation of hydraulic conditions, a physical scale model can give insight into the problems under investigation with a high degree of accuracy and reliability [5]. Physical scale models are also beneficial for studies related to the performance of the sediment trapping basin. This allows visual observation of the hydraulic phenomenon occurring in the basin and allow direct measurements.

The scale model of any hydraulic structures represents the prototype with some degree of simplification. Thus, the model needs to be designed based on applicable model laws , proper choice of model scale and appropriate representation of model boundaries to minimize the influence of these simplifications. These factors also influence the cost of the model study and hence the final model design is the compromise between cost and accuracy [5].

3.1 Modelling laws

Euler number is a dimensionless value used for analyzing a fluid flow dynamics problem where the pressure difference between two points is important. The Euler number can be interpreted as a measure of the ratio of the pressure force to inertial force. Thus, for flows which are dominated by pressure forces and inertial reactions, the Euler's model law is applicable. [1,3]

For a fully pressurized incompressible flow in the tunnel with a velocity V, for a tunnel length L, and diameter D, the flow shows a pressure difference ΔP.

A perfect frictionless flow corresponds,

$$Eu = \frac{\Delta P}{\rho V^2}, \qquad (1)$$

If for a fluid flow, the inertial reaction may also be influenced by viscosity and/or gravity. Then, the Euler's number is the function of form of the flow boundaries, Reynold's number and Froude's number [3].

i.e, Eu= f (shape, R_e, F_r)

Then, the drop-in pressure can be affected by velocity, viscosity, gravity, geometry and density of the fluid

$$\Delta P = (V, \mu, g, \rho, D, L, k) \quad (2)$$

In such a case, Reynold's or Froude's model law should be applied for the model study based on the parameter dominating the flow. However, the Euler's similitude is preserved once the Reynold' number of Froude's number similitude is maintained [2].

For highly turbulent flow which is generally the case in pressurized sand traps, the Reynolds number are quite high, and the viscous forces become negligible compare to inertial forces. In such a case, the model can be designed according the Froude's model law provided, the Reynold's number is also maintained sufficiently high in the model to avoid viscosity effect. The Froude's model law relates gravity and inertia force, neglecting viscous and surface tension force. [1,3]

$$F_{r=}\frac{\mathrm{V}}{\sqrt{gL}} = 1 \quad (3)$$

3.2 Scaling of Tonstad sand trap

The flow condition in the pressurised sand trap III of Tonstad HPP is turbulent having Reynolds number in the range of 10^6. At higher Reynold's number, the flow is independent of viscous forces. Thus, Froude's model law can be applied for the scaling of the Tonstad sand trap III. A model scale of 1:20 was chosen for the study. This scale was chosen such that it could fit in the available space and discharge capacity at the laboratory without severe scaling effects. The resulting scale ratios for the model are presented in Table 1.

Table 1: Model scale ratios

Parameter	**Unit**	**Relative**	**Scale**
Length	m	Lr	1:20
Velocity	m/s	$Lr^{1/2}$	1:4.472
Time	sec	$Lr^{1/2}$	1:4.472
Discharge	m^3/s	$Lr^{5/2}$	1: 1788
Area	m^2	Lr^2	1:400
Volume	m^3	Lr^3	1:8,000
Pressure	m	Lr	1:20

3.2.1 Sediment transport characteristics and scaling of sediment

There are two main modes of sediment transport, it can be transported as bed or and suspended load. The scaling criteria for these two modes of transport are different. The boundary shear stress plays a prominent role in the movement of bed load while movement of particles as suspended load is dependent on the fall velocity. Applying one of the modes of sediment transport in the model therefore involves scale effects associated with the other [2].

3.2.1.1 Bed load

Little or no information is available on the characteristic of incipient motion in tunnels. It is a reasonable assumption however that the characteristics of incipient motion in open channels and tunnels are principally the same [4]. The shield's diagram is useful for characterizing the condition of incipient motion of particles on a bed and for describing the intensity of bed particle movement. It relates the shields number Θ, which is the dimensionless ratio of nominal bed shear stress to the submerged weight of the average bed particle and the particle Reynold's number Re_*, that relates particle size to the thickness of the laminar sub layer [2].

For lower values of particle Reynold's number ($Re_* < 60$) the viscous forces play an increasingly important role in particle entrainment and thus should be considered to ensure similarity of flow around particles and particle entrainment by flow. However, if the particle Reynolds number exceed about 400, the dimensionless shear stress or the shield parameter is constant for any changes in the particle Reynolds number. Then, the particle motion is independent of viscous shear forces and the Froude's law is applicable keeping the shields parameter (Θ) same as that of the prototype [2].

3.2.1.2 Suspended load

For the similitude of suspended load, the ratio of shear velocity and particle fall velocity needs to be equal in prototype and the model. However, when Reynold's number based on particle diameter (particle Reynold's number) is approximately between 400 to 20,000, the coefficient of drag is nearly equal to unity and the relationship for suspended particle scaling would be similar to the shields number criterion [2].

3.2.2 Sediment scaling considerations

Similitude parameter of sediment motion relate particle diameter to fluid properties (viscosity and density) and is independent of local flow conditions. As water is the practical fluid used in

the model studies, the dynamic similarity in the reproduction of sediment transport in a small-scale model is almost impossible .Then, it is important to compromise some of the parameters to make modelling in smaller scale possible[11]. The basic requirement for sediment modelling would be that the model bed particles move in about the same way as do the particles in the prototype [2].

The geometric scaling of particle diameter more often necessitates using very fine sediments which may introduce the undesired effect of cohesion forces. For particles below 0.1mm in diameter, particle behaviour becomes increasingly dependent on ionic forces rather than gravity. Hence, minimum particles size for model studies is limited to 0.1 mm to avoid cohesive forces. A further consideration arises because of the propensity for beds of medium and fine sands (0.13mm < d < 0.5 mm) to ripple under some flow conditions. Thus, if the same sediment is used in the model as that of a prototype i.e. sand, it is important to ensure that the model sediment size is greater enough to avoid these effects. This limitation in the scaling of the particle diameter can be addressed by adjusting one variable, i.e. the density of the particle ($d_r = l_r/(\rho_s - \rho_w)_r$) [2]. However, finding a particle of defined density and right diameter is practically challenging and financially demanding.

The suspended load is in principle not possible to scale as the geometric scaling of sediments and the hydraulic scaling do not comply. However, it is still possible to get an indication of the suspended sediment transport through Froude scaling [9]. The water temperature influences the sinking velocity and thus the sedimentation process. Therefore, the effect of the temperature also needs to be taken into account while conducting model studies as temperature in model are in general higher than that in the prototype [10].

3.2.3 Sediment scaling for Tonstad sand trap

With higher velocities of about 2.5 m/s in the headrace tunnels, fine to coarse particles are transported to the sand trap. Most of this sand is transported as bedload while some fines may come in suspension [4]. The Tonstad sand trap was designed to trap a critical sediment size of 2 mm in diameter. This is based on the fact that Norwegian rivers transport a limited amount of sediments to the power plants. Unlike other countries, sediment less than 2 mm is considered acceptable to pass to the turbine [6].

The sand trap of Tonstad HPP is drained and cleaned regularly (yearly or bi-yearly). As per the field report 2018, sediment samples were collected from 10 different locations in the sand trap as shown in Figure 6. The particle size distribution (PSD) curves of the samples collected at

these locations are shown in Figure 7 and the sieve analysis data are presented in Appendix B-1 [7].

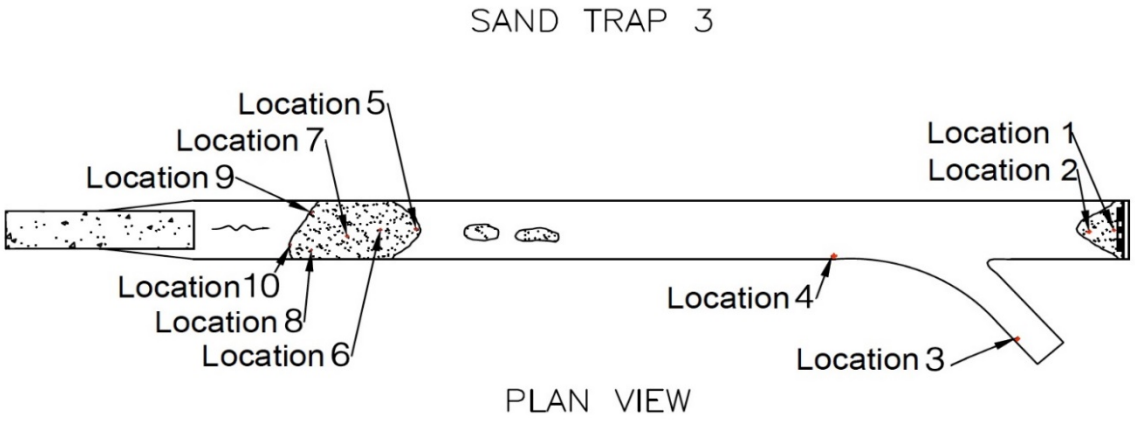

Figure 6: Sampling location in sand trap III [7]

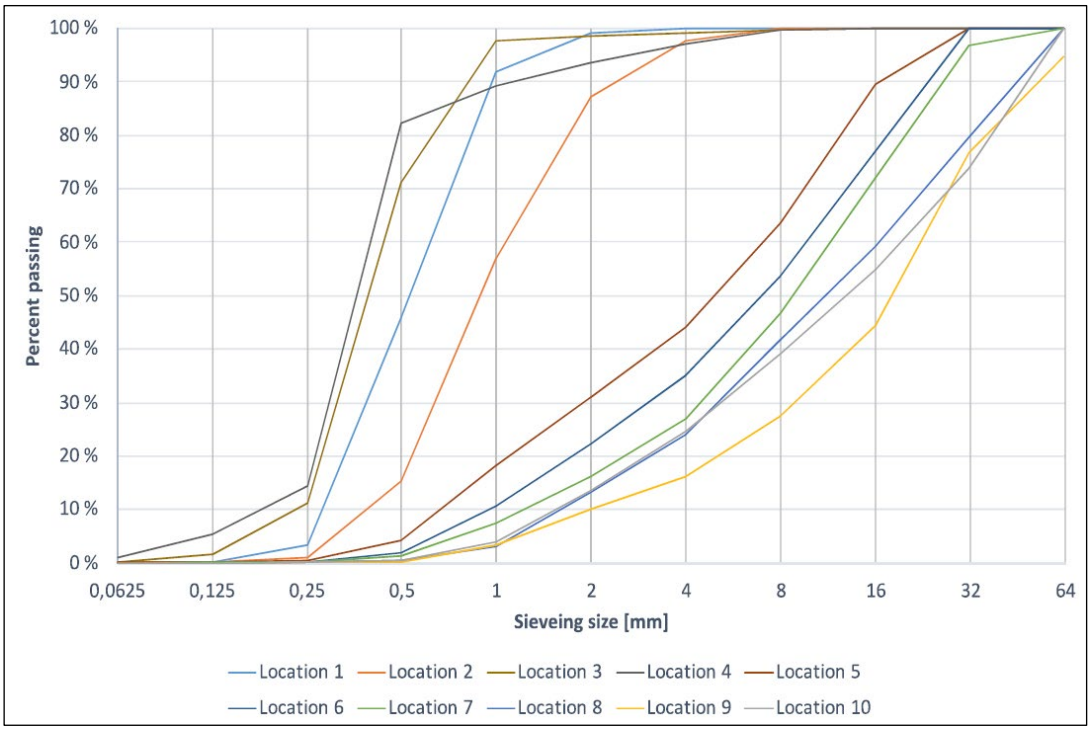

Figure 7: PSD curve of the sediment samples collected from the prototype in sand trap [7]

There are two main areas of deposition, in the upstream part of the sand trap and in front of the trash rack. Based on the PSD curve, about 90 % of the sediments in front of the trash rack are below 2 mm. Almost 65 % of the total sediment collected was deposited in the upstream part of the sand trap [8]. Particles from 100 mm to about 0.1 mm were found in this location.

About 70% of the sediment collected in the sand trap was above 2 mm size. As stated earlier, the sand trap of Tonstad HPP was designed to traps sediments up to 2 mm in diameter and

transport of sediment below 1mm to the turbines is considered acceptable. Hence, it is assumed that improving the trap efficiency for this grain size ensures improvement in trap efficiency of the larger fraction of the sediment transported to the sand trap.

Based on its availability sand was chosen as a model sediment. The minimum grain size to be used in the model was set to 0.1 mm to avoid effects of cohesive forces in the model test. The Particle Reynold's number is greater than 400 in this case. The shield's number is therefore independent of the particle Reynold's number or the viscous forces. Hence, Froude's law holds applicable. This 0.1mm sand therefore corresponds to the sand grain of 2 mm in the prototype when geometrically scaled according to the Froude's law. Uniform grain size of 2 mm in prototype was therefore considered to be used to evaluate the performance of the sand trap.

Due to the unavailability of the sand of required size, model test using uniform grain size was not possible. Thus, sediment between 5 mm to 2 mm was used for the initial tests. This sediment was derived sieving the commercially available sand with grain size below 14 mm. This process was very rigorous and time-consuming. It is worth mentioning that even though the sand was derived sieving between 5 m to 2 mm, it contained some fraction below 2 mm. The commercially available sand had very less fraction above 5 mm and below 2 mm. The d_{50} for both the sieved and un-sieved sand was also about 3mm. Therefore, a test was carried out to check if the commercially available sand (un-sieved sand) can be used instead. As the test results showed no significant difference, un-sieved sand was used in the later stage of the study. The details on the test, are presented in section 5.2.1.2. The comparative graph showing the PSD curve of the sieved sand and the commercially available sand /un-sieved sand in prototype scale is presented in Figure 8. The PSD details are presented in Appendix B-2. The d_{50} for both the sieved and un-sieved sand was about 3mm.

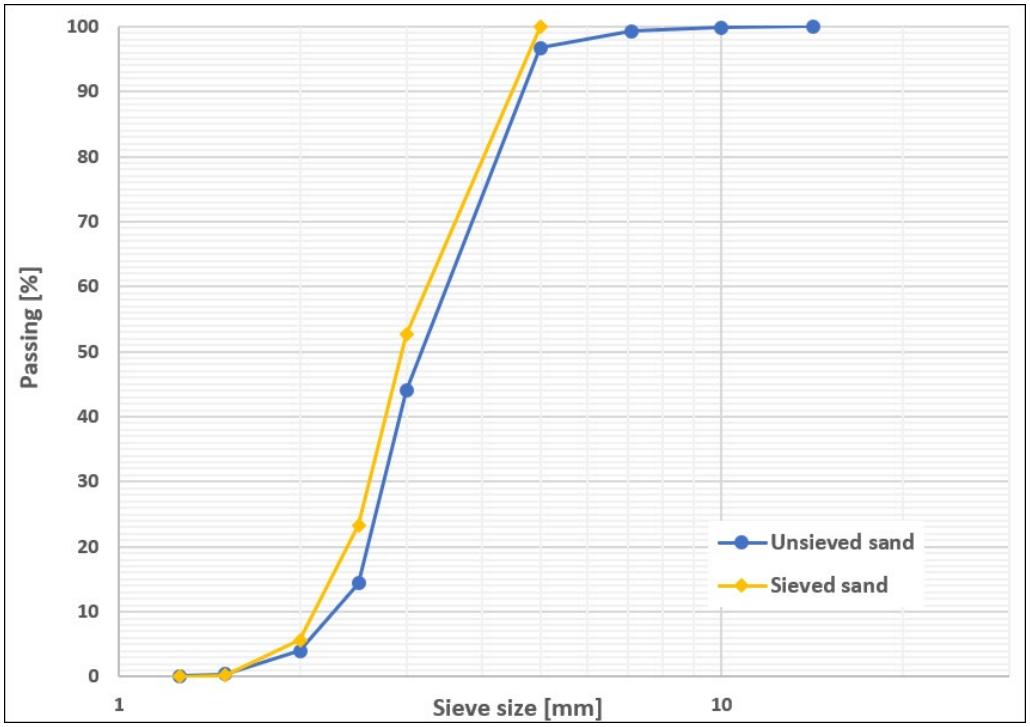

Figure 8: PSD curve of sediment used for testing in model (grain size in prototype scale)

4 Sand trap model construction

4.1 Basis for model construction

The Tonstad sand trap III model in the hydraulic laboratory is constructed in the scale of 1:20. The model construction was based on the prototype drawings provided by the client. The drawings provided by the client are presented in Appendix A-1 to A-8. The prototype drawings were scaled down as per the scale chosen for the model study and working drawings were prepared to fabricate different parts of the model. One of the prototype drawings showing the sand trap detail is presented in Figure 9.

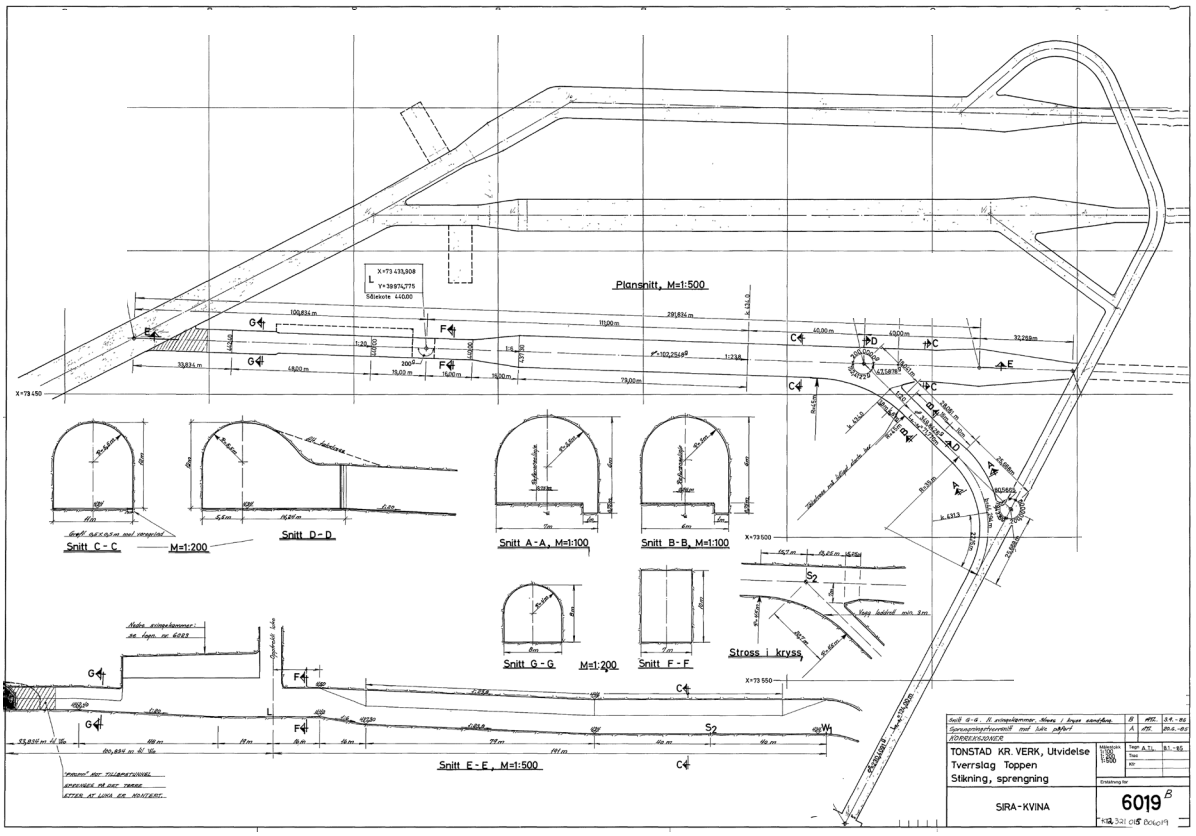

Figure 9: One of the Tonstad sand trap III drawings used as a base for model construction

Simplifications were made in some components of the sand trap during construction. The scaled height of the surge tank is not fully included in the model so as to fit into the available laboratory space and facilities. It was assumed that lowering the height of the surge will not significantly influence the model test results under the current scope of the study. The top geometry of the lower surge chamber, as well as access tunnel, are simplified to half hexagon shape instead of semi-circular structure.

4.2 Model components

The model starts at the headrace tunnel and ends at the transition to the penstock. It consists of the lower surge chamber, the surge shaft and the sand trap including the access tunnel (till the concrete plug). To ensure correct inflow to the sand trap, the model includes about 49 m of the headrace tunnel upstream of the lower surge chamber. In the downstream, the model is constructed till the transition section to the penstock, ensuring correct acceleration of water out of the sand trap. The model is about 16 m long reproducing about 320 m of the prototype section. The width of the model is about 1 m (including the steel support) while the maximum height of the model is about 3.8 m. The turbine is represented by a valve at the end of the model. The surge tank gate is constructed of thick acrylics which is operated manually. The sand trap model is constructed such that it can be deepened if necessary, at the later stage of the study. The schematic sketch of the sand trap III model is shown in Figure 10. The plan and longitudinal section of the model are shown in Figure 11. The detail drawings of the sand trap model are presented in Appendix A-9 and A-10.

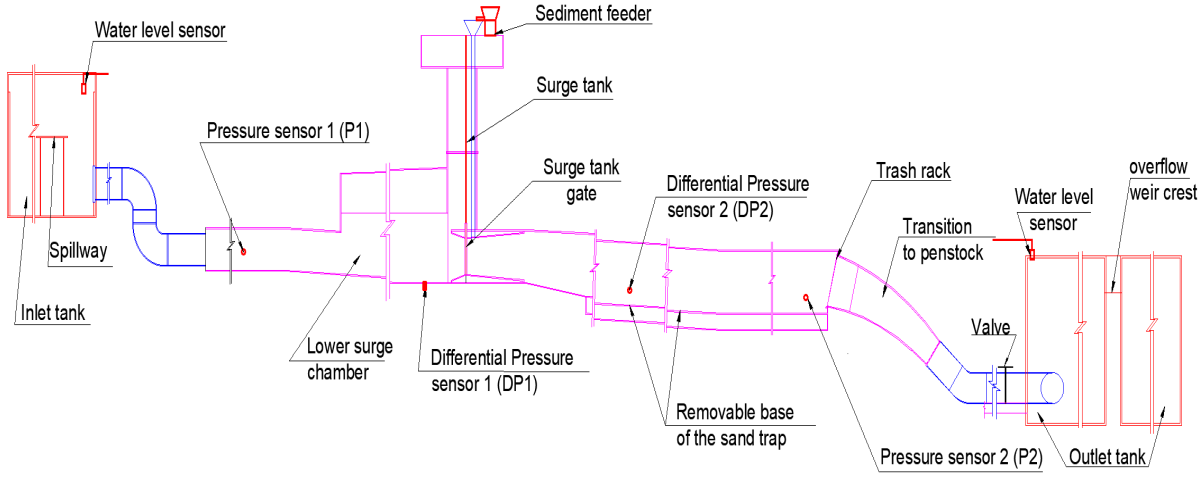

Figure 10: Schematic overview of the sand trap III model at the laboratory

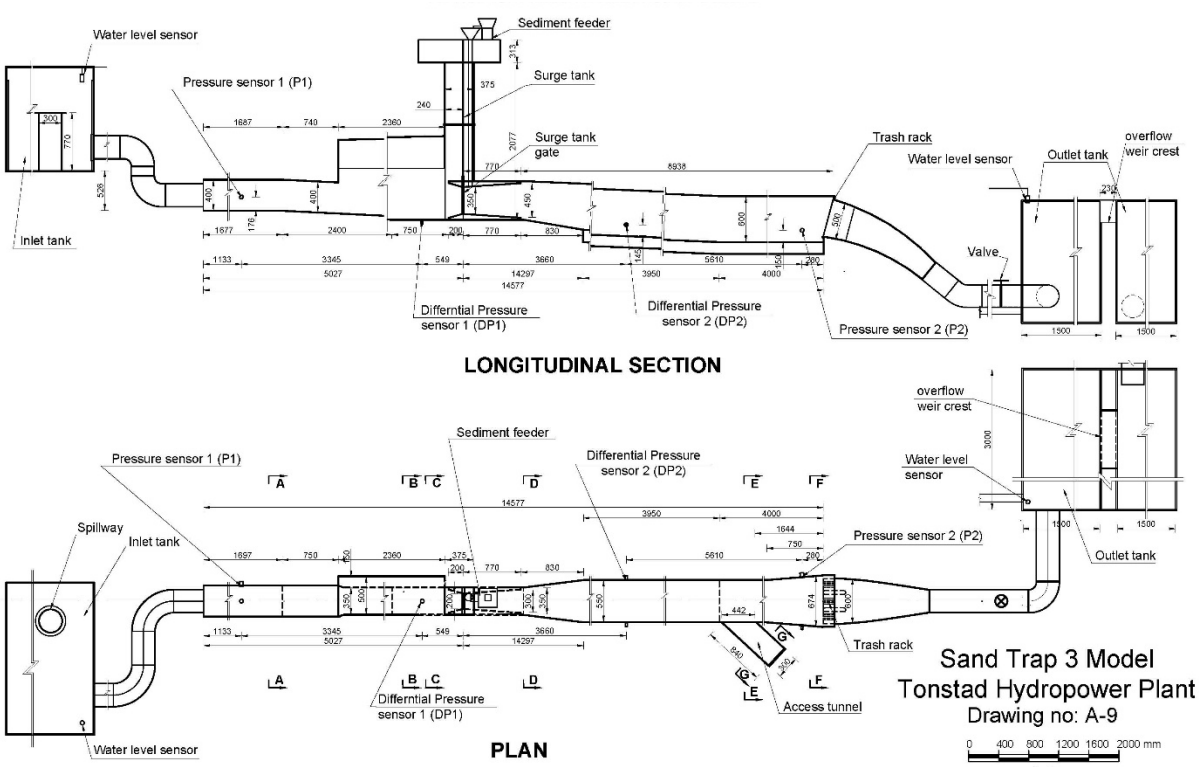

Figure 11: Plan and longitudinal section of sand trap III model at the laboratory

4.3 Model construction and general considerations

The sand trap model is built using acrylic sheets for the visibility of flow pattern and sediment movement as well as its flexibility for moulding into different shapes. The model structure is exposed to a maximum pressure of about 3 m in the model. The plexiglass has density of 1.18 kg/m^3, tensile strength of 70 MPa and modulus of elasticity of 3. 3GPa.The sand trap model is mounted in steel frames for easy dismantling and transport of the model components to Sira-Kvina after the completion of the model tests.

The sand trap and the tunnels in prototype are unlined except for some areas with weak zones. However, for this study, the roughness of the rock surface is neglected for the ease in construction as well as to keep the visibility of the acrylic model intact.

An overview of the sand trap model indicating the distances in the model scale is shown in Figure 12. The distances are marked to locate the photographs taken with respect to its specific location in the sand trap.

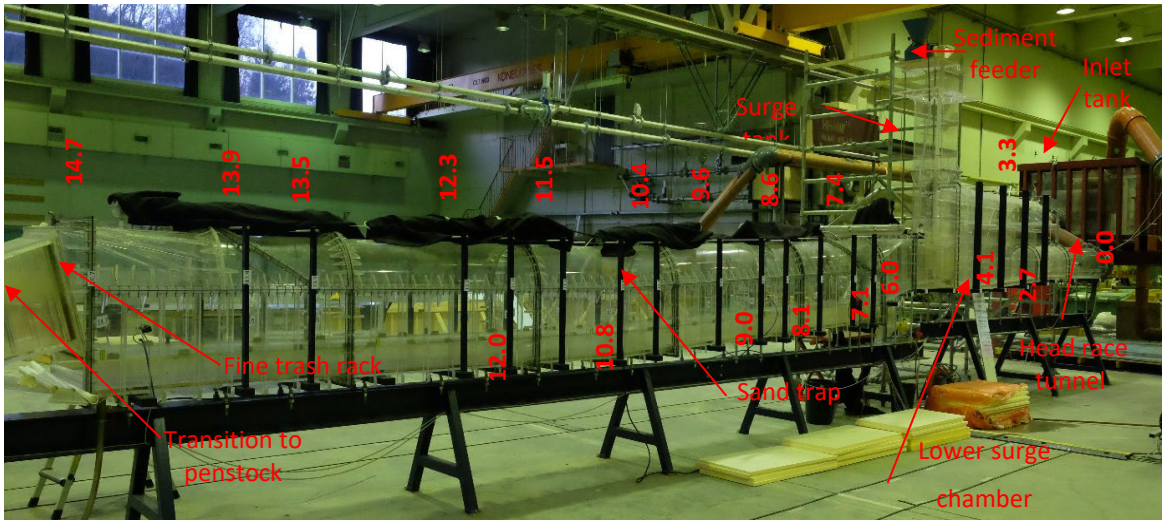

Figure 12: Overview of the sand trap III model in the laboratory

The distance measurement in Figure 12 starts at the start of the headrace tunnel in the model (0 m). The distance marking is in model scale. The distance of the surge tank gate is 5 m from the start of the headrace tunnel and the uniform section of the sand trap starts at 6.6 m.

4.4 Inflow and outflow arrangement in the model

An inlet tank supplies water to the sand trap model. Water is supplied to this inlet tank via pipeline connected to the main overhead tank of the laboratory. The laboratory has underground reservoirs from which the water is pumped to this overhead tank that supplies water to the model at a constant head. A valve is provided in the pipeline to regulate inflow to the model. The inlet tank is also facilitated with a spillway to avoid flow overtopping in case of backflow. A view of the inlet tank is shown in Figure 13.

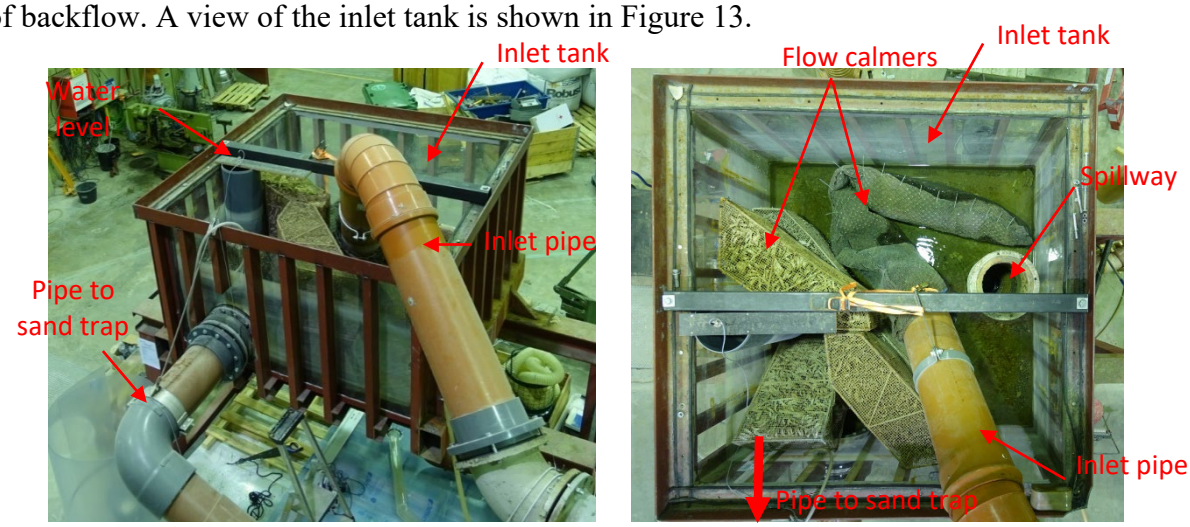

A. Perspective view B. Plan

Figure 13: Overview of the inlet tank

At the end of the model, a pipeline connects the model to the outlet tank furnished with a spillway. The water from this outlet tank, overflow to the other tank and back to the return canals and the main reservoir. The outlet tank also functions as a sedimentation tank for the sediments that pass through the sand trap model. This basin also ensures stable downstream pressure for the operation of the valve to ensure repeatability. A view of the outlet tank is shown in Figure 14.

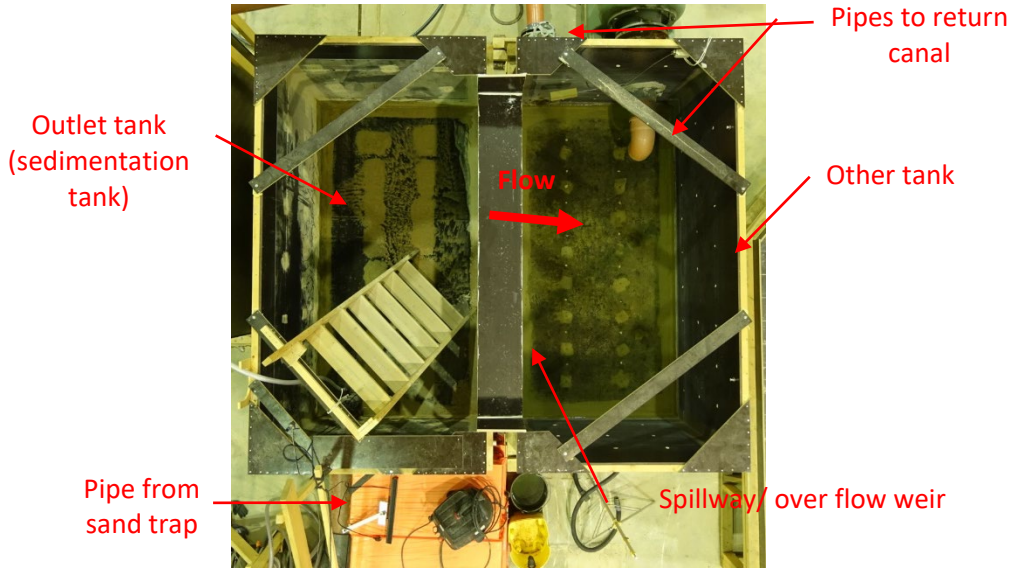

Figure 14: Plan view of the outlet tank

4.5 Measurements and instrumentation in the model

Model test parameters require proper measurement facilities and arrangements which can give consistent measurement with an acceptable level of accuracy. At normal condition, a simple direct method of measurement is convenient and acceptable. However, for a very complex flow condition, a more advanced and sophisticated instrument would be preferable depending on its availability. In some circumstances, the flow pattern, sediment transport and deposition pattern study in the model can be assisted by photograph, video and dye tests. The instruments used in Tonstad sand trap III model study is described in the following sections.

4.5.1 Flow measurement

An electromagnetic flowmeter is provided in the inlet pipe to keep track of the incoming discharge to the inlet tank. A flow meter is also provided to measure the spillage discharge from the inlet tank. The flow meters used are SITRANS FM MAG 5100 coupled with MAG 5000 transmitter, with an accuracy of 0.25% and 0.4% of flow rate respectively. The

repeatability is 0.1% for velocities > 0.5m/s and conductivity >10μS/cm. The photograph of the flow meter is presented in Appendix D-1(A).

A rating curve for the spillway in the overflow tank was also generated to ensure the discharge coming through the sand trap when the spillage discharge from the inlet tank is relatively less for the ensured accuracy in measurement by the flow meter. It also guides in adjusting the downstream valve during tests. The rating curve for the spillway is presented in Appendix C-1. The table showing the details of the rating curve is shown in Appendix B-3.

4.5.2 Water level measurement

Water level measurements are carried out in two areas. In order to know the pressure acting in the system, a water level sensor is provided in the inlet tank. A water level sensor is also installed in the outlet tank to measure head over the crest of the overflow weir in the outlet tank/ sedimentation tank. The water level sensors used are ultrasonic sensors with an accuracy of $\pm$1% and repeatability of $\pm$0.15 % and has a measurement range of 350 to 65 mm. Photograph of this sensor is presented in Appendix D-1(B).

4.5.3 Pressure measurement

A differential pressure sensor is installed to measure pressure difference at four different locations in the model, enabling to study how different arrangement or modification in the design, influence the head loss in the system and thereby influence the power production. The differential pressure sensor used was Aplisen's smart differential pressure transmitter (APR-2000/AL) with an accuracy of 0.375%, and a maximum measurement range of 0 to 25 Kpa/2.5 m of H_2O. The span set for measurement is 0.5 m during testing. The photograph of this sensor is presented in Appendix D-1(C).

Two pressure sensors (P1 and P2) are also provided at the inlet tunnel and before the trash rack in the sand trap to measure the pressure head at these locations. Wika S11 pressure transmitters are used which has a measurement range of 0 to 0.4 bar/4 m of H_2O. The accuracy of the instrument is $\leq \pm$0.5 % and the repeatability is $\leq$ 0.1%. The photograph of this pressure sensor is presented in Appendix D-1(D).

The pressure sensor, P1 is placed in the headrace tunnel, 78 m upstream of the surge tank gate while the pressure sensor P2 is located at the end of the sand trap just before the fine trash rack. The differential pressure sensor is connected about 11 m upstream and about 78 m downstream of the surge tank gate, namely DP1 and DP2 respectively and the rest two at the same two

locations of the pressure sensors, P1 and P2. The measurement locations are represented as P1, P2, DP1 and DP2 in this report. An overview of the locations of the pressure sensors and the measurement point for the differential pressure sensors is shown in Figure 15. The location of the pressure sensor and the differential pressure sensor measurement point are shown in drawing in Appendix A-9.

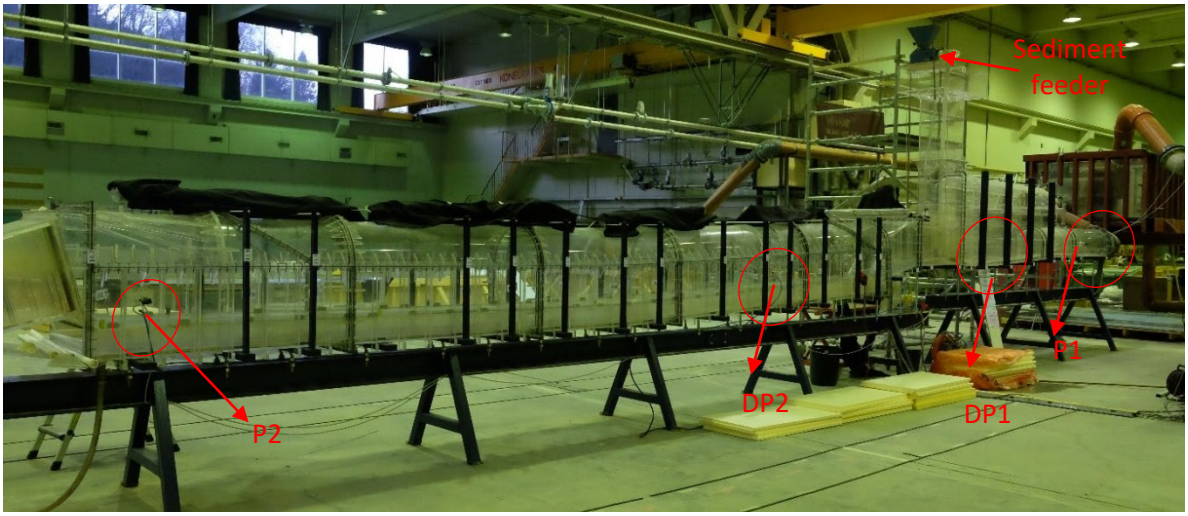

Figure 15: Location of the pressure sensors and differential pressure sensor in the model

4.5.4 Thermometer

A thermometer is placed in the overflow tank to keep track of the water temperature in the laboratory. The water temperature has a significant effect in the fall velocity of the sediment particle. The water temperature in the prototype is assumed to be approximately 4 degrees which is normally between 10 to 20 degrees in the laboratory [10].

4.5.5 Sediment feeding arrangement

Information on sediment inflow, outflow and deposition are necessary to measure the trap efficiency of the sand trap. Calibrated vibrating sediment feeder was used to supply a known quantity of sediment into the model. Mass oscillations may lift and mix the sediments in transition between the surge tank and the sand trap. This is accounted for by adding sediments from the top of the surge tank. The assumption was that, if the performance of the sand trap would be acceptable with sediments entering the basin on suspension mode, then much better trapping efficiency can be expected when sediment is transported as bed load to the basin.

The sediment feeder is placed on the top of the surge tank which releases sediment to a cone connected to a pipe that releases the sediment on the invert of the tunnel, just after the surge

tank gate. The sediment was fed in the slurry form by adding water pumped from the same system to this cone. A photograph of this arrangement is shown in Appendix D-1(E).

4.5.6 Collection of sediment deposited in the model

The sediment trapped in the sand trap was collected using a vacuum cleaner after it is dried using an air blow dryer. This sediment from the outlet tank was collected using a vacuum cleaner but in its slurry form. All the sediments collected was then dried in the oven at 105 degrees until no further change in weight of the sediment occurs on increasing the span of drying. The dried samples are then further investigated.

4.5.7 Gate operation and opening control

In the prototype, the surge tank gate is hydraulically controlled with a maximum lifting and lowering speed of 1cm/s. However, the surge tank gate is operated manually in the model. It has threaded rod and wheel connection such that horizontal rotation at one end raises or lowers the surge tank gate. A measuring scale is placed along the side of the gate that indicates the opening of the surge tank gate.

In the following chapters, the procedures and results of the model tests are presented and discussed.

5 Model test of the existing situation of the sand trap

This chapter presents the model tests carried out to assess the performance of the existing sand trap III. This information will be essential to assess the impact of the modification in the design, with respect to trap efficiency in its current state. The tests carried out under this heading are briefly described below.

The test plan includes the following.

i. Existing design test in terms of pressure head loss and trap efficiency in steady flow condition

ii. Trap efficiency test with un-steady flow condition

iii. Model test on the impact of sand trap filling on trap efficiency in the existing geometry of the sand trap

iv. Model test to observe the influence of sediment feeding mechanism on the performance of the sand trap in the existing design

The pressure head loss tests were carried out at four different discharges 20, 40, 60 and 80 m^3/s while the trap efficiency tests were carried out for 80 m^3/s which is the design discharge of the sand trap. All the measurements and data given in this report are in prototype scale unless specified otherwise**.**

5.1 Pressure head losses

This test was carried out to evaluate the impact of design modifications on the head loss in the sand trap which directly influences the power production of the plant. The head loss measured in the existing design of the sand trap will provide a basis for evaluation of the modification in the design.

The head loss test was carried out at four different steady discharges, including the design discharge, without feeding sediment. These discharges are shown in Table 2. After the steady discharge is maintained in the model, the pressure measurements and the differential pressure measurements were taken at four different locations as described in section 4.5.3. The pressure head changes measured are presented in this report, considering the velocity head remains constant for one particular discharge, as the cross-sectional area remains the same. Thus, it was

assumed that the comparison of pressure head between two different tests at the same discharge will indicate the impact of the modification on the design.

During the test, the major flow passed through the upper portion of the sand trap inlet transition and this was prevalent up to certain distance downstream in the sand trap. A view of the flow scenario captured during the dye test at the design discharge of 80 m^3/s is presented in Figure 16. The geometry of the sand trap i.e., the higher slope at the bottom of the inlet transition, as well as sloping of the sand trap downwards may have contributed to this phenomenon. It was difficult to exactly determine where the flow was uniform over the depth in the sand trap. However, based on the dye test, the flow seemed to be uniform over the depth within 80 m distance from the start of the sand trap. A video taken during the dye test is presented in Appendix E-1.

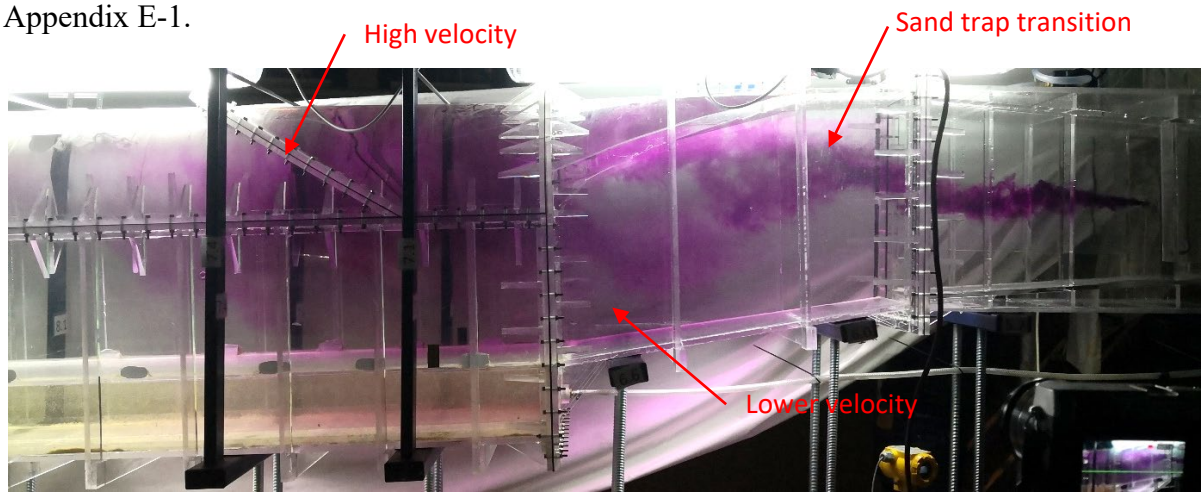

Figure 16: Flow scenario in the upstream part of the sand trap including sand trap transition during dye test

The pressure head loss measured at different locations in the model by the differential pressure sensor during the tests is shown in Table 2. The pressure head changes recorded at different steady discharges is also presented in Figure 17. However, it is important to consider the accuracy range of the instrument that is used in the model (i.e. 0.375 mm in model scale=7.5 mm prototype), during analysis.

Table 2: Pressure head loss measured along the sand trap

S.NO	Inflow to the tunnel	Pressure head loss based on differential pressure sensor			
		From P1 to P2	From P1 to DP1	From DP1 to DP2	From DP2 to P2
	m^3/s	mm	mm	mm	mm
1	20	1	2	1	-2
2	40	10	4	9	-4
3	60	21	7	20	-6
4	80	38	12	34	-8

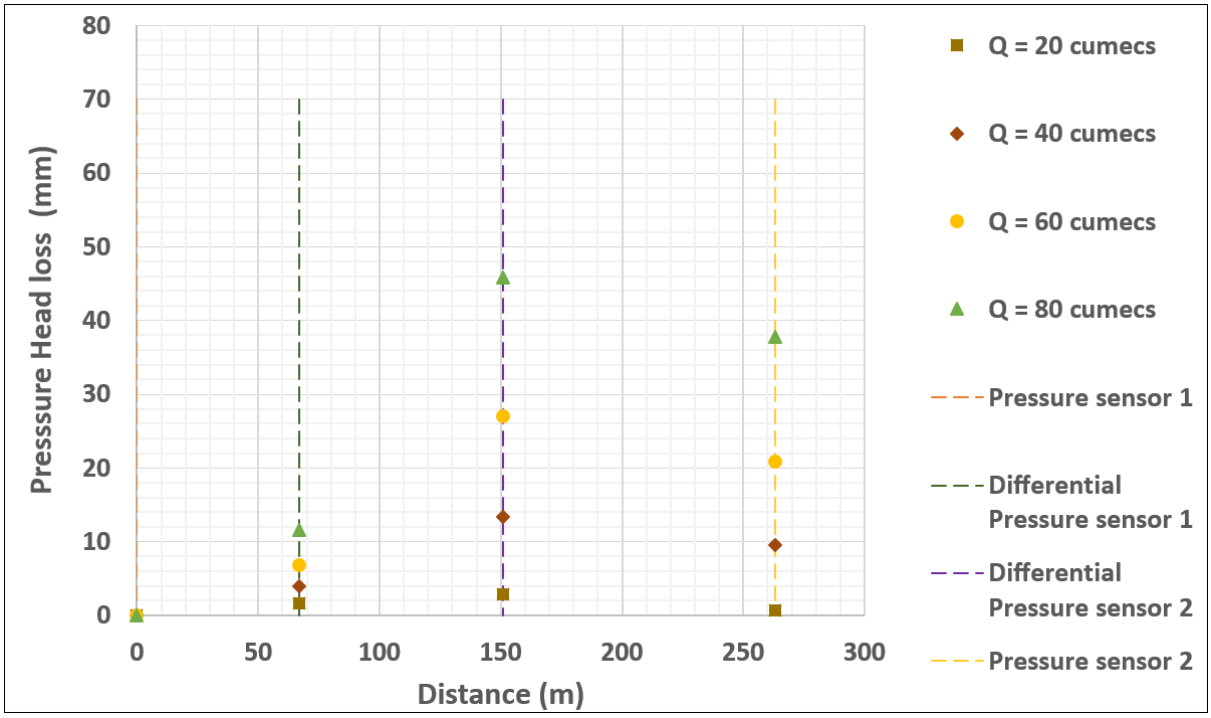

Figure 17: Change in pressure head along the sand trap

The pressure head changes are very minimal as the surface of the sand trap is smoother than in the prototype. As shown in Table 2, the pressure head loss increased when the discharge increased at all the measurement location. . An increase in pressure head was about 25 % on average between DP2 and P2, at the end of the sand trap. This could be due to the decrease in velocity head as a result of the increase in the cross-sectional area of the sand trap, before the trash rack.

The overall pressure head loss in the system, from inlet tunnel till the end of the sand trap (P1 to P2) measured with the pressure sensors are slightly different from the pressure head loss

measured by the differential pressure sensor. However, the trend in pressure head loss is the same for both the measurements. It is worth mentioning that the difference in the pressure head loss measured is only around 1 mm in model scale which is within the accuracy range of the instruments used.

Based on the specification, the accuracy of the pressure sensor is 0.5 % i.e. 20 mm in model scale. This is quite high, in the context where the head losses being measured are below 1mm in the model scale. However, the pressure head loss recorded from the differential pressure sensor was used for the analysis of the model test results. For comparison purpose, the head loss measured by both the pressure sensor and differential pressure sensor is presented in Appendix B-4.

The pressure head loss is also recorded for design discharge feeding sediment in order to show the difference in pressure head loss with and without sediment in the flow. There was no significant variation between the measurements. Therefore, the head loss tests were simplified and carried out without feeding the sediment henceforth. Table 3 shows the head losses measured with and without feeding the sediment.

Table 3: Pressure head loss measured along the sand trap at design discharge with and without feeding sediment

S.NO	**Inflow to the tunnel**	**Pressure head loss based on differential pressure sensor**			
		From P1 to P2	**From P1 to DP1**	**From DP1 to DP2**	**From DP2 to P2**
	m^3/s	**mm**	**mm**	**mm**	**mm**
1	Without feeding sediment				
	80	38	12	34	-8
2	Feeding sediment				
	80	38	13	33	-7

5.2 Trap efficiency test

The general purpose of the sand trap is to reduce the flow velocity in the basin and increase the effect of gravity relative to the flow turbulence in the water flow such that, the sediment is deposited and relatively clear water is transported to the turbines. The higher the trapping efficiency the better is the performance of the sand trap. The trap efficiency of a sand trap is mainly influenced by the geometry of the basin. A larger basin facilitates the exclusion of more

sediment load if terms of both volume and size while the shape of the sand trap determines the flow distribution in it.

The trap efficiency tests were carried out in the model for both steady and unsteady state operation of the powerplant. The tests were carried out at design discharge (80 m^3/s). Sediment size of d_{50} = 3 mm was used for the tests. The particle size distribution (PSD) curve of this sediment represented as sieved sand is presented in Figure 8. After the steady discharge is maintained, the sediment was fed in from the top just after the surge tank gate, as described in section 4.5.5. It is also worth mentioning that the water temperature was about 17.5 ˚C in the model during the tests.

The sand collected from the sand trap in the prototype varied in amount every year. Some of the recorded amount of sand removed during the inspection is shown in Figure 18.

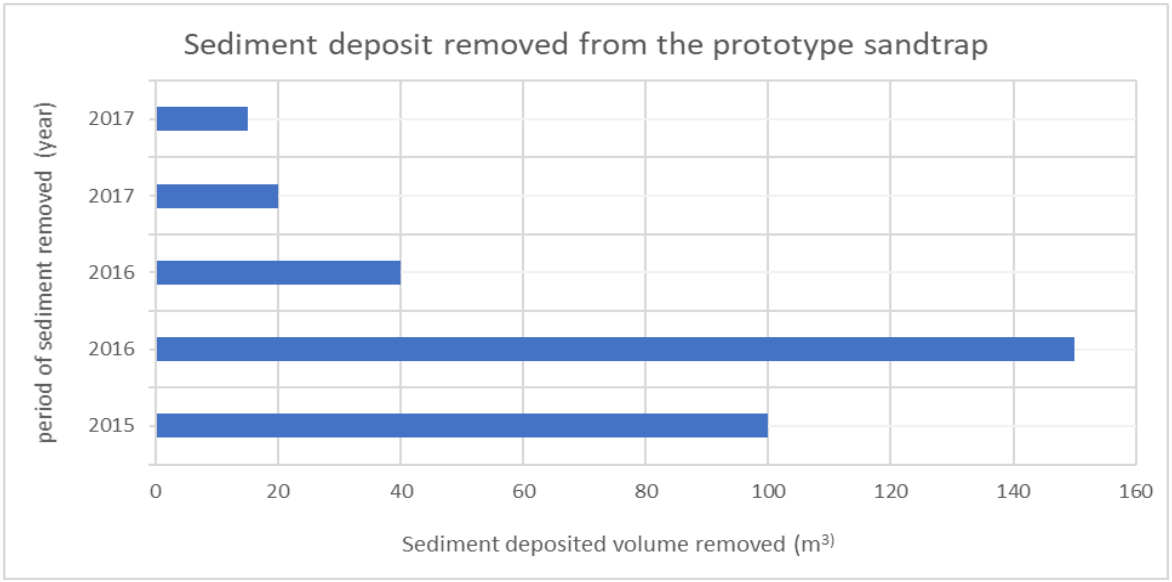

Figure 18: An overview of periodic removal of sediment deposit from Tonstad sand trap III

In terms of volume, it was decided that about 60 m^3 of sand (20 kg of sediment in model scale) shall be fed in the model for the trap efficiency test. This was based on the sediment collected in the sand trap in 2018 [7]. To represent one year in the model, it would take 82 days. This is not possible due to time and resource limitation, so it was simplified and the equivalent amount of sediment was fed in over a period of about 4.47 hours (equivalent to one hour in the model). A test was also done by feeding about 242 m^3 of sediment (80 kg of sediment in model scale). However, this did not increase the depth of deposition in the sand trap significantly. Thus, feeding about 60 m^3 of sediment was accepted for the tests.

During sediment feeding in the model, it was observed that sediment transported in full suspension along the entire length of the sand trap. The videos taken during the feeding of sediment is presented in Appendix E-2. Sediment deposition started at the inlet transition of the sand trap and continued further downstream in the model. There was deposition over the entire length of the sand trap unlike in the prototype where deposition pattern was concentrated in two major areas, as described in section 3.2.3. This could have occurred because of feeding the sediment from the top. The sediment size used in the model could also be another factor. In the model, fine sand below 5 mm grain size was used, whereas in the prototype about 50 % of the collected sample from the upstream part of the prototype was below this size.

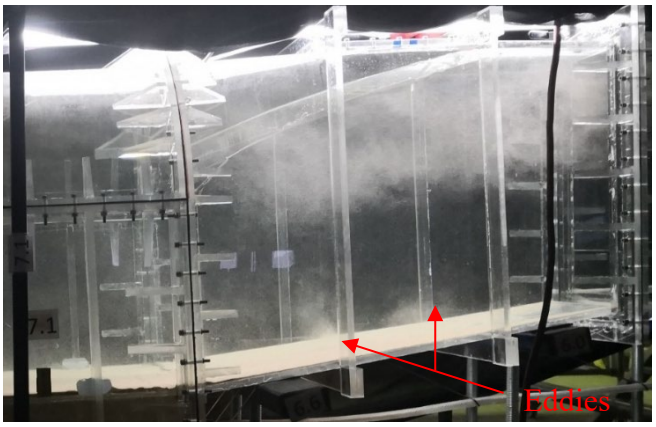

Figure 19: Localised eddies seen in the sand trap transition

Minor eddies occurred at times in the sand trap transition during the test, upheaving the sediment deposited in this area, as seen in Figure 19. These eddies occurred occasionally within the first 20 m of the uniform section of the sand trap. However, movement of the sediment, deposited at the bottom of the sand trap was not observed along the entire length of the sand trap.

The sediment deposited in the central part, at the start of the inlet transition to the sand trap, eroded over time as seen in Figure 20. Sedimentation and erosion actively took place in this area; however, the extent of erosion, expanded over time. The length of this erosion was about 6.5m (from the start of the inlet transition) by the end of the sediment feeding process.

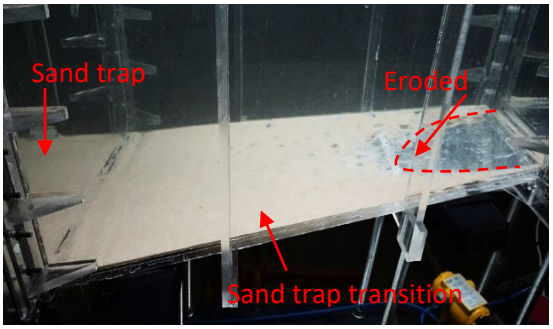

Figure 20: Sediment deposition in sand trap transition

The depth of deposition was very less, in millimetres in the model along the entire length of the sand trap. Thus, it was difficult to be accurately measured due to practical problems

especially unclarity in vision. Observation and documentation using photos and videos were made for visual comparison. The deposition was relatively higher on the left side of the model compared to the right side. This could be due to the feeding of sediment from the left side of the model. It was also difficult to visualize the change in sediment grain size distribution along the length of the sand trap, as sediment fed was quite fine in the model. However, it was clear that the sediment deposited in front of the trash rack was relatively fine compared to that in the initial length of the sand trap. A video taken after the completion of the feeding sediment is presented in Appendix E-3.

Some fraction of the sand fed in the model was also observed to pass through the sand trap. A part of this was deposited in the downstream of the trash rack, as shown in Figure 21. This sediment will finally be transported downstream to the turbines in case of the prototype.

After the sediment feeding was complete, the tests continued at different flow conditions, for evaluating the trap efficiency of the sand trap.

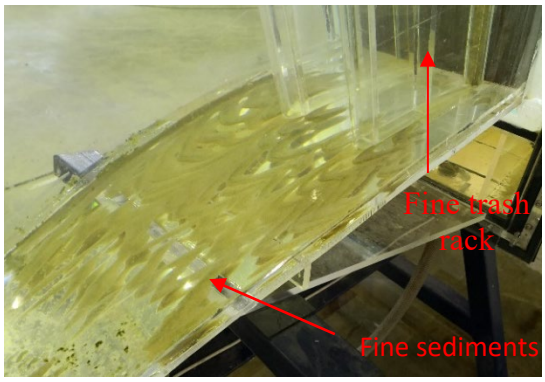

Figure 21: An overview of fine sediment deposited downstream of trash rack

These tests are presented in the following sections.

5.2.1 Steady state trap efficiency

The steady state trap efficiency test was carried out to check the trap efficiency of the sand trap at steady flow situation in the sand trap. The steady state test was carried out using both the sieved and the un-sieved sand.

5.2.1.1 Sieved sand

During the steady state test, the model was run at a steady discharge of 80 m^3/s for 22.4 hours equivalent to 5 hours in the model after the completion of feeding sediment. The sand trap was then slowly emptied without disturbing the sediment deposition pattern inside the sand trap. The sediment, while inside the sand trap, was then air-dried overnight using an air blower and collected using a vacuum cleaner. The collected sediment was then dried in the oven to 105 ˚C to make sure that all the moisture is evaporated. Finally, the sediment was cooled down and then measured. To make sure that all the sediment is collected as far as possible, water jet was

injected to remove sand from the corners of the sand trap and was then collected in slurry form. It was then dried in the oven and measured as stated above. The sediment from the access tunnel was also collected and measured similarly. Sand collected in the outlet tank was also measured to keep track of the sediment lost in the system.

After running the model at a steady discharge of 80 m^3/s for 22.4 hours, the erosion seen in the sand trap transition extended further downstream by about 2 m. This erosion was about 8.5 m long from the start of the sand trap transition. The comparative view of the deposition pattern left after completion of sediment feeding and at the end of the test is shown in Figure 22. The change in the deposition pattern in the sand trap transition over time is also presented in Appendix D-2.

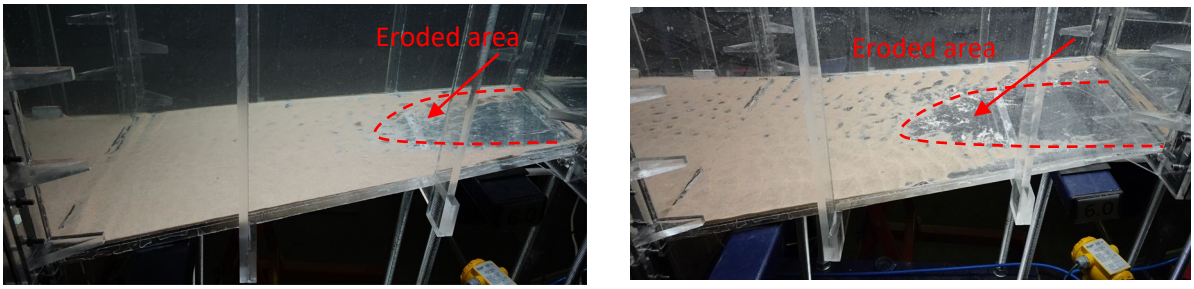

A. After completion of sediment feeding B. At the end of the test

Figure 22: Deposition pattern in the sand trap transition

An increase in ripples was observed which indicate initiation of motion in the upstream part of the sand trap. The ripples were quite prominent in the first 40 m length of the sand trap (uniform section) while mild undulations were observed further downstream, in about 20 m of the sand trap. Defined ripples was observed, at a construction joint 30 m downstream from the start of the sand trap (uniform section) and also in an area about 40 m from the start of the sand trap as shown in Figure 23.

Figure 23: A view of ripples formed at 40 m distance from the start of the sand trap

Uniform deposition was observed in the rest of the area of the sand trap. However, irregularity in the deposition pattern was observed in areas where there were construction joints in the model.

The deposition was higher in the starting section of the sand trap. The deposition was highest in an area about 30 m from the start of the sand trap. The deposition thickness slowly decreases, and very shallow deposition occurs at the end of the sand trap in front of the trash rack. The rough measurement showed that highest deposition measured was about 190 mm in the initial part of the sand trap and the lowest was around 10 mm before the trash rack. However, it is to be noted that the deposition was not uniform across the width of the sand trap. Deposition was higher on the left side and lower on the right side of the sand trap as stated earlier. An overview of the deposition pattern at various location in the sand trap can be found in photo Appendix D-3. The video of the sediment deposition pattern after the test is presented in Appendix E-4.

The trap efficiency of the sand trap including the sand collected in the access tunnel, was on average about 87% as show in Table 4. The details on the trap efficiency test are presented in Appendix B-5. It was observed that there was some loss of sediment from the bottom of the sand trap. Thus, the trap efficiency could be a bit higher than 87%. Details on the sediment losses in the system are discussed under the limitations of the model in section 7.4.

Table 4:Trap efficiency of the sand trap for steady state test

Test type	**Average Steady state**
Sediment	**%**
Collected in sand trap	86.9
Collected in access tunnel	0.3
Collected in sand trap including access tunnel	87.2

The PSD curves of the sediment collected at different locations of the sand trap are presented in Figure 24. The PSD data is presented in Appendix B-6. Relatively coarser sand was deposited at the start of the sand trap while relatively fine sediment was deposited before the trash rack. The sediment deposited in the access tunnel was the finest. The sediment of about 5 mm grain size was observed to be transported downstream of the sand trap even though the sand trap was designed to trap sediments up to 2 mm. The PSD curve shows that coarse sediment grains were transported to the outlet tank.

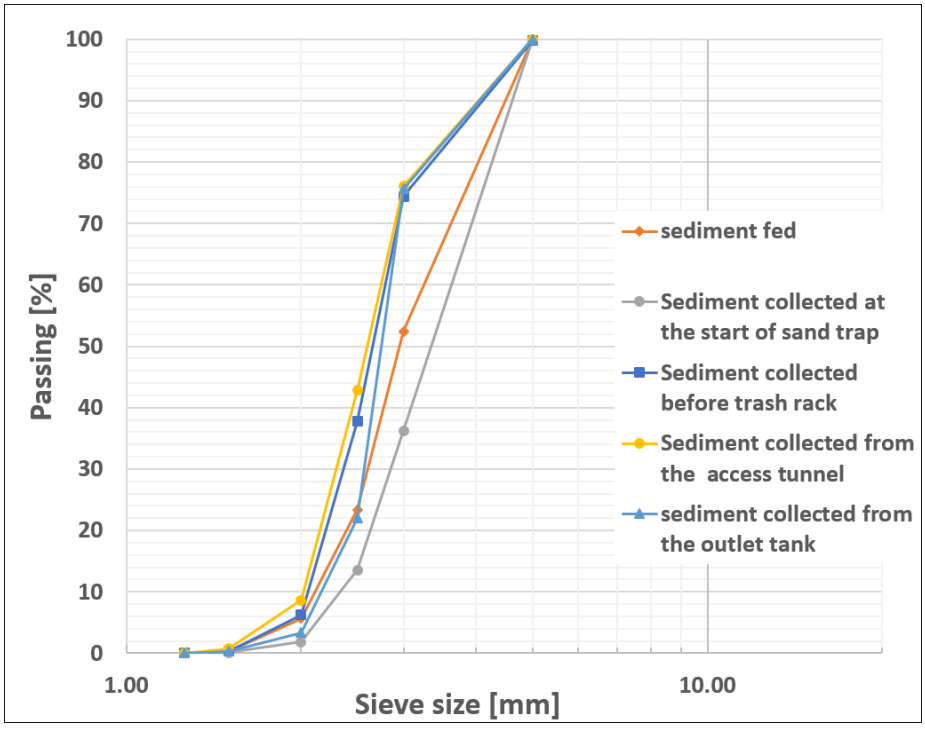

Figure 24: PSD curve of sediment collected at various location in the sand trap after steady state trap efficiency test using sieved sand

5.2.1.2 Un-sieved sand

A steady state trap efficiency was also carried out using commercially available (un-sieved) sand . As the commercially available sand had smaller fraction with grains above and below the range of the sieved sand, the test was carried out to check if this sand could be directly used as model sediment and the sieving of the sand could be avoided. The PSD curve of this commercially available sand is presented in Figure 8. The d_{50} of this sand is 3 mm. The same test procedures were followed as for the test described earlier.

The deposition pattern was similar to the test with sieved sand except for mild changes in the formation of the ripples. The deposition depth was almost the same with higher deposition in the upstream part of the sand trap that decreased slowly in the downstream part of the sand trap. Photographs showing the deposition pattern at various location of the sand trap taken at the end of the test is presented in Appendix D-4. A video showing the deposition pattern left after the test is presented in Appendix E-5.

The trap efficiency of the sand trap including the access tunnel was found to be around 89 %. The details on the trap efficiency are presented in Appendix B-7. This was 2% higher than the trap efficiency of the sand trap with sieved sand. Due to alternate expansion and contraction in the model, leakages occurred through the joints in the model over time. In such a case, the trap efficiency of the sand trap was found to be 87 % . This was similar to the trap efficiency test result with sieved sand. A comparative table showing the trap efficiency for both sieved and as shown in Table 5. This indicates that the assumption of trap efficiency to be slightly higher than that measured in the steady state trap efficiency test with sieved sand is valid.

Table 5: Trap efficiency of the sand trap for sieved and un-sieved sand at steady state test

Sediment	**Sieved sand**	**Un-sieved sand**
	%	**%**
Collected in sand trap	86.9	86.5
Collected in access tunnel	0.3	0.4
Collected in sand trap including access tunnel	87.2	86.9

The graph showing the PSD curves of the samples collected at various locations in the sand trap during the test, is shown in Figure 25 and the related data is presented in Appendix B-8.

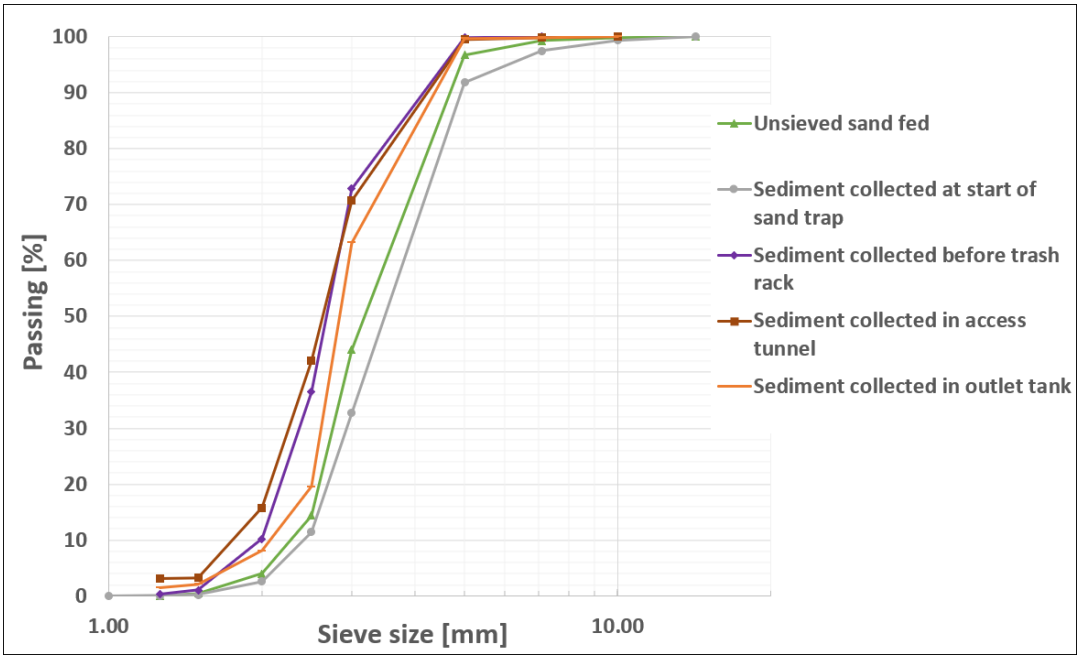

Figure 25: PSD curve of sediment samples collected at various location in the sand trap after steady state trap efficiency test using un-sieved sand

The PSD samples collected at various location in the sand trap shows that coarser particles get deposited at the start of the sand trap while relatively fine particles get deposited before the trash rack. Particles of about 5 mm also passed through the trash rack during this test. A comparative graph showing the PSD of the samples collected at various locations in the sand trap during the tests with both sieved and un-sieved sand is presented in Appendix C-2.

As the trap efficiency was almost the same for both sieved and un-sieved sand, to make optimum use of the resource, un-sieved sand was used for further study. In addition, the use of graded sediment corresponds to the natural phenomenon of graded sediment that occurs in the sand trap, where sediment of variable sizes is carried by the water.

Another test was carried out to check the impact of operation hours on trap efficiency. The test involved shorter test hours after the completion of the feeding of sediment. In this test, the model was run at a steady discharge of 80 m^3/s for 9 hours after the completion of feeding the sediments. It was also observed that the change in the trap efficiency was not significant even though the test was carried out for a shorter period. The trap efficiency of the sand trap including the access tunnel was about 87%. Here, the comparison was made with the test results for steady state test with some leakages in the model as the model condition was similar in this test as well. The details on the trap efficiency and the PSD data of the samples collected during the test is presented in Appendix B-9 and B-10 respectively. However, as the total run time

was not considered to be the critical path for the complete test, the test time of 22.4 hours was adopted for further testing.

5.2.2 Unsteady state trap efficiency test

As the power plant has been running with frequent load changes to meet the power demand, it is important to check its impact on the trap efficiency of the sand trap. A sudden opening of the power plant is considered critical in terms of sediment movement and the impact of this scenario was studied in the model.

In the prototype, the turbine can be opened from 0 to full load within 100 secs while the turbine can be shut down in less than 10 secs. As the valves are opened manually in the model, discharge close to the required amount could be achieved within the time frame. However, further fine-tuning was necessary. The closure of the turbine is considered to be not that significant in terms of scouring and transporting of the sediments. Thus, closing the valve within 45 secs was considered acceptable for the model test.

The unsteady state trap efficiency test was carried out with sieved sand as this test done before the steady state test with un-sieved sand. After completion of feeding sediment in the model as described earlier, the valve in the downstream of the sand trap, representing the turbine was closed in about 45 secs and was then instantly opened in 100 secs to simulate sudden closure and opening of the turbine. The model was then continued running at the same steady discharge for the next 4.47 hour (1 hour in the model). This cycle of sudden closure and opening to run at steady discharge was repeated 5 times such that the test continued for a total of 22.4 hours (5 hours in the model), after the completion of sediment feeding.

During sudden opening and closure of the valve, sediment movement was not observed in the sand trap. For further insight to the process, the videos taken at different locations of the sand trap during sudden closure and opening of the sand trap is presented in Appendix E-6.

The sediment deposition pattern as well as the depth of sediment deposit in the sand trap after the completion of the unsteady state test was very similar to the steady state test. The erosion of sediment in the sand trap transition increased by about 2 m compared to the steady state test after the completion the test. Figure 26 shows an overview in the sand trap transition during steady state test and unsteady state test for comparison. The central part of the initial 10 m of the base of the sand trap transition was exposed at the end of the test.

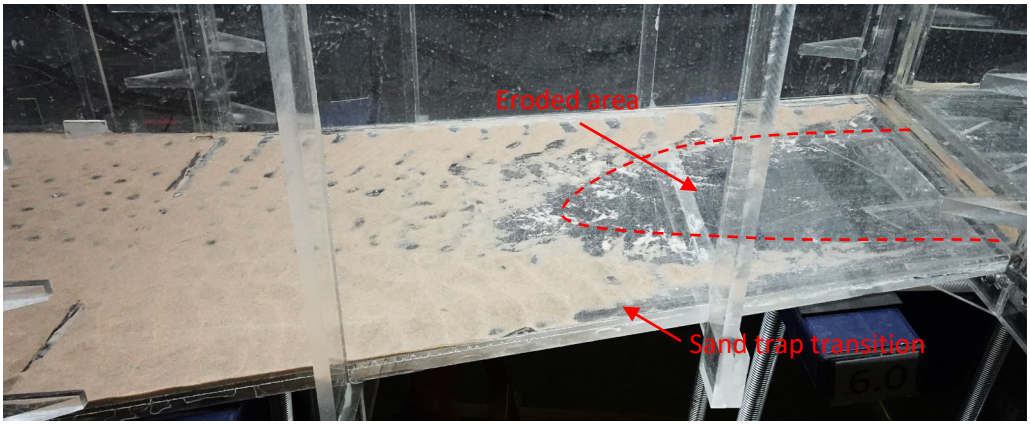

A. Steady state test

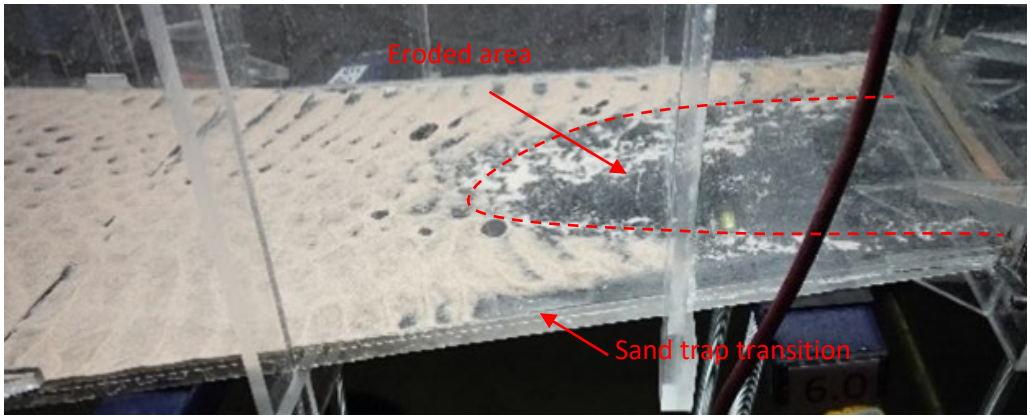

B. Unsteady state test

Figure 26: Sediment deposition in the sand trap transition

The sediment ripples were more prominent in this test compared to the steady state test as shown in Figure 27. Mild ripples extended till the upstream 70 m of the sand trap while the sediment deposit was flat further downstream. A video of the deposition pattern in the sand trap is presented in Appendix E-7 while an overview of the deposition pattern at various locations of the sand trap is presented in Appendix D-5.

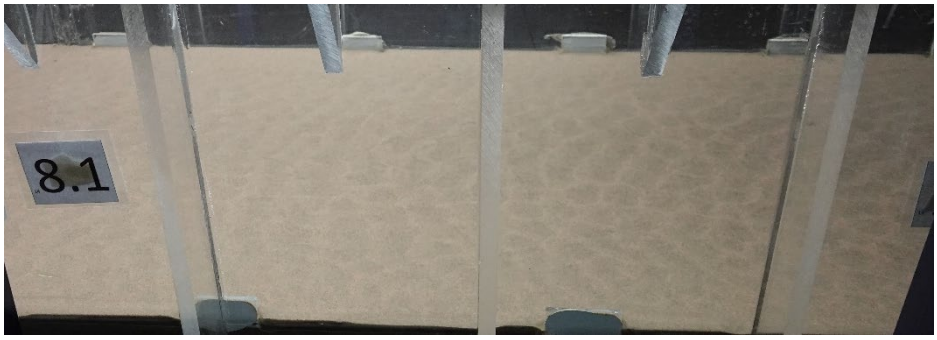

A. Steady state test

B. Unsteady state test

Figure 27: Ripple marks seen on the sediment deposited in the sand trap during steady and unsteady state test

The trap efficiency of the sand trap during the unsteady state test was calculated to be around 87 %. The trap efficiency for unsteady state test was similar to the trap efficiency measured during steady state test. The trap efficiency during steady state test and unsteady state test is presented in Table 6. Further details on the trap efficiency is also presented in Appendix B-11.

Table 6: Trap efficiency of the sand trap for steady and unsteady state test

Test type	**Steady state**	**Unsteady state**
Sediment	**%**	**%**
Collected in sand trap	86.9	87.0
Collected in access tunnel	0.3	0.3
Collected in sand trap including access tunnel	87.2	87.2

The PSD curves of the sediment collected at various locations in the sand trap after the unsteady state test are presented in Figure 28. The table showing the PSD data is presented in Appendix

B-12. The grain size of the sediment deposited in the sand trap was similar to earlier tests, relatively coarser particles at the start of the sand trap and finer before the trash rack. Particles of about 5 mm size were transported downstream of the sand trap. The PSD curves of the sediment collected in the sand trap during steady state and unsteady state test is presented in Appendix C-3.

As the impact of steady and unsteady flow on trap efficiency was not significant, no further unsteady state tests were carried out in the model.

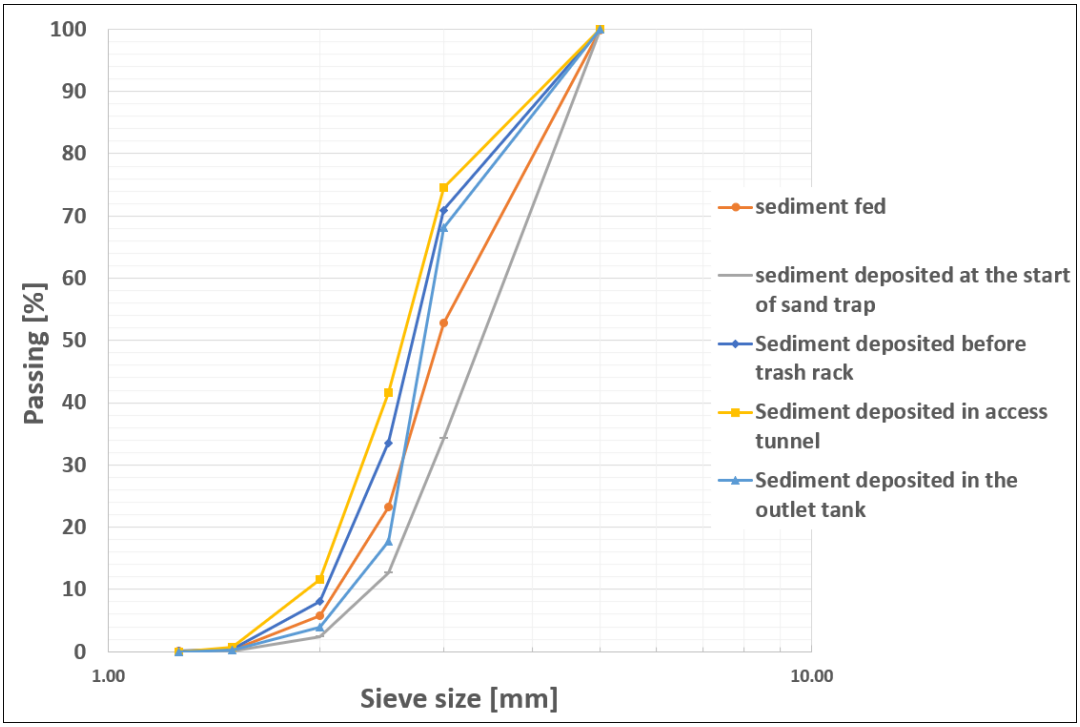

Figure 28: PSD curve of sediment collected at various location in the sand trap after unsteady state test

5.2.3 Sand trap filling test

The sand trap filling test was carried out to check if sediment from the sand trap is transported to the turbine during the filling of the sand trap.

For the test, about 60 m^3 of un-sieved sand was fed in the model at a steady discharge of 80 m^3/s within 4.5 hours. The downstream valve representing the turbine was first closed, followed by the surge tank gate and the inflow valve. The sand trap was then drained slowly without disturbing the sediment deposition pattern. After complete draining of the sand trap, the surge tank gate was opened 50 mm for filling of the sand trap. No additional inflow was provided during this process and only the water stored upstream of the surge tank gate was

used. During the sand trap filling or draining of the water from the surge tank, free surface flow was maintained over the weir crest before the trash track to reproduce critical condition for the erosion of sediment in the sand trap.

The high-velocity flow from the surge tank gate eroded the sediment deposited till the 34 m length of the sand trap. More erosion occurred along the right part of the sand trap with maximum erosion to a distance of about 95 m in the sand trap, almost creating a triangular zone of erosion, after the initial 34 m stretch of the sand trap as shown in Figure 29.

Figure 29: Erosion/deposition pattern after sand trap filling test

The erosion stops and mild deposition occur along this reach as the water level in the sand trap increases until it reaches the top of the weir crest in the fine trash rack. The video taken during the filling of the sand trap is presented in Appendix E-8. It was observed that no sediment was carried to the penstock/ turbine in the process. The scenario in front of the trash rack during the filling of the sand trap is presented in Appendix E-9.

The sediment eroded from the upstream is deposited in the area between 100 to 120 m as shown in Figure 30. Based on the deposition pattern left after the end of the test, it can be concluded that sediment movement occurs in the sand trap almost up to 140 m length of the sand trap including the access tunnel. The deposition pattern in the vicinity of the access tunnel, at around 120 to 140 m of the sand trap can be seen in Figure 31. However, the deposition seemed undisturbed before the trash rack. A video showing the sediment deposition pattern in the sand trap after the sand trap filling test is presented in Appendix E-10. The deposition pattern at various location in the sand trap is presented in Appendix D-6.

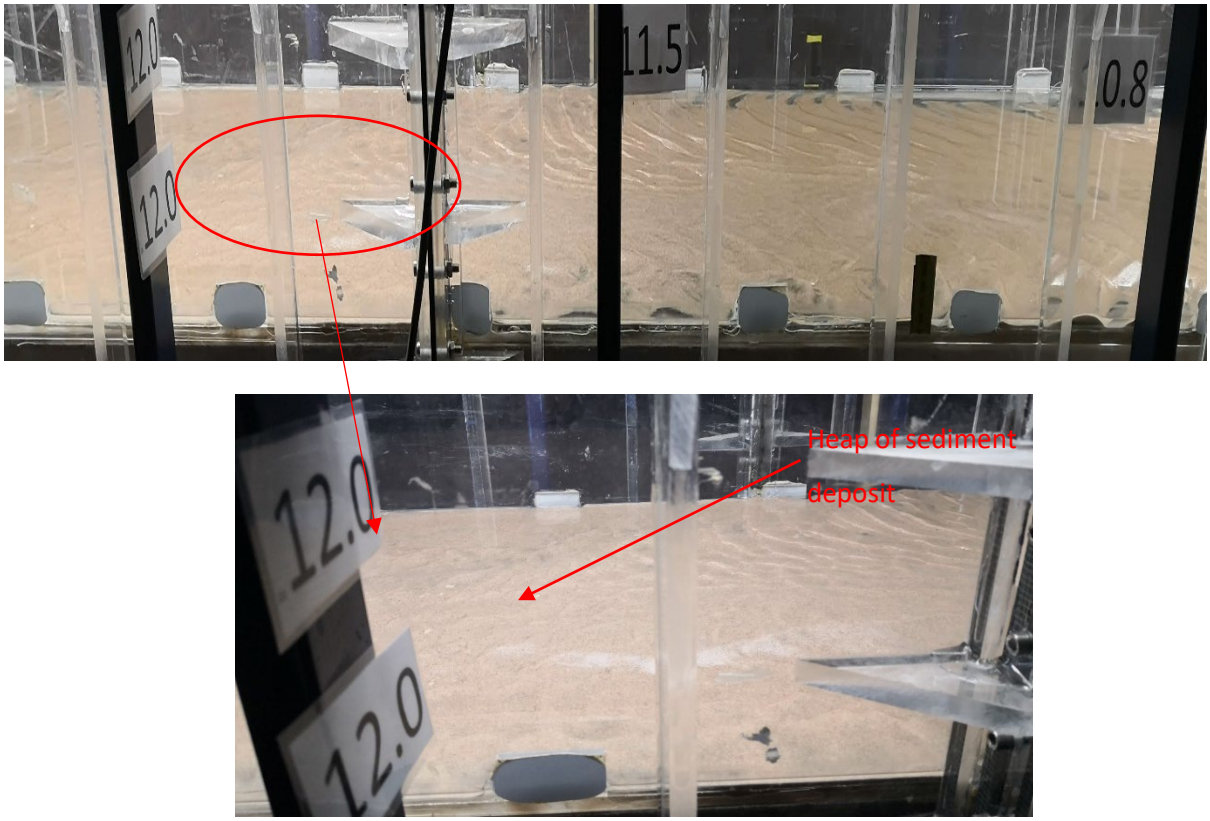

Figure 30: A view of the deposition pattern just downstream of the eroded area left at the end of the sand trap filling test

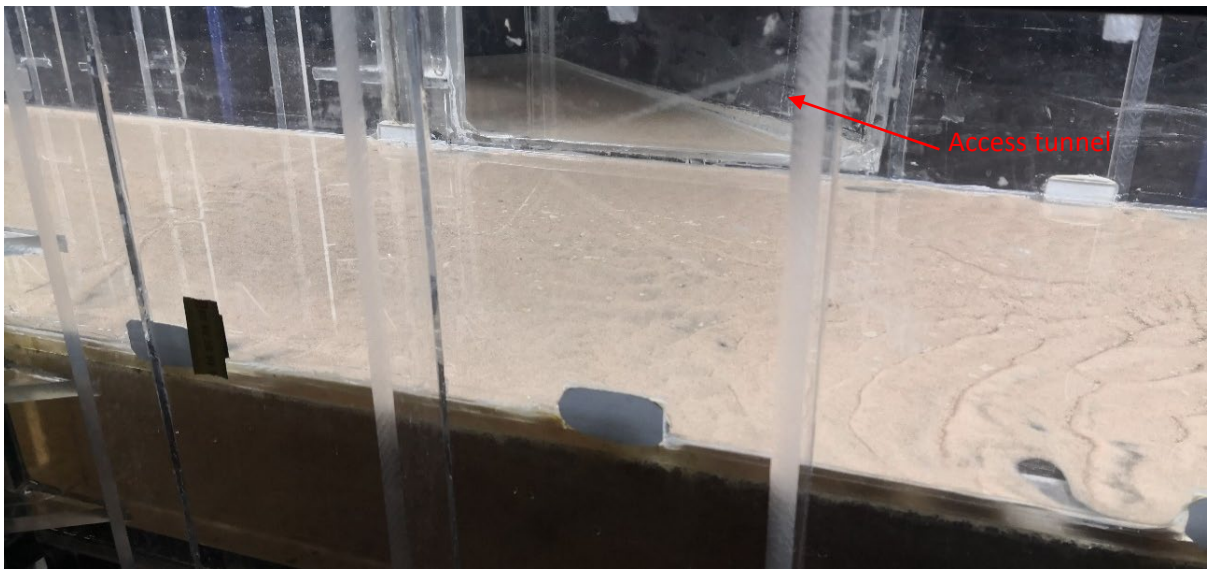

Figure 31: Ripple marks seen in the vicinity of the access tunnel after the sand trap filling test

The trap efficiency of the sand trap was found to be unaffected by erosion during the filling of the sand trap. The trap efficiency was found to be 89 %. However, there was an increase in the amount of deposit in the access tunnel, indicating there was sediment movement even in the vicinity of the access tunnel. This indicates that displacement of the deposited sediment of the

sand trap takes place during the filling of the sand trap. Table 7 shows the trap efficiency measured during steady state test and sand trap filling test. Further details on trap efficiency are presented in Appendix B-13.

Table 7: Trap efficiency of the sand trap during steady state test and after sand trap filling test

Test type	**Steady state test**	**Sand trap filling test**
Sediment	**%**	**%**
Collected in sand trap	88.7	88.6
Collected in access tunnel	0.3	0.5
Collected in sand trap including access tunnel	89.0	89.1

The PSD curves of the sediment collected at various location of the sand trap after the test compared to that of the steady state test are shown in Figure 32. Though slightly finer, not much variation was observed in the grain size of the sediment collected in the sand trap between these tests. Also, the maximum size of the particle carried downstream of the trash rack was about 5 mm, same as that of the steady state trap efficiency test. This indicates that there was no transport of particles from the sand trap to the turbine downstream. The PSD data and PSD curve of the sediment collected in the sand trap is presented in Appendix B-14 and Appendix C-4.

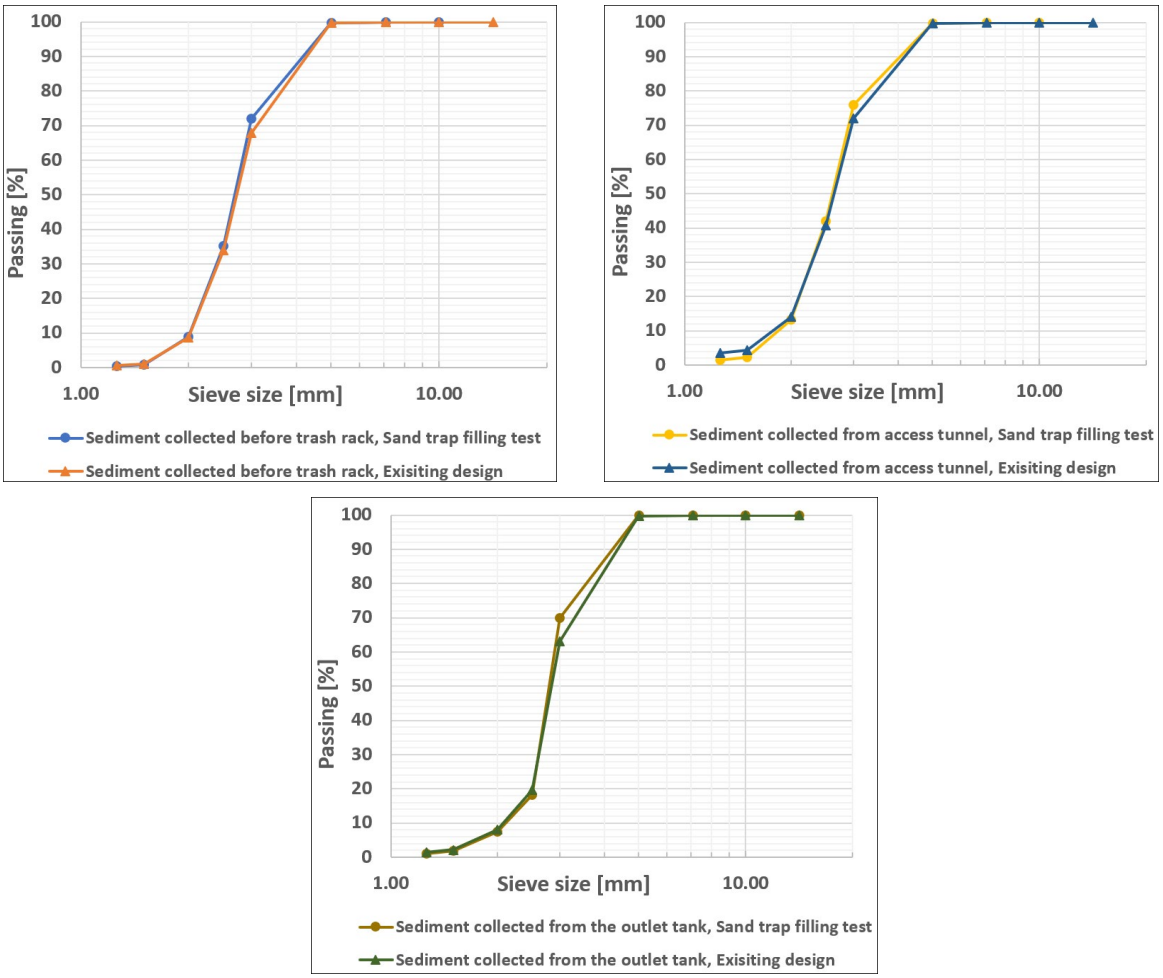

Figure 32: PSD curve of sediment collected at various location in the model after the sand trap filling test compared to steady state test

It is important to mention that, in prototype with a maximum lifting speed of the gate of 1 cm/s, the gate can be opened in 5 seconds. However, as the gate is opened manually in the model, the surge tank gate could be lifted only within 10 to 15 secs. The flow velocity through the surge tank gate is higher in the prototype than in the model. Thus, the erosion capacity of the flow is higher than that observed in the model. Moreover, as the water in the surge tank and inlet tank is drained for the filling of the sand trap without any inflow, the velocity decreases over time unlike in case of the prototype, which maintains constant inflow during filling.

5.2.4 Trap efficiency test with sediment feeding from bottom

A test was carried out feeding the sediment from the bottom to observe the impact of change in the sediment feeding mechanism on the trap efficiency of the sand trap. The sediment was

fed from the opening, centrally located at the invert just after the surge tank gate. As in earlier tests, about 60 m^3 of un-sieved sand was fed in about 4.47 hours at the steady discharge of 80 m^3/s (20 kg of sand is fed in 1 hour in the model). The test was then further continued for about 22.4 hours (5 hours in the model) at the same steady discharge.

The sediment that entered the model from the bottom, slowly came in suspension as it moved downstream during the feeding process. By the time the sediment reached the end of the sand trap transition, it was already in suspension and was distributed over the depth of the sand trap cross-section as shown in Figure 33. A video taken during the sediment feeding process is also presented in Appendix E-11.

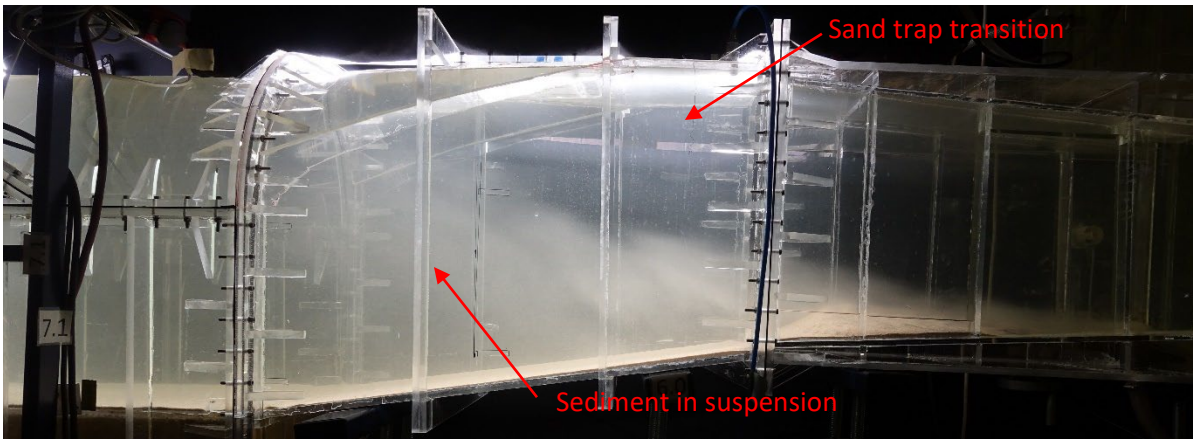

Figure 33: Sediment movement seen from the point of sediment feeding till sand trap transition during sediment feeding from bottom

The sediment deposition at the bottom of the sand trap increases with time until the end of the sediment feeding. At the end of the sediment feeding, the deposition was observed even in the transition from the surge tank gate to the start of the sand trap transition. This sediment deposit slowly eroded over time and was deposited in the sand trap transition by the end of the test as shown in Figure 34. A time-lapse video showing this movement of sediment over the period of the test is presented in Appendix E-12.

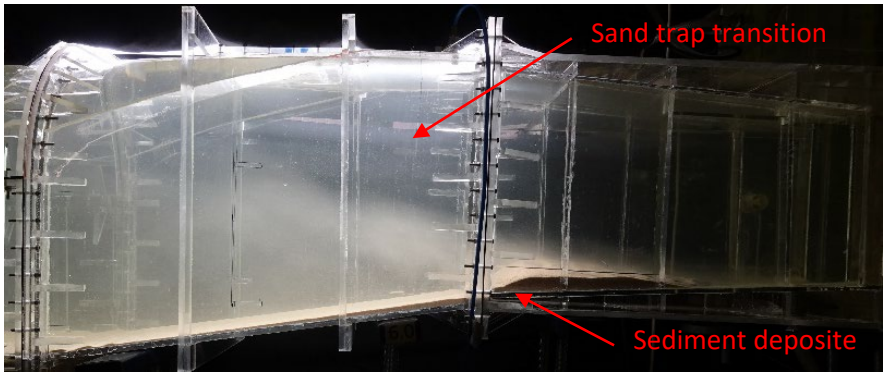

A. At the end of sediment feeding

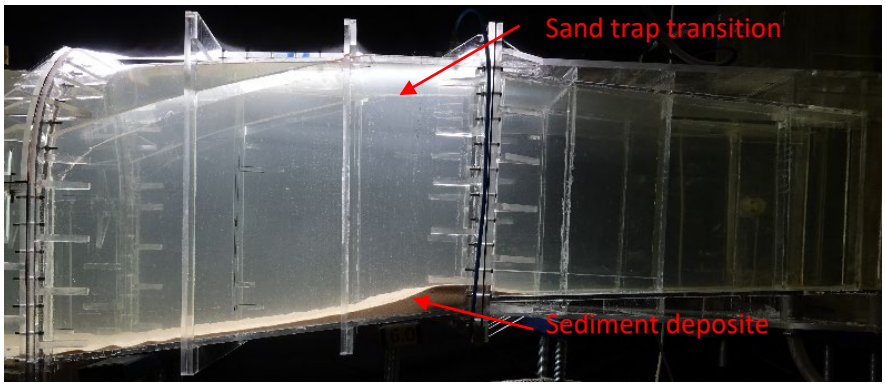

B. At the end of the test

Figure 34: Sediment movement in the sand trap transition during steady state test with sediment feeding from bottom

No noticeable movement of sediment occurred in the rest of the part of the sand trap during the test. At the end of the test, large deposition of sediment occurred in the sand trap transition. in the sand trap. This deposition was higher compared to the deposition when the sediment was fed from the top as shown in Figure 35. The deposition was higher at the start of the sand trap transition that decreased further downstream. Maximum deposition of about 1 m occurred at the start of sand trap transition which decreased to about 20 cm towards the end. This deposit was almost half the total amount of sediment deposited in the sand trap.

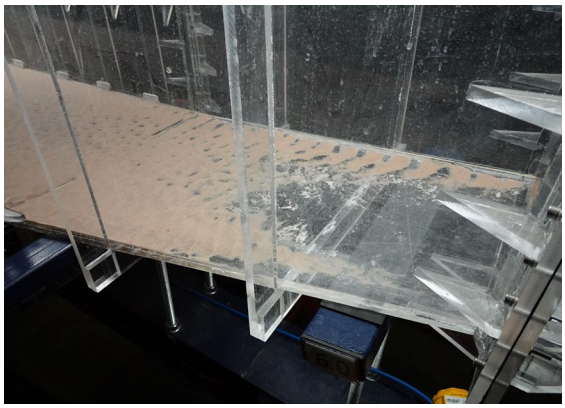

A. Plan view (sediment feeding from top)

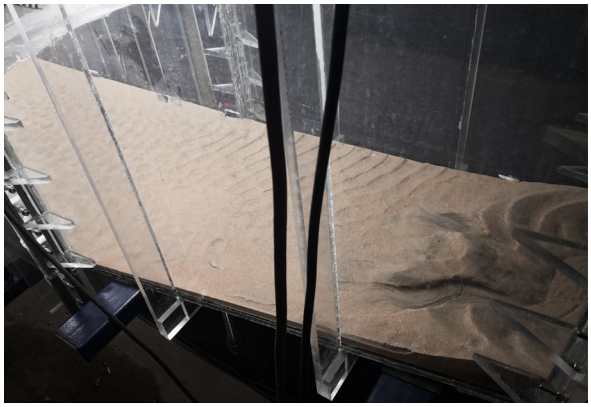

B. Plan view (sediment feeding from bottom)

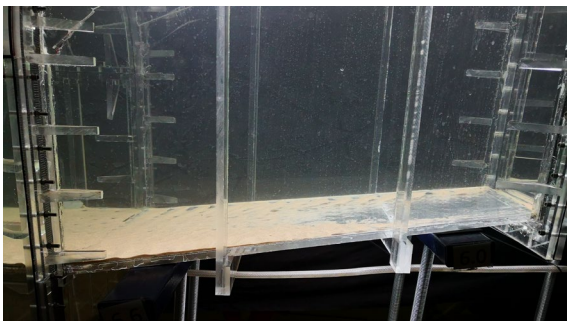

C. Side view (sediment feeding from top)

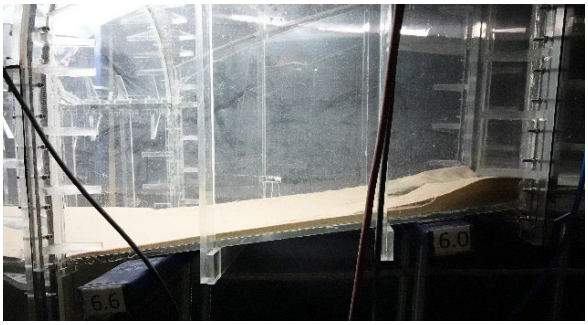

D. Side view (sediment feeding from bottom)

Figure 35: Comparative photograph showing deposition pattern in sand trap transition as a result of sediment feeding from top and bottom

The deposition pattern in the sand trap was similar to the steady state test carried out by feeding sediment from the top. However, the depth of deposition was almost uniform over the width of the sand trap in this test as the sediment was fed in from the centre. The deposition gradually decreased from the start of the sand trap until its end. The depth of deposition was roughly about 20 cm at the start of the sand trap that decreased to about 2 cm at mid-length. The deposition was about 1cm by the end of the sand. It is to be noted that the depth measurements are given only for an overview of the deposition pattern as it was roughly measured from outside the sand trap wall without any deposition details along the cross-section. Thus, the actual amount of deposited sediment could differ.

The ripple marks were noticed until 80 m from the start of the sand trap as shown in Figure 36. The deposition further downstream was flat. An overview of the deposition pattern at various locations in the sand trap is presented in Appendix D-7. The video of the sediment deposition pattern at the end of the test is shown in Appendix E-13.

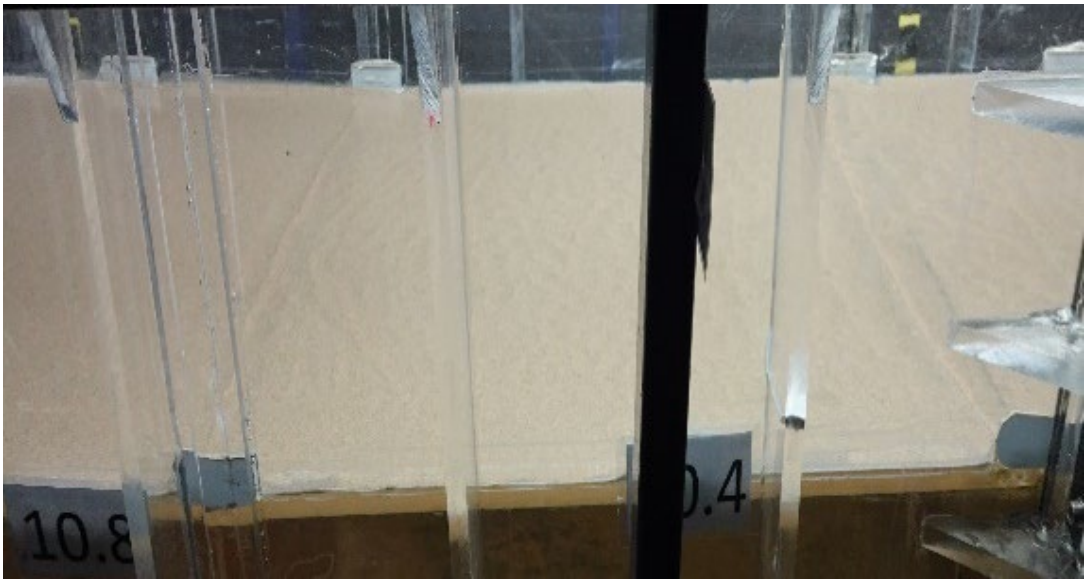

Figure 36: Deposition pattern at around 70 to 80 m of the sand trap after steady state trap efficiency test with sediment feeding from bottom

The trap efficiency of the sand trap, with sediment feeding from bottom was found to be 93.5% which was 4.5 % higher than the steady state test with sediment feeding from top. Table 8 shows the details on the trap efficiency of the sand trap when sediment was fed from the top compared to sediment feeding from the bottom. Additional data on the trap efficiency can be found in Appendix B-15.

Table 8: Trap efficiency of the sand trap for sediment feeding from top and bottom

Sediment feeding method	**From Top**	**From bottom**
Sediment	**%**	**%**
Collected in sand trap	88.7	93.3
Collected in access tunnel	0.3	0.2
Collected in sand trap including access tunnel	89.0	93.5

The PSD data and PSD curve of the sediment collected at various location in the sand trap after the test is presented in Appendix B-16 and Appendix C-5 respectively. Comparative graph showing the PSD curves of the samples collected in the sand trap when feeding sediment from the top and the bottom is shown in Figure 37.

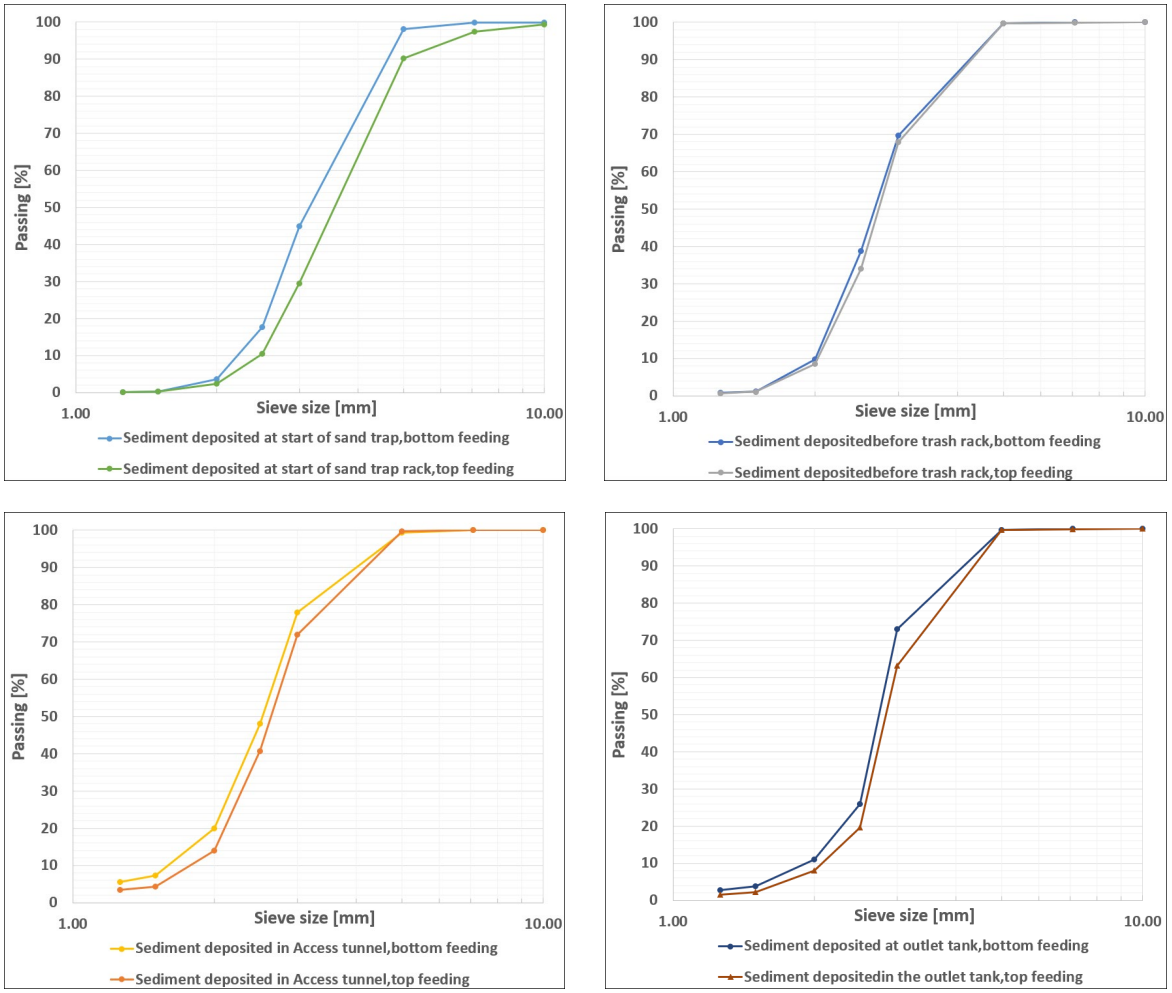

Figure 37: Comparative graph showing PSD curve of sediment collected at various location in the sand trap with sediment feeding from top and bottom

Based on the PSD diagram, the sediment deposited at the sampling locations were relatively fine compared to the test feeding the sediment from the top. However, sediment size up to 5 mm passed through the sand trap to the penstock in this case as well.

6 Model test with modifications in the sand trap

The model test under this section includes modifications made to improve the sand trap performance. The following arrangement of the modifications were tested in the model.

a) Modification 1: To evaluate the impact of flow calming structure on the performance of the sand trap

b) Modification 2: To evaluate the impact of raising the weir crest level height on the sand trap performance

c) Modification 3: To evaluate the influence of installation of ribs on the trap efficiency of the sand trap

6.1 Modification 1: Inclusion of flow calming structure in the sand trap transition

In order to reduce the impact of the incoming jet from the surge tank gate, flow calming structures were placed in the sand trap transition under this modification. Two flow calmers were installed as recommended in the master's thesis report [1]. The flow calmers consisted of vertical L-shaped rods with its tips facing in the downstream. They were placed 7 m apart with the last flow calming structures being placed just at the end of the sand trap transition. The L shaped rods were 0.2 x 0.2 x 0.02 m with the centre to centre spacing of 0.8 m. The arrangement of the flow calming structures in the sand trap transition in the model is shown in Figure 38. The drawing showing the arrangement of the flow calming structures is shown in Figure 39.

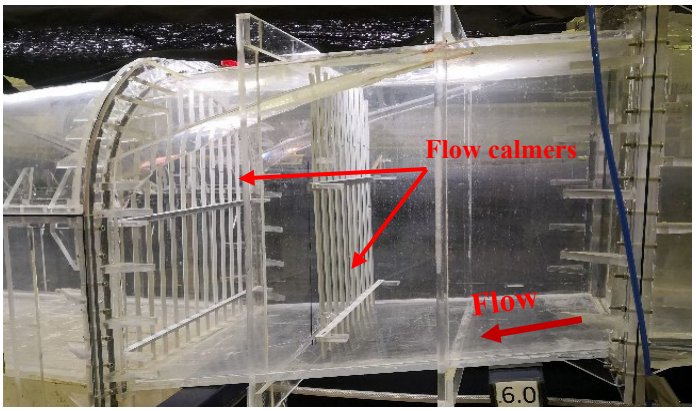

A. Arrangement of flow calmers

B. Flow calmers seen from downstream

Figure 38: A view of flow calming structures placed in the sand trap transition in the model

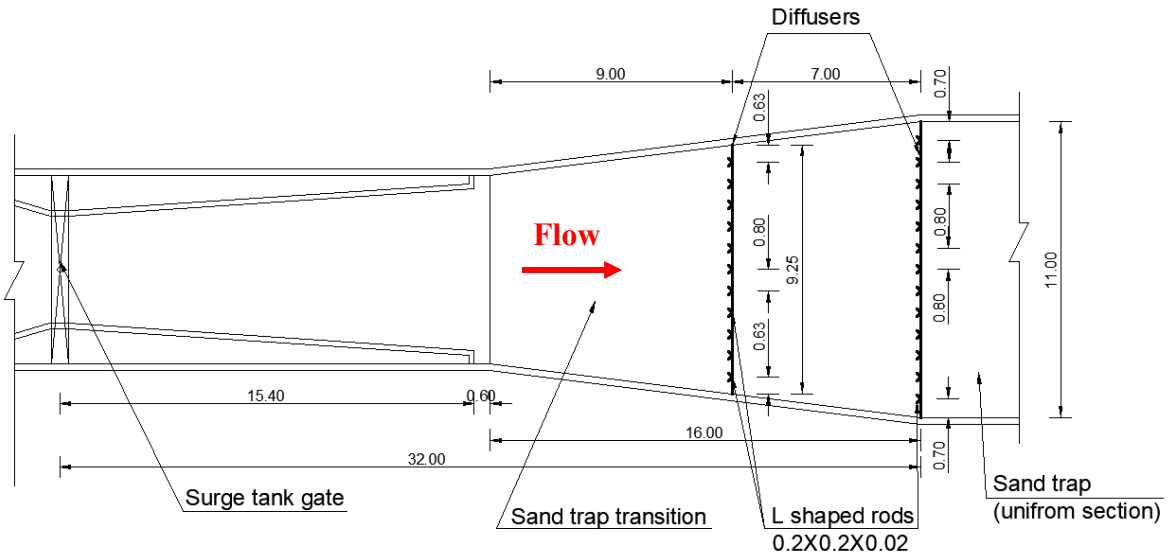

Figure 39: Drawing showing the plan view of the sand trap with the placement of the flow calming structures

Both the head loss and the trap efficiency test were carried out to assess the impact of this modification.

6.1.1 Pressure head loss test

Pressure head loss test was carried out at four different steady discharges including the design discharge, similar to the other tests described in Section 5.1. The decrease in pressure head increased with increasing discharge. The pressure head dropped significantly at the section with surge tank gate and the flow calmers. The total decrease in the pressure head was about 130 mm at design discharge. Compared to the existing situation design of the sand trap, the total pressure head loss increased by almost 3.4 times at design discharge. The head losses measured at various locations at these discharges before and after modification is presented in Table 9. The pressure head losses measured by both the pressure sensor and differential pressure sensor during the test is presented in Appendix B-17.

Table 9: Pressure head loss measured in the sand trap with and without flow calming structures

S.NO	Inflow to the tunnel	Pressure head loss			
		From P1 to P2	From P1 to DP1	From DP1 to DP2	From DP2 to P2
	m^3/s	mm	mm	mm	mm
Existing Design (without flow calming structures)					
1	20	1	2	1	-2
2	40	10	4	9	-4
3	60	21	7	20	-6
4	80	38	12	34	-8
Existing design with flow calming structures					
1	20	7	0	8	-1
2	40	32	3	31	-2
3	60	73	6	70	-3
4	80	130	9	120	0

6.1.2 Trap efficiency test

Similar to earlier tests, about 60 m^3 of sand was fed in about 4.47 hours at the steady discharge of 80 m^3/s. This means 20 kg of sand was fed in 1 hour in the model. The test was then continued at the same discharge for 22.4 hours (5 hours in the model). Un-sieved sand with grain size below 14 mm was used during the test.

With the inclusion of flow calmers, no secondary currents occurred at the bottom of the sand trap. The dye tests showed that the water jet is diffused by the flow calmers resulting in more uniform distribution of discharge over the depth of the sand trap as shown in Figure 40. However, the velocity in the lower part of the sand trap transition up to certain length at the start of the sand trap, was relatively low.

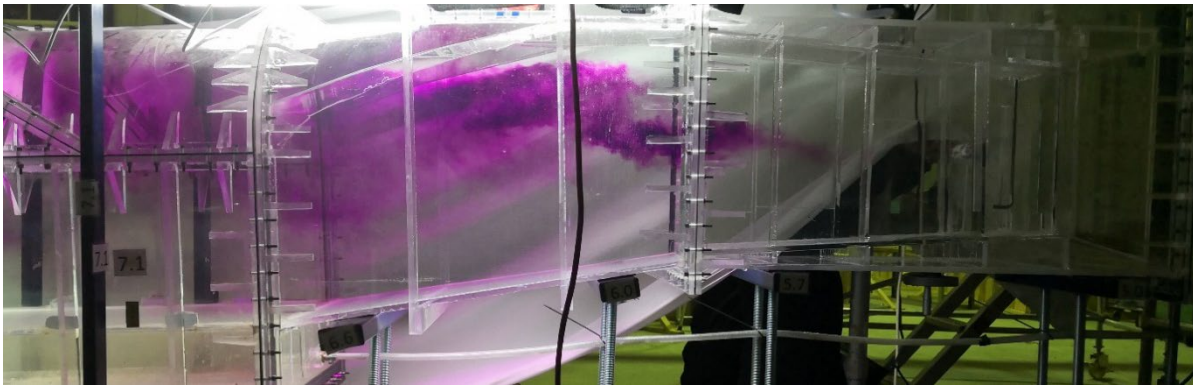

A. Existing design

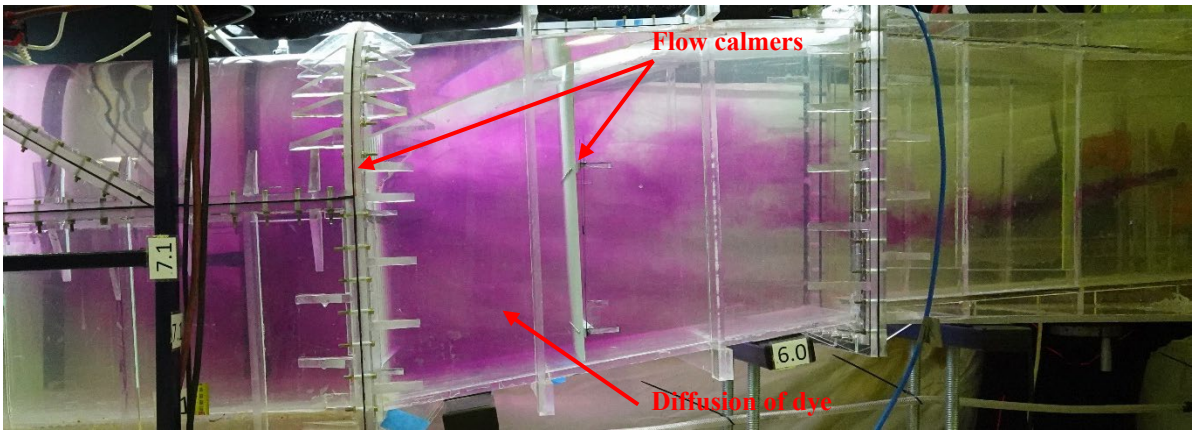

B. Modification1

Figure 40: A scenario of dye test at existing design (A) compared to modification 1 (B)

The flow was roughly uniform over the depth within 40 m length from the start of the sand trap (uniform section) as shown in Figure 41. For more insight, the video of the dye test is presented in Appendix E-14.

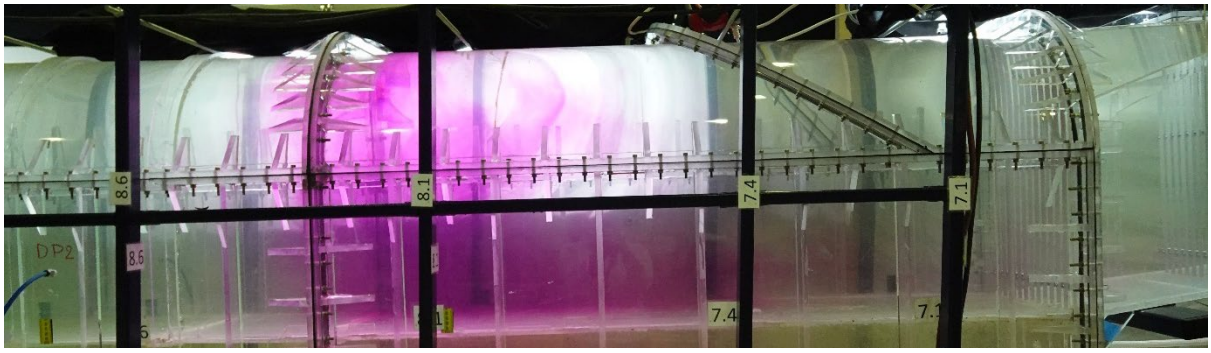

Figure 41: A scenario of dye test after modification 1

The effect of sediment feeding from the left was more visible in this case as no deposition occurred in the right side of the sand trap transition and with negligible deposition for the first

25 m of the sand trap. The sediment deposition pattern in the sand trap transition is shown in Figure 42.

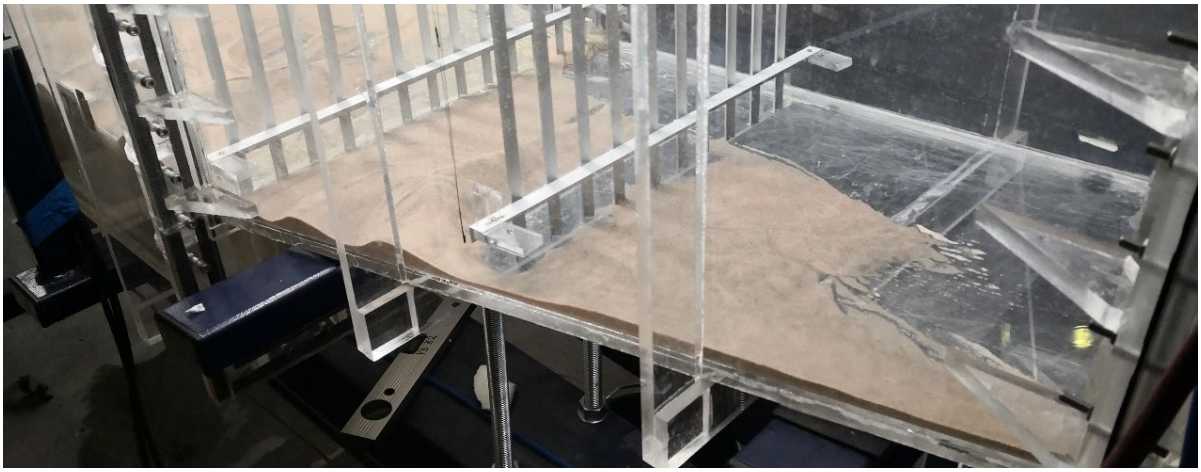

Figure 42: Deposition pattern at the sand trap transition after modification 1

The sediment deposition was higher along the left bank at the upstream 40 m stretch of the sand trap. Undulations in the deposition were formed in this area as shown in Figure 43 with a maximum depth of around 40 to 50 cm. By the end of the test, these undulations and ripples were observed only within the first 30 m of the sand trap and the deposition was flat further downstream as shown in Figure 44. This indicates that the flow was relatively calm in the sand trap and the impact of the jet with secondary currents were reduced with the inclusion of the flow calming structures. Time-lapse video showing how these dunes shifted over time is presented in Appendix E-15.

Figure 43: Deposition pattern at the start of the sand trap after modification 1

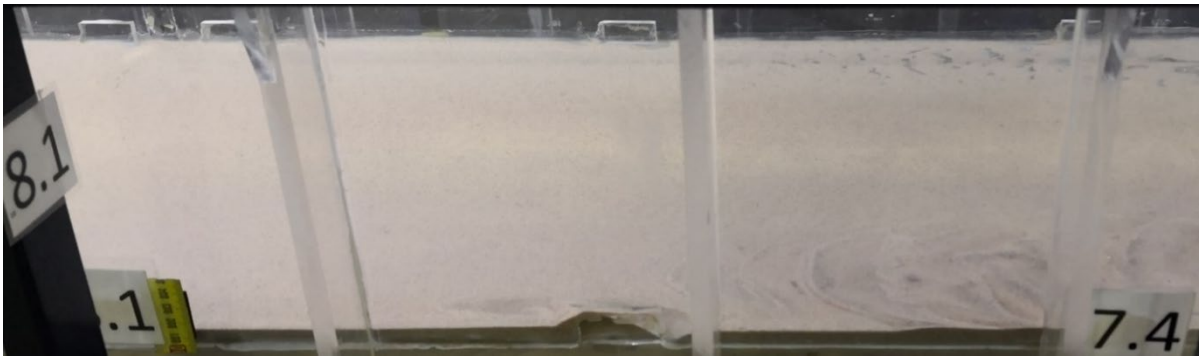

Figure 44: Deposition pattern within 20 to 30 m of the sand trap after modification 1

Sediment deposit of about 18 cm was seen at the left bank at the start of flat deposition after 30 m of the uniform section of the sand trap while the depth was about 2 cm at the right bank in this area. The sediment deposit decreases along the left side while increases along the right side of the sand trap. The deposit is roughly uniform over the width at mid-length of the uniform section of the sand trap. The sediment deposit was about 4 cm in this area of the sand trap which gradually decreases to about 1 cm before the trash rack. An overview of the sediment deposition pattern at various location of the sand trap are presented in Appendix D-8. The video of the sediment deposition pattern is presented in Appendix E-16.

The trap efficiency of the sand trap increased by about 5 % after modification 1 compared to the trap efficiency of the existing sand trap. The trap efficiency of the sand trap before and after modification 1 is shown in Table 10 and further details are presented in Appendix B-18.

Table 10: Trap efficiency of the sand trap before and after modification 1

Sand trap design	**Existing design**	**Modification 1**
Sediment	**%**	**%**
Collected in sand trap	88.7	94.1
Collected in access tunnel	0.3	0.1
Collected in sand trap including access tunnel	89.0	94.2

The PSD data and the PSD curve of the sediment collected at various location of the sand trap are presented in Appendix B-19 and Appendix C-6 respectively. PSD curves of the sediment collected in the sand trap before after modification 1 are presented in Figure 45.

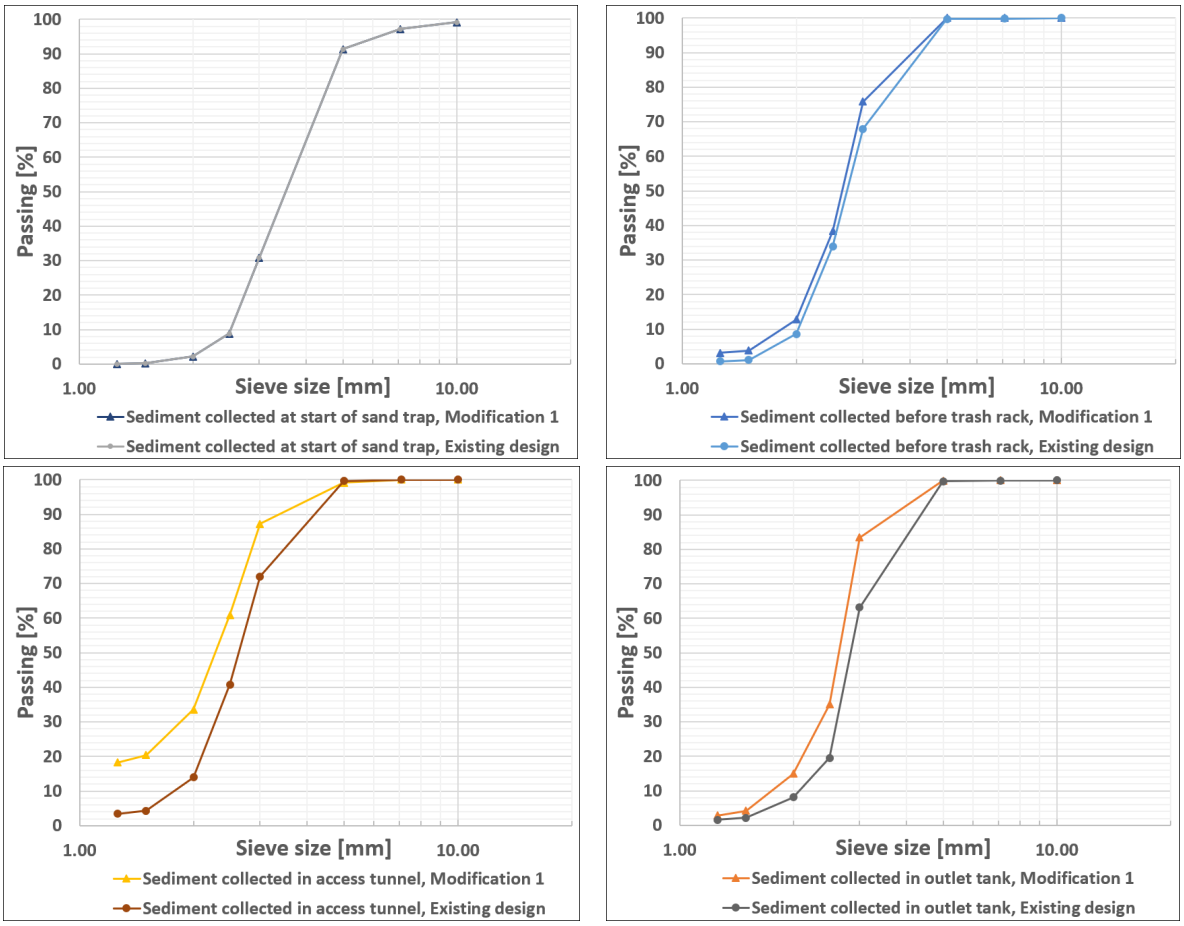

Figure 45: PSD curve comparison of sediment collected in the sand trap before and after modification 1

The curves indicate that the sediment deposited were relatively fine before the trash rack as well as in the access tunnel after the inclusion of the flow calmers. The sediment passing to the turbines as indicated by the sediment collected in the outlet tank is relatively fine showing an improvement in the functioning of the sand trap. However, particles of about 5 mm were still passing through the sand trap to the penstock/ turbines.

6.2 Modification 2: Increased weir crest level before the trash rack

This modification involves the increase in height of the weir at the end of the sand trap where the fine trash rack is placed. The weir crest level was increased by 4.8 m such that the opening of the trash rack 50% of the original opening. An overview of this modification is shown in Figure 46.

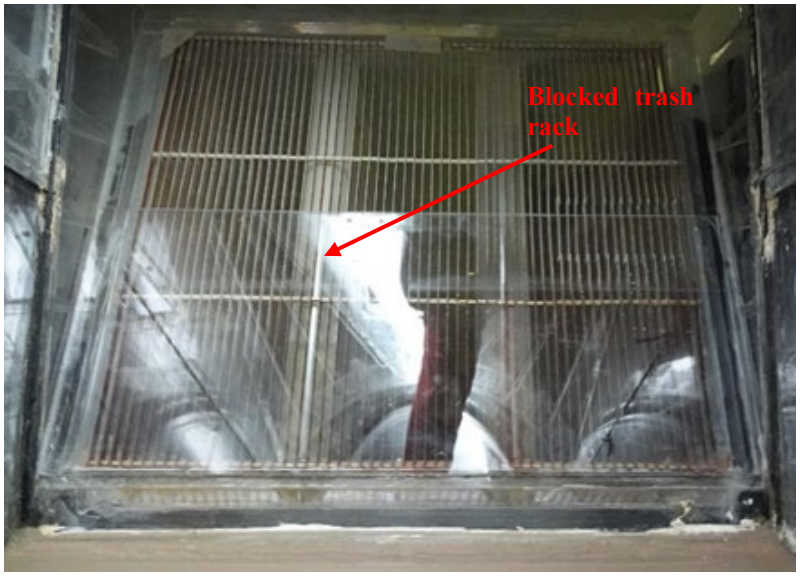

Figure 46: An overview of the weir height at trash rack after modification 2

6.2.1 Pressure head loss test

Pressure head loss test was carried out at four different discharges including the design discharge. Similar to previous tests, the pressure head decreased with increasing discharge. The pressure head loss measured was about 5 mm lower at design discharge compared to the existing design. The pressure head measured at various locations of the sand trap before and after modification 2 is presented in Table 11. Further information on the total pressure head loss measured with the pressor sensor is presented in Appendix B-20.

Table 11: Pressure head loss in the sand trap before and after modification 2

S.NO	Inflow to the tunnel	Pressure Head loss			
		From P1 to P2	From P1 to DP1	From DP1 to DP2	From DP2 to P2
	m^3/s	mm	mm	mm	mm
Existing situation test					
1	20	1	2	1	-2
2	40	10	4	9	-4
3	60	21	7	20	-6
4	80	38	12	34	-8
Modification 2					
1	20	2	0	4	-2
2	40	12	2	11	-2
3	60	22	5	22	-5
4	80	33	15	31	-13

6.2.2 Trap efficiency test

The trap efficiency test was carried out at steady discharge. About 60 m^3 of un-sieved sand was fed in about 4.47 hours at the steady discharge of 80 m^3/s (20 kg of sand was fed in 1 hour in the model). The test was then continued at the same discharge for the next 22.4 hours which means 5 hours in the model.

The sediment deposition pattern was similar to the existing design test of the sand trap. Sediment deposition started from the sand trap transition and continued the whole length of the sand trap. Sediment deposition was higher in the left side and lower along the right side of the sand trap. The sediment deposit was almost negligible along the right side of the sand trap transition and further downstream to a length of about 30 m of the sand trap. Erosion of the sediment deposited in the sand trap transition occurred over time exposing its bottom at the central portion. This erosion was about 8.5 m in length as seen in Figure 47. Additional information on on the erosion and deposition in the sand trap transition is available in the time-lapse video presented in Appendix E-17.

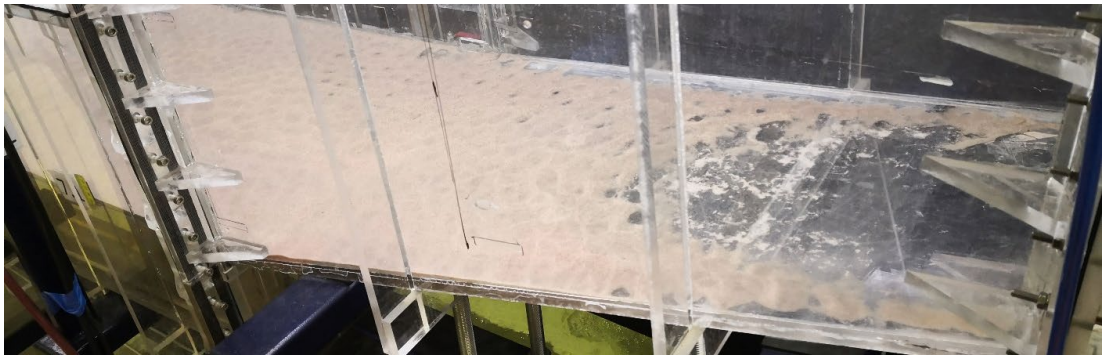

Figure 47: Sediment deposition in the sand trap transition after modification 2

The sediment deposition was higher in the upstream 30 m length of the sand trap along its left part. Ripples marks were quite prominent in this section with sediment deposit about 15 to 18 cm deep along the left side of the sand trap. A view of the sediment deposit in the first 30 m length of the sand trap can be seen in Figure 48.

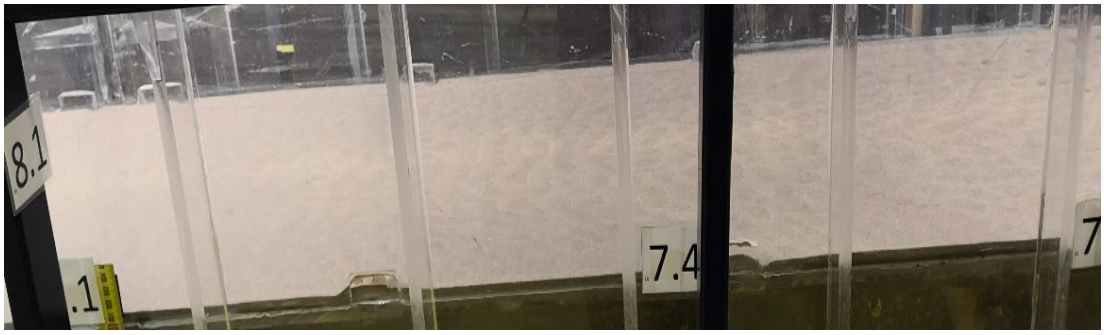

Figure 48: Sediment deposition in the initial part of the sand trap after modification 2

Mild ripples occurred further downstream within 50 m length of the sand trap while the deposition was flat further downstream. The depth of sediment deposited along the left side of the sand trap decreased slowly downstream while it increased along the right side of the sand trap. The deposition was almost uniform along its width at half-length of the sand trap. This deposit was about 80 mm thick. A view of the deposition pattern at mid-length of the sand trap is shown in Figure 49.

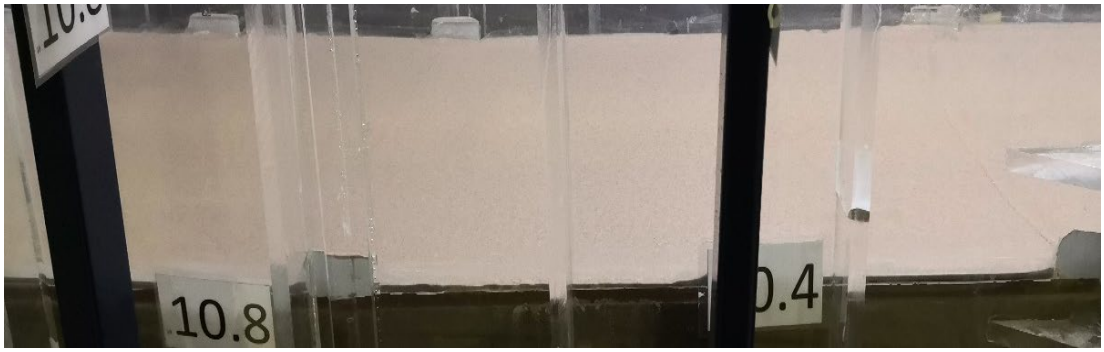

Figure 49: Sediment deposition at mid-length of the sand trap after modification 2

The depth of the sediment deposit decreased gradually further downstream and was about 1 cm in depth in the vicinity of the access tunnel and before the trash rack. The sediment deposition pattern before the trash rack can be seen in Figure 50. The effect of increment in the weir height on the sediment deposition pattern could not be visually detected.

Figure 50: Sediment deposition before the trash rack after modification 2

An overview of the sediment deposition pattern at various location of the sand trap is presented in Appendix D-9. For more insight, the video of the sediment deposition pattern is presented in Appendix E-18.

The trap efficiency of the sand trap was almost equal to the trap efficiency of the existing design test i.e. 89 %. The trap efficiency of the sand trap before and after the modification is shown in Table 12 while further details are presented in Appendix B-21.

Table 12: Trap efficiency of the sand trap before and after modification 2

Sand trap design	**Existing design**	**Modification 2**
Sediment	%	%
Collected in sand trap	88.7	88.5
Collected in access	0.3	0.3
Collected in sand trap including access tunnel	89.0	88.9

The PSD data and the PSD curve of the sediment collected at various location of the sand trap during the test are presented in Appendix B-22 and Appendix C-7 respectively. The PSD curve of the sediment collected in the sand trap after modification 2 compared to the existing design of the sand trap is presented in Figure 51. There was no change in the maximum grain size of the sand that passed through the sand trap to the turbines even after this modification. Sand particles of about 5 mm were still passing through the sand trap.

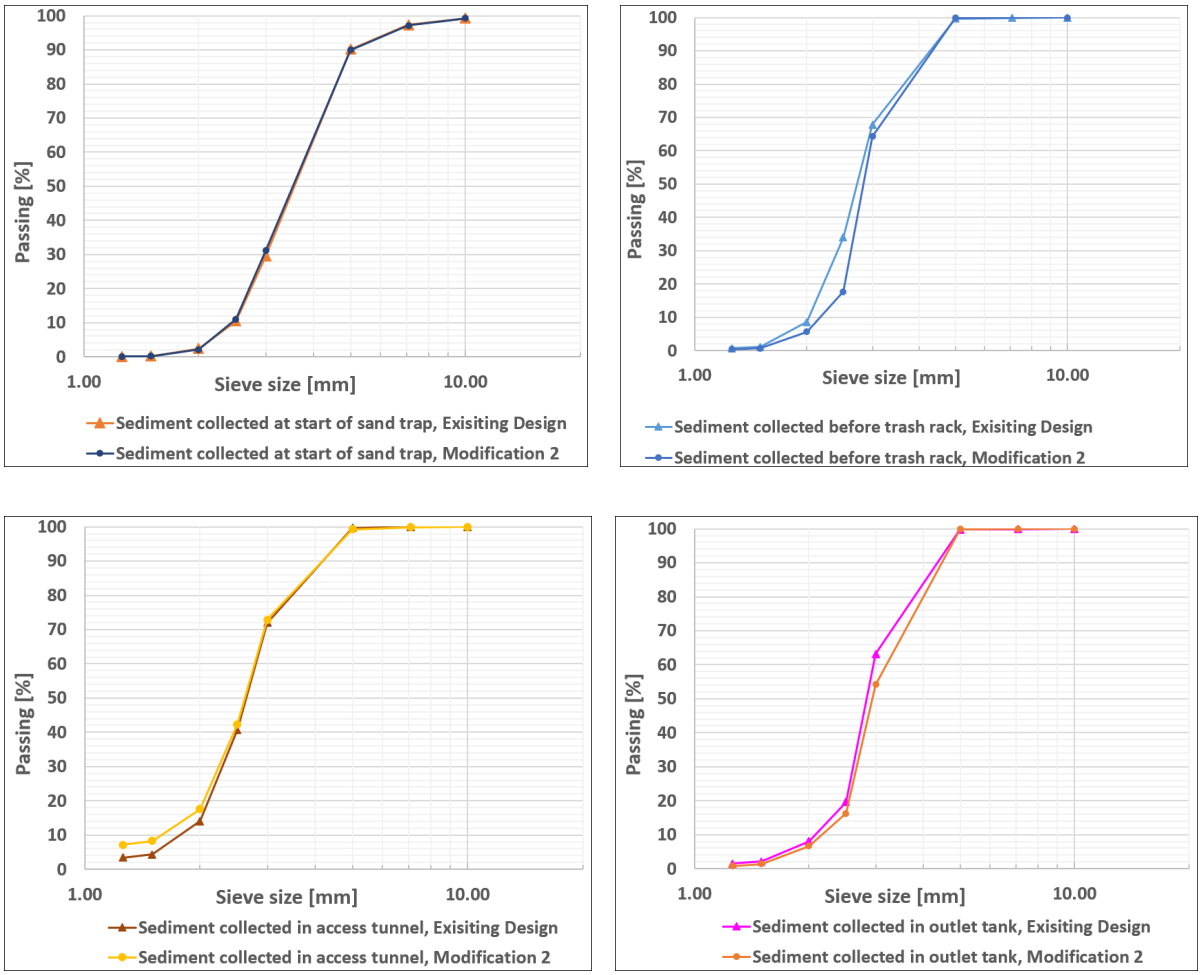

Figure 51: PSD curve of sediment collected in the sand trap before and after modification 2

6.3 Modification 3: Provision of ribs above the bottom of the sand trap

Under this modification, ribs were placed in the sand trap to prevent the deposited sand from coming to suspension and passing to the turbines. The ribs were placed at regular intervals above the sand trap floor as shown in the schematic drawing presented in Figure 52.

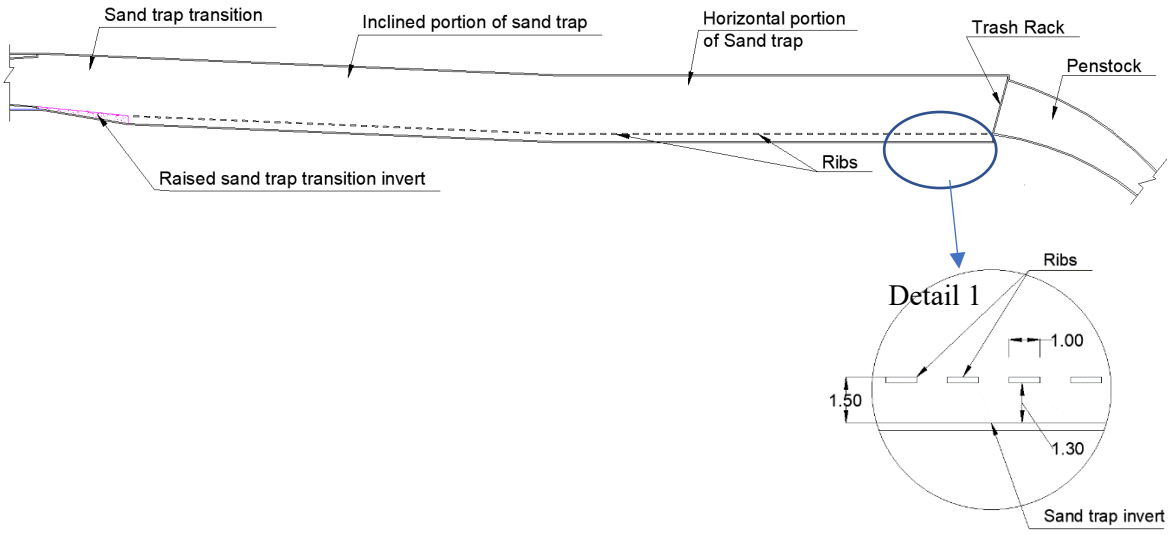

Figure 52: Schematic drawing showing the ribs arrangement in the sand trap

These ribs were 1m wide and 0.16 m thick that extended over the width of the sand trap. They were placed 1.3 m higher from the sand trap floor. The sand trap with ribs placed before the trash rack is shown in Figure 53.

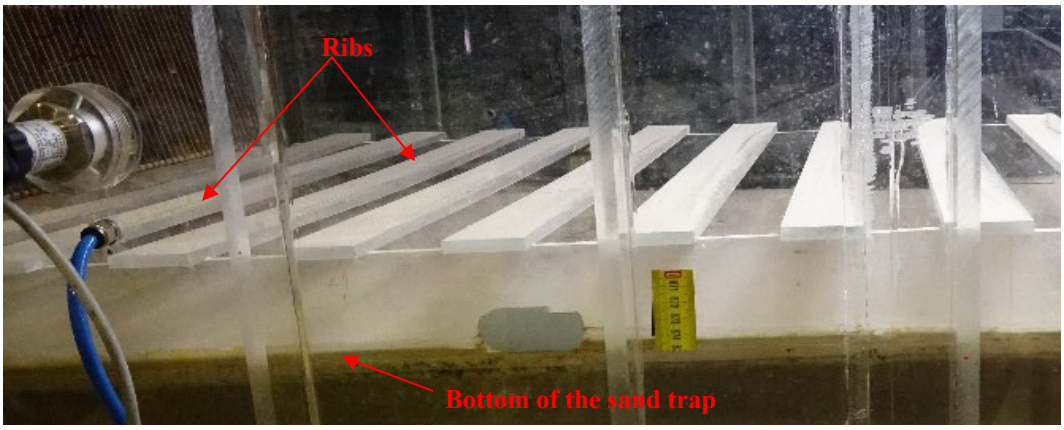

Figure 53: The ribs placed in the sand trap transition

The invert of the sand trap transition was raised to provide room for sediment deposition below the ribs in the sand trap. The drop at the start of the sand trap transition was filled and its invert was raised by 1.5 m at its end (at the start of the sand trap). Thus, the slope of the sand trap transition was changed from 1:6 to 1:9.4. This can be seen in Figure 54.

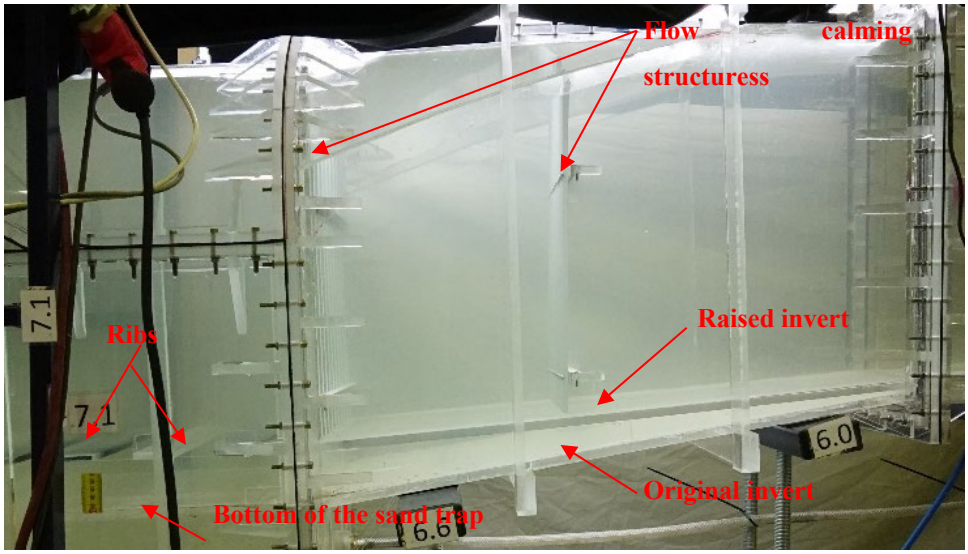

Figure 54: An overview of the arrangement in the sand trap transition under modification 3

Flow calming structures were also provided together with the ribs in this modification to calm the incoming jet flow from the surge tank gate. The configuration of the flow calmers was as in modification 1 i.e. vertical L-shaped rods with its tips facing in the downstream and the flow calmers placed 7 m apart. The L shaped rods were 0.2 x 0.2 x 0.02 m with the centre to centre spacing of 0.8 m for the flow calmer at the end of the sand trap transition as in modification 1. The centre to centre spacing of the rods was 1m for the upstream flow calmer. It is to be noted that the flow calmers placed did not cover the full height of the sand trap transition on the top curved part. An overview of the flow calming structures placed in the model is shown in Figure 55.

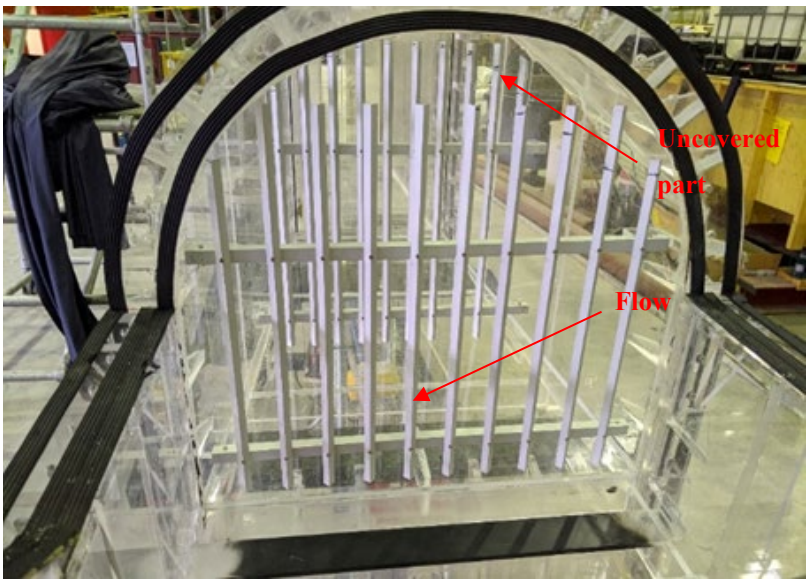

Figure 55: Flow calming structures placed in the sand trap transition, looking upstream

6.3.1 Pressure head loss test

Pressure head changes were recorded at four different discharges including the design discharge. The drop-in pressure head along the sand trap at design discharge is about 2.7 times higher after the modification 3. The pressure head losses measured along the sand trap before and after the modification is presented in Table 13. Further information on pressure head losses measured with the help of pressure sensors are presented in Appendix B-23.

Table 13: Pressure head loss in the sand trap before after modification 3

S.NO	Inflow to the tunnel	Pressure Head loss			
		From P1 to P2	From P1 to DP1	From DP1 to DP2	From DP2 to P2
	m^3/s	mm	mm	mm	mm
Existing situation test					
1	20	1	2	1	-2
2	40	10	4	9	-4
3	60	21	7	20	-6
4	80	38	12	34	-8
Modification 3					
1	20	2	1	2	-1
2	40	29	4	26	-1
3	60	71	5	64	2
4	80	126	6	113	8

6.3.2 Trap efficiency test

The trap efficiency test for this modification was also carried out at steady discharge of 80 m^3/s. About 60 m^3 of un-sieved sand was fed in about 4.47 and the test was then continued at the same discharge for the next 22.4 hours.

As the flow calmers were included under this modification, the jet effect was relatively reduced. However, the flow calmers did not cover the top portion of the sand trap, thus higher velocities were still observed on the top portion of the sand trap. Flow separation was observed at the bottom i.e. below the ribs in the initial stretch of the sand trap. Thus, the flow velocity was lower beneath the ribs in the initial few meters of the sand trap as seen in Figure 56. A video taken during the dye test is also presented in Appendix E-19.

Figure 56: A scenario captured during dye test at the initial section of the sand trap

The sediment deposition started at the sand trap transition and deposition occurred along the entire length of the sand trap including the top of the ribs during sediment feeding in the model. To provide an overview of the process, a video taken during sediment feeding in the model is presented in Appendix E-20. Recirculatory flows were observed between the ribs which can be observed in a video in Appendix E-21.

After the end of the sediment feeding process, the sediment deposited in the sand trap transition eroded over time. The deposition pattern in the sand trap transition at the end of the test can be seen in Figure 57. The sediment deposition is large on the left side of the sand trap as in earlier cases due to sediment feeding from the left. The sediment deposition was almost uniform over the width only on the downstream half of the sand trap.

Figure 57: Sediment deposits seen in the sand trap transition

Undulation/dunes were observed in the sediment deposited along the left side of the sand trap along the initial 40 m length of the sand trap as shown in Figure 58. The maximum depth of the dune was about 0.45 m at the start of the sand trap. However, sediment deposition was negligible along the right side of the sand trap in this area as shown in Figure 59.

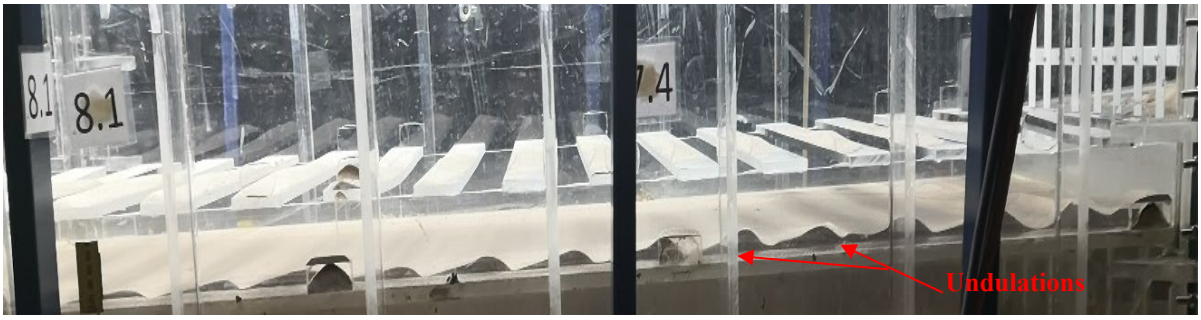

Figure 58: Sediment deposits seen in the ladder placed inside the overflow tank

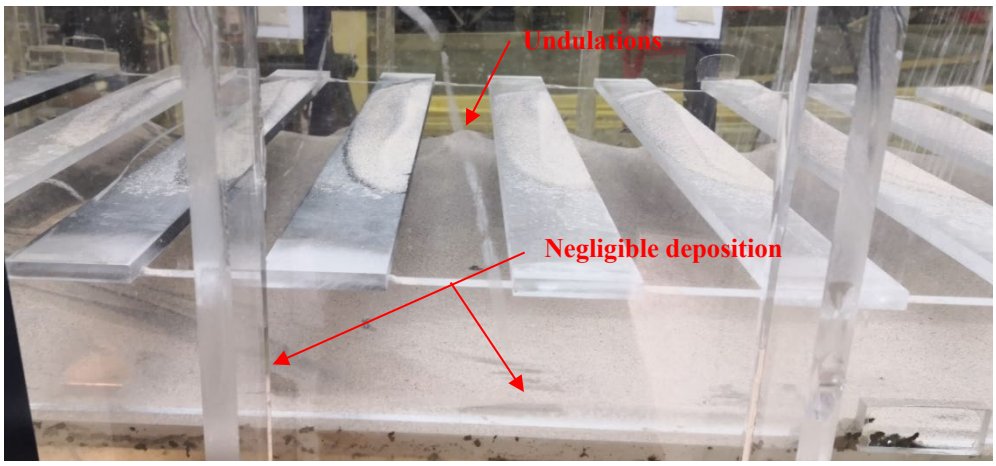

Figure 59: Sediment deposit along right side at the start of the sand trap

The sediment deposited on top of the ribs also eroded over time. It was observed that erosion also occurred on the bars closer to the trash rack. The sediment deposition pattern on top of the bars at various locations in the sand trap is shown in Figure 60.

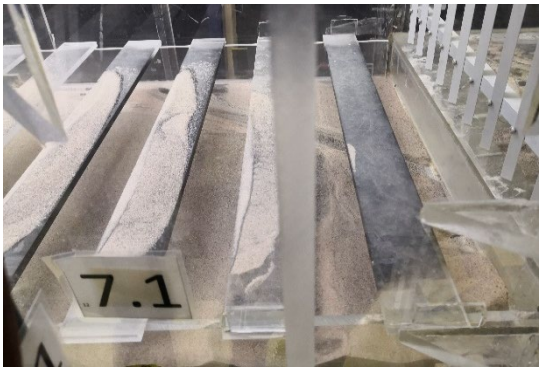

A. At start of the sand trap

B. At mid-length of the sand trap

C. Before the trash rack

Figure 60: Sediment deposition on top of the bars at different location in the sand trap

Measuring depth of sediment deposition was difficult in this case as there were acrylic supports for the ribs along the walls of the sand trap that impaired vision. Moreover, some of these supports were also opaque in nature. An estimate of the depth of deposition at mid-length of the sand trap was about 80 mm. Very shallow deposit below 10 mm was seen in front of the trash rack. An overview of the sediment deposition pattern at various locations in the sand trap are presented in Appendix D-10. For more insight into the sediment deposition pattern, a video is presented in Appendix E-22.

The trap efficiency of the sand trap after this modification is 87.5 % which is 0.6 % higher than the sand trap efficiency during existing design as shown in Table 14. There was relatively less sediment deposit in the access tunnel after this modification. Further details on trap efficiencies are presented in Appendix B-24.

Table 14: Trap efficiency of the sand trap before and after modification 3

Sand trap design	**Modification 3**	**Existing design**
Sediment	%	%
Collected in sand trap	87.4	86.5
Collected in access tunnel	0.1	0.4
Collected in sand trap including access tunnel	**87.5**	**86.9**

The PSD data and the PSD curve of the sediment collected at various location of the sand trap during the test are presented in Appendix B-25 and Appendix C-8 respectively. The PSD curve of the sediment collected in the sand trap before and after modification 3 is presented in Figure 61.

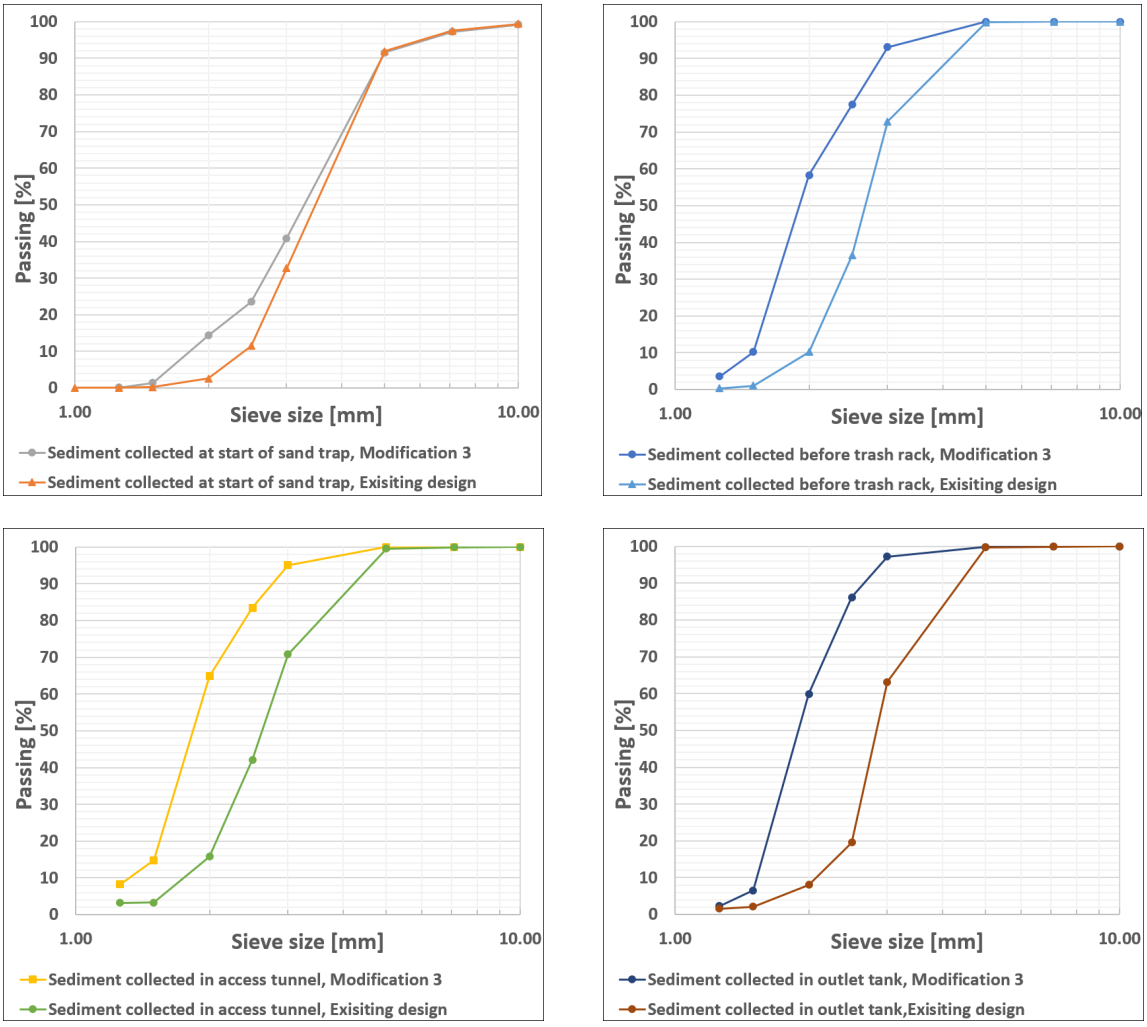

Figure 61: PSD curve of sediment collected in the sand trap before and after modification 3

Based on the PSD curves, it can be seen that the sediment deposited before the trash rack, access tunnel as well as that carried to the outlet tank was relatively fine after modification 3. However, even in this test there was no change in the maximum grain size of the sand that passed through the sand trap. Sand particles of about 5 mm were still passing through the sand trap.

7 Model test results, discussion and limitations

The model study was mainly focussed on evaluating the trapping efficiency of the sand trap under existing and modified design arrangements.

The performance of the existing design was analysed by

i. Assessing the pressure head losses and trap efficiency at steady and unsteady flow conditions.

ii. Assessing the impact of sand trap filling on trap efficiency.

iii. Assessing the influence of sediment feeding mechanism on the performance of the sand trap.

To improve the trap efficiency of the sand trap, different modifications were made and tested in order to evaluate,

i. Evaluation of the impact of flow calming structures

ii. Effect of lifting the weir crest level before the trash rack and

iii. Inclusion of ribs separating the sediment deposition zone together with flow calming structures

These modifications were evaluated based on parameters like the pressure head losses and trap efficiency.

The pressure head loss tests were carried out at four different discharges 20, 40, 60 and 80 m^3/s while the trap efficiency tests were carried out at 80 m^3/s which is the design discharge of the sand trap. It is also worth mentioning that the water temperature was between 17.5 to 18.5 ˚C in the model during the tests.

7.1 Model test on existing design

The pressure head losses measured in the model are very minimal as the boundary roughness is not included in the model. The head loss increased with the increase in discharge at all the measurement location. The corresponding pressure head loss in the model increased by about ten times when the discharge increased by four times. The pressure head loss was higher between the lower surge chamber (before the surge tank gate) and the start of the sand trap. An increase in pressure head was recorded before the trash track which could be due to the

increase in cross-sectional area of the sand trap at that location as well as the effect of trash rack on the flow velocity.

The trap efficiency of the existing sand trap both for the steady state and unsteady state operation of the power plant was found to be around 87 %. The trap efficiency was tested with sediments of about 5 mm and less (sieved sand) with d_{50} of about 3 mm. No significant changes in the deposition pattern were present between these tests. However, more erosion occurred in the sand trap transition and more ripples occurred in the sand trap as a result of unsteady state test operation compared to the steady state test. For both the tests, particles of size up to 5 mm passed through the sand trap to the penstock downstream.

The performance of the sand trap was also tested with un-sieved sand with sediment size below 14 mm and d_{50} of about 3 mm. The trap efficiency of the sand trap for this case was also found to be about 87 %. Thus, un-sieved sand was used for further testing in the model. Using un-sieved sand was also assumed to represent a wider band of sediment sizes that come to the sand trap as in the prototype. During the process of model testing, leakage was observed and thus another test was carried out having controlled the model leakages and the trap efficiency of the existing sand trap was found to be 89 % . As the model test without leakage reflect the reality, the trap efficiency of the sand trap would be 89 %.

To check the impact of sediment feeding mechanism on the trap efficiency, a steady state test with sediment feeding from the bottom was carried out. The test result showed that the trap efficiency was 4.5 % percent higher than the trap efficiency when the sediment was fed from the top. This indicates that the trap efficiency obtained by feeding the sediment from the top is more conservative and safely represents the prototype trap efficiency.

Filling of the sand trap is one of the crucial conditions when free surface flow occurs in the sand trap with the possibility of eroding the sand from the sand trap downstream to the penstock or turbine. Thus, a sand trap filling test was carried out by opening the surge tank gate by about 5 cm. The high flow velocity coming through the gate eroded the sediment deposited along the 95 m length of the uniform section of the sand trap. It is to be noted that the flow velocity through the surge tank gate is lower in the model compared to the prototype as the full height of the surge tank is not represented in the model. Moreover, the speed of the opening of the gate is almost one third in the model. All these suggest that even higher scouring occurs in the prototype than that in the model. Transport of sediment from the sand trap to the penstock downstream was not visible during the test. Also, there was no significant change in the trap

efficiency of the sand trap. This indicated that there was no or negligible sediment transport downstream of the trash rack during the sand trap filling process except for displacement and relocation of the sand within the sand trap.

7.2 Model test on modified design of the sand trap

Tests were carried out to evaluate the performance of the sand trap with different arrangements that were intended to improve the trap efficiency.

As a first modification, flow calming structures were provided in the sand trap transition to reduce the impact of the water jet coming from the surge tank gate. Two flow calmers were installed which consisted of vertical L-shaped rods with its tips facing in the downstream. It was observed that the flow calming structures improved the flow pattern in the sand trap and increased the effective length of the sand trap for settling of the particles. The trap efficiency of the sand trap increased by 5%. However, there was an increase in the head loss in the system due to introduction of the flow calming structures. The pressure head loss almost tripled after this modification. Sediment with the grain size up to 5mm passed through the sand trap to the penstock downstream.

The second modification involved lifting the weir crest level located at the trash rack. The weir was lifted such that the opening of the trash rack is 5 m, which is half the initial opening. There was no significant change in the trap efficiency as a result of this modification. No significant improvement was seen on reducing the maximum particle size that can be transported through the sand trap downstream. However, this modification ensures safety in preventing sand transport downstream to the penstocks in the context of free-surface flow in the sand trap. There was decrease in head loss by about 5mm at design discharge after this modification. Thus, further studies are necessary to justify its costs over its advantages.

The third modification was placement of ribs at a certain height in the sand trap that separated the sediment deposition zone, avoiding sediment to come back in suspension. The ribs were placed at regular intervals above the bottom of the sand trap. The top of the ribs was placed at the height of the weir crest before the sand trap, this means 1.5 m above the sand trap invert. The invert of the sand trap transition was also raised to end at this height. In addition to this, flow calming structures were also installed in the sand trap transition. However, the flow calmers didn't cover the full height of the cross-section. With this modification, the trap efficiency of the sand trap was increased by about 0.6 %. However, particles of grain size up

to 5 mm still transported through the sand trap into the penstock downstream while the pressure head loss almost tripled after this modification.

7.3 Discussion and interpretation of test results

The trap efficiency of the existing sand trap was found to be 89 %. The highest trap efficiency of about 94% was obtained when flow calming structures were installed in the sand trap transition under modification 1. There was 0.6 % increment in the trap efficiency with the installation of rib and the flow calming structure under modification 3. The increase in the weir crest level before the trash rack under modification 2 showed no improvement in the trap efficiency of the sand trap. The maximum size of the particle that passed through the sand trap was about 5mm for all the tests. The pressure head losses increased when flow calming structures were installed. The head loss was almost tripled for both modification 1 and 3 at design discharge. The pressure head loss was not significantly changed after modification 2 but a decrease in head loss of about 5 mm was measured at design discharge after modification 2.

Based on the test results it can be seen that it is necessary to improve the inflow hydraulics of the sand trap to fully utilize the sand trap. The inclusion of flow calmers helped in diffusing the flow at the inlet transition thus increasing the effective settling length of the sand trap. Thus, an improvement in the trap efficiency was observed due to modification 1. However, as stated above, it introduces more head loss in the system. Thus, the possibility of improving trap efficiency over head loss needs further investigation and optimisation.

The impact of the increase in weir height (modification 2) was not positive in terms of improvement in the trap efficiency of the sand trap. However, this modification ensured higher safety in connection to free surface flows in the sand trap and transport of sediment further downstream.

Very less improvement in the trap efficiency, less than 1% was achieved with the inclusion of the ribs under modification 3. This suggests that resuspension of the deposited sediment was not an issue in this case. Even though the diffusers were placed, the improvement in the trap efficiency was less compared to modification 1 where diffuser were only installed. This could be because the diffusers did not cover the top part of the cross-section where the velocity is higher. Also, the diffuser configuration was slightly different with more flow area in the flow calmer placed at the end of the sand trap. The bottom of the sand trap transition was also raised

under this modification reducing the sectional area thus having relatively higher velocity in comparison to modification 1 at the start of the sand trap.

Particle of about 5mm were transported to the penstock even after the modification in all the arrangements tested. However, the PSD curves suggest that the amount of the coarser fraction transported downstream was reduced after the modifications.

7.4 Model limitations

Before relating the model test results with the prototype conditions, it is important to understand and consider some of the limitations in the model.

The roughness in not included in the model due to practical problems. Adding sand roughness along the walls impairs visibility. Even the use of rubber seals along the tunnel for simulating the net head loss was not possible in this case, as it interferes the sediment transport pattern. Thus, the head loss is underestimated in the model. But the measured pressure head loss can provide a basis for comparison between different modifications.

Scaling of the suspended sediments in model experiments is more complex. This is due to the change in properties that happen when originally small sediment particles are scaled down. If suspended sediments scale down, the particles would be so small that the cohesive forces become dominant.

Ripples were seen in the model that is less likely to occur in the prototype. The presence of fine sediment below 0.5 mm in the model sediment could be the reason for this.

The reproduction of the time scale for the sediment transport and deposition was quite complicated for the model test. Based on the scaling factor, the sediment deposition that took place in one year would take 82 days in the model. This is not possible due to time and resource limitation. Thus, a simplified approach was adopted for the study.

For simplicity in model construction, the geometry of some of the structures were changed ensuring no impact on the test results. The invert of the lower surge chamber is simplified from a semi-circle geometry to semi hexagonal geometry. The access tunnel invert is also simplified in the same manner. No curvature is provided at the junction between the access tunnel and the sand trap. The access tunnel is also shifted upstream by about 3 m for structural safety reasons.

Sediment was fed in the model from the left portion of the model. Thus, uneven deposition of sediment occurs in the sand trap at least up to half of its length. The deposition was also uneven across the width of the sand trap. The acrylic plates that were glued to hold the sand trap bottom/invert in the model was also seen to influence the deposition pattern in its vicinity.

The sediment deposit was very less in the model and was often below the translucent glue used in sealing the sand trap invert in the model. The depth of deposition in the sand trap could be only measured from outside the walls. Thus, the deposition measurements are presented in the report only to provide an overview of the deposition pattern.

There was some amount of sediment loss in the system. Some of these losses occur due to leakages through the joint along the sides of the sand trap while some of the losses occur downstream of the sand trap due to deposition on the groves of the valves. It was also evident that some of the fine sediment was also lost from the outlet tank during the test. Moreover, at the end of the tests, the sand trap was drained by opening the valve in the lower portion of the outlet tank. This could also possibly transport some fine sediments out of the outlet tank. This could be the reason for the coarse gradation of the sediment collected in the outlet tank.

In the prototype, the turbine can be opened from 0 to full load within 100 secs while the turbine can be shut down in less than 10 secs. Manually operated valve represents the turbine in the model. The valves can be opened as per the prototype condition, obtaining discharge very close to the required amount. However, further fine-tuning to the exact discharge requires some more minutes. As the closure of the turbine is not that significant concerning dragging of the sediment to the turbines, it was considered acceptable to close the valve within 45 secs in the model.

The total height of the surge tank was not replicated in the model as it was not possible to be adjusted at the model scale chosen for the study. This was considered acceptable as there is no significant effect of this limitation on the tests that were carried out. However, the impact of the head on the sand trap filling test cannot be ignored as it governs the velocity of the water coming through the surge tank gate and the resulting erosion.

The surge tank gate in the prototype are mechanized, the lifting or closing speed of the gates is 1 cm/s. However, as the gate is opened manually in the model, the opening speed was almost one third the speed of the prototype. Thus, the erosion capacity of the flow is underestimated in the model during the sand trap filling test.

The water in the surge tank and inlet tank is drained for the filling of the sand trap during sand trap filling test without any inflow. The velocity of the incoming jet is thus reduced over time which is constant in case of the prototype. This also underestimates the possible erosion in the sand trap during the sand trap filling test.

8 Conclusion and recommendation

A physical model of 1:20 scale for Tonstad sand trap III is built at the hydraulic laboratory at NTNU. The physical model was used to get insight and understand the hydraulic flow conditions in the existing sand trap and to assess pressure head losses, trap efficiency at steady and unsteady flow conditions, to evaluate the impact of sand trap filling on trap efficiency and also observe the influence of sediment feeding mechanism in the model on the performance of the sand trap.

The model was also used to evaluate the impact of flow calming structures, ribs and effect of lifting the weir crest level before the trash rack on the trap efficiency of the sand trap. The trap efficiency tests were carried out at design discharge of the sand trap i.e. 80 m^3/s and using sediment size equivalent with d_{50}=3 mm. This chapter presents the main conclusion of the model tests and its recommendations.

8.1 Conclusion

The trap efficiency of the existing sand trap is found to be 89 %. However, the friction at the boundary walls of the model is much less than that in the prototype. It is expected that the higher friction along the boundary gives different trapping efficiency in the prototype.

The effect of the sediment feeding mechanism in the model was also assessed by comparing the trap efficiency of the sand trap by feeding sediment from top and bottom in the sand trap model. The trap efficiency increased by 4.5 % when the sediment was fed from the bottom. To be on safe side, all model tests were carried out by feeding sediment from the top. Thus, the trap efficiency in the prototype is expected to be higher than that measured in the model.

The pressure head loss measurements in the model showed that there is a higher-pressure head loss at the upstream part of the sand trap between the upstream and downstream of the surge tank gate. The model test also depicted higher hydraulic pressure head at the downstream end of the sand trap close to the trash rack. This increase in the hydraulic head at the downstream part of the sand trap, close to the trash rack could be due to wider cross-section of the sand trap at that location and also may be due to the influence of the trash rack and the weir. In both the cases, the pressure head loss measured from the model can provide an overview on the trend and can be used as a basis for comparison between the modifications. However, the values does not represent the prototype head loss values as the boundary friction is not reproduced in the model.

At design discharge of 80 m^3/s, the trap efficiency measured under the unsteady operation of the power plant was not significantly different from the trap efficiency of the sand trap under the steady state operation conditions.

During sand trap filling test, erosion of sediment deposited within the sand trap was observed but there was no visible movement of sand through the trash track to the penstock. There was also no difference in the trap efficiency after the sand trap filling test compared to the trap efficiency during steady state operation. This indicates that no transport of sediment downstream of the trash rack during the sand trap filling process except for displacement of the sediment from upstream to downstream of the sand trap.

The flow calming structures under modification 1, improved the flow pattern in the sand trap. It distributed the inflow uniformly over the basin flow area and introduced the flow at minimum turbulence level. The jet impact is reduced increasing the effective length of the sand trap for sedimentation. The trap efficiency increased by about 5 % whereas the pressure head loss almost tripled. Thus, the negative effect of head loss in the system and the possibility of improving the trap efficiency needs further investigation and optimization before the installation of the flow calming structures in the Tonstad sand trap III. The maximum grain size transported downstream of the sand trap was unaltered by this modification.

The lifting of the weir crest level by 5 m at the trash rack under modification 2 showed no improvement in the trap efficiency or on reducing the size of the particles passing through the trash rack to the penstocks. However, this modification showed slight decrease in head loss at design discharge.

Another modification made during the model test was the provision of ribs that separated the sediment deposition zone. In addition to this, flow calming structures were also installed in the sand trap transition under modification 3. The improvement in the trap efficiency due to this modification is less compared to the trap efficiency achieved with the installation of only flow calming structures. However, it is worth mentioning that the flow calming structures placed under this modification had slightly different configuration and did not cover the full height of the cross-section of the sand trap transition, which could possibly be the reason for this. The head loss almost tripled after this modification as well.

Though an improvement in the trap efficiency of the sand trap could be achieved by modification 1 and 3, there is no improvement in the maximum grain size of the sediment that is transported downstream the penstocks. However, based on the PSD curves it can be seen

that there is reduction in the volume of the coarser fraction transported downstream after the modification.

8.2 Recommendation

Based on the conclusions drawn from the test results, the following recommendations are made.

(a) Amongst the modification tested, the inclusion of flow calming structures in the sand trap transition is recommended as it significantly improved the flow patterns in the sand trap and increased its trap efficiency despite an increase in the head loss.

Inclusion of one more flow calming structure may further increase the effective settling length of the sand trap. The spacing between the rods may be varied to achieve the required result with acceptable head loss. Therefore, further optimization study is recommended to decide on the number of flow calming structures and for economic justification for its installation in Tonstad sand trap III.

(b) The geometry of the sand trap is such that it has a higher slope at the bottom of the inlet transition as the elevation of the sand trap is lower. This also facilitated for higher velocity in the upper portion of the sand trap. Smoothening of the invert of this transition will help reduce flow stagnation and secondary current at the bottom of the sand trap. However, this might not be of that significance in the context when the flow calming structures are installed in this area.

(c) The Tonstad sand trap was designed to trap sediments up to 2 mm, However, particles greater than this size was observed transported downstream of the sand trap even though the trap efficiency of the sand trap is improved. Thus, further modifications are recommended to be tested in this regard. Though expensive, increasing the cross-section of the sand trap to decrease the velocity could be an effective means and is recommended to be tested in the model.

(d) Modification involving the provision of ribs for separation of sediment deposition zone was carried out without increasing the cross-section of the sand trap. Test involving this modification with the increase in the cross-section of the sand trap is recommended. The spacing of the ribs can be varied and tested for effective deposition of sediments while avoiding them to come in suspension.

(e) Provision of automated sediment flushing system is recommended to avoid loss in cross-section of the sand trap due to sediment deposition. Moreover, this will also decrease the power loss due to drawn down during cleaning of the sand trap. This can also be used as a

means for complete draining of the sand trap. Deepening of the sand trap for the adjustment of this setup is recommended to avoid decreasing the available settling area in the sand trap.

(f) Increasing the weir height before the trash rack did not improve the trap efficiency of the sand trap. However, an increase in this height helps to ensure less transfer of sediment to the turbines during free flow in the sand trap. Either increasing this weir height and/or lower the bottom in front of it could be an option for increased safety during the free-flow situation in the sand trap as flushing of the gravels to the turbines was experienced by the power plant.

(g) As the lower surge chamber is integrated with the water way, decreases in velocity occurs with deposition of sediment in this area before reaching the sand trap. Provision of shear plates to decrease this area to prevent sedimentation in this zone is recommended. This will also help in reducing the expansion-contraction head losses in this area.

9 References

[1] Daxnerova, J., "Hydraulic scale modelling of flow calming structures for hydropower plants", Master's thesis in Civil and Environmental Engineering, 2017

[2] Ettema, R., Arndt, R., Roberts, P., wahl,T., ASCE Manuals no 97, "Hydraulic Modelling Concept and Practice", American Society of Civil Engineers, 1982

[3] Kobus, H.E., Abraham, G., "Hydraulic Modelling", German Association for water resources and land improvement, Bulletin 7, 1980

[4] Lysne, D.K., "Summary of laboratory investigation on sand trap arrangements in power plant tunnels", Articles and summaries of project reports, Bulletins of the river and harbour research laboratory, Bulletin No:10E, 1967

[5] Lysne, D. K., Glover, B., Støle, H. and Tesaker, E., Hydraulic Design, Hydropower Development, Volume no:8, 2003

[6] Richter, W., Vereide, K., and Zenz, G., "Upgrading of a Norwegian pressurized sand trap combined with an open-air surge tank", Geomechanics and tunnelling. Vol. 10 (5), 2017

[7] Steinkjer, S.M., "Hydraulic Scale modelling of sediments for pressurized sand traps", Master's thesis in Civil and Environmental Engineering, 2018

[8] Vereide, K., Svingen, B. and Guddal, R., "Case study: Damaging effects of increasing the installed capacity in an existing hydropower plant", Proceedings, 12th International Conference on Pressure Surges, Fluid Transients and Water Hammer, Dublin, Ireland, 2015

[9] Vereide, K., Richter, W., Lia, L., Havrevoll, O.H. and Jakobsen, T., "Upgrading of sand traps in Existing Hydropower plants", Hydro conference, 2017

[10] Vereide, K., Richter, W.and Belete, K., "Project Description- Physical Scale Model of Sand trap 3-Tonstad", Sira Kvina Kraftselskap, 2017

[11] Yalin, M. S., Theory of Hydraulic models, The Macmillan Press Ltd, 1971

[12] Zenz, G. and Richter, W., "Intermediate Report Tonstad HPP Sand Trap-3D CFD", Graz University of Technology, Institute of Hydraulic Engineering and Water Resource Management, 2017

Ola Haugen Havrevoll
Kaspar Vereide, Nils Rüther and Leif Lia

PIV experiments on ribs in the Tonstad rock trap model

Trondheim – 19.01.2021

Report

NTNU
Norwegian University of Science and Technology
Faculty of Engineering
Department of Civil and Environmental Engineering

NTNU
Norwegian University of Science and Technology

Norwegian University of Science and Technology

Report

PIV experiments on ribs in the Tonstad rock trap model

VERSION
04

DATE
19.01.2021

AUTHOR(S)
Ola Haugen Havrevoll
Kaspar Vereide, Nils Rüther and Leif Lia

PROJECT NUMBER
90572600

NUMBER OF PAGES
17

CLIENT(S)
Sira-Kvina kraftselskap DA

CLIENTS REF.
5644

ABSTRACT
Experiments with particle image velocimetry (PIV) have been conducted to study the flow field around ribs in the Tonstad rock trap model. The objective was to investigate how a rib setup equivalent to 1 m wide ribs with 1 m spacing in prototype scale influence the flow field in the rock trap. The working hypothesis was that the ribs separate the flow field resulting in higher velocities above the ribs and lower velocities below the ribs. The results from the experiments confirm the hypothesis and show that the ribs successfully separate the flow field. The ratio between the flow velocity above and below the ribs is increasing with higher discharges. Detailed measurements and analyses of the flow field around and in between the ribs are presented in this report.

CORRESPONDING AUTHOR
Ola Haugen Havrevoll

CONTROLLED BY
Kaspar Vereide, Nils Rüther, Leif Lia

APPROVED BY
Leif Lia

REPORT NUMBER
B1-2021-2

ISBN
978-82-7598-121-7 (electronic)
978-82-7598-122-4 (printed)

CLASSIFICATION
Open

Contents

1. Introduction

The Hydraulic Laboratory at NTNU was commissioned by Sira-Kvina kraftselskap to conduct physical models tests of rock trap no. III in the Tonstad hydropower plant. As a part of the work, experiments should be done with particle image velocimetry (PIV) to map the flow field around ribs in the rock trap model. This report presents the results from the initial PIV experiments. The work with PIV experiments of ribs in sandtraps will continue, and this report presents the results from the initial tests.

The main objective of the PIV experiments was to investigate how a rib setup equivalent to 1 m wide ribs with 1 m spacing in prototype scale influence the flow field in the rock trap. The working hypothesis was that the ribs separate the flow field resulting in higher velocities above the ribs and lower velocities below the ribs. To answer the objective and evaluate the hypothesis, a detailed study of the flow field has been undertaken. The results will also serve as a reference in future studies of optimum rib design.

The main purpose of ribs in rock traps is to increase the trap efficiency for sediments. However, in the present study the effect of the ribs on sediment transport is not quantified, only the effect on the flow field. Some preliminary observations are provided in the discussion chapter, but further quantification of the effect on sediment transport is a topic for future studies.

The work was conducted by PhD candidate Ola Haugen Havrevoll, Post Doc. Ushanth Navaratnam, and Researcher Usha Shrestha. Laboratory technicians included Thai Mai, Geir Tesaker, and Eirik Nygård. Scientific advisors included Prof. Nils Rüther, Prof. Leif Lia and Adj. Ass. Prof. Kaspar Vereide, all from NTNU. The project has been a part of the “Fleksible sandfang” research project with project number 269062 funded by the Regionale Forskningsfond for Agder.

2. Model construction

The work was conducted in an already existing model of the rock trap no. no. III in Tonstad power plant. The prototype rock trap is about 200 m long, has a cross section of over 100 m^2 and has a design discharge of about 80 m^3/s. The existing model in geometrical scale 1:20 of the prototype was modified by installing a flow calming structure at the inlet, and ribs along the tunnel invert. Figure 1 presented a photo of the physical model, Figure 2 present a schematic drawing of the model, and Figure 3 presents the horizontal ribs that were installed in the model.

Construction drawings for the fitting of the ribs into the rock trap were produced in June 2020. Fitting of the ribs started in July and went on through August. Ribs with the thickness 8 mm were used instead of 10 mm, that is equivalent to 160 mm thick ribs in prototype scale. The ribs were 50 mm wide and spacing between them was 50 mm. The removable floor in the model was not removed, to allow for the commercial experiments to be done intermittently between the rib experiments. The observation window for the PIV was placed as far downstream in the model as possible, to mitigate model effects and get as well distributed and generic flow as possible from the inflowing water. The calibration of the PIV setup was done on 28th of August.

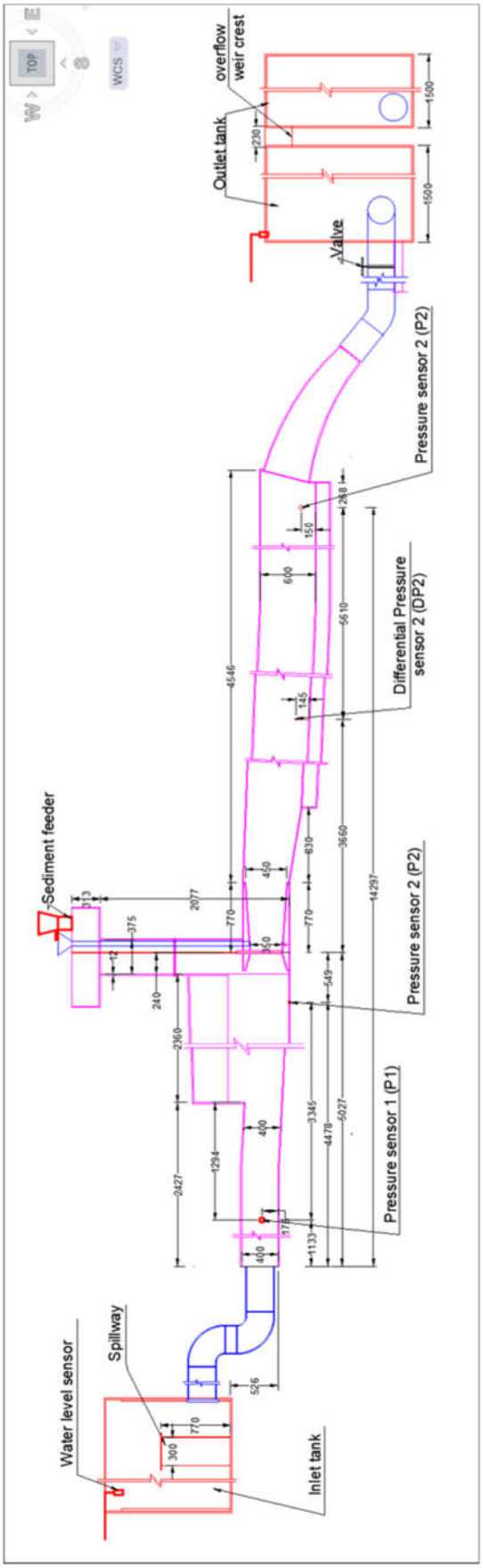

Figure 1 and Figure 2: Schematic drawing and photo of the 1:20 scale model of rock trap no. III in Tonstad power plant. From left, the reservoir, headrace tunnel and inlet gate going to the rock trap and trashrack to the right.

Figure 3 Ribs installed in the model

The model of the rock trap is built in scale 1:20. All the results in this report are presented in model scale. Since the flow is pressure-driven, the ratio between the pressure difference and the inertial forces must be the same in the model and prototype. The ratio between the pressure difference (i.e. head loss) and the inertial forces is called the Euler number:

$$Eu = \frac{\Delta p}{\rho U^2}$$

where Δp is the pressure difference, ρ is the fluid density and U is the flow velocity. The requirement of the ratio of forces being equal is called a scaling law. The Euler scaling law gives this relation between velocity scale (V_r) and length scale (L_r):

$$V_r = \sqrt{L_r}$$

If we represent Δp with an empirical formula for head loss, for example the Darcy-Weisbach formula, the requirement of $Eu_p = Eu_m$ gives $f_r = 1$, that is the friction coefficient must be the same in the model and prototype. The model is built in acrylic glass, and the surfaces are therefore much smoother than the prototype, which has very rough unlined walls of blasted rock. However, the floor and the ribs which are the subjects of the experiments, are built with concrete in the prototype. The roughness of concrete in the prototype scaled down will be roughly the same roughness as the acrylic glass in the model. Therefore, around the ribs, we assume the Euler number scaling law to be fulfilled around the ribs and the invert, even if this is not the case for the model as a whole.

3. Experimental setup

The experiments with width/spacing ratio = 1 started on 3rd of September. Test with this rib setup was with a range of discharges from 20 l/s to 140 l/s with increments of 20 l/s.

The PIV method was selected to study the flow in the model. The PIV method is conducted by inserting tracer particles, small particles with the same density as water, that reflect the light from a laser sheet placed in conjunction with a camera. A software coordinates the laser and the camera to allow accurate photographing of the particle movement over time. The pictures are thereafter postprocessed to obtain the results.

Velocity measurements were taken with 2D PIV (2-dimensional 2-component velocimetry) using a TSI stereoscopic particle image velocity system. The laser sheet was formed by a Nd:YAG (neodymium-doped yttrium aluminum garnet) double-pulsed laser and was aligned normal to the horizontal plane and parallel to flow direction. Two high speed 4 Mega Pixel CCD (charge-coupled device) cameras captured the particle images at 20 Hz frequency over 3 minutes, which gives 3600 samples of the flow field for each discharge. The images were post-processed and analyzed using the TSI Insight 4G software. Figure 4 shows the setup of the camera.

The experiments were done with two different camera setups. For the first setup, the camera was placed having one rib in the center of the picture. The flow field above the ribs was completely visible, but the view to the area immediately below the ribs, as well as a small area to the left and right of the rib in the center was blocked. The tests were done for the following discharges (all in l/s): 20, 40, 60, 80 and 100.

For the second setup, the camera was moved, so the center point of the image coincided with the downstream, upper corner of one rib. This point of view made one opening between two ribs completely visible, while still the area below the ribs was obstructed. The tests were done for the following discharges (all in l/s): 20, 40, 60, 80, 100, 120, 140. For the discharges over 100 l/s, the downstream tank spillway had to be extended.

Figure 4 The camera pointing at the ribs. The camera focuses on the calibration object in the middle of the tunnel, therefore the near end of the ribs obstruct the view below the ribs. The flow is from left to right.

3.1 The PIV field of view

For the image capture, a 28 mm lens was used. This was a compromise between long focal length and available space outside the model, as a longer focal length, e.g., 50 mm, would have given less perspective distortion, but would have been impractical to work around, as the safety tent around the equipment is quite small, and personnel must work in the close vicinity of the camera.

The PIV field of view was 186 x 184.5 mm. The point in center between the ribs in the length axis, and on the middle of the rib in the width-axis is in focus, resulting in that half of the rib upstream and half of the rib downstream extends into the field of view. The nearest end of the rib, closest to the camera, will obstruct parts of the flow field, and it is a challenge to find the optimal point of view where the largest possible part of the flow field is visible.

3.2 Challenges

It was challenging to keep the discharge constant over time owing to the model setup. The standard deviation of the flow was in the range 0.778 to 1.088 l/s for the 20 and 140 l/s test respectively. The influence on the results is assumed to be limited as the measurements are averaged over time.

For the measurement of the discharge, an electromagnetic flowmeter at the inlet was used. The water supply pipe feeds into an upstream reservoir with two outlets, one leading to the model and one for overflow to keep the water level in the reservoir constant in case of fluctuating incoming water. The spillway was also fitted with an electromagnetic flowmeter. However, this flowmeter did not give reliable measurements, as air was entrained in the spilled water. Therefore, it was decided to keep the water level in the upstream reservoir below the spillway crest, so the discharge in the model was measured directly from the inlet flowmeter. To keep the water level below the spillway crest, the inflow and outflow had to be balanced by manually adjusting the outlet valve downstream the sandtrap model.

Another major challenge has been the size of the model, resulting in significant hydraulic forces acting on the Plexiglas-walls. Even though the wall were supported by a steel frame, several cracks encountered causing delays in the progress. Because the model was fragile, it was desirable to keep the internal pressure as low as possible, thus keeping the upstream water level as low as possible, without entraining air into the model.

4. Results

The flow field around and in between the ribs was measured with the PIV equipment. Measurements were taken with different discharges, illustrating the influence for different velocities for the equivalent 1 m wide 1 m spacing setup, but also for different rib width and spacing in relation to the flow velocity for the prerequisite that the width = spacing.

The experiments gave flow field measurements for a wide range of flow velocities. For every sample, the horizontal and vertical velocity was captured with a resolution of 126×127 datapoints, over an area of 186×184.5 mm in the model (grid size = 1.5 mm). Spatial velocity variations smaller than this are not captured.

Figure 5 shows an image from the camera. The samples are taken in pairs, so the movement of the seeding particles (white) indicate the velocity at that point. The red rectangles mark the positions of the ribs at the focus plane. The protruding ribs cover parts of the interesting flow field.

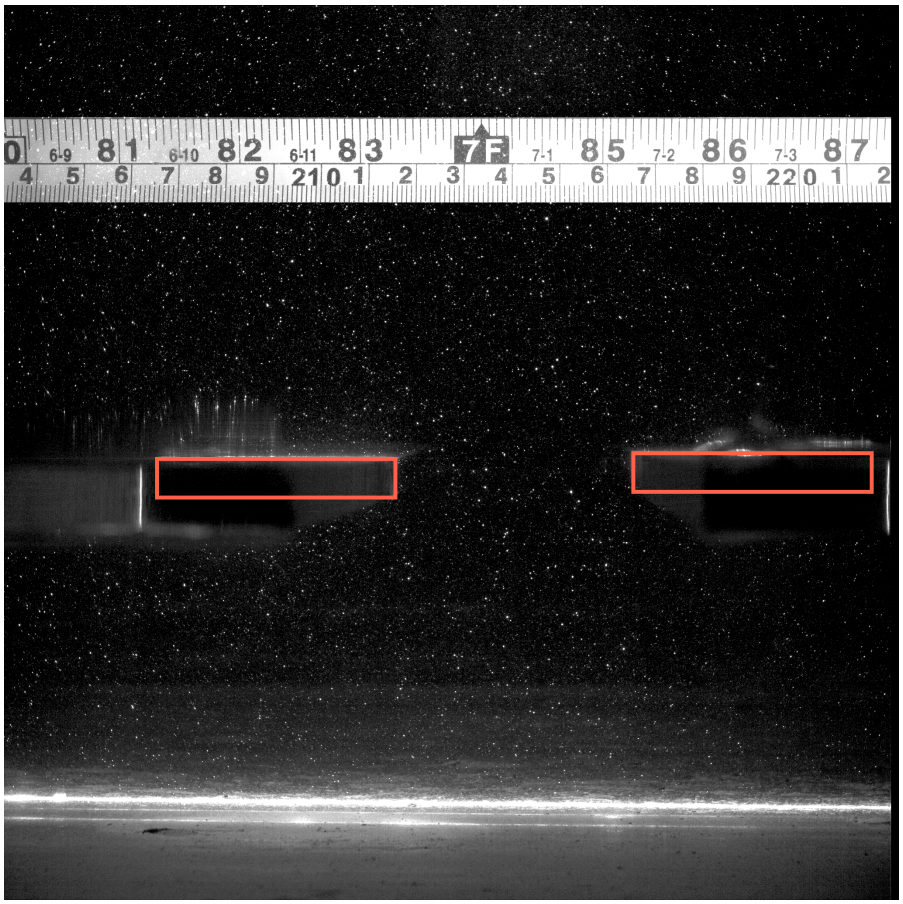

Figure 5 Sample raw capture with overlaid ruler and markings for the part of the ribs in focus. The seeding particles are seen as white points.

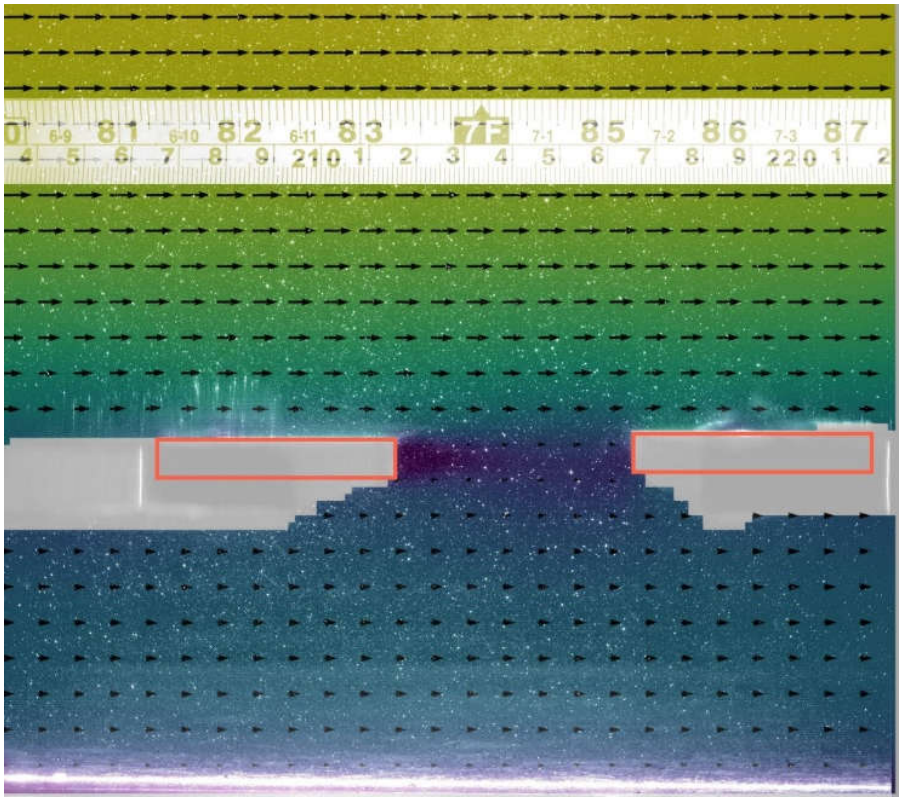

Figure 6 The analyzed flow field, overlaid on a raw image.

Figure 6 shows the analyzed vector velocity field with both color gradients and arrows to indicate the magnitude and direction of the flow. The data plot is overlaid on the raw image to show where the obstructing ribs prevents data acquisition. We can see from the figure that the ribs separate the flow into a zone with lower velocity below the ribs and higher velocity above the ribs.

In the project plan, two parameters for calculating the sedimentation efficiency of the ribs were suggested, namely the vorticity and integrated mean mass flux through the slits. In the following, the velocity, vorticity and integrated mean mass flux are analyzed.

4.1 Velocity

Figure 7 shows the velocity profiles of the horizontal velocity component averaged along the horizontal axis for all the discharges that were tested. The velocities are approximately linearly correlated with increasing discharges. The local and global maximum and minimum velocities are shown in Figure 8.

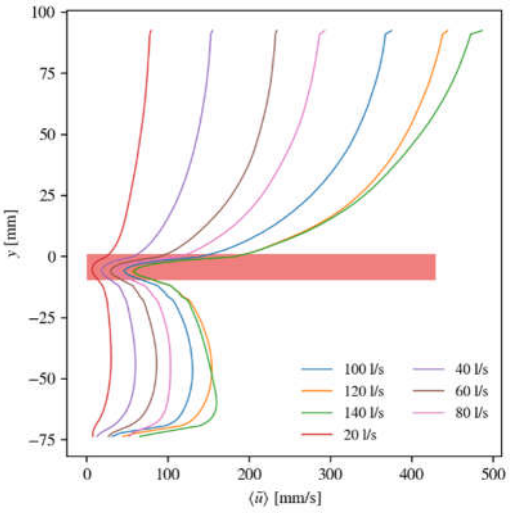

Figure 7 Horizontal velocity profiles for different discharges. The red bar indicates the location of the ribs.

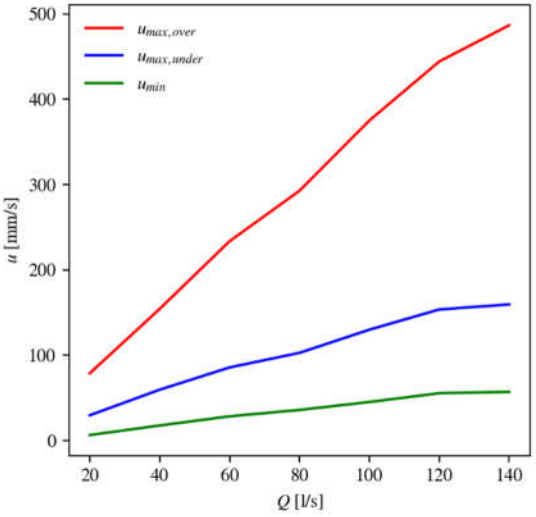

Figure 8 Maximum and minimum horizontal velocities for discharges

4.2 Flux between ribs

The net vertical flow between the two studied ribs is fluctuating over time, but on average it is slightly positive, which means a net flux upwards.

4.3 Vorticity

The vorticity is a measure of the local rotation of each individual fluid particle, or in this case, each discrete datapoint. The vorticity $\omega_{i,j}$ in each datapoint with velocity $U_{i,j}$ is calculated as (Luff et al. 1999):

$$\omega_{i,j} \cong \frac{1}{\Delta l}\left[\frac{U_{i,j-1} - U_{i,j+1}}{2} + \frac{U_{i+1,j} - U_{i-1,j}}{2}\right]$$

Figure 9 shows a vector field for the 20 l/s measurements which gives an impression of the flow field. In the area immediately downstream of the rib, a vortex is set up, as seen on Figure 9 and Figure 10. The time-averaged flow field has been used for these figures. It is seen, though, that the location of the vortex is fluctuating with time, so the averaged flow calculation might smear out the characteristics of the vortex. The vortices are only seen immediately downstream of the ribs, but for the majority of the space between the ribs, there is no vortices.

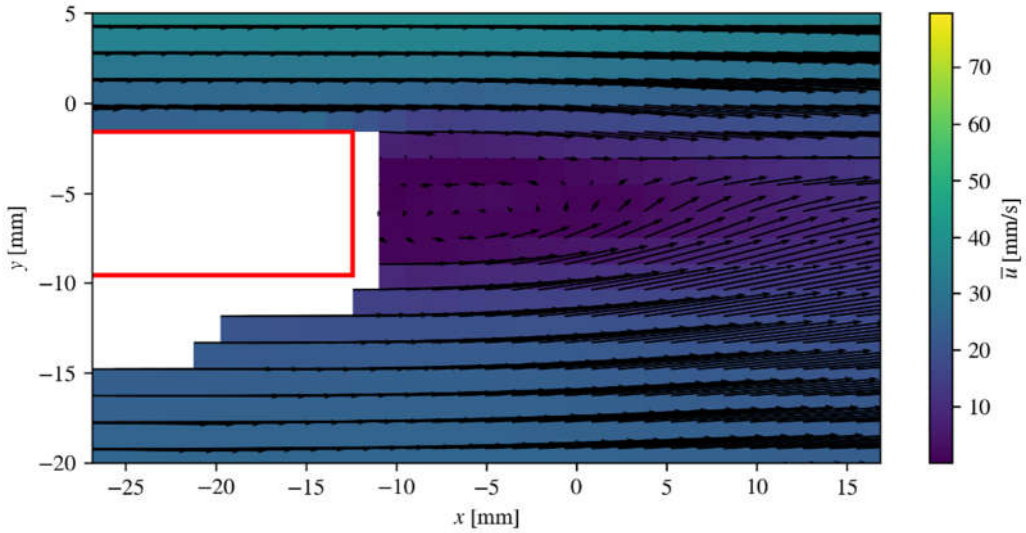

Figure 9 The vortex downstream of the rib for Q = 20 l/s. The black arrows are time-averaged velocity vectors, showing the vortex forming on the downstream end of the rib.

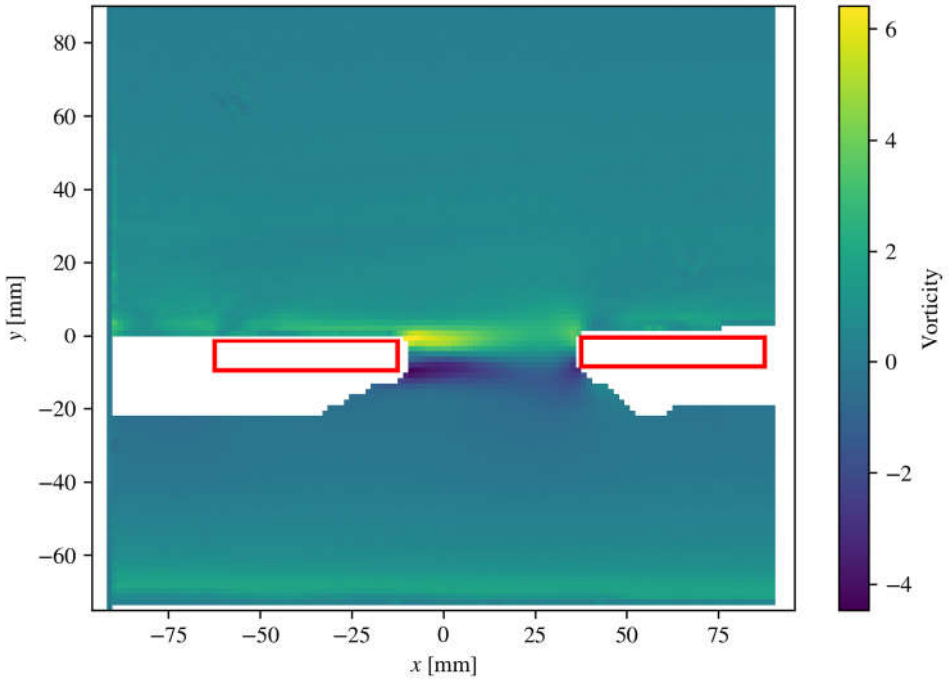

Figure 10 Mean vorticity calculated for Q = 20 l/s.

4.4 Reynold's shear stress

The Reynolds shear stress, or the turbulent shear stress, is computed based on the measured values with this formula:

$$\tau_t = -\rho\overline{u'v'}$$

Here, u' and v' are the velocity fluctuations as calculated by Reynolds decomposition and ρ is the water density. A bar over the velocity fluctuations means the average over time, that is the average over the 3600 samples. Figure 11 shows the Reynolds' shear stress for the whole measurement area.

By averaging the time-averaged Reynolds' shear stress over the horizontal space, which is a part of the Double Averaging Concept (Nikora et al. 2001), we get a vertical profile similar to the velocity profile in Figure 7. The spatial averaging is denoted by angle brackets. The result of the double averaging is seen in Figure 12.

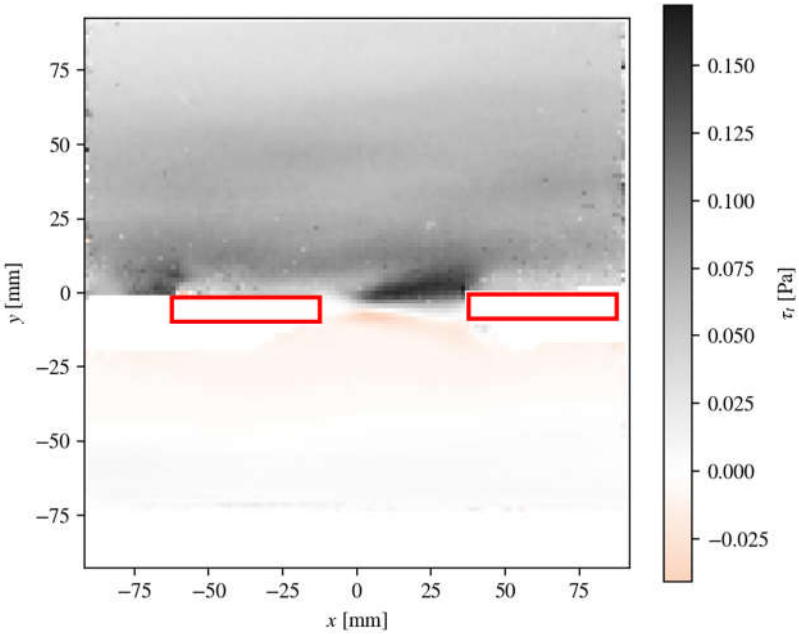

Figure 11 Reynolds shear stress for Q = 40 l/s

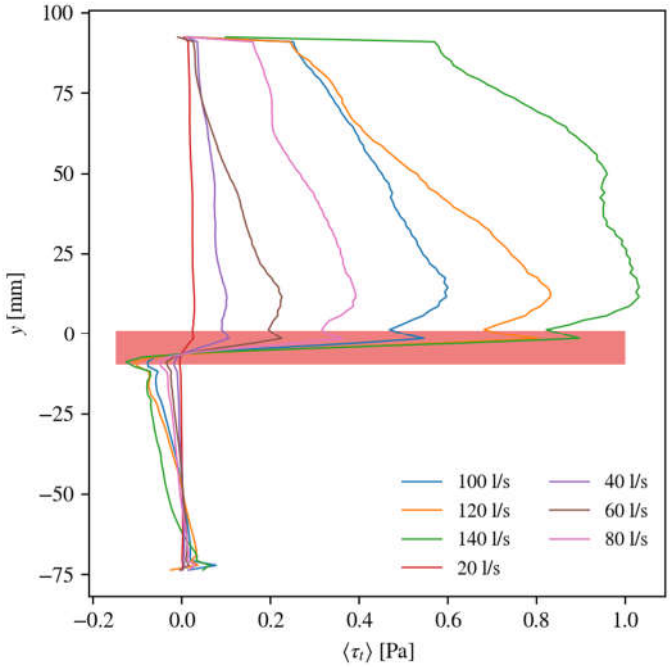

Figure 12 Reynolds' shear stress profiles for all the discharges, averaged over time and horizontal space. The red bar indicates the location of the ribs.

4.5 Quadrant analysis

Quadrant analysis has been conducted similar to the analysis of flow over rough beds such as described in Pokrajac et al. (2007). But in this case, there is also a flow below the roughness elements (ribs), which makes the flow more complicated.

The spatial deviations from the time-averaged, space-averaged flow velocities are denoted $\tilde{u}$ and $\tilde{v}$. They are calculated as follows:

$\tilde{u} = \langle \overline{u} \rangle - \overline{u}$ and $\tilde{v} = \langle \overline{v} \rangle - \overline{v}$

Here, $\overline{u}$ and $\overline{v}$ are the time-averaged velocities, they are functions of x and y coordinates. The spatial deviations in horizontal and vertical direction will in each point in the measured area belong to a quadrant, depending on the sign of the two variables. See Figure 13 and Pokrajac et al. (2007) for more information.

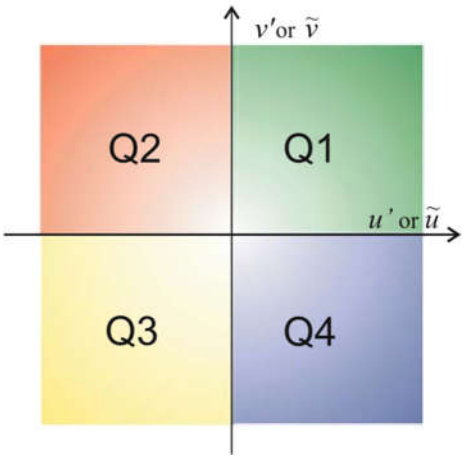

Figure 13 Sketch for quadrant numbers and color code (Pokrajac et al. 2007)

The quadrant analysis was done for all the discharges. The quadrant map in Figure 14 shows one cycle, from the middle of one rib to the middle of another rib. Above the rib, in the upstream end of the area, the vertical velocity is below the average, while the horizontal velocity is above the average (blue region). When the flow gets above the opening between the ribs, the vertical velocity still is below the average, and here the horizontal velocity also is less than average, i.e. the flow is decelerating as the area marked in yellow expands over the space between the ribs. Near the upstream end of the next rib, the flow is still decelerating in horizontal direction but has an upward accelerating vertical component, as the flow is split along the rib (red region). Below the ribs, the velocity deviations are similar but mirrored, so the vertical directions are opposite of the flow above the ribs. This means the quadrant diagram would be a path with opposite direction from the plots of the flow above the ribs.

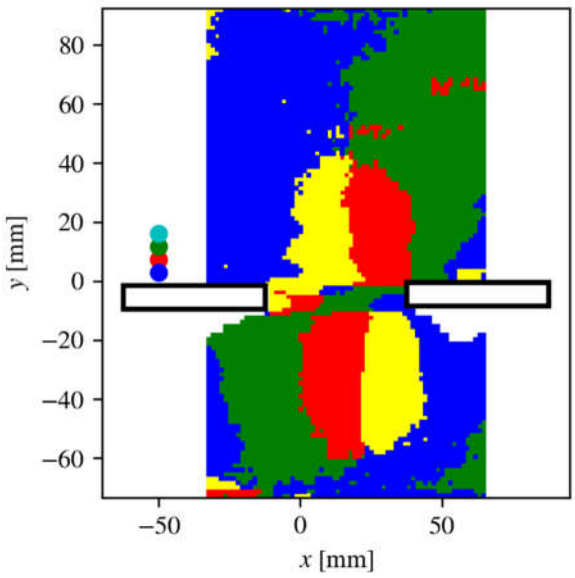

Figure 14 Quadrant map for 40 l/s

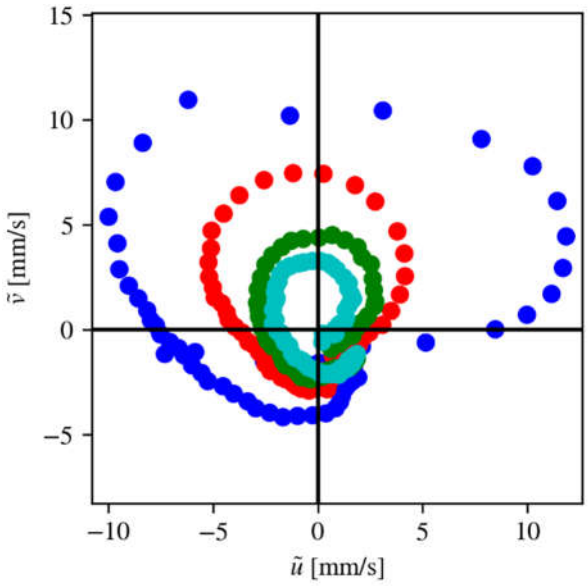

Figure 15 Quadrant diagram for 40 l/s

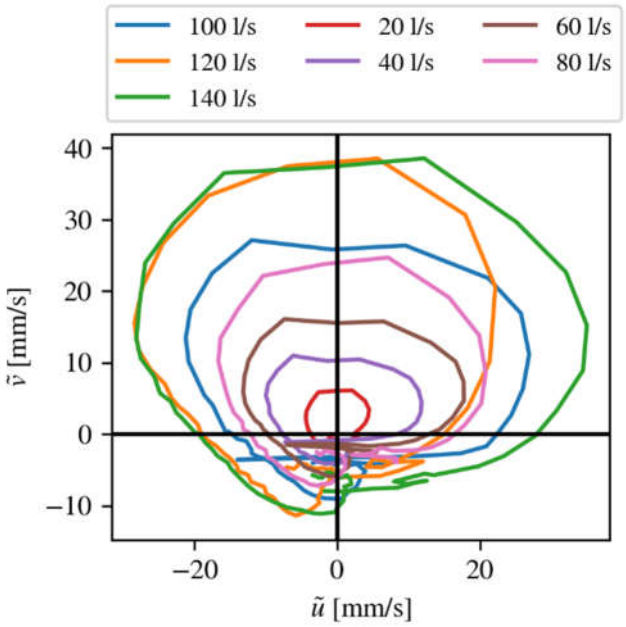

Figure 16 Quadrant diagram for all discharges, 3 mm above the ribs

The plots in Figure 15 show the values of $\tilde{u}$ and $\tilde{v}$ in a horizontal line at the vertical positions that are indicated in Figure 14. In Figure 15 we thus see where in the quadrants the spatial velocity fluctuations belong, and that they go in cycles. That is expected, as the downstream end of the quadrant map in Figure 14 ideally should be equivalent to the upstream end. In Figure 16, the values of of $\tilde{u}$ and $\tilde{v}$ at 3 mm above the ribs are shown for all the discharges.

5. Discussion

A discussion on the ribs effect on the flow field is given in this chapter. In addition, a preliminary discussion of observations relevant for the rock trap efficiency is provided. However, the main scope of this report is to present the effect of ribs on the flow field, and the effect on sediment transport is a topic for further studies.

The results show that the ribs have a significant effect on the flow and separate the flow field into lower velocities below the ribs and higher velocities above the ribs. The effect is higher for higher discharges, where the ratio of maximum horizontal velocity is about 2.5:1 for 20 l/s and almost 5:1 for 140 l/s. This may indicate that a larger distance between the ribs is acceptable for higher discharges. The prototype discharge of 80 m^3/s is equal to about 45 l/s in model scale and gives a factor of about 3:1 for flow velocity above and under the ribs.

The vorticity plots show that a vortex is forming on the trailing edge of the ribs. This is as expected. This vortex may cause both higher headloss and reduce sedimentation, but these effects have not been quantified. The vorticity is highest on the top corner on the downstream side of the ribs. There is also a higher vorticity at the top corner on the upstream side, but this is less significant compared with the downstream side. It may be possible to reduce the vorticity by adapting the geometrical shape of the ribs, for example with round corners. The Reynolds shear stress plots show positive values above the ribs and negative values below the ribs. The highest values are in between the ribs. This shows that the highest turbulence is in this area and the highest variability of the velocity.

The quadrant analysis has been done similar to the analysis of flow over rough beds. The resulting diagrams are very similar to the results in Pokrajac et al. (2007), but in this case, there is also a flow below the roughness elements (ribs). In this work, we are especially interested in the sedimentation between roughness elements to evaluate the rock trap design.

The quadrant analyses show that the highest variability in velocity in the flow just above the ribs is in the upward vector. This may be result in higher likelihood of sediments being resuspended or lifted over the spacing between the ribs, which may indicate a negative consequence for the sediment trap efficiency. However, since the measured ribs are in the downstream section of the rock trap, this effect may be opposite in the upstream end.

The net flux of water between the ribs is upwards. This is as expected since the water enters at the upstream end of the rib section and must exit in the downstream rib section (the studied ribs are in the downstream end). This is expected to give slightly unfavorable conditions for settling of particles, but the effect might not be very strong. Since the net vertical flow over the whole rock trap must be zero, more water is flowing down into the sediment compartment at another position. If this position is at the upstream end of the ribs, the effect could be very favorable since the upstream end of the ribs is the position most likely to trap sediments. The effect of the vertical flux has not yet been compared to the sediment weight and falling velocity, but it might be quite small.

For future studies, a promising method to visualizing the effect of the ribs is to calculate the particle paths of sediment particles entering the flow field based on the PIV-measurements. The particles are mainly influenced by the drag and gravity forces, which can be simulated over time. Figure 17 shows a preliminary calculation of weightless particles (density of particle is equal to density of water) that entered the flow field at the same time and same horizontal position but distributed vertically. After a certain time, the particles spread, as they are influenced differently by the flow field. Yellow color indicates higher velocities and blue color indicate lower velocities. Work to improve this method will be done in future studies.

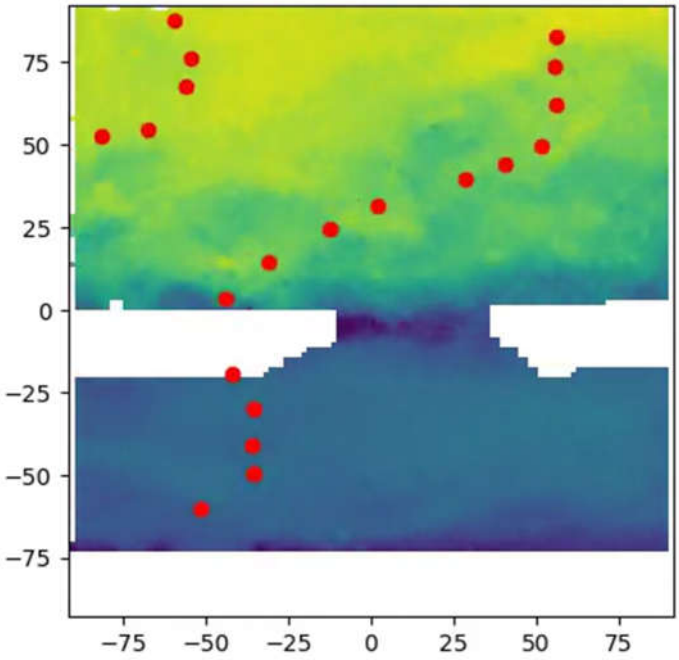

Figure 17 Particle positions calculated for weightless particles. The particles originated at the left end at the same time.

6. Conclusion

The experiments confirm the hypothesis that the rib setup equal to 1 m wide and 1 m spacing in the prototype successfully separate the flow field resulting in higher velocities above the ribs and lower velocities below the ribs. The effect is higher for higher discharge, ranging from 2.5:1 and 5:1 for discharges 20 l/s and 140 l/s respectively.

In the present study, we have not quantified the effect or created a correlation between sediment transport and spatially varying velocity, but this is a topic for future studies. In this report, the data from the experiments are presented, and deeper analysis will have to be done at a later stage. The experiments will continue with different rib configurations, and the effect of varying width/spacing ratio is planned to be investigated.

References

Luff, J. D., et al. (1999). "Experimental uncertainties associated with particle image velocimetry (PIV) based vorticity algorithms." Experiments in Fluids 26(1): 36-54.

Nikora, V., et al. (2001). "Spatially Averaged Open-Channel Flow over Rough Bed." Journal of Hydraulic Engineering 127(2): 123-133.

Pokrajac, D., et al. (2007). "Quadrant analysis of persistent spatial velocity perturbations over square-bar roughness." Experiments in Fluids 42(3): 413-423.

Attachments

Attachment 1: PIV raw data

Attachment 2: Processed data for all flow situations

Attachment 3: Plots for all flow situations

Institute of Hydraulic Engineering and Water Resources Management

Report

Hydraulic Investigation

Numerical Simulations

Flexible Sandtrap (FlekS) 1.0

December 2020

Project Partner and Client

Keywords: **Tonstad HPP pressurized sand trap situation evaluation, Tonstad HPP upgrade, 3D CFD, 3D CFD particle tracking simulation, mass oscillation in headrace system, extension chamber, semi-air cushion surge tank**

PROJECT PARTNERS

CLIENT

Sira-Kvina kraftselskap

Postboks 38

4441 Tonstad

Norway

Project leader: Kaspar Vereide, Phd

CONTRACTOR

Graz University of Technology

Institute of Hydraulic Engineering and Water Resources Management

Stremayrgasse 10/II

A-8010 Graz

Austria

Head of institute and project leader: Univ.-Prof. Dipl.-Ing. Dr. Gerald Zenz

Project co-leader and research consultant: Dipl.-Ing. Dr. Wolfgang Richter

1. Content

2. Introduction

2.1 Power plant – pilot study

Tonstad Hydro Power Plant is located in the south west part of Norway. This hydro power plant is the largest in Norway with respect to annual production, yielding 3,6 TWh. Total installed capacity is 960 MW, divided on five units. Four units each of 160 MW were installed in 1968. The capacity was enlarged in 1988, with a fifth unit of 320 MW. The water from to rivers is regulated for production. An 18 km long transfer tunnel from the river Sira intake connects with the 7,6 km long tunnel from the river Kvina intake at Ljosdal, before continuing 5,8 km to the forked headrace tunnel above Tonstad, as shown in Figure 1

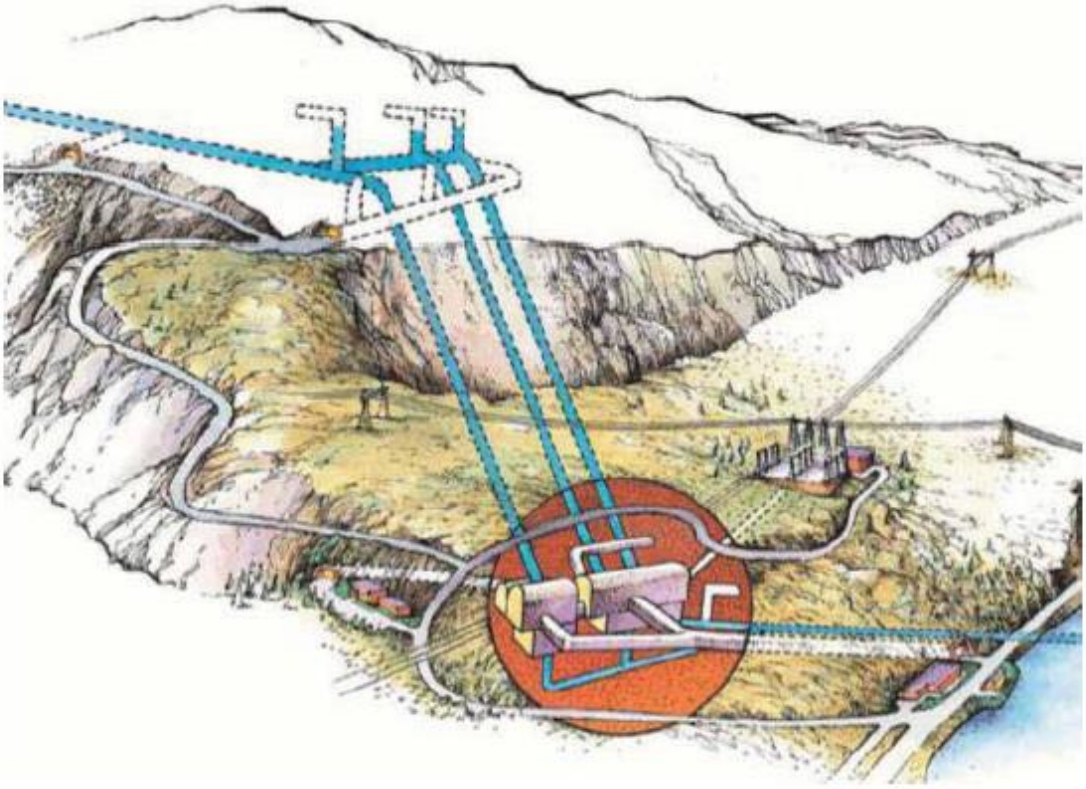

Figure 1: Surge tank position and power cavern of Tonstad HPP

Figure 2 shows the overview of the HPP system with the main headrace reservoirs Ousdalsvann and Homstølvann as well as the creek intakes.

The power plant was constructed in the 1960s with 4 machines and surge tank no1 and no2 also including sand trap no1 and no2.

In 1988 the fifths unit was installed as well as the surge tank no3 and sand trap no3 were constructed. But the original main tunnel was used.

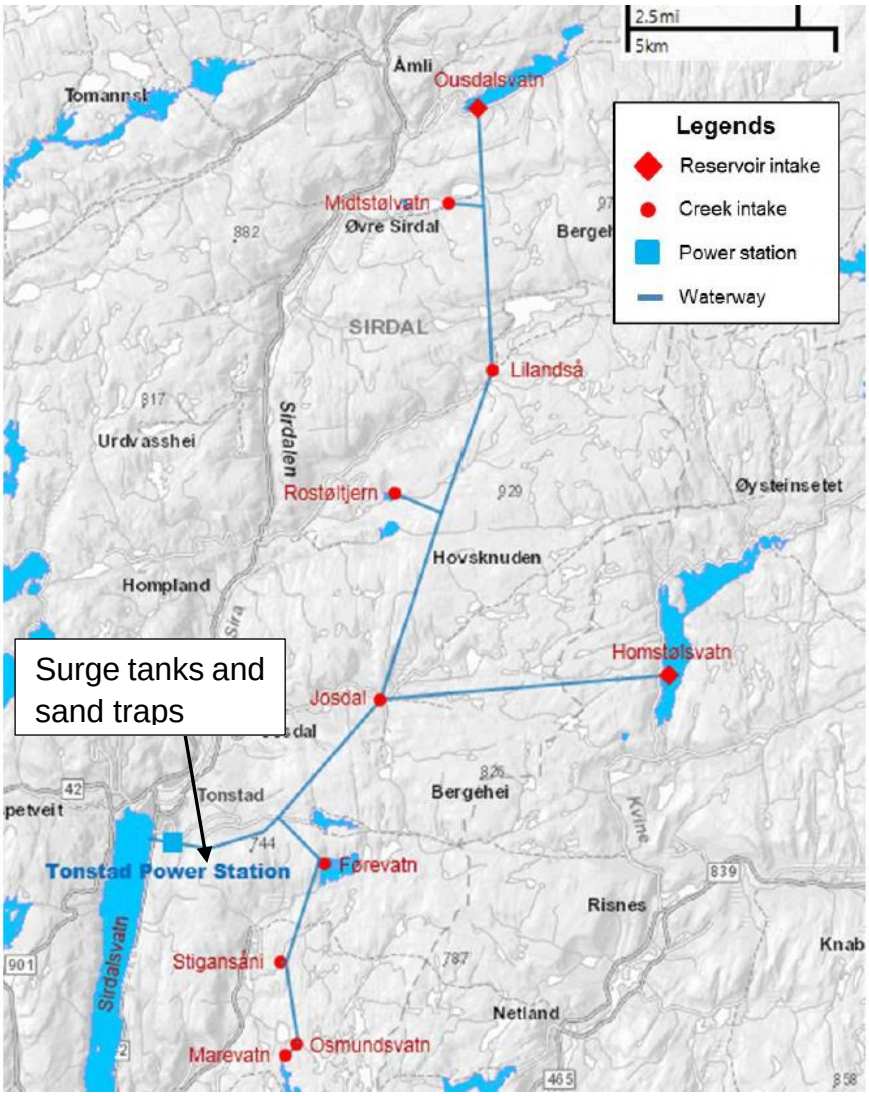

Figure 2: Overview of Tonstad HPP with headrace main reservoirs Ousdalsvatn and Homstolsvatn

2.2 Tonstad Hydropower plant

The municipality Tonstad is situated in the Sirdal valley, in the south west of Norway at the northern end of the lake Sirdalsvann. The power plant is part of the Sira-Kvina development project and owned by the Sira-Kvina hydro power scheme and owned by the Sira-Kvina power company. The power plant is part of a series of seven power plants illustrated in Figure 3.

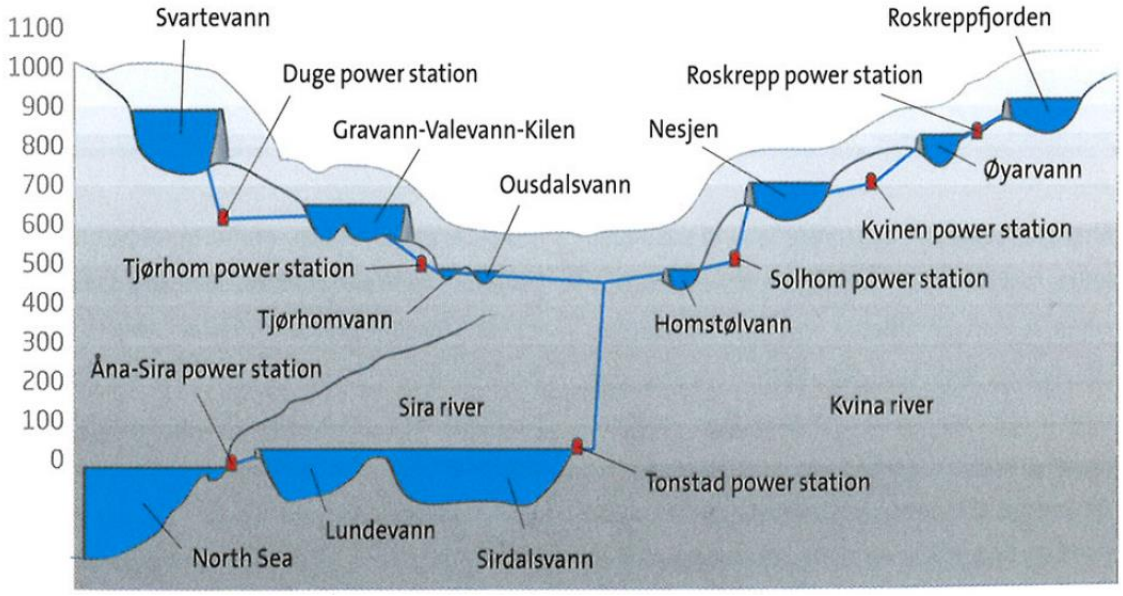

Figure 3: - Overview Sira-Kvina waterway system **(Møller 2009)**

All seven power plants together have an installed capacity of 1760 MW and provide a large portion of the Norwegian power output (Møller 2009). The installed capacity of the Tonstad power plant is 960 MW and is in respect to the annual produced energy of nearly 4 TWh the largest power station in Norway. The capacity is distributed to five vertical Francis turbines that have a combined discharge of about 250 m^3/s and a gross head of 450 m. The power plant was put in service in 1968 by starting energy production with two turbines, each with a capacity of 160 MW. In 1971 two additional turbines with a capacity of 160 MW were commissioned. The final addition until now was the fifth turbine with a capacity of 320 MW in 1988 (Sira-Kvina Kraftselskap n.d.).
Table 1 sums up the key information regarding the design discharge.

Table 1: Key information Tonstad power plant **(Sira-Kvina Kraftselskap n.d.)**

Units	Capacity	Design discharge
M1 & M2	each 160 MW	each 42.5 m^3/s
M3 & M4	each 160 MW	each 42.5 m^3/s
M5	320 MW	80 m^3/s
Overall	960 MW	250 m^3/s

2.3 Waterway and reservoirs

The power waterway is part of a greater system. This system gets fed by the Sira and Kvina rivers. There are two power stations along the Sira river and three along the Kvina river (Figure 3). The two upper reservoirs of Tonstad power plant are the downstream reservoirs of the foregoing power stations.

The Tonstad power plant gets mainly fed by two upper reservoirs and additional eight brook inlets along large headrace tunnel. The reservoir on the Kvina river side is the Homstølvann and the respectively on the Sira river side the Ousdalsvann. Due to the excellent rock quality, the main part of the system consists of unlined tunnels, only small sections with poor rock or weakness zones had to be lined.

The tunnel branch from the Ousdalsvann has a length of 16 km and a flow section area of 65 m^2, the water tunnel from the Homstølvann reservoir has a length of 7.5 km and a flow area of 55 m^2. These two merge into one tunnel with a cross section of 100 m^2 and a length of 6 km until it splits into three branches. All three branches have the same structure and consist of a surge tank with an associated sand trap. The brook inlets have a significant impact on the behaviour of the power plant because of the dampening effect, which is connected to them. The brook inlets function as small surge tanks along the headrace system (Vereide , Richter , et al. 2017).

Figure 4 shows the full Sira-Kvina hydropower system in ground view. The specific area of the Tonstad scheme is indicated.

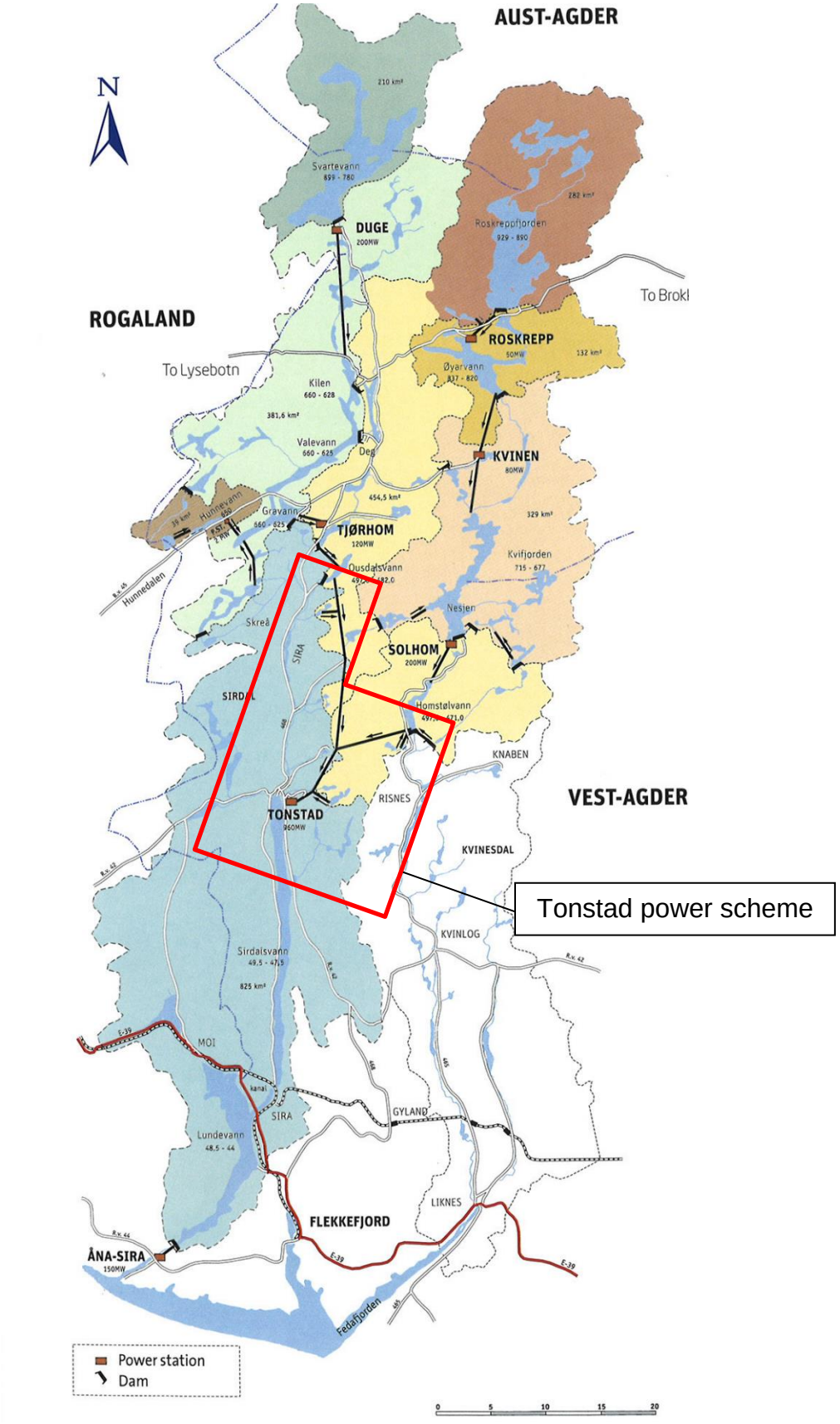

Figure 4: - Overview Tonstad power plant waterway **(Møller 2009)**

2.4 Sand traps

The sand traps of the HPP are located at the end of the pressure tunnel, after the surge tanks and right before the pressure shaft.

The main purpose of the sand traps are the separation and deposition of sediments from the main tunnel. Sediments are still in the power water way because of construction reasons. The system has worked properly until some years ago, when stones and sand was even destroying the parts of machine no5.

The incidents are described more detailed at Vereide, Bjørnar und Rolv 2015

Figure 5 shows the section of surge tank 3 with the investigated object: sand trap no3. It is also visible that the lower chamber of the surge tank is integrated in the pressure tunnel as a widening of the flow area. Figure 6 shows all 3 sand traps in ground view.

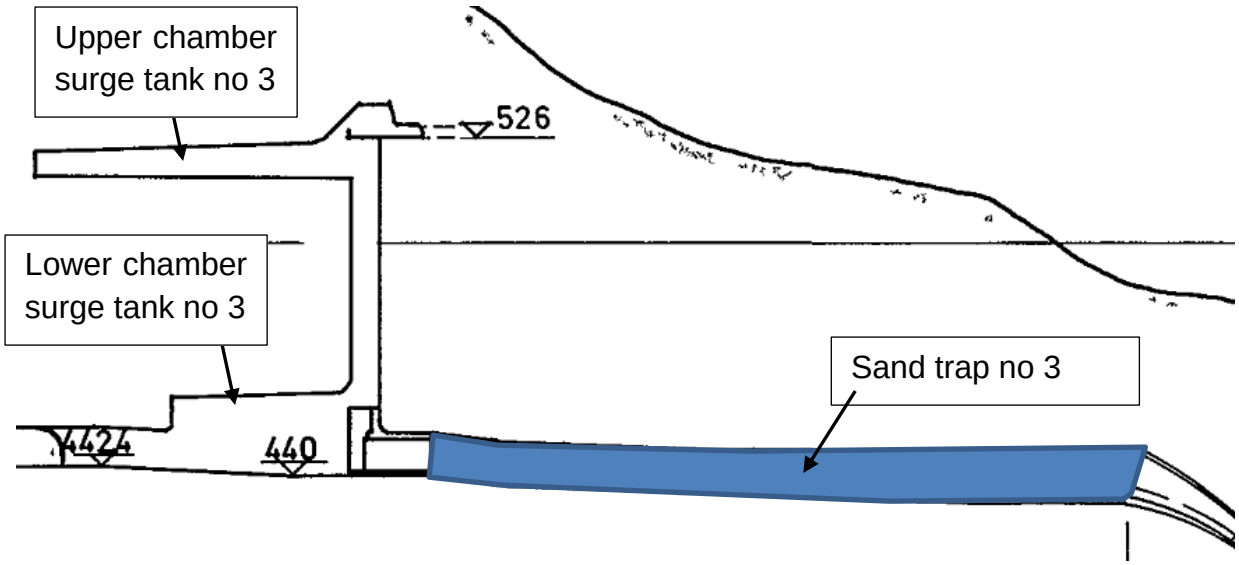

Figure 5: Section of surge tank 3 with sand trap no 3, overburden

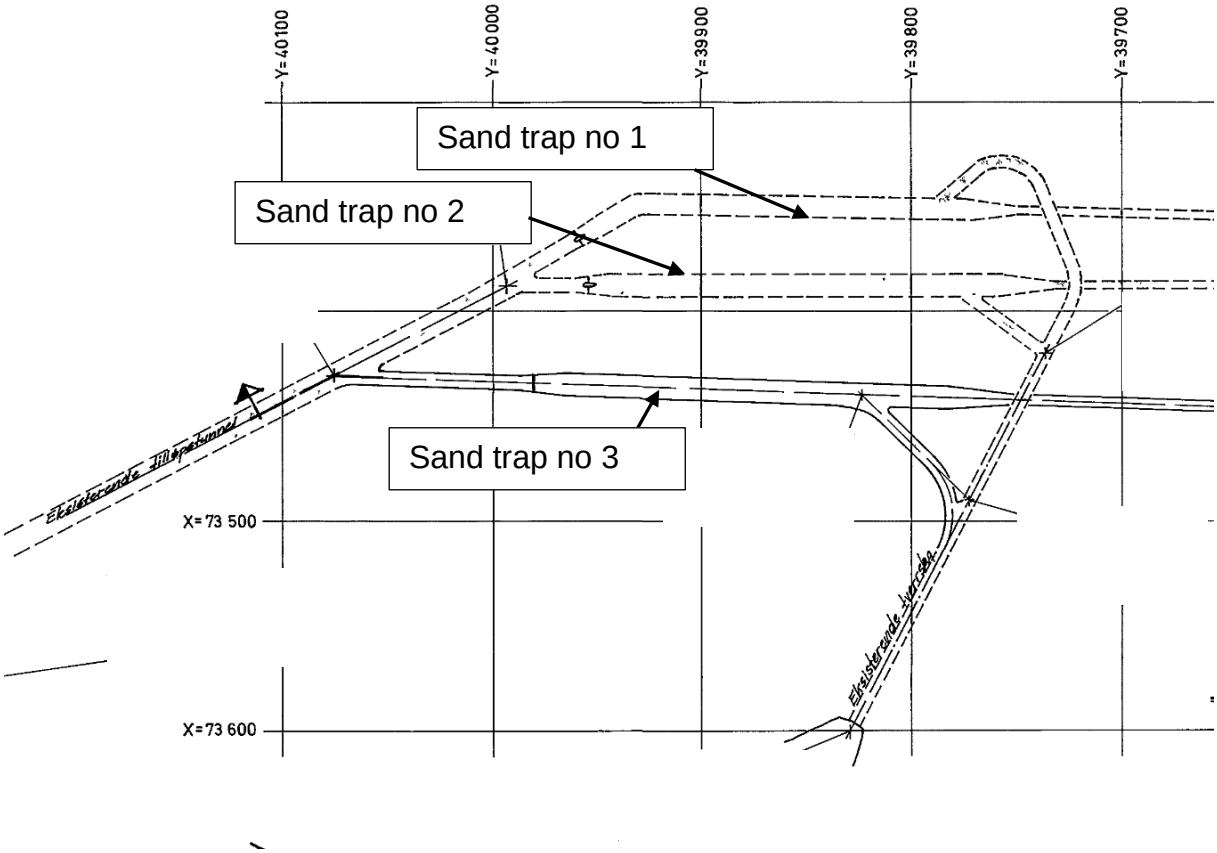

Figure 6: Ground view of the sand traps of Tonstad HPP

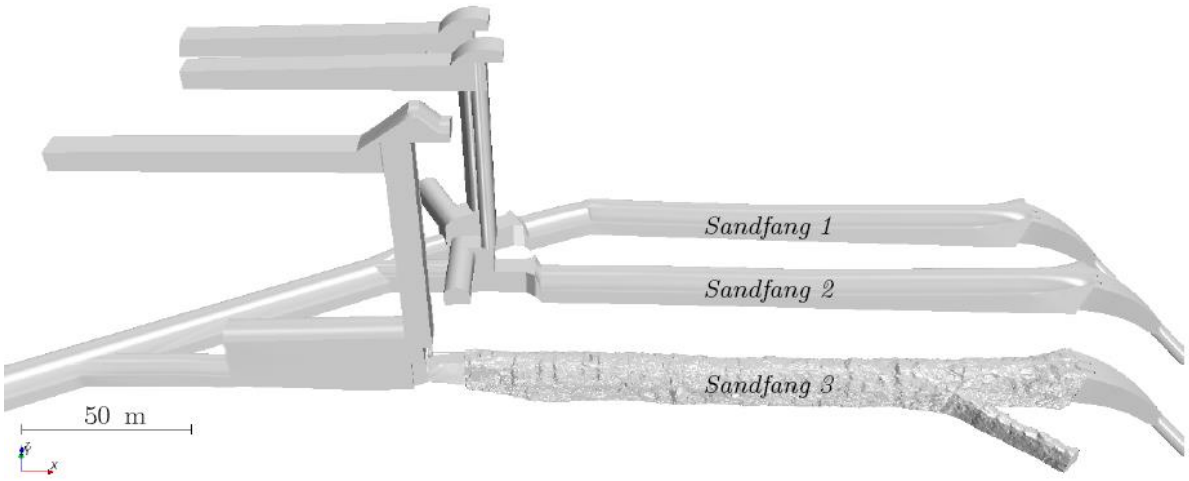

Figure 7: Isometric view of the three surge tanks with sand traps and the unlined pattern of sandtrap No.3 (Brevik 2013)

Following pictures visualize the prototype sand trap.

Figure 8: Rake from sand trap to pressure shaft after sediment removing (picture: Sira Kvina)

Figure 9: View inside the sand trap no3 while manual sand removing (picture: Sira Kvina)

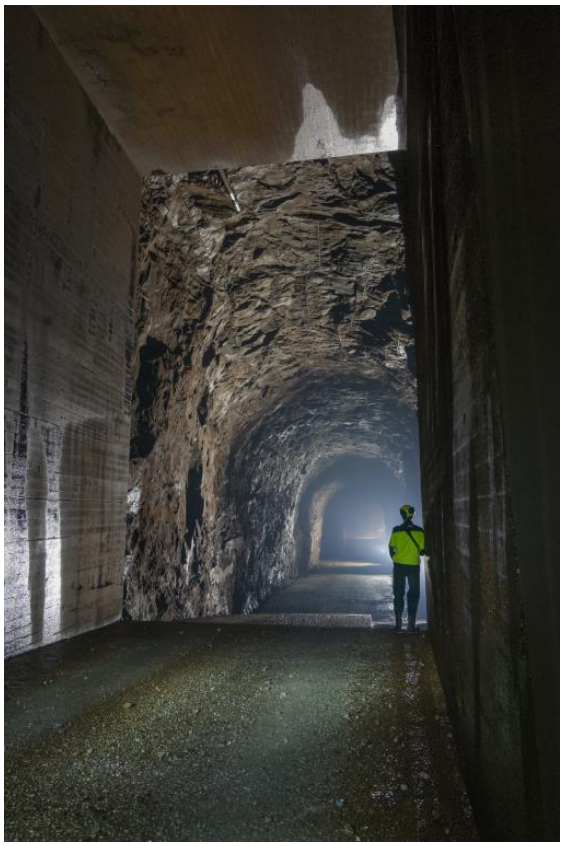

Figure 10: View from the gate area of sand trap no3 into the unlined part (picture: Sira Kvina)

Figure 11 shows sand depositions in front of the stairs of the rake. The backflow zone is visible that is obviously lifting sand up and through the rake.

Figure 11: Sediments in front of the rake to the p**ressur**e shaft (picture: Sira Kvina)

Figure 12 shows the widening section at the access gate on the right. This widening is believed to introduce a backflow zone and negatively influences the sedimentation process.

Figure 12: Flow widening at the adit (picture: Richter/TUG)

2.5 Summary of suspected sediment issues

This section describes shortly the suspected incidents of the sediment problems in connection with sand trap no 3.

1. Limit design grain size deposition (design size about 1 mm)

2. Deposition in area of lower chamber due to flow section widening
   - Suspected to be increased by mass oscillation in the system
   - Filling of the sand trap by gate opening → formation of a hydraulic jump and moving also of larger grains through the rake – hints regarding simulations of Brevik 2013 → Especially in connection with Point no 2
   - The gate has to be used because a filling valve has not properly operated

3. Free surface flow in the desander due to mass oscillation in succession of quick power changes due an installed power feedback controller
   - Too small dimensioning of the lower chamber volume of the surge tank volume

The question may arise why sand trap no 1 and no 2 with the machine units 1-4 are not affected as significantly as sand trap no 3 with machine unit 5 so far by the sediment problems. Following arguments can be listed:

1. Limit design grain size is the same for all three sand traps → these arguments seems to be the least relevant
2. Lower chamber of surge tank no 1 and no 2 are not integrated in the main tunnel → this seems to be an important factor.

So, the sediments in will be directly transported to the sand traps no1 and no 2.

3. Two smaller gates are installed at surge tank no 1 and no 2. So, the filling process
   can be done more smoothly.
4. The access tunnels are much closer to the rake in sand trap no 1 and no 2. This is believed to improve the deposition of sediments in front of the rake for this two sand traps

Figure 13 shows the three sand traps in comparison.

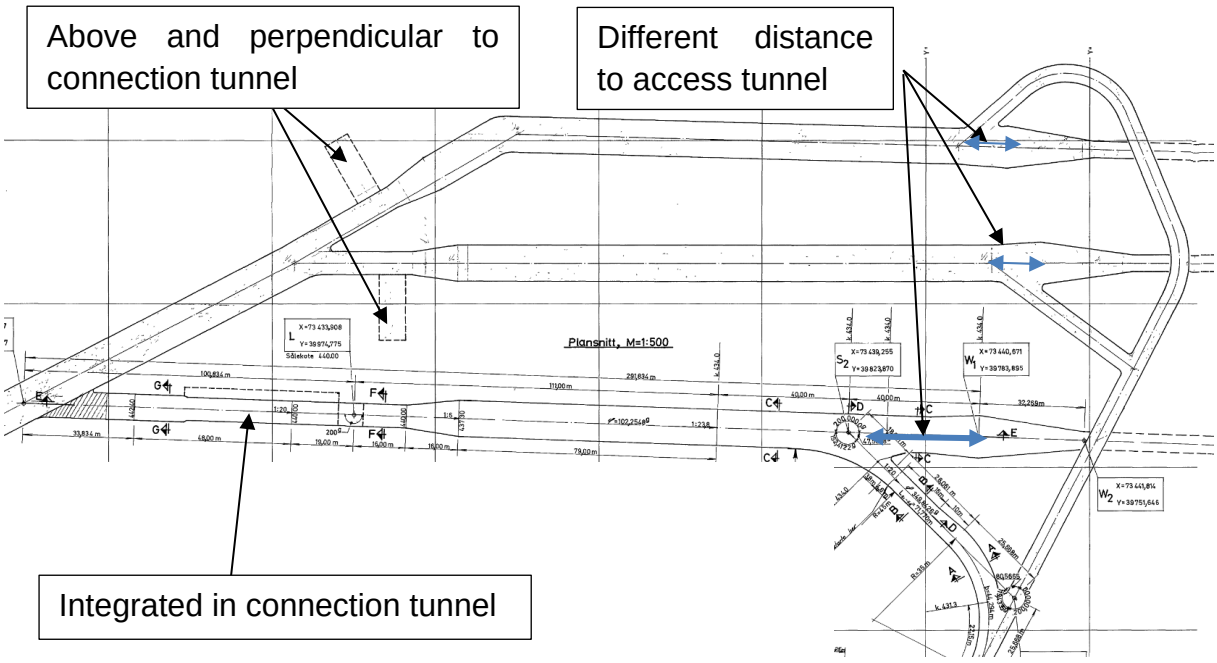

Figure 13: Ground view of the sand traps of Tonstad HPP, with lower chamber placing

2.6 Relevant issues for 3D CFD and physical model

1. Deposition in front of gate due to steady state operation, and if possible due to mass oscillation

Figure 14 shows a sediment issue that is relevant to be measured in situ. For the 3D CFD simulations the particle injection is placed at the crown right after the gate.

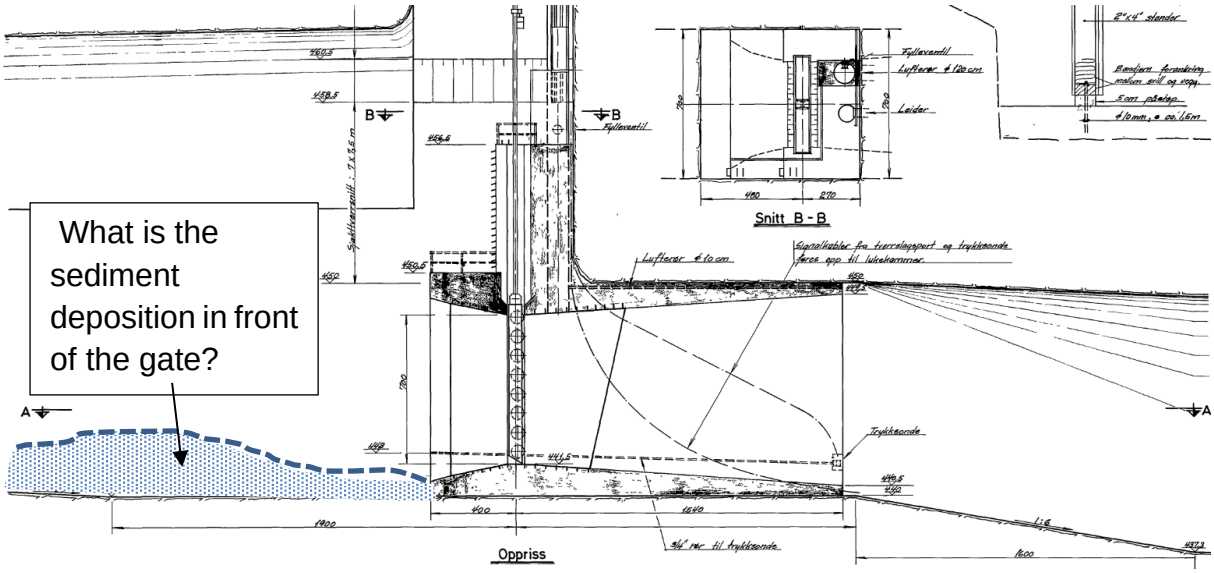

Figure 14: Detail of the gate of surge tank No.3

2. Sand grain separation and flow behaviour inside the sand trap
   - Evaluation of limit grain size
   - Flow behaviour due to roughness
   - Shear stresses on bottom
   - Investigation of structural objects and variants to improve the flow behaviour

➔ This is the main task in this present intermediate report. Regarding these results suggestions for further investigation for sand removal and flow optimizations are made by TU Graz

3. Filling of the sand trap after emptying the chamber. Suggested in combination with point no 1 above.
   For model test also with valve.

2.7 1D numerical simulations

1D-numerical simulations have been elaborated by TU Graz to investigate mass oscillation in the main tunnel system of HPP Tonstad and the impact to the sand trap (Figure 15).

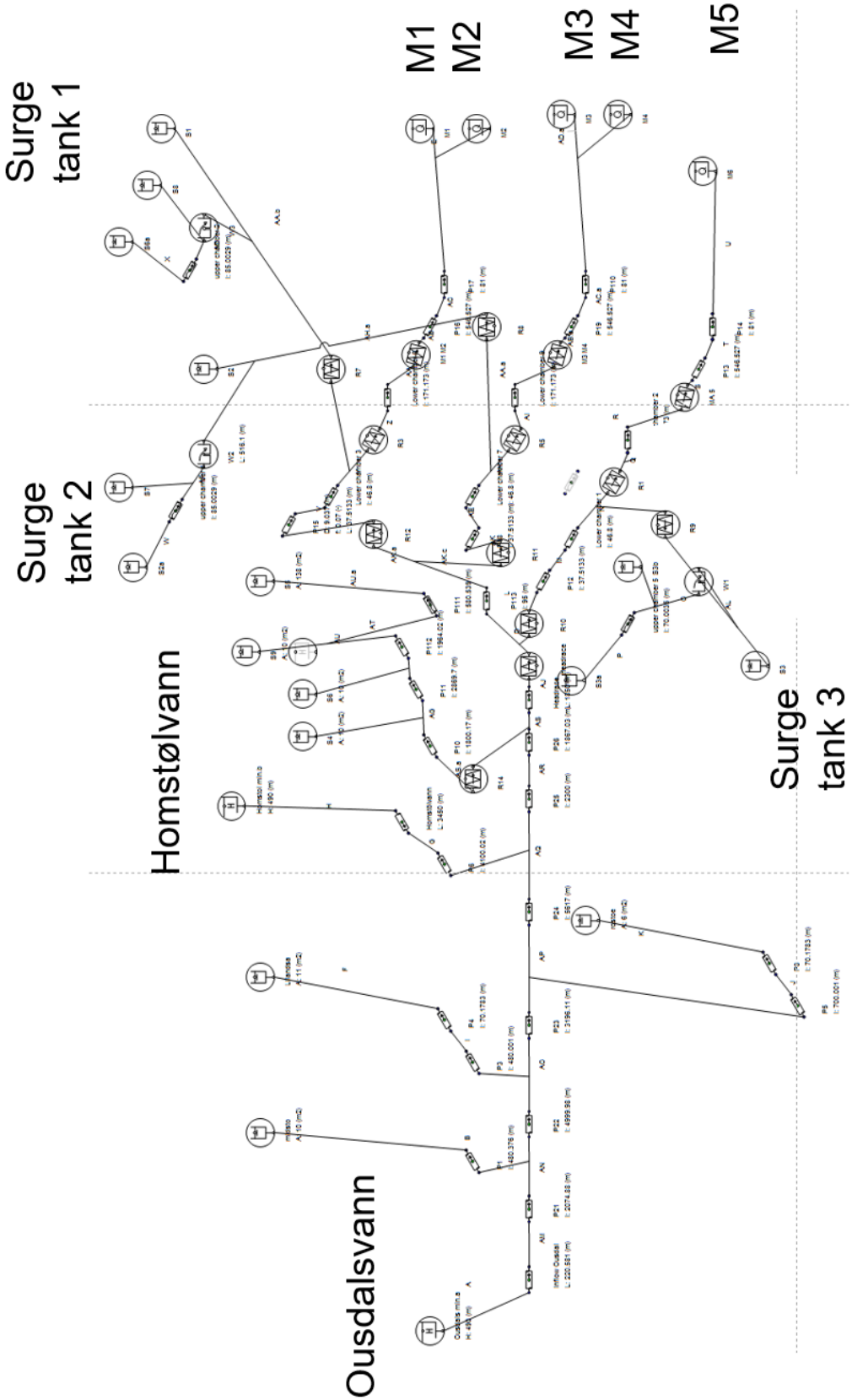

Figure 15: 1D-numerical scheme of Tonstad power plant, Wanda software

3. 3D CFD Sand Trap investigations

This chapter describes the 3D CFD sand trap investigation of TU Graz.

3.1 Software and modelling approach

The 3D numerical simulations are conducted with the software package ANSYS CFX V15.

The sand trap geometry was modelled in scale 1:15 to safe calculation expenses. For a design discharge of 80 m³/s a model flow rate of 0.092 is calculated. The simulations are transient and also include the start-up of the turbines in a reasonable time span to investigate the flow development in the sand trap.

Table 2: Scale factor and discharge

Scale	15	[-]
Q_P	80	m³/s
Q_M	0.092	m³/s

For the simulation of sand grains, the particle tracking model is used. For the current result one-way coupling was chosen. This leads to faster results but does not include an inner collision model of particles. The aim of this simulations is to see the behaviour of different grain sizes and its transient flow behaviour inside the sand trap.

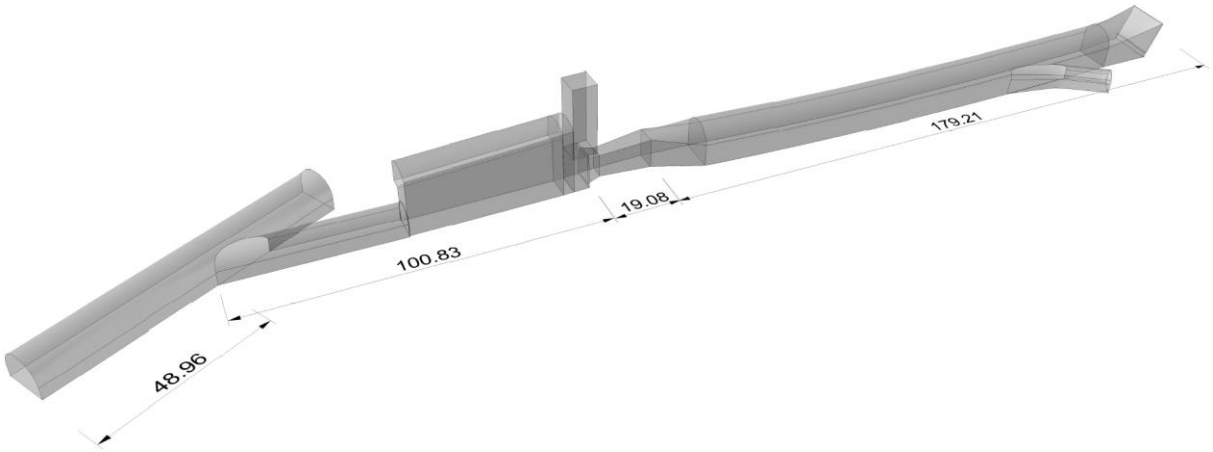

Figure 16: Geometry of the investigated zone of the sand trap with prototype dimensions [m]

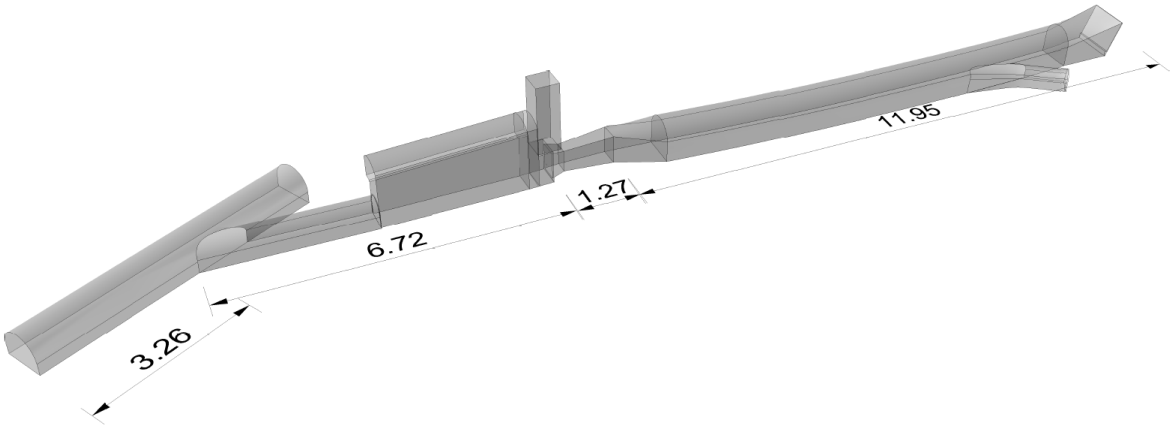

Figure 17: Geometry of the investigated zone of the sand trap in scale 1:15 dimensions [m]

3.2 Roughness of unlined rock

The roughness of unlined rock at the walls as well as the concrete bottom is considered in the simulations. The unlined rock roughness for prototype size is estimated to Strickler value 34 [$m^{1/3}/s$] or Manning value of 0.0294 [$s/ m^{1/3}$]. In conversion to sand grain roughness it is 200 mm and a friction factor of 0.045 [-].

Table 3 shows the conversion from Strickler roughness to sand grain roughness via the Colebrook-White formula. The conversion to the scaled roughness in the simulations is assumed to be scaled by factor the chosen scale factor 1:15. Since the sand grain roughness is used in the 3D CFD Simulations this results in a roughness of 200 mm/15= 13.33 mm. This approach fits very well to the suggested procedure by ASCE (1942) expressed in (Webb, Barfuss und Johnson 2010) and shown in Equation (1).

The roughness factor of Strickler value 34 [$m^{1/3}/s$] was chosen because back calculation of tunnel measurements from the Tonstad unlined tunnel system leads to the conclusion that the roughness varies between Strickler value of 32 [$m^{1/3}/s$] to 42 [$m^{1/3}/s$] between various hydraulic measurement runs. In this case the value of 34 [$m^{1/3}/s$] is more on the rough side.

In measurements it was a friction factor found of 0.059 [-] (Bråtveit, Lia und Olsen, An efficient method to describe the geometry and the roughness of an existing unlined hydro power tunnel 2012). So, it can be discussed if simulations with an increased roughness to this factor will influence the simulations. Comparison to that fact is planned to be included in an updated version by following simulation runs. Table 5 shows the roughness conversion for prototype scale and Table 6 for 1:15 scale model.

Table 3: Conversion of chosen wall roughness from Strickler value 34 [$m^{1/3}/s$] to 200 mm sand grain roughness

Strickler value				**34** [$m^{1/3}/s$]											
Q [m^3/s]	L [m]	D_i [m]	A [m^2]	k [mm]	T [C°]	ν [m/s]	E kin	ν [m^2/s]	Re [-]	C-W-1	C-W-1	λ	h_{vr} [m] sand grain roughness	alpha	head loss strickler [m]
80	140	12	113.1	**200**	20	0.71	0.03	1E-06	8 471 321	4.695	4.695	0.045	0.0135	2.1E-06	0.0137

Table 4: Conversion of chosen wall roughness from Strickler value 34 [$m^{1/3}/s$] to 13.3 mm sand grain roughness for present 3D CFD simulations

Strickler value				**53** [$m^{1/3}/s$]	factor	$15^{1/6}$	→		33.74 [$m^{1/3}/s$]						
Q [m^3/s]	L [m]	D_i [m]	A [m^2]	k [mm]	T [C°]	v [m/s]	E kin	ν [m^2/s]	Re [-]	C-W-1	C-W-1	λ	h_{vr} [m] sand grain roughness	alpha	head loss strickler [m]
0.0918	0.667	0.4	0.126	**13.49**	20	0.73	0.03	1.00E-06	291 638	4.082	4.082	0.060	0.00272	0.3238	0.002729

Table 5: Conversion of friction factor 0.06 [-] to wall roughness 412 mm sand grain roughness, prototype.

Strickler value				**30** [$m^{1/3}/s$]										
Q [m^3/s]	L [m]	D_i [m]	A [m^2]	k [mm]	T [C°]	v [m/s]	E kin	ν [m^2/s]	Re [-]	C-W-1	C-W-1	λ	h_{vr} [m] sand grain	alpha	head loss Strickler [m]
80	140	12	113	**412**	20	0.71	0.03	1.00E-06	8 471 321	4.067	4.067	0.060	0.0180	2.81E-06	0.0180

Table 6: Conversion of friction factor 0.06 [-] to wall roughness 27.5 mm sand grain roughness in 1:15 scale model

Strickler value				**47** [$m^{1/3}/s$]										
Q [m^3/s]	L [m]	D_i [m]	A [m^2]	k [mm]	T [C°]	v [m/s]	E kin	ν [m^2/s]	Re [-]	C-W-1	C-W-1	λ	h_{vr} [m] sand grain roughness	alpha	head loss strickler [m]
0.092	9.3	0.73	0.42	**27.5**	20	0.22	0.00	1.00E-06	159 141	3.991	3.991	0.0628	0.00192	0.22714	0.001914

$$n_r = L_r^{1/6}$$ Equation **(1)**

3.3 Boundary conditions of 3D CFD

This chapter describes the boundary condition approach for the 3D CFD simulations. The3D CFD simulations are conducted with Ansys CFX.

3.3.1 Scale factor hydrodynamic

The simulations were conducted in a 1:15 numerical scale model. The idea of this scaling are savings in computational resources. Subsequently the discharge, the flow velocity and time has to be scaled. Therefore, the Froude similitude law is applied.

$$Fr_r = \frac{Fr_p}{Fr_m} = \frac{v_r}{\sqrt{g \cdot L_r}} = 1 \qquad (2)$$

Index [r] ratio [P/M]

Index [p] prototype

Index [m] scale model

Following ratios are given by scale factor 1:15 ($L_R = L_N/L_M = 15$):

Area: $A_R = A_p / A_m = L_R^{\,2} =$ 225 (3)

velocities: $v_R = v_p / v_m = \sqrt{L_R} =$ 3,87 (4)

time: $t_R = t_p / t_m = \sqrt{L_R} =$ 3,87 (5)

discharges: $Q_R = Q_p / Q_m = L_R^{5/2} =$ 871,42 (6)

3.3.2 Flow simulations

The 3D CFD simulations are conducted as transient RANS simulations, taking the roughness of the walls into account as well as the gravitational force. The chosen turbulence model is the implemented SAS-SST in Ansys CFX. Figure 18 shows the input conditions for the transient simulation of the original sand trap geometry with particle injection region.

Figure 18 shows the flow inlet, outlet and the injection area. The sand grain injection area is chosen to be at an unfavourable position in order to generate conservative results.

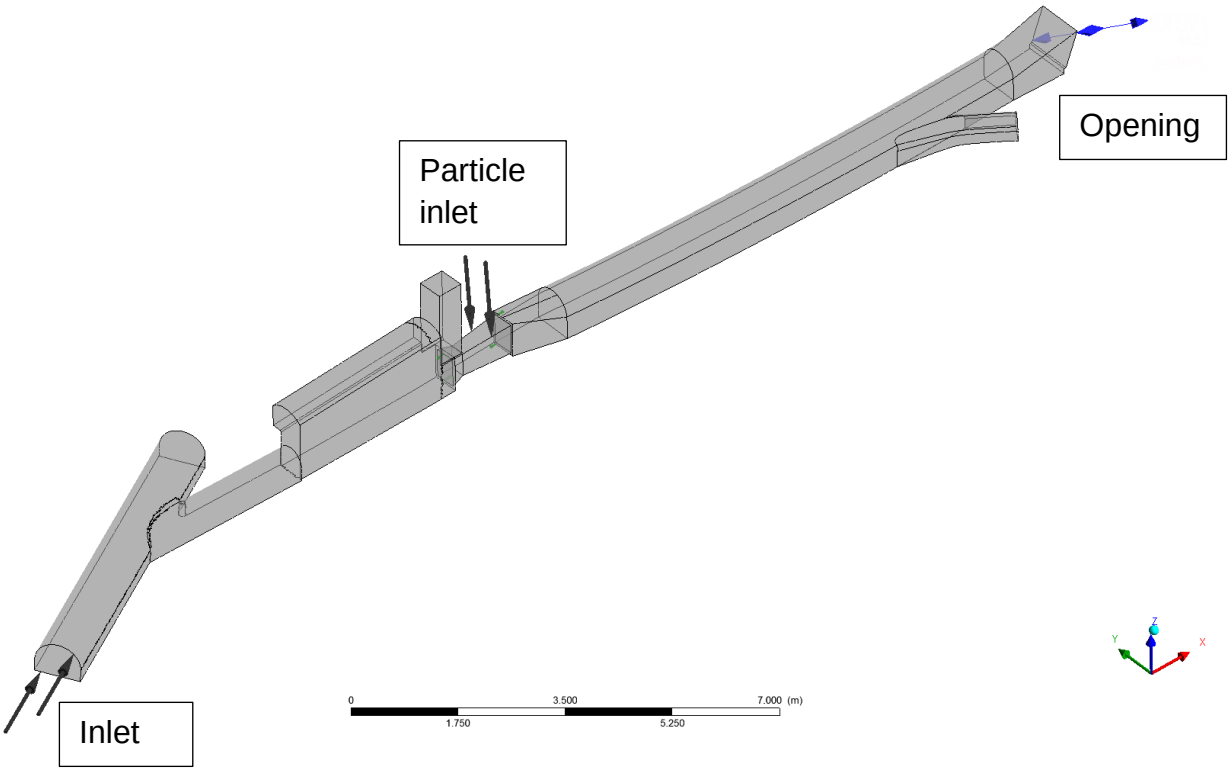

Figure 18: Boundary conditions for transient simulation incl. particle injection

3.3.3 **Sediment input**

Sand grain particles with density of 2300 kg/m³ are added. The simulations are conducted with one-way coupled sand grains. So, no interaction between the grains are modelled. As drag force the Schiller-Naumann scheme is used and found to be appropriate for the investigations (Schiller und Naumann 1933).

where C_D is the drag coefficient given by Schiller and Naumann (1933):

$$\begin{cases} C_D = \dfrac{24}{\mathrm{Re}_p}(1 + 0.15\,\mathrm{Re}_p^{0.687}) & \mathrm{Re}_p < 1000 \\ C_D = 0.44 & \mathrm{Re}_p > 1000 \end{cases}$$

A good approach was found to add 150 particles per second and a mass flow rate of 0.03_m kg/s. For the particle diameter distribution, it was chosen to use a uniform distribution by number between minimum diameter of 0.08_m mm and a maximum diameter of 0.5_m mm.

The sediments are simulated via a Lagrangian particle tracking model in Ansys CFX.

3.3.4 Scale of sediments in the simulation

Since the simulation is scaled via Froude similitude law also the sediments have to be scaled and the results interpreted respectively.

Table 7 shows the fall velocity of sand grains in still water for prototype. The aim of the simulation is to accurately combine the sink velocity and the drag force of the turbulent flow in the sand trap. The settling velocity of the grains is used to define the scaling of the grain diameters between scaled simulation and prototype.

It is indicated that also the water temperature has an influence on the fall velocity. Grains fall slower when the water is colder. This is believed to be connected with viscosity properties of water. Simulations in this report are conducted with water of 10 ° Celsius.

Table 7: fall velocity of sand grains in still water (Giesecke und Mosonyi 2009)

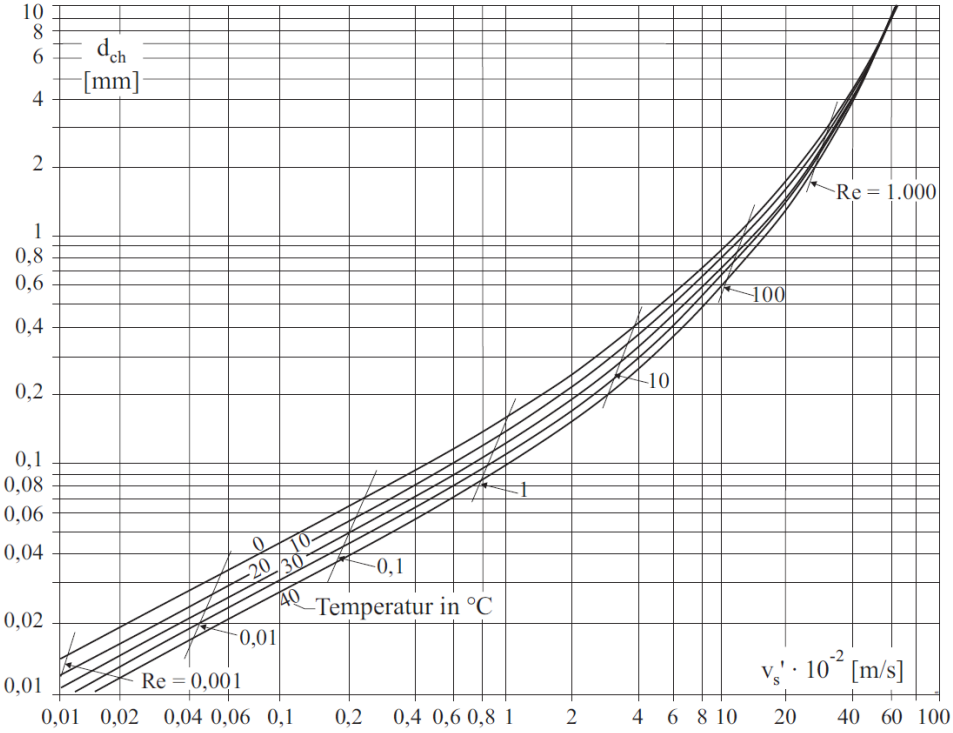

Abb. 7.8: Sinkgeschwindigkeit v_s' in ruhendem Wasser in Abhängigkeit des charakteristischen Korndurchmessers d_{ch} für Quarzkugeln ($\rho_F = 2650$ kg/m^3) bei verschiedenen Temperaturen mit den zugehörigen Reynolds-Zahlen [7.7]

The settling velocity of the diagram was first tested via a simple box of water in 3d CFD with particles. Two diameters were tested via 3D CFD, a 1mm grain and a 0.2 mm grain. It was found that the simulations have a very high accordance (Figure 19).

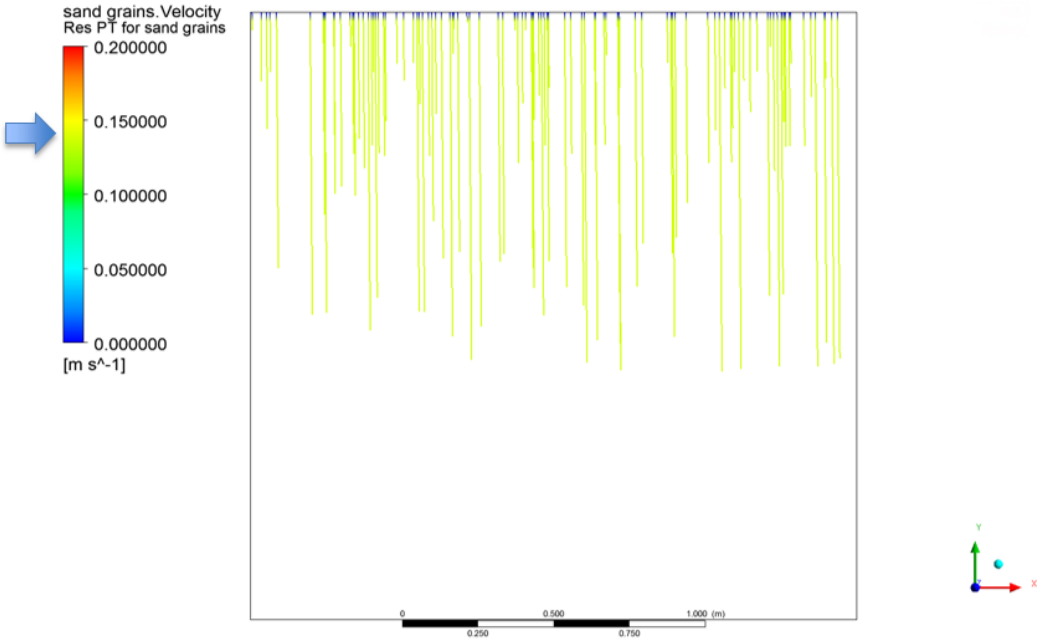

Figure 19: 3D-CFD simulation of 1mm sand grain settling velocity, literature 0.14 m/s equally to the results from 3D CFD

Figure 20 shows the scaling of the sand grains for the 1:15 Froude modelled numerical simulation. The scaling is based on the fall velocity of the sand grain. A 0.2 mm sand grain in prototype is scaled to a 0.09 mm sand grain particle in the 1:15 numerical simulation.

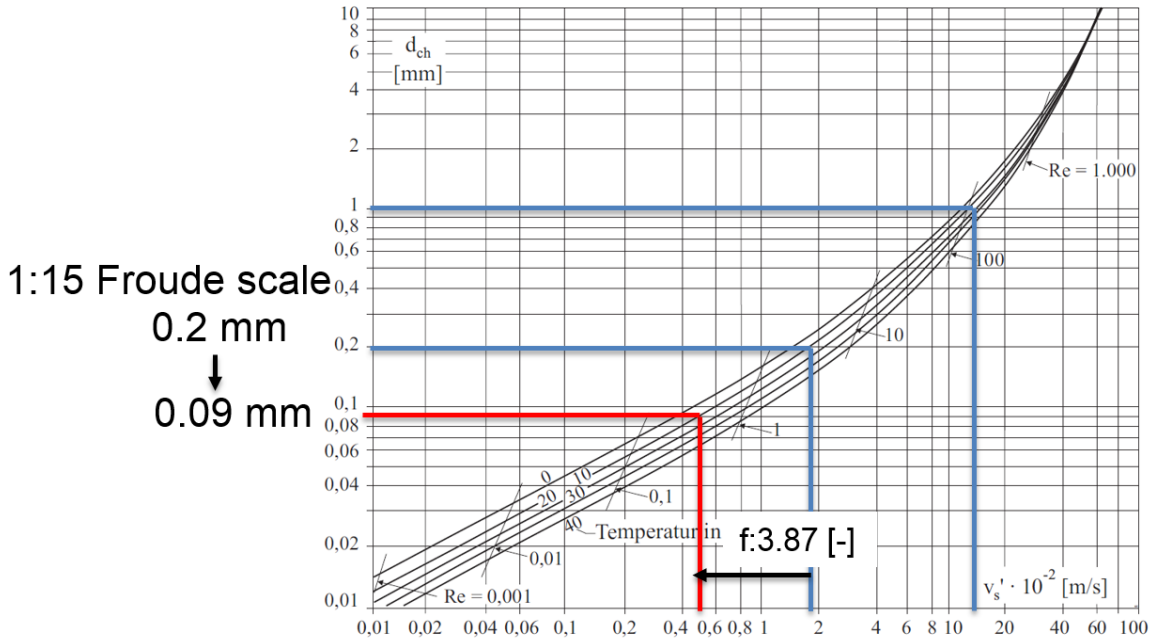

Figure 20: Scaling from Prototype to model scale, in this case 0.2_p mm correlate to 0.09_m mm

3.4 Roughness of measurements in tunnel system

This chapter shows the hydraulic losses in the Tonstad power water way from measurements and converts it to Strickler roughness, sand grain roughness and friction factor. The sections were separately measured. An average cross section was also taken from the same report as basis for back calculation.

It has to be stated that the total roughness is believed to be higher than the average value from the measurements below. This show calibration of mass flow and the roughness measurement by laser scan in the sand trap (Bråtveit, Lia und Olsen, An efficient method to describe the geometry and the roughness of an existing unlined hydro power tunnel 2012).

3.4.1 Homstøl – Ljostal

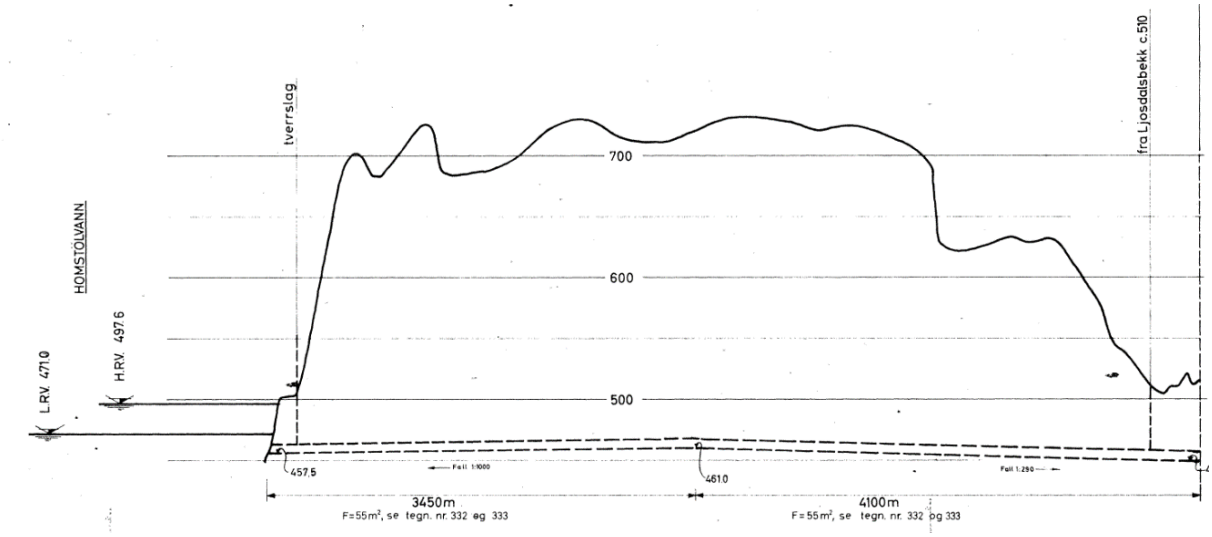

Figure 21: Longitudinal section from Homstøl to Ljostal

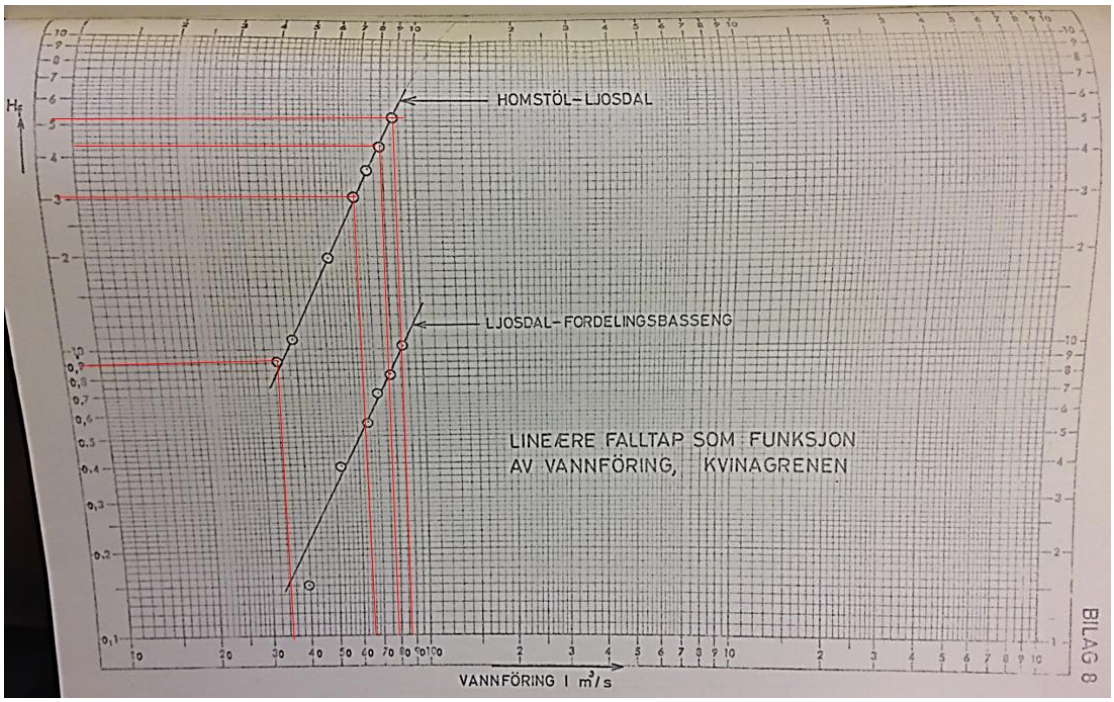

Figure 22: Measurement results from section from Homstøl to Ljostal

Table 8: Roughness values from back calculation in section Homstøl to Ljostal with average values

Conversion Strickler Value						[m$^{1/3}$/s]				Tunnel Section Homstöl - Ljostal							
	K_{ST}	Q [m³/s]	L [m]	D_i [m]	A [m²]	k [mm]	T [C°]	v [m/s]	E kin	ν [m²/s]	Re [-]	C-W-1	C-W-1	λ	h_{vr} [m]	alpha	hv
Average	**33**					**248**								0.055			
K_{ST}	34	86	7550	8.58	57.8	**213**	20	1.49	0.11	1.00E-06	12 736 601	4.347	4.347	0.053	5.25	0.0007	5.22
K_{ST}	33	65	7295	8.58	57.8	**242**	20	1.12	0.06	1.00E-06	9 626 501	4.238	4.239	0.056	3.05	0.0007	3.05
K_{ST}	32	35	7295	8.58	57.8	**288**	20	0.61	0.02	1.00E-06	5 183 501	4.088	4.088	0.060	0.95	0.0008	0.95
K_{ST}	34	80	7295	8.58	57.8	**209**	20	1.38	0.10	1.00E-06	11 848 001	4.367	4.367	0.052	4.35	0.0007	4.35

3.4.2 **Ousdal - Liland**

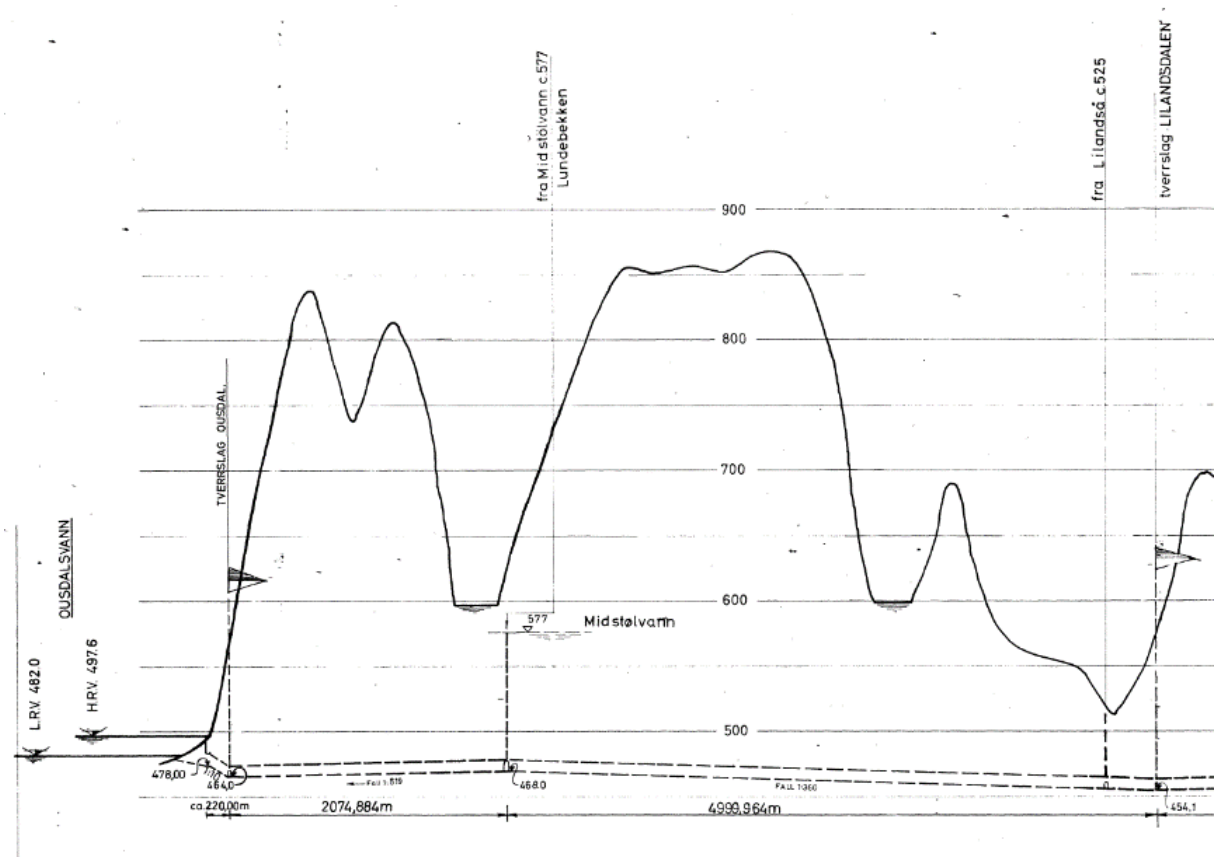

Figure 23: Longitudinal section from Ousdal to Liland

Table 9: Roughness values from back calculation in section Ousdal to Liland with average values

Conversion Strickler Value						[m$^{1/3}$/s]				Tunnel Section Ousdal - Liland							
	KST	Q [m³/s]	L [m]	D_i [m]	A [m²]	k [mm]	T [C°]	v [m/s]	E kin	ν [m²/s]	Re [-]	C-W-1	C-W-1	λ	h_{vr} [m]	alpha	hv
Average	**41**					**81**								**0.036**			
K_{ST}	39	84	7295	9.18	66.1	**95**	20	1.27	0.08	1.00E-06	11 631 104	5.112	5.112	0.038	2.50	0.0004	2.50
K_{ST}	42	50	7295	9.18	66.1	**67**	20	0.76	0.03	1.00E-06	6 923 276	5.413	5.413	0.034	0.79	0.0003	0.79
K_{ST}	40	70	7295	9.18	66.1	**81**	20	1.06	0.06	1.00E-06	9 692 587	5.244	5.244	0.036	1.65	0.0003	1.65

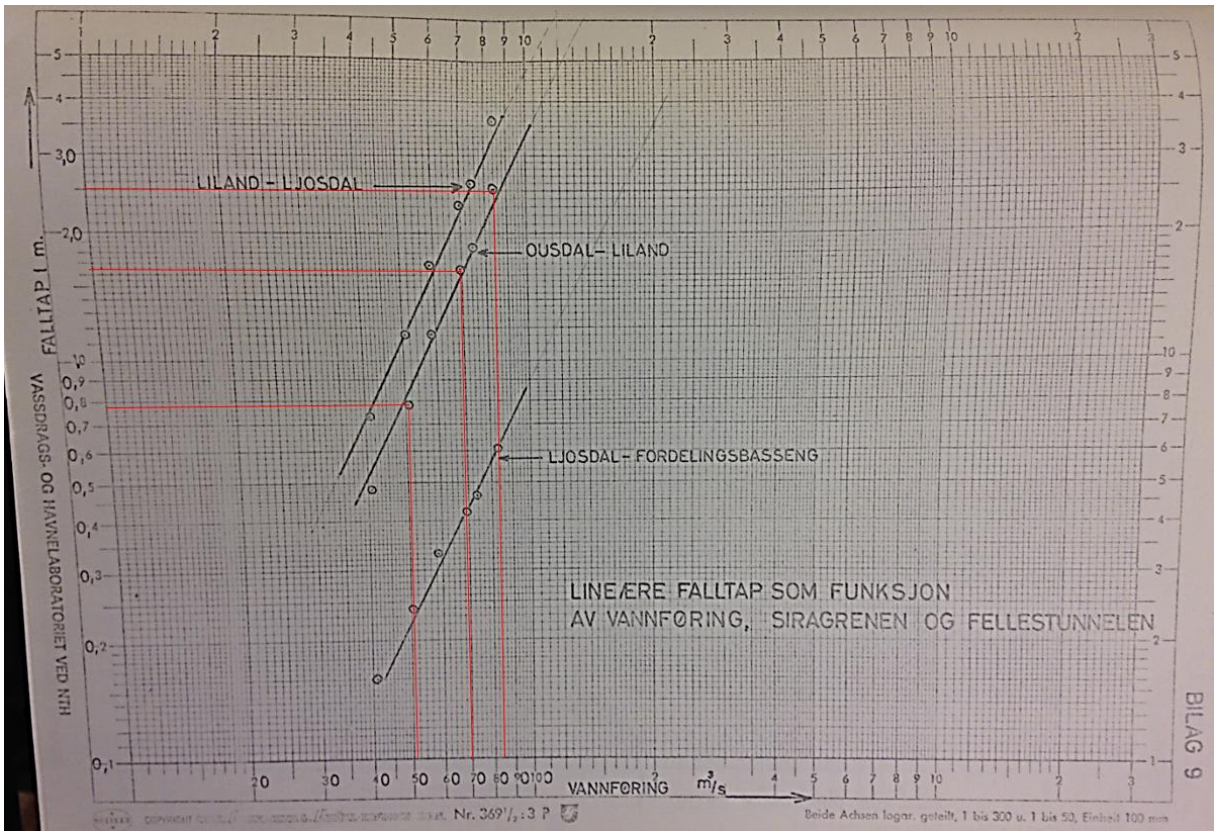

Figure 24: Measurement results from section from Ousdal to Liland

3.4.3 **Liland – Ljosdal**

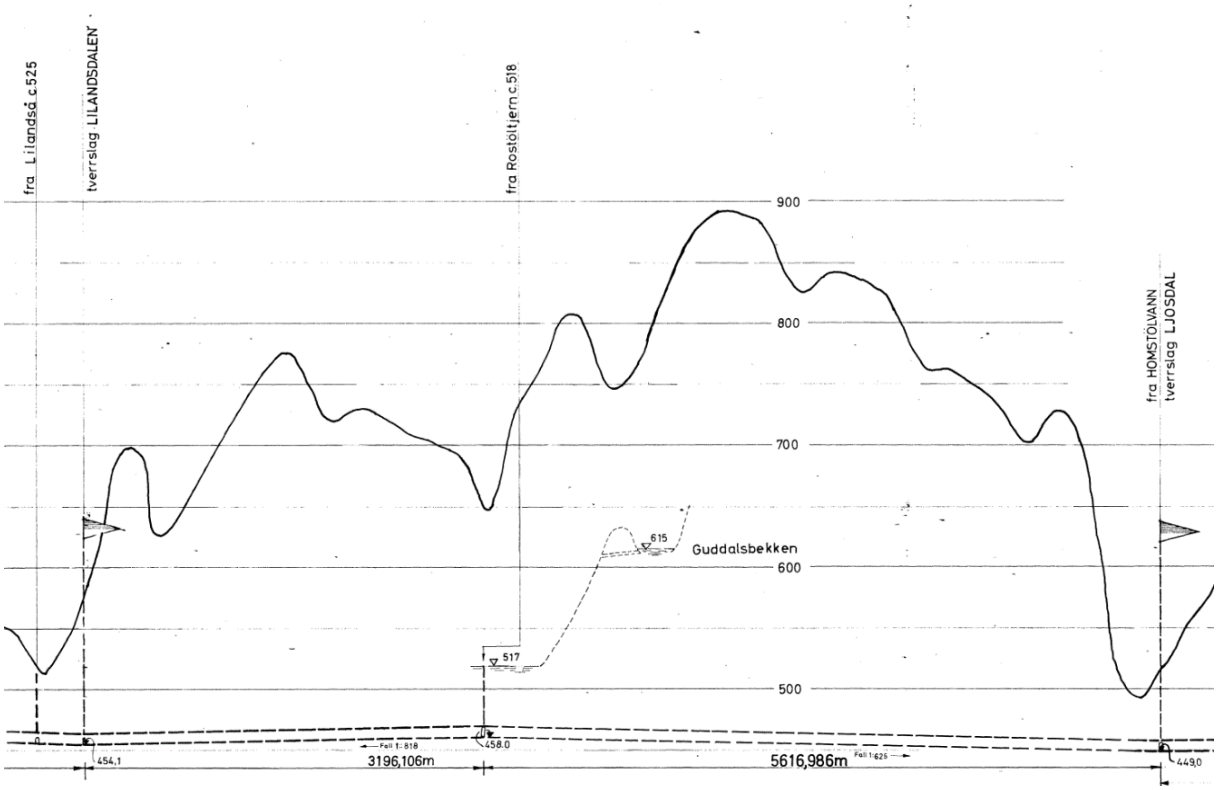

Figure 25: Longitudinal section from Liland to Ljosdal

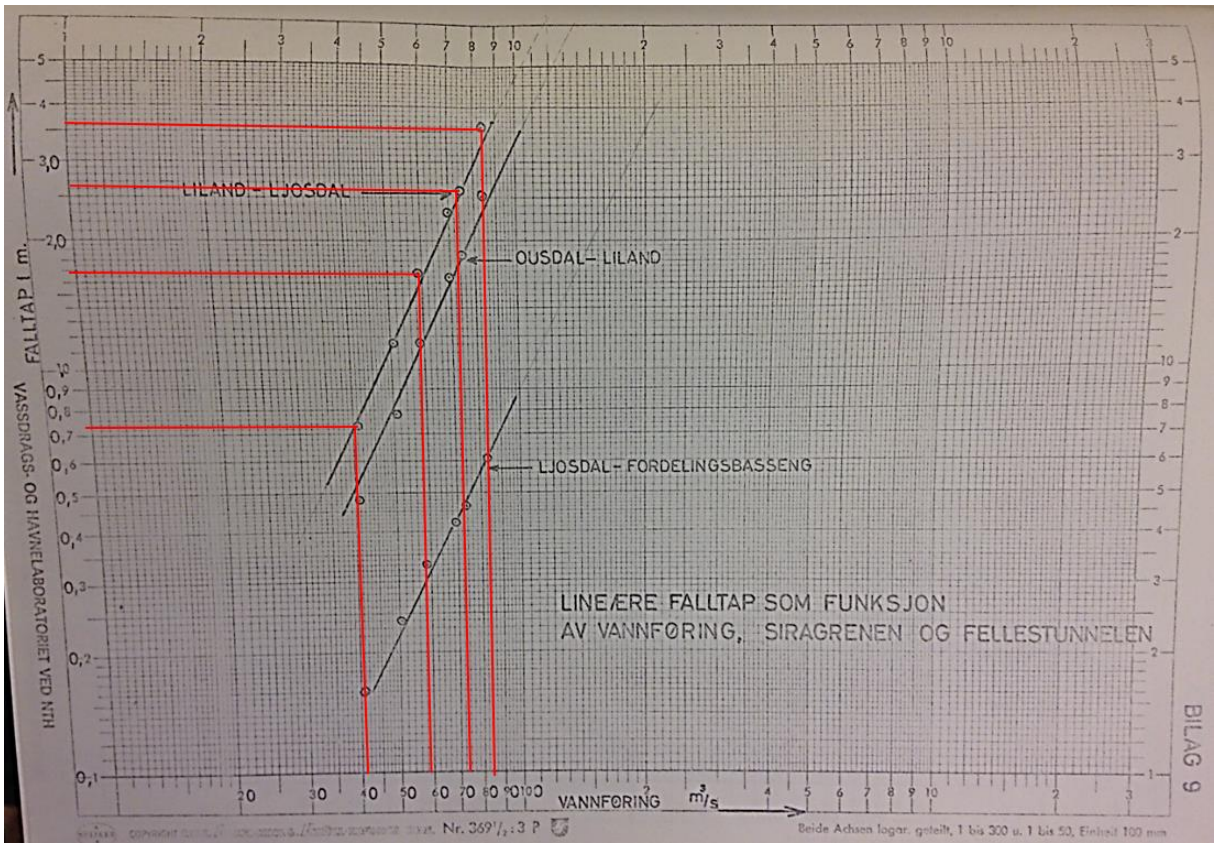

Figure 26: Measurement results from section from Liland to Ljosdal

Table 10: Roughness values from back calculation in section Liland to Ljosdal with average values

Conversion Strickler Value								[m$^{1/3}$/s]			Tunnel Section Liland - Ljosdal						
	KST	Q [m³/s]	L [m]	D_l [m]	A [m²]	k [mm]	T [C°]	v [m/s]	E kin	ν [m²/s]	Re [-]	C-W-1	C-W-1	λ	h_{vr} [m]		alpha	hv
Average	**35**					**199**								**0.052**				
K_{ST}	33	84	8813	9.14	65.61	**239**	20	1.28	0.08	1.00E-06	11 678 189	4.304	4.305	0.054	4.35		6E-04	4.35
K_{ST}	34	59	8813	9.14	65.61	**214**	20	0.90	0.04	1.00E-06	8 202 537	4.399	4.399	0.052	2.05		6E-04	2.05
K_{ST}	37	42	8813	9.14	65.61	**144**	20	0.64	0.02	1.00E-06	5 839 094	4.746	4.746	0.044	0.89		5E-04	0.89
K_{ST}	34	74	8813	9.14	65.61	**144**	20	1.13	0.06	1.00E-06	10 287 928	4.461	4.746	0.050	3.14		6E-04	3.14

3.4.4 **Ljosdal – Fordelingsbasseng**

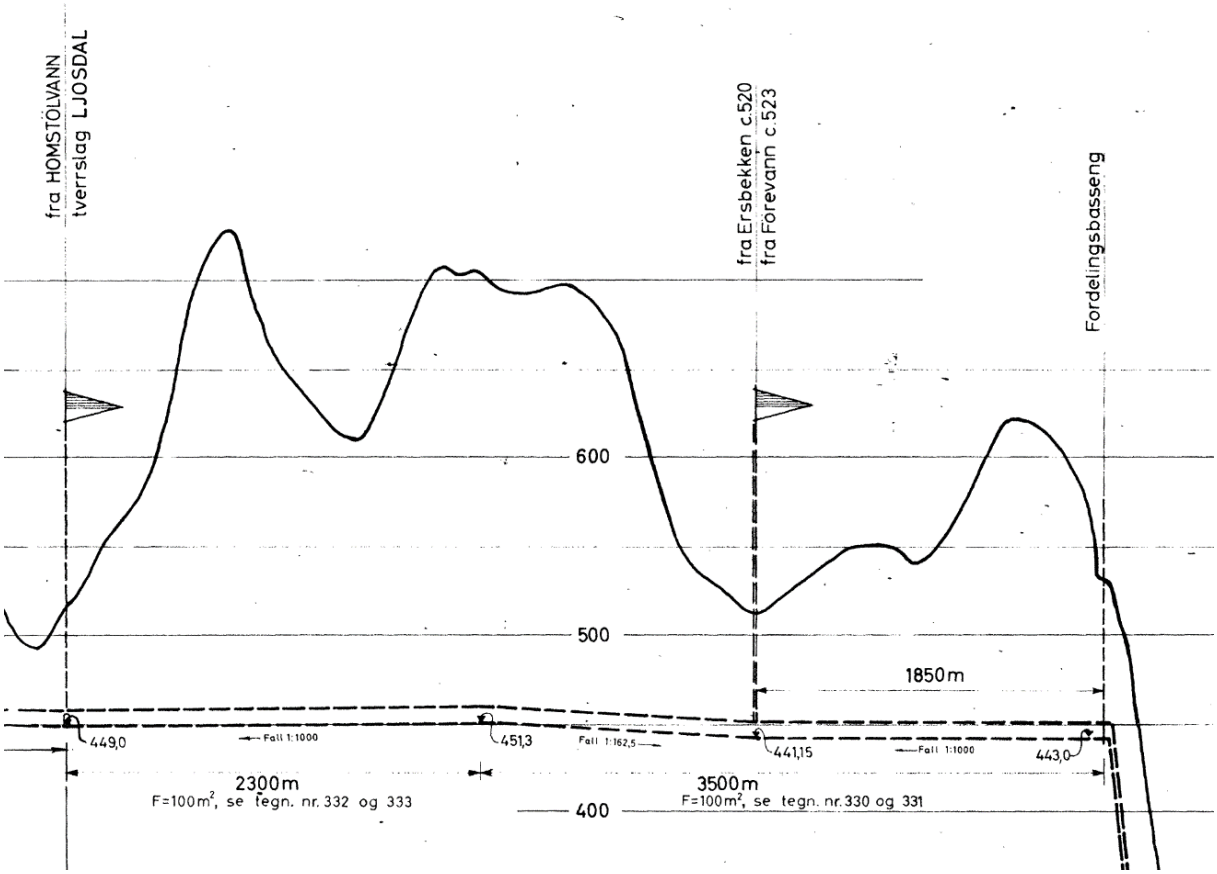

Figure 27: Longitudinal section from Ljosdal to Fordelingsbasseng

Table 11: Roughness values from back calculation in section Ljosdal to Fordelingsbasseng with average values

Conversion Strickler Value								[m$^{1/3}$/s]				Tunnel Section Ljosdal - Fordelingsbasseng						
	KST	Q [m³/s]	L [m]	D_i [m]	A [m²]	k [mm]	T [C°]	v [m/s]	E kin	ν [m²/s]	Re [-]	C-W-1	C-W-1	λ	h_{vr} [m]		alpha	hv
Average	**37**					**144**								**0.041**				
K_{ST}	37	82	5800	11.6	105.7	**134**	20	0.78	0.03	1.00E-06	8 982 521	5.015	5.015	0.040	0.61		9E-05	0.61
K_{ST}	39	74	5800	11.6	105.7	**107**	20	0.70	0.02	1.00E-06	8 106 178	5.212	5.212	0.037	0.46		8E-05	0.46
K_{ST}	35	59	5800	11.6	105.7	**193**	20	0.56	0.02	1.00E-06	6 463 034	4.697	4.697	0.045	0.36		1E-04	0.36
K_{ST}	37	51	5800	11.6	105.7	**140**	20	0.48	0.01	1.00E-06	5 586 690	4.973	4.973	0.040	0.24		9E-05	0.24

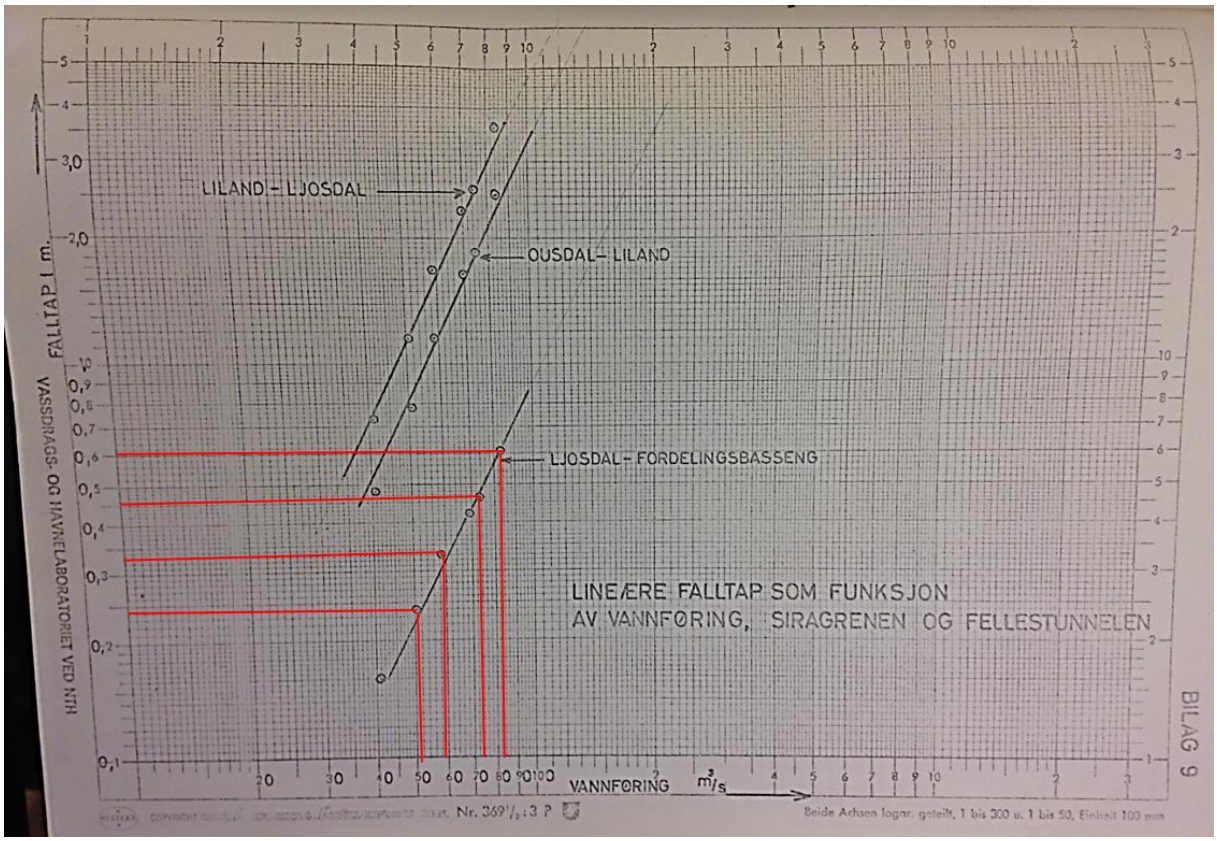

Figure 28: Measurement results from section from Ljosdal to Fordelingsbasseng

4. Sand Trap Geometry Variation and 3D CFD simulations

This chapter describes the simulations and the evolution of the sand trap variants

4.1 Original Geometry

The simulations are increased in its complexity by investigation process. Firstly, smooth wall and steady state simulations are conducted. This has shown that a very stable jet is formed (Figure 28). But from the ADCP measurements inside the sand trap and from the DES simulations it was known that the flow field is much more complex, even at steady flow conditions (Figure 30). Therefore, it was chosen to use transient simulation with the SAS SST turbulence model including wall roughness of the unlined part and the concrete part.

Figure 31 shows a single frame the transient simulation. Although it is not as detailed resolved and a shift between the discharge of 73.5 m³/s to 80 m³/s one can see that the flow pattern is matching quite well. The flow pattern is highly transient and fluctuate. The aim of this simulations is to investigate the transient behaviour of the shear stress at the bottom of the sand trap.

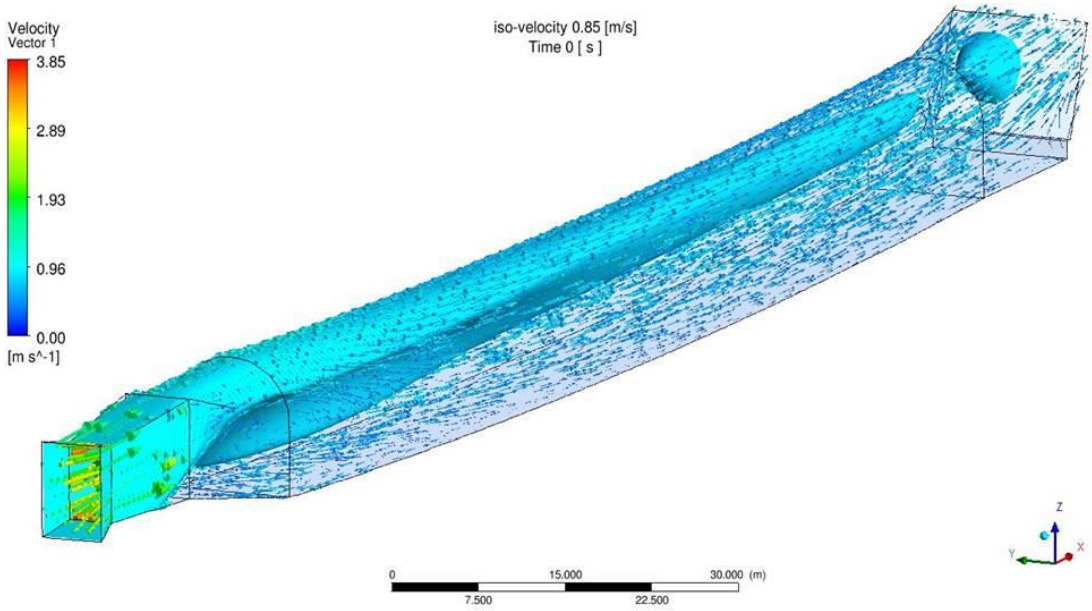

Figure 29: Steady state simulation, iso-velocity of 0.85 m/s (m) → 3.29 m/s (p)

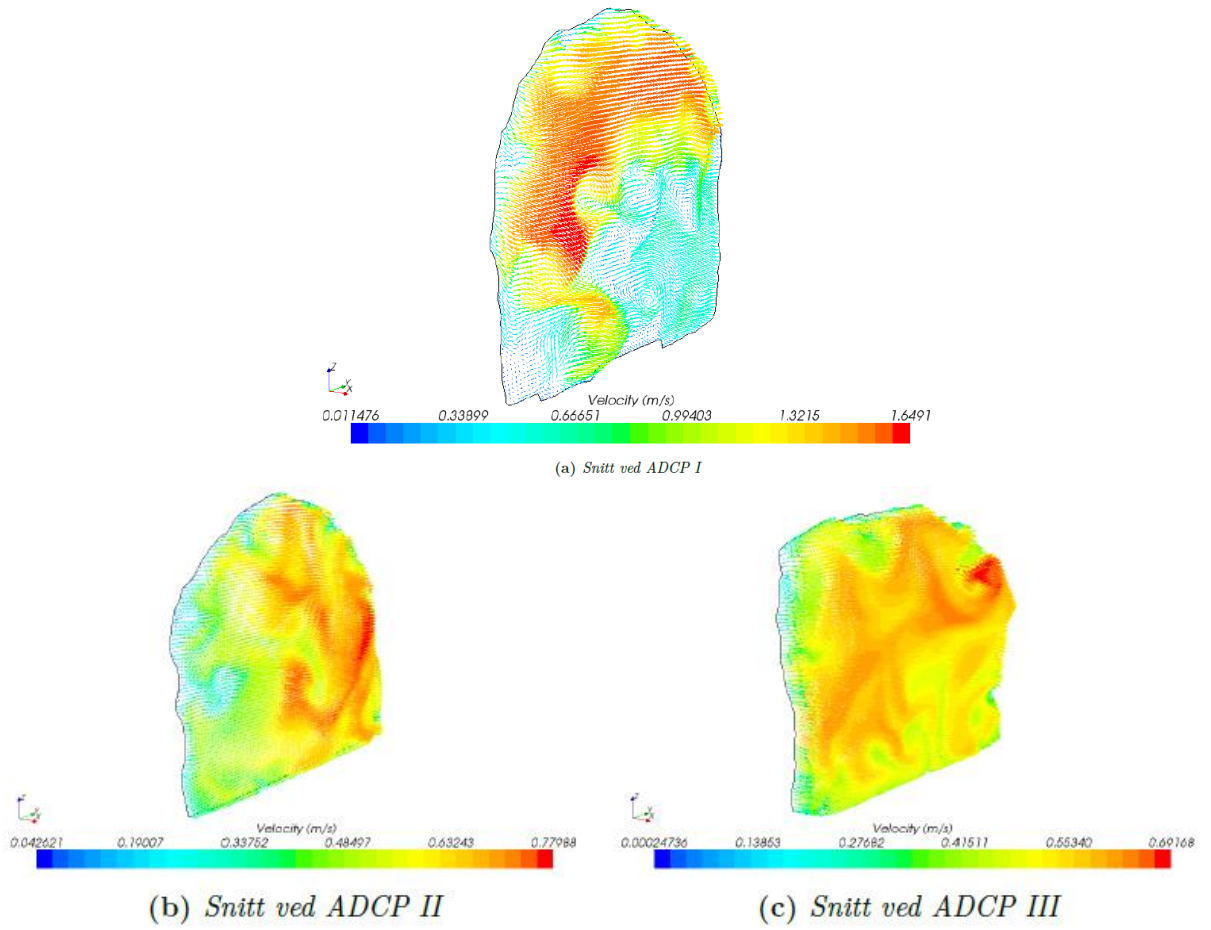

(a) *Snitt ved ADCP I*

(b) *Snitt ved ADCP II*

(c) *Snitt ved ADCP III*

Figure 30: Results from DES simulations (Brevik 2013), Discharge 73.5 m³/s

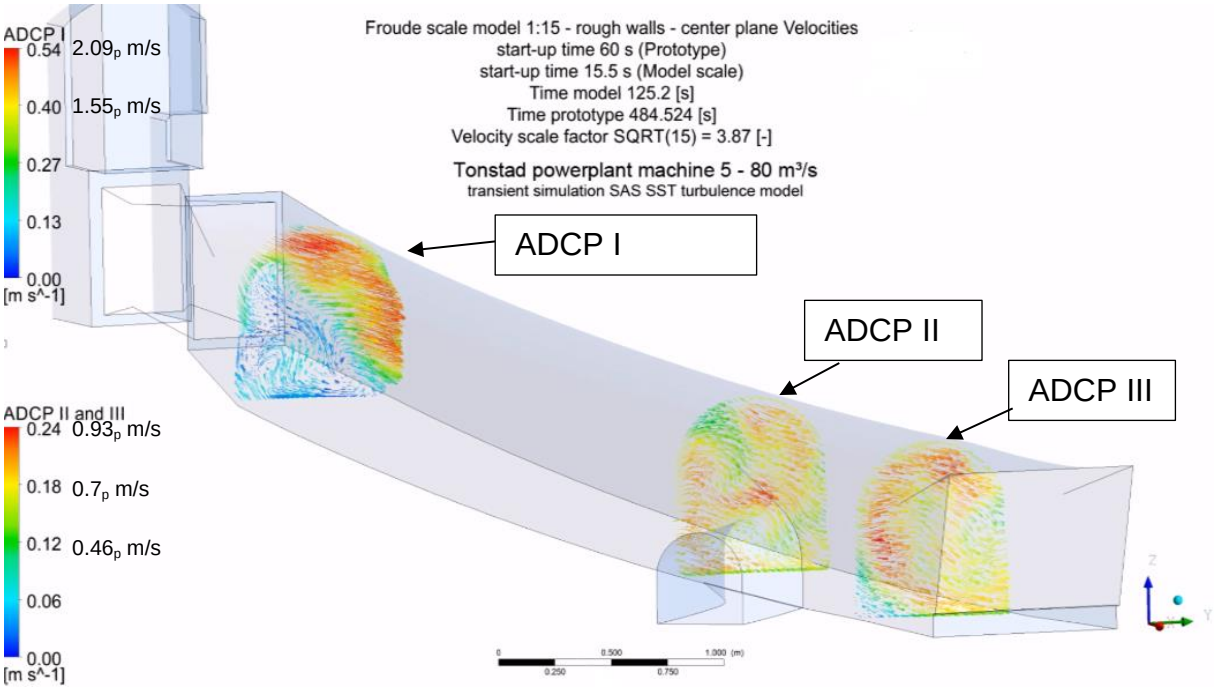

Figure 31: Results from transient RANS model with SAS SST simulation, linear machine start-up and then steady machine operation at 80_p m³/s or 97.5_m l/s, rock roughness K_{ST}=34 $m^{1/3}/s$, timeframe at $484.524s_p$ after start-up of the unit, velocities in prototype (p) and model scale – proving the measurements

Figure 32 to Figure 40 show the velocity evolution in the centre plane when the turbines are linear loaded to a resulting discharge of 80m³/s. A jet coming from the gate is formed and enters the sand trap to a distance of about 40 m to 50 m. This Jet is highly transient and

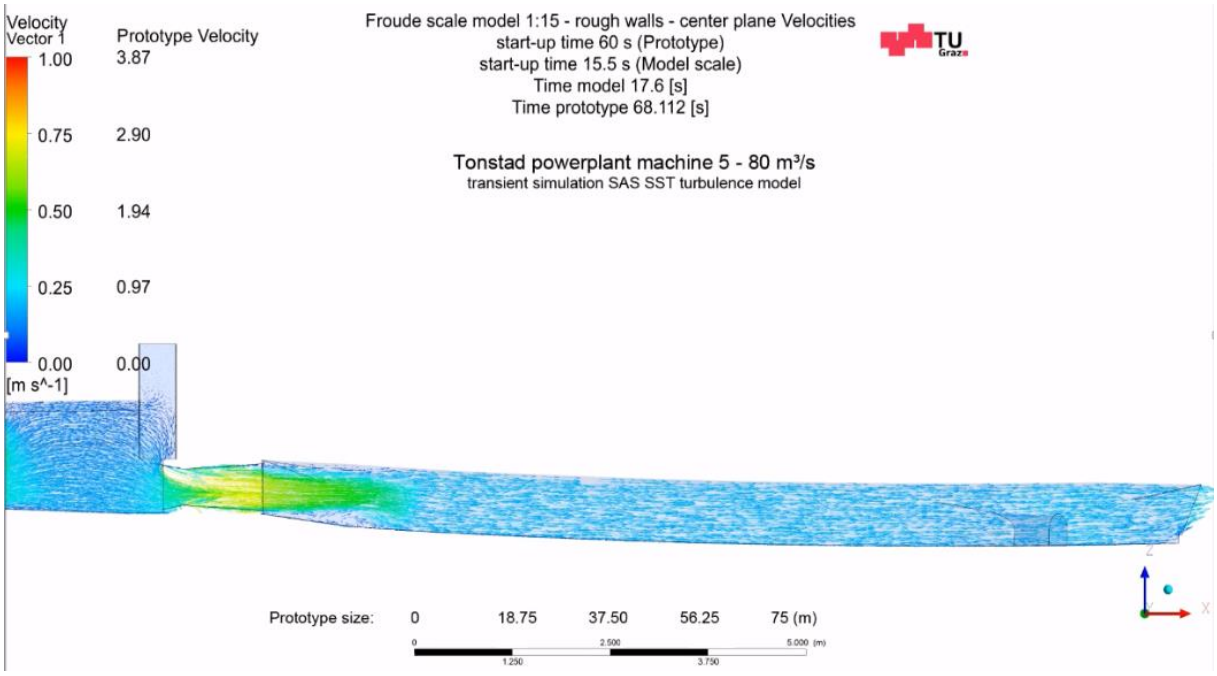

Figure 32: Results from transient RANS model with SAS SST simulation, linear machine start-up and then steady machine operation at 80_p m³/s or 97.5_m l/s, rock roughness K_{ST}=34 $m^{1/3}$/s, timeframe at $68.11s_p$ after start-up of the unit, velocities in prototype (p) and model scale

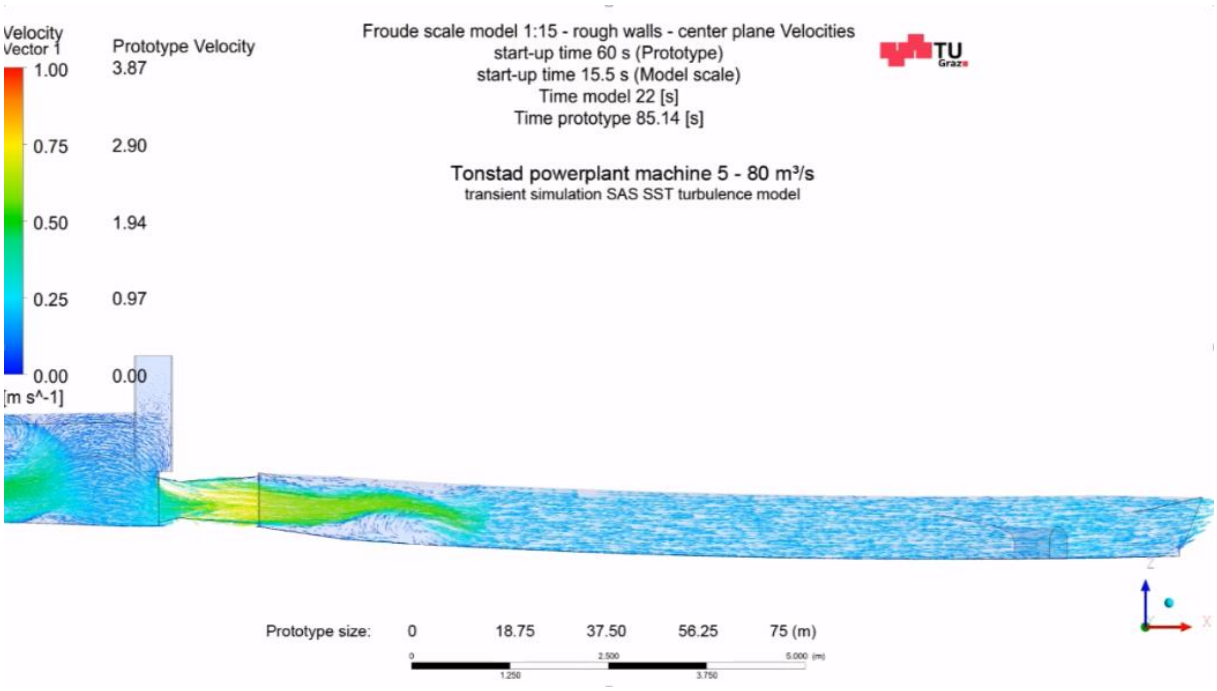

Figure 33: Results from transient RANS model with SAS SST simulation, linear machine start-up and then steady machine operation at 80_p m³/s or 97.5_m l/s, rock roughness K_{ST}=34 $m^{1/3}$/s, timeframe at $85s_p$ after start-up of the unit, velocities in prototype (p) and model scale

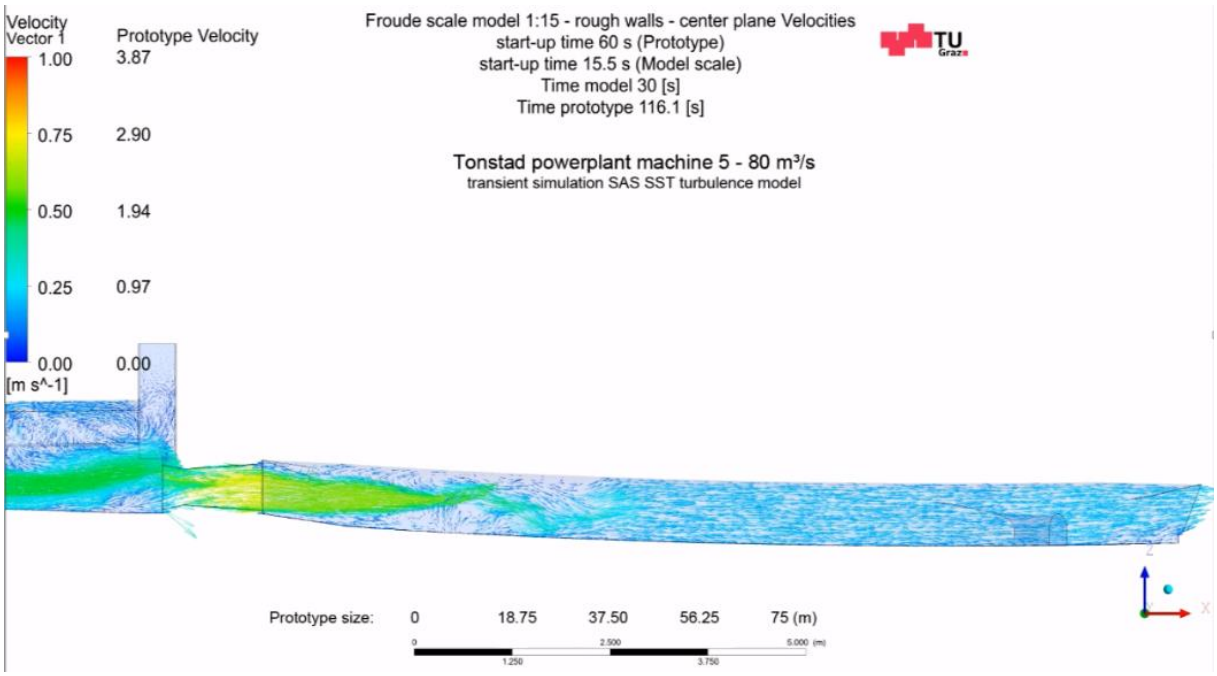

Figure 34: Results from transient RANS model with SAS SST simulation, linear machine start-up and then steady machine operation at 80_p m³/s or 97.5_m l/s, rock roughness K_{ST}=34 $m^{1/3}/s$, timeframe at $116.1s_p$ after start-up of the unit, velocities in prototype (p) and model scale

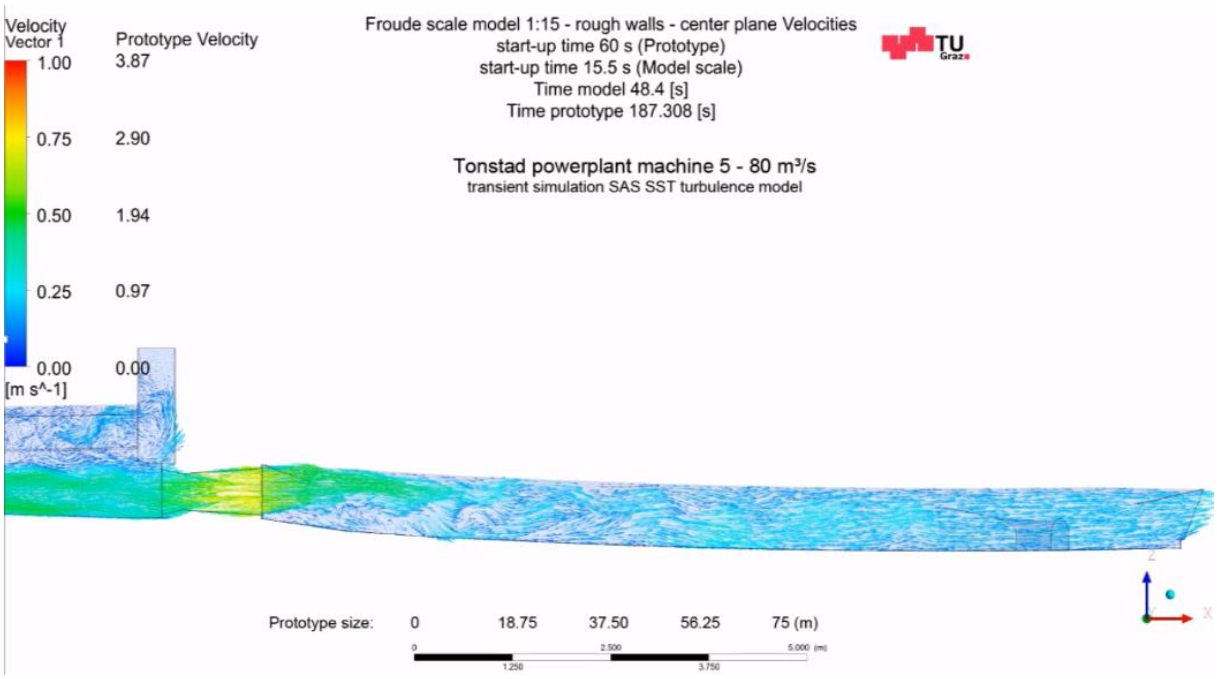

Figure 35: Results from transient RANS model with SAS SST simulation, linear machine start-up and then steady machine operation at 80_p m³/s or 97.5_m l/s, rock roughness K_{ST}=34 $m^{1/3}/s$, timeframe at $187.3s_p$ after start-up of the unit, velocities in prototype (p) and model scale

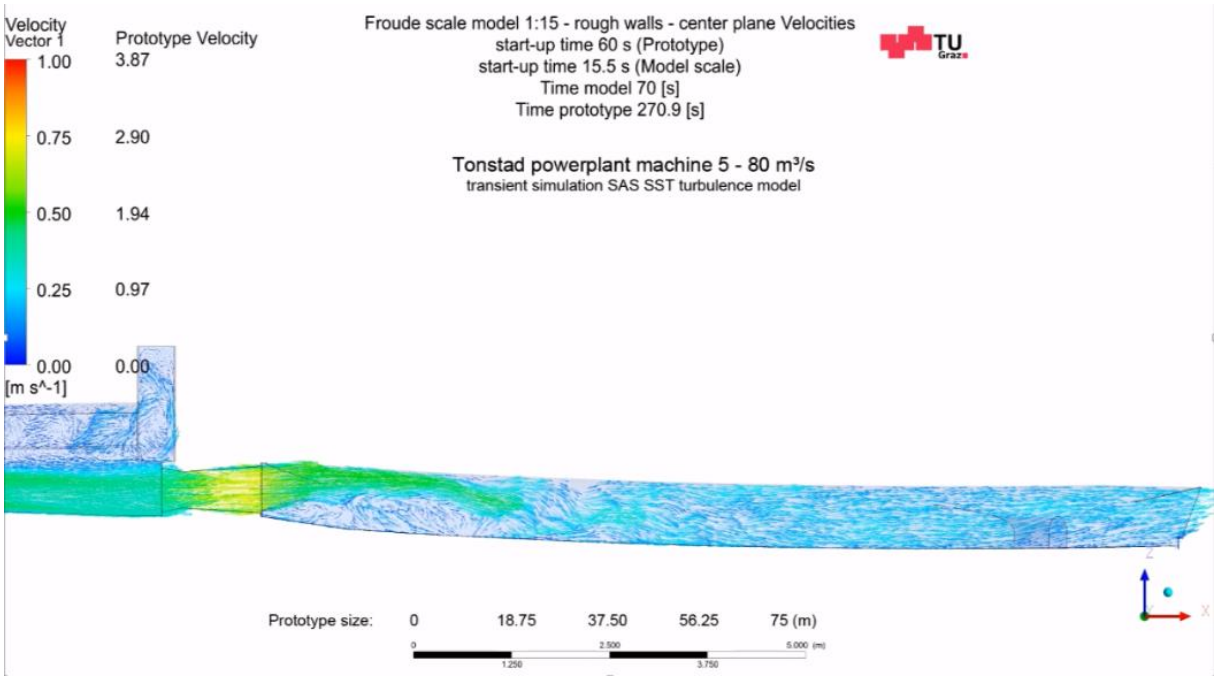

Figure 36: Results from transient RANS model with SAS SST simulation, linear machine start-up and then steady machine operation at 80_p m³/s or 97.5_m l/s, rock roughness K_{ST}=34 $m^{1/3}$/s, timeframe at $270.9s_p$ after start-up of the unit, velocities in prototype (p) and model scale

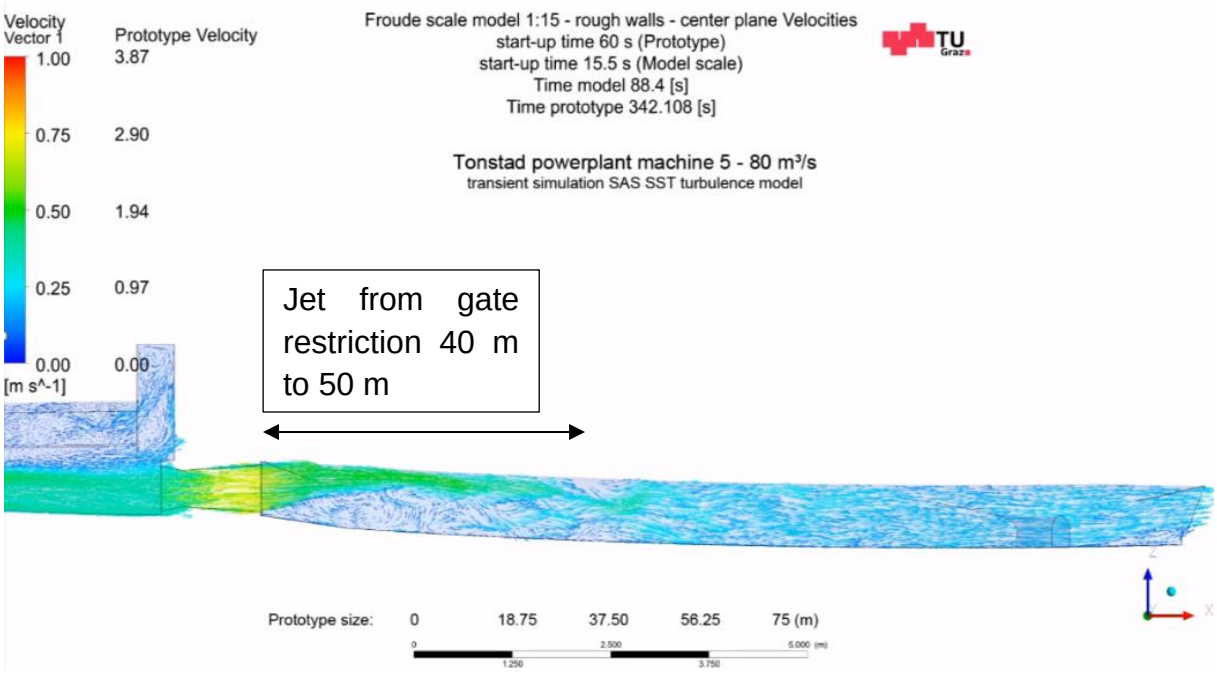

Figure 37: Results from transient RANS model with SAS SST simulation, linear machine start-up and then steady machine operation at 80_p m³/s or 97.5_m l/s, rock roughness K_{ST}=34 $m^{1/3}$/s, timeframe at $342.1s_p$ after start-up of the unit, velocities in prototype (p) and model scale

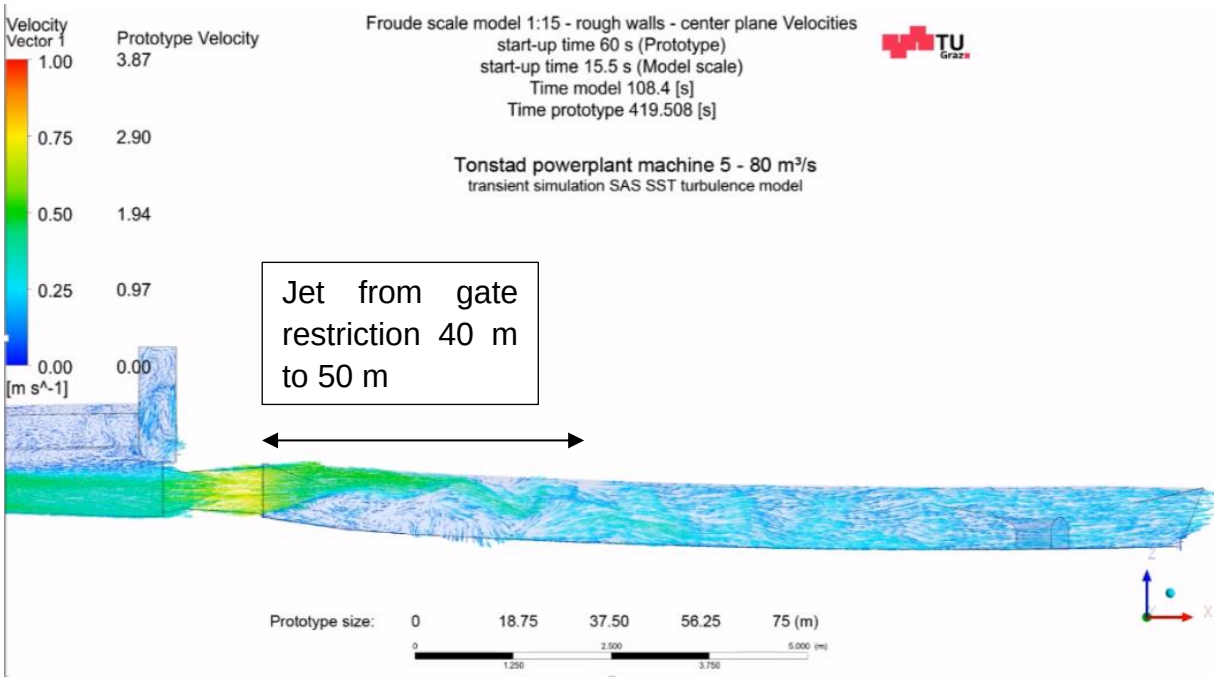

Figure 38: Results from transient RANS model with SAS SST simulation, linear machine start-up and then steady machine operation at 80_p m³/s or 97.5_m l/s, rock roughness K_{ST}=34 $m^{1/3}$/s, timeframe at $419.5s_p$ after start-up of the unit, velocities in prototype (p) and model scale

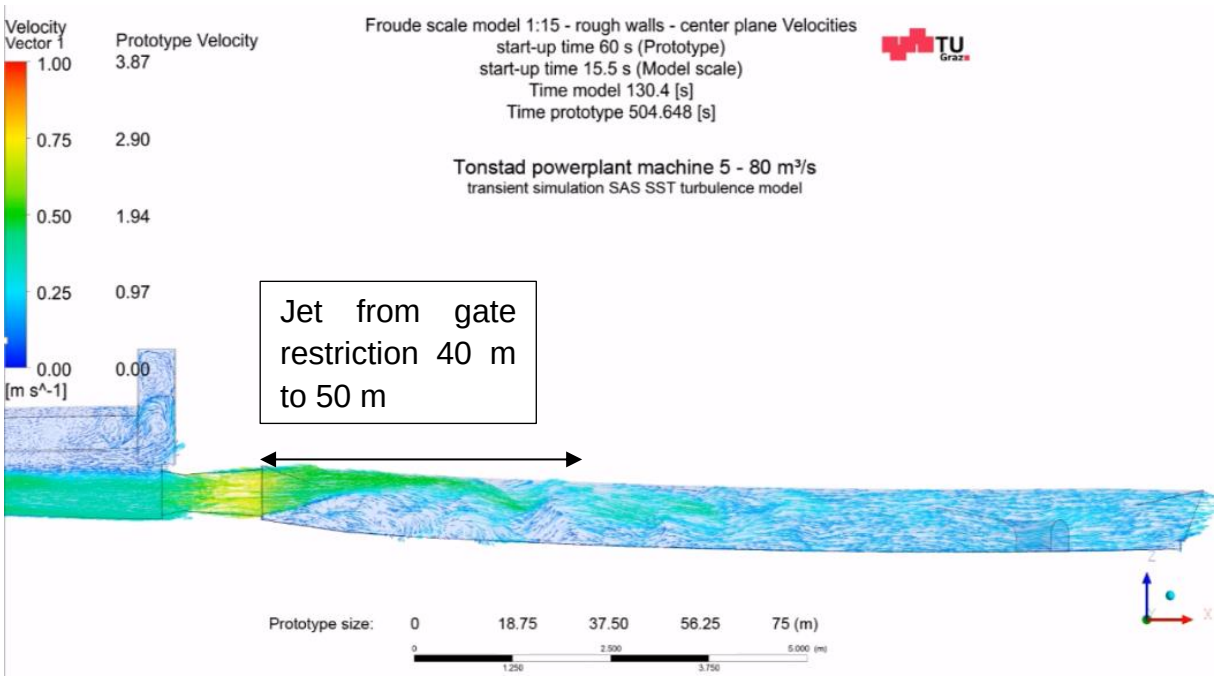

Figure 39: Results from transient RANS model with SAS SST simulation, linear machine start-up and then steady machine operation at 80_p m³/s or 97.5_m l/s, rock roughness K_{ST}=34 $m^{1/3}$/s, timeframe at $504.6s_p$ after start-up of the unit, velocities in prototype (p) and model scale

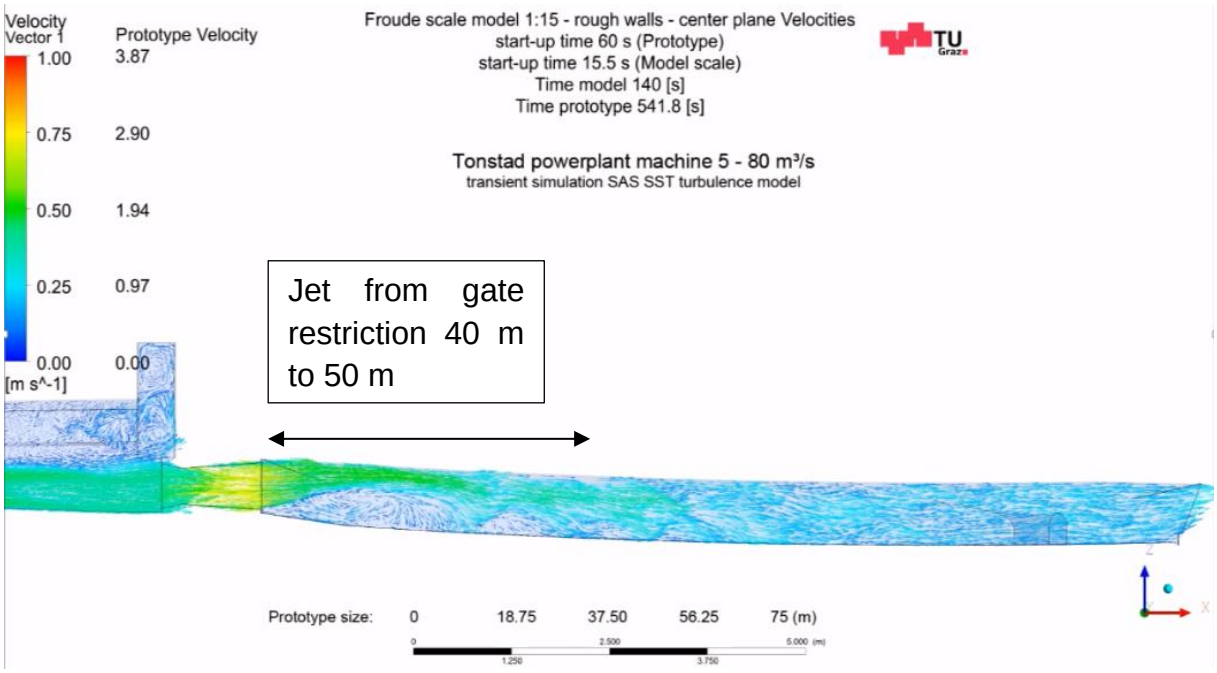

Figure 40: Results from transient RANS model with SAS SST simulation, linear machine start-up and then steady machine operation at 80_p m³/s or 97.5_m l/s, rock roughness K_{ST}=34 $m^{1/3}$/s, timeframe at $541.8s_p$ after start-up of the unit, velocities in prototype (p) and model scale

Figure 41 and Figure 42 show a result from the transient simulation in prototype scale, plotting the wall shear stress. Until about half of the sand trap a wall shear stress of about 4 N/m² is generated. This results in a possible moving of fine gravel of 4-8 mm diameter just due to steady state operation.

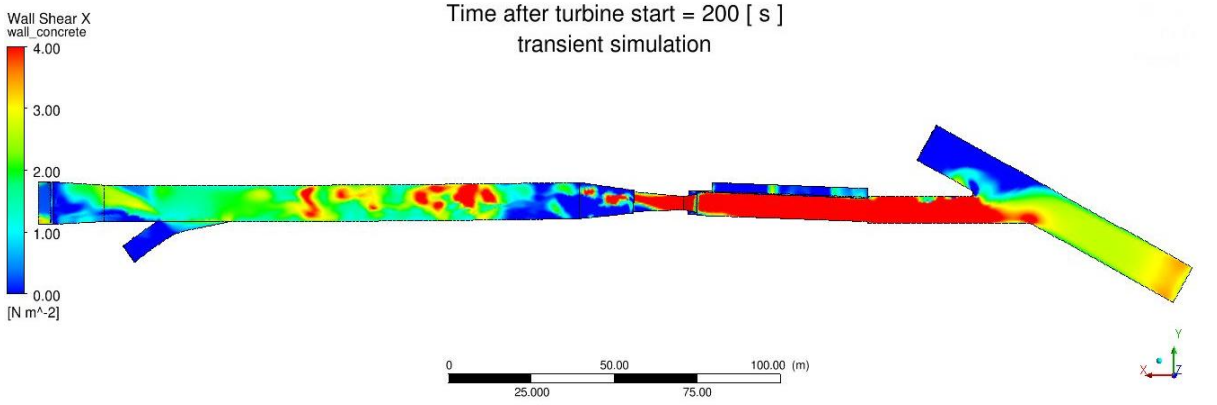

Figure 41: Results from transient RANS model with SAS SST simulation, linear machine start-up and then steady machine operation at 80_p m³/s or 97.5_m l/s, rock roughness K_{ST}=34 $m^{1/3}$/s, timeframe at $200s_p$ after start-up of the unit, Wall shear stress, prototype size simulation

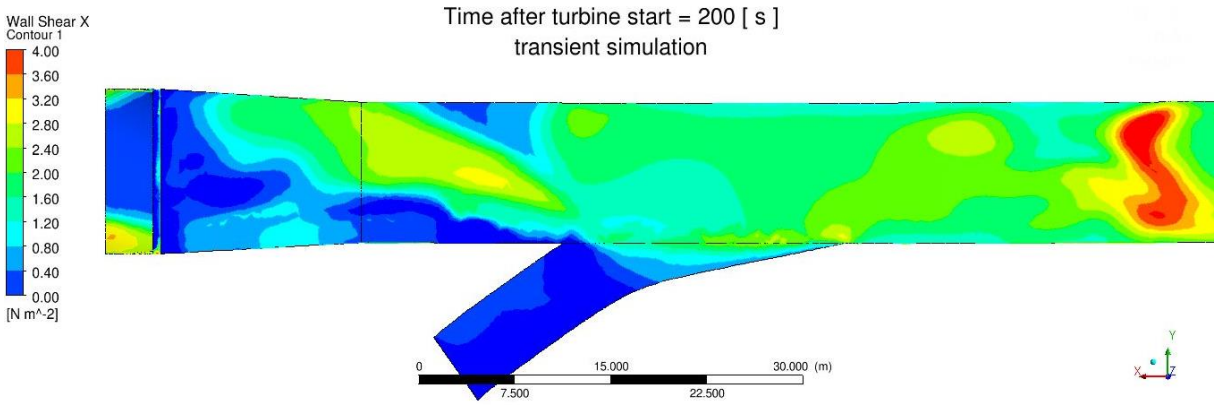

Figure 42: Results from transient RANS model with SAS SST simulation, linear machine start-up and then steady machine operation at 80_p m³/s or 97.5_m l/s, rock roughness K_{ST}=34 $m^{1/3}$/s, timeframe at $200s_p$ after start-up of the unit, Wall shear stress, detail Prototype size simulation

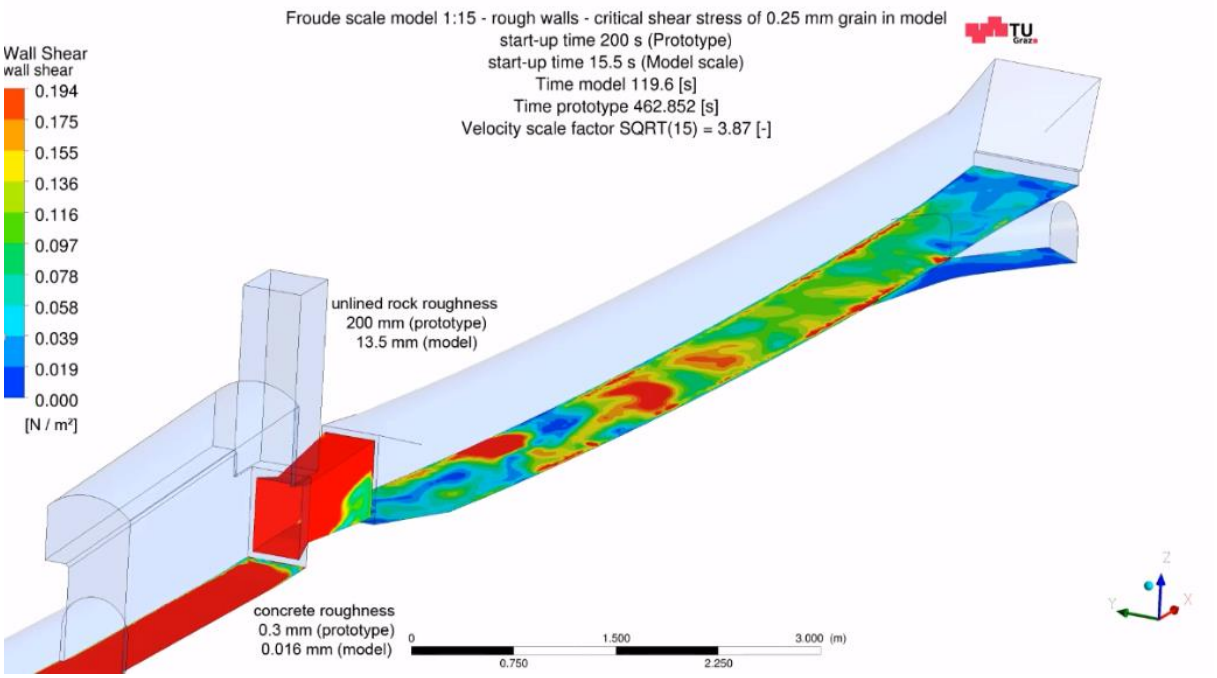

Figure 43: Results from transient RANS model with SAS SST simulation, linear machine start-up and then steady machine operation at 80_p m³/s or 97.5_m l/s, rock roughness K_{ST}=34 $m^{1/3}$/s, timeframe at $452s_p$ after start-up of the unit, wall shear stress at the bottom

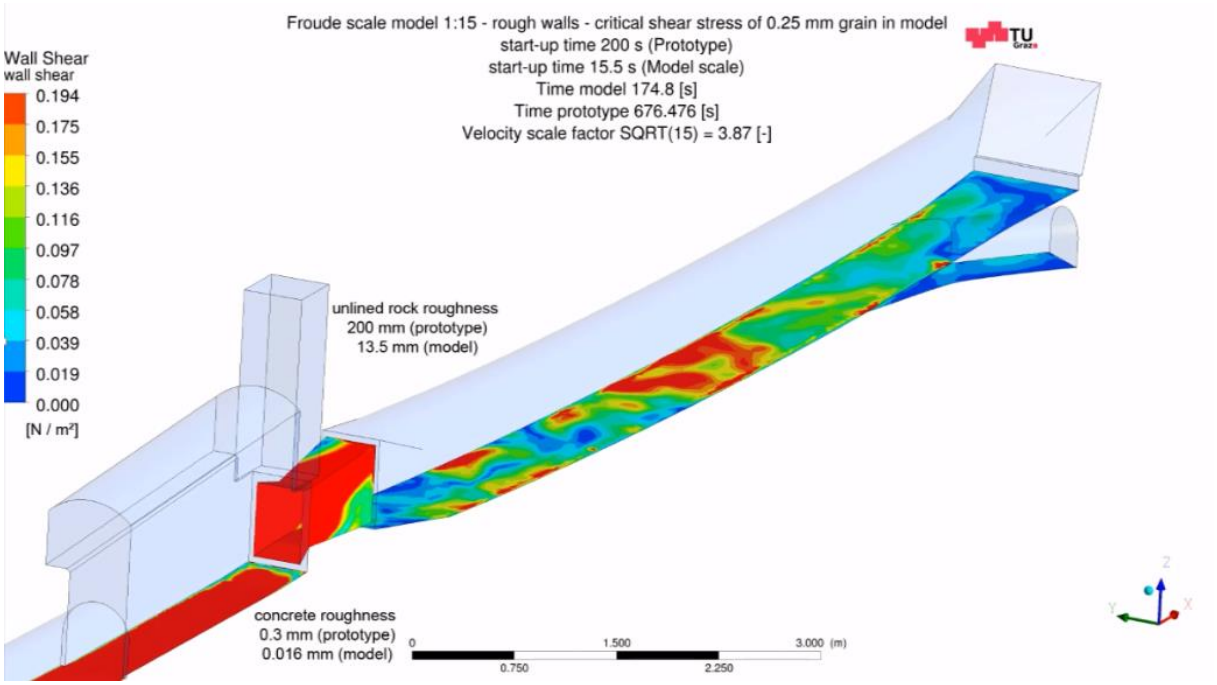

Figure 44: Results from transient RANS model with SAS SST simulation, linear machine start-up and then steady machine operation at 80_p m³/s or 97.5_m l/s, rock roughness K_{ST}=34 $m^{1/3}$/s, timeframe at $676s_p$ after start-up of the unit, wall shear stress at the bottom

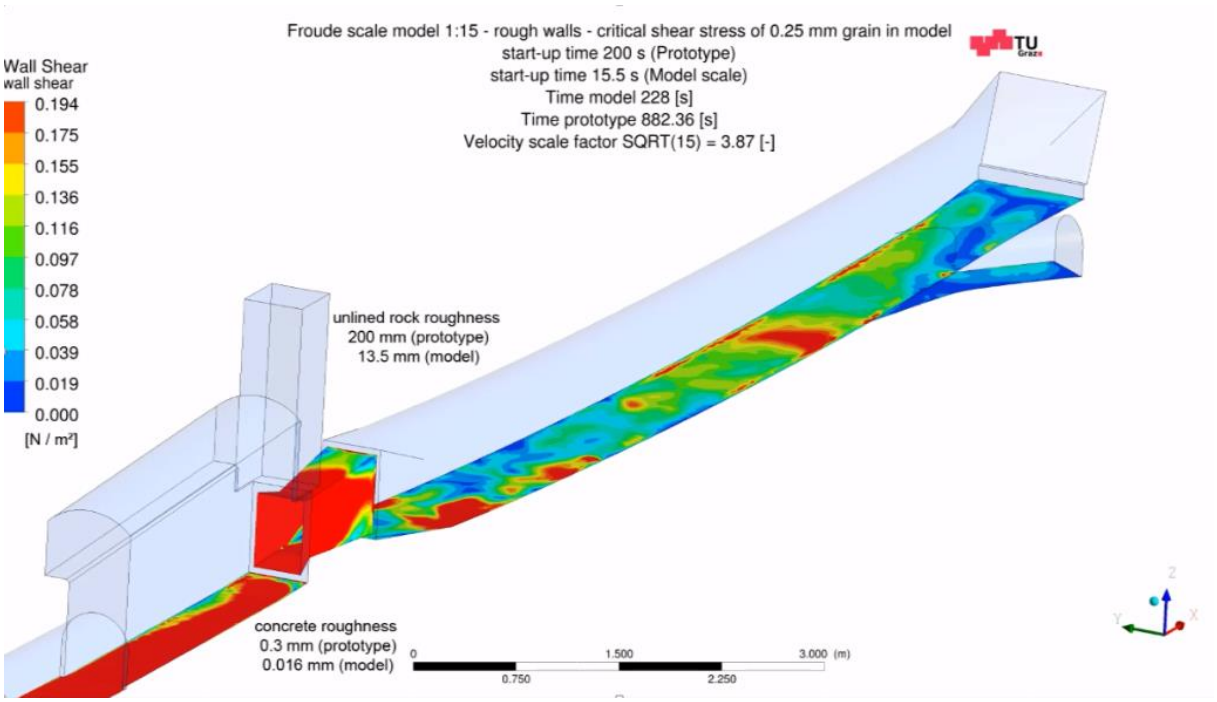

Figure 45: Results from transient RANS model with SAS SST simulation, linear machine start-up and then steady machine operation at 80_p m³/s or 97.5_m l/s, rock roughness K_{ST}=34 $m^{1/3}$/s, timeframe at $882s_p$ after start-up of the unit, wall shear stress at the bottom

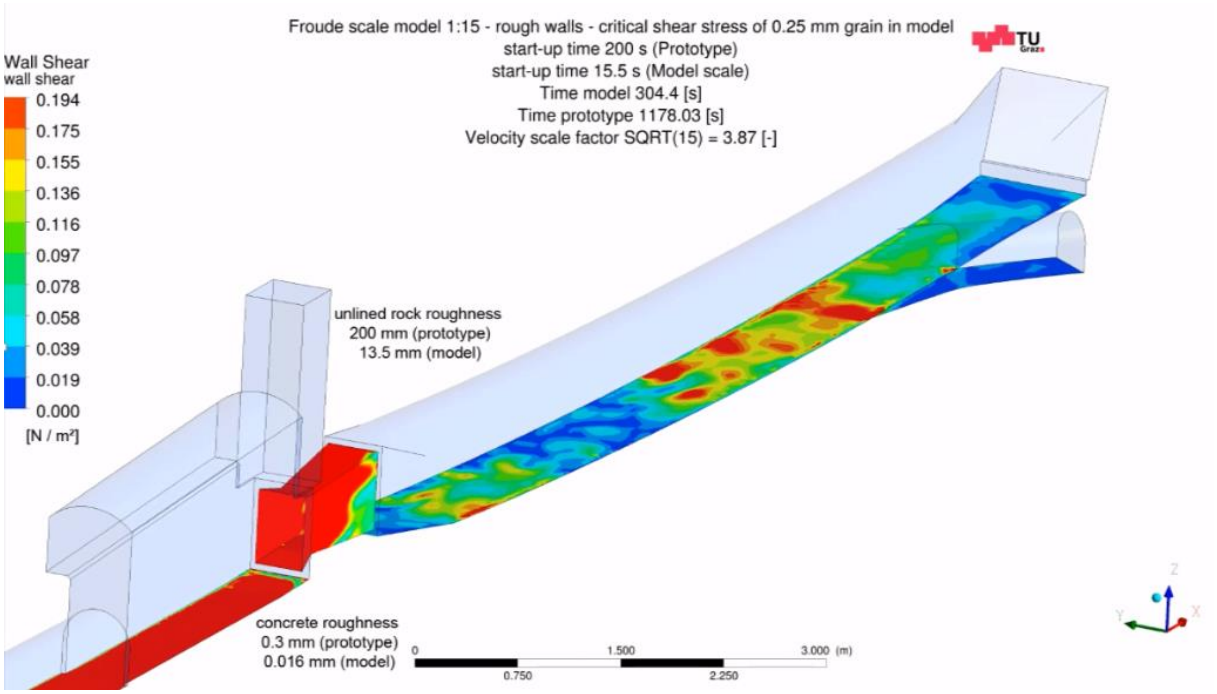

Figure 46: Results from transient RANS model with SAS SST simulation, linear machine start-up and then steady machine operation at 80_p m³/s or 97.5_m l/s, rock roughness K_{ST}=34 $m^{1/3}/s$, timeframe at $1178s_p$ after start-up of the unit, wall shear stress at the bottom

Figure 47 shows the evolution of sand grains in the sand trap after turbine start-up and steady state operation. The time frame is 200 s in prototype. It is visible that 2mm sand grains are able to settle in the sand trap. But it is also visible that the sand grains are transported at the bottom of the sand trap.

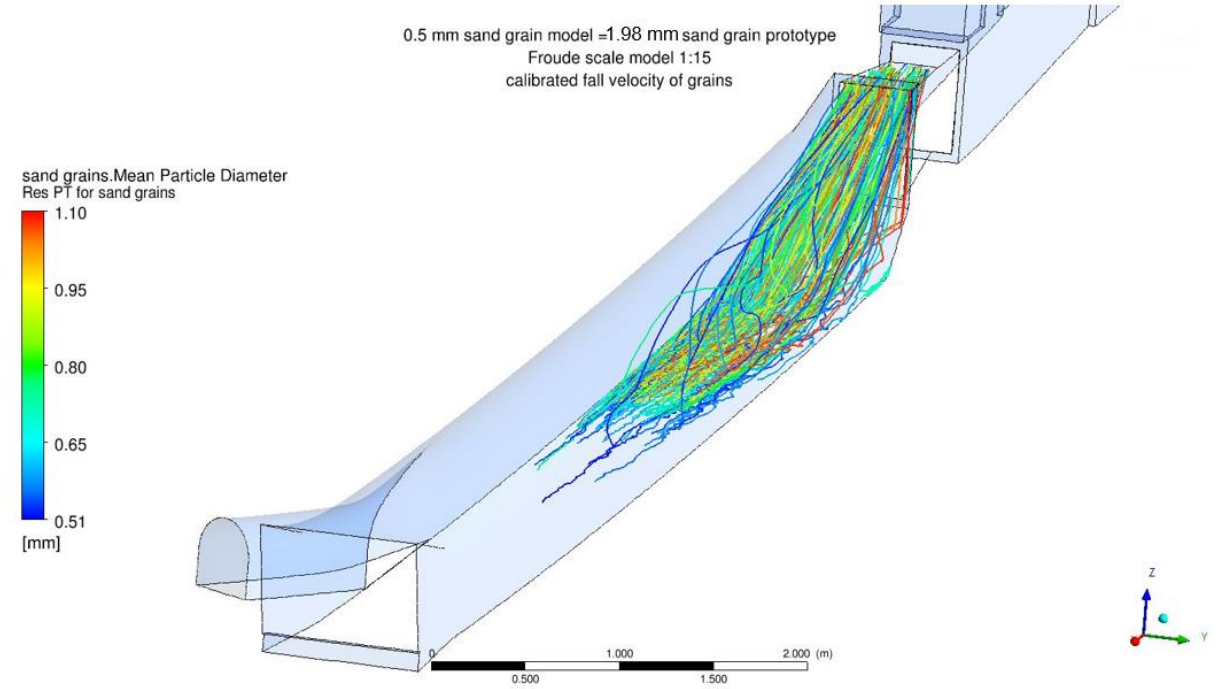

Figure 47: Results from transient RANS model with SAS SST simulation, linear machine start-up and then steady machine operation at 80_p m³/s or 97.5_m l/s, rock roughness K_{ST}=34 $m^{1/3}/s$, min diameter 0.51_m mm respectively 1.98_p mm, isometric view

Figure 48 shows the same simulation as Figure 47. It is visible that 1.1_m mm grains (10_p mm) are settled very quickly to the bottom, but also moved on the ground.

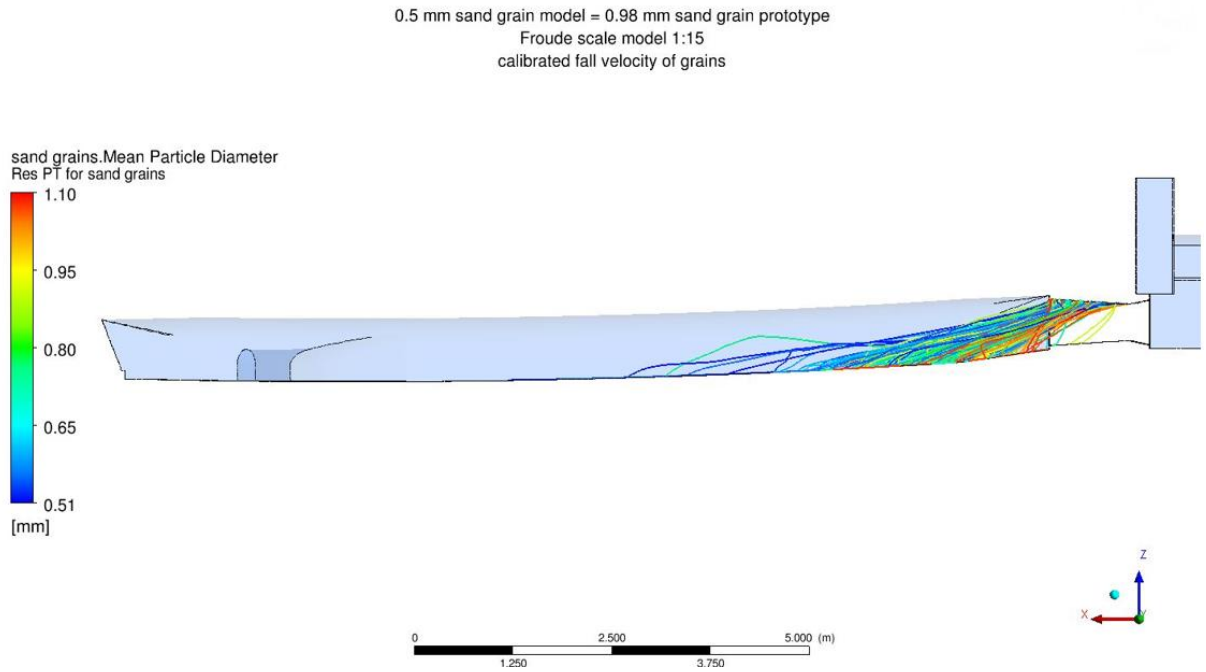

Figure 48: Results from transient RANS model with SAS SST simulation, linear machine start-up and then steady machine operation at 80_p m³/s or 97.5_m l/s, rock roughness K_{ST}=34 $m^{1/3}$/s, min diameter 0.51_m mm respectively 1.98_p mm, side view

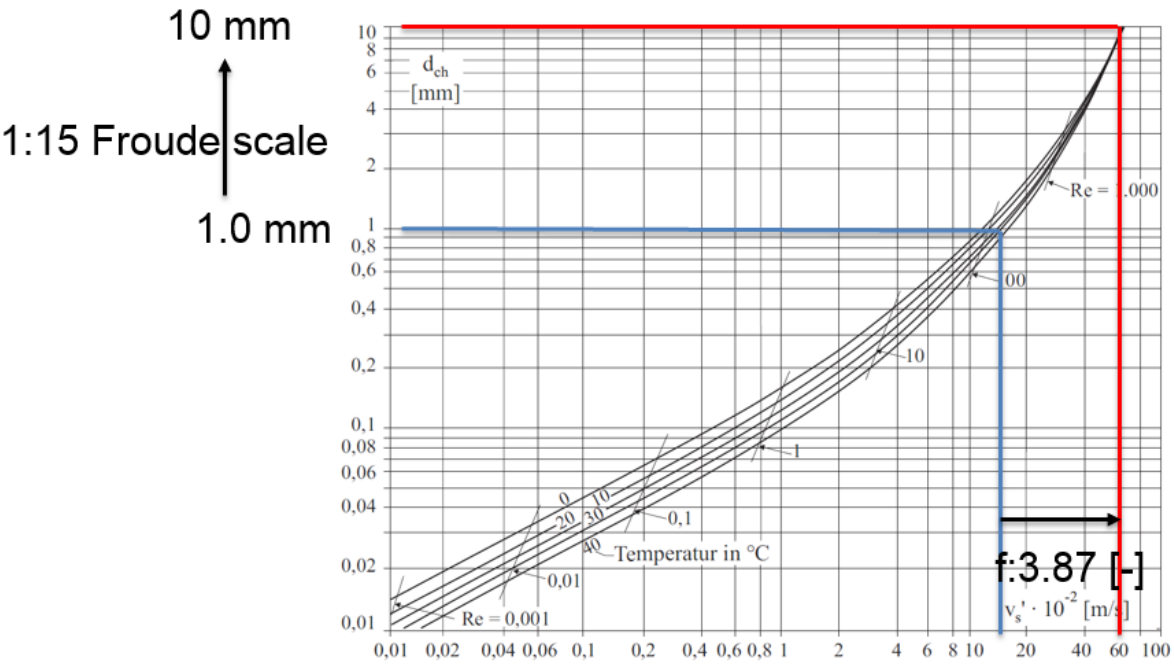

Figure 49: Scaling of sediments via fall velocity – for Froude flow approach.

Figure 50 shows the same simulation as above but with different particle details. Calculations show that particles from 0.8_p mm to 0.9_p mm are possible to be transported by steady state flow through the desander without settling. The approximate limit for totally water filled sand trap with steady state flow of 80m³/s was found to be about 1.2_p mm.

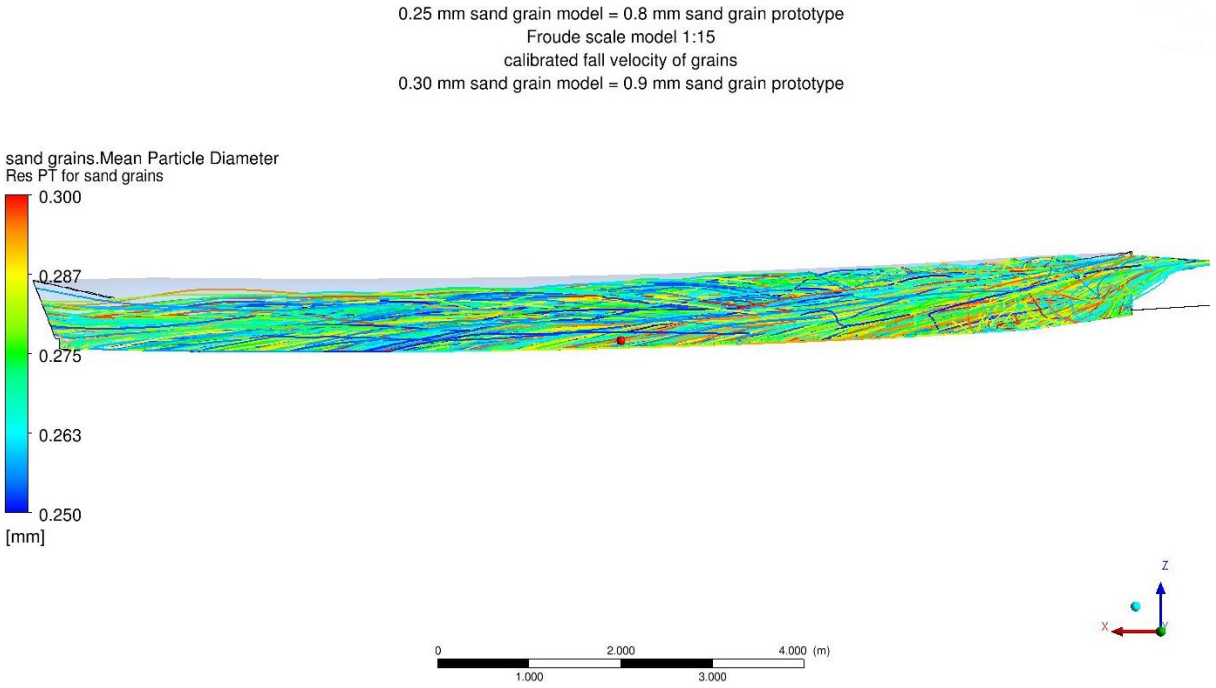

Figure 50: Results from transient RANS model with SAS SST simulation, linear machine start-up and then steady machine operation at 80_p m³/s or 97.5_m l/s, rock roughness K_{ST}=34 $m^{1/3}$/s, min diameter 0.8_p mm to 0.9_p mm

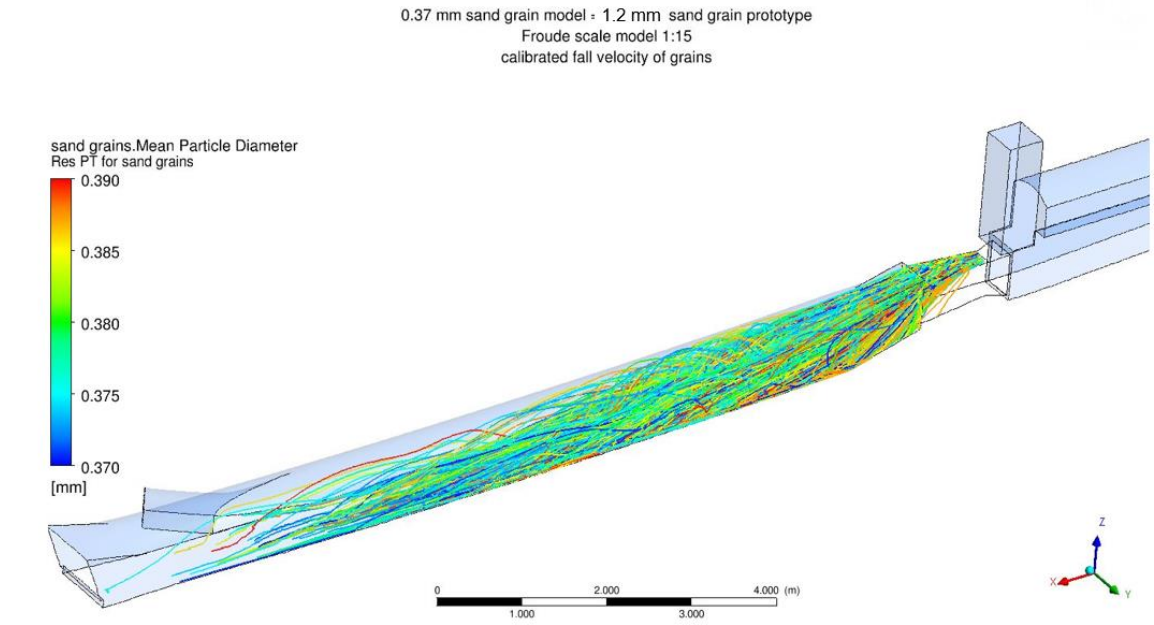

Figure 51: Results from transient RANS model with SAS SST simulation, linear machine start-up and then steady machine operation at 80_p m³/s or 97.5_m l/s, rock roughness K_{ST}=34 $m^{1/3}$/s, min diameter 1.2_p mm to 1.25_p mm

Following conclusions are drawn from 3D CFD simulations of the original sand trap no 3 simulations:

- Limit grain size of about 1.2_p mm of existing sand trap for full turbine operation and if fully filled with water.
- Compared with conservative sand trap limit grain sizes of 0.2 mm to 0.3 mm it is very high. But to achieve such settling efficiency the sand trap would need to be 3 times as long. This should not be necessary since information's from operation show that the machines are withstanding sand grains with such diameters. Problems occurred with larger grains from specific incidents.
- Significant transient flow is generated inside the sand trap – this is established by both a dominating jet coming from the gate opening and the rough unlined rock walls.
- The jet reaches about 40 m – 50 m inside the sand trap and shortens this way the sand trap efficiency.
- Up to fine gravels of 10 mm are moved on the bottom of the sand trap near to the rake due to transient shear stresses up to about 4 N/mm² in filled sand trap a steady operation of 80 m³/s

For the simulations the sand grains are added unfavourably from the crown of the gate section. The simulations are done with 10° C Water, so if the water is colder settling is even less effective due to the viscosity of water.

Following considerations are made resulting from the simulations above for further steps:

- A flow calming device in the diffusor may mitigate the oscillation and significant jet influence in order to improve the settling behaviour.
- Obstacles on the ground may block the moving of grains on the floor.
- Automated sediment removing may help

Following considerations are seen as boundary conditions and restrictions for sand trap improvement:

- Measures need to be installed very quickly
- Measures should be multipurpose and automated grain removing is needed
- Filling of the sand trap should be much safer without moving large particles to the gates
- Measures should be able to be installed when the other machines no 1 to no 4 are in operation.

4.2 Variant 1 – sand trap modification

Variant 1 to improve the desander shows a geometric adaptation with a smoother diffusor by filling the gap at the bottom at a length of about 44 m. Additionally the bottom for a length of 115 m is excavated by about 2.0 m. the weir in front of the rake is heightened by both excavation and adding of concrete to 5.45 m. This results in a remaining flow height of 8.42m above the weir.

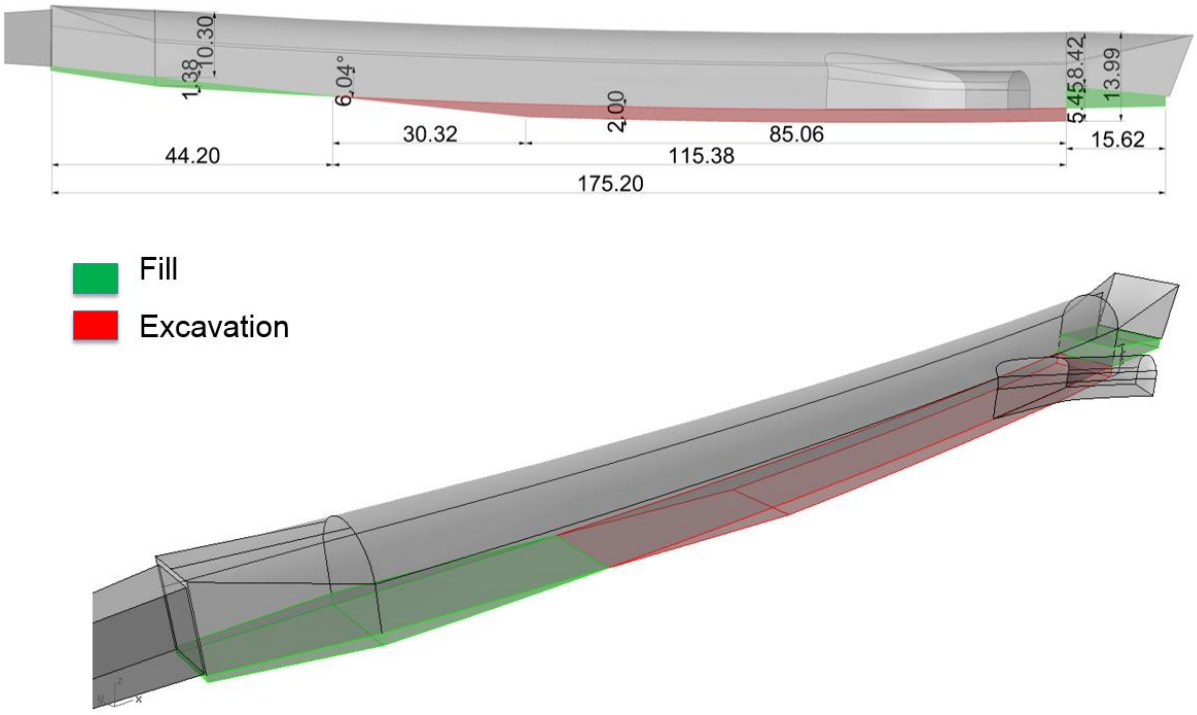

Figure 52: Variant 1 geometrical measures to improve the sand trap

4.3 Variant 2 – sand trap modification

Variant 2 is an addition to variant 1. Additionally, to the excavation at the bottom inclined baffles are placed. In the middle between the baffles a sluicing trench is placed. The baffles should guide the sediments into the trench and should increase the roughness on the bottom to improve settling. The baffles are placed over a length of about 84 m. the height of the baffles is 0.8 m and need a thickness of 1 m. In the middle trench the automated sluicing pipe can be placed.

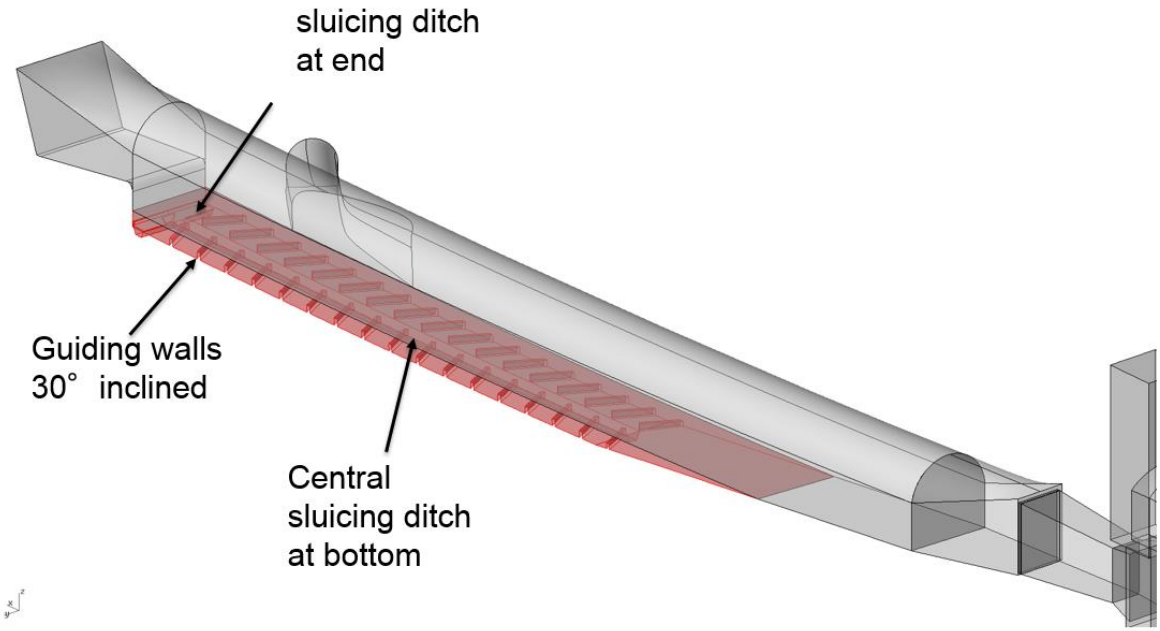

Figure 53: Variant 2 geometrical measures to improve the sand trap with inclined baffles

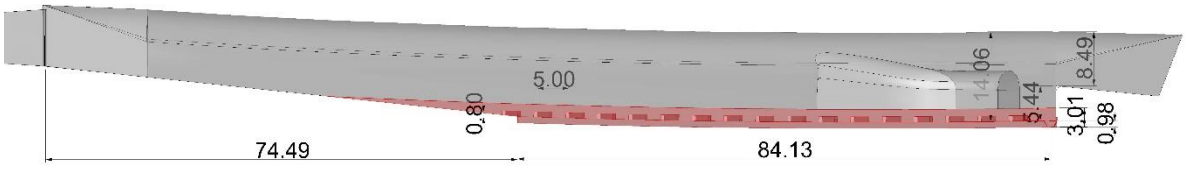

Figure 54: Variant 2 geometrical measures to improve the sand trap with inclined baffles

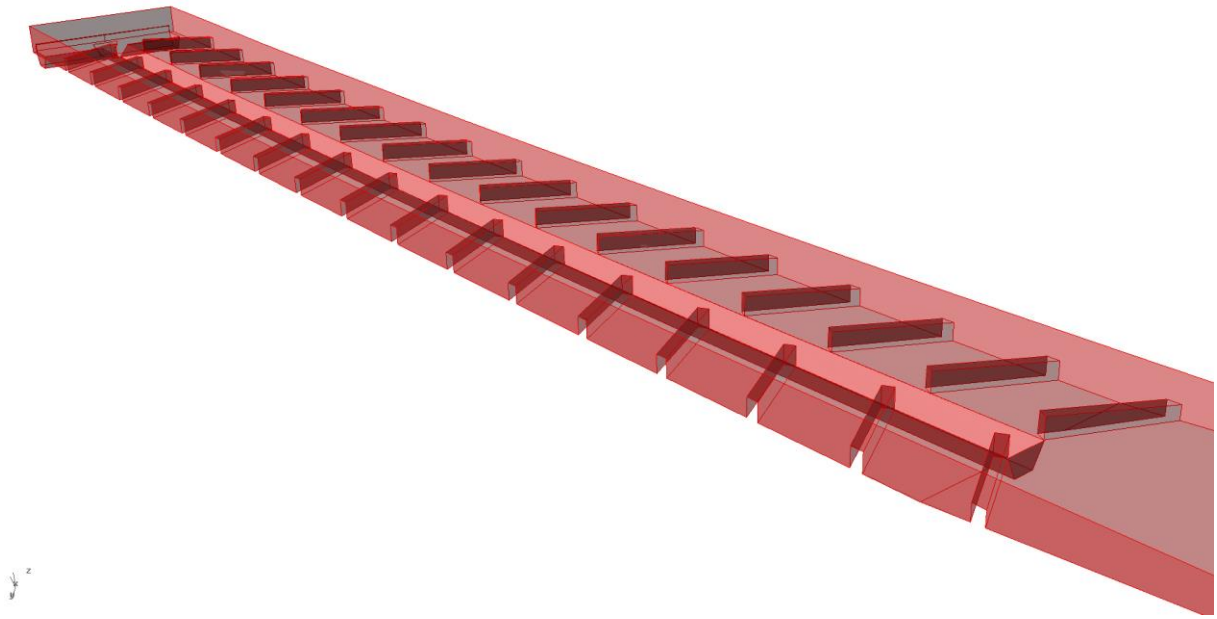

Figure 55: Variant 2, detail of baffles and middle trench

4.4 Variant 3 – sand trap modification

Variant 3 introduces a flow calming device in the diffusor section about 8 m after the concrete section of the gate tunnel. To calm the flow about 52 steel pipes with 1 m diameter are place. The aim is to mitigate the transient turbulent action of the jet. Important also seems that steel pipes rigidly connected and fixed in the sand trap are believed to be installed very quickly. The pipes both guide the flow in order to support the diffusion and calm the turbulent impact of the jet.

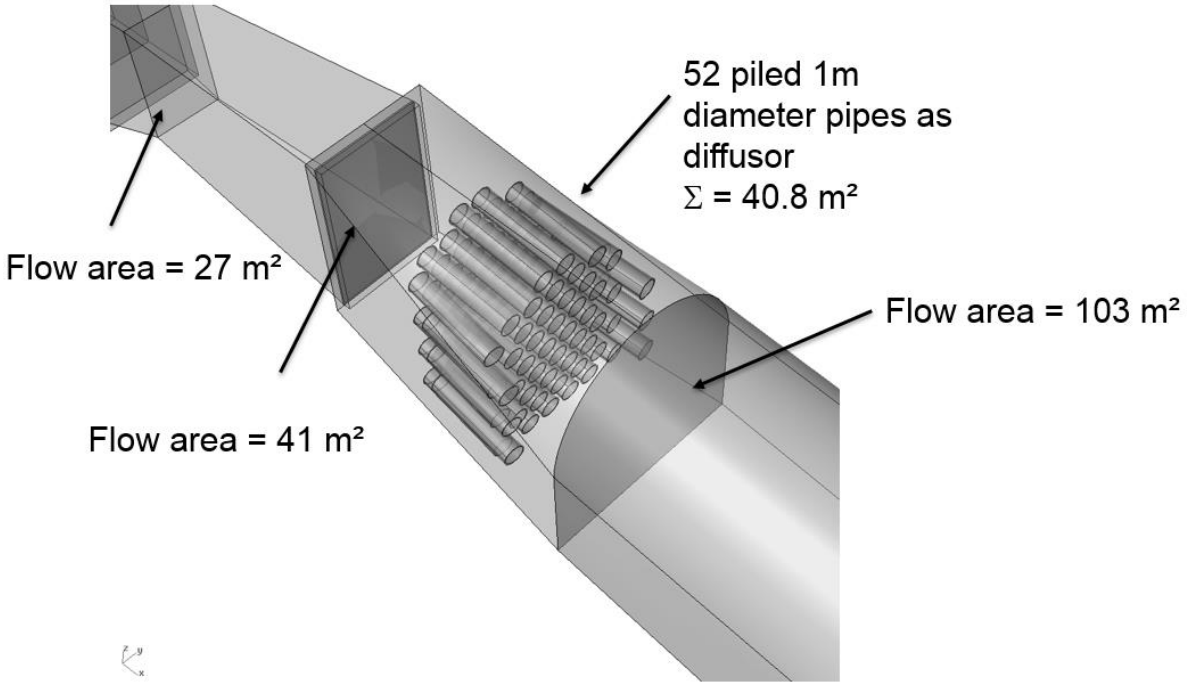

Figure 56: Variant 3 has additionally to variant 1 and 2 flow calming pipes after the gate

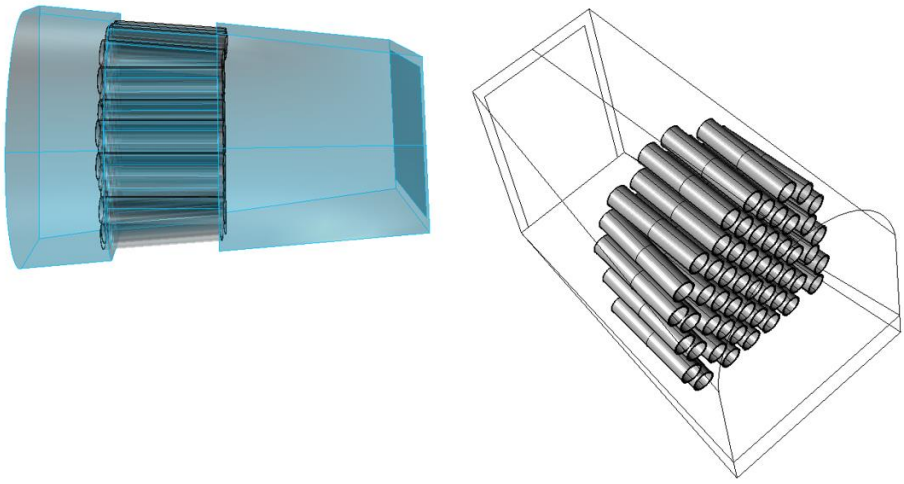

Figure 57: Variant 3 flow calming pipes

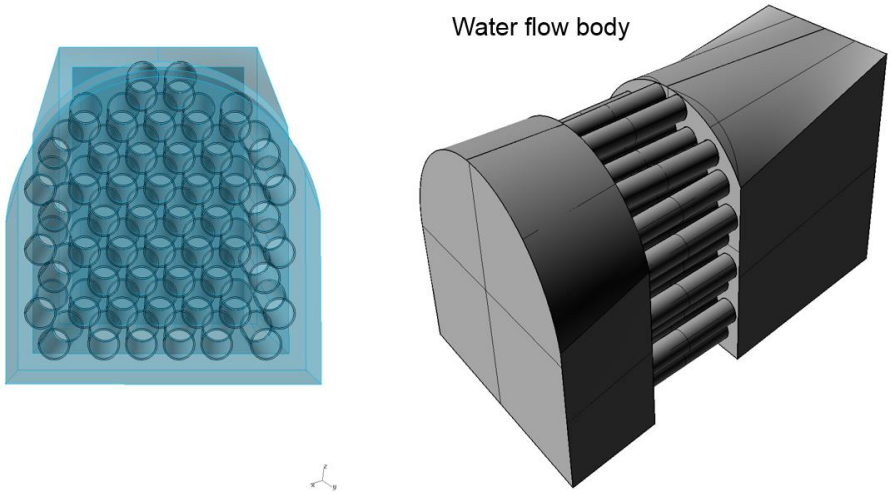

Figure 58: Variant 3 flow calming pipes

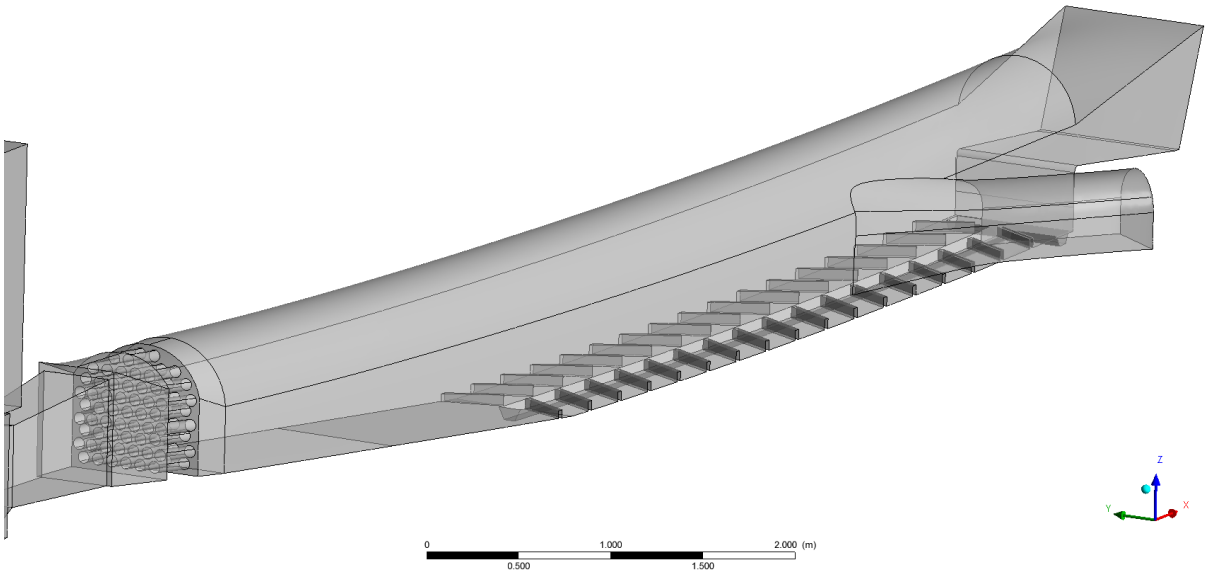

Figure 59: Variant 3 flow calming pipes, deeper bottom and baffles with sluicing trench

4.5 Variant 4 – sand trap modification

Variant 4 is geometric version of variant 3 but without the baffles.

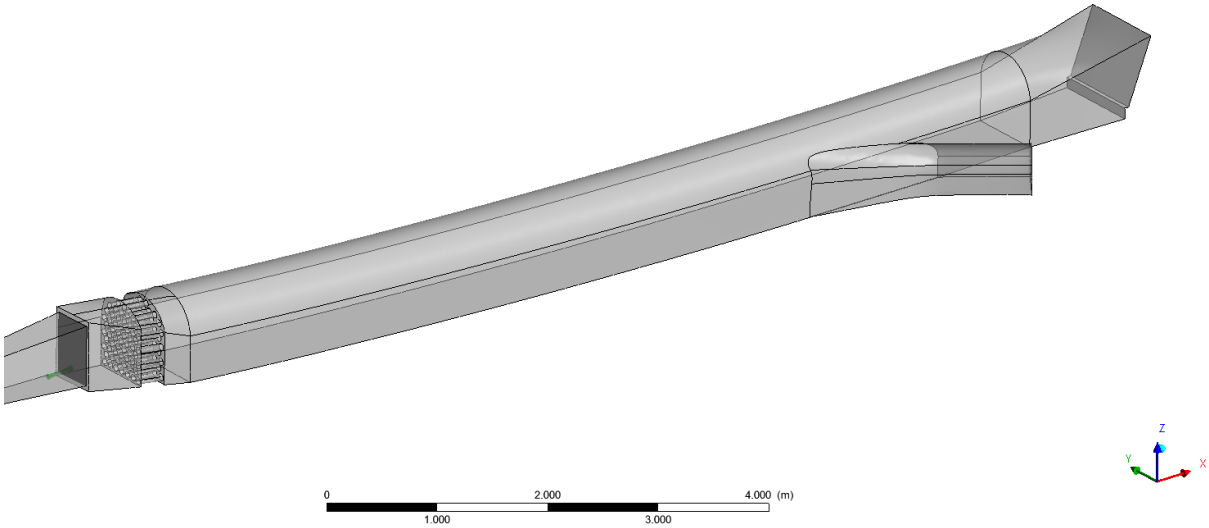

Figure 60: Variant 4 with flow calming pipes and no baffles and trench.

4.6 Variant 5 – sand trap modification

Variant 5 is a combination of variant 4 with the flow calming pipes and an excavation at the bottom of the sand trap. The excavated and concreted trench has a wall inclination of 35° in order to allow sediments to be concentrated in the centre. There a sluicing. Additionally, a horizontal rake can be placed to allow traffic on top of the trench. The depth of the trench for the simulation is about 3.4 m. The automatic sluicing system does not necessarily be placed over the total length as **Figure 63** indicates with a connecting ramp between the pipes and the trench.

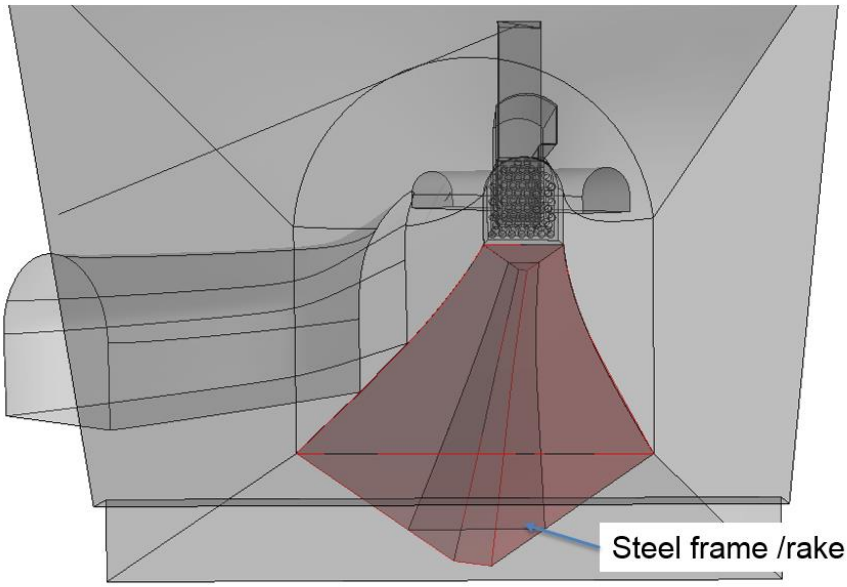

Figure 61: Variant 5 with flow calming pipes and bottom trench for sluicing facility, view from front

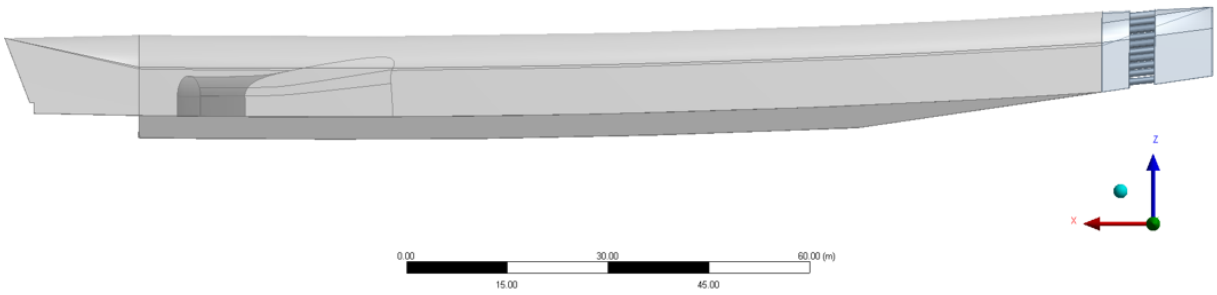

Figure 62: Variant 5 with flow calming pipes and bottom trench for sluicing facility, side view

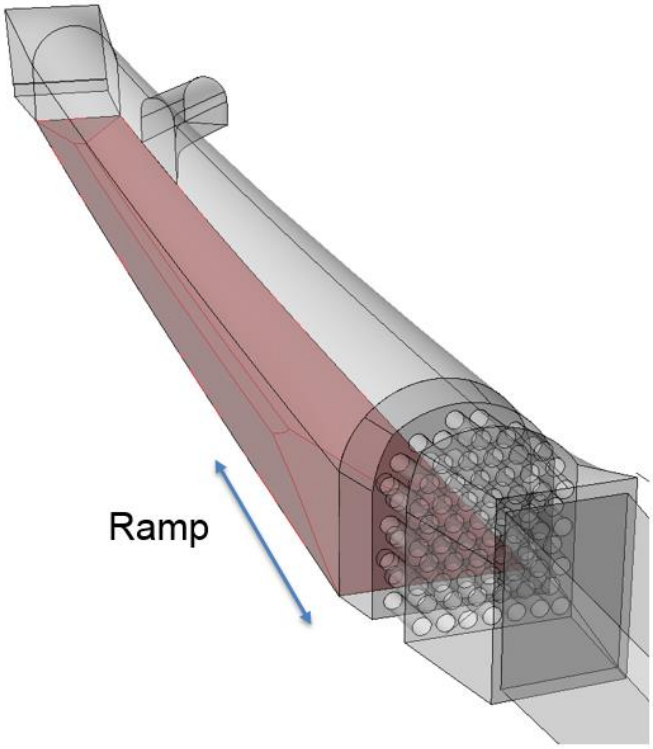

Figure 63: Variant 5 with flow calming pipes and bottom trench for sluicing facility, view of ramp

4.7 Results of Variant analysis

This chapter shows the results from particle simulations of the sand trap variants and discusses the aim of the suggested measures. The simulations are basically elaborated for opening of the turbines in 60$_p$s and then steady operation with 80m³/s. the simulations time was as long as to assure that the water has more than enough time to move through the total sand trap length. This load case is the comparing case between the variants.

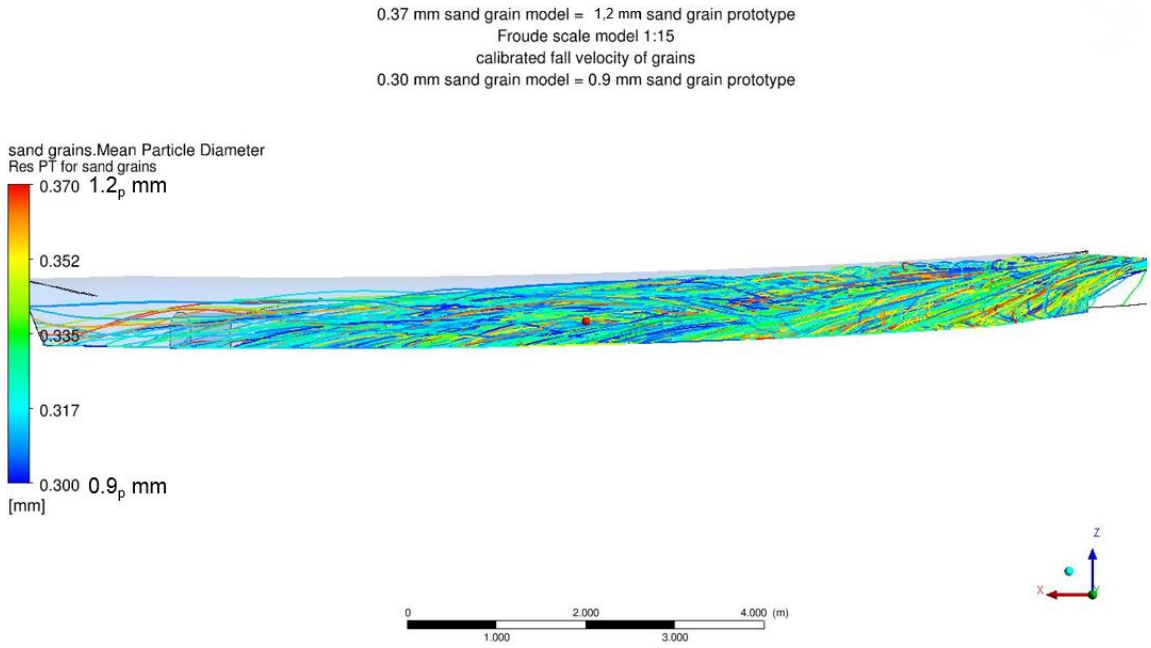

Figure 64: Variant 0 particle simulation in a range of 0.9$_p$ mm (0.3$_m$ mm) to 1.2$_p$ mm (0.37$_m$ mm)

Figure 66 and Figure 65 show the effect of the flow calming pipes.

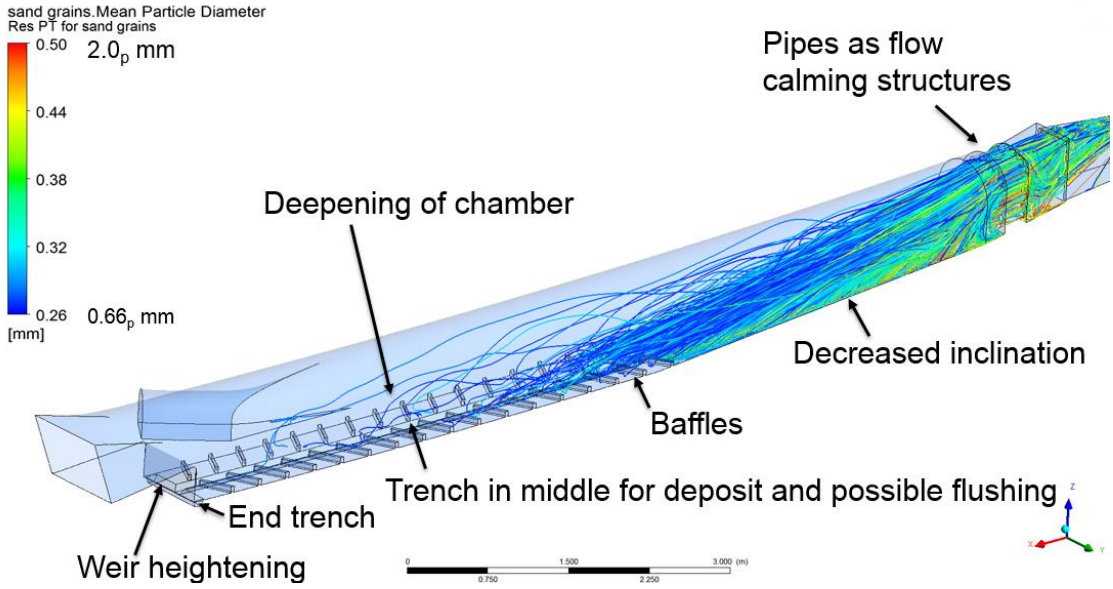

Figure 65: Variant 3 particle simulation in a range of 0.66$_p$ mm (0.26$_m$ mm) to 2.0$_p$ mm (0.5$_m$ mm)

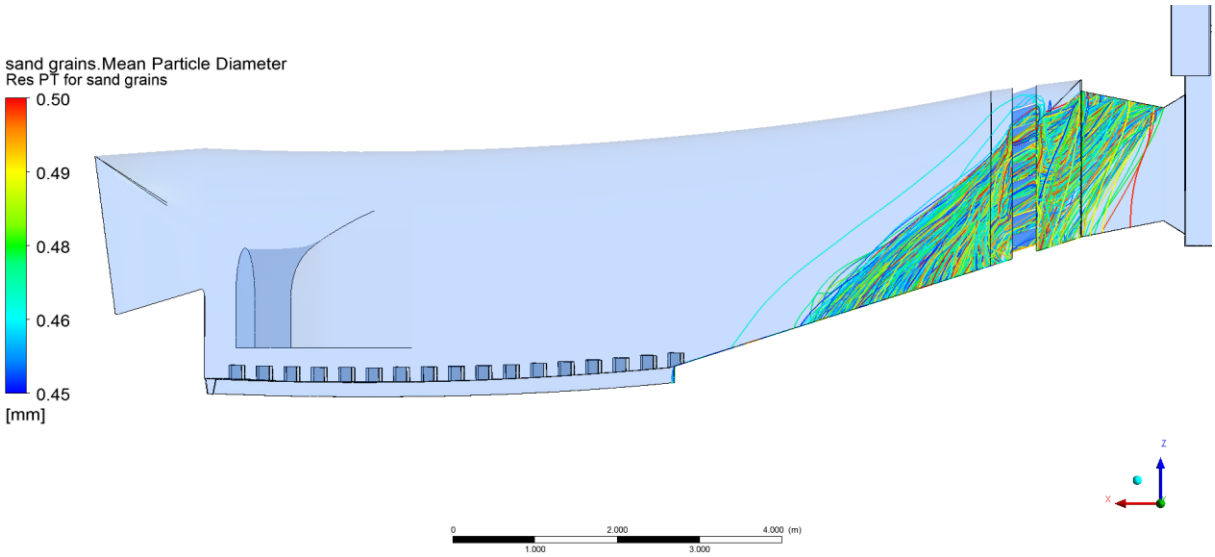

Figure 66: Variant 3 particle simulation

Figure 67 visualizes the effect of the measures of variant 3 to improve the particle settling in the sand trap. Especially the flow calming pipes decrease significantly the impact of the jet onto the flow inside the sand trap.

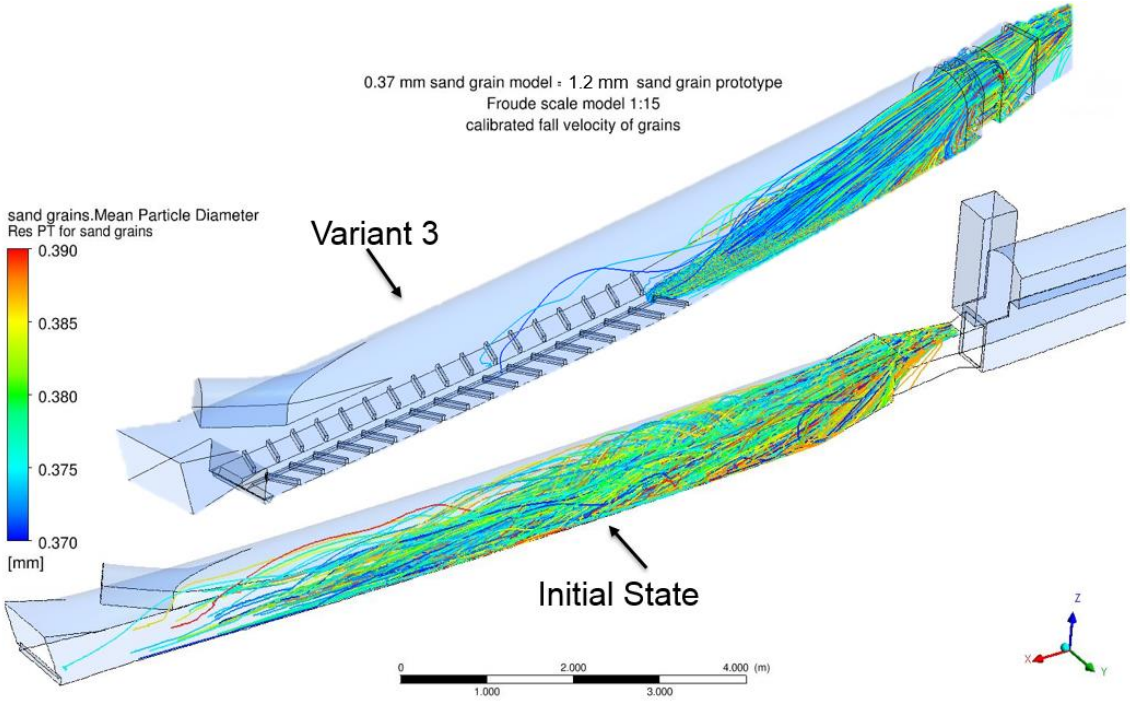

Figure 67: Variant 3 particle simulation and comparison of variant 0 (initial state) and variant 3

Figure 68 highlights the improvement by the flow calming pipes inside the sand trap after the gate. It also shows the smaller particles then about 0.7 mm will also be passed to the units. An improvement of max. Particle diameter can be established by the flow calming measures.

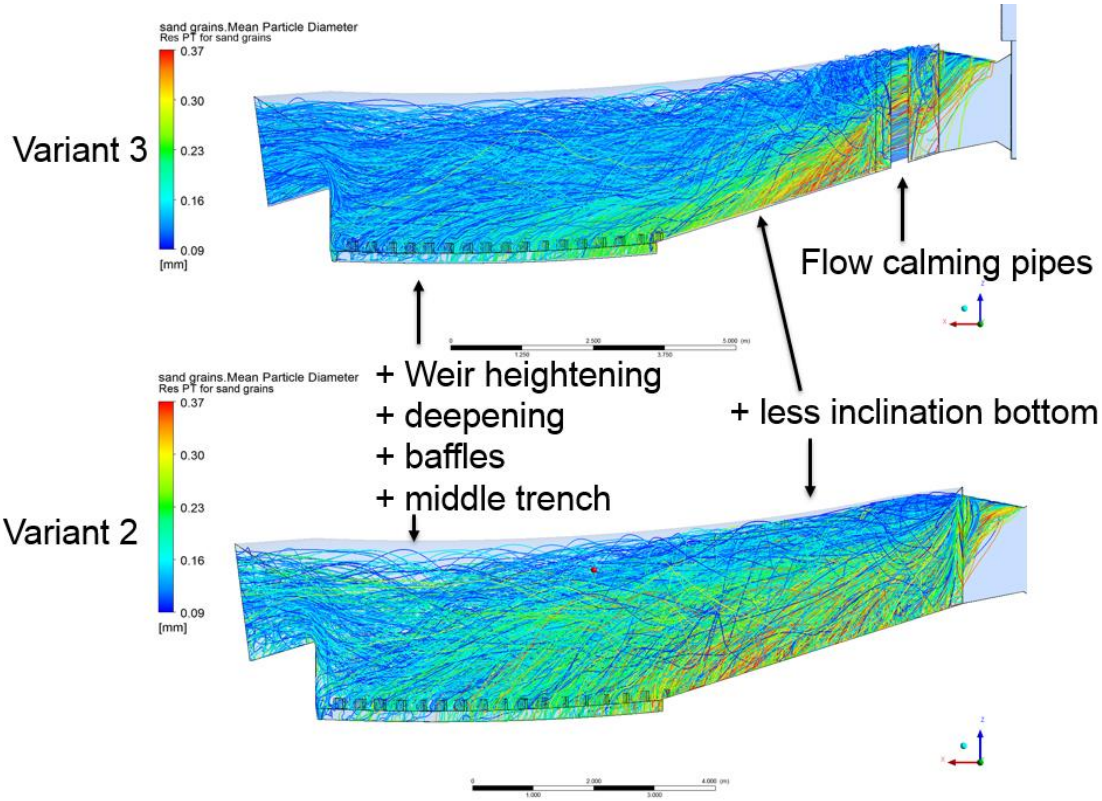

Figure 68: Particle simulation and comparison of variant 3 vs variant 2

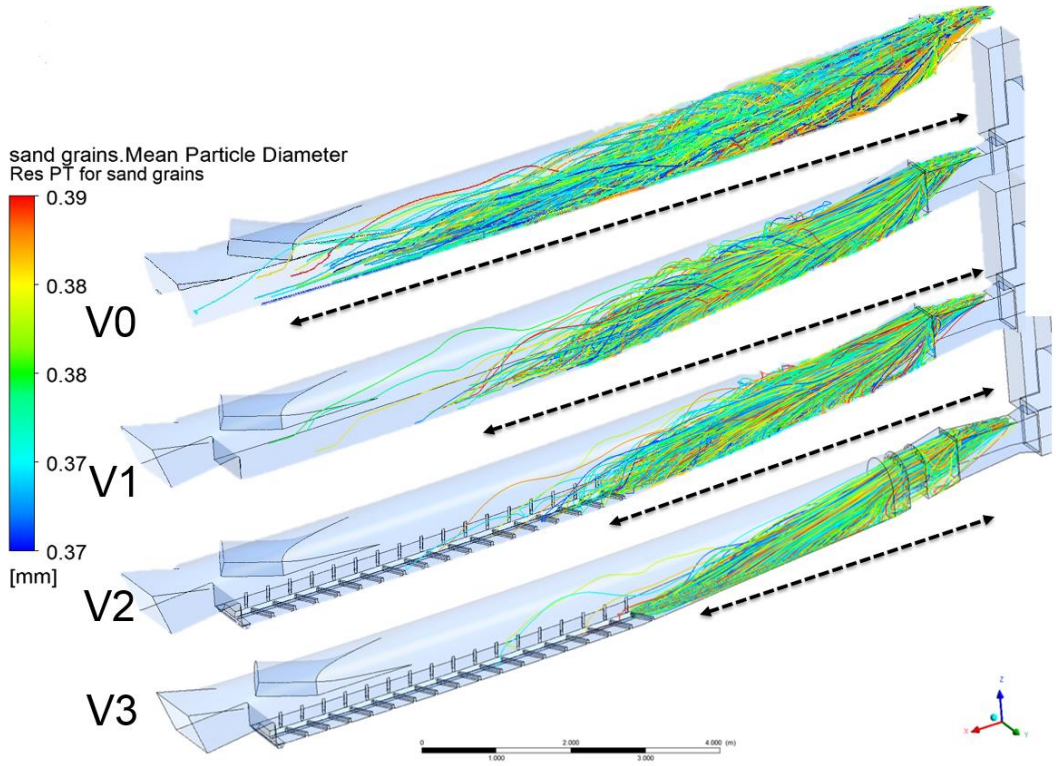

Figure 69: Particle simulation and comparison of variant 0 vs variant 1, variant 2 and variant 3

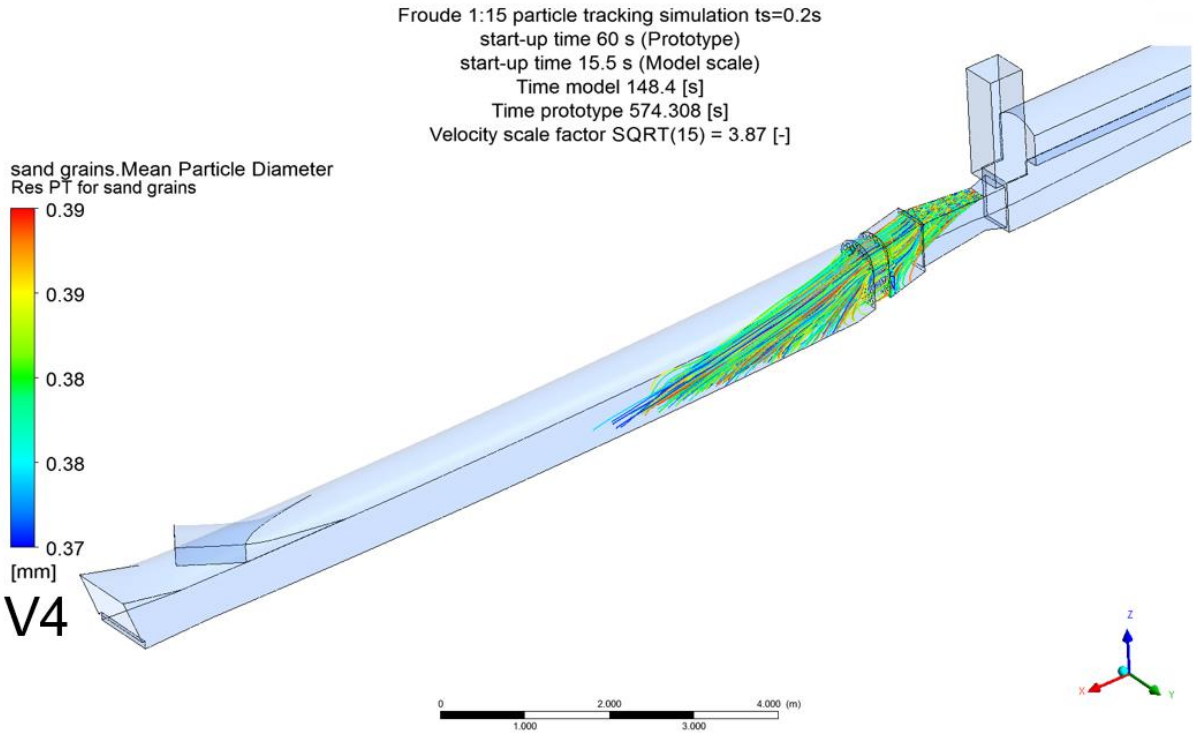

Figure 70: Particle simulation of variant 4 in comparison to Figure 69

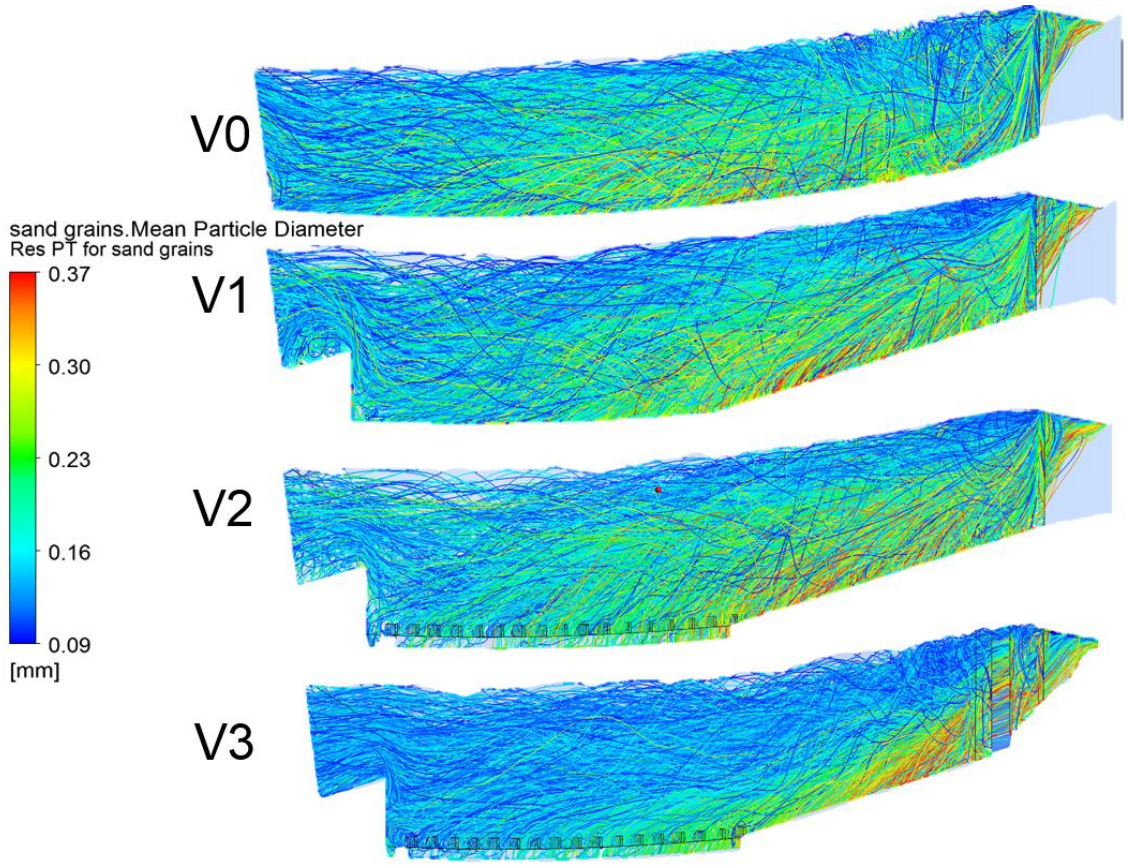

Figure 71: Particle simulation of variant 0 to V1, V2 and V3

Figure 72 shows the comparison for variants V0 to V5.

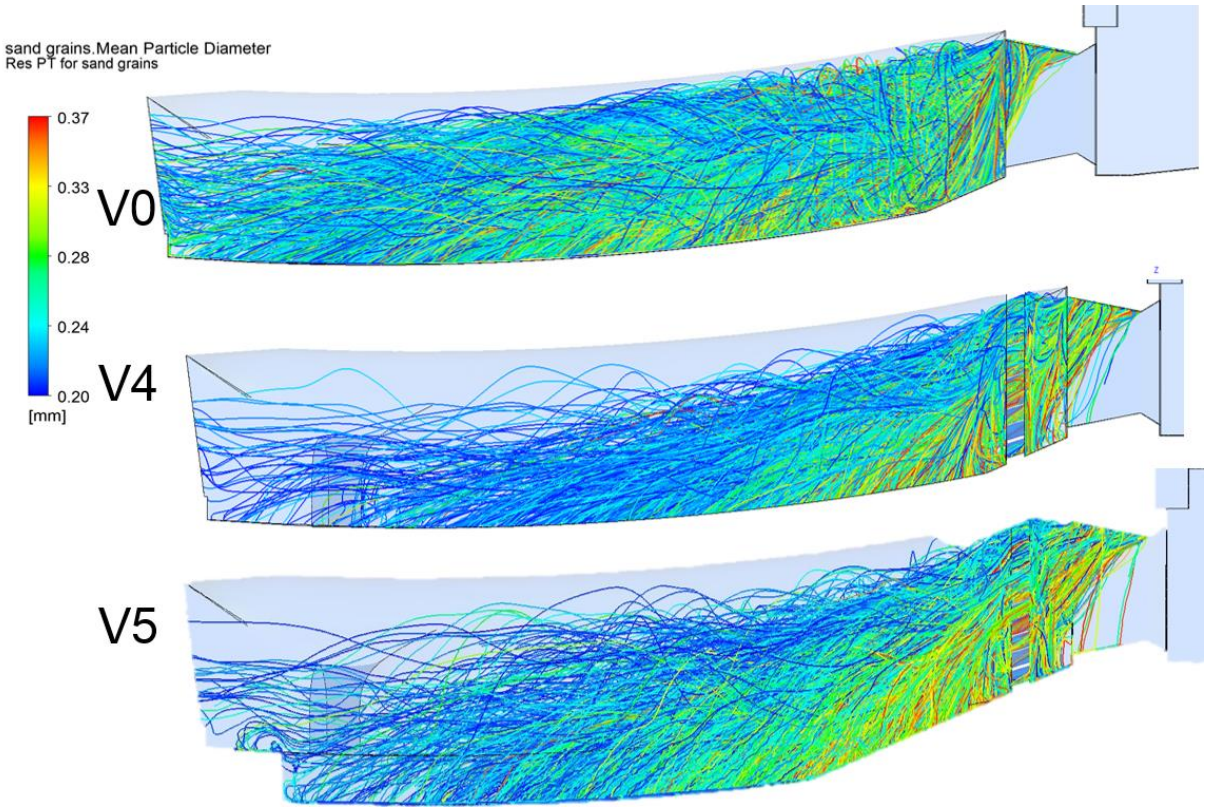

Figure 72: Particle simulation of variant 0 to V4 and V5

Figure 73 shows that particles larger up to at least 0.6 mm are very likely to be transported through the sand trap. But it also indicates that the sluicing trench in combination with the flow calming pipes is very positive for the settling in the pipe.

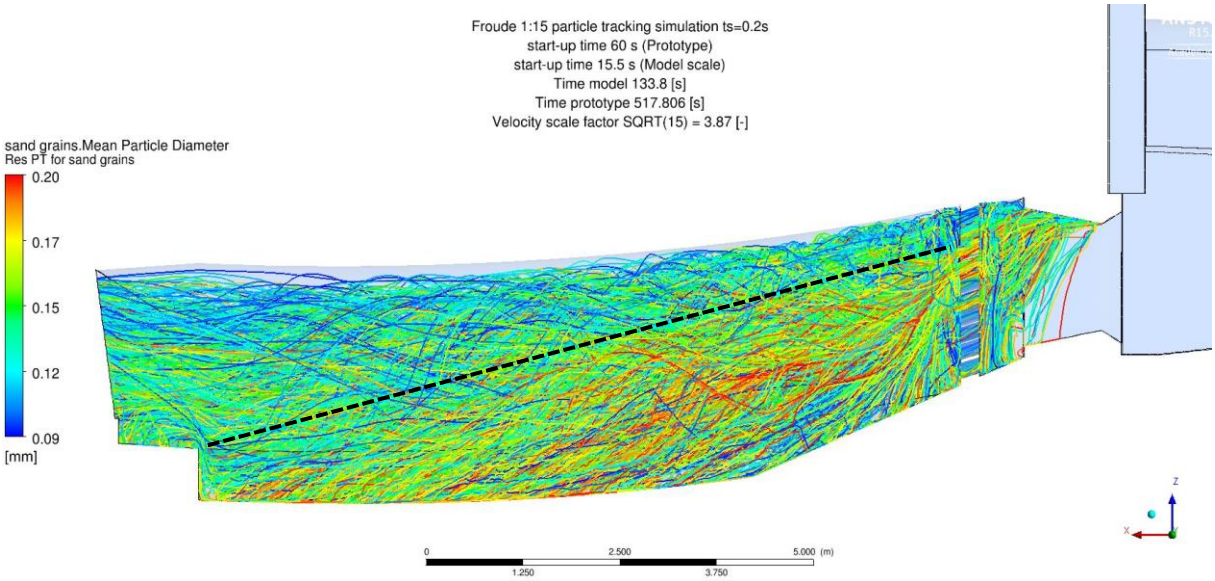

Figure 73: Particle simulation of variant V5 for particle diameters 0.21_p mm to 0.6_p mm

5. 3D CFD particle simulations – scale 1:20

This chapter describes the particle tracking and flow simulations in the 1:20 scale sand trap as it is constructed at NTNU Trondheim in a physical model test, applying the prototype inflow velocity.

Various simulations were undertaken to show the particle tracking simulations in that scaling.

5.1 Prototype velocity according to 80 m³/s

Inflow velocity of 1.64 m/s at the gate inlet. This is the 1:1 velocity for 80 m³/s in the sand trap.

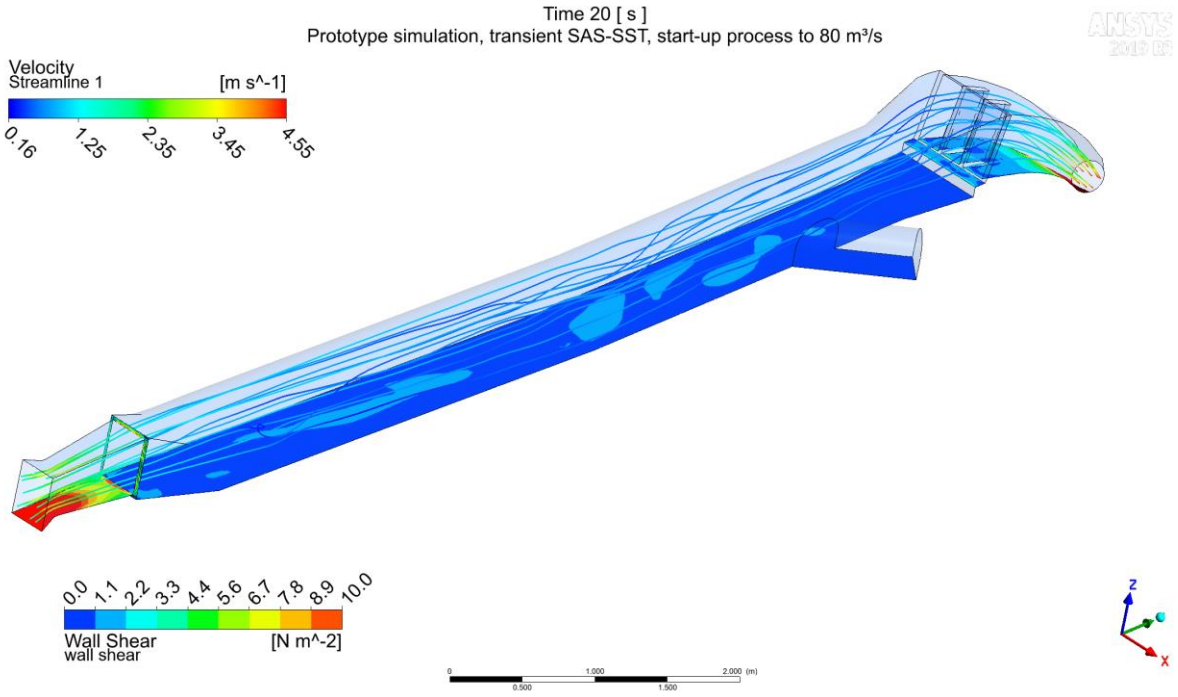

Figure 74: 1:20 scale simulation as NTNU model test comparison, inflow velocity as prototype 1.64 m/s, flow velocity, and wall shear for a certain timestep

Figure 75 shows the wall shear stress on the bottom of the sand trap for a certain time step during the transient simulation. Compared with the particles critical bed shear stress this explains the bed load transport in the chamber for this discharge.

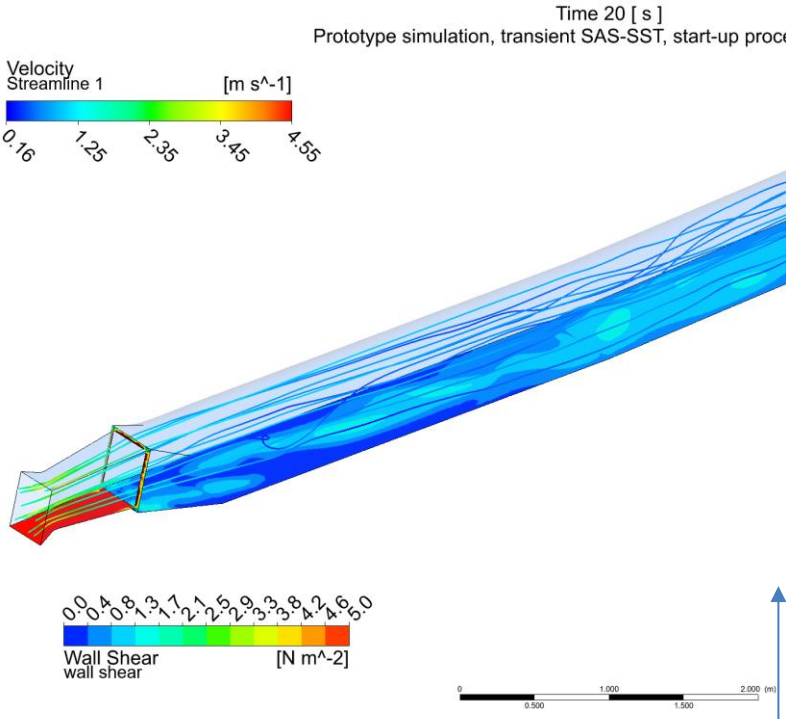

Particle classification name	Ranges of particle diameters mm	Critical bed shear stress (τ_c) (N/m²)
Coarse cobble	128 – 256	112 – 223
Fine cobble	64 – 128	53.8 – 112
Very coarse gravel	32 – 64	25.9 – 53.8
Coarse gravel	16 – 32	12.2 – 25.9
Medium gravel	8 – 16	5.7 – 12.2
Fine gravel	4 – 8	2.7 – 5.7
Very fine gravel	2 – 4	1.3 – 2.7
Very coarse sand	1 – 2	0.47 – 1.3
Coarse sand	0.5 – 1	0.27 – 0.47
Medium sand	0.25 – 0.5	0.194 – 0.27
Fine sand	0.125 – 0.25	0.145 – 0.194
Very fine sand	0.0625 – 0.125	0.110 – 0.145
Coarse silt	0.0310 – 0.0625	0.0826 – 0.110
Medium silt	0.0156 – 0.0310	0.0630 – 0.0826
Fine silt	0.0078 – 0.0156	0.0378 – 0.0630

Figure 75: 1:20 scale simulation as NTNU model test comparison, inflow velocity as prototype 1.64 m/s, flow velocity, and wall shear detail for a certain timestep, SAS SST

Figure 76 shows the transportation of the spherical quartz grains of the size of 15 mm to 20 mm on smooth plexiglass wall. The large spheres are transported to the very end of the sand trap chamber. This is in contradiction to the observations in the prototype; thus, factors are investigated such as grain shape, bottom roughness or grain roughness. However, grain roughness in recommended to be carefully applied.

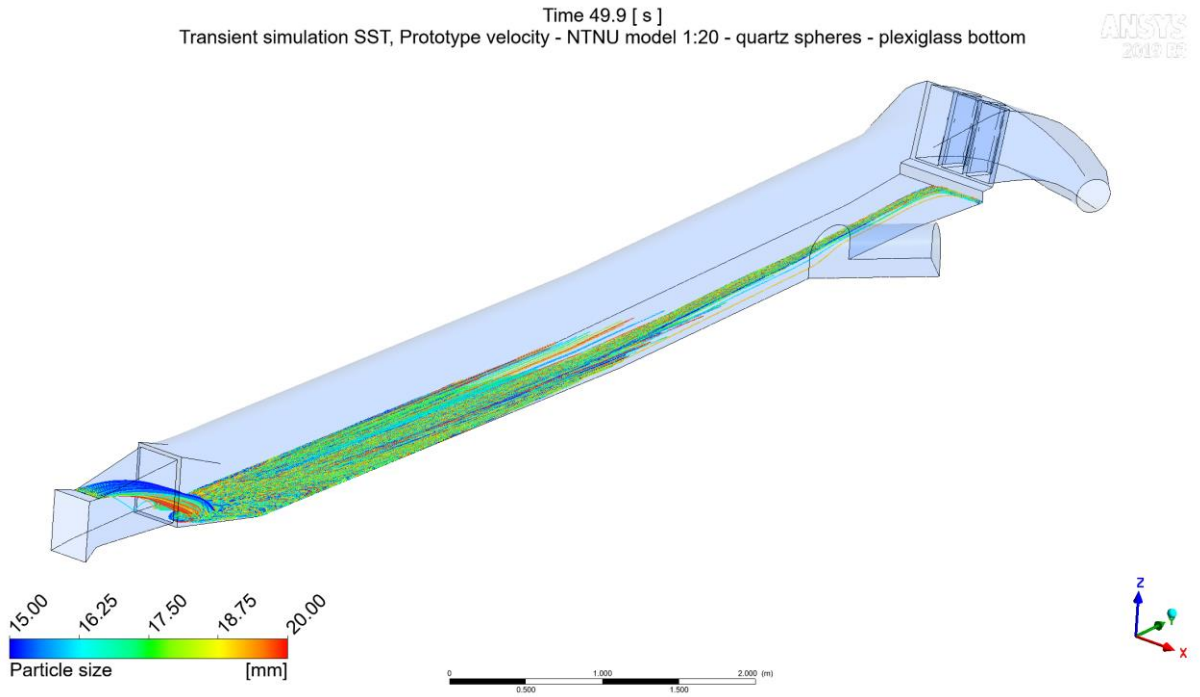

Figure 76: 1:20 scale simulation as NTNU model test comparison, inflow velocity as prototype 1.64 m/s, flow velocity, and wall shear detail for a certain timestep, SST, bed load transportation on Plexiglas, quartz spheres 15 mm – 20 mm

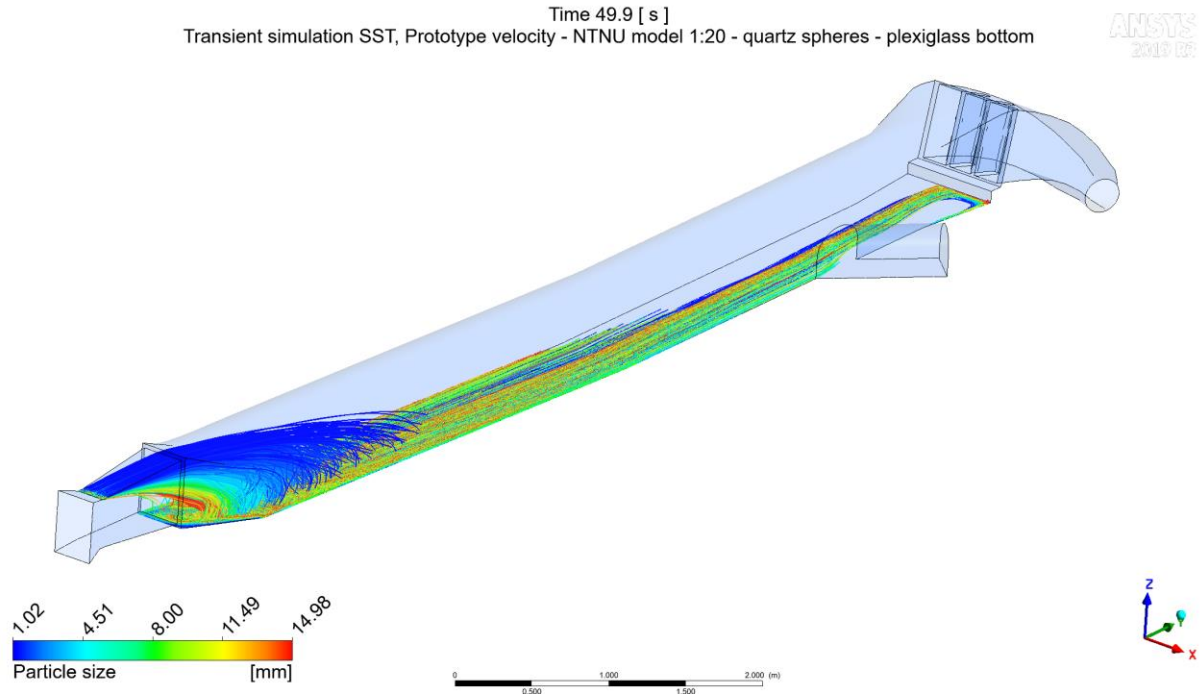

Figure 77: 1:20 scale simulation as NTNU model test comparison, inflow velocity as prototype 1.64 m/s, flow velocity, and wall shear detail for a certain timestep, SST, bed load transportation on Plexiglas, quartz spheres, 1 mm – 15 mm

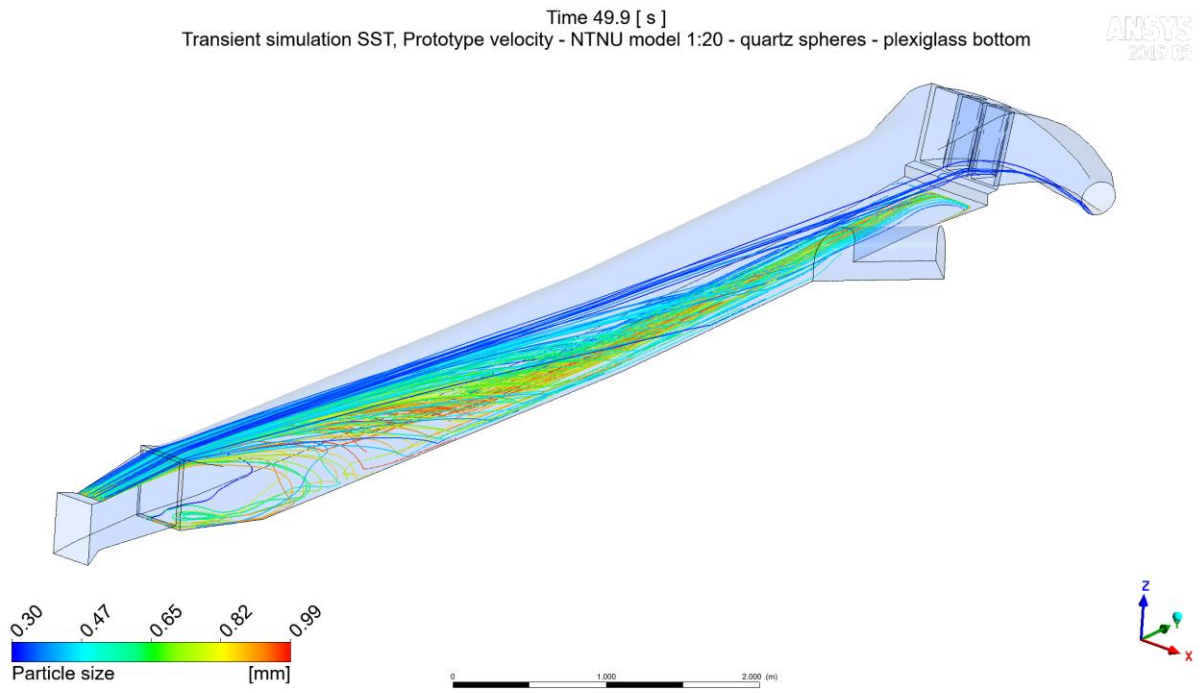

Figure 78: 1:20 scale simulation as NTNU model test comparison, inflow velocity as prototype 1.64 m/s, flow velocity, and wall shear detail for a certain timestep, SST, bed load transportation on Plexiglas, quartz spheres, 0.3 mm – 1 mm

5.2 Froude scaled velocity in 1:20 scale

This chapter shows the particle tracking and velocity simulations for the 1:20 scaled model with Froude scaled velocity of the design discharge of 80 m³/s, leading to an inflow velocity of 0.373 m/s.

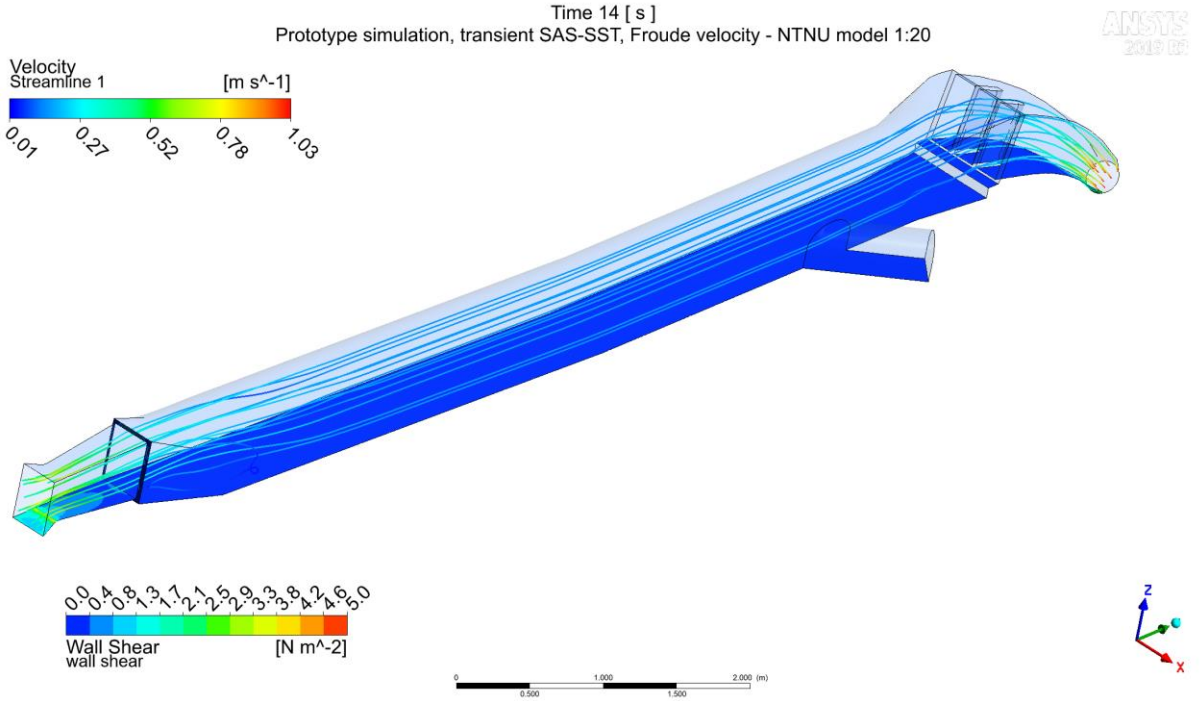

Figure 79: 1:20 scale simulation as NTNU model test comparison, inflow velocity as Froude scaled 0.373 m/s, flow velocity, and wall shear for a certain timestep, SAS SST

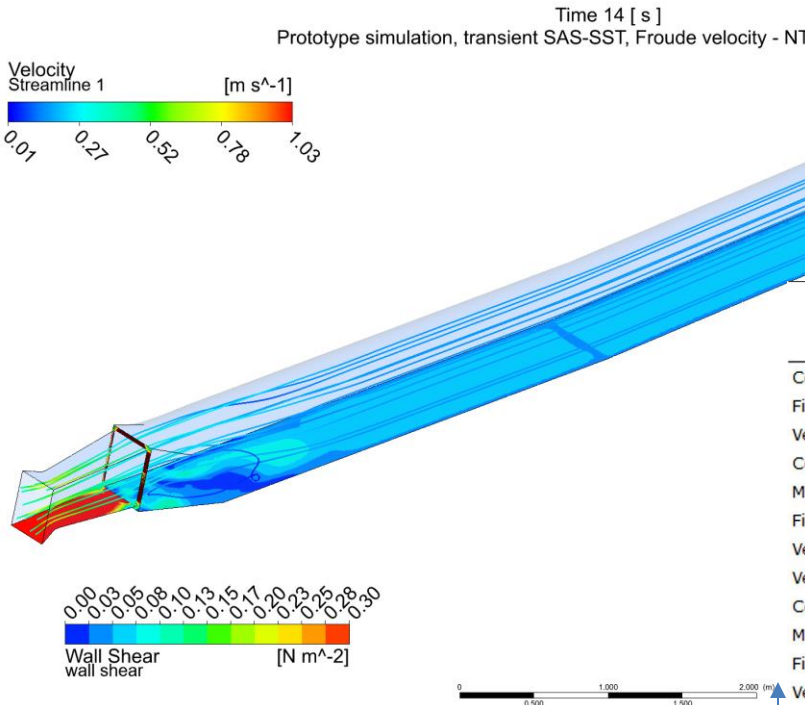

Particle classification name	Ranges of particle diameters mm	Critical bed shear stress (τ_c) (N/m²)
Coarse cobble	128 – 256	112 – 223
Fine cobble	64 – 128	53.8 – 112
Very coarse gravel	32 – 64	25.9 – 53.8
Coarse gravel	16 – 32	12.2 – 25.9
Medium gravel	8 – 16	5.7 – 12.2
Fine gravel	4 – 8	2.7 – 5.7
Very fine gravel	2 – 4	1.3 – 2.7
Very coarse sand	1 – 2	0.47 – 1.3
Coarse sand	0.5 – 1	0.27 – 0.47
Medium sand	0.25 – 0.5	0.194 – 0.27
Fine sand	0.125 – 0.25	0.145 – 0.194
Very fine sand	0.0625 – 0.125	0.110 – 0.145
Coarse silt	0.0310 – 0.0625	0.0826 – 0.110
Medium silt	0.0156 – 0.0310	0.0630 – 0.0826
Fine silt	0.0078 – 0.0156	0.0378 – 0.0630

Figure 80: 11:20 scale simulation as NTNU model test comparison, inflow velocity as Froude scaled 0.373 m/s, flow velocity, and wall shear detail for a certain timestep; SAS SST

6. 3D CFD shear plate variant simulations – scale 1:20

This chapter describes the 3D CFD simulations in 1:20 scale with particle tracking including shear plates (ribs) in the Tonstad sand trap. Hydraulic investigations regarding these questions are being done the hydraulic laboratory at NTNU (discussion Figure 81 Figure 82). The simulations in this report represent the comparison between model test and 3D CFD as anticipated initially. The investigations contain three variants of ribs. Further rib investigations in small scale 1:36.67 model tests were undertaken for the FlekS 2.0 project expansion. Table 12 shows the physical values and boundary conditions of the specific investigations. The ribs have a geometric size in prototype of 1 m width, and 1 m gap at a height of 1.2 m.

The inlet velocity of 1.64 m/s represents the 1:1 prototype scaling velocity for 80 m³/s. The sediments show a 0.3 mm to 1.0 mm diameter distribution.

Table 12: Data for simulations Variant (1), (2) and (3)

Scale	1:20	Geometry	Tonstad plan
Particle injection	Above gate	Symmetry	yes
Particles Diameter	0.3 -1.0 mm	Wall roughness	Smooth wall
Time	100 s	Software	CFX
Timestep	0.05	Inlet	Velocity 1.64 m/s
Particles Density	2650 kg/m³	Outlet	Pressure 0 Pa
Particle roughness	Non	Mesh (Variant 1) number of nodes	1’240’613
Particle Drag	Schiller-Naumann	Element size	3 mm
Turbulence Modelling	SAS-SST	Inflation first layer	0.3 mm
Mesh (Variant 2) number of nodes	1’551’480	Mesh (Variant 3) number of nodes	2’429’099

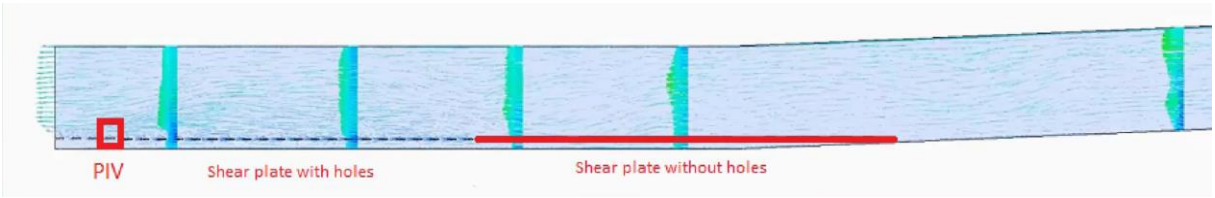

Figure 81: Discussion sketch with PIV investigation position at NTNU

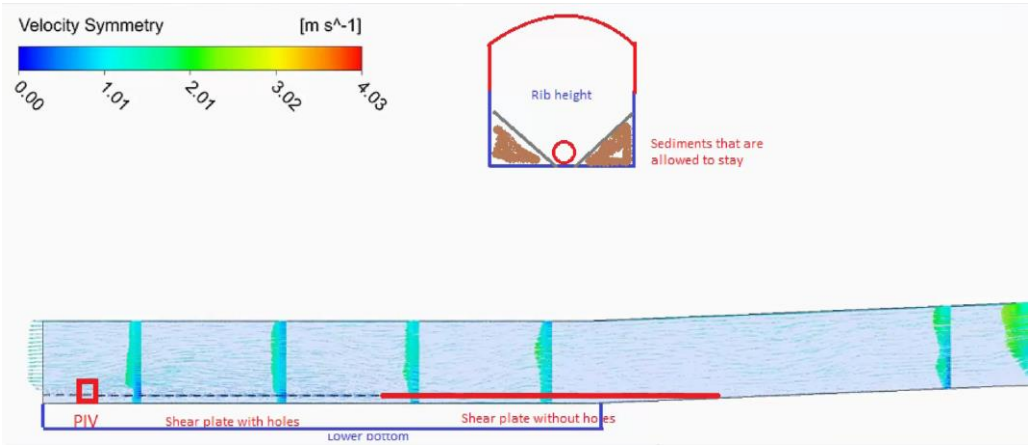

Figure 82: Discussion sketch of potential sand trap upgrade with PIV investigation position at NTNU

6.1 1:20 Variant 1) shear plate first part - particle simulation geometry

This variant contains ribs for a length of 50 m (prototype) upstream of the weir at the downstream part of the sand trap. Particles are injected on top of the gate restriction.

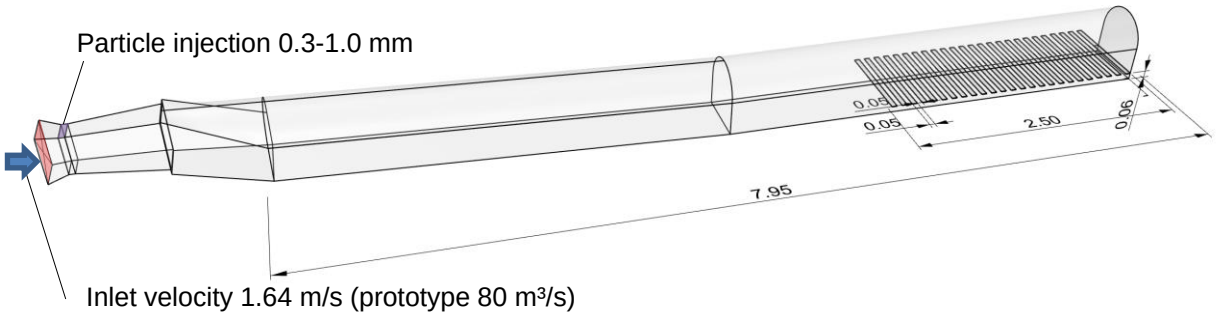

Figure 83: 1:20 Variant 1, 3D geometry for shear plate simulation, first 2.5 m in model, of the sand trap

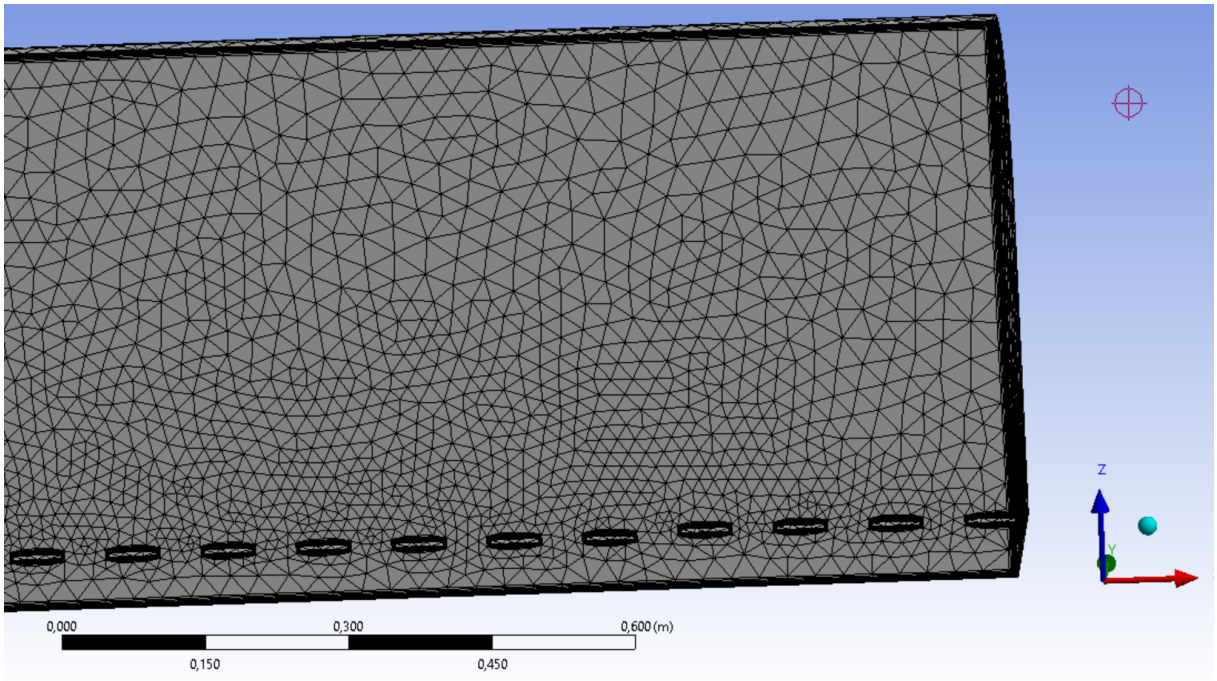

Figure 84: 1:20 Variant 1, 3D geometry for shear plate simulation, first 2.5 m in model, of the sand trap, mesh detail

6.2 1:20 Variant 2) shear plate flat part - particle simulation geometry

This variant contains ribs for a length of 80 m (prototype) upstream of the weir at the downstream part of the sand trap. Particles are injected on top of the gate restriction.

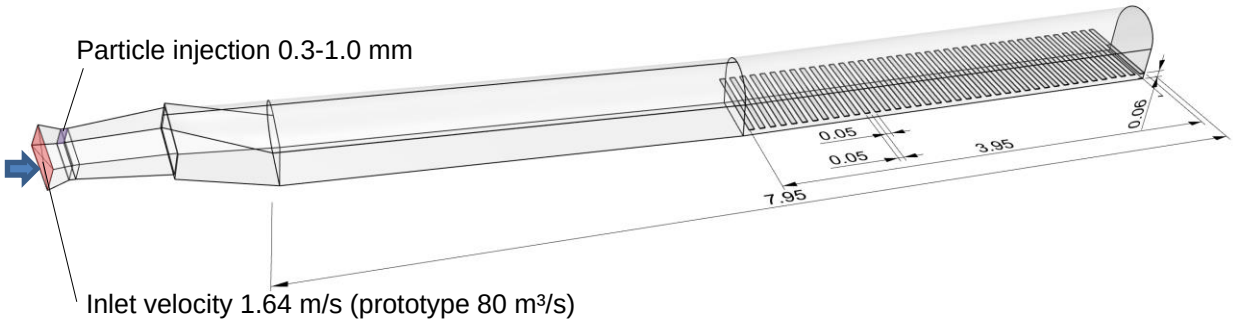

Figure 85: 1:20 Variant 2, 3D geometry for shear plate simulation, flat part of the sand trap

6.3 1:20 Variant 3) shear plate full length - particle simulation geometry

This variant contains ribs for a length of 159 m (prototype) over the full length up to the diffusor section parallel to the bottom. Particles are injected on top of the gate restriction.

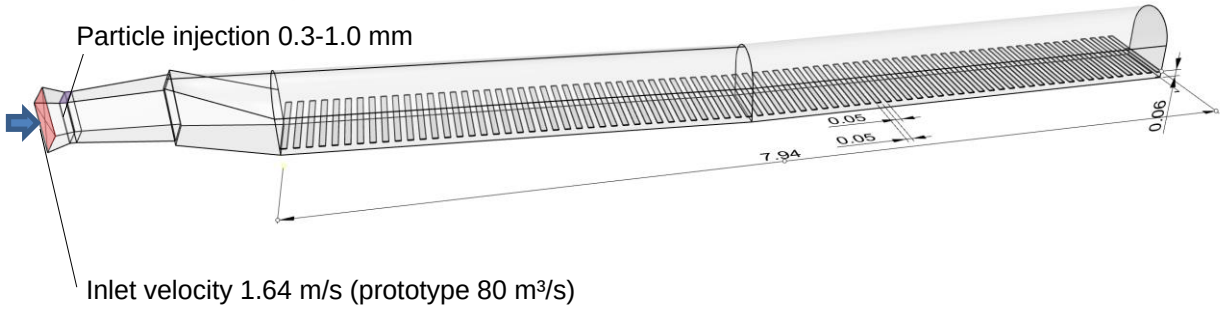

Figure 86: 1:20 Variant 3, 3D geometry for shear plate simulation, full length of the sand trap

6.4 Results 3D CFD shear plate variants

This chapter describes the results of the 3D CFD simulations of the 1:20 scaled particle tracking simulation with various rib designs.

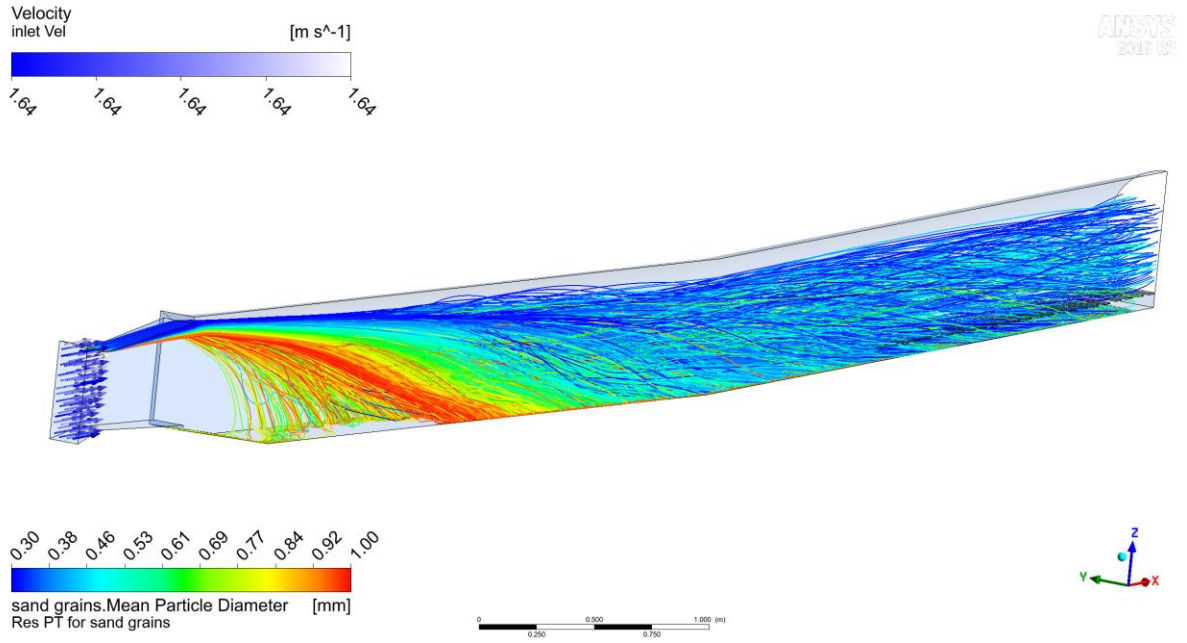

Figure 87: 1:20 Variant 1, particle settling and movement 0.3 mm to 1.0 mm

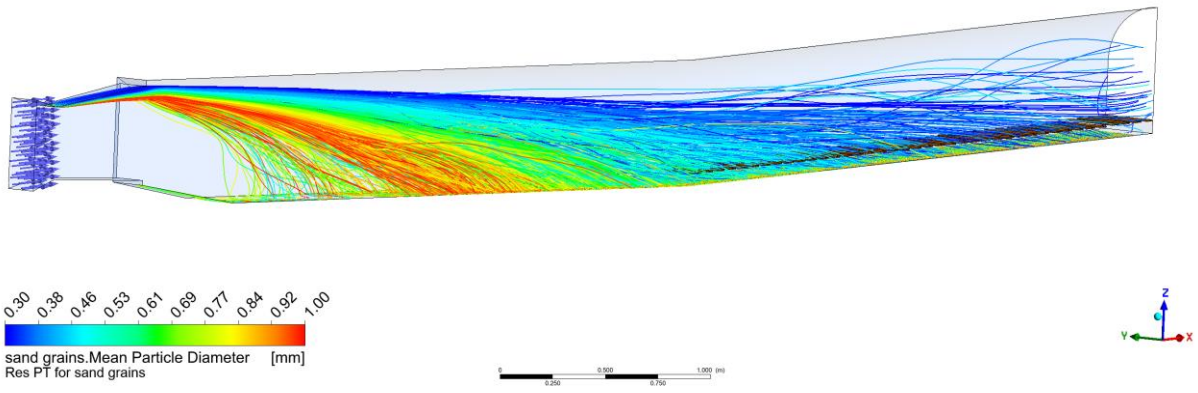

Figure 88: 1:20 Variant 2, particle settling and movement 0.3 mm to 1.0 mm

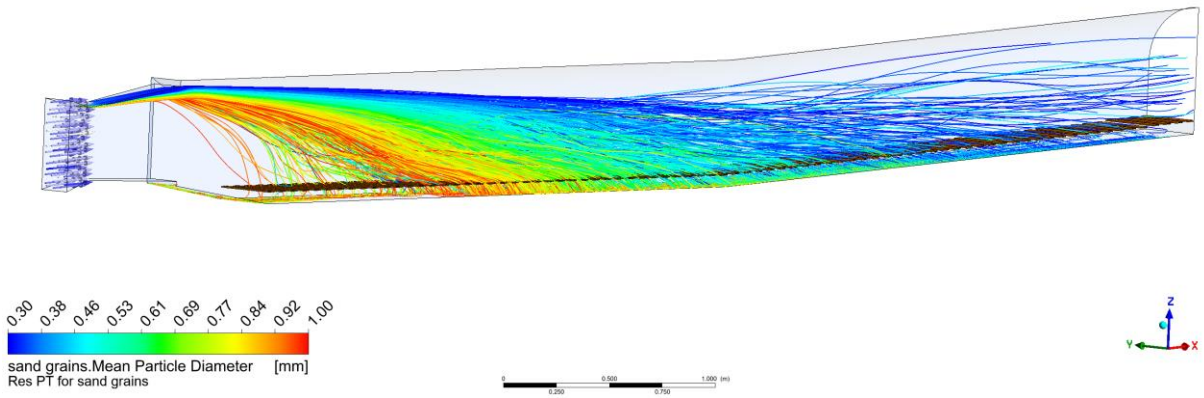

Figure 89: 1:20 Variant 3, particle settling and movement 0.3 mm to 1.0 mm

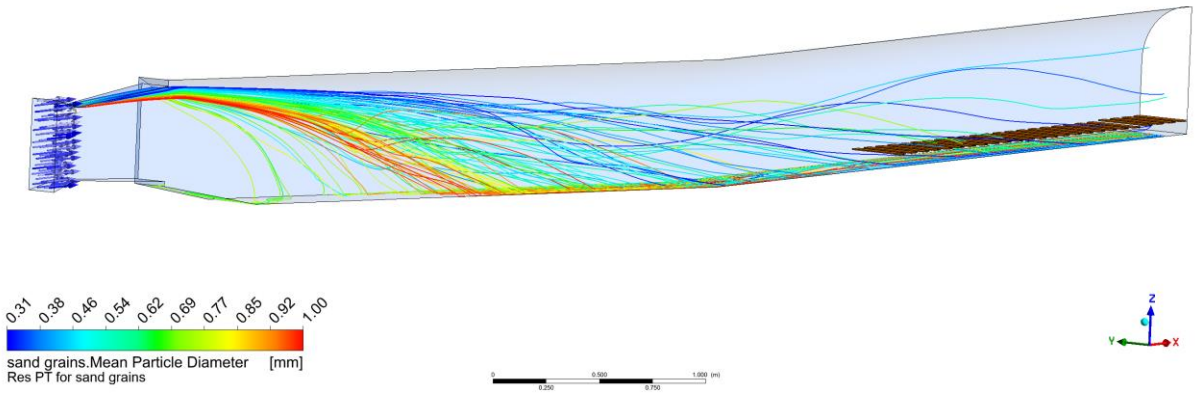

Figure 90: 1:20 Variant 1, 100 particle tracks of sediment, particle settling and movement 0.3 mm to 1.0 mm

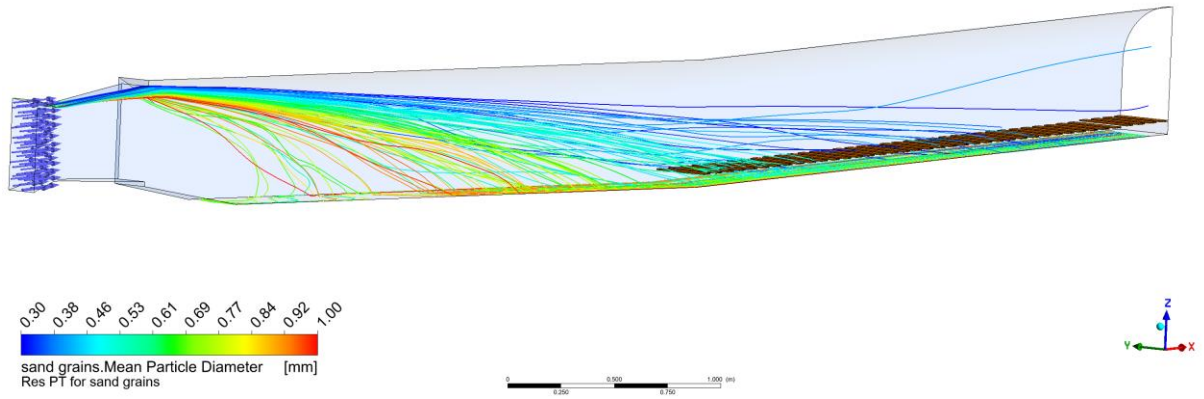

Figure 91: 1:20 Variant 2, 100 particle tracks of sediment, particle settling and movement 0.3 mm to 1.0 mm

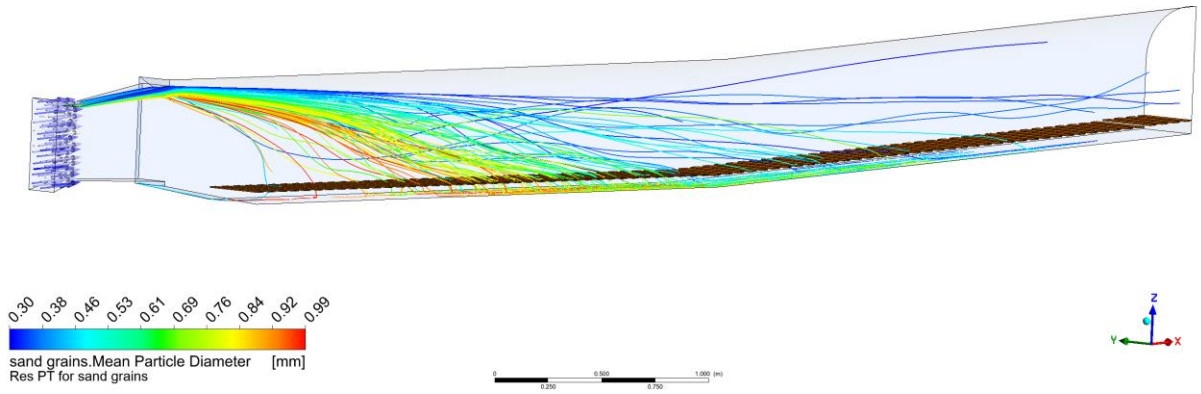

Figure 92: 1:20 Variant 3, 100 particle tracks of sediment, particle settling and movement 0.3 mm to 1.0 mm

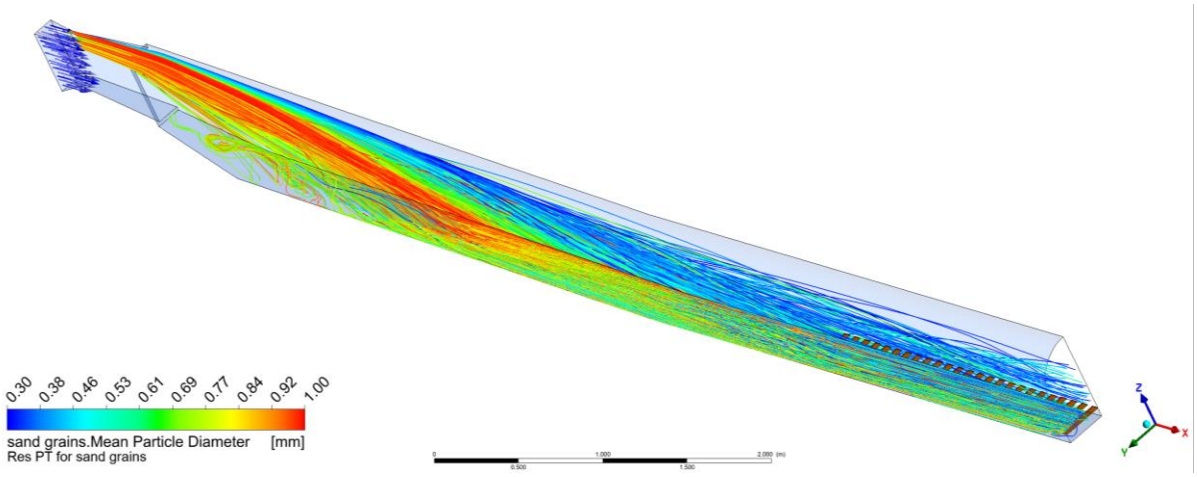

Figure 93: 1:20 Variant 1, 1000 particle tracks of sediment, bottom view

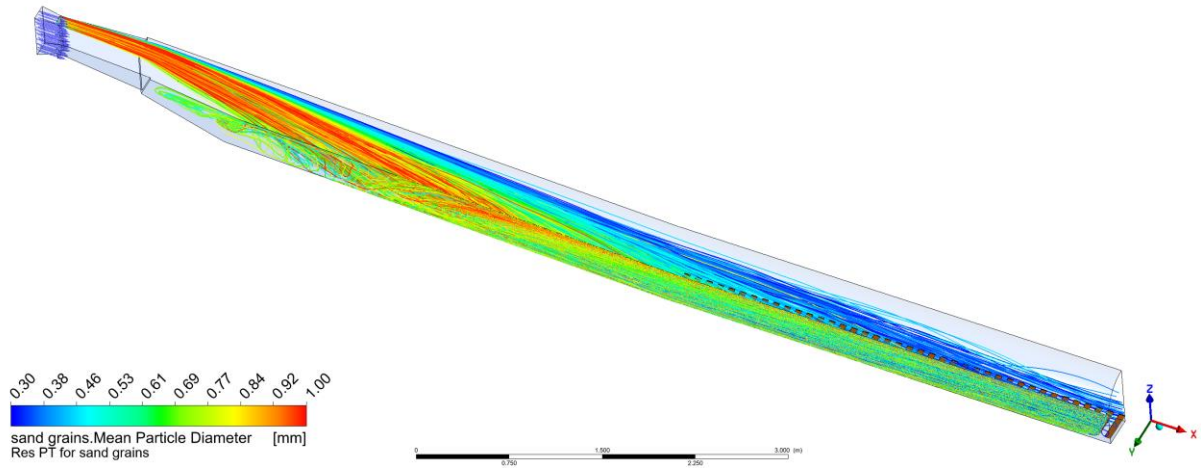

Figure 94: 1:20 Variant 2, 1000 particle tracks of sediment, bottom view

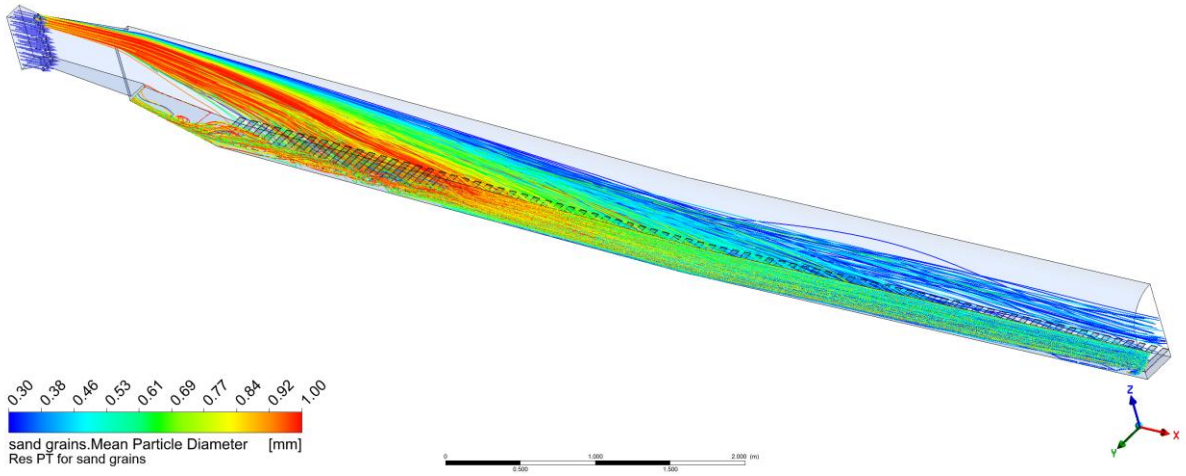

Figure 95: 1:20 Variant 3, 1000 particle tracks of sediment, bottom view , particle settling and movement 0.3 mm to 1.0 mm

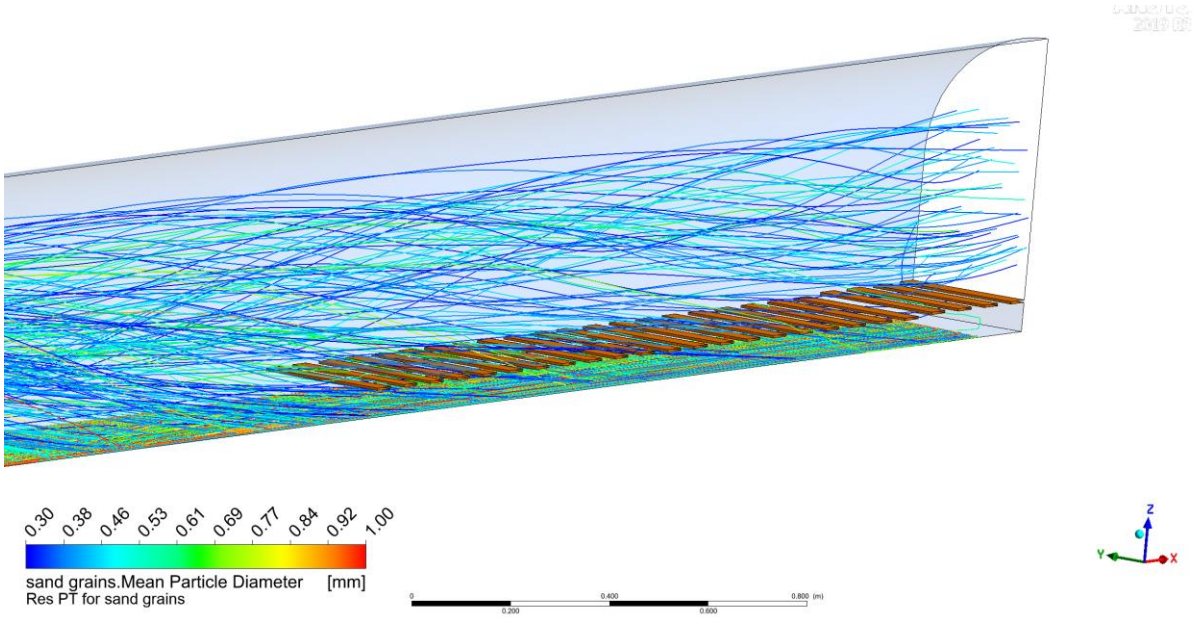

Figure 96: 1:20 Variant 1, particle settling and movement 0.3 mm to 1.0 mm

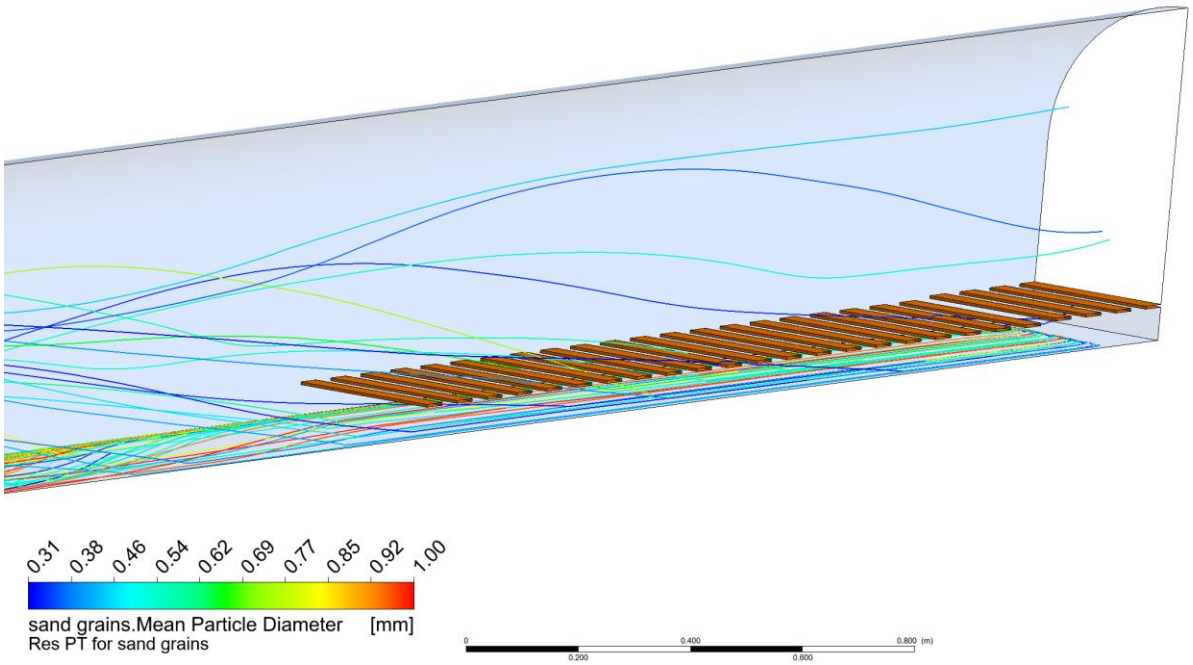

Figure 97: 1:20 Variant 1, particle settling and movement 0.3 mm to 1.0 mm, detail

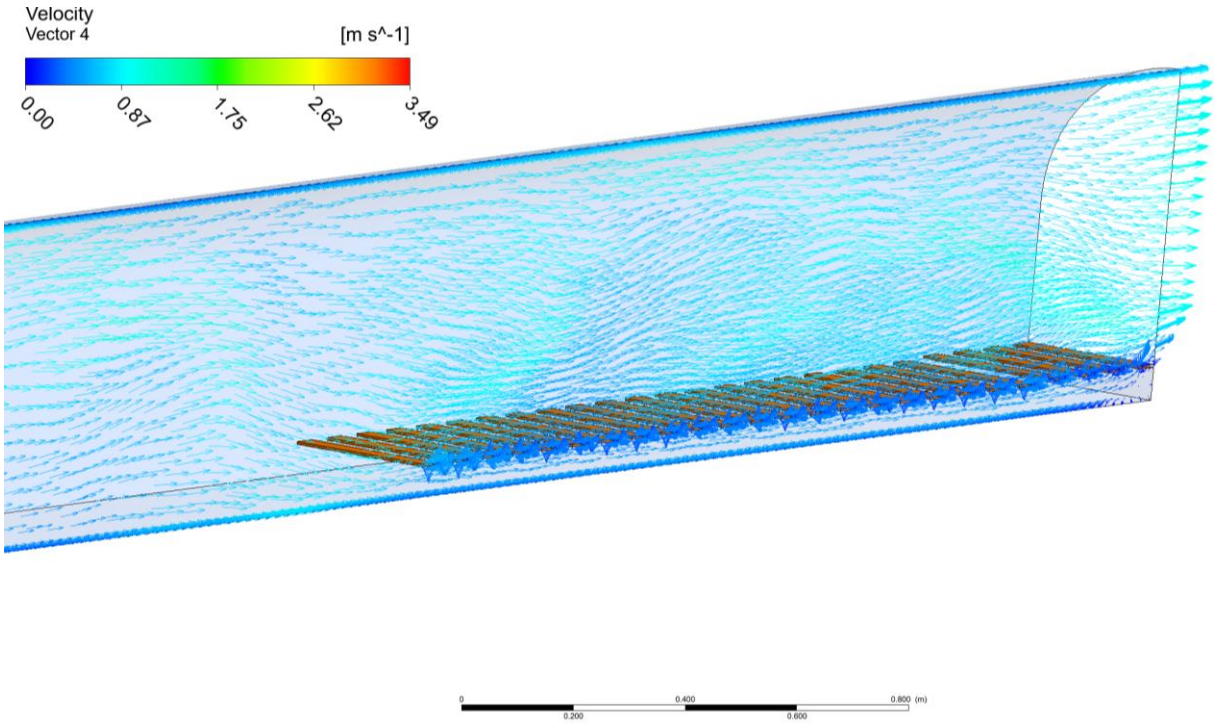

Figure 98: 1:20 Variant 1, flow velocity vectors

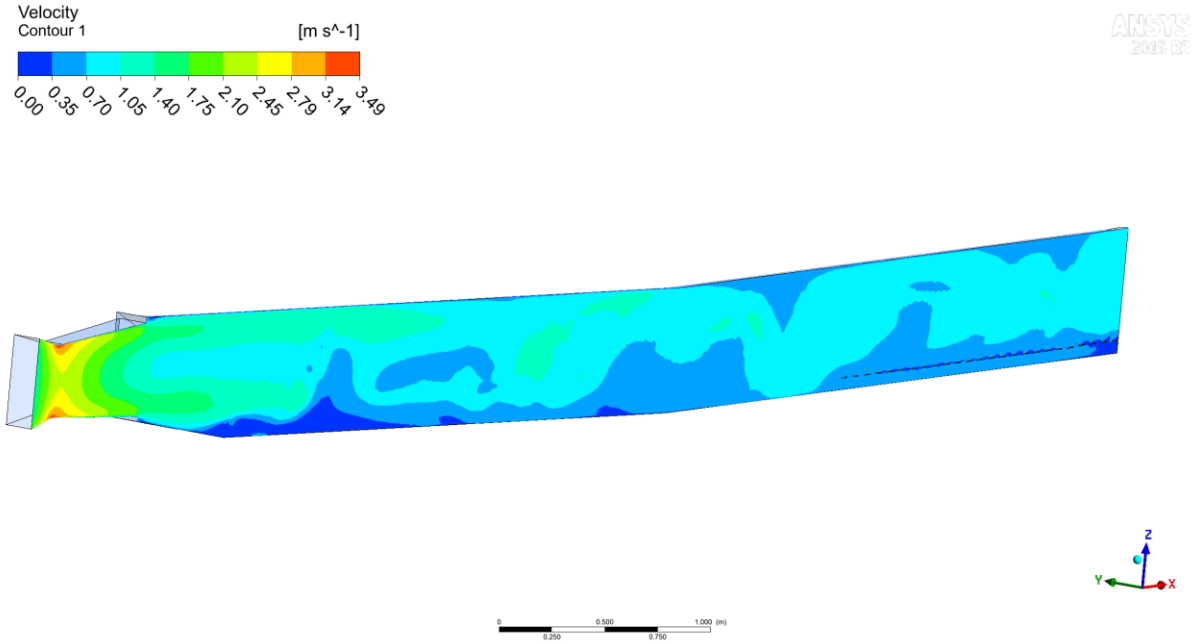

Figure 99: 1:20 Variant 1, flow velocity contour plot in symmetry

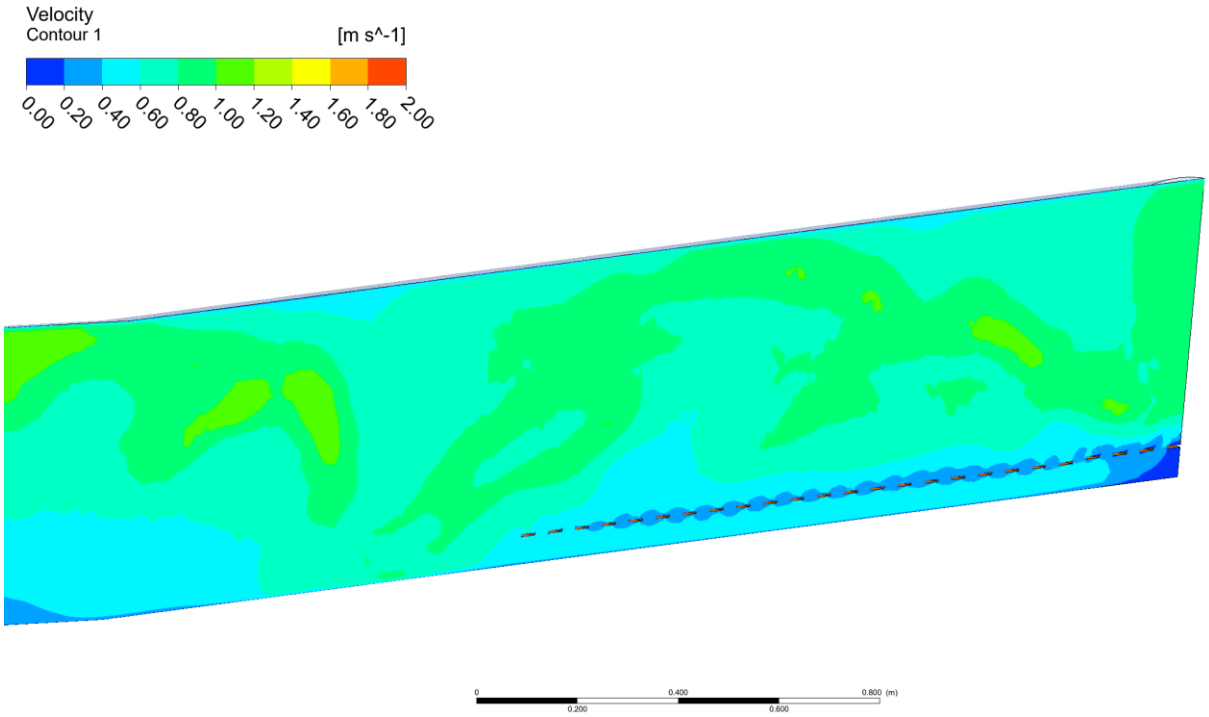

Figure 100: 1:20 Variant 1, flow velocity contour plot in symmetry, detail at ribs

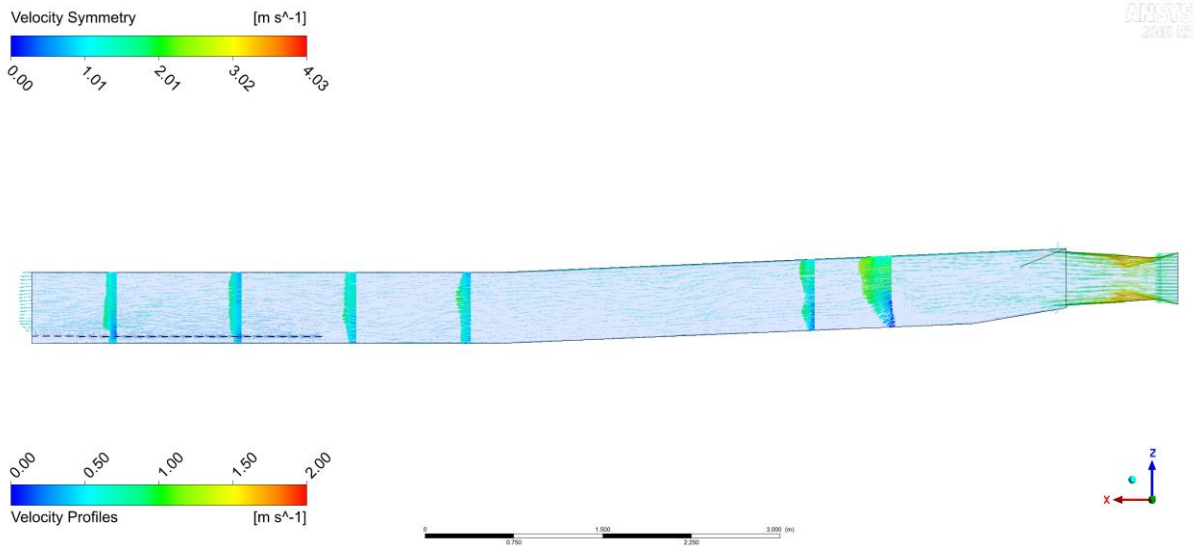

Figure 101: 1:20 Variant 1, flow velocity vectors in symmetry plane

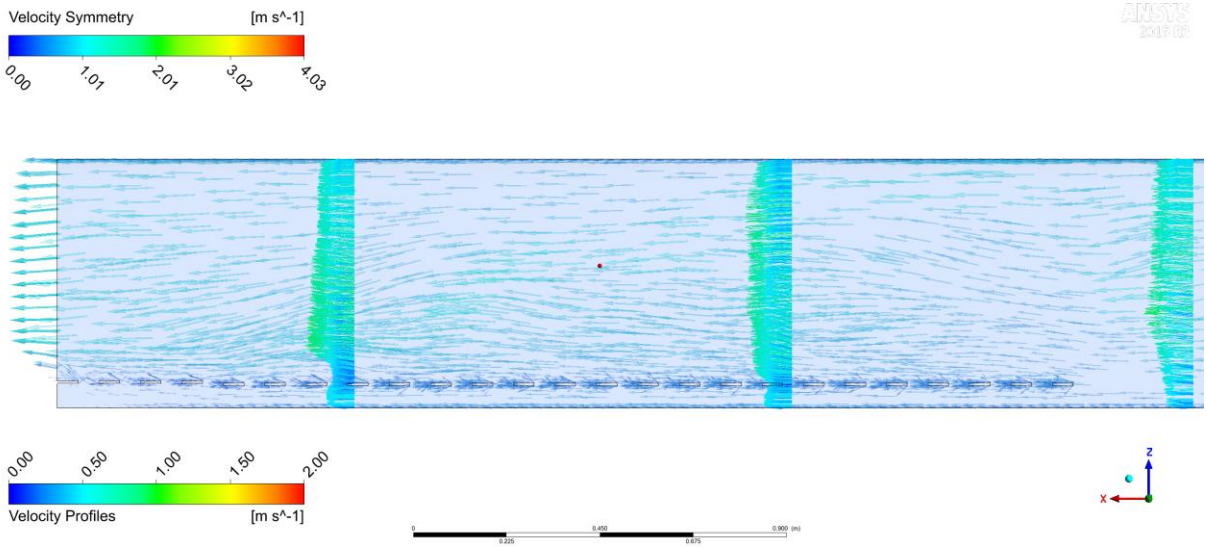

Figure 102: 1:20 Variant 1, flow velocity vectors in symmetry plane, detail

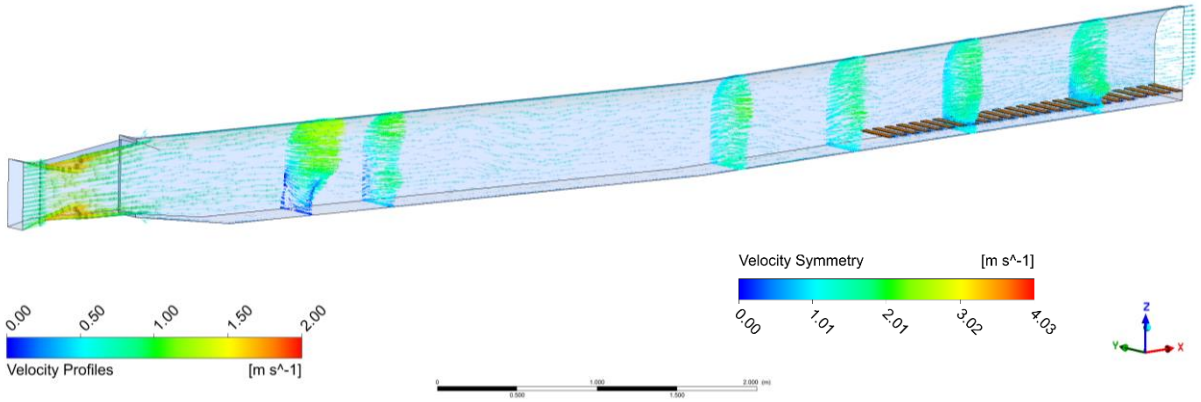

Figure 103: 1:20 Variant 1, flow velocity in symmetry section

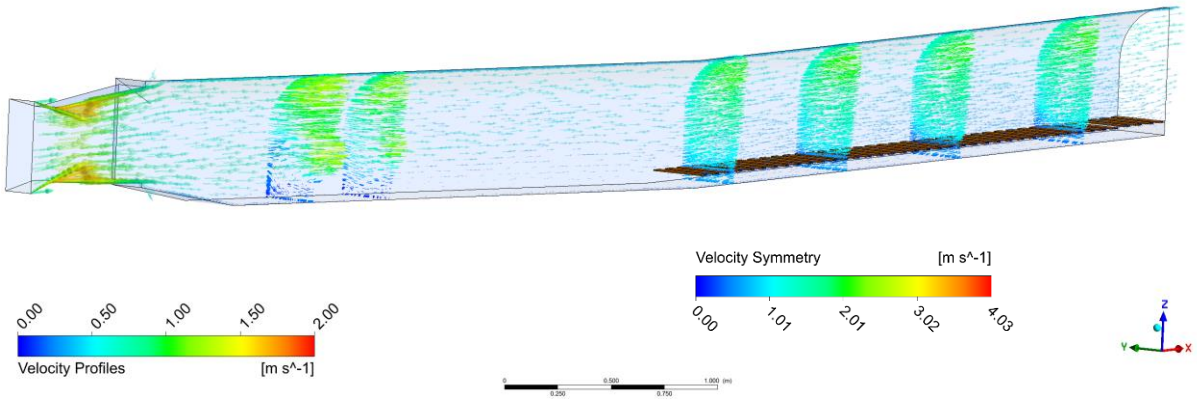

Figure 104: 1:20 Variant 2, flow velocity in symmetry section

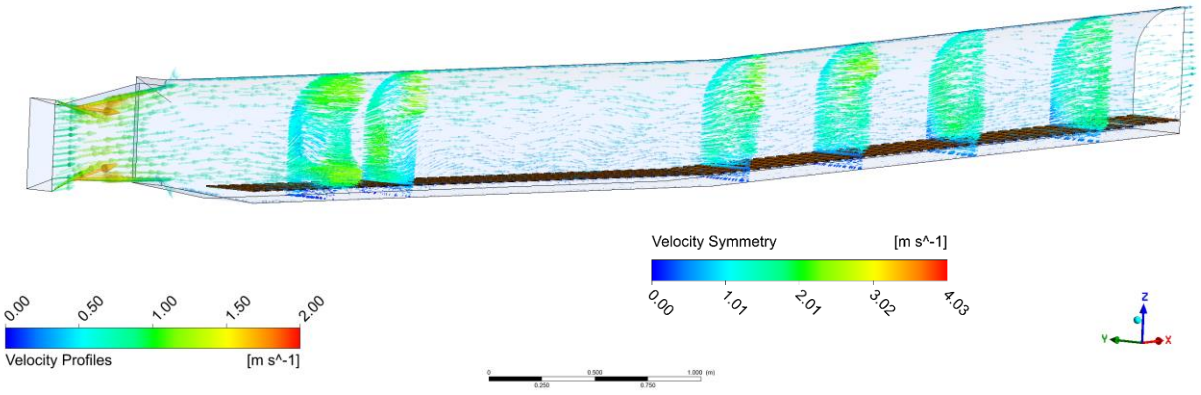

Figure 105: 1:20 Variant 3, flow velocity in symmetry section

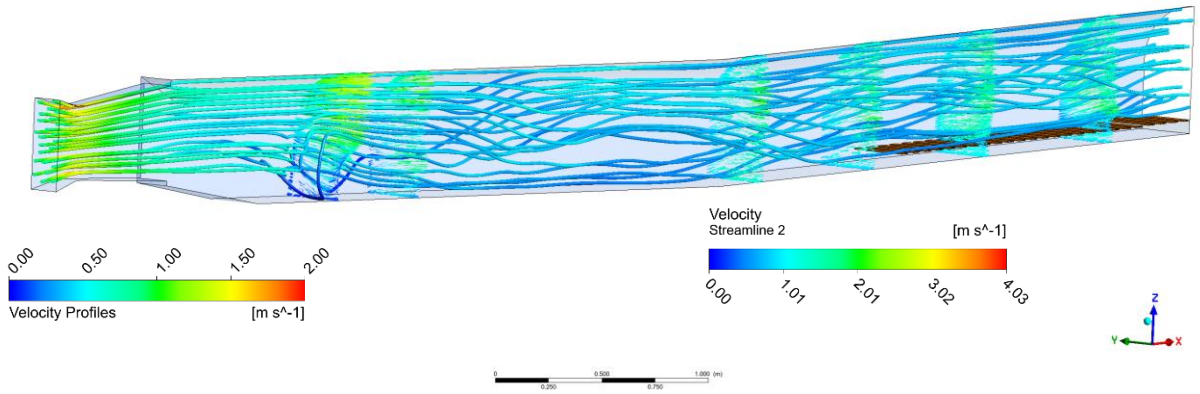

Figure 106: 1:20 Variant 1 - shear plates in front section, streamlines, velocity profiles

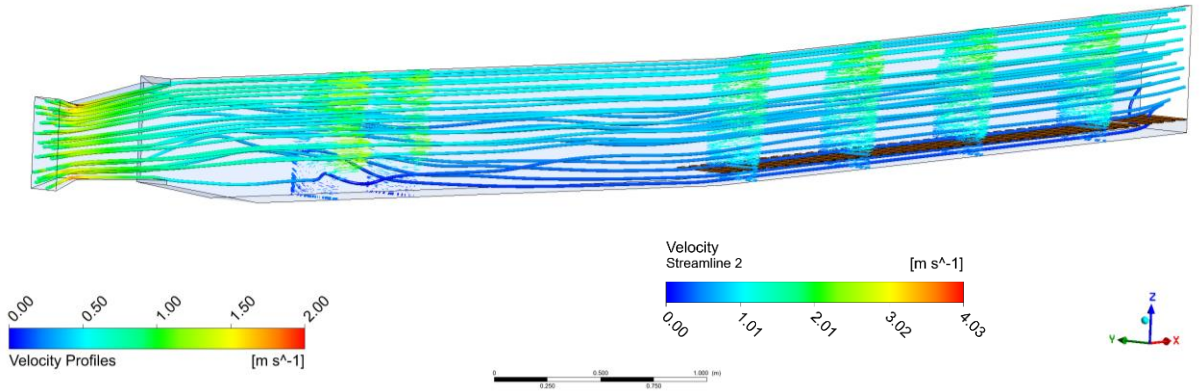

Figure 107: 1:20 Variant 2 - shear plates in flat part, streamlines, velocity profiles

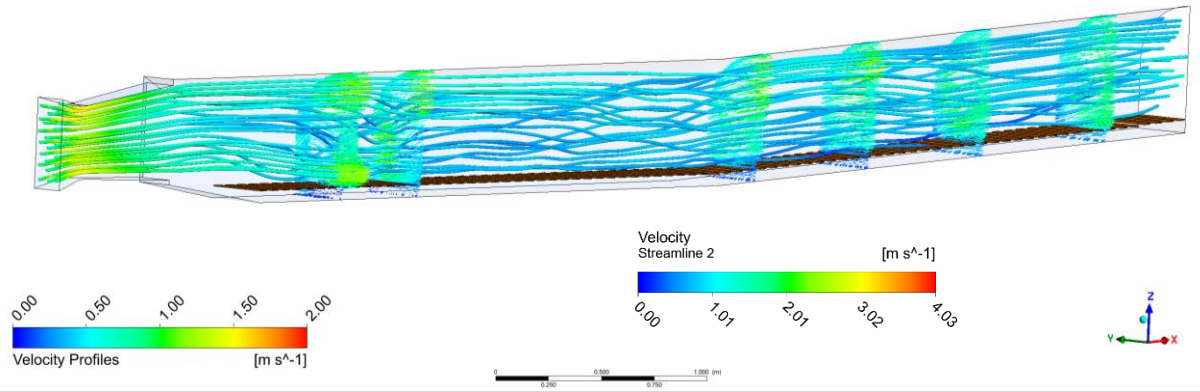

Figure 108: 1:20 Variant 3 - shear plates full length, streamlines, velocity profiles

7. Tonstad upgrade- Surge tank expansion

During the investigations it was found that the Tonstad power plant can be significantly upgraded in power output by increasing the discharge using the existing power water ways. The goal upgrade is investigated to increase the discharge up to 25%. This would mean a possible power upgrade of about 20%. The water level in the surge tank is less due to higher friction in the power water tunnels and thus, less head is available on the machines. But the higher discharge allows for significant higher power output. The surge tanks need to be upgraded to allow a reasonable acceleration of the water and also avoid the creation of free surface flow in the sand traps. Figure 109 shows a schematic view of a possible arrangement of the surge tank expansion to be attached to the existing system.

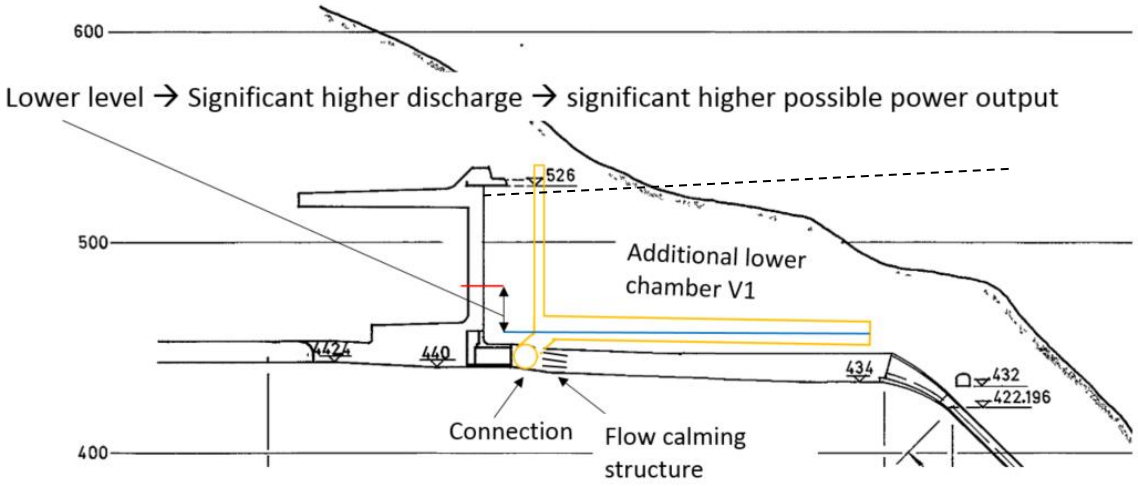

Figure 109: Schematic section of surge tank expansion with added lower chamber, critical overburden

Since Figure 109 shows a critical overburden, the extension chamber was chosen in different alignments as shown in chapter 8.1.

7.1 1D Numerical simulation of Tonstad power plant upgrade

Figure 110 visualizes the 1D numerical model of Tonstad power plant to model the discharges and mass oscillations.

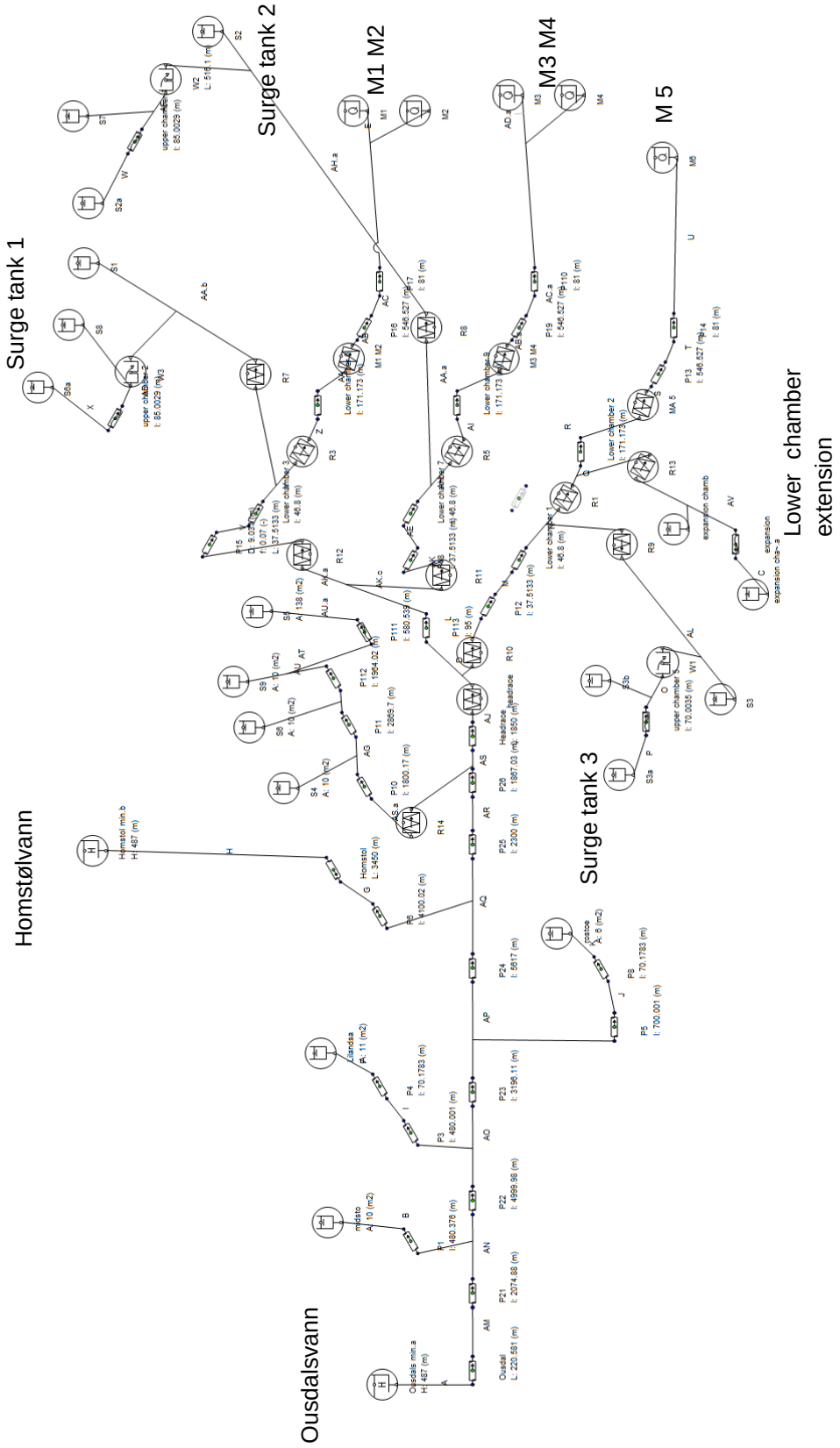

Figure 110: 1D-numerical model of Tonstad power plant

Figure 111 shows the fluid level in the surge tank and the discharge in the headrace tunnel after an emergency shutdown in 12s from 250 m³/s, reaching and filling the upper chambers. The surge waves are visible in this simulation. Figure 112 shows a similar behaviour after start-up in 10 minutes.

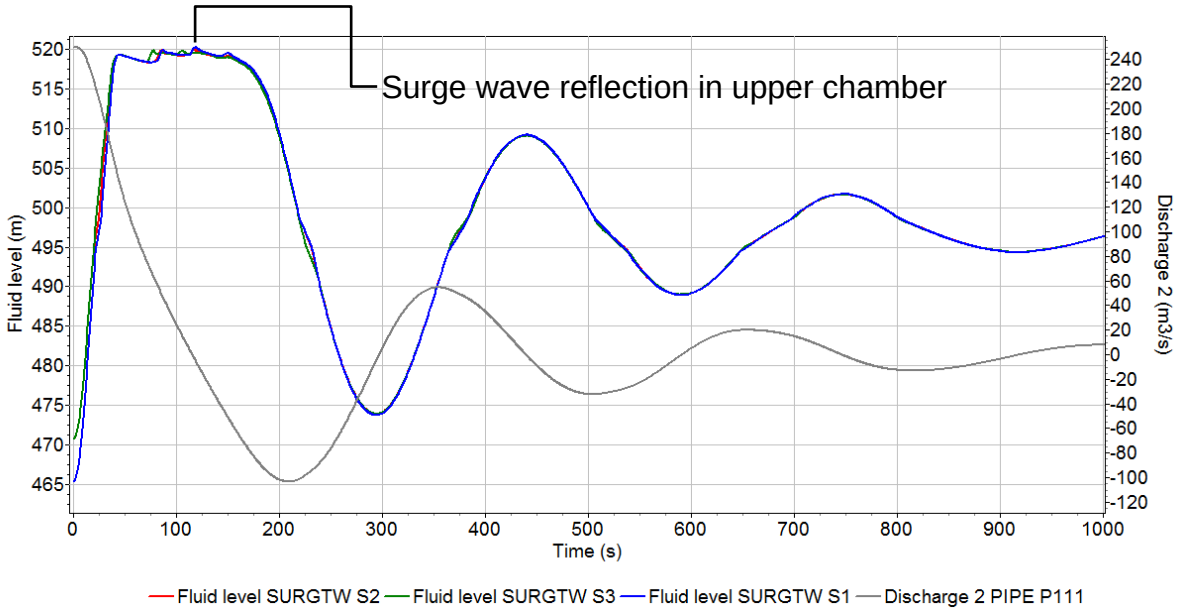

Figure 111: 1D-numerical simulation - Emergency shutdown in 12 sec from 250 m³/s, up-surge in upper chambers

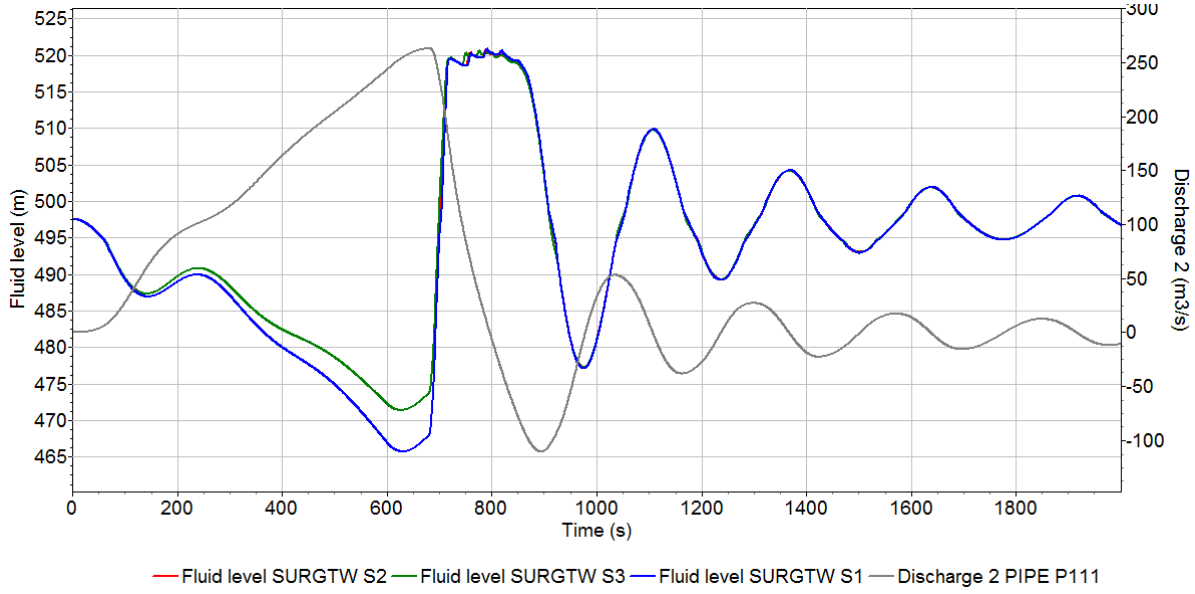

Figure 112: 1D-numerical simulation - Emergency shutdown in 12 sec after start-up in 10 minutes from 250 m³/s, up-surge in upper chambers

7.2 Surge tank geometry of Tonstad power plant

7.2.1 Initial geometry of Tonstad surge tanks

The initial geometry design represents the current state of the surge tank. It consists of the three surge tanks and the associated sand traps and penstocks. In Figure 113, the geometry is visualized.

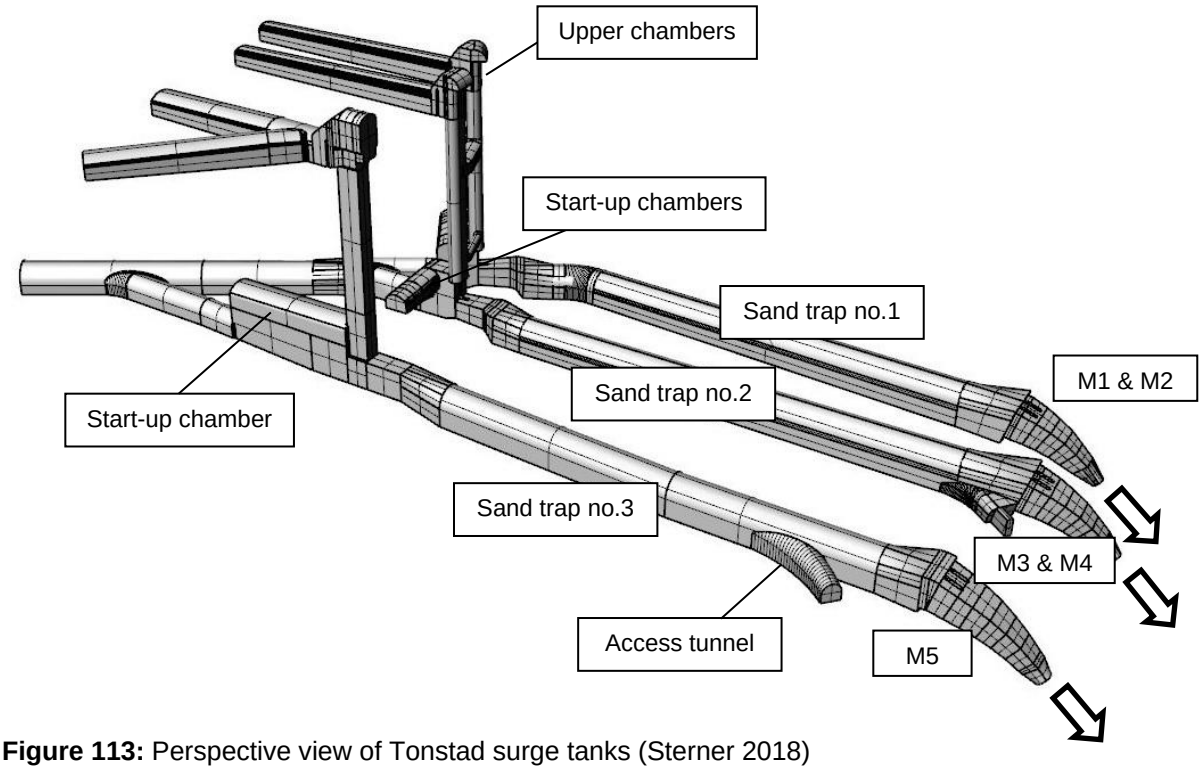

Figure 113: Perspective view of Tonstad surge tanks (Sterner 2018)

Following some of the features of the current state design is described.

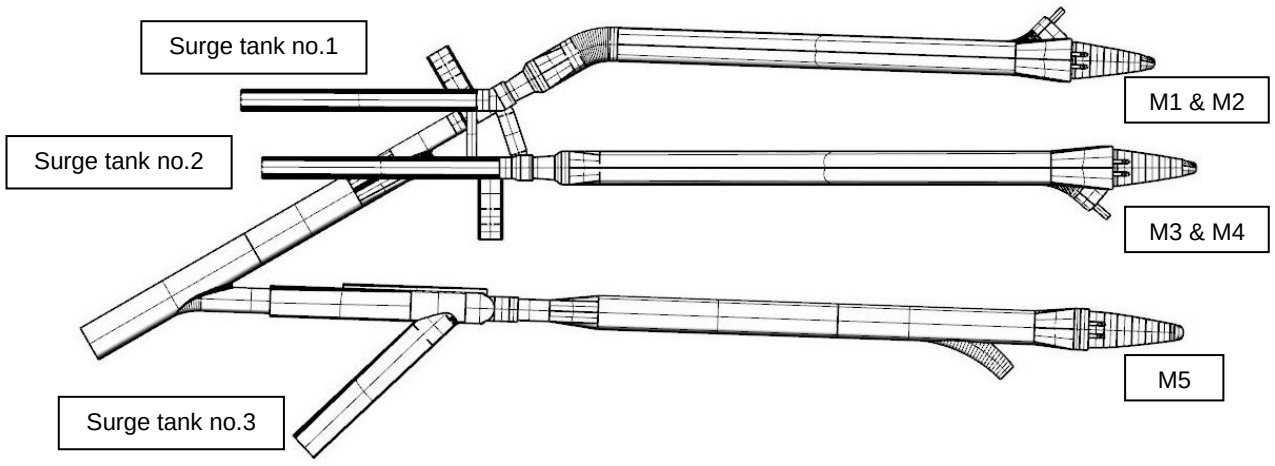

Figure 114: Ground view of Tonstad surge tanks (Sterner 2018)

The system ground view is shown in Figure 114. The main headrace tunnel has a flow area of about 100 m^2. According to the flow direction, the first diversion from the main tunnel is surge tank no.3. After the diversion the main tunnel splits into two separate branches, each branch leading to one of the surge tanks no.1 and no.2. Sand trap no.2 and no.3 follow the direction of the headrace. Sand trap no.1 is an exception, the route of this trap bends parallel to sand traps no.2 and no.3 shortly after the widening of the cross section.

The important elevations of the system are shown in Figure 115. Additional marked is the water level limitation of the current system. This limitation was defined to mitigate the danger of free surface flow in the sand traps. This limitation is the limit water level for steady state flow in full operation. One aim of this work is to find a structural way to avoid this limitation.

For the 3D CFD simulations a reference coordinate system was defined with the origin at 0,0,0 [x,y,z] at the middle of the main tunnel invert. All elevations in the 3D CFD simulations are referring to this coordinate system.

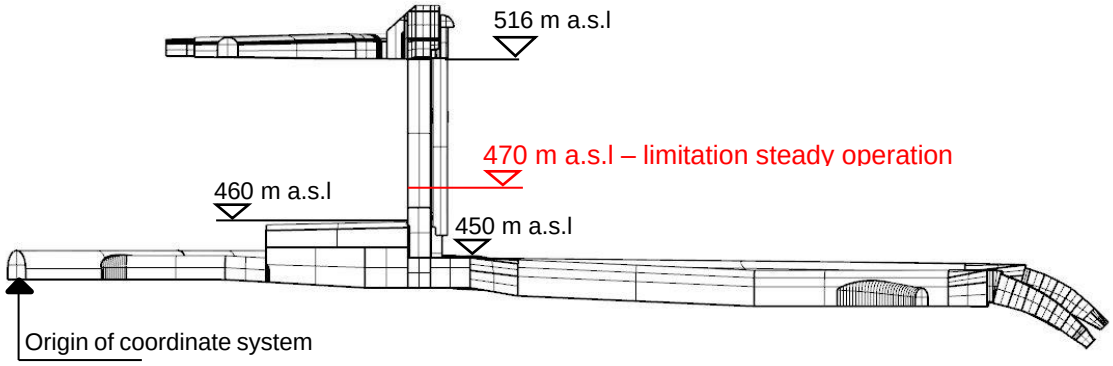

Figure 115: Side view of reference geometry of Tonstad surge tanks with elevations (Sterner 2018)

7.2.2 **Start-up chambers**

The design for surge tank no.1 and no.2 is very similar, the only difference is the orientation of the chambers. The chambers are aligned in a 90° angle to the tunnel axis. The cross sections are shown in Figure 116.

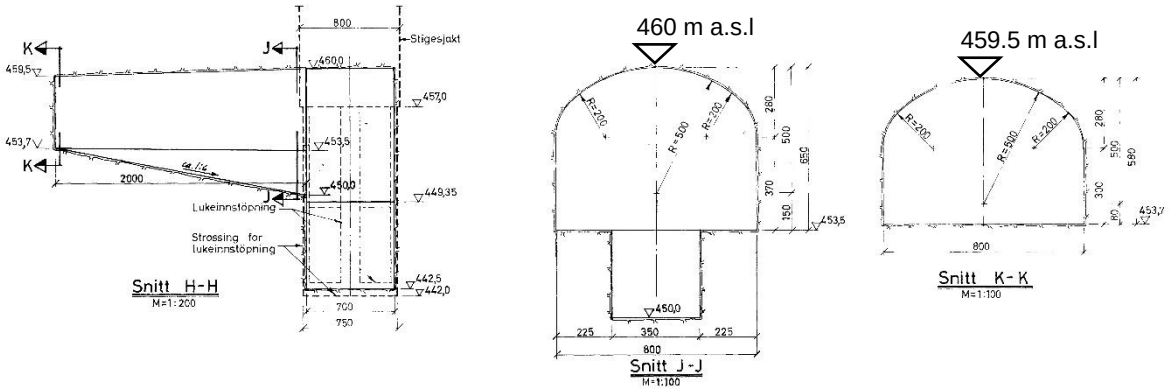

Figure 116: Start-up chamber layout surge tank no.1 & no.2

The design of the start-up chamber for surge tank no.3 is different and constructed as an extension of the lower tunnel cross section and is shown in Figure 117. This shape is somehow disadvantageous regarding an increased possibility of sediment deposition due to decreased flow velocity.

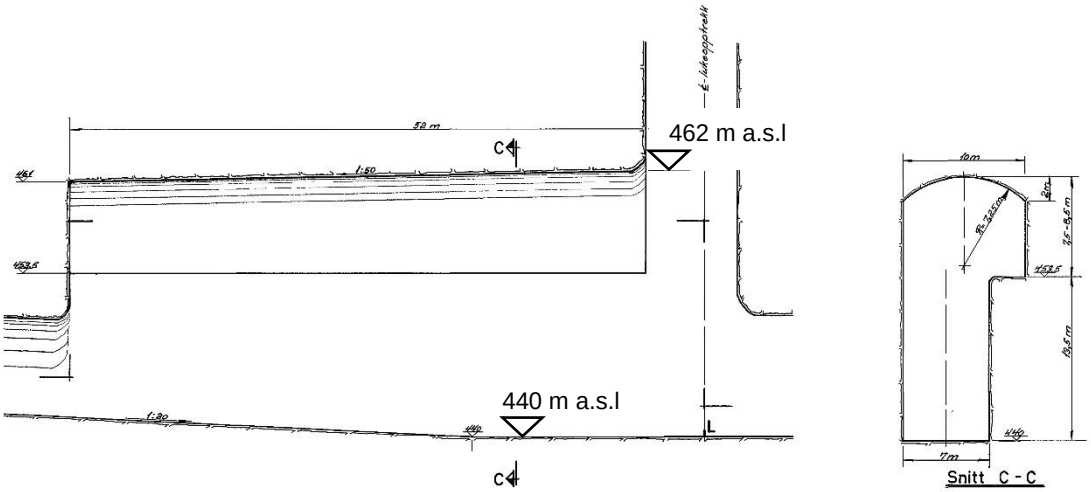

Figure 117: Start-up chamber layout surge tank 3

7.2.3 **Upper chambers**

The shape as well as size of the upper chambers were discussed above. In this part, the focus will be on the design of the throttle in the upper chambers. All upper chambers are equipped with such a throttle at the inlet, only the opening size varies. These throttles limit the run-off into the chamber at filling and into the surge shaft at emptying. The reason for their existence is the fact that the limited run-off into the chamber keeps the upsurge water level higher. The higher the water level in the surge improves the situation for the decelerating of the water mass in the main tunnel in sense of improving the differential effect of the surge tank. The same goes for the other way, the limited run-off back into the surge shaft leads to a lower water level in the shaft that corresponds as pressure level in the system.

The width of the opening is 2.3 m for the surge tanks no.1 and no.2 and slightly larger at surge tank no.3 with the width of 2.5 m. The opening height is from the chamber floor until the maintenance platform. This platform was neglected in the model because it is not attached to water. Obviously is it strictly forbidden that water can overflow the platform.

Figure 118 gives an impression of the throttles, as example only the throttle of one surge tank is shown due to the fact that they are nearly the same for all three.

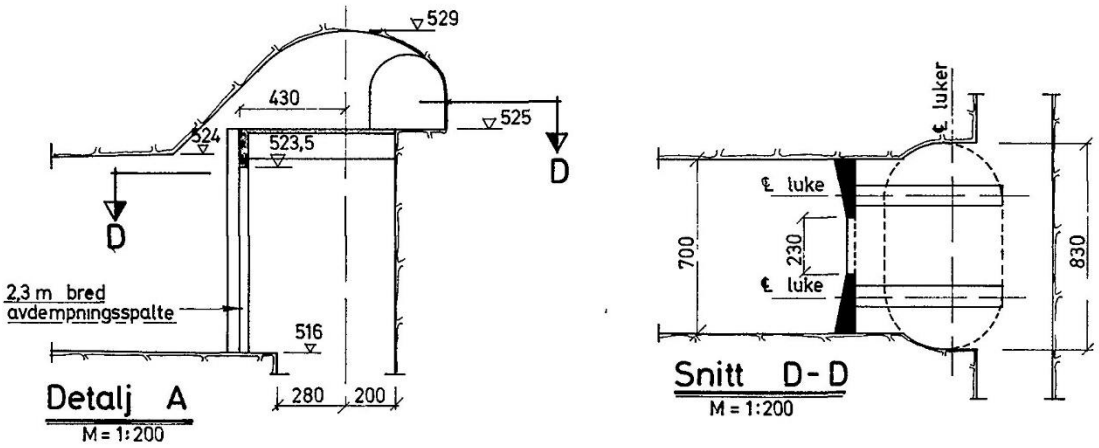

Figure 118: Upper chamber throttle surge tank no.1

7.2.4 **Penstocks**

The penstocks are connected at the end of the sand traps. The inlet edges are about 1.5 m higher than the floor of the sand trap. Due to the position at the end of the sand trap, this space is needed for the deposited material. The two penstocks for the machines M1 & M2 and M3 & M4 have a diameter of 3.7 m and the one for M5, a diameter of 4.8 m. The entries of the penstocks start with a rectangular shape and evolve into a circle shape. Each penstock inlet is covered by an inclined rake (13.5 m by 11 m), which is supported by two pillars. Each pillar has a width of about 1.5 m and extends over the whole cross section. The rake covers as well as the pillars have nearly the same area for all three inlets. The rakes are not modelled because they have little to no effect on the mass oscillation and the investigated issue.

Figure 119 provides an impression of the transition to the penstocks.

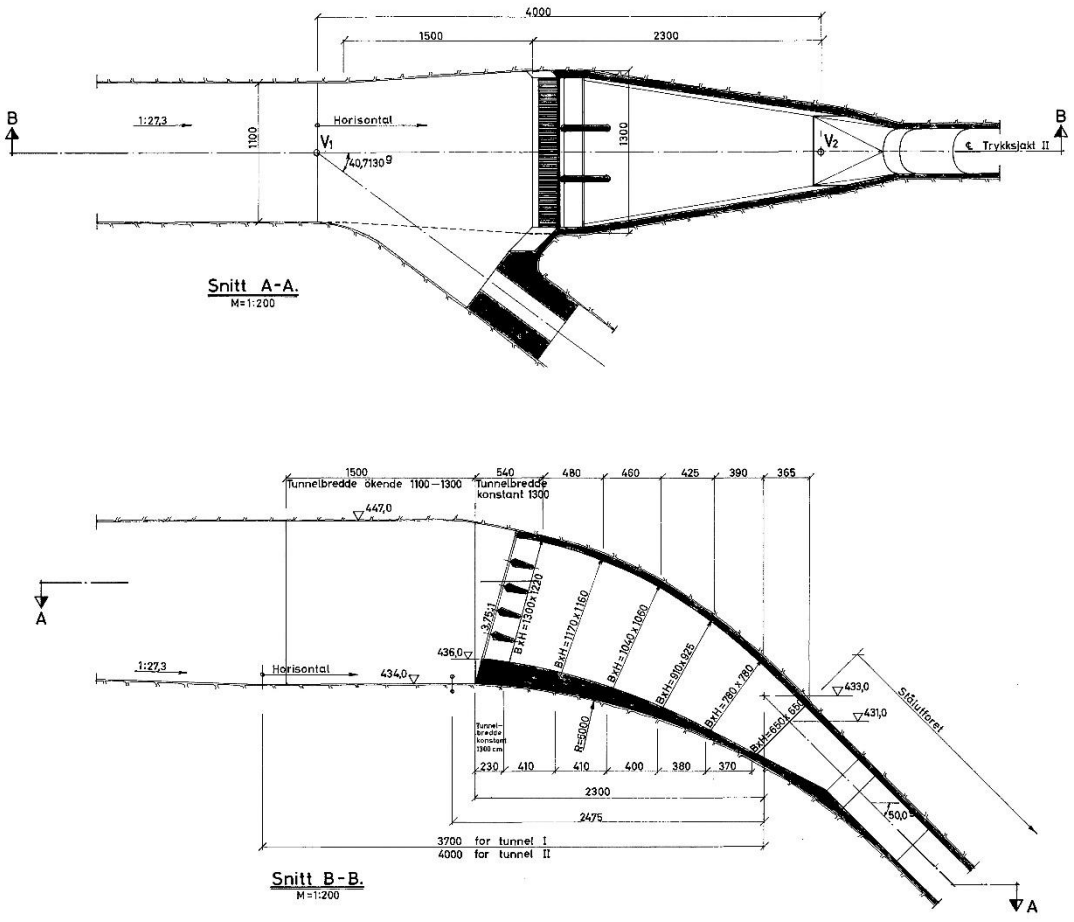

Figure 119: Penstock layout of surge tank no.2

8. Extension chamber for upgrade of headrace tunnel

This chapter describes the findings of the master thesis from (Sterner 2018). In this thesis the approach from the 1D numerical simulations allowing an upgrade of the Tonstad scheme with 25% discharge was applied by introducing the geometry of an extension chamber. The main findings and the main geometry are described below.

Further details regarding the semi-air cushion surge tank are investigated in the FlekS 2.0 report.

Figure 120 shows the result of the 1D numerical simulation applying the extension chamber and running the system with 300 m³/s followed by an emergency shutdown. It shows that the water level drops to about 456 m a.s.l. in all surge tanks. The up-surge due to the shut-down creates an upsurge in to the existing upper chambers, showing still sufficient capacity with this load case. The semi-air cushion (FlekS 2.0 project) is not applied here.

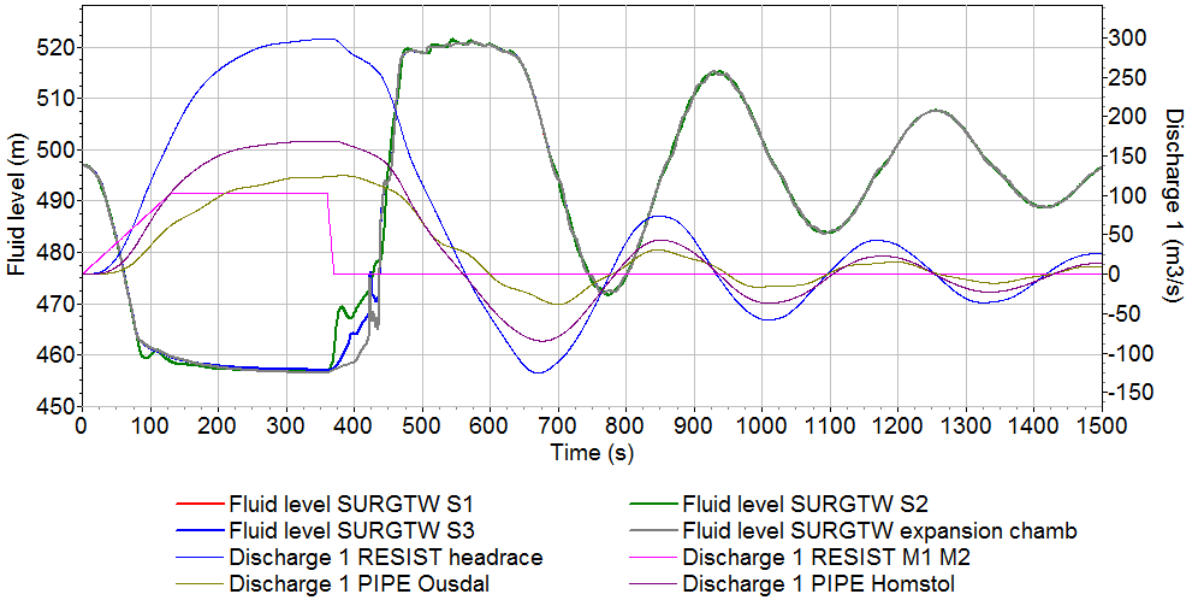

Figure 120 – Result 1D numerical simulaitons – start-up to 300 m³/s – emergency shut down – with extension chamber

8.1 Extension chamber

The final variant of the extension chamber has to solve the filling and emptying demand for the mass oscillation. The lack of sufficient overburden is the reason for the layout that shows a bend upstream as shown in Figure 121.

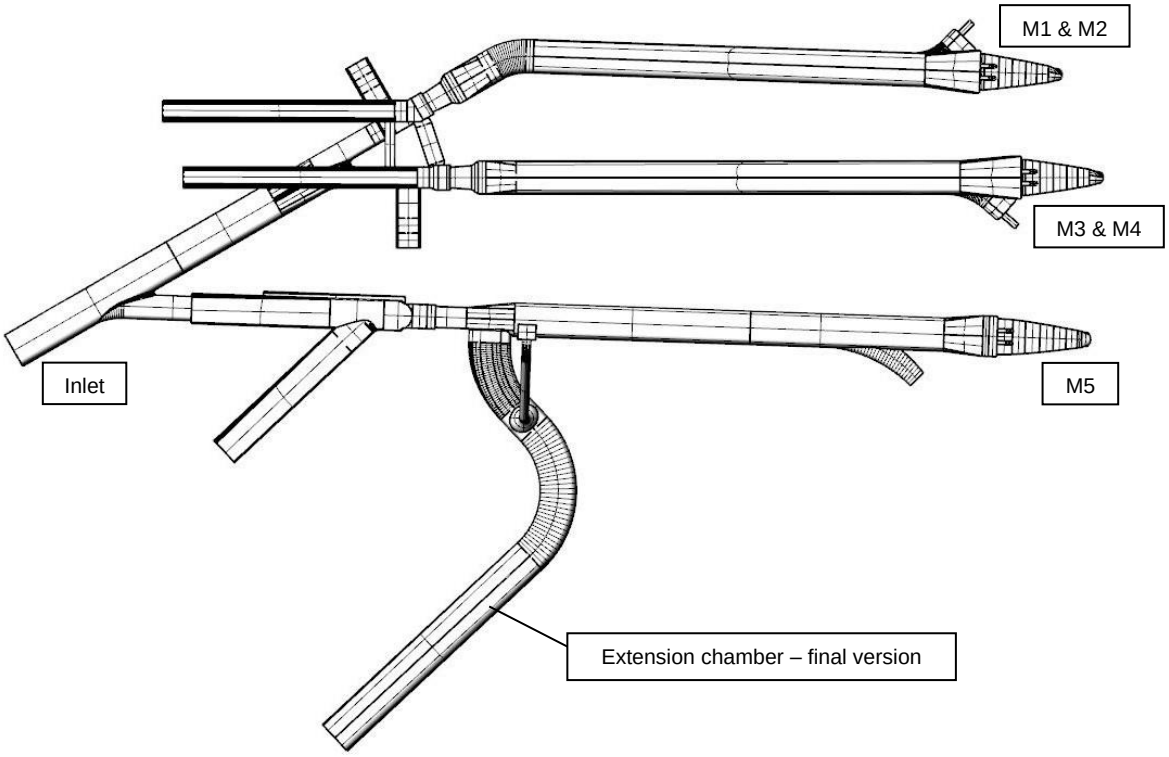

Figure 121 - Ground view extension chamber, ground view (Sterner 2018)

Figure 122 represents the system in a front view and should serve for the sake of completeness. It shows that the elevation of the chamber and the connection to the existing system stayed the same and the only change made is the route.

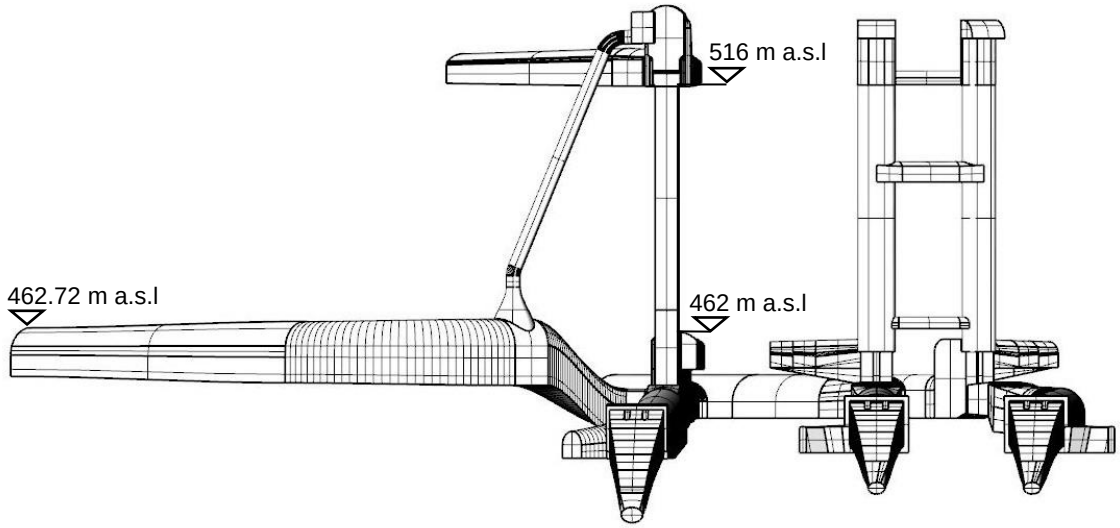

Figure 122 - Front view of the extension chamber (Sterner 2018)

The extension chamber provides a satisfying degree of overburden throughout the alignment. The comparison between the terrain model and the extension chamber is shown in Figure 123.

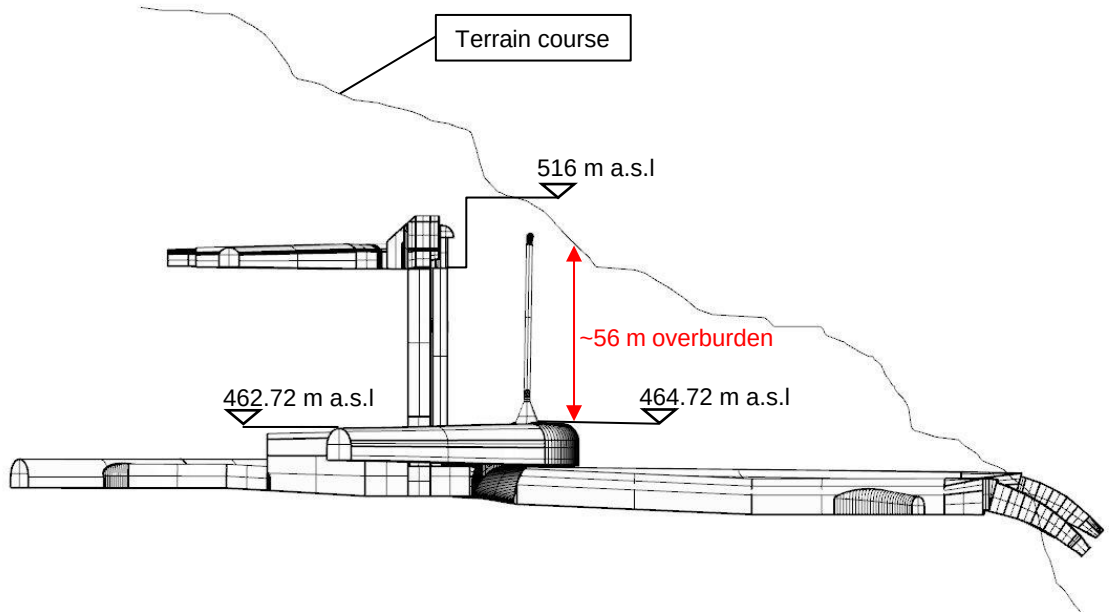

Figure 123 - Comparison of V2 with terrain (Sterner 2018)

The extension chamber at least an overburden of about 56 m. The general procedure would be to construct an unlined chamber with concrete on the bottom.

In Norway, due to the very good rock quality it was already often proven that lower ratios of 1.0 between overburden/internal pressure is possible (Palmstrom 1987) (Kjørholt 1991).

This means that the pressure in the chamber can be slightly higher or equal than the provided coverage, as it is also present in the existing surge tanks. Additionally, it can be seen that the surrounding terrain has a very steep inclination at the end of the sand traps.

8.1.1 **Results and Findings extension chamber**

At the start of the simulation, the hydraulic system shows, that the extension chamber is supplying the full system with water, meaning that the single extension chamber plays a role for all three surge tanks at start-up.

To evaluate the mass oscillation in the surge tank with expansion chamber 3D CFD simulations were undertaken to show and compare with 1D CFD and to develop a suitable surge tank concept.

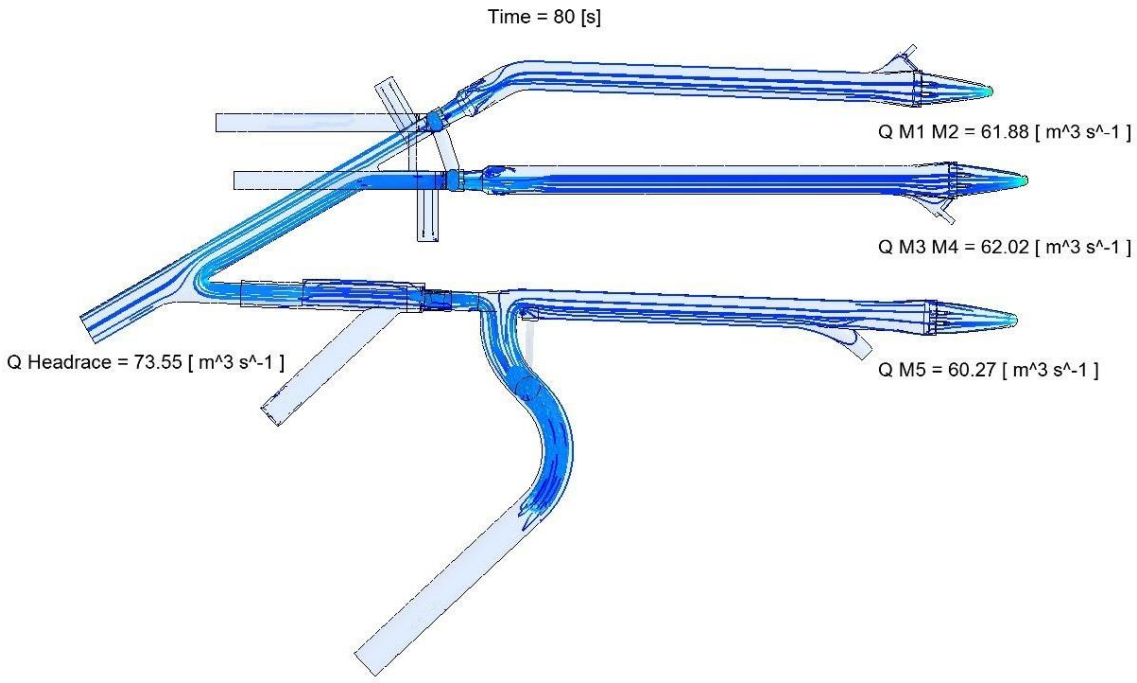

Figure 124 - Streamlines at start-up full system ground view (Sterner 2018)

The turbines are fed on the on side by the reservoirs and on the other side by the extension chamber until full acceleration of the water in the headrace tunnel is completed. This is indicated by the streamlines in Figure 124 originate from the extension chamber as well as from the headrace inlet.

Figure 125 shows a two-minute sequence (120 seconds) showing the effects during the mass oscillation. The start of the sequence is at 360 seconds after the turbine start-up (Figure 125a) and the end at 480 seconds (Figure 125d). It can be seen that at the start of the sequence, the water is only provided by the headrace inlet or reservoirs. This is indicated by the velocity vectors in sand trap no.3.

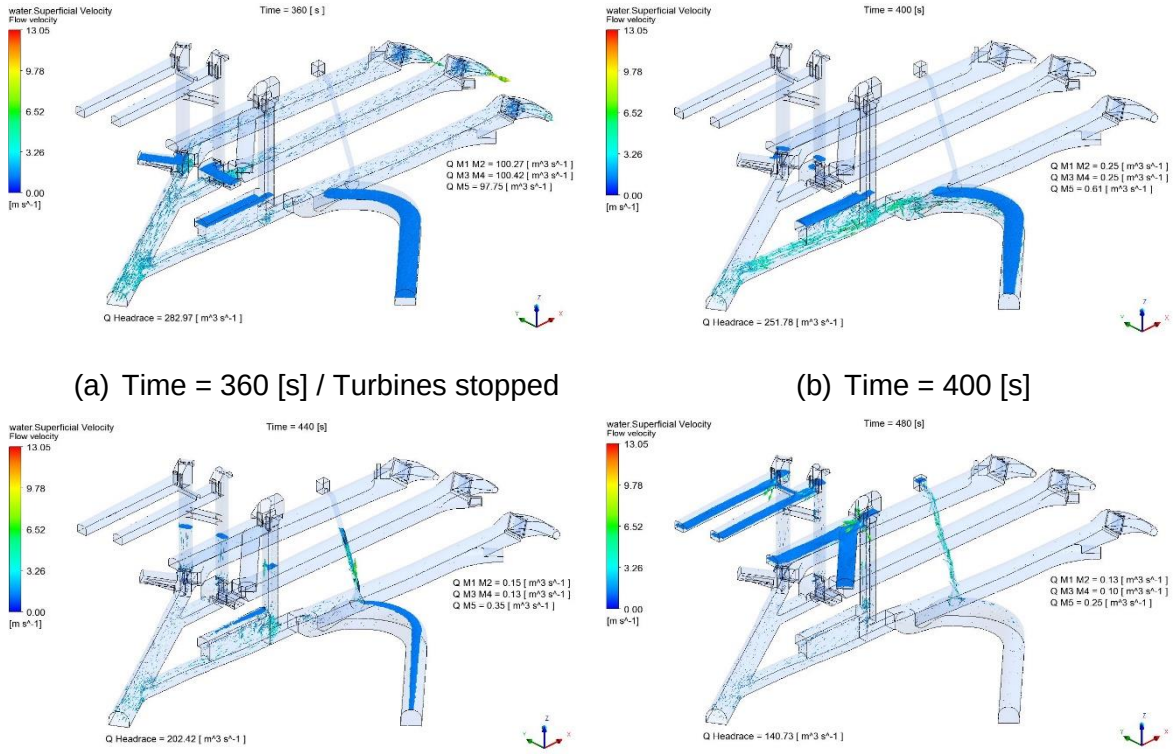

(a) Time = 360 [s] / Turbines stopped

(b) Time = 400 [s]

(c) Time = 440 [s]

(d) Time = 480 [s] / ~max. upsurge

Figure 125 - Sequence of mass oscillation with extension chamber (Sterner 2018)

The upswing can be noticed after 40 seconds of the turbine shut-down (Figure 125b). The rise of the water level is until this time step only limited to the lower chambers. The additional volume of the extension chamber takes on a large portion of the mass oscillation at the beginning. After 80 seconds (Figure 125c) the mass oscillation can additionally be noticed in the surge shafts as well as in the aeration pipe. The maximum upsurge can be seen two minutes after the stopping of the turbines (Figure 125d). The retention cavern is needed, due to the continuing issue of the air water mix spraying. The widening of the diameter of the aeration pipe does not provide the desired result indicated by the relative high-water level in the cavern.

On the basis of these observations it is needed to investigate the issue of the air water mix further. The forming of the air water mix can be best seen at the time step of 440 seconds. The result of the air water mix is shown at the time step of 480 seconds. Therefore, a time step between these two is picked to explain the development.

Figure 126 represents the time step of 460 seconds and illustrates the evolving air water mix in the combined air-water riser.

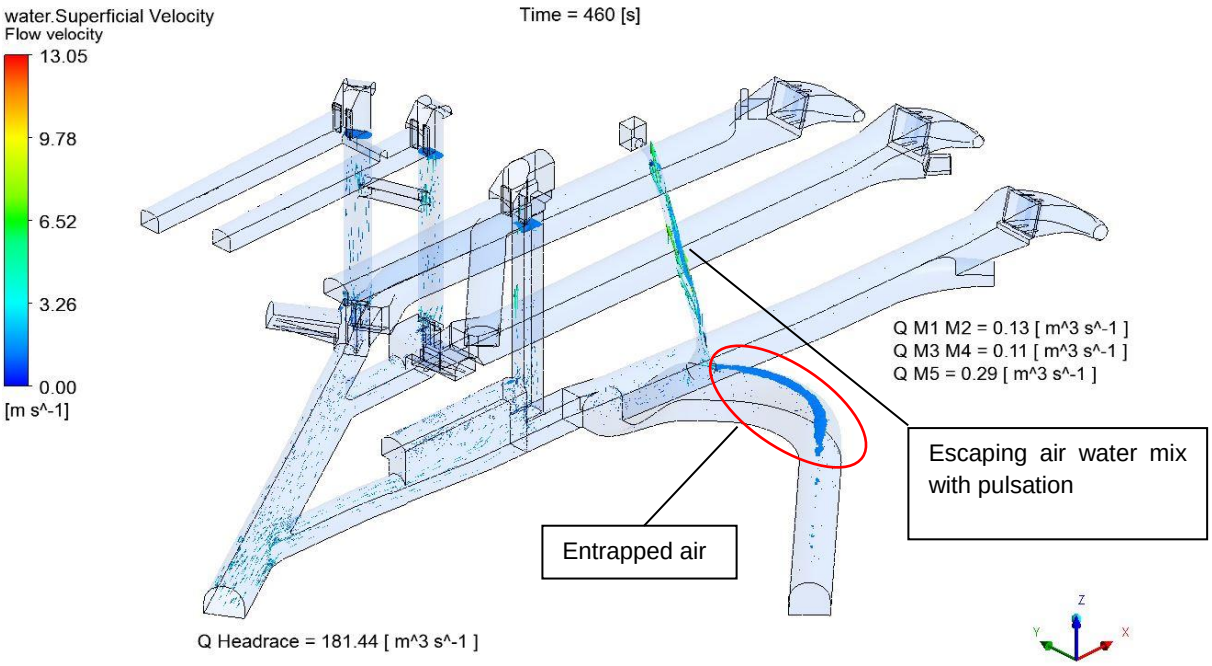

Figure 126 - Development of the air water mix spraying (Sterner 2018)

During the rising of the water level air gets entrapped in the extension chamber crown. This is a very natural behavior since the crown is not steep inclined. In addition, the surge wave influences the creation of entrapped air. The surge waves move towards the end of the chamber and get reflected at the end. These waves push some amount of air in front of them due to the reflection. This leads to a pulsation effect at the aeration cone. This effect is amplified by the oncoming waves due to the entrapped air. The pulsation in combination with the amplification leads to the unsteady air-water release in the pipe. This is seen to make no damages but also is not a beneficial and desirable property.

These findings show that there is need for improvement, especially for the aeration pipe. The additional results show that an ongoing widening in small steps of the pipe diameter is not straightforward, since the idea is to keep the aeration pipe as small as possible. The problem is the entrapped air in the rear part of the extension chamber.

8.2 Extension chamber – separation of air and water riser

The results above show that there is need for improvement according to the water-air mixture flow in the aeration pipe. The taken measures up to this point are not sufficiently solving the problem with the air water mix spraying out of the pipe. Further considerations on the issue lead to the introduction of an aerated crown throttle.

8.2.1 Aerated Crown throttle

By the simulations above, it was found that the effect of the pulsating air release and significant spraying (geyser effect) has its roots in the entrapped air in the rear part and along the chamber crown. This entrapped air causes a sloshing of water into the aeration cone at the beginning of the chamber. The resulting spraying effect is based on the pulsation of the surge waves and the accompanied amplification due to the high interval of the waves. Based on these investigations, a structure was developed to mitigate the surge waves, which results in a decreasing of the sloshing effect. The concept is to place a bar shortly after the aeration pipe. In the following is this bar referred as crown throttle. The throttle reduces the cross section of the chamber and creates a large cavity behind, that is only de-aerated by a small pipe (Figure 127).

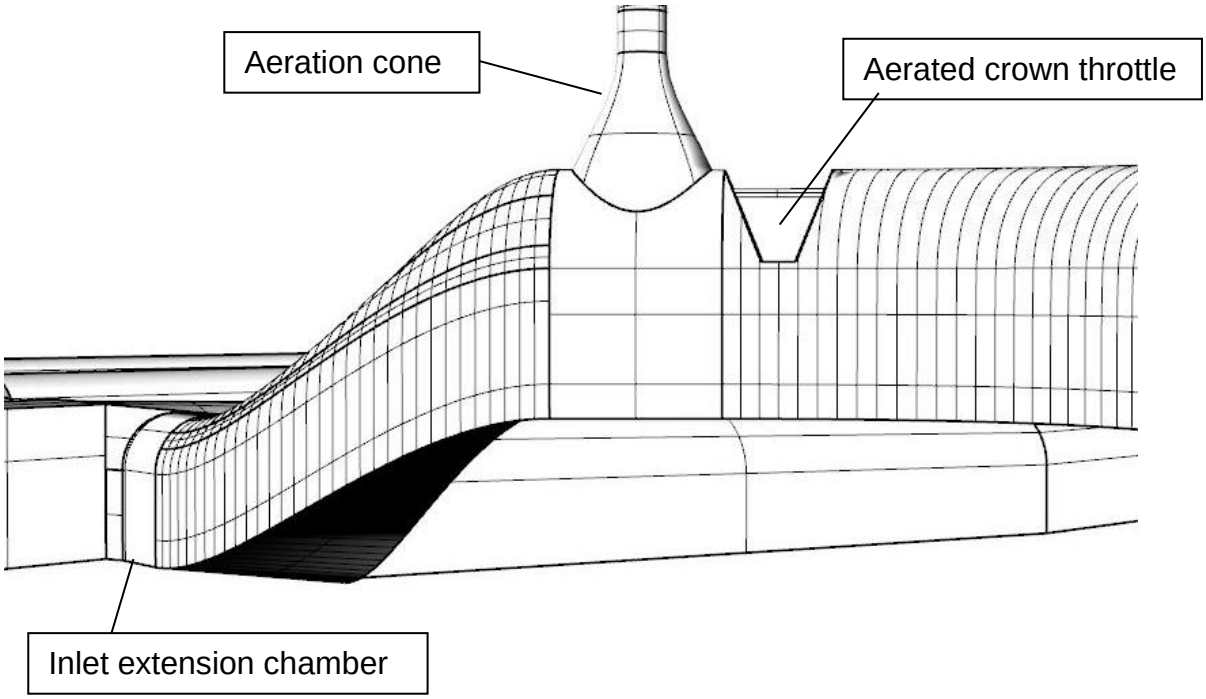

Figure 127 - Aerated crown throttle in side view (Sterner 2018)

The crown throttle has a trapezoidal shape and gets pierced, as shown in Figure 127, by a round opening (DN 500). The opening is needed to aerate the resulting rear part of the chamber. The dimensions of the crown throttle as well as the elevation at the top are shown in Figure 128. This design is a first and principal design proposal.

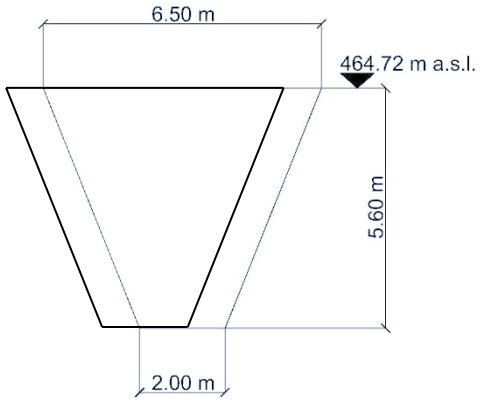

Figure 128 - Cross section of the crown throttle **(Sterner 2018)**

The crown throttle has an influence on the overall process of the mass oscillation. Not only is the effect of the sloshing and the combined spraying of the air water mix influenced. Additional is it investigated that the extension chamber in some way shares effects which else can be found at the upper chambers. This way the crown throttle improves the differential effect of the surge tank system with the extension chamber. The rather small de-aeration opening creates a so-called semi-air cushion in the rear part which has a significant impact on the water level in the inlet area of the chamber. The effect of the semi-air cushion will be further explained in the following analysis of the simulation results.

8.2.2 **Results and Findings with crown throttle**

The impact of the crown throttle can be noticed right at the beginning of the simulation. The separation into two parts, a front and rear one, of the chamber can already be noticed after a short period of time (Figure 129).

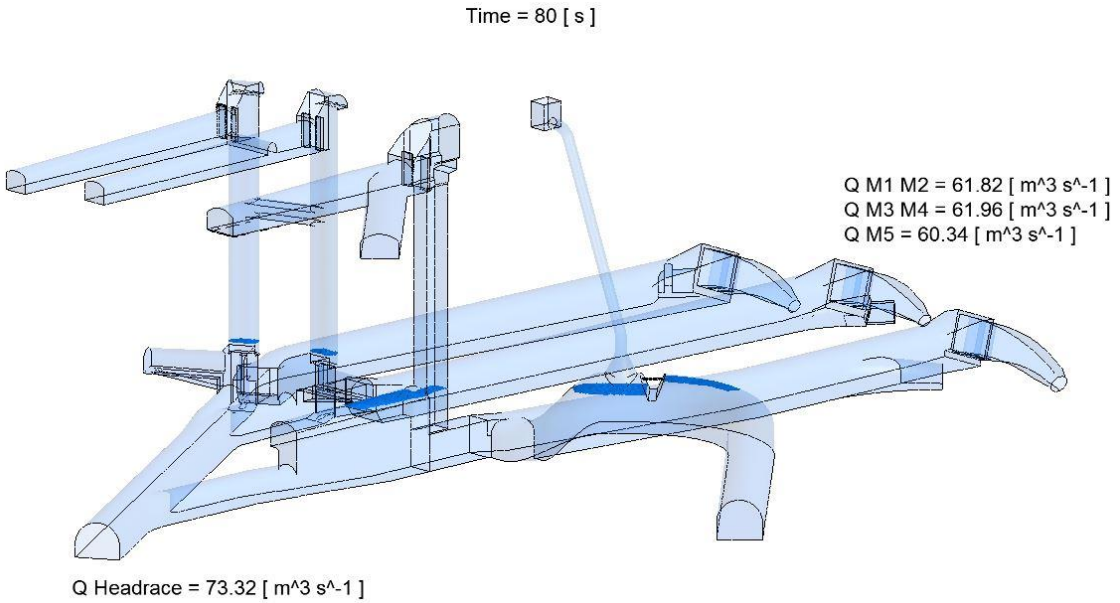

Figure 129 - Effect of crown throttle at start-up, extension chamber with crown throttle (Sterner 2018)

The extension chamber provides water for all three start-up chambers. After about 80 seconds (Figure 129) is the water level lowered to a point where the extension chamber parts into two sections. The water level at the aeration pipe in front of the throttle is lowered faster due to the bigger area of the connection to the existing system. The rear water level stays at a higher level and the flow situation approaches to an outflow under a gate. The reduced cross section leads to an acceleration of the outflow below the throttle. The flow velocity is higher until the point where the water levels are balanced out between the two parts. After the balancing, the level is lowered over the whole route of the chamber. This observation already gives consensus with the considerations of the semi-air cushion effect during the mass oscillation.

The previous simulations stated already that free-surface flow in the sand traps is avoided at any point. This is also the case for the extension chamber with the additional installed aerated crown throttle.

8.2.3 **Semi-air cushion effect**

The semi-air cushion effect is best explained at the first upswing of the mass oscillation. The upswing starts after the closing of the turbines at 360 seconds and can be noticed by a differential filling of the parts before and after the crown throttle. Figure 130 shows a two-minute sequence with steps of 40 seconds.

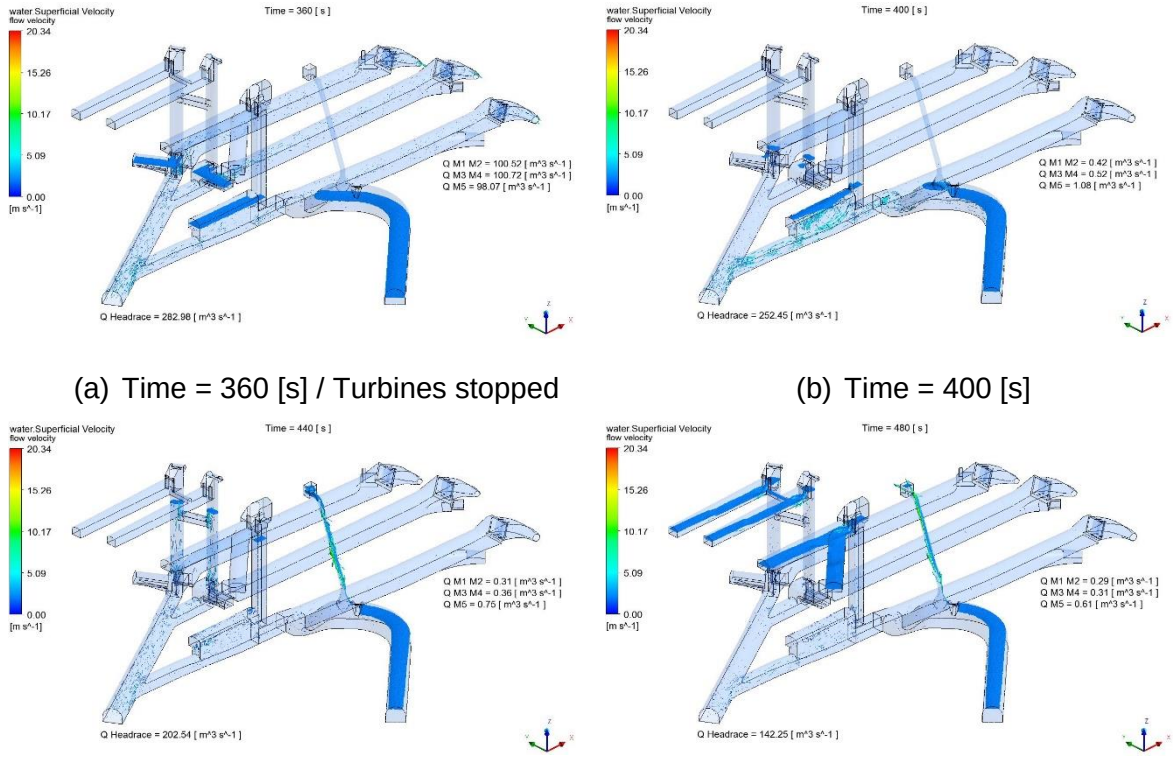

(a) Time = 360 [s] / Turbines stopped

(b) Time = 400 [s]

(c) Time = 440 [s]

(d) Time = 480 [s] / ~max. upsurge

Figure 130 - Sequence of mass oscillation, extension chamber with crown throttle (Sterner 2018)

Figure 130a shows that the water level is at its lowest just as the turbines are shut. The lowest water level is the same as for the foregoing simulations due to the fact that the dimension of the chamber is not changed and that the input data for the transient load case is the same. The water level is rising in the whole system simultaneously until the crown throttle is reached. After surpassing the bottom of the throttle, the water level in the rear part is rising at a slower rate than in the front part due to the limited discharge of air through the throttle. This behaviour creates a pressure inside the semi-air cushion. The semi-air cushion can be seen as fully adiabatic because the time exposed is relatively short. This means no significant heat exchange with the rock. The rising of the water level in the system can be seen in Figure 130b and Figure 130c. In both figures, the mentioned effect of the limited run-off can be seen, indicated by the different water level with respect to the level in the rear part of the chamber. The maximum upsurge at the system noticed is shown in Figure 130d. At this point it can be observed that the extension chamber somehow works just the same as the upper chambers – except the pressure by elevation it is an air pressure that is creating the delayed filling. The limited run-off at the upper chambers generates a higher water level in the surge shaft. The same effect can be seen one to one at the crown throttle.

The water level in the front part is much higher than in the rear part. Therefore, an additional water mass is provided that helps to slow down the flow in the main tunnel. The term semi-air cushion for this effect is based on the small de-aeration opening. Due to this, the volume can be used instead of volume in an upper chamber. This way the semi-air cushion increases the safety of the upper chamber volume.

The sequence of the mass oscillation shows that the issue concerning the spraying of the air water mix out of the pipe into the cavern could not be fully eliminated. But the air escape with spraying and pulsation was significantly mitigated. The semi-air cushion effect based on the throttle has such a positive impact on the system that it nearly overshadows this fact. The sloshing of the water into the aeration cone is fixed but due to the changed pressure situation the aeration pipe needs to be revisited.

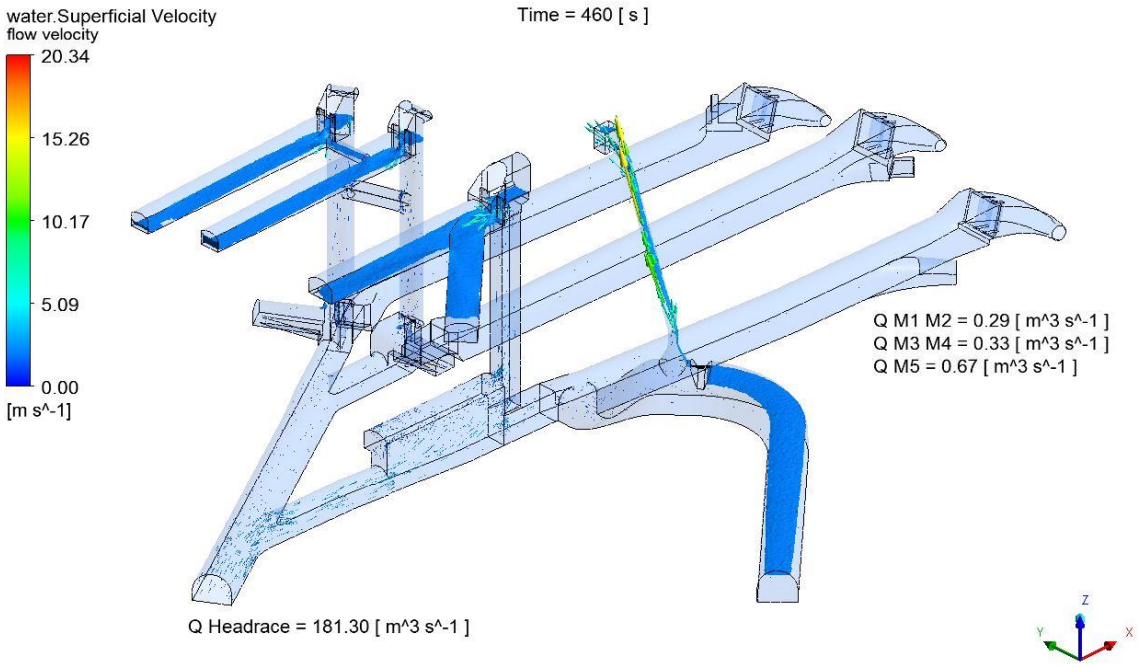

Figure 131 - Maximum upsurge after 460 seconds, extension chamber with mixed air – water riser (Sterner 2018)

Figure 131 shows the system at the maximum upsurge. It shows that the velocity of the air water mix in the ventilation pipe is very high. This leads to the assumption that the air needs to be fully separated from the water. The rising water level compresses the entrapped air in the chamber. The rather small opening (DN 500) leads to the forming of an air jet at the aeration opening. The air jet blasts the water into the ventilation pipe and upwards resulting in a higher water level in the aeration pipe and further on in the spraying of the air water mix.

It appears that the solution for this problem is an independent aeration for the rear part of the chamber. An additional aeration pipe generates two separate air situations in the chamber. The generating of an air jet due to the compressed air is therefore eliminated. During the mass oscillation, the pipe only has to transport air and the aeration of the front part only has to aerate the small front section.

8.3 Results of extension chamber with separated air and water riser

The situation for the extension chamber design with separated air and water riser during the start-up of the turbines is equivalent to the variant above. A negative effect due to the flow diffusor cannot be noticed. The lowering of the water level happens almost in the same way as for variant with combined air water riser. In Figure 132 the system is shown at the time step of 80 seconds after the start of the simulation. The turbines are starting up and the water in the headrace gets accelerated.

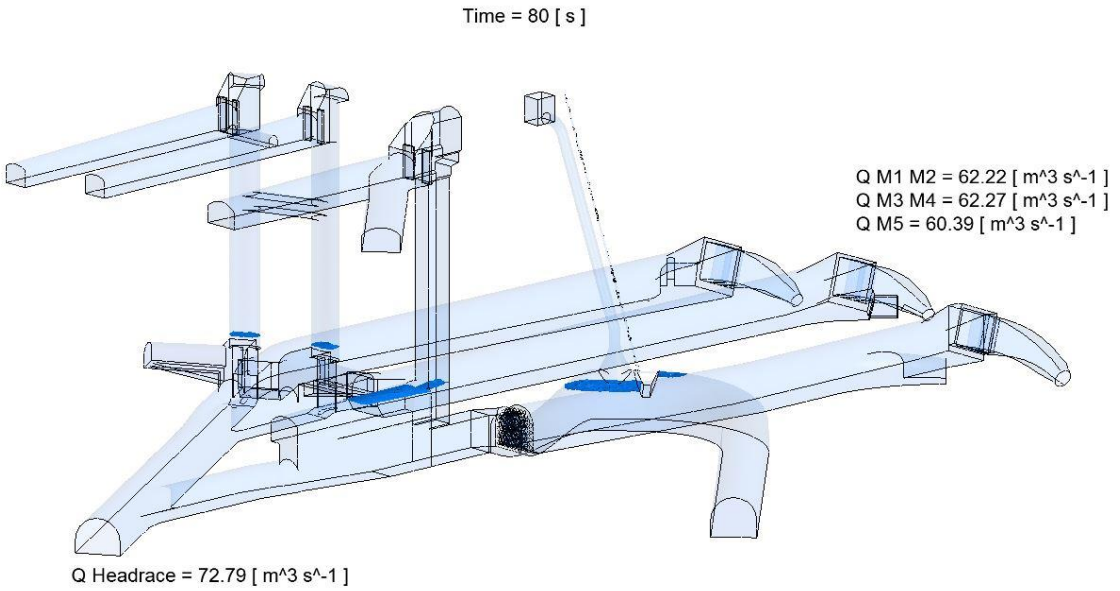

Figure 132 - Water level at start-up, extension chamber with separated air and water riser (Sterner 2018)

As above, the mass oscillation is investigated over a time sequence of two minutes, starting at the exact moment were the stopping of the turbines is initiated.

The Figure 133a represents exactly this moment. The water level is at its lowest and is high enough to ensure no free surface flow in the sand traps. The additional installation of the flow diffusor has therefore no significant impact in the case of steady operation. Although the effect of potential inlet vortices has to be studied more in detail. The water level starts to rise due to the stopping of the turbines, this situation can be seen in Figure 133b. The semi-air cushion effect behaves exactly the same as in variant with mixed phase risers of the system. The impact of the additional aeration pipe for the rear part of the chamber can be seen just 40 seconds after the stopping. Figure 133c shows that the positive effect of the extra aeration pipe lasts on for the whole upswing event. The water levels are nearly the same in all three surge tanks and in the aeration pipe of the front part. In Figure 133d the system is shown two minutes after the stopping of the turbines. Nearly the maximum water level in the system is reached. The system shows over this two-minute sequence no negative effects or situations.

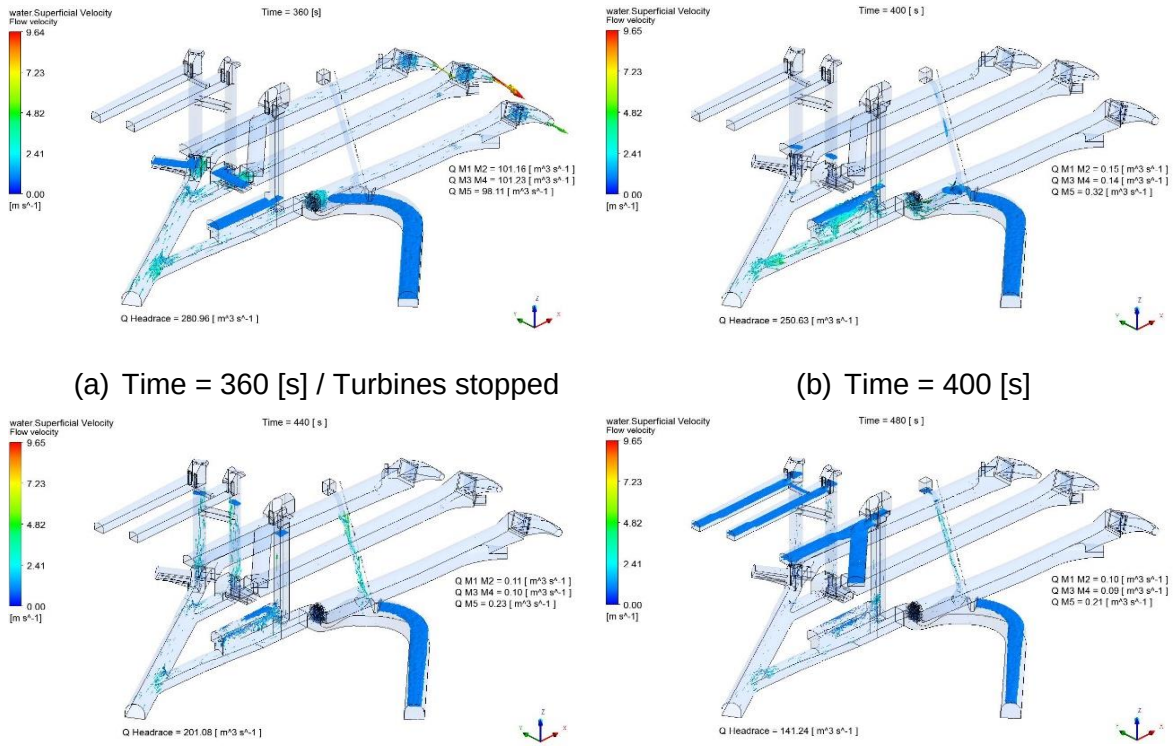

(a) Time = 360 [s] / Turbines stopped

(b) Time = 400 [s]

(c) Time = 440 [s]

(d) Time = 480 [s] / ~ max. upsurge

Figure 133 - Sequence of mass oscillation, extension chamber with separated air and water riser (Sterner 2018)

The point of the maximum upsurge is reached at about 460 seconds and can be seen in Figure 134. This time step is further analysed to make a statement about the additional aeration pipe and the retention cavern.

The main aeration pipe works very promising without pulsations and water spraying. Also, the small extra aeration pipe functions very well. Although, still some spraying can be detected. The solution for this is that the extra pipe will be bended inside the small retention cavern. Thus, water is kept in the system without any spill and air can fully access the pipe and the air cushion.

The retention cavern is still necessary which can be seen in Figure 133d and Figure 134. In both figures is the floor of the cavern covered with water.

The positive effect is that the amount of water sprayed or spilled into the cavern is much lower than before. The size of the retention cavern is sufficiently large.

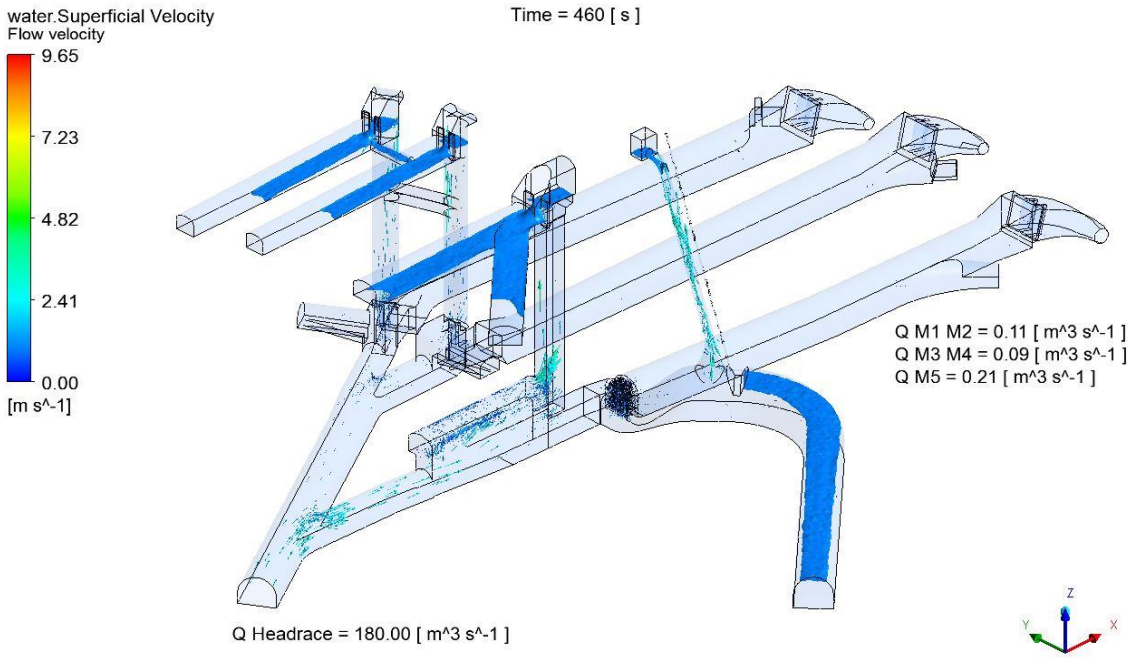

Figure 134 - Maximum upsurge after 460 seconds, extension chamber with separated air and water riser (Sterner 2018)

The simulation of the variant with separated air and water pipes shows that the combination of an upgraded discharge and sand trap is compatible and realisable. The flow diffusor is just one structural measure from the preliminary results. The next step would be to implement more of the structural measures of the preliminary results and further investigate the effects in a bigger scale than just for the sand trap no.3.

Figure 135 shows the comparison of the 1D simulations and the 3D simulations. A very well accordance can be seen. The difference and shift in some simulations with the crown throttle show the positive behaviour onto the mass oscillation. Three effects can be identified.

1. Faster down surge due to the crown throttle to faster accelerate the mass flow
2. Faster upsurge to faster react on the flow to slow it down
3. Volume of the semi-air cushion to be used instead of upper chamber

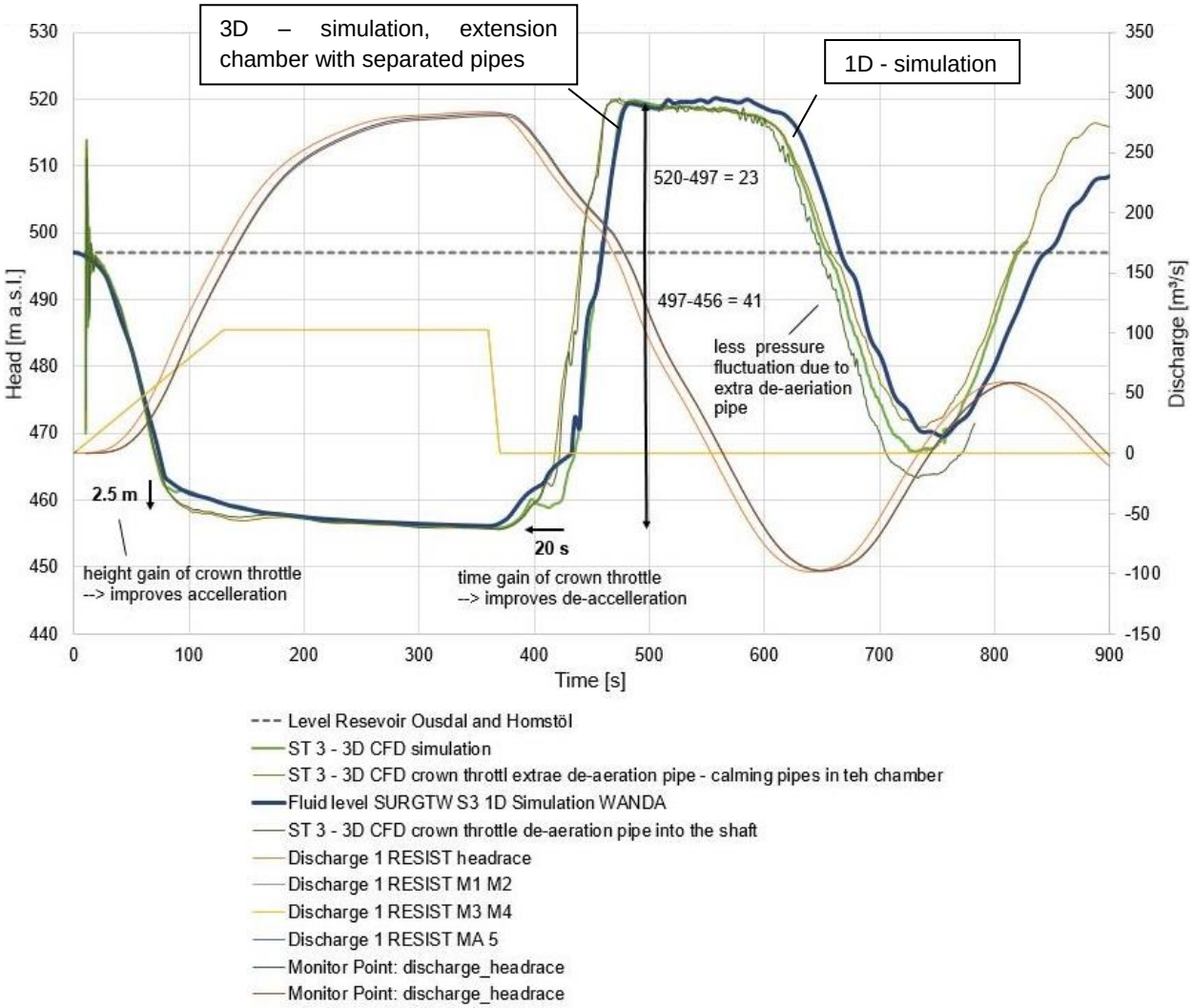

Figure 135 - Comparison of 3D and 1D simulation at the example of, extension chamber with separated air and water riser (Sterner 2018)

9. Suggestions for further steps and Improvements on sand trap

This chapter describes some specific findings and discussions as input for the FlekS 2.0 project.

The 3D CFD simulations of the original no 3 sand trap with potential geometry measures has shown that such measures can significantly improve the settling behaviour of the sand trap. Also, the measures of possible automated sluicing are included in the considerations of the geometrical measures. Two possible geometric measures at the bottom are investigated. First a middle trench with baffles (V3) that guide the flow and the sediments to the middle trench and secondly a 35° inclined trench where sluicing facilities can be placed. Especially a flow calming structure has positive effects on the flow inside the chamber. It was found and suggested to use steel pipes with about 1m diameter as flow calmer to support the diffusion effect for the jet coming from the gate flow.

The placing of the flow calming device is suggested be around 8 m after the unlined section has started.

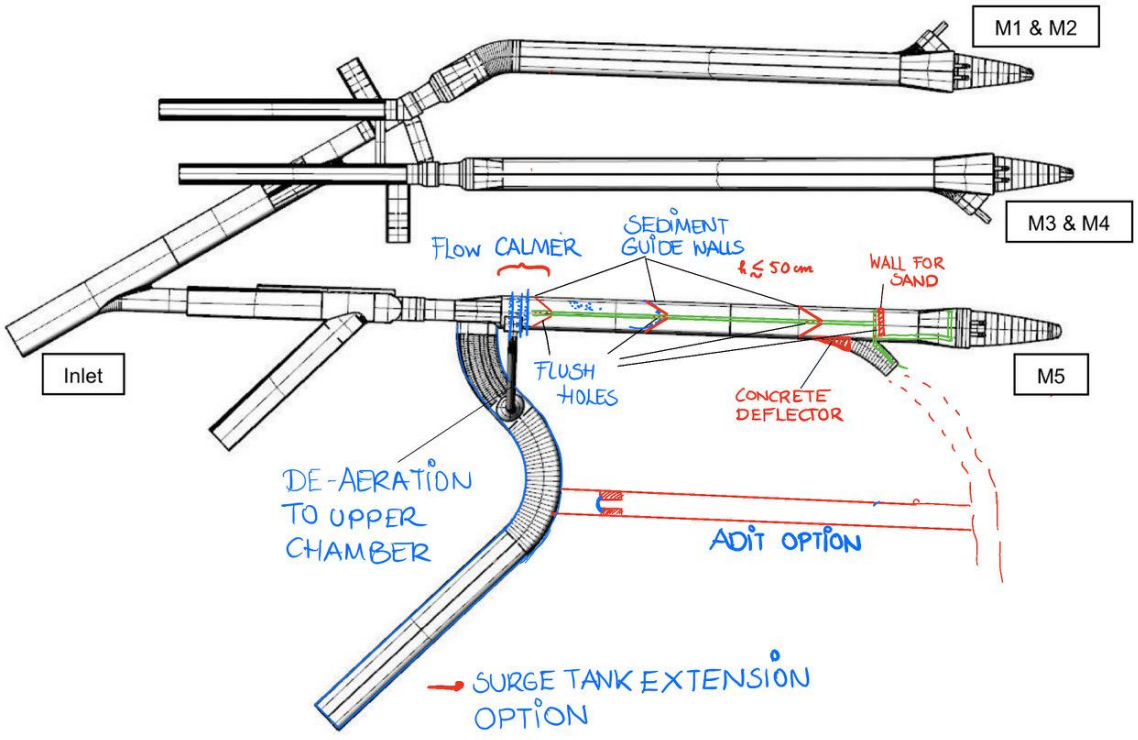

Figure 136: Suggestions for possible combined upgrade and sand trapping

1) Suggested steps that are promising for further improvements:
- Flow calming device
- Wall or deflector in front of the access tunnel to keep the main profile constant

2) Discussion suggestions for the sediment trapping and efficient removal:
- Sediment guide walls or guiding blades to lead the sediment into the centre of the sand trap
- Flushing pipes with holes near the sediment guide blades → functionality of the sluicer has to be discussed with the manufacturer
  - ➔ If this works I think no shear plates are necessary
  - ➔ If critical sediment can be removed before entering the turbine there will always be some sediment in the trap between the blades in order to locally reach transportation equilibrium, the rest is flushed out but does not harm the turbines, filters or influences leaking water
- A sediment wall at the widening section for efficient sand grain exclusion with direct flushing pipe

3) Optional aspects including the upgrade:
- Surge tank extension chamber to allow more discharge and power output of Tonstad plant
- Adit to this surge tank extension can substitute the existing access so that traffic does not intervene the sand trap facilities

Figure 137: Suggestion of concrete wall wedge to keep the flow patter equally to improve sedimentation

10. Conclusions and Summary

Tonstad hydropower power plant has been investigated in terms of 3D CFD and 1D numerical simulations. The main focus was the pressurized sand trap no. 3 at this power plant, with a design discharge of 80 m³/s for turbine no. 5.

The sand trap has encountered problems with sediments. The 3D CFD simulations with transient RANS approach could show and prove with indirect results (wall shear) and direct results (particle tracking) the movement of sediments in the chamber. With the 3D CFD RANS approach and rough walls in the simulation the transient flow effects of the jet resulting from the gate restriction could be resolved according to measurements in the prototype.

A major impact on the case study sand trap is the predominant jet flow from the gate section of the upstream surge tank creating a significant back flow zone.

Several structural variants were investigated in terms of 3D CFD with particle tracking to mitigate the sediment transport. Particle tracking method was found to be a very helpful tool to support hydraulic investigations with sediments involved.

Three ribs variants were investigated in terms of 3D CFD particle tracking simulations. It can be shown that particles settle in the sand trap accordingly as without the ribs. Significant flow velocity is still observed underneath the ribs. Further investigation during a 1:36.67 scaled hydraulic model test (Fleks 2.0) shows the inefficiency of ribs only. There, only a few ribs at the end of the sand trap are found to be efficient to trap sediments by adding a ramp that guides the flow over the ribs and allows absence of significant flow underneath the ribs to trap sand and gravel if transported. The 3D CFD simulation above with particle tracking also show the significant bed load transport of sediments underneath the ribs.

By 1D numerical simulations and the proposal of an expansion chamber it can be shown that the headrace tunnel system of Tonstad power plant can be upgraded by 25% discharge, leading to 20% potential power upgrade.

For the potential upgrade a new surge tank type; the semi-air cushion surge tank (semi ACST) has been proposed. Further results and design proposals were conducted in FlekS 2.0 report.

Questions and suggestion resulting from the hydraulic investigations from this report have led to further investigations presented in FlekS 2.0 report.

11. Bibliography

Bråtveit, K., and N. R.B. Olsen. “Calibration of Horizontal Acoustic Doppler Current profilers by three dimensional CFD simulations.” *Engineering Applications of Computational Fluid Mechanics*, 2015.

Bråtveit, K., L. Lia, and N.R.B. Olsen. “An efficient method to describe the geometry and the roughness of an existing unlined hydro power tunnel.” *Energy Procedia 20 (2012)* , 2012: 200 – 206.

Brevik, Oddmund. *3D numerisk modellering av deler av vassvegen til Tonstad kraftverk.* Master thesis NTNU, Trondheim, 2013.

Giesecke, Jürgen, and Emil Mosonyi. *Wasserkraftanlagen, Planung, Bau und Betrieb.* 5. Auflage: Springer Heidelberg, 2009.

Kjørholt, H. “Gas Tightness of Unlined Hard Rock Caverns.” Dissertation: NTH Trondheim, 1991.

Møller, Inge. *Norwegian dams, volume I.* Oslo: Energi Forl, 2009.

Palmstrom, Arild. “Norwegian design and contruction of unlined pressure shafts and tunnels.” Oslo: Proceedings of the International conference on Hydropower, Norway, 1987.

Schiller, L., and A. Naumann. “Über die grundlegende Berechnungen bei der Schwerkraftaufbereitung.” *Zeitschrift des Vereines deutscher Ingenieure*, 1933: Leipzig.

Sira-Kvina Kraftselskap. *Tonstad kraftverk.* n.d. https://www.sirakvina.no/ tonstad-kraftverk/tonstad-kraftverk-article260-919.html (accessed October 18, 2017).

Sterner, L. *3D CFD Simulations for Tonstad Surge Tanks Upgrade, Master Thesis, Graz University of Technology.* Graz, 2018.

Vereide , Kaspar, Wolfgang Richter , Leif Lia , Tom Jacobsen , and Ola H Havrevoll. “Upgrading of Sand Traps in Existing Hydropower Plants.” Sevilla: Proceedings of the Hydro conference, 2017.

Vereide, Kaspar, Svingen Bjørnar, and Guddal Rolv. “Case study: Damaging effects of increasing the installed capacity in an existing hydropower plant.” *BHR Pressure Surges.* Dublin, 2015.

Webb, C., S. Barfuss, and M. Johnson. “Modelling roughness in scale models.” *Journal of Hydraulic Research*, 2010: 260-264.

Institute of Hydraulic Engineering and Water Resources Management

Report

Hydraulic Investigation

Numerical and Physical Model Test

Flexible Sandtrap (FlekS) 2.0

Project extension

December 2020

Project Partner and Client

Keywords: **Tonstad HPP sand trap upgrade, pressurized sand trap, physical sand trap model test, 3D CFD, 3D CFD particle tracking simulation, Tonstad HPP upgrade, extension chamber, semi-air cushion surge tank**

PROJECT PARTNERS

CLIENT

Sira-Kvina Kraftselskap
Mr. Kaspar Vereide, PhD
Postboks 38
4441 Tonstad

CONTRACTOR

Graz University of Technology

Institute of Hydraulic Engineering and Water Resources Management
Stremayrgasse 10/II
A-8010 Graz
Austria

Project leader, researcher: Dipl.-Ing. Dr. Wolfgang Richter
Project assistant, researcher: Gašper Mauko, MSc
Head of institute: Univ.-Prof. Dipl.-Ing. Dr. Gerald Zenz

1. Content

2. Abbreviations

CFD	Computational Fluid Dynamics
CST	Chamber surge tank
ESD	Emergency shutdown
HPP	Hydro power plant
IFM	Inductive Flowmeter
LC	Load case
LCh	Lower chamber of a surge tank
m a. s. l.	Meters above sea level
MT	Physical model test (hydraulic small-scale test)
MHT	Main Headrace Tunnel
MS	Main Shaft
MW	Mega Watt
mwc	Meter water column
PSH	Pumped Storage Hydropower
PVE	Power Vision Engineering Sàrl
Q	Discharge
ST	Surge tank
TUG	Graz University of Technology, Institute of Hydraulic Engineering and Water Resources Management
TU	Turbine load case
PU	Pumping load case
UCh	Upper chamber of a surge tank

3. General description of the task

The present report describes the hydraulic investigation of the sand trap No. 3 and associated parts of the surge tank of Tonstad HPP. The investigations were done both in 3D CFD and small-scale physical model test.

The goal is to investigate the sand trap behaviour of the chamber and how it can be improved and automated.

The goal of the associated surge tank investigation is to investigate the hydraulic behaviour of an extension chamber to the sand trap No. 3 in order to allow more flow discharge and possibly install a unit No. 6 to Tonstad HPP, possibly being also a reversible pump turbine. The surge tank extensions is investigated to be a semi-air cushion chamber to optimize the hydraulic implementation to the existing scheme and to investigate this new design approach.

4. Technical proposal

The Tonstad Flexible Sand Trap project by TU Graz in cooperation with NTNU and Sira-Kvina contained the investigations of the sand trap improvements for the Tonstad pressurized sand trap, including the 3D CFD modelling in collaboration with physical model testing by NTNU Trondheim.

Additional outcome of the studies was the possibility of significant power upgrade of the Tonstad power plant. This upgrade can be achieved by allowing additional water flow through the power water way allowing deeper water level in the surge tanks. A significant discharge upgrade of 25% was found to be possible, enabling about 20% power upgrade. The discharge increase for the existing pressure tunnel system is possible by upgrading the surge tanks in order to expand the volume available at the level of the start-up chambers. The existing power plant can further be upgraded by the measures for significant higher flexibility by structurally expansion of the surge tank. In order to enable an economic and convenient surge tank expansion by minimized outage time, a concept was developed to attach one large lower chamber serving for all units that can also be constructed in some portion during operation of the power plant. The investigations covered 1D numerical simulations and supervised master theses by TU Graz to develop a single extension chamber of the lower surge tank system of the Tonstad power plant scheme. A promising solution is to improve the single extension chamber with a novel developed semi air cushion development, described in Sterner 2018 (Sterner 2018) and Richter 2020 (W. Richter, Surge Tank Design for Flexible Hydropower 2020).This extension project addresses the key two structures to be further improved for specific applications; (i) the design details for the semi-air cushion chamber and (ii) improving the flow calmer for the pressurized chamber, especially to investigate a design that is passable for persons and vehicles.

Keywords: Semi-air cushion surge tank, crown-throttle, throttled aeration pipe, Surge tank upgrade, Surge tank design, power plant upgrade, Pressurized Sand Trap, Flow Calmer, Unlined surge tank, Crown throttle

Publications from FlekS and outcome dissemination:
Final report of the FlekS investigation at Graz, University of Technology.

Sterner L. Master thesis TU Graz: *3D CFD simulations for Tonstad surge tanks upgrade* 2018 (Sterner 2018)

Mauko G. Master thesis TU Graz: *Water hammer simulation for Tonstad HPP upgrade* (ongoing) (Mauko, WaterHammer Simulation for Tonstad HPP upgrade 2020 - ongoing)

Richter W. Dissertation TU Graz Title: *Surge Tank Design for Flexible Hydropower* 2020 (W. Richter, Surge Tank Design for Flexible Hydropower 2020)

Rakel Næss Master Thesis *CFD Simulations of Open and Close Sand Trap Design for Tonstad Hydropower Plant,* (Naess 2020)

Steinkjer S. Master Thesis NTNU *Hydraulic scale modeling of sediments for pressurized sand trap,* 2018 (Steinkjer 2018)

Daxnerová J Master Thesis NTNU, *Hydraulic scale modelling of flow calming structures for Hydropower Plants* (Daxnerová 2019)

Richter W., Vereide K. and Zenz G., *Upgrading of a Norwegian pressurized sand trap combined with an open air surge tank*, 2017 (Richter, Vereide and Zenz, Upgrading of a Norwegian pressurized sand trap combined with an open air surge tank 2017)

Vereide K., Richter W., Lia L., Havrevoll H., and Jakobsen T., Upgrading of sand traps in existing hydropower plants, 2017 (Vereide, et al. 2017)

Richter W., Vereide K., Mauko G., and Havrevoll O. H. (2021). Retrofitting of existing sand traps in hydropower plants. Manuscript

4.1 Investigation proposal

The proposed research investigations are separated in three specific positions;

Pos. 1: Semi-Air Cushion Surge Tank
Pos. 2: Passable Flow Calming Device
Pos. 3: Optimum Sand trap and Surge Tank Arrangements

Pos. 1 aims for the development of the novel semi-air cushion surge tank device, that combines the aspects of chamber and air cushion surge tanks. The purpose is to minimize excavation expenses and optimize the power plant operation.

Pos. 2 aims for the development of a flow calming device to be applied in pressurized sand traps to allow both flow tranquilization for improved particle settling and make such permanent structures passable for inspection or construction vehicles and personnel.

Pos. 3 aims to study the optimum construction arrangement layout for power plants and pumped storage plants with pressurized sand traps and surge tanks. This task will be performed as a desk study and will results in drawings and descriptions of different variant with different benefits.

The development for all positions is studied exemplary for Tonstad power plant and Kuli pumped storage plant in southern Norway to improve its upgrade options. The results aim to be generalized and applied for other facilities. The goal is to provide meaningful applicable results and additionally publish the structural solution approach via scientific journal publications.

4.1.1 Semi-air cushion surge tank – pos. 1

The semi-air cushion surge tank is a novel construction approach to optimize surge tank design for upgrades of power plants and new plants, especially large facilities.

Figure 1 shows the 3D geometry of the complex Tonstad headrace surge tank with pressurized sand traps, start-up chambers, upper chambers, as well as the proposed extension chamber to be utilized as semi-air cushion chamber. This design, that already contains significant research and developing output is taken as starting geometry of further research, including additionally further specific aspects in relation to a potential Tonstad power plant upgrade utilizing this extension chamber.

The investigations are proposed to be done by multiphase 3D-CFD simulations. Additionally, a new 1D-numercal model Tonstad power plant is proposed to be set-up by utilizing the comprehensive 1D-numerical software SIMSEN including possible Tonstad upgrade opportunities and to further study the behavior of various transient aspects of the semi-air cushion surge tank.

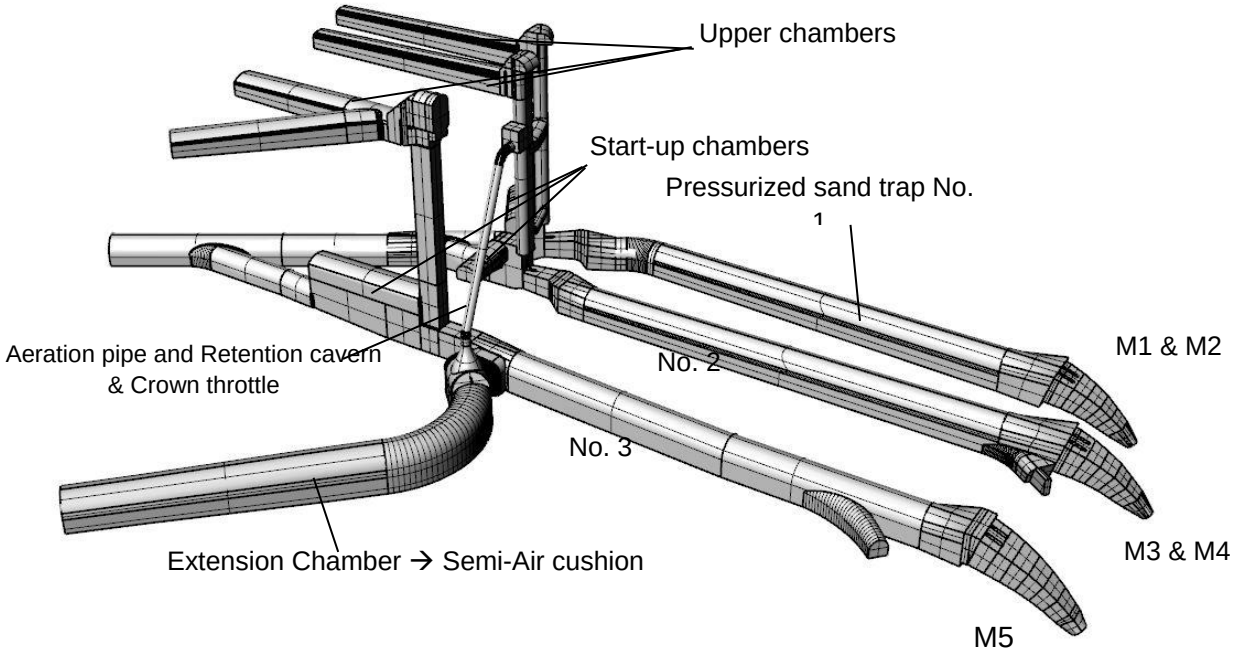

Figure 1: 3D-Geometry of the Tonstad Surge Tank with extension chamber, semi-air cushion chamber, initial design state (Sterner 2018)

Goals and Questions:

Development of general design guidelines for surge tank upgrade with expansion chamber utilizing semi-air cushion principle. Investigation of semi-air cushion behaviour for implementation in surge tank chamber including:

(i) Thermodynamics of relevant parts, (ii) development of crown-throttle and (iii) aeration pipe. The aeration pipe operates as an air throttling device. Air in the crown region of the semi-air cushion surge tank is released through the pipe in case of air compression. Due to the compression, high velocities and temperature gradients arise in the aeration pipe. Investigations need to answer the required pipe diameter and pipe mouth design to avoid freezing or other unwanted effects. It is aimed to investigate the semi-air cushion surge tank application for several purposes such as upgrades of surge tanks and for application in new hydropower and pumped storage schemes, both in order to minimize the excavation expenditures as well as to improve the flexibility of the system by allowing quick water mass response.

A question at the Tonstad semi-air cushion application is to include also a sand trap facility for potential power plant extension via the surge tank extension in combination with the semi-air cushion design.

The investigations may both highlight the opportunities as well as uncovering further questions for detailed design.

Figure 2 shows a sketch of the semi-air cushion chamber already developed in principle for the Tonstad upgrade feasibility as an initial design state for the proposed research. However, several questions remain to be solved in detail, which is the aim of the proposed research initiative. The specific hydropower plant is taken exemplary for further developments in order to design the main riser for best construction and operational functionality. Since an upgrade for Tonstad power plant was already proposed, this may be applied also via the expansion chamber for a new unit, that may also be a pumped turbine unit. The functionality will be investigated including a gate and to allow for best accessibility to construct the extension for minimized operational interruption.

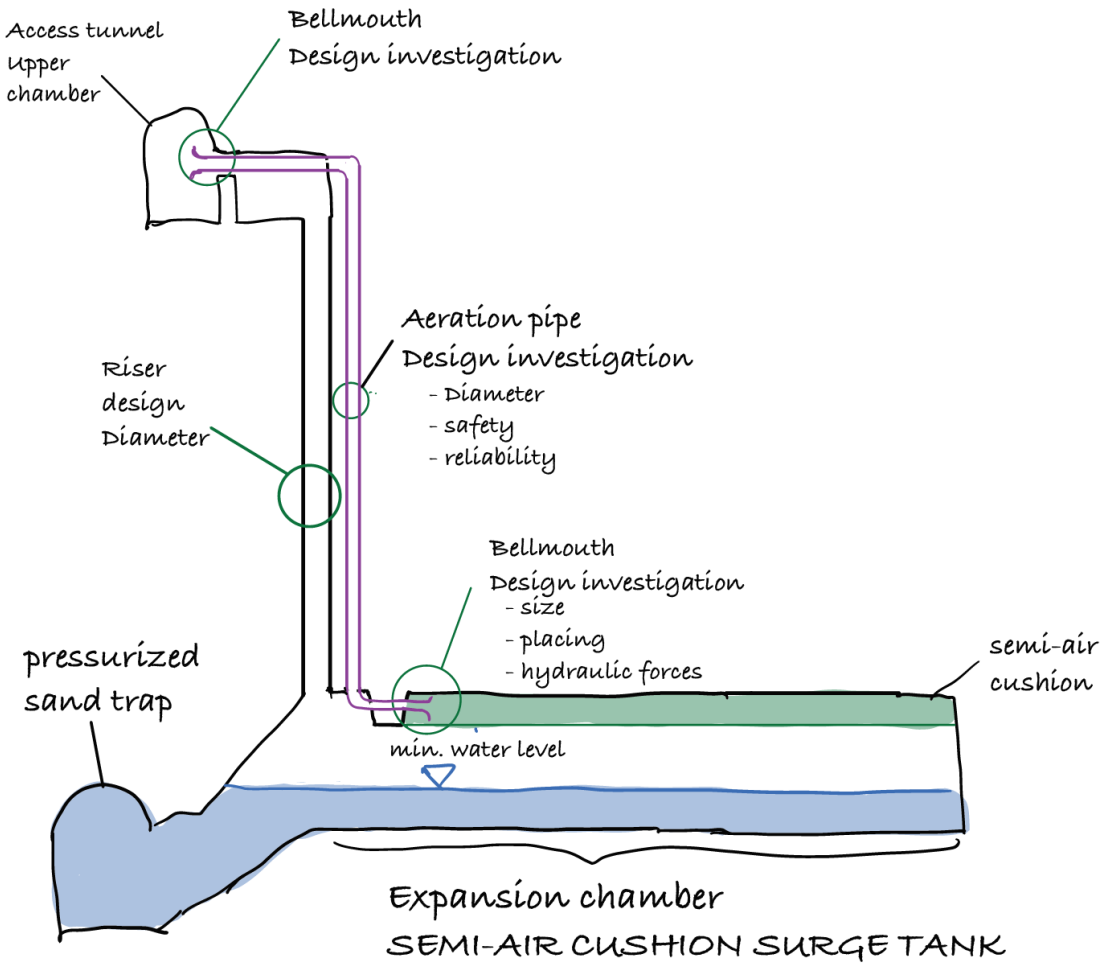

Figure 2: Sketch of semi-air cushion surge tank as expansion chamber for Tonstad HPP

4.1.2 **Passable flow calming device - pos.2**

The proposed research intents to develop a passable flow calming device to be applied at pressurized sand traps for upgrades and new constructions.

Figure 3 shows the physical testing at the flume at NTNU in Trondheim at free surface flow, pre-evaluating the implementation of a flow calming device.

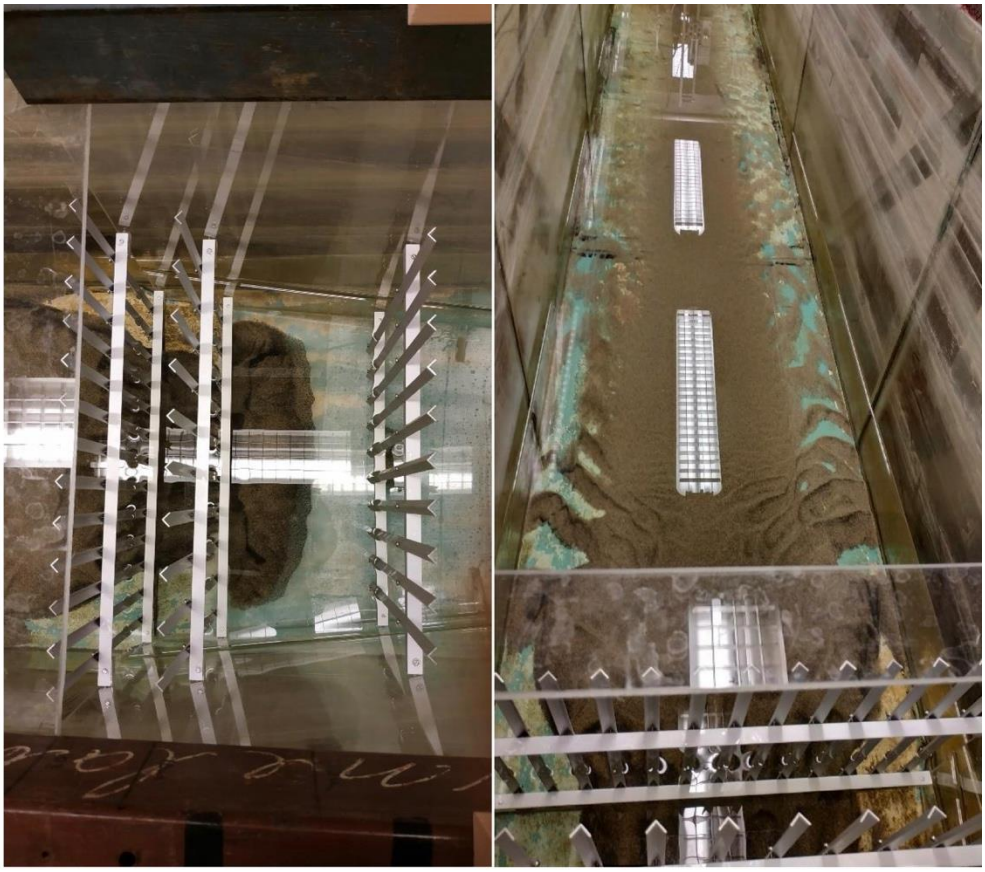

Figure 3: Flow calming device studied by Daxnerová at NTNU (Daxnerová 2019)

The investigation for the passable flow calming device is proposed to be done in the laboratory flume at Graz University of Technology. The flume has a width of 30 cm, which gives a scale ratio of 36.67 [-]. The flume will be covered by a transparent acrylic glass lid to utilize pressurized flow conditions. The investigations will include the sediment behaviour of the tranquilizing structures to improve the particle settling in the pressurized sand trap. The sediment is intended to be chosen on aspects in order to allow qualitatively comparing the best solution of the flow calming structure.

The flume with the relatively high scale ratio allows an effective implementation of particle image velocimetry (PIV) to investigate the flow behaviour due to the diffusor and also the flow impact of the final design.

Goals and Questions:

The desired flow tranquilizer design should be applicable for pressurized sand traps, but also for free surface sand traps with diffusors.

The flow calmer design aims to be utilized for upgrade of sand traps demanding quick installation and robust design. In combination with Pos.1 the flow tranquilizer may also allow to be combined with a semi-air cushion surge tank. The structural design aims to allow

adequate settling of particles and to be passable by persons and vehicles in case of maintenance.

Figure 4 shows a sketch of the proposed initial design for a passable flow calming structure with the requirements to be installed very quickly and robust.

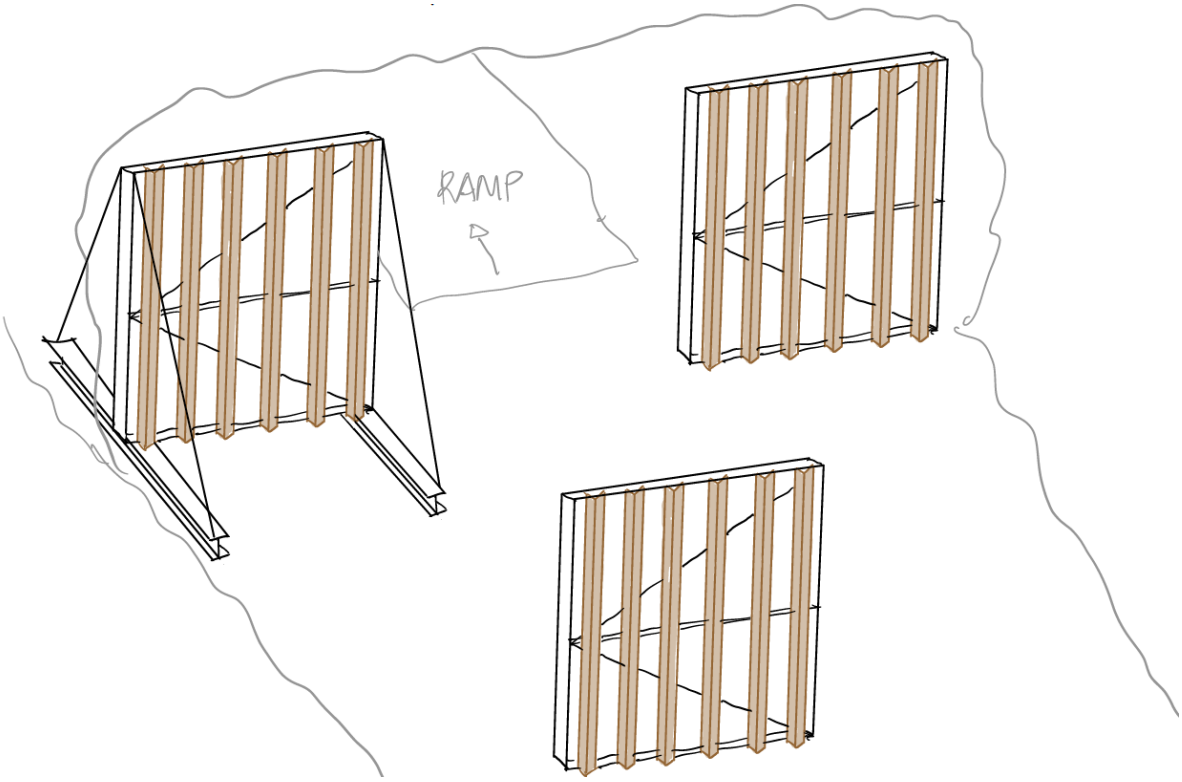

Figure 4: Proposed approach for passable flow calming device in pressurized sand trap, principle sketch

4.1.3 **Optimum sand trap and surge tank arrangements - pos.3**

In many hydropower plants in Norway, the sand trap and surge tank are constructed in close vicinity of each other, to utilize the same access and the position at the end of the headrace tunnel, close to the pressure shaft. It is seen that the surge tank should be placed upstream the sand trap to avoid mass oscillations occurring inside the sand trap, and to enable the installation of a gate in the surge tank, to allow dewatering and emptying of the sand trap. As such, there are many interdependencies and mutual benefits of such arrangements.

Goals and Questions:

The proposed research intents to develop new layouts for combination of sand traps and surge tanks including air cushion surge tanks in hydropower plants and pumped storage plant. This work will be carried out as a desk study and the deliverables will be drawings of different possible variants and descriptions of the benefits and challenges.

4.2 **Deliverables**

This chapter describes the proposed deliverables of the research investigation.

All data generated is made accessible for the client and will be transmitted after completion of the project.

A digital lecture (video) is produced for dissemination (at an online conference) of the research item of the semi-air cushion chamber including explaining; (i) problem, (ii) methods, (iii) solution (iv), discussion, dedicated for joint lecture purposes (NTNU and TU Graz) and other people involved in the power industry.

The proposal includes 10% of the working time to be dedicated specifically in the learning zone and 90% in the performing zone. The learning zone includes the study of literature and tutorials for improving the performance and also includes feedback meetings with the client on a regularly biweekly basis.

An online dissemination conference will be organized to present and discuss the aspects and solutions of the research.

Monthly intermediate report parts are delivered to the client and are anticipated to be part of the final report.

Deadline for final intermediate report: 10th September 2020

Deadline for the final report including the invoice is 22nd December 2020

4.2.1 **Semi-air cushion – pos. 1**

The development of the semi-air cushion surge tank is intended to allow its specific design for the Tonstad surge tank upgrade including further opportunities by the extension chamber and is aimed to practically applicable.

A further main outcome is aimed to be a joint scientific journal paper, describing the semi-air cushion surge tank for general application and guidelines for aeration pipe and air throttle design.

Additionally, a report with project specific aspects for Tonstad surge tank upgrade, including an upgrade proposal for Tonstad power plant for a pumped storage facility enabling;

(i) increased power production,
(ii) increased flexibility of the exiting scheme,
(iii) increased flexibility of upgraded scheme,
(iv) allowing negative regulation power,
(v) reliable redundancy for air throttling (aeration shaft),
(vi) minimized outage time of unit 5 for connection
(vii) energy shift by storing electricity, including
(viii) 3D CAD drawing of surge tank expansion prototype.

The work includes the basis for a further joint scientific conference paper describing the Tonstad surge tank upgrade.

Following variant studies are contained by this proposal:

A) Semi-ACST with Aeration system utilizing a gate equipped shaft
    a. Minimum three geometric variants
    b. Implementation in 1D code (anticipated cooperation with PVE)
B) Semi-ACST with Aeration system with separate water riser and air riser (air throttle)
    a. Minimum three geometric variants
    b. Implementation in 1D code (anticipated cooperation with PVE)
C) Extension chamber design proposal including a sand trap and considering this to operate as free surface flow desander and pressurized desander allowing automated flushing

The report will contain construction time (utilizing standard values provided by the client) with the volume estimation as well as part estimation to construct the semi-air cushion chamber as an extension chamber for Tonstad power plant. Next to economic aspects the focus is to minimize the construction time of the connection tunnel between the extension chamber and the existing surge tank and allow best possible serviceability. A specific delivery is the setup of a 1D-numerical model of Tonstad powerplant including the semi-air cushion in SIMSEN software. Budget is reserved for cooperation with Power Vision Engineering (PVE) to create a surge tank module to capture the semi-air cushion chamber, possibly including a potential Tonstad power plant expansion.

4.2.2 **Passable flow calming device - pos.2**

The research is aimed to propose a hydraulically functional flow calming device to tranquilize the flow in the pressurized sand trap by the initial gate restriction flow at the Tonstad power plant. The flow calming design aims to allow;

(i) to be passable for both vehicles and personnel in case of maintenance or constructional work,
(ii) upgrades of pressurized sand traps
(iii) the implementation at new pressurized sand traps,
(iv) comparing the results with previous research of the Tonstad pressurized sand trap,
(v) transient flow patterns by measurements in terms of PIV

The deliveries are collected in a research report with the investigation results. A joint scientific journal paper is anticipated to be written with draft deadline 20 December 2020.

In this proposal at least three geometric variation (either design or position) of passable flow calming devices are included. The report includes at least two variant proposals of how to place flushing devices at a flat concrete bottom of a pressurized sand trap.

The report will include a time schedule estimation and an estimation of parts or amount demand of construction works to place the flow calming devices in the pressurized sand trap Tonstad sand trap No.3.

4.2.3 **Optimum sand trap and surge tank arrangements - pos.3**

The research is aimed to propose new and improved combined arrangements of sand traps and surge tanks. The design aims to allow;

(vi) Reduce the amount of access tunnels,
(vii) Allow installation of closing devices,
(viii) Optimum performance of the sand trap and the surge tank,
(ix) Reduced construction costs.

The work will be conducted as a desk study. The deliveries are collected in a research report with the investigation results. A joint scientific conference paper is anticipated to be written with draft deadline 22nd September 2020.

In this proposal at least three geometric variation (either design or position) of combined sand trap and surge tank arrangements are included.

4.3 **Tools and references**

4.3.1 **1D-numerics for investigation of mass oscillation**

For 1D-numerical simulations the software *Wanda* and *SIMSEN* is planned to be used for the described purpose. At the Institute of Hydraulic Engineering at TU Graz several projects and research initiatives could successfully be conducted by using this software. A comprehensive 1D model to investigate the transient mass oscillation for Tonstad was already built and being the basis for proofing the possibility of a 25% discharge upgrade. Also a LVTrans model was built in terms of a supervised master thesis investigating the upgrade regarding the capability of the pressure relief valves (Mauko, WaterHammer Simulation for Tonstad HPP upgrade 2020 - ongoing). The following list provides the references for having successfully used / applied Wanda for research projects:

- Cavern storage simulation and development of a surge tank shaft
- Hydraulic investigation in terms of 1D-numerical simulations of the surge tank configurations of the hydro power plant extension Prutz-Imst
    - Tailrace system with surge tank upgrade of the existing plant
    - 1D-numerical simulation to dimension a new tailrace open air surge tank
    - Developing a new headrace surge tank system in connection with the existing power water way
    - Total simulation of the whole hydro power plant with old and new power water way to investigate the stability criterion
- Master thesis: Investigation of a storage tunnel design
    - 1D-numerical simulation of 4 km tunnel that is to be used as a storage tunnel with free surface flow
- Hydraulic Investigation of the pumped storage hydropower plant Obervermuntwerk 2
    - Simulation of the headrace system with dimensioning of the surge tank and the throttle design
- Water hammer and mass oscillation investigation of the PSH Reisseck II
- Hydraulic Investigations of PSH Atdorf – Mass oscillation of the tailwater system with surge tank design evaluation

Additionally, this research approach proposes to introduce the software SIMSEN for the Tonstad, modelling the development of the semi-air cushion surge tank device for this software. The software was successfully utilized to model the complex waterpower system of

Reisseck II with the S-shape characteristics of the pump turbine units to model the water hammer for load rejection events.

It is proposed to incorporate the developers of SIMSEN, Power Vision Engineering (PVE) into the development of the novel semi-air cushion surge tank within this proposal.

4.3.2 **3D-numerics – *CFX***

It is proposed to simulate the complex hydraulics and thermodynamic behaviour for the semi-air cushion surge tank with capable 3D-numerical Software. For several projects and research initiatives the software CFX have been used. References are listed below:

- Development of a pressure tunnel junction for a cavern storage to find the design with least hydraulic loss
- Hydraulic investigation in terms of 3D-numerical simulations of the surge tank configurations of the hydro power plant extension Prutz-Imst
    - 3D-simulation of mass oscillation with generation of free surface and air enclosure in the pressurized tailrace tunnel – for study purpose
    - Simulation and visualization of the total geometry of two combined headrace surge tank for filling and emptying load case
- Hydraulic Investigations of the pumped storage power plant Obervermuntwerk II – surge tank (Krespa) investigations – and developments
    - Upper chamber design – optimization study – free surface flow
    - Waterfall simulations – variant study – development of a waterfall dampening device
    - Throttle simulations - variant study – development of a differential throttle, comparison with physical model test
- Hydraulic Investigations of the PSH Atdorf – surge tank simulations
    - Multiphase simulations of air intrusion due to waterfall occurrence
    - Vortex core simulations at transition of lower chamber into the power tunnel
    - Throttle optimization study
- Hydraulic Investigation of PSH Reisseck II – surge tank simulations
    - Optimization studies and development of the differential throttles, comparison with physical model test

4.3.3 **PIV measurements**

It is proposed to additionally investigate the pressurized sand trap with flow calming device in terms of particle image velocimetry (PIV). Two states of flow are of interest:

(i) The jet behaviour generated by the gate restriction into the pressurized sand trap without structural measures – this allows also a comparison with 3D CFD simulations already done for the Tonstad pressurized sand trap.

(ii) The jet behaviour generated by the gate restriction into the pressurized sand trap with the final structural measures found by the flume tests with the lid.

The PIV is mounted to observe in general (especially) the centred flow in the longitudinal flow direction.

References of transient PIV measurements by the involved persons and institution are:

- for the throttle in the Reisseck II tail race surge tank (Richter, Dobler and Knoblauch 2012)
- for the waterfall dampening device for surge tank for PSH Obervermuntwerk II (supervised master thesis (Ruetz 2014))
- for the waterfall jet intrusion behaviour for surge tank for PSH Obervermuntwerk II (supervised master thesis (Urach 2015))
- PIV flow measurements in the flume to investigate the flow for removal of cohesive particles (Harb 2013)

Figure 5 shows the application of the PIV system, intended to be applied for the described research initiative (from (W. Richter, Surge Tank Design for Flexible Hydropower 2020), (Richter, Dobler and Knoblauch 2012)).

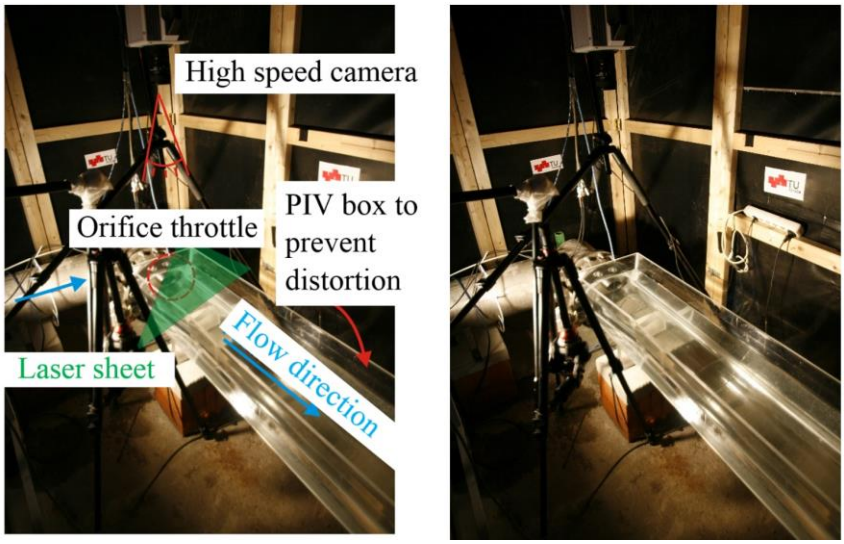

Figure 5: PIV Measurements for a transient throttle flow

4.3.4 **Flume in the hydraulic laboratory**

Figure 6 shows the 30 cm flume in the hydraulic laboratory of Graz, University of Technology to be used for the pressurized sand trap investigations.

Figure 6: 30 cm wide flume proposed for the pressurized sand trap investigations

4.4 Time schedule

This chapter describes the proposed time schedule for Pos.1 and Pos. 2 respectively. Pos. 3 is adapted to utilize available time in between, as it is not time critical.

The time schedule described below is adapted to the deadline of the overall FlekS project of 2nd October. The client has informed that it has been applied for an extension owing to the ongoing Covid-19 pandemic. If the extension application is approved, the deadline for the work at TU Graz will be adapted correspondingly without additional costs.

Time Schedule 2020

Semi-Air Cushion Chamber – Pos.1

Team: W. Richter (Post-Doc), G. Zenz (Professor)

May 2020

3D-CFD model setup

3D-geometry of the semi-air cushion model
Meshing, defining physical boundary conditions
Variant Study setup
Calibration simulations
First 3D-numerical simulations studies
Setup of 1D model of Tonstad with SIMSEN

June

3D CFD – Simulation emphasis on: Thermodynamic behaviour of the chamber and the aeration shaft

Variant study simulations of the semi-air cushion
Setup of 1D model of Tonstad with SIMSEN

July

3D CFD – Simulation Variation

Post processing of results – defining design parameters for the critical aspects of the aeration shaft details

August – vacation

Passable Flow Calming Device – Pos.2

Team: W. Richter (Post-Doc), G. Zenz (Professor), University Assistant (Pre-Doc), Technicians

May 2020

Model test planning for Flume

Theoretical approaches – literature study. Decision of particles used as sediment. Design of the flow calmers

June

Flume setup with construction of (i) the lid and the to make the flow pressurized. Construction of the flow calmers. First laboratory tests to check the behaviour

July

Model tests – Variant studies to find the optimized position for passable design. Consideration of how to place sluicing. Preparations of the PIV measurements.

August – vacation

September

Report writing, Model test operation. Discussing the design suggestions for the sand trap upgrade for Tonstad power plant including in the report. PIV-measurements of

September

Report writing, Post processing, Journal paper writing. Discussing the design suggestions for the surge tank and power plant upgrade for Tonstad hydropower plant.

October

Delivering of the report. Feedback consideration for the final report. Dissemination seminar – online conference. Journal paper writing in collaboration with NTNU for the new semi-air cushion surge tank device, deciding of paper submission process.

November – December 2020

Feedback consideration for the final report. Finalizing the journal paper.

Further outlook

Evaluation of possible Scientific Theses – Collaboration TU Graz – NTNU – Sira-Kvina for Teaching, Research and improving existing power plants

the initial geometry of the diffusor without flow calmer and the final geometry with the flow calmer.

October

Delivering of the report. Feedback consideration for the final report. Dissemination seminar – online conference

November – December 2020

Feedback consideration for the final report. Finalizing the journal paper.

Further outlook

Evaluation of possible Scientific Theses – Collaboration TU Graz – NTNU – Sira-Kvina for Teaching, Research and improving existing power plants

Notes to the proposed content and schedule:

Additional investigation from TU Graz were undertaken during the investigation that were expanding the volume of the proposed content. Additional investigations were:

- Finding an appropriate sediment scaling law with 1:1 particle size
- Improving and destabilizing the model test geometry of the Tonstad sand trap
- Running the physical model test with 1:1 sand particle for three characteristic discharges
- Developing a sand trapping device with ribs that allow automatic flushing

These aspects enrich both the specific output and also the output for the scientific papers that will be written in continuation of this report in combination with an appropriate dissemination seminar.

5. Geometry representation

The figures below show several presentation geometries of the sand trap no.3 of Tonstad HPP.

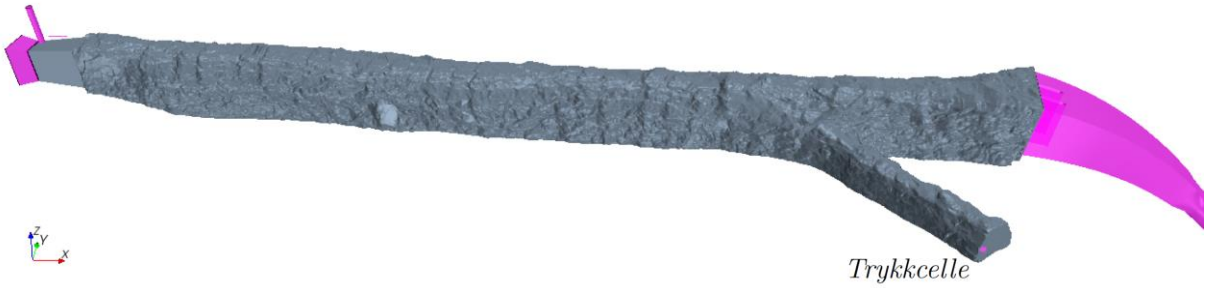

Figure 7: 3D laser scan geometry of the sand trap No. 3

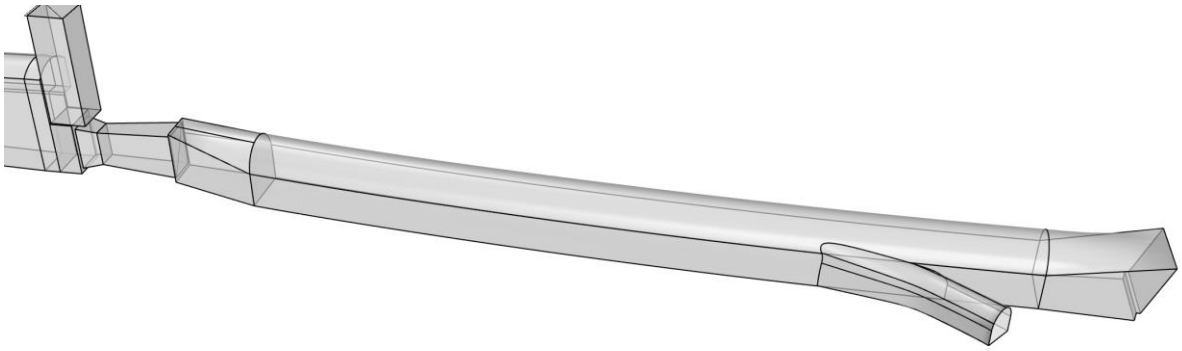

Figure 8: Sand trap geometry from design plans

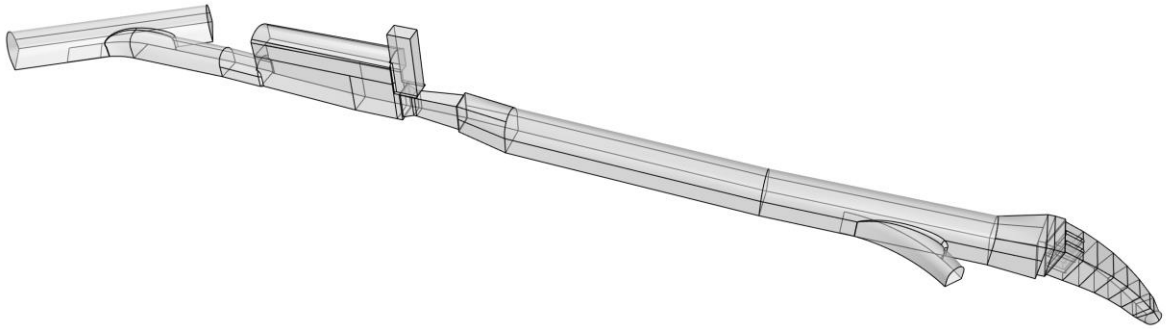

Figure 9: Relevant geometry for approach flow to the sand trap

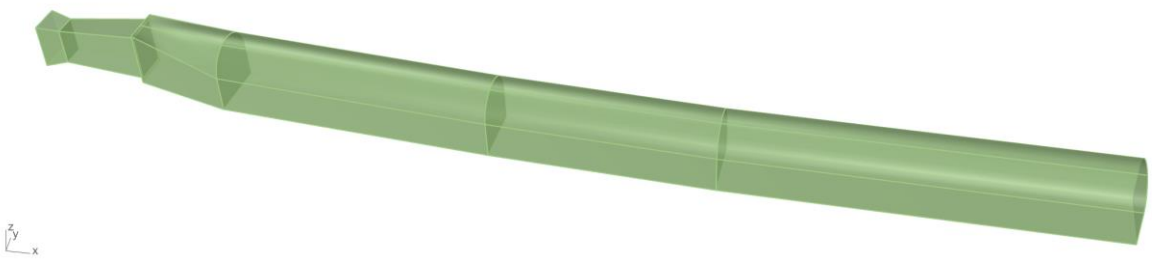

Figure 10: 30 cm wide flume proposed for the pressurized sand trap investigations

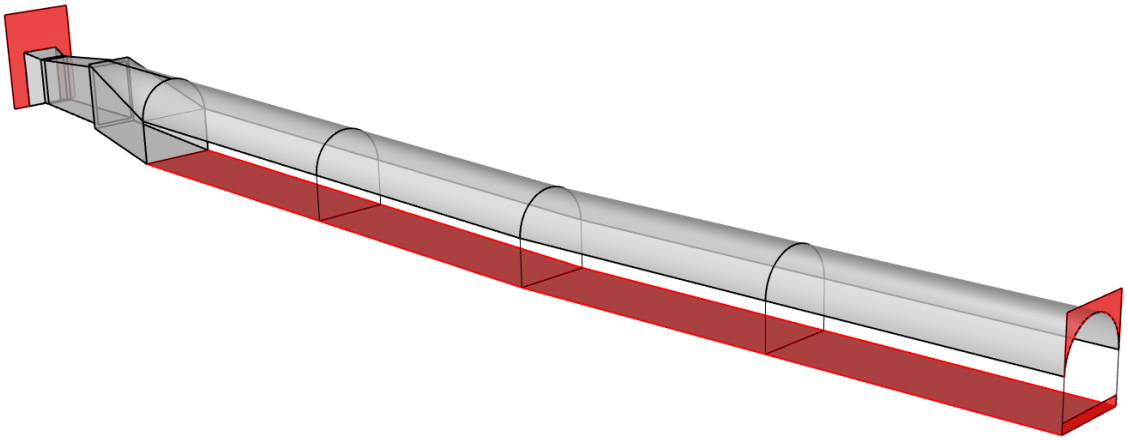

Figure 11: 30 cm wide flume proposed for the pressurized sand trap investigations, based on design plans

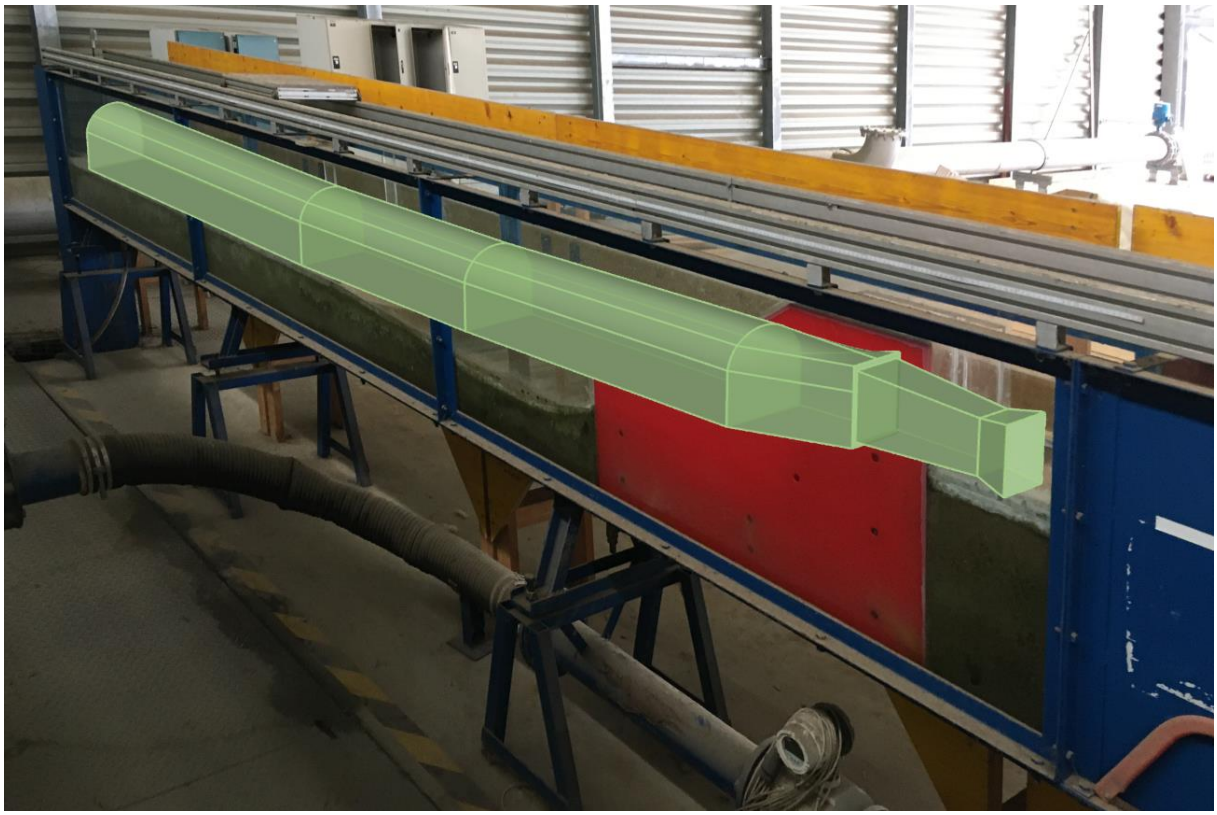

Figure 12: composition of flume with planned sand trap geometry

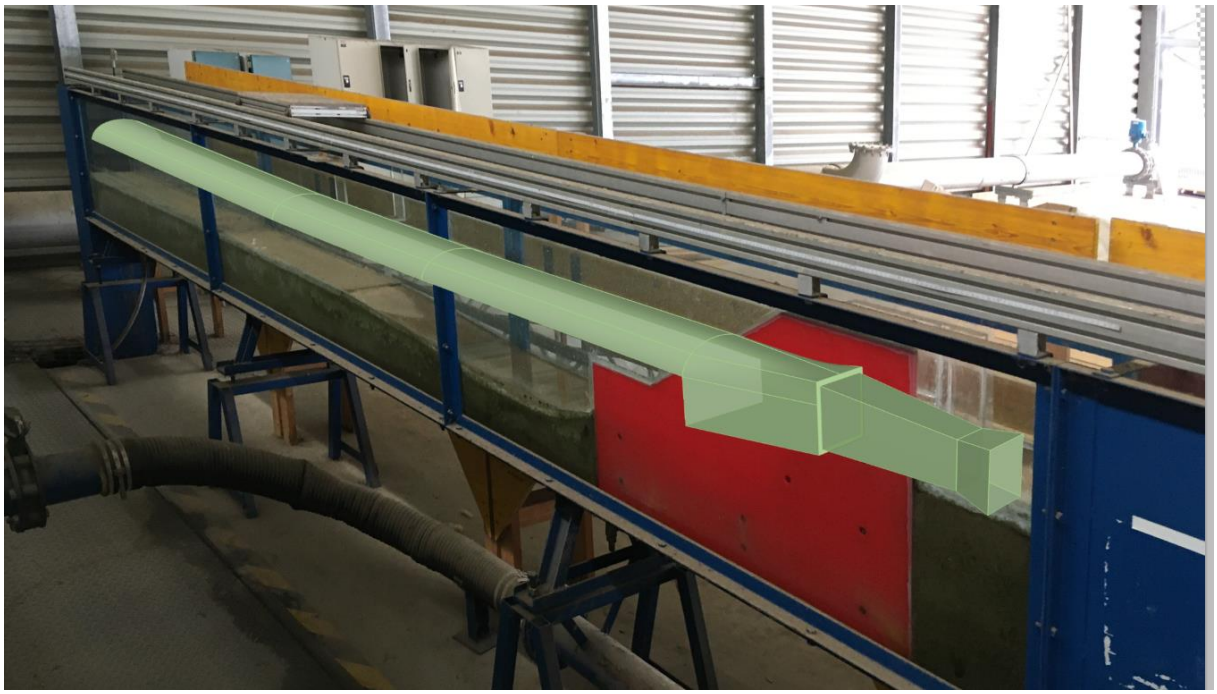

Figure 13: composition of flume with planned sand trap geometry, plexi glass parts

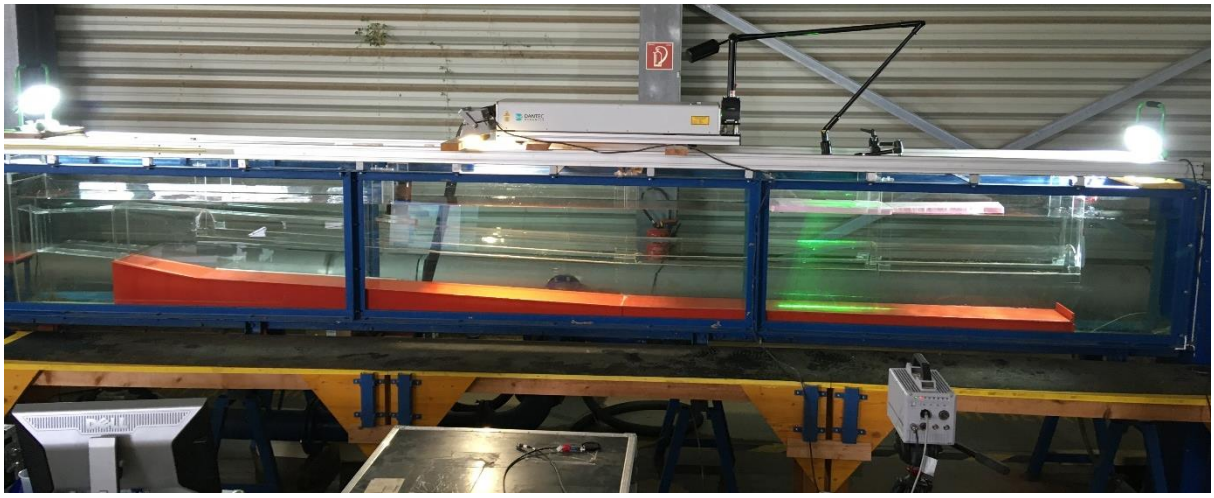

Figure 14: Sand trap geometry with PIV equipment

6. Meetings and communication

This chapter lists briefly the Joure fix meetings that were basically hold in a weekly period and improve the investigations due to flexible adaptations that could be made.

6.1 Joure fix meetings:

- **Jour Fixe 01**

4.05.2020 Vereide K., Richter W.; Project Planning Discussions, sluicer design evaluation. Pictures below show the discussed content and intermediate output:

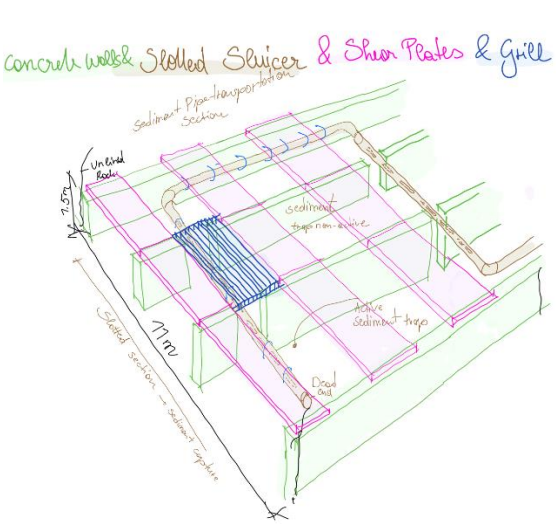

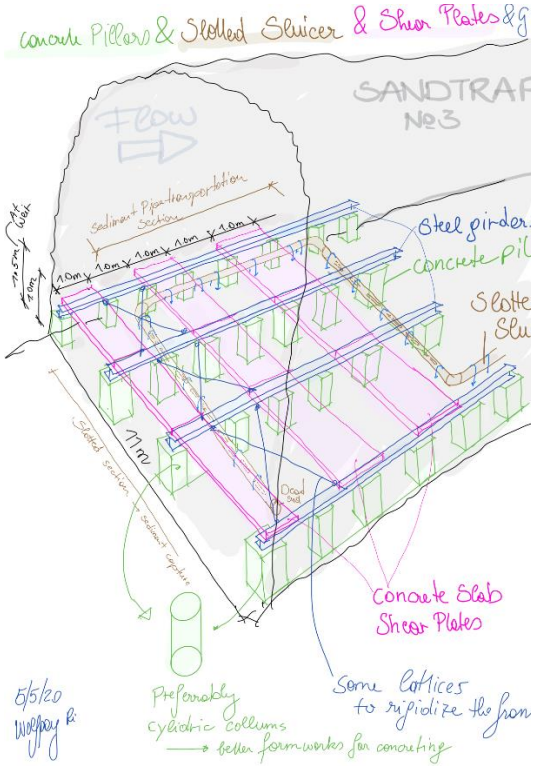

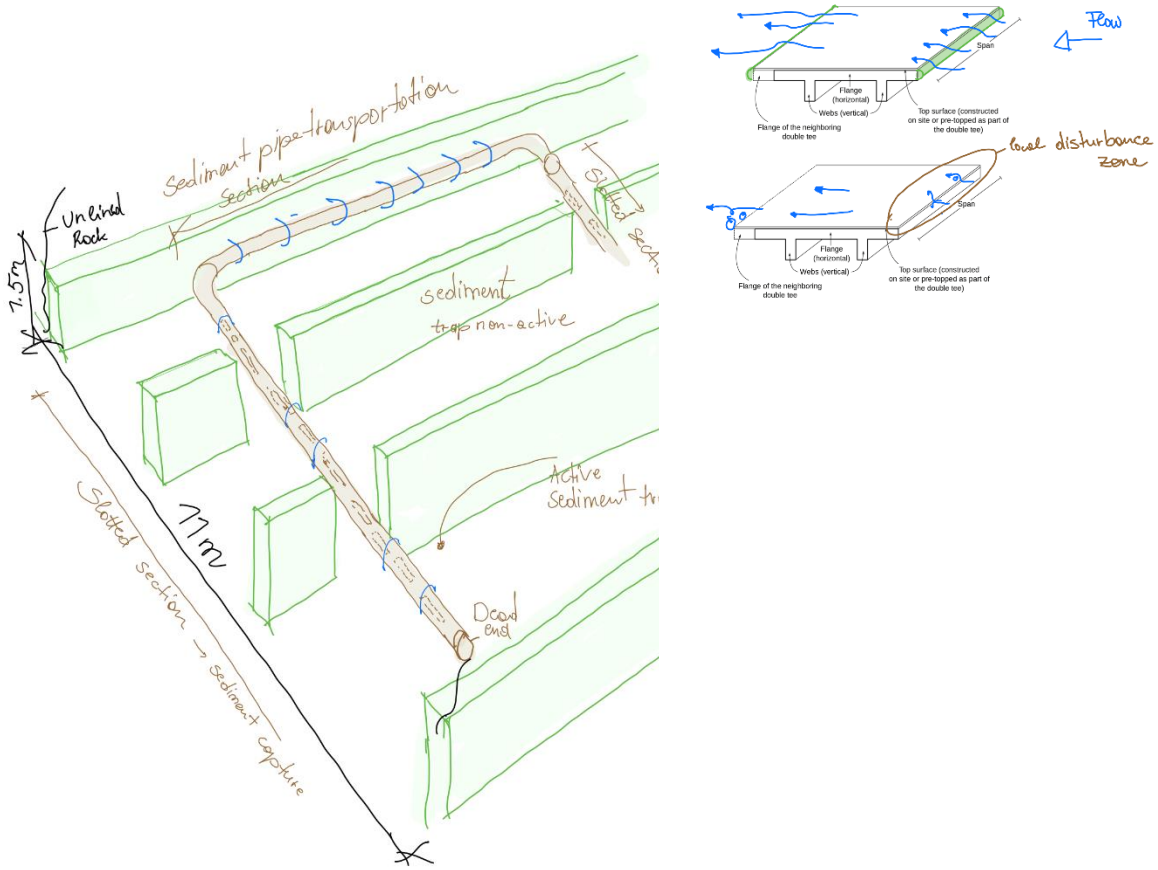

- **Jour Fixe 02**

11.05.2020 Vereide K., Havrevoll O., Pummer E., Naess R., video conference about settings for Particle Simulation in Fluent for master thesis of Naess R. for Tonstad pressurized sand trap

Pictures and notes below show the discussed content and output

Particle Simulation Fluent

```
Advancing DPM injections ....
number tracked = 0, escaped = 0, aborted = 0, trapped = 0, evaporated = 0, incomplete = 0,
incomplete_parallel = 0
Flow time = 200s, time step = 800
```

```
Advancing DPM injections ....
number tracked = 20997, escaped = 0, aborted = 0, trapped = 47, evaporated = 0, incomplete =
0, incomplete_parallel = 0
Flow time = 65s, time step = 260
540 more time steps
```

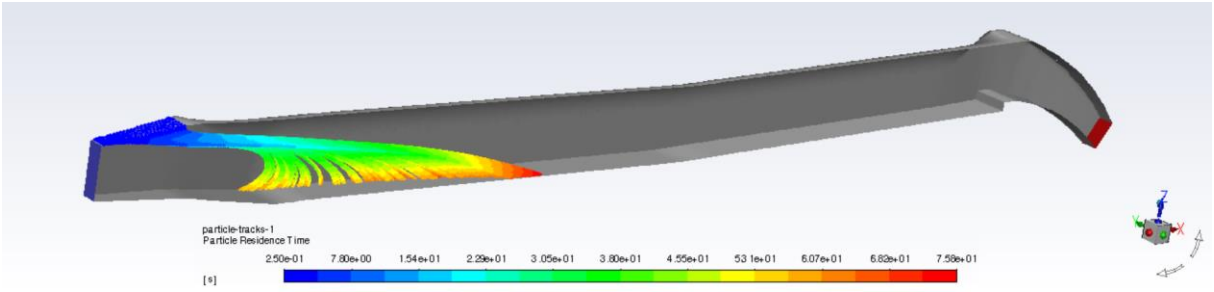

200s water flow and 200 s particle injection 1 mm grain size sand

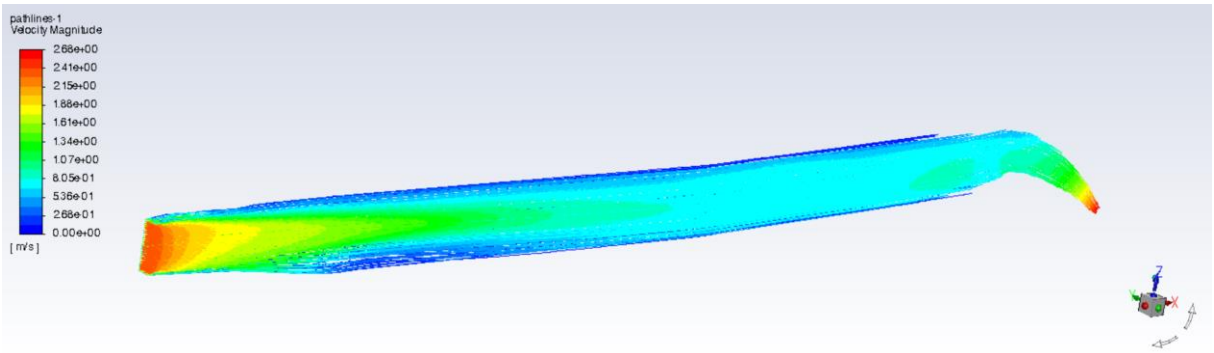

velocities 80 m³/s in sand trap

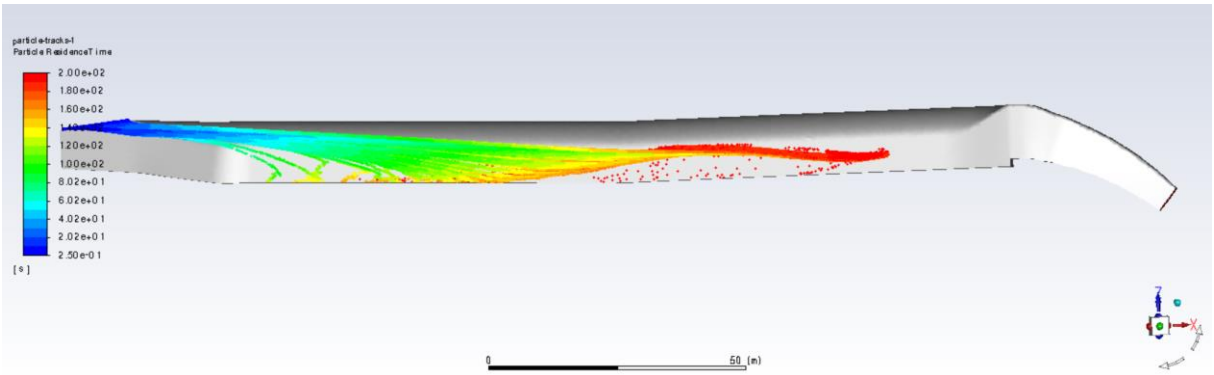

200s water flow and 200 s particle injection 0.3 mm grain size sand

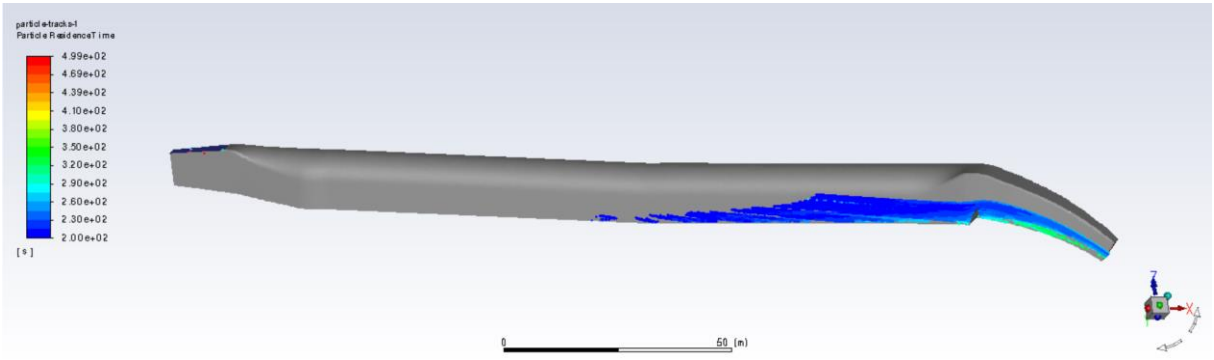

200s – 300s water flow and particle 0.3 mm grain size sand

- **Jour Fixe 03**

18.05.2020 Vereide K., Havrevoll O., Pummer E., Videoconference about settings for Particle Simulation – scaling law of sediments in pressurized flow, Model testing at NTNU, Flextrap 1.0 further approach, idealized 3D CFD Box simulations for sediment scaling comparison.

- **Jour Fixe 04**

25.05.2020 Vereide K. Richter W. Sediment scaling discussion for pressurized sand trap. 3D CFD approach to model the sediment scaling via a idealized box flow with particle tracking.

- **Jour Fixe 05**

08.06.2020 Vereide K. Richter W., Mauko Gasper, Havrevoll O. discussing the results of the systematic particle tracking simulation to evaluate the scaling law for pressurized sand traps. Discussing and reviewing the results of the three-shear plate variant simulations.

- **Jour Fixe 06**

15.06.2020 Vereide K. Richter W., Mauko Gasper, Havrevoll O. short discussion of sand trap.

Purpose: - separated Sluices
- guided flow
- quick and safe to install
- Ramp as vertical flow column + sediment mover

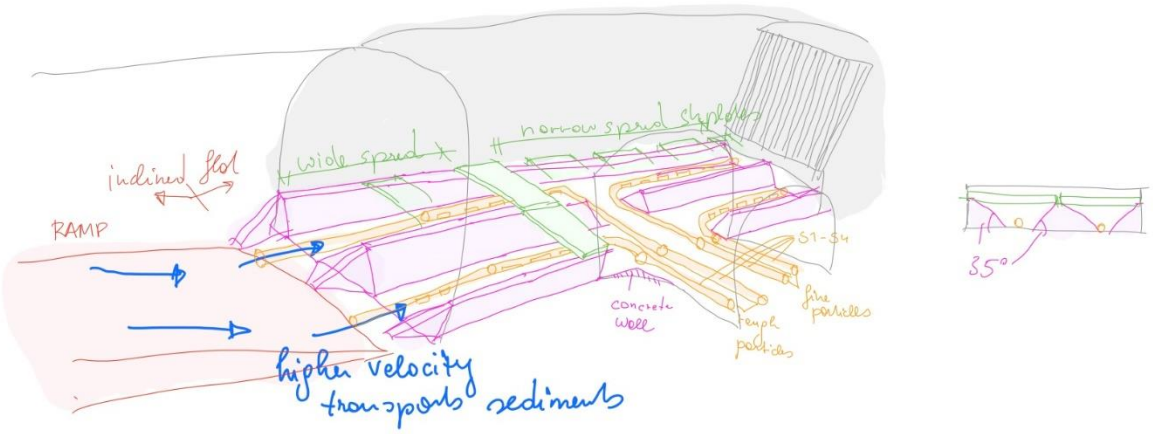

To be defined:
- length of abutment / concentration walls
- length of sluices
- length of placing shear

Figure 15: sketch of sand trap with sluicer proposal for discussion

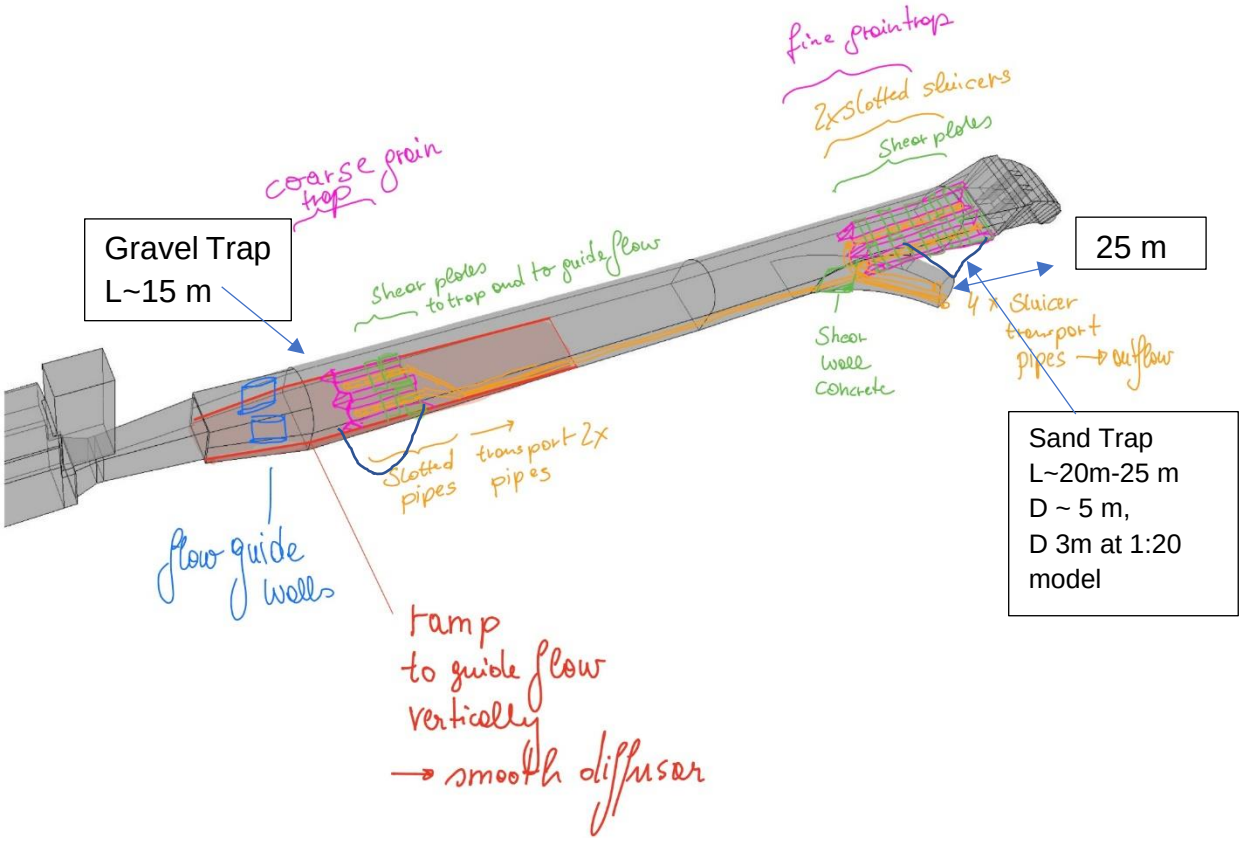

Figure 16: sketch of sand trap with sluicers for discussion

- **Jour Fixe 07**

22.06.2020 Vereide K. Richter W., Mauko Gasper, Havrevoll O. discussion of upper chamber filling and emptying coefficient, sand trap sluicing design in continuation to joure fixe 06, grain origin at the sand trap, PIV measurements at NTNU.

- **Jour Fixe 08 - Workshop with Sedicon, NTNU, TUG**

25.06.2020 Vereide K. Richter W., Havrevoll O., Jacobson T., Belete K., Online workshop to discuss the sluicing options.

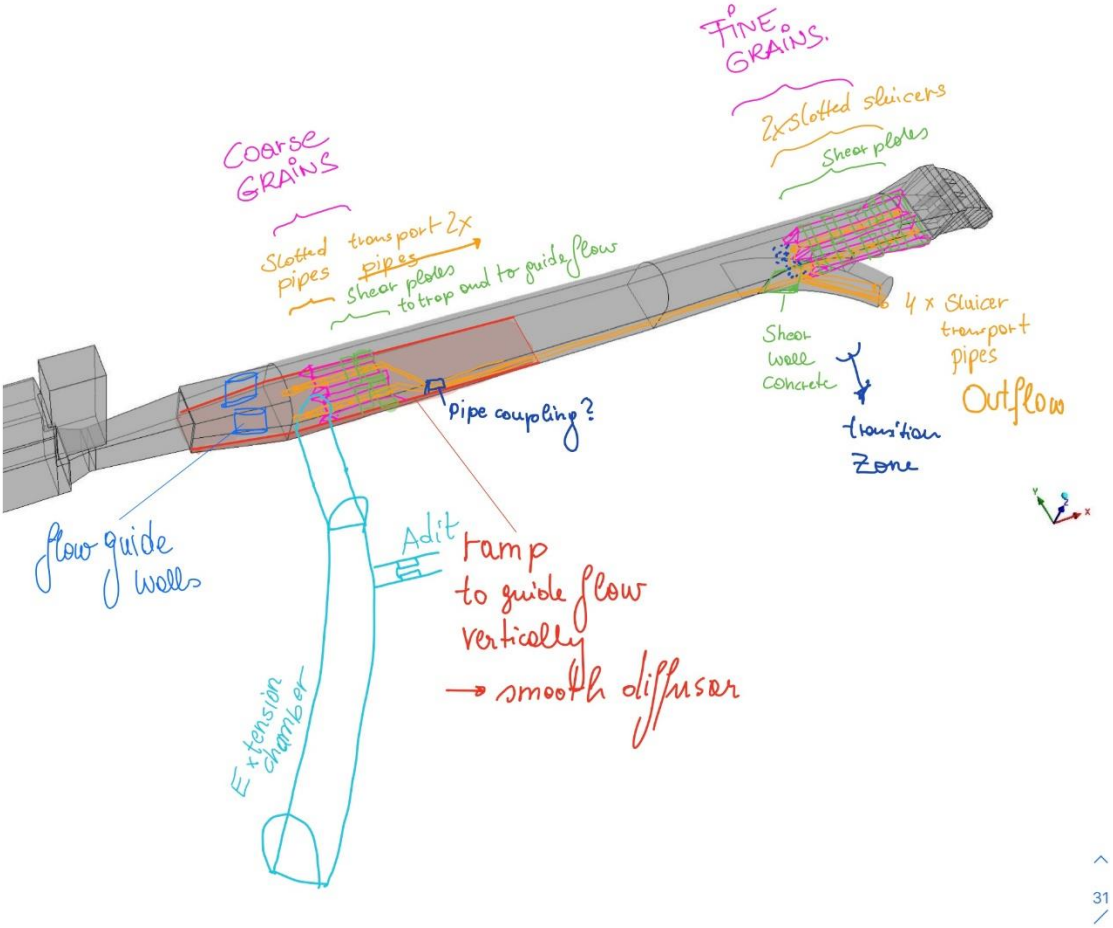

Figure 17: sketch of sand trap with sluicers and with extension chamber for discussion

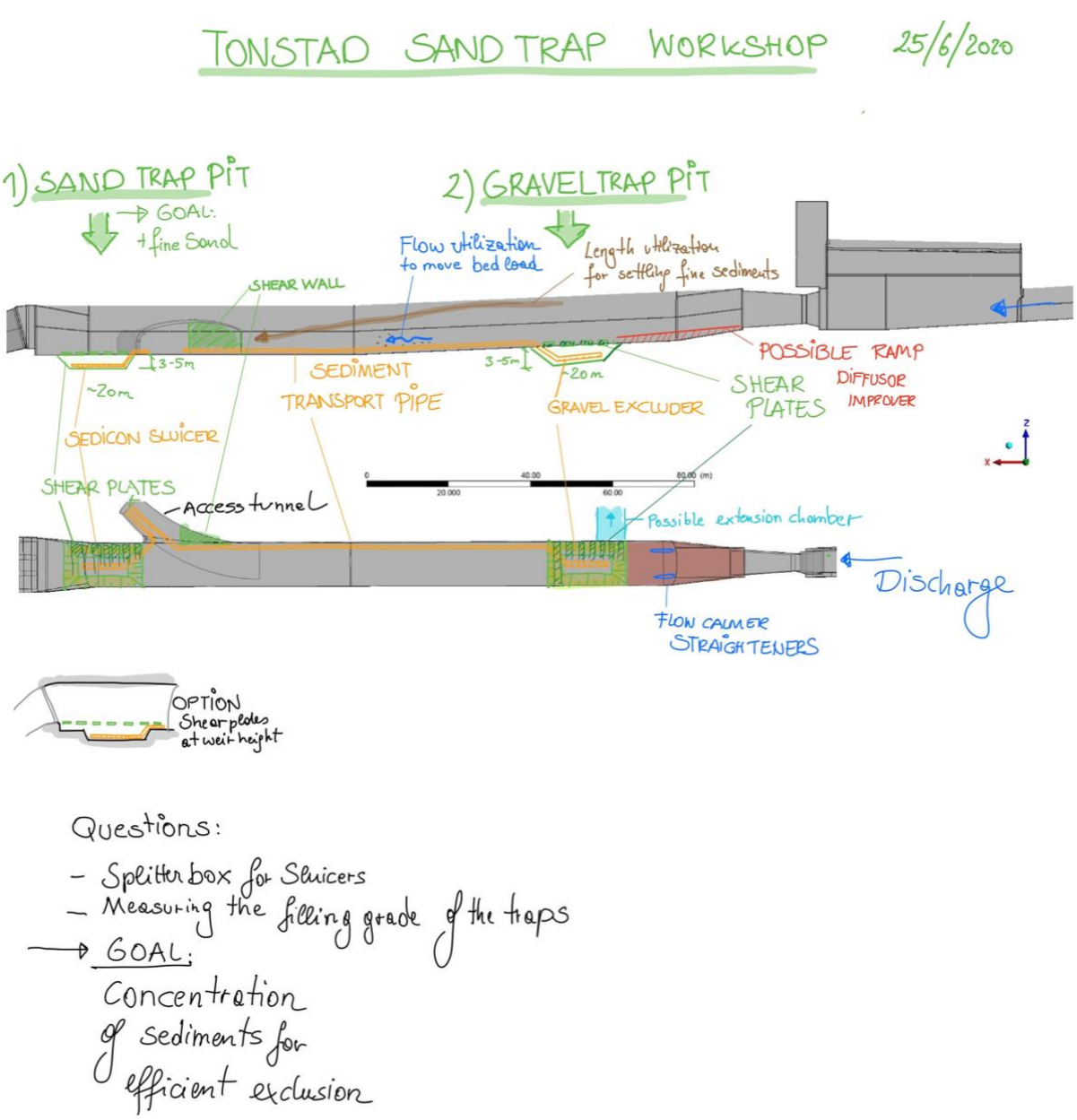

Figure 18: sketch of sand trap with sluicers in a gravel trap pit- and a sand trap pit

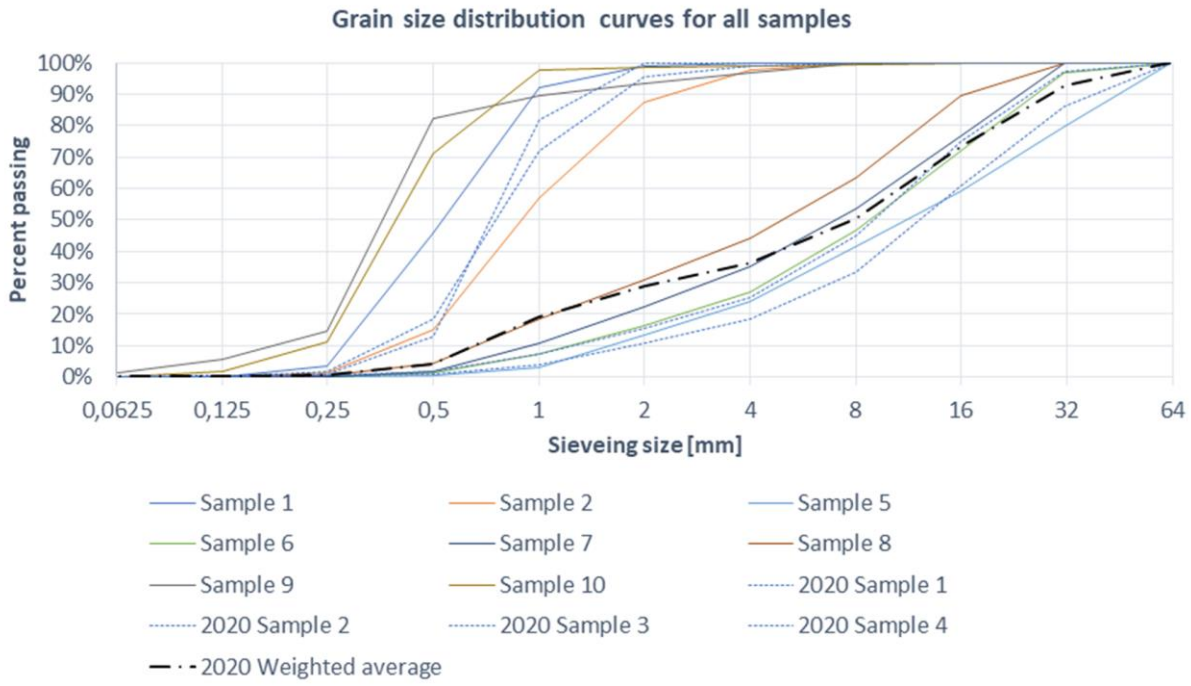

Figure 19: Grain size distribution of sediment in the sand trap

Email Havrevoll O. 2020 06 29 referring to Figure 19: *The dotted lines are from 2020. They fit nicely in the pattern that was evident already in 2018. Also, I've included a line with a weighted average of the sediments from 2020. The coarse material amounted to 80 m³ and the fine material to 20 m³, so I added all the samples and made a new curve, but multiplied the mass of the coarse samples by 4. This is the thick black dot-dash-line.*

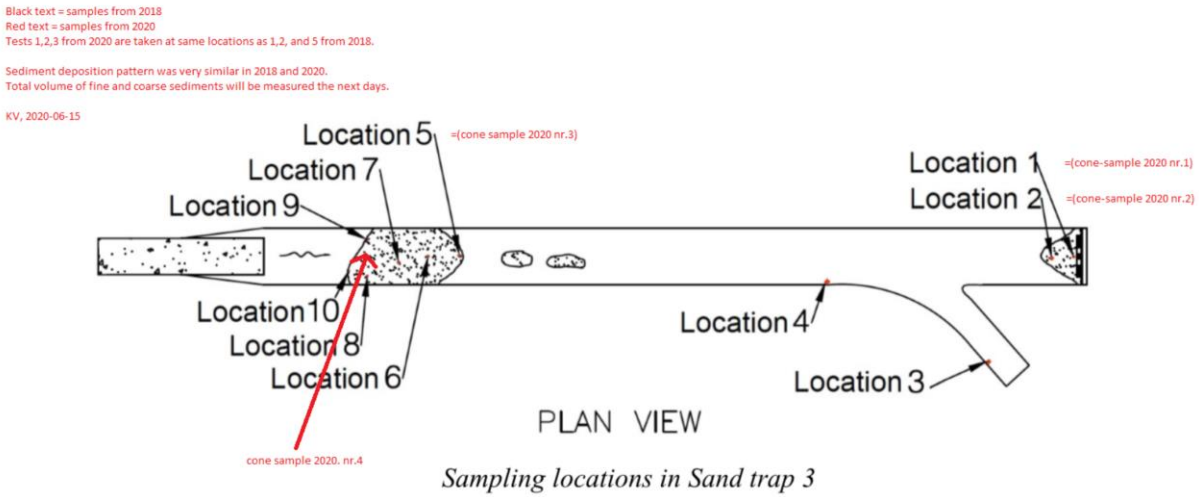

Figure 20: sediment specimen for the sieve curves

- **Jour Fixe 09**

03.08.2020 Vereide K. Richter W., Mauko Gasper, Havrevoll O. Presenting the work of TU Graz in the meantime since the last conference;

- SIMSEN model of Tonstad power plant
- Model test in the flume
- PIV in the model test
- 3D CFD of diffuser design
    - Ramp and tranquilizer rakes – 7 variants

- **Jour Fixe 10**

24.08.2020 Vereide K. Richter W.,

Discussion about the sand trap flow behavior and best options to improve the situation.

- **Jour Fixe 11**

31.08.2020 Vereide K. Richter W., Mauko G., presenting PIV results and discussion of the SIMSEN model of TU Graz

- **Jour Fixe 12**

07.09.2020 Vereide K. Richter W., Mauko G., presenting PIV results and discussion of weir heightening

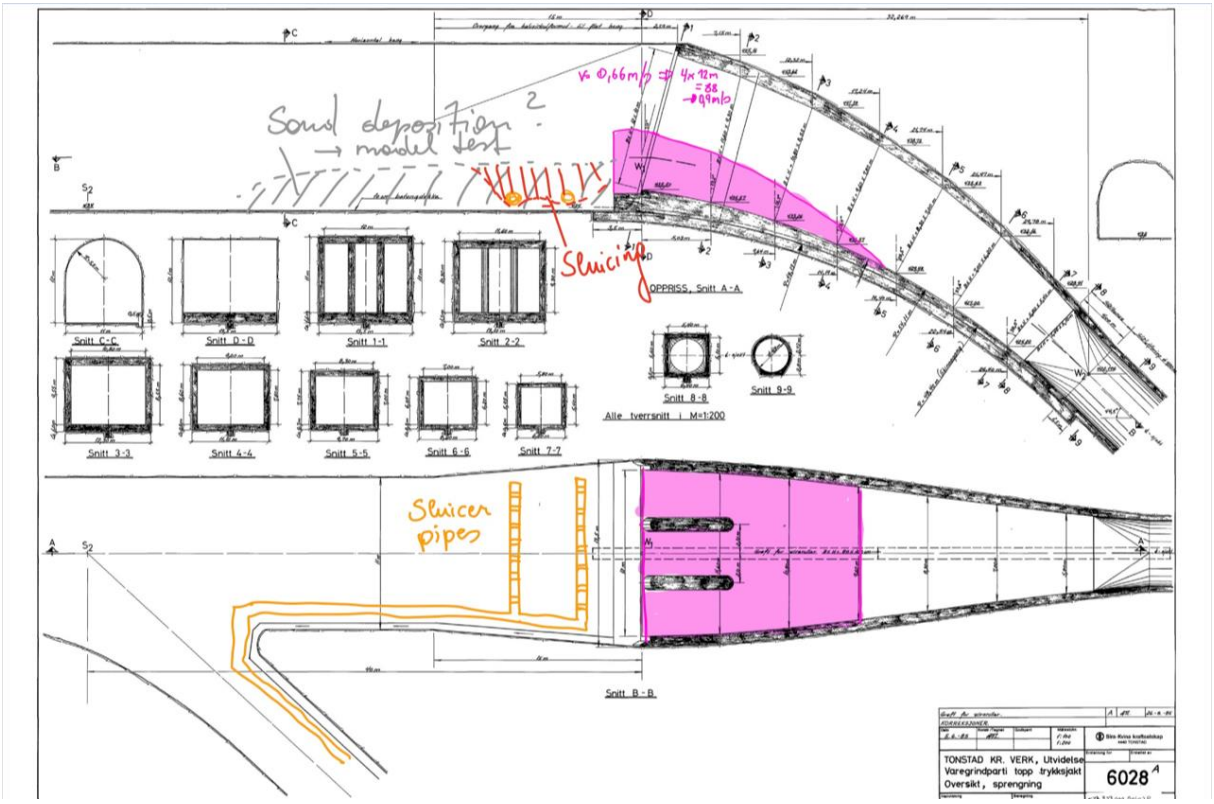

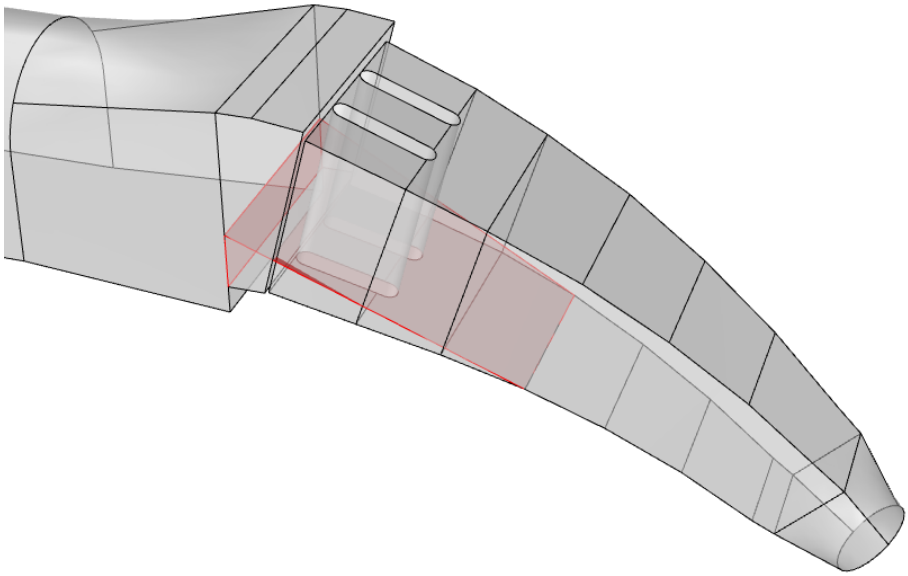

- **Jour Fixe 13**

14.09.2020 Vereide K. Richter W., Mauko G., presenting PIV results as well as discussing PIV results at NTNU. Presenting results of weir heightening on sand transportation effects. Discussion about rib investigations in Graz.

- **Jour Fixe 14**

30.10.2020 Vereide K. Richter W., Mauko G., Presenting SIMSEN results by G. Mauko and discussion about pump trip and SIMSEN model. Presenting of the semi-air cushion simulation by W. Richter as fig belwo

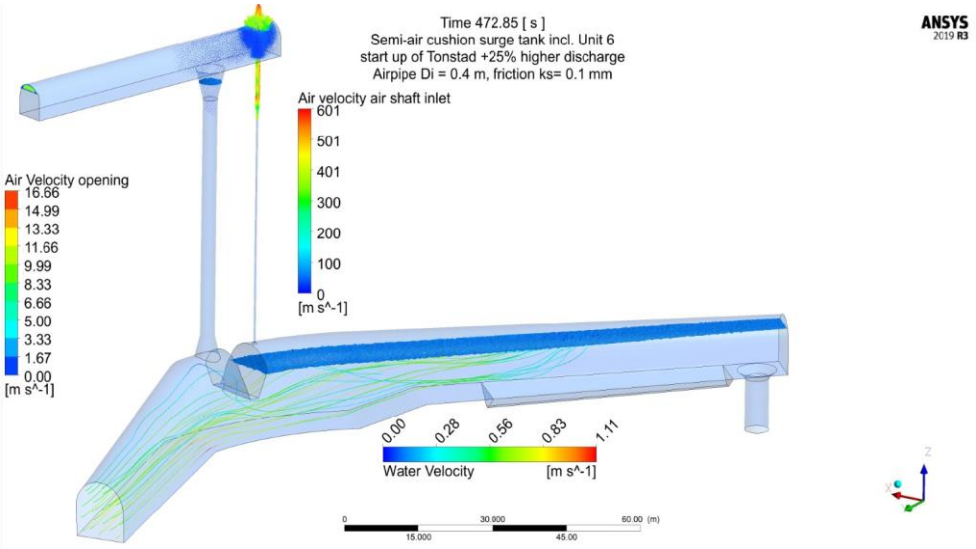

- **Jour Fixe 15**

23.11.2020 Vereide K. Richter W., Talks about finalizing the report and the project.

7. Surge tank investigation

The sand trap of the investigation is the number 3 sand trap of the Tonstad HPP. The sand trap is located directly downstream of the surge tank. No.3 surge tank and sand trap are upstream of the unit number 5 of the Tonstad HPP.

8. Geometry

8.1 Tonstad sand trap geometry

Figure 21 shows the geometry of the surge tank system with the sand trap of Tonstad HPP and the specific sand trap no. 3.

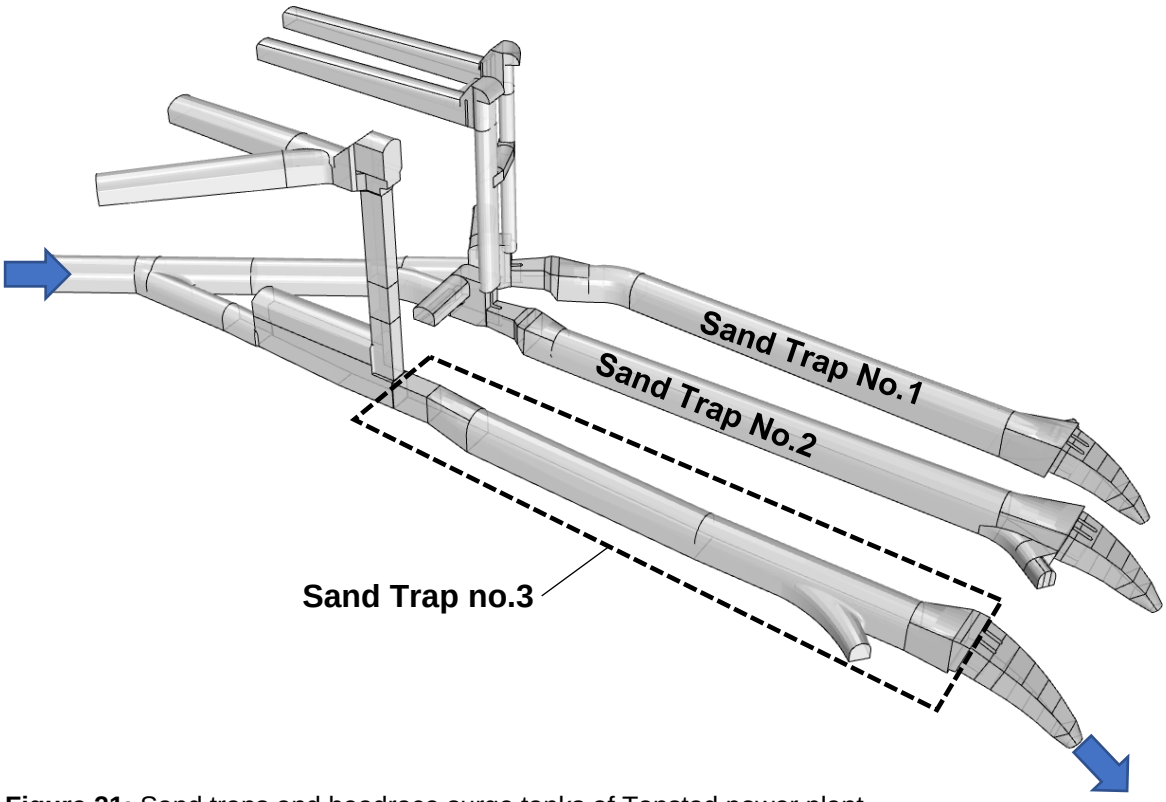

Figure 21: Sand traps and headrace surge tanks of Tonstad power plant

Table 1 shows the key numbers of the Tonstad high-head hydropower plant.

Table 1: Key numbers of *Tonstad* HPP (source: *Sira-Kvina*)

Installed capacity	960 MW
Head variation	430.3 m – 450.1 m
Machine concept	5 Francis turbines
Main headrace tunnels length and flow section area	L = 16000 m, A_i = 66 m² L = 7500 m, A_i = 57 m² L = 6000 m, A_i = 100 m²
Design discharge	Q_{Tu} = 240 m³/s

Figure 22 shows the geometry of the three surge tank structures of Tonstad HPP, except the gate section, that are concrete lined all other parts of the surge tank are unlined. The pressure shaft is steel lined. Surge tank no. 3 has one gate, both other surge tanks have two gates, separated by a middle pillar.

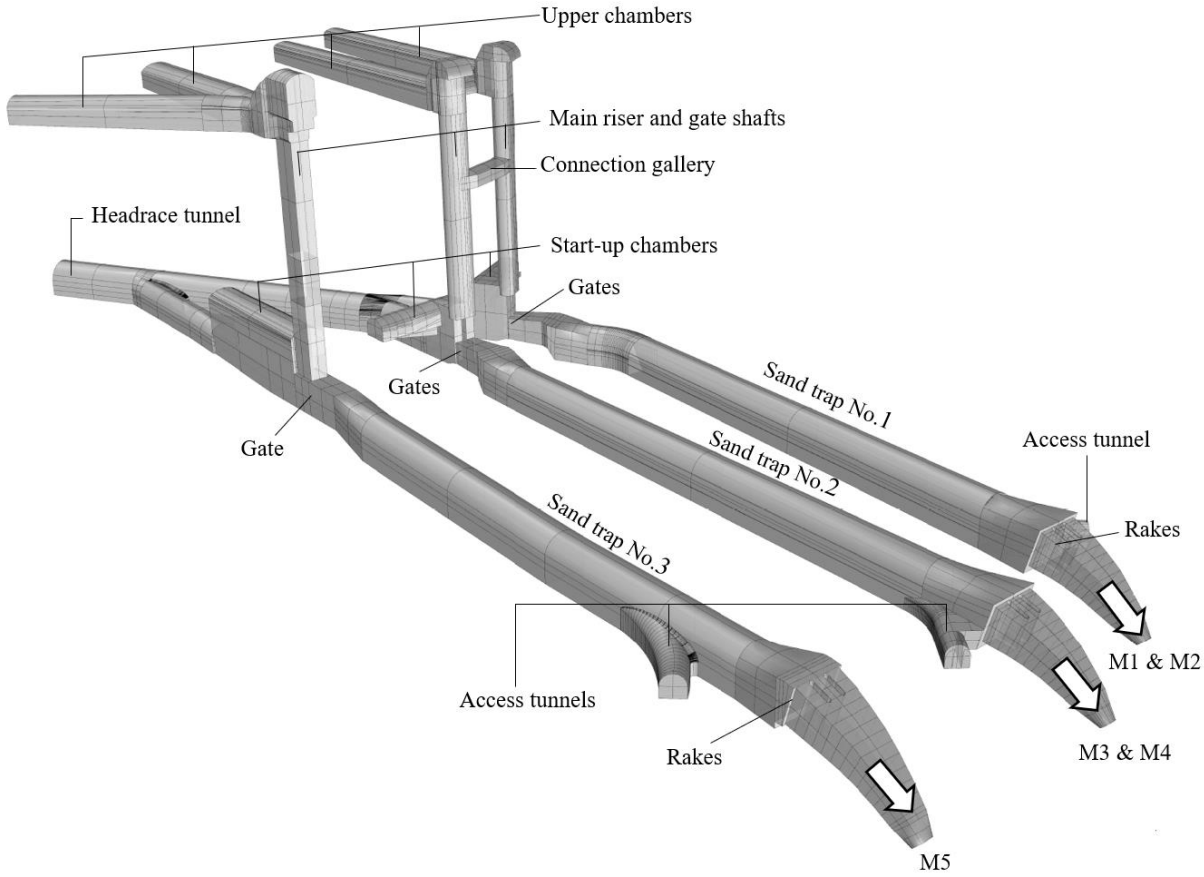

Figure 22: Tonstad surge tank, perspective view (Richter, 3D model by Sterner (Sterner 2018))

Figure 23 and Figure 24 show the gate section of surge tank no.3 and the dimensions for the 3D geometry used for the modelling in 3D CFD and small-scale model test.

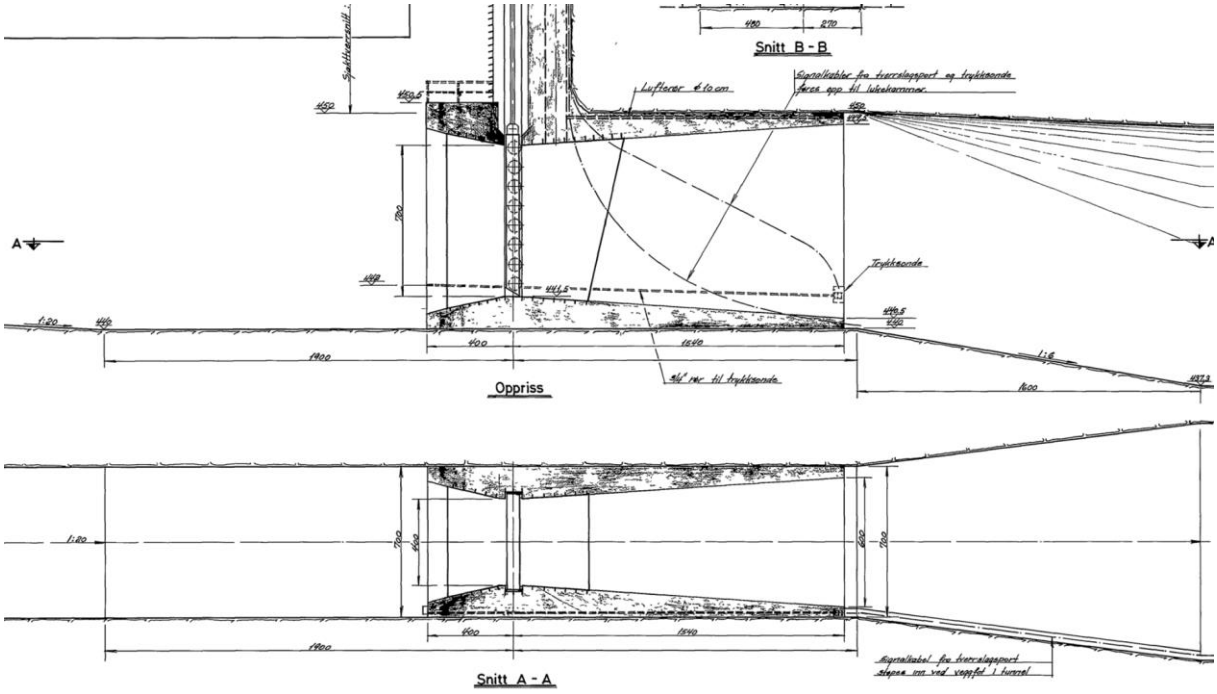

Figure 23: section View and Ground view of gate inlet of sand trap No. 3

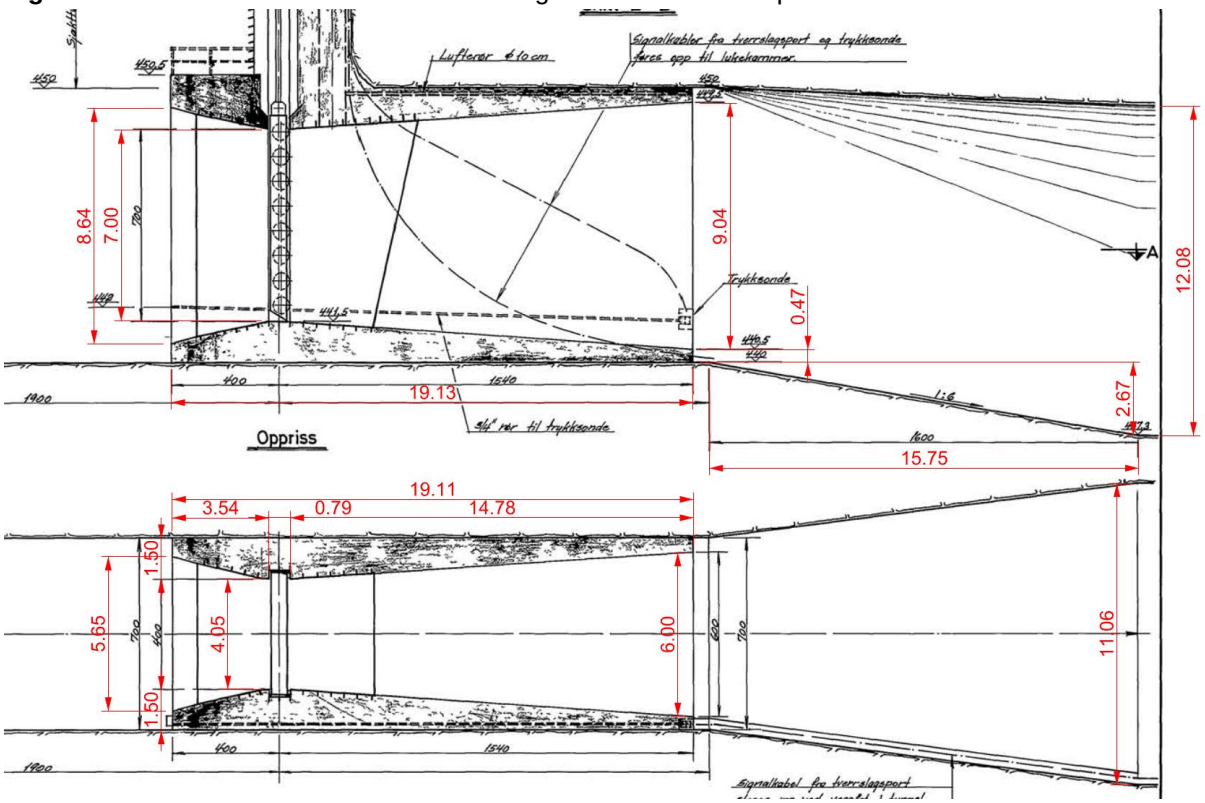

Figure 24: section View and Ground view of gate inlet of sand trap No. 3, with dimensioning

Figure 25 shows the longitudinal section and the plan view of surge tank no.3 Figure 26 shows the detail of the weir and the geometry of the concrete connection confusor to the pressure shaft of unit no. 5.

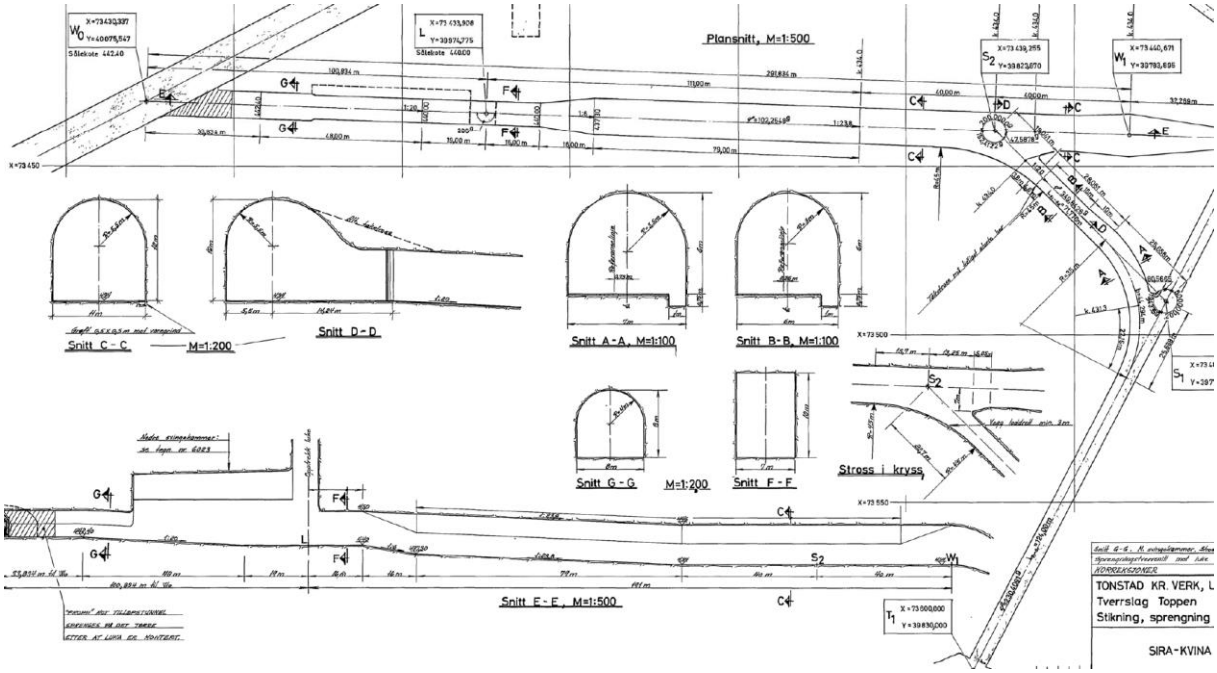

Figure 25: Sand trap no.3, design plan

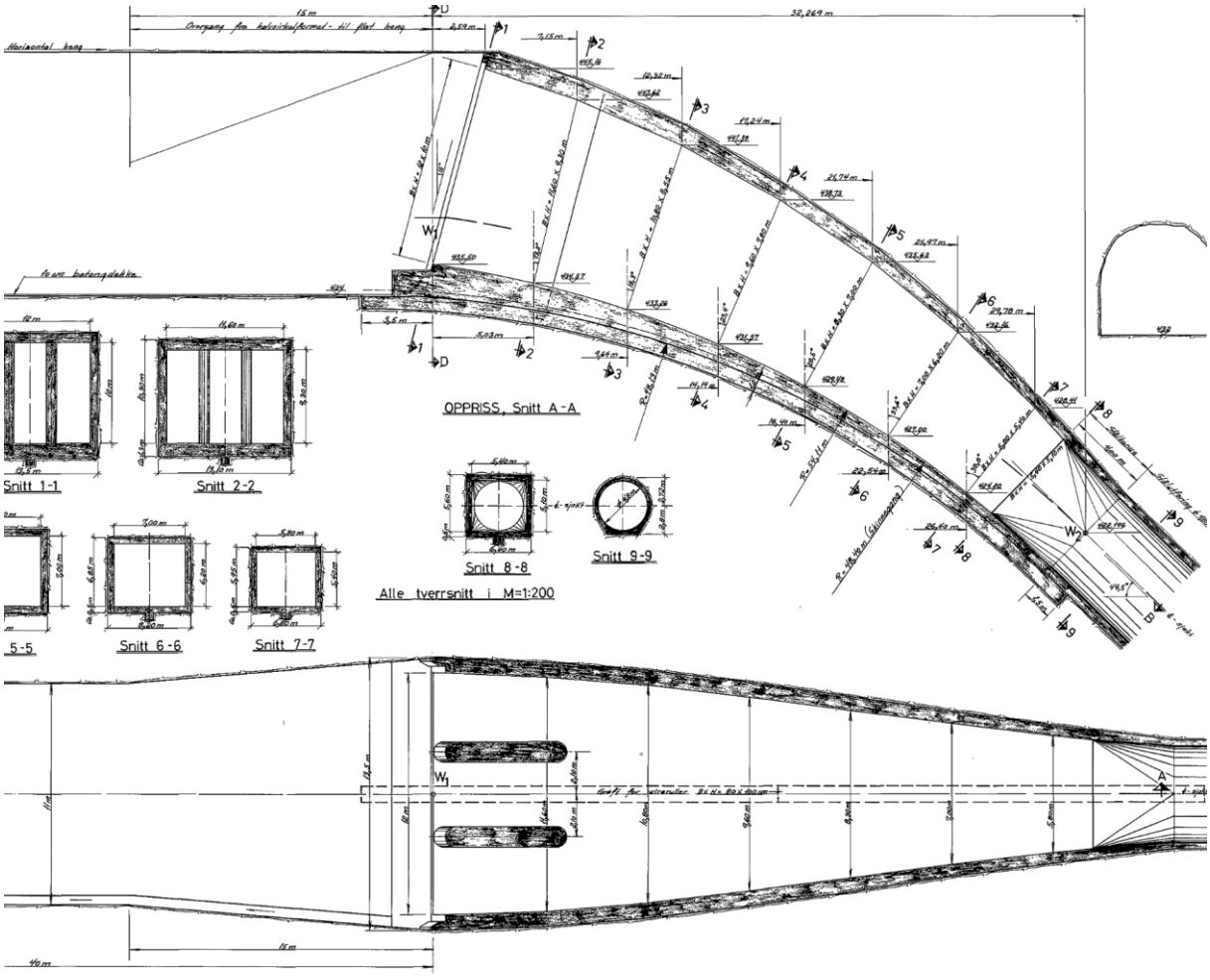

Figure 26: Weir section and transition to pressure shaft for unit no.5

Figure 27 shows the 1:20 scaled geometry for the *Fluent* particle meshing.

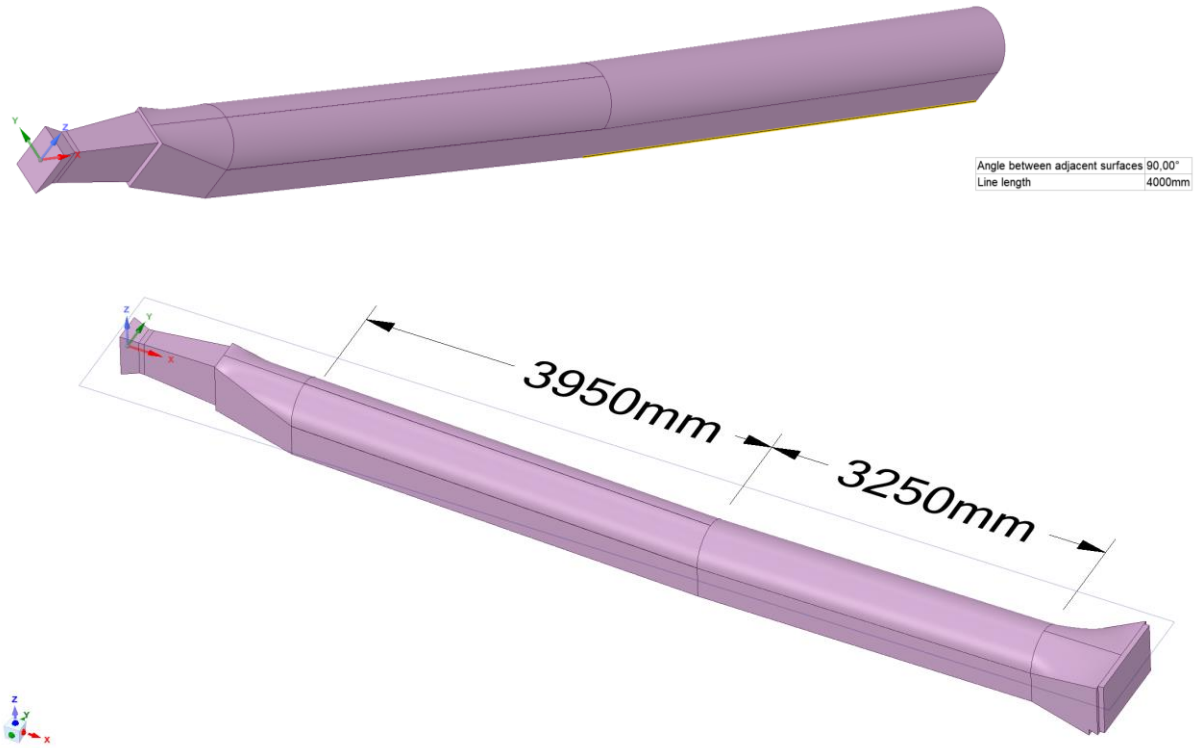

Figure 27: 1:20 scale of plan geometry of the sand trap no 3

8.2 **Meshing**

Figure 28 and Figure 29 show the meshing of the sand trap in *Fluent*. For the main 3D CFD simulations the software *CFX*, both Ansys was used with different meshing approach.

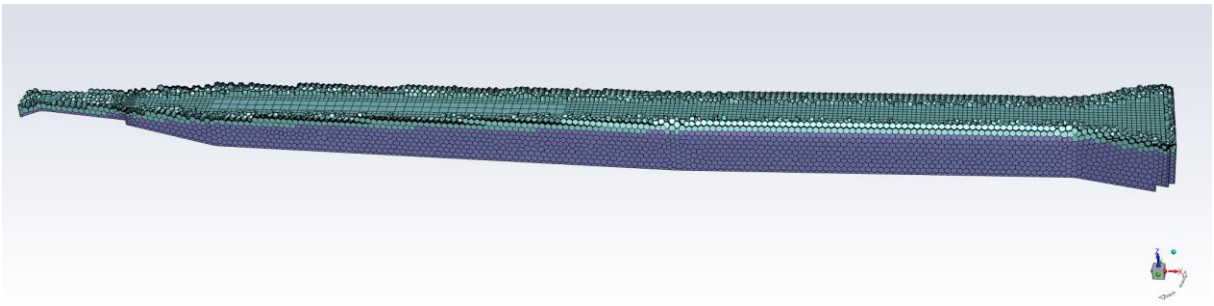

Figure 28: 1:20 meshing of sand trap with clipping plane

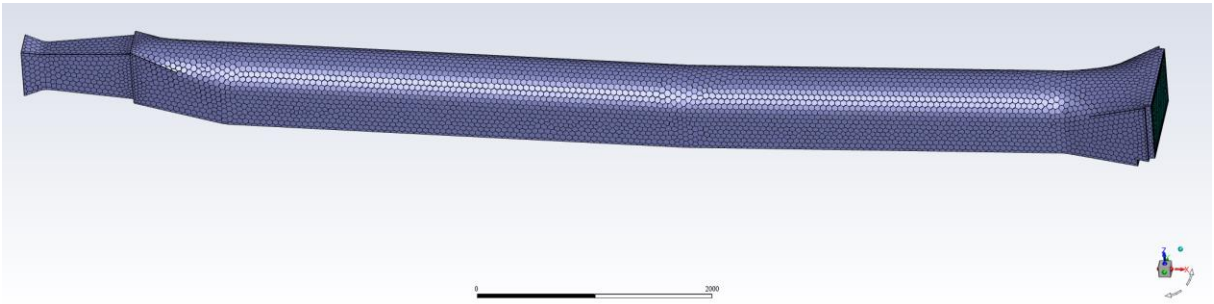

Figure 29: 1:20 meshing of sand trap

8.3 **Theory particle drag implementation in 3D CFD**

Figure 30 including the table from (Zhou, et al. 2019) shows different particle drag models implemented in 3D CFD. The drag model from Schiller and Naumann 1930's (Schiller und Naumann 1933) is implemented in CFX and is used for the particle tracking simulations in the investigations.

Table 2. Some well-established correlations of the drag force coefficient for spherical particles.

Name	Year	Correlation	
Newton [46]	1687	0.44	$Re_p \geq 100$
Stokes [47]	1880	$\frac{24}{Re_p}$	$Re_p \leq 40$
Schiller and Nauman [48]	1935	$\begin{cases} \frac{24}{Re_p}(1+0.15Re_p^{0.687}) \\ 0.44 \end{cases}$	$Re_p \leq 1000$ $Re_p \geq 1000$
DallaValle [49]	1948	$(0.63+\frac{4.8}{\sqrt{Re_p}})^2$	/
Brown and Lawler [50]	2003	$\frac{24}{Re_p}(1+0.15Re_p^{0.681})+\frac{0.407}{1+\frac{8710}{Re_p}}$	/

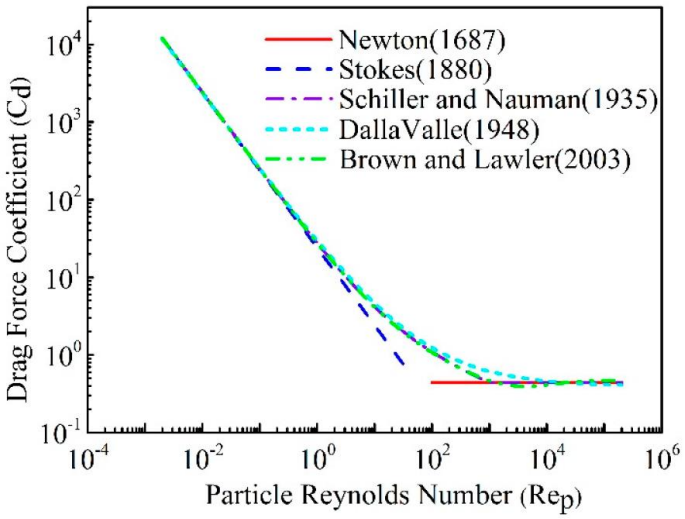

Figure 2. Correlations of the drag force coefficient.

Figure 30: Drag law implementation in 3D CFD (Zhou, et al. 2019)

8.3.1 **Sediment scaling in pressurized sand trap**

This chapter briefly describes some aspects of sand scaling for pressurized sand trap investigation.

The research was done via 3D CFD using particle tracking at prototype scale and physical model testing at 1:36.67 scale. For the latter investigations a scaling with 1:1 sediment size was used utilized with 1:1 velocity.

This approach could also produce very comparable sediment pattern with the prototype sand trap.

A reason for the approach is the conservation of the particle Reynolds number. Sediment settling follows the same pattern for the scaled model test and the prototype.

In order to avoid cohesive sediments in the flume test it is aimed for running the model test simulations with prototype size sediments for the range of the particle of critical size defining the sand trap.

The approach was utilized also for a model test investigation at TU Delft by (Develay, et al. 1996) and (de Jong, et al. 1992) for a large desilter in a realized hydropower project.

Sphere in a fluid

For a sphere in a fluid, the characteristic length-scale is the diameter of the sphere and the characteristic velocity is that of the sphere relative to the fluid some distance away from the sphere, such that the motion of the sphere does not disturb that reference parcel of fluid. The density and viscosity are those belonging to the fluid. Note that purely laminar flow only exists up to Re = 10 under this definition.

Under the condition of low Re, the relationship between force and speed of motion is given by Stokes' law

Fall velocity

The particle Reynolds number is important in determining the fall velocity of a particle. When the particle Reynolds number indicates laminar flow, Stokes' law can be used to calculate its fall velocity. When the particle Reynolds number indicates turbulent flow, a turbulent drag law must be constructed to model the appropriate settling velocity (Wikipedia Reynoldsnumber kein Datum).

Particle Reynolds number:

$$Re = \frac{uD_p\rho}{\mu}$$

u : velocity of fluid stream
D_p : diameter of the particle
ρ : density of fluid
μ : viscosity of fluid

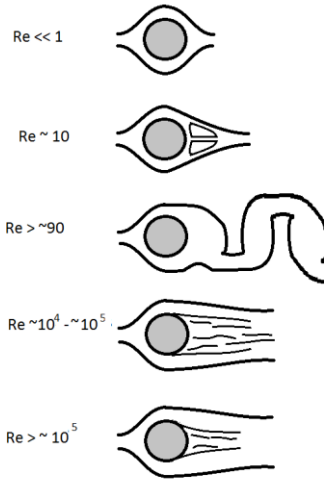

Figure 31: Flow on articles depending on Reynolds number Source: Wikipedia https://en.wikipedia.org/wiki/Reynolds_number

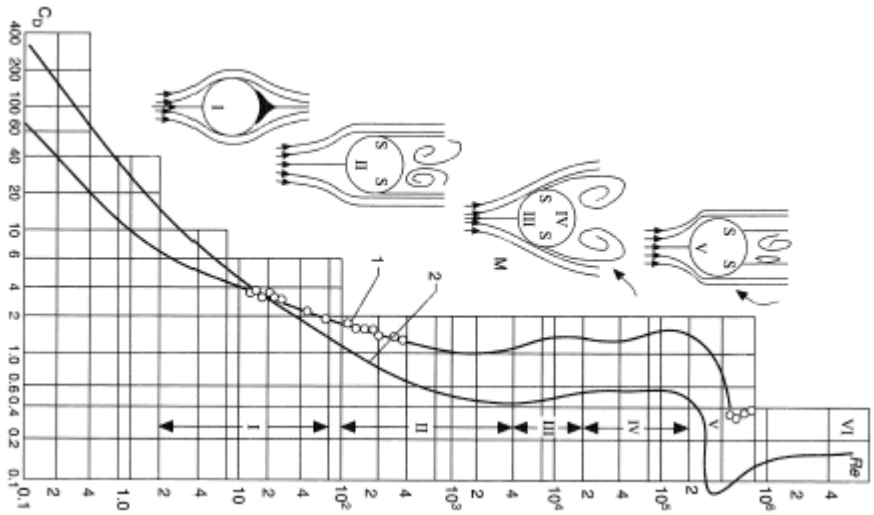

Figure 32: Drag coefficient for cylinders (1) and spheres (2) as a function of Reynolds number (Re) (Source: http://www.thermopedia.com/content/707/)

Table 2 shows the relation of particle fluid properties that can be correlated with hydrodynamic flow behaviour and results. Especially critical bed shear stress is a very significant property to outline the bed load capacity of the flow in the sand trap without particle tracking simulation.

Table 2: critical bed shear stress for several grain sizes (U.S. Geological Survey 2013)

[Modified from Julien, 1998, table 7.1. Sediment mobility for a given particle size occurs when the bed shear stress exceeds the critical shear stress. This only determines whether or not a given particle size is mobile. **Critical bed shear stress** (τ_c) calculated from equation 4 using particle diameters from this table. **Abbreviations:** φ, phi scale where $\varphi = -\log_2$ (diameter in mm); mm, millimeter; N/m^2, Newtons per square meter]

Particle classification name	Ranges of particle diameters		Shields parameter (dimensionless)	Critical bed shear stress (τ_c) (N/m^2)
	φ	mm		
Coarse cobble	-7 – -8	128 – 256	0.054 – 0.054	112 – 223
Fine cobble	-6 – -7	64 – 128	0.052 – 0.054	53.8 – 112
Very coarse gravel	-5 – -6	32 – 64	0.05 – 0.052	25.9 – 53.8
Coarse gravel	-4 – -5	16 – 32	0.047 – 0.05	12.2 – 25.9
Medium gravel	-3 – -4	8 – 16	0.044 – 0.047	5.7 – 12.2
Fine gravel	-2 – -3	4 – 8	0.042 – 0.044	2.7 – 5.7
Very fine gravel	-1 – -2	2 – 4	0.039 – 0.042	1.3 – 2.7
Very coarse sand	0 – -1	1 – 2	0.029 – 0.039	0.47 – 1.3
Coarse sand	1 – 0	0.5 – 1	0.033 – 0.029	0.27 – 0.47
Medium sand	2 – 1	0.25 – 0.5	0.048 – 0.033	0.194 – 0.27
Fine sand	3 – 2	0.125 – 0.25	0.072 – 0.048	0.145 – 0.194
Very fine sand	4 – 3	0.0625 – 0.125	0.109 – 0.072	0.110 – 0.145
Coarse silt	5 – 4	0.0310 – 0.0625	0.165 – 0.109	0.0826 – 0.110
Medium silt	6 – 5	0.0156 – 0.0310	0.25 – 0.165	0.0630 – 0.0826
Fine silt	7 – 6	0.0078 – 0.0156	0.3 – 0.25	0.0378 – 0.0630

8.4 3D CFD Boundary conditions

This chapter describes the boundary conditions for the model test simulations and the 3D CFD simulations.

8.4.1 Pressurized sand trap simulations

Figure 33 shows the geometry of the sand trap with chamber widening before the weir, in the main simulations this was substituted by a constant geometry to simplify the model to place it in the flume.

Particles: density: 2650*0.8 (safety reduction) = 2120 kg/m³. This safety reduction was initially anticipated. The main simulations were done with 2650 kg/m³ particle density.

Froude scale model: 1:20
Discharge scale factor: $20^{2.5}$ = 1788.85 [-]

Comment: Due to the improved approach of 1:1 velocity in the inlet, the Froude scaled velocity was not further investigated.

Discharge $_P$ … 80 m³/s
Discharge $_M$ … 80 m³/s / 1788.85 = 0.04472 m³/s = 44.72 l/s
Velocity Boundary condition inlet $_P$ = 1.637 m/s
Velocity Boundary condition inlet $_M$ = 0.3651 m/s

Pressure Boundary condition outlet $_M$ = 0 Pa

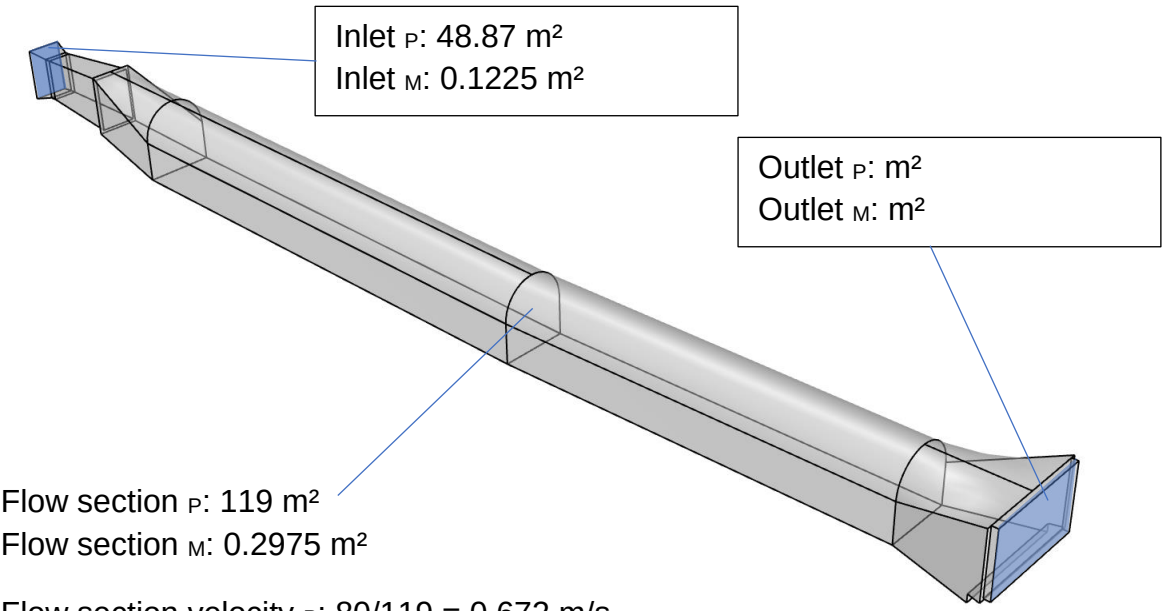

Flow section $_P$: 119 m²
Flow section $_M$: 0.2975 m²

Flow section velocity $_P$: 80/119 = 0.672 m/s
Flow section velocity $_M$: 0.04472 / 0.2975 = 0.1503 m/s

Length: 9.68 m / 0.1503 m/s = 64.4 s – ref. time to pass

Figure 33: Sand trap model boundary conditions

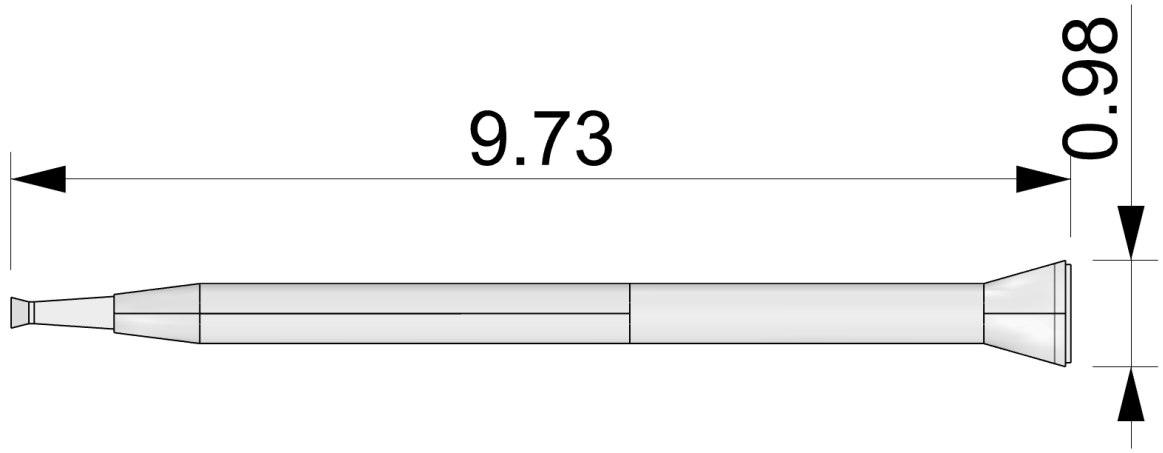

Figure 34: Sand trap model size 1:20

8.4.2 **1:36.67 scaled geometry for flume tests**

Figure 35 and Figure 36 show the sand trap geometry idealized as given in the design plans. The flow section was set to be constant. This unification of the flow section, also the sparing of the adit tunnel section improved the ability to simulate the geometry and the aspect to place it in the flume of the hydraulic laboratory.

The effects of the adit were investigated in the Fleks project 1.0, where hydraulic investigations and have shown unbeneficial behaviour.

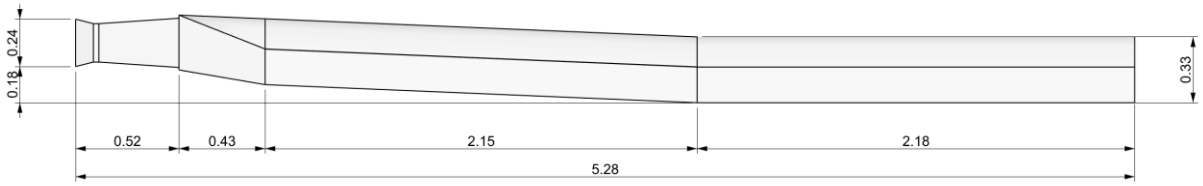

Figure 35: Geometry of the sand trap in 1:36.67 scale for the flume test

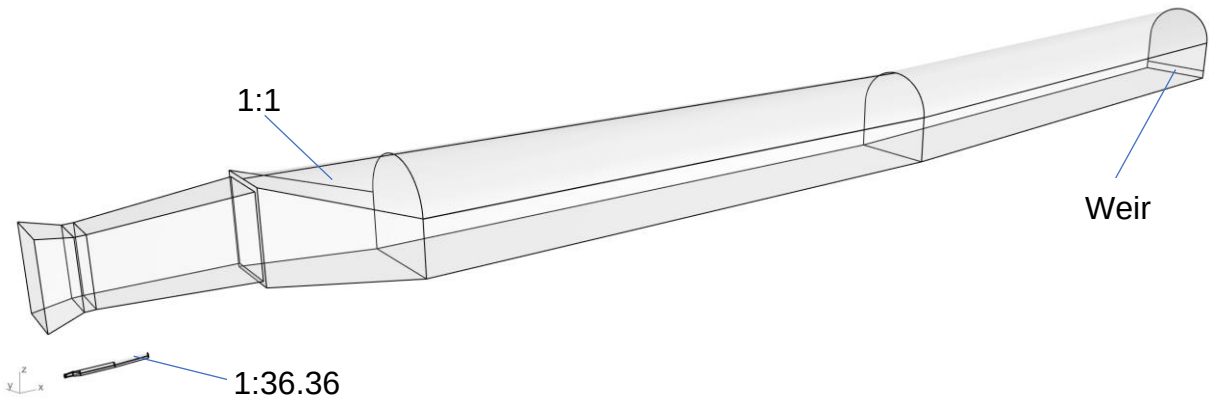

Figure 36: Scale comparison 1:1 to 1:36.67

8.4.3 **Boundary conditions**

Following boundary conditions are basis of the hydraulic investigations described in this report.

8.4.3.1 Idealized box simulation

These simulations are dedicated to study the particle tracking flow for different scaling in order to study the particle scaling laws for pressurized flow. The simulations based on the box flow confirm the 1:1 velocity scaling for the sediment investigations.

Figure 37 and Figure 38 show the dimensions of the box that are related to the size of the sand trap chamber in its length and width.

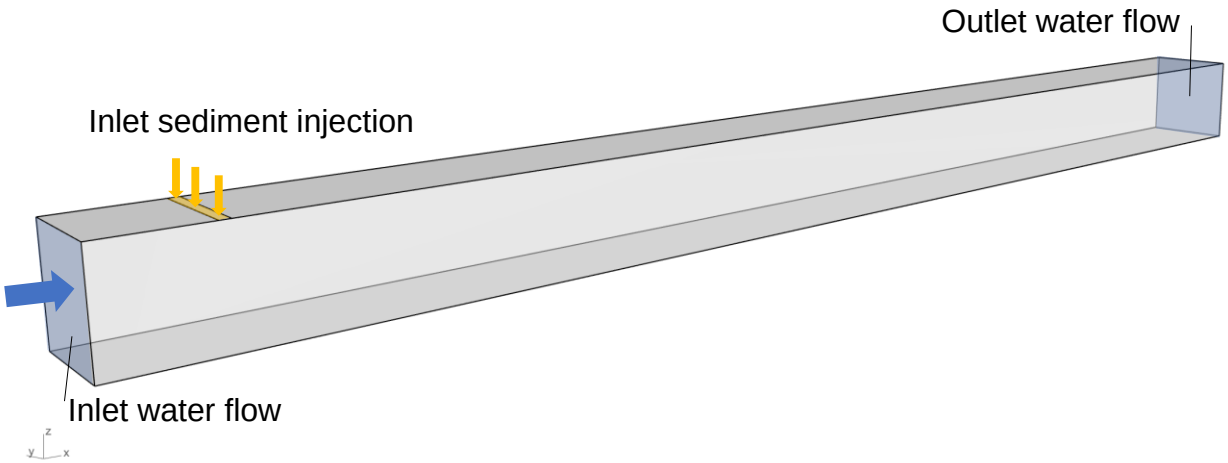

Figure 37: Geometry of a rectangular box for the idealized particle simulations

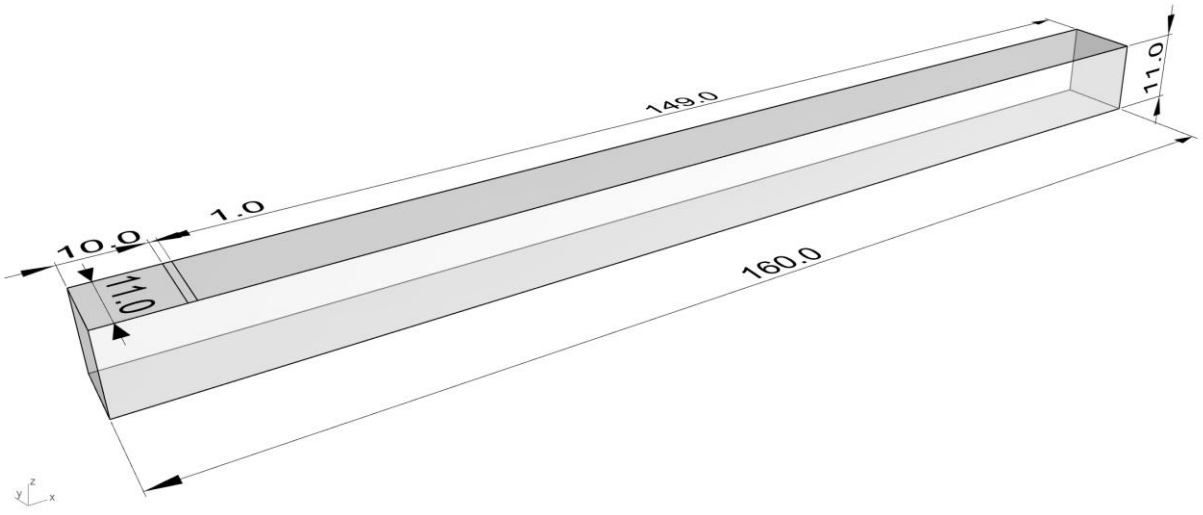

Figure 38: Geometry of a rectangular box for the idealized particle simulations, dimensions

8.4.3.2 Prototype scale 1:1 velocity Boundary condition

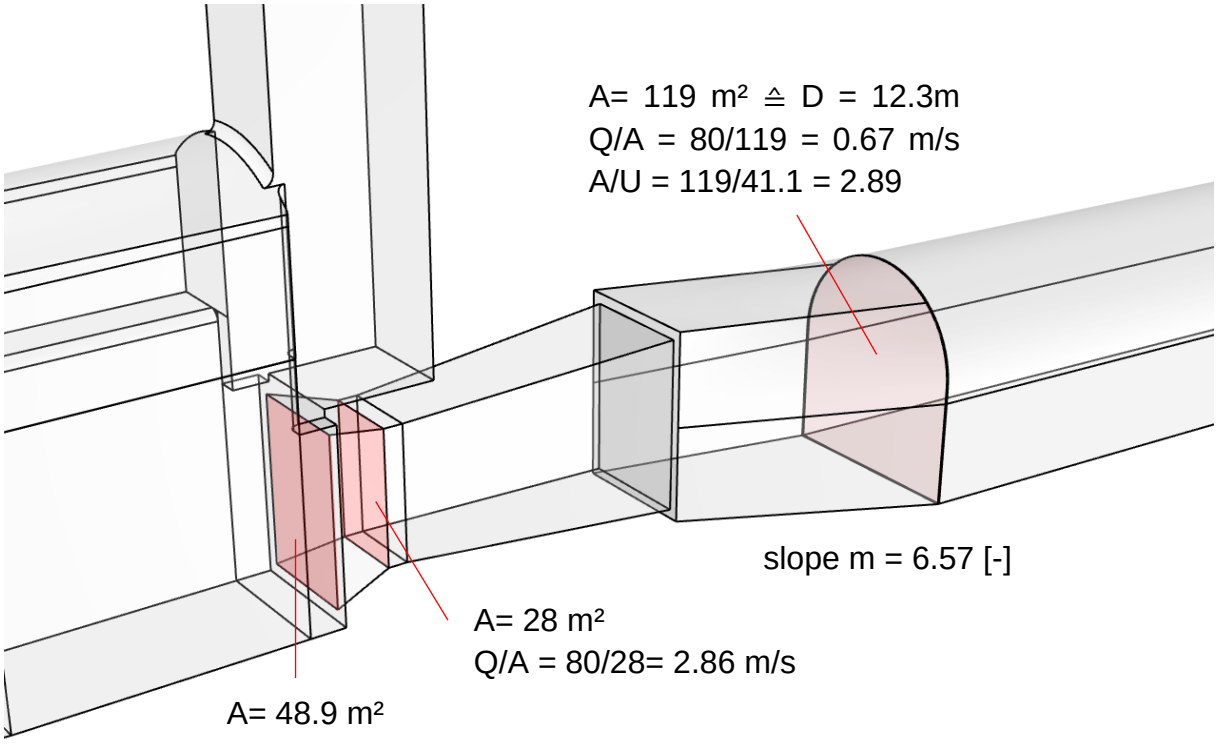

Note: Additionally, asymmetric and rotational flow concentrate max. velocity rotational flow concentrate max. velocity peaks. Creating a “catapult effect”. Sediment disposal in front worsens the situation.

Re in sand trap 1:1: $\frac{v0 \cdot D}{\nu} = \frac{0.67 \cdot 12.3}{0.000001} = 8.2 \cdot 10^6$

Figure 39: Geometry of a rectangular box for the idealized particle simulations, dimensions, Froude scaled velocity **prototype scale**

8.4.3.3 Model scale 1:20 velocity Boundary condition

Figure 40 shows the inflow section dimensions and the associated uniform velocities of the 1:20 scale geometry, as it is applied in the hydraulic laboratory in Trondheim.

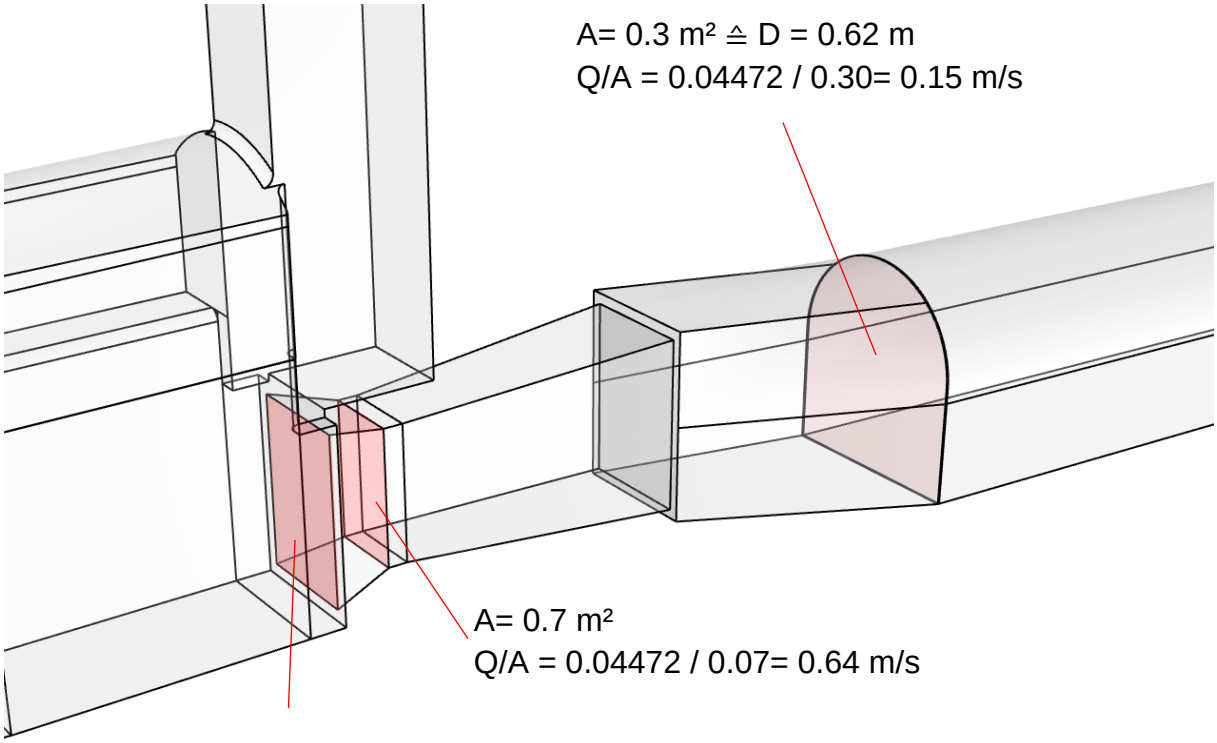

A= 0.12 m²
Q/A = 0.04472 / 0.12 = 0.373 m/s

Discharge if $v_M \triangleq v_P$ = 1.64 m/s
1.64 m/s * 0.12 m² = 0.197 m³/s

Re in sand trap 1:20: $\frac{v0 \cdot D}{\nu} = \frac{0.67 \cdot 0.62}{0.000001} = 4.15 \cdot 10^5$

Note: Additionally, asymmetric and rotational flow concentrate max. velocity peaks. Creating a “catapult effect”. Sediment disposal in front worsens the situation.

Figure 40: Geometry of a rectangular box for the idealized particle simulations, dimensions, Froude scaled velocity **model scale 1:20**

8.4.3.4 Model scale 1:36.667 velocity Boundary condition

Figure 41 shows the inflow section dimensions and the associated uniform velocities of the 1:36.67 scale geometry as it is applied in the hydraulic laboratory in Graz. The size was defined by the given width of the flume and a reasonable length to represent the sand geometry.

Froude scale for velocity: $\sqrt{36.667}$= 6.055 [-]
Froude scale Discharge: 36.667^2.5 = 8141.2 [-] → 80 m³/s ≙ 0.0098 m³/s

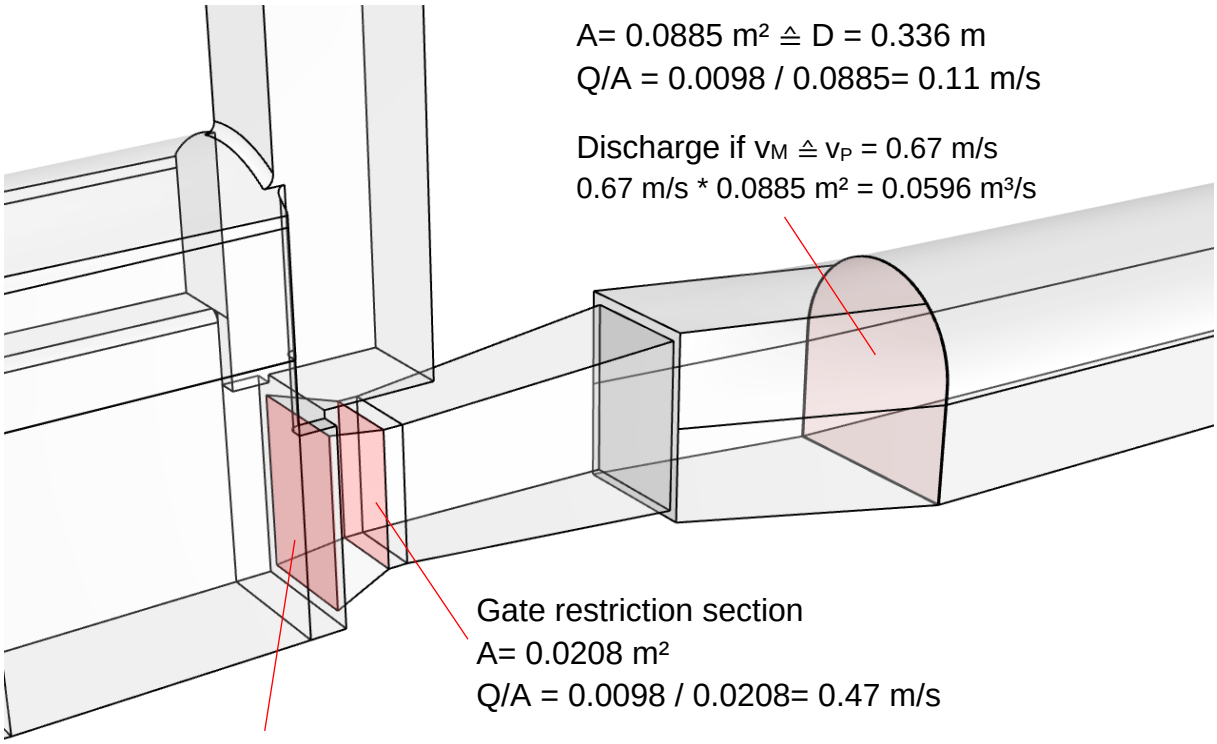

Note: Additionally, asymmetric and rotational flow concentrate max. velocity rotational flow concentrate max. velocity peaks. Creating a "catapult effect". Sediment disposal in front worsens the situation.

Re in sand trap 1:36.67: $\frac{v0 \cdot D}{\nu} = \frac{0.67 \cdot 0.336}{0.000001} = 2.25 \cdot 10^5$

Figure 41: Geometry of a rectangular box for the idealized particle simulations, dimensions, Froude scaled velocity **model scale 1:36.67**

Velocity scale:	1:1
Discharge scale:	80000 / 59.6 = 1342 [-]
Length and Timescale:	36.67 [-]

8.4.3.5 Discharge for sand trap

The discharges for the sand trap model tests were assumed based on a typical discharge plot at unit no. 5 leading to three discharges as shown below.

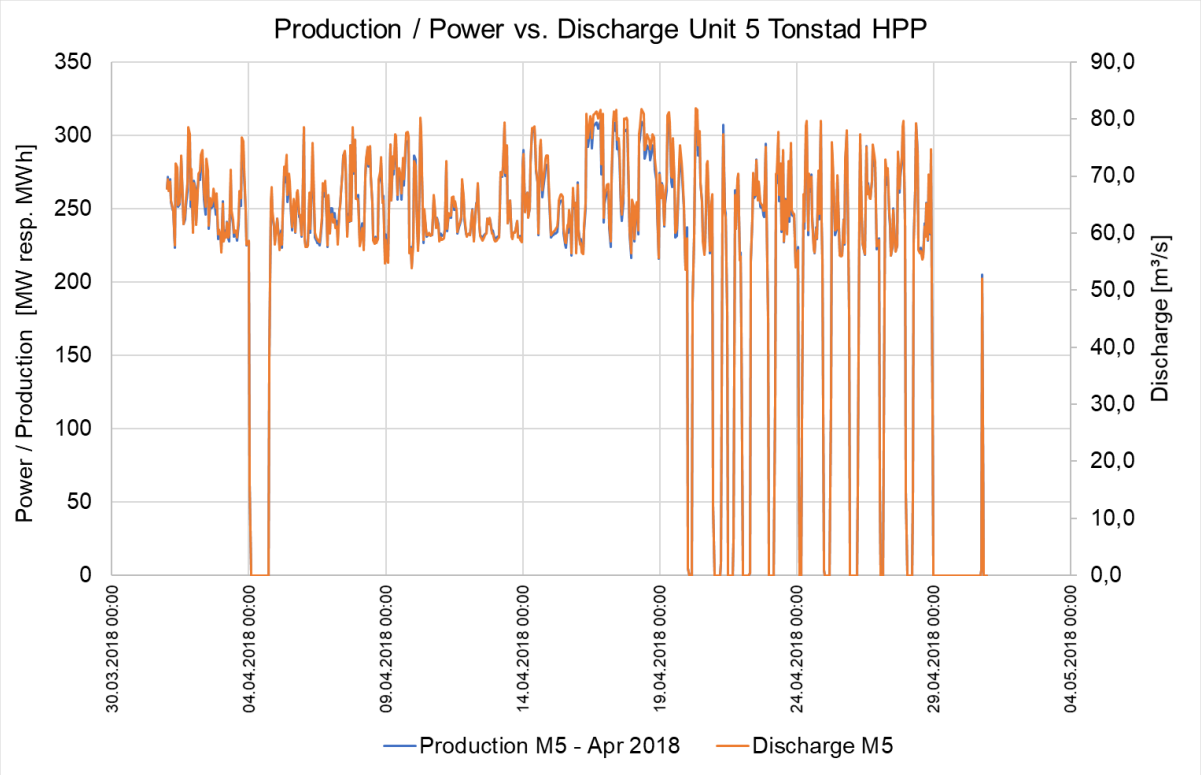

Figure 42: Discharge plot of the operation of unit no. 5 in Tonstad power plant

The discharges below are the main input flows for the model test investigations:

Upper limit discharge: 80 m³/s / 1342 [-] → 59.6 l/s

Mean discharge: 65 m³/s / 1342 [-] → 48.4 l/s

Lower limit discharge: 55 m³/s /1342 [-] → 41 l/s

8.4.3.6 Assumed sediment disposition at surge tank no.3 behind gate

It was observed that the widening of the flow section at the start-up chamber allows sediment deposition. The assumed deposition geometry in Figure 43 is investigated by a 3D CFD simulation towards its influence on the flow pattern entering the pressurized sand trap. The sedimentation pattern is assumed by a circular arc with 2m height at the maximum, filling also the gap at the entrance to the gate restriction. Figure 44 shows the excavation work upstream of the gate with the removed deposition similar to the anticipated deposition as shown in Figure 43.

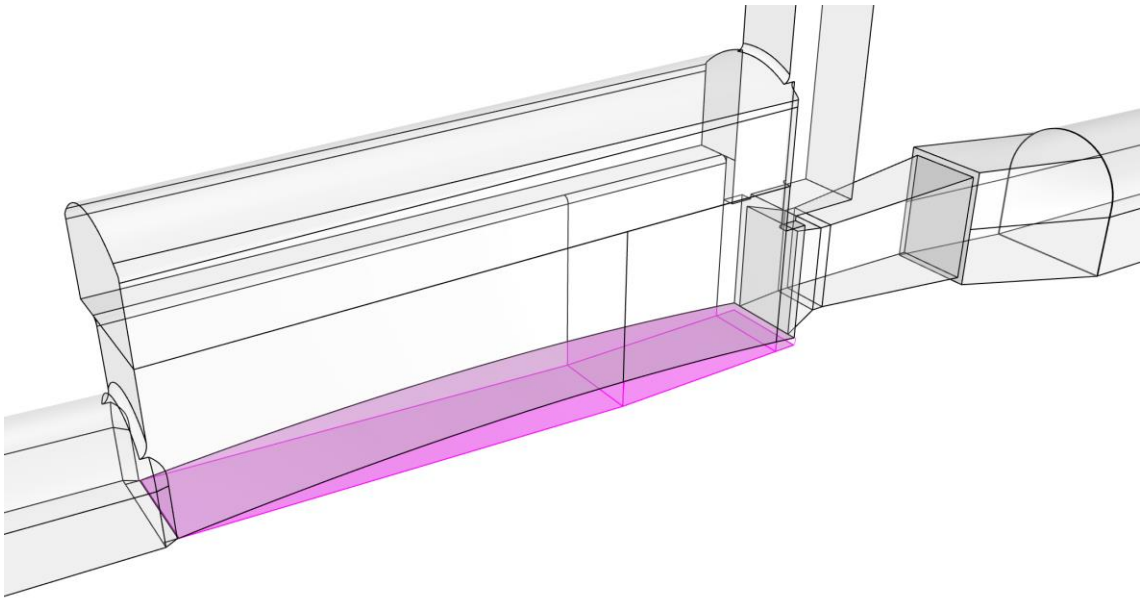

Figure 43: Geometry of surge tank No.3, tunnel widening at start-up chamber, assumed sediment deposition for 3D CFD flow simulation study

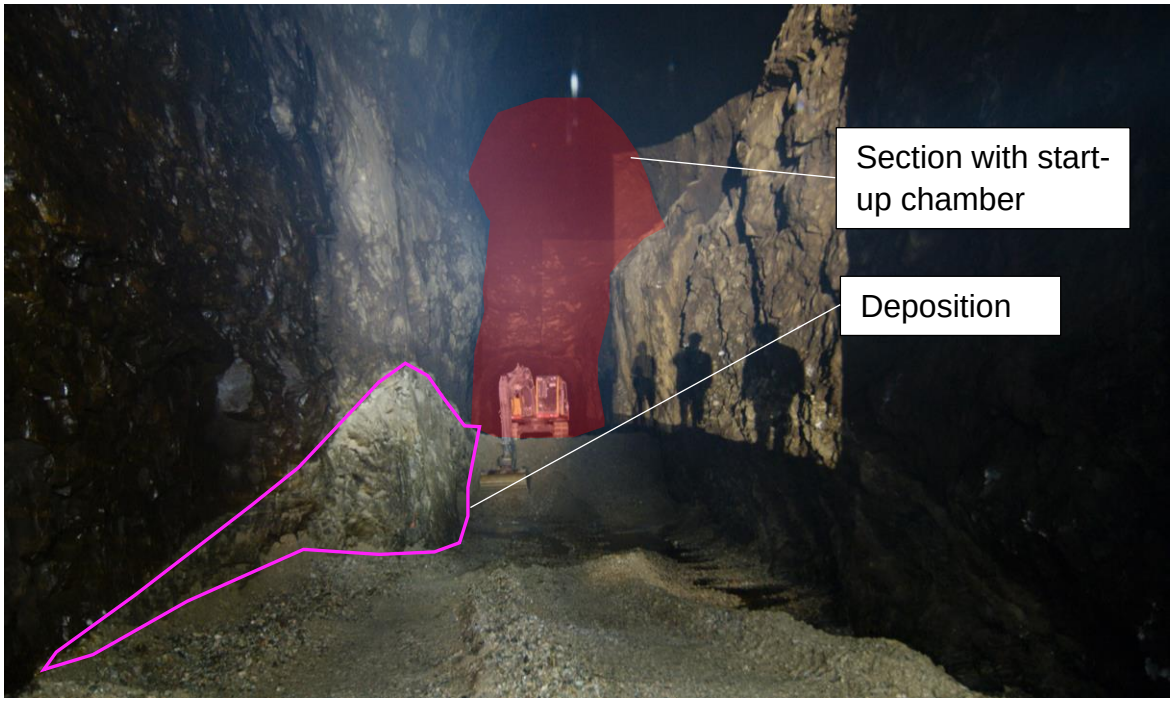

Figure 44: Excavated Sediment in the Tunnel Section at the start-up chamber upstream of the gate section

8.4.3.7 Rotational flow at gate section

Due to the bend in the branch from the main headrace tunnel a rotational flow is induced reaching the gate section of the surge tank and thus enters with a rotational motion into the sand trap that is negatively influencing the settling behaviour. From the simulations shown below a value of 2.75 m³/s from 80m³/s is flowing in y-direction entering the gate section. This is 3.44%. With sand depositions at the widening section it is believed that the rotational flow can be even more significant. The 3.44% for rotation flow input are taken as boundary condition for reduced geometry simulations.

Further in this report it is shown that rather than a rotational inflow conditions a specific velocity boundary condition generated from a simulation including the surge tank and the headrace tunnel are more straightforward.

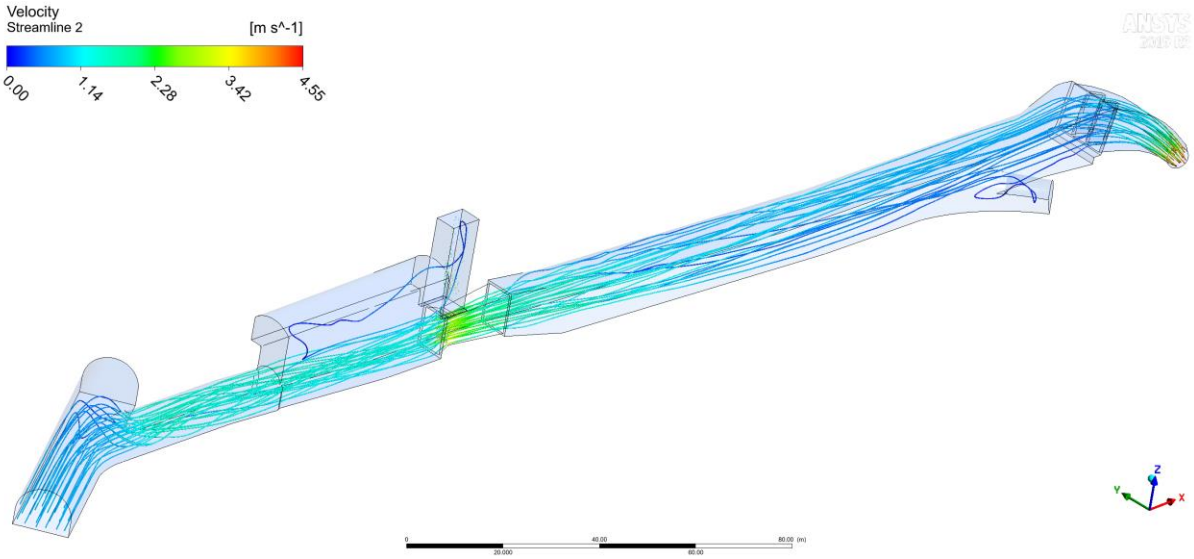

Figure 45: 3D flow situation with 80m³/s full geometry with approach flow

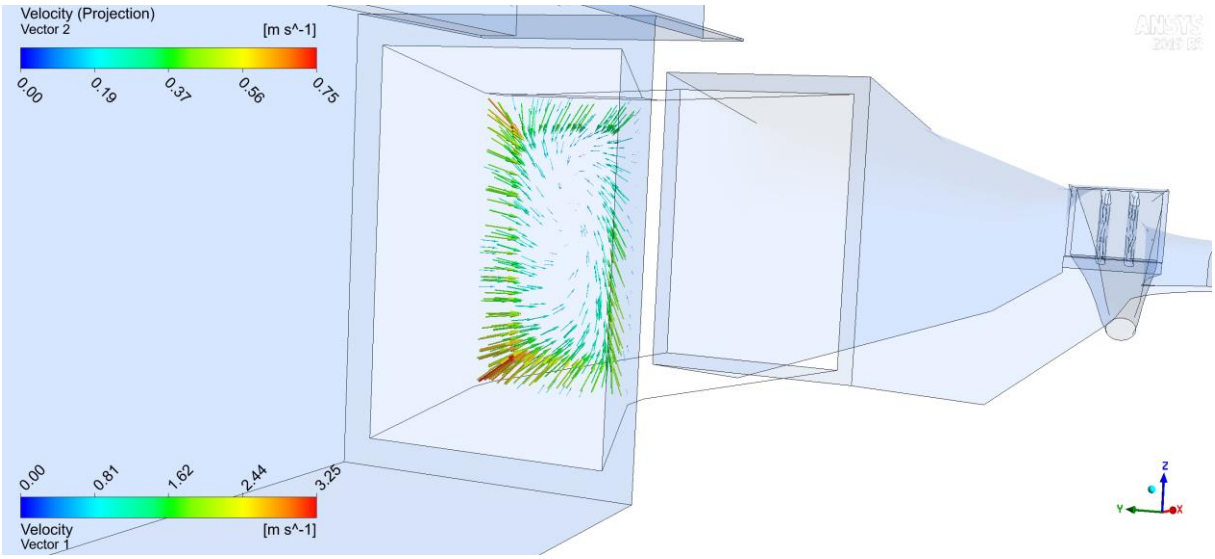

Figure 46: 3D flow situation with 80m³/s full geometry with approach flow, detail of rotational flow in gate section

8.4.3.8 Inlet velocity profile taking approach flow into account

The inlet velocity profile is significantly influencing the jet behaviour inside of the sand trap expansion chamber. The asymmetry of the profile is influenced by the curved flow from the headrace tunnel and flow fluctuations in the start-up chamber region as well as sediment depositions there. Figure 45 shows the profile as a result from a simulation with the approach geometry applied onto a simulation without approach flow geometry.

This approach was further used to simulate the flow behaviour for variant study and particle tracking simulations.

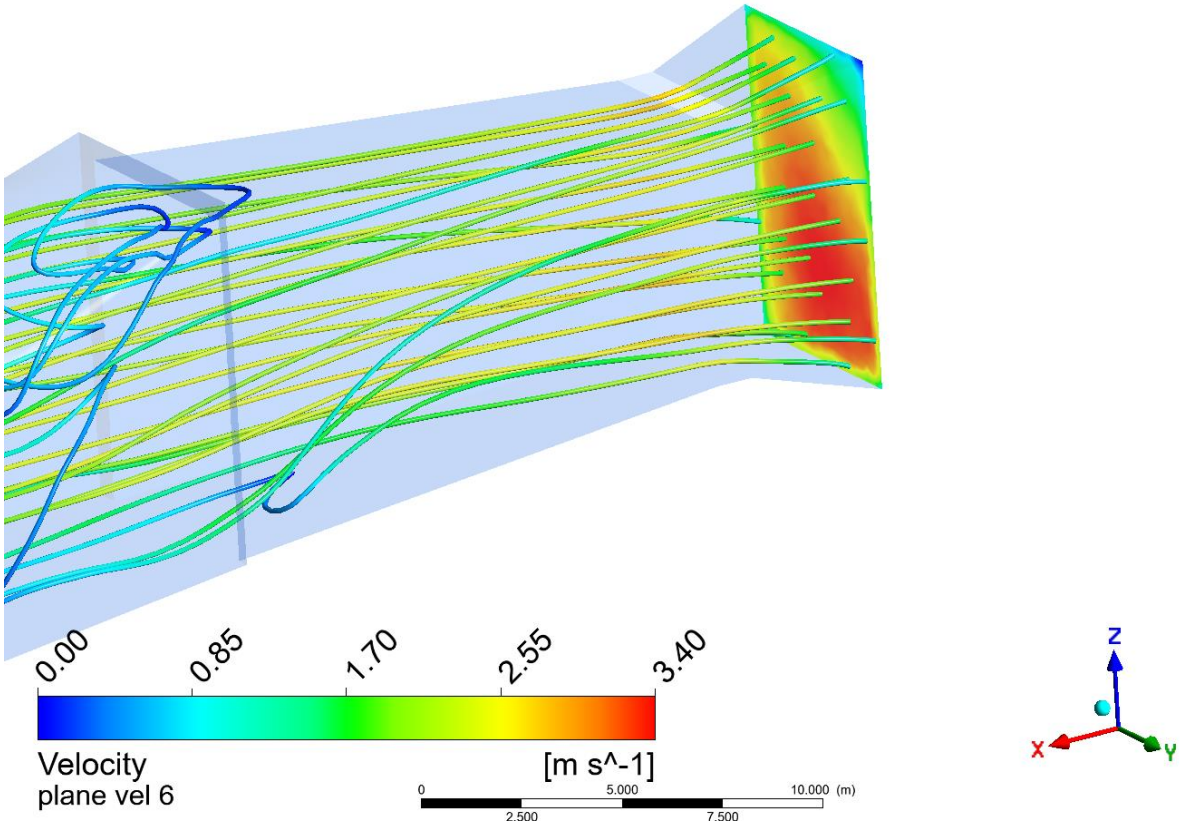

Figure 47: Inlet velocity plane as result from simulation with approach flow from tunnel and surge tank

8.5 **Literature sand trap design approach**

A comparison is done with the literature source (Ortmanns 2006) utilizing the formula:

$$L = \frac{H \cdot U}{w_0 - \frac{0.21}{K}} \quad [m] \qquad K = \frac{1}{U^{0.4} \cdot U_E^{0.3}} \cdot m \cdot \frac{1}{(g \cdot R)^{0.15}} \quad [m/s]^{-1}$$

U … average flow velocity in the sand trap [m/s]

U_E … average flow velocity in the approach channel to the sand trap [m/s]

R … hydraulic radius of the sand trap at chamber start [m]

m … inclination of ramp transition into the chambers [-]

H … flow depth in the sand trap chamber [m]

w_o … settling velocity of the design particle [m/s]

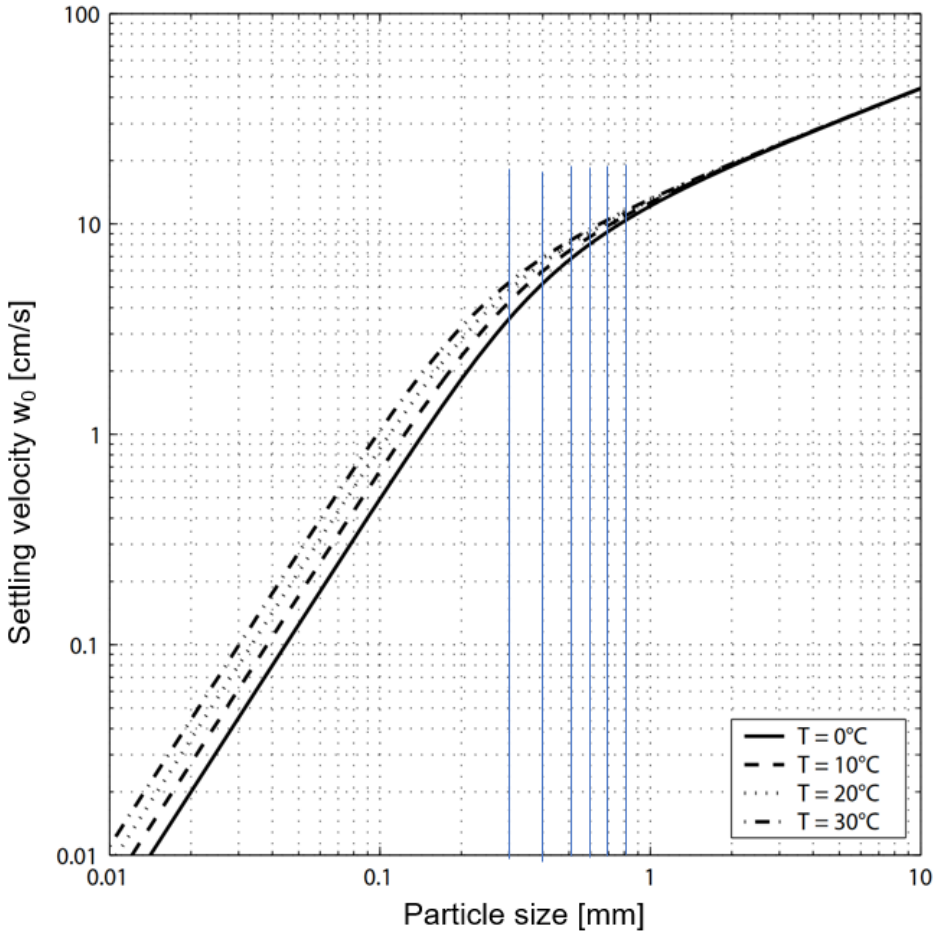

Figure 48: Settling velocity of quartz sediment particles in still water (Ortmanns 2006)

Table 3: Results for applying the *Ortmanns* formula on the Tonstad geometry

Particle	w0	A	Q	U	H	m	K	L
mm	[m/s]	m²	m³/s	m/s	m	[-]	[m/s]	[m]
1	0.103	119	80.0	0.7	10.0	6.6	6.2	97.6
0.8	0.1	119	80.0	0.7	10.0	6.6	6.2	102.1
0.7	0.09	119	80.0	0.7	10.0	6.6	6.2	120.4
0.6	0.08	119	80.0	0.7	10.0	6.6	6.2	146.6
0.5	0.068	119	80.0	0.7	10.0	6.6	6.2	198.6
0.4	0.05	119	80.0	0.7	10.0	6.6	6.2	424.0
0.3	0.04	119	80.0	0.7	10.0	6.6	6.2	1148.5

Figure 49 shows that theoretically after the Ortmanns formula a minimum grain of about 0.55 mm can be settled. One may notice that the conventional approaches of desander design do not take into account resuspension as it can be observed in the Tonstad sand trap.

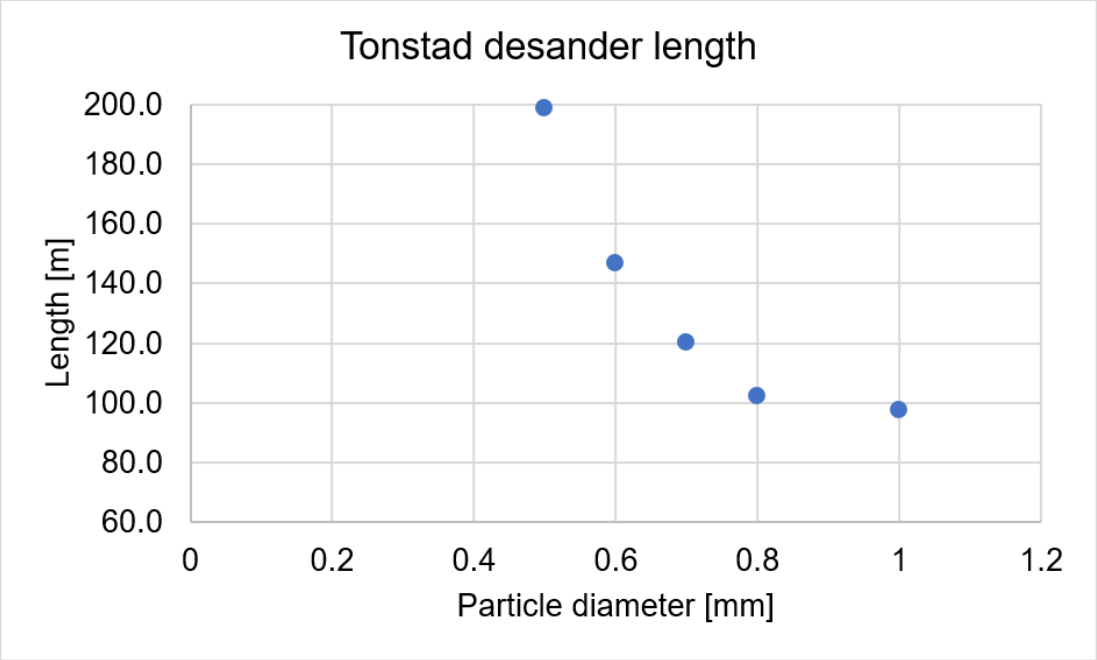

Figure 49: Demanded desander length for specific particles if Tonstad desander would be an open channel sand trap

9. Idealized box - 3D CFD particle tracking simulations

Idealized Box flow simulation are made to investigate and compare the different ideal sediment settling and drag flow behaviour for prototype scale 1:1 and model test scale 1:20. The simulations proof the sediments scaling behaviour for pressurized sand traps to be independent from Froude number, but in relation to Reynolds number. The findings allow a sediment scaling for the model scale by tuning the flow velocity and thus allow to increase the particle sizes to model fine sediment settling behaviour.

The particles are fed from a section above the inlet and in a diameter range of 0.25 mm to 1.0 mm.

The inclination of the particle settling tracks were compared and led to the conclusion that the 1:1 sediment scaling for 1:1 velocity is feasible.

9.1 Box flow with unrestrained flow

The simulations below were conducted with free slip wall boundary condition.

Table 4: Data for idealized box flow simulations

Scale	1:20 and 1:1	Geometry	Box
Particles Diameter (1:1)	0.25-1.0 mm	Particle injection	Above gate
Particles Diameter (1:20)	0.05-0.5 mm	Wall roughness	Free slip
Time (1:20 resp. 1:1)	80s resp. 300 s	Software	CFX
Timestep	0.1 resp. 0.2 s	Inlet	Velocity
Particles Density	2650 kg/m³	Outlet	Pressure
Particle roughness	Non		
Particle Drag	Schiller-Naumann		
Turbulence Modelling	SST		

- **Box flow 1:1 velocity 0.67 m/s**
  This velocity represents the Q/A velocity of 80 m³/s in the main flow section in the sand trap no.3.

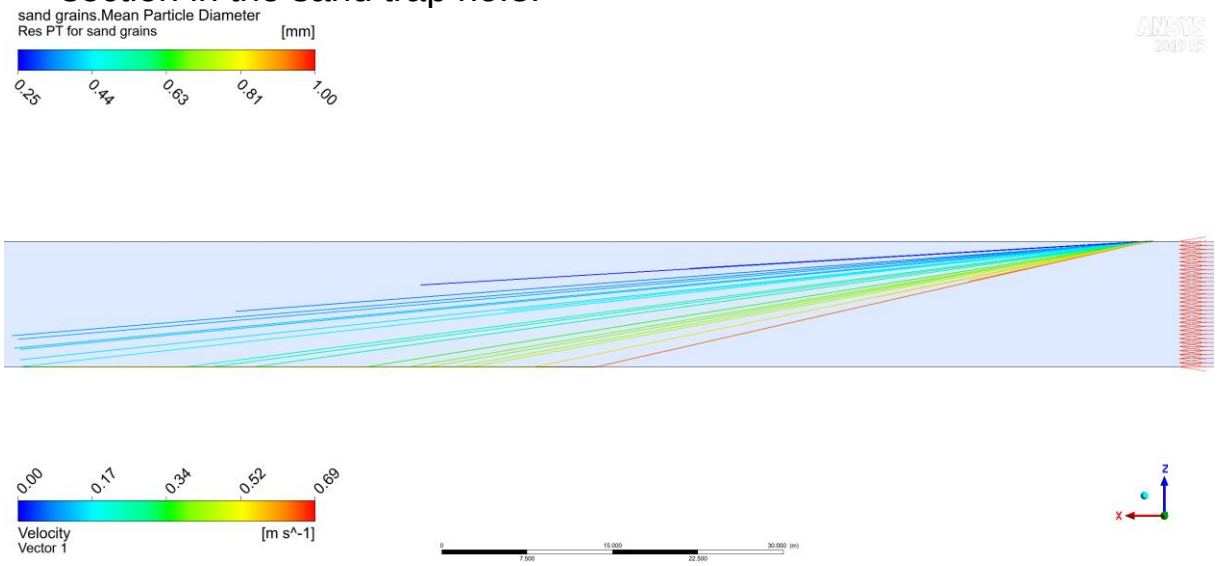

Figure 50: Particle tracking flow in 1:1 scaled box with average flow velocity of the sand trap chamber

- **Box flow 1:1 velocity 2.86 m/s**

This velocity represents the Q/A velocity of 80 m³/s in the gate restriction flow section in the sand trap no.3.

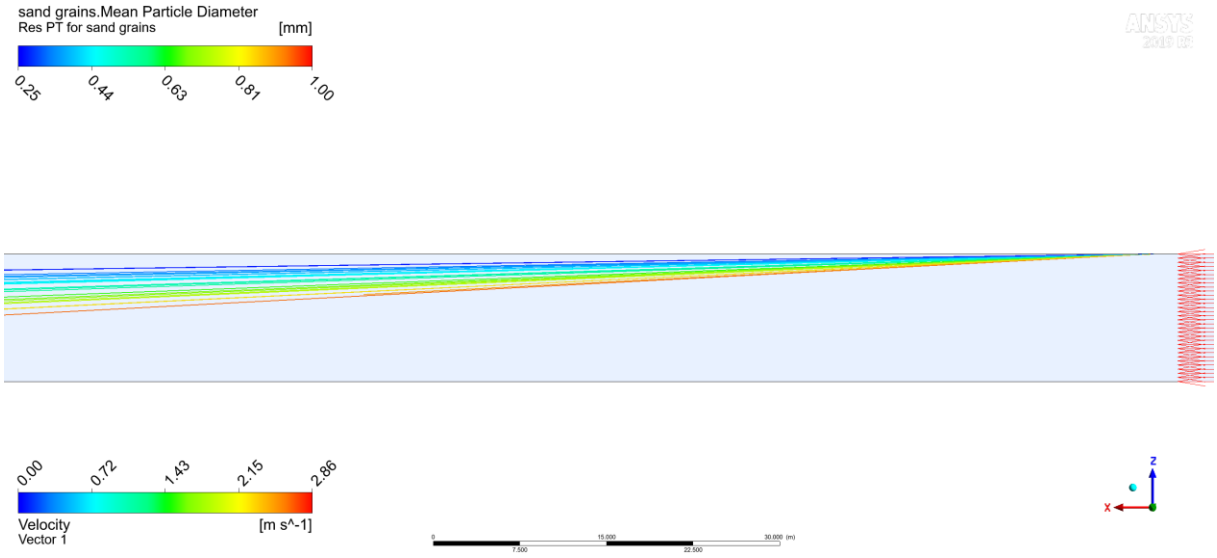

Figure 51: Particle tracking flow in 1:1 scaled box with average flow velocity at the gate restriction

- **Box flow 1:20 velocity 0.15 m/s**

This velocity represents the Q/A velocity of 80 m³/s in main flow section in the sand trap no.3, if Froude scaled for the 1:20 model test.

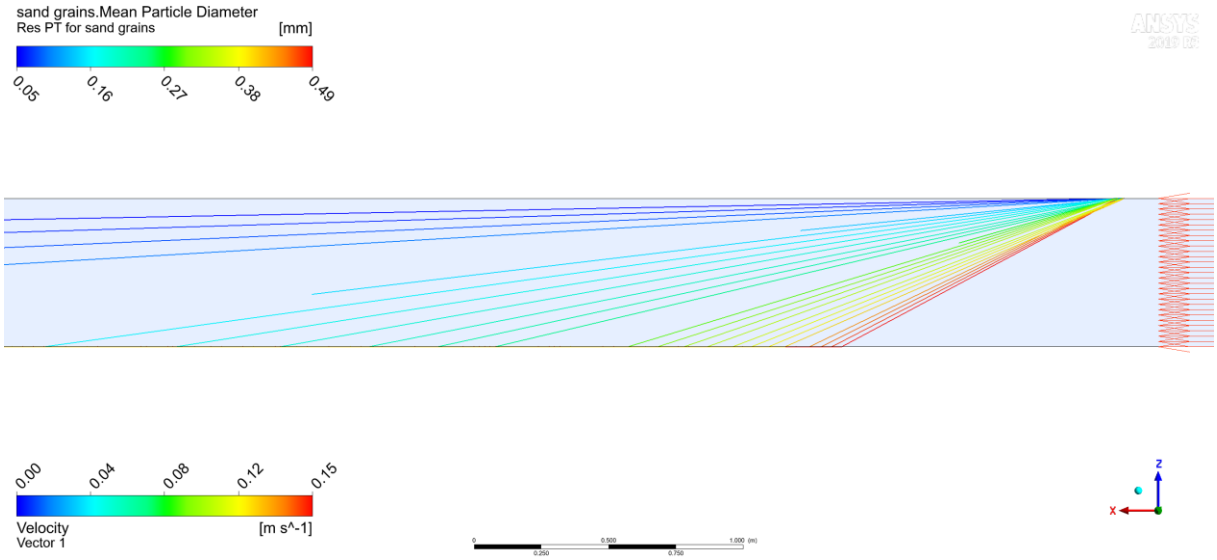

Figure 52: Particle tracking flow in 1:20 scaled box with average flow velocity in the main chamber section for Froude scaled discharge of 80 m³/s

- **Box flow 1:20 velocity 0.64 m/s**

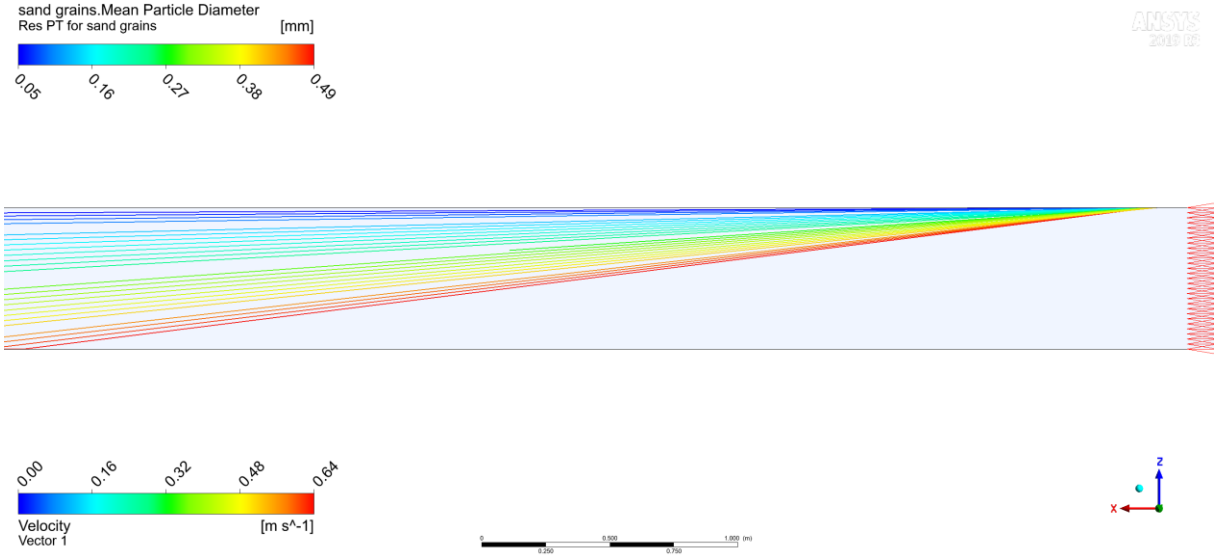

Figure 53: Particle tracking flow in 1:20 scaled box with average flow velocity from the gate restriction section for Froude scaled discharge of 80 m³/s

- **Box flow 1:20 velocity 0.30 m/s**

This flow velocity represents the factor 2x average velocity in the sand trap chamber compared to 1:20 Froude scaled velocity.

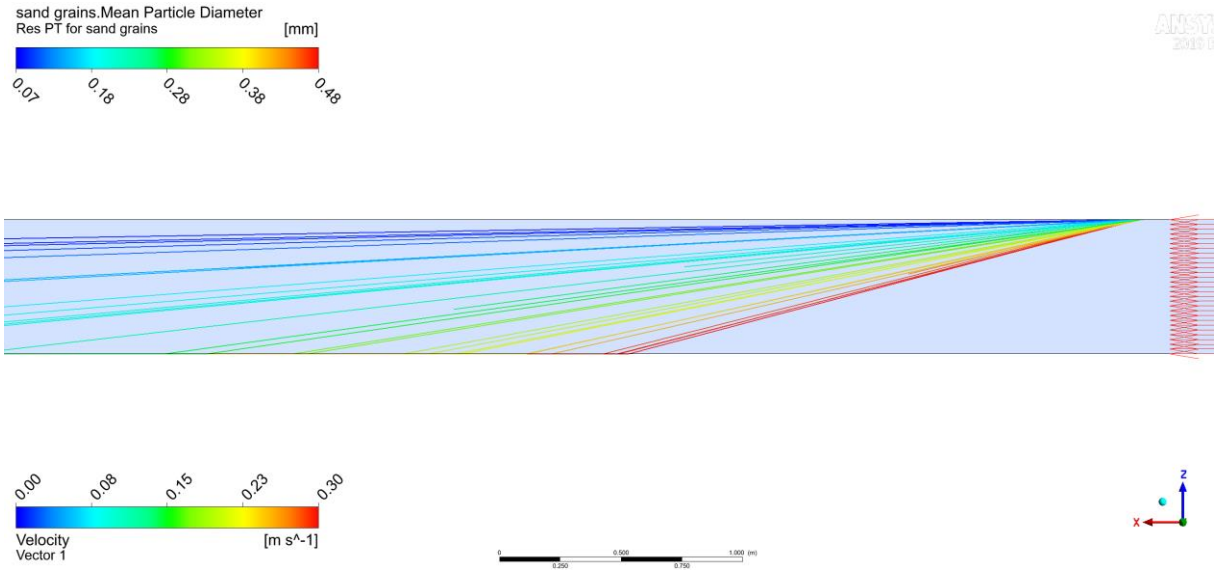

Figure 54: Particle tracking flow in 1:20 scaled box with 2x average flow velocity in the main chamber section for Froude scaled discharge of 80 m³/s

- **Box flow 1:20 velocity 1.28 m/s**

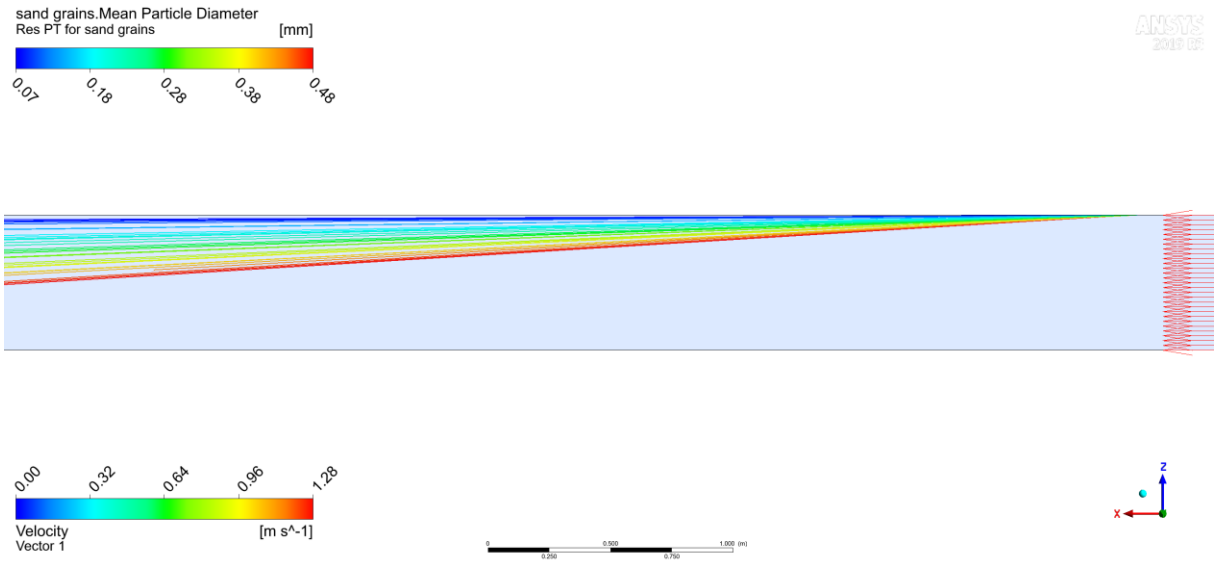

Figure 55: Particle tracking flow in 1:20 scaled box with 2x average flow velocity from the gate restriction section for Froude scaled discharge of 80 m³/s

9.2 Box flow with wall restriction

The simulations below include an obstacle to investigate the flow separation effect on particle tracking simulation. The box simulation were done for scale 1:20 and 1:1 to compare the particle settling inclination tracks.

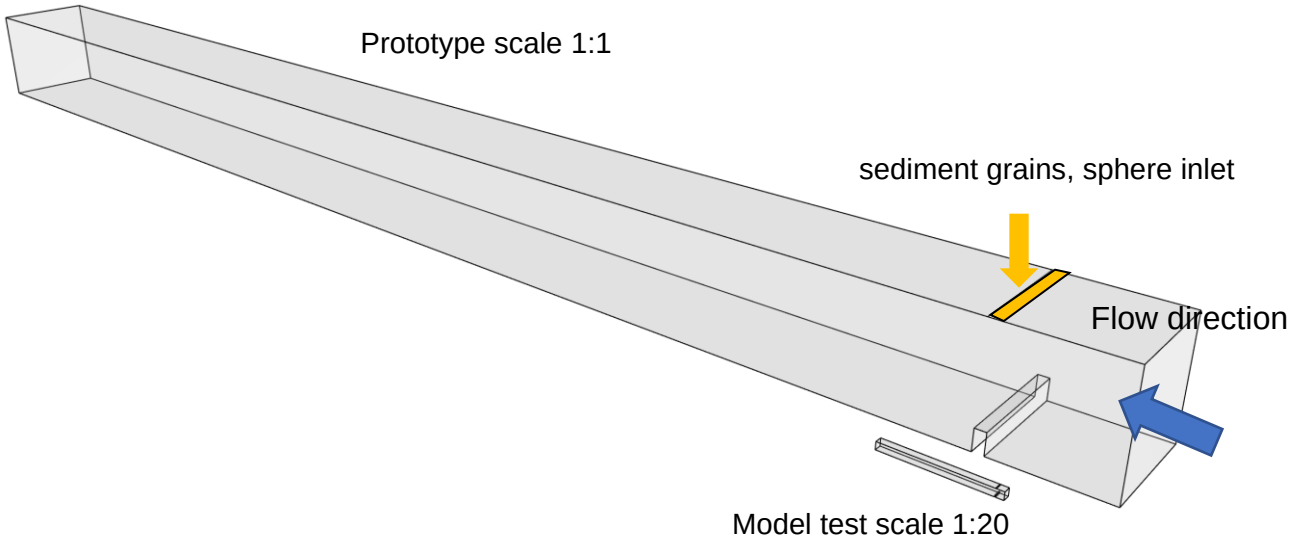

Figure 56: Geometry and flow boundary conditions of idealized box flow with wall restriction

- **Box flow with wall 1:1 velocity 0.67 m/s**

Figure 59 shows the particle tracks for the flow velocity of 0.67 m/s, which is the design discharge of 80 m³/s in the main sand trap chamber.

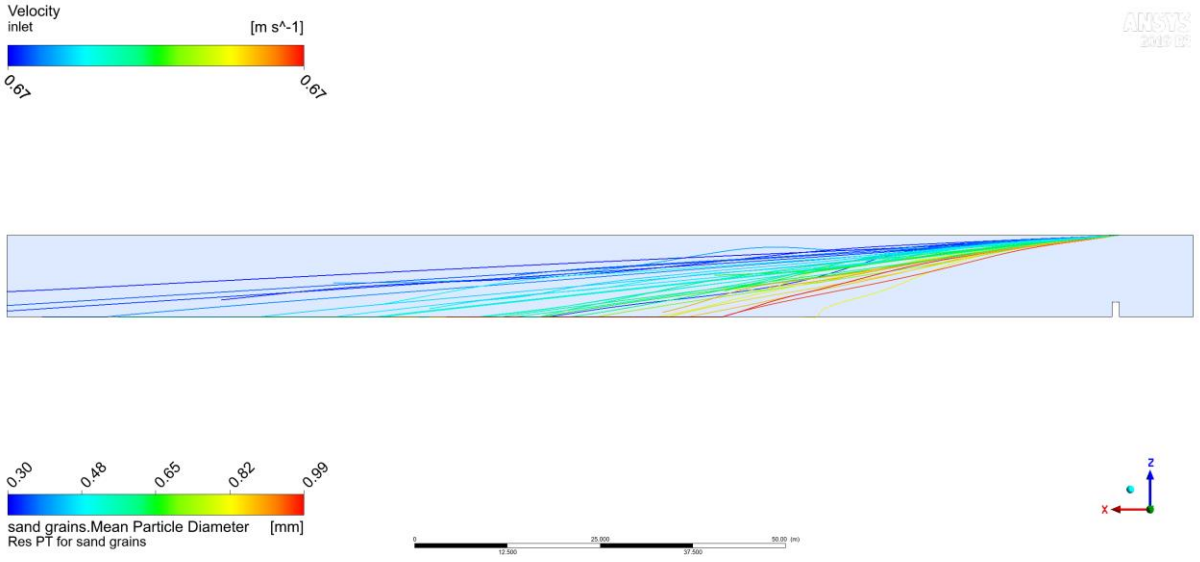

Figure 57: 1:1 scale of box flow with wall restriction, 0.67 m/s inlet velocity (80m³/s / main flow section), longitudinal view

- **Box flow with wall 1:20 velocity 0.15 m/s**

Figure 58 shows the particle tracks for the flow velocity of 0.15 m/s, which is the design discharge of 80 m³/s in the main sand trap chamber for Froude scaled velocity in the 1:20 model. Figure 59 additionally shows the wall shear stress for the simulation.

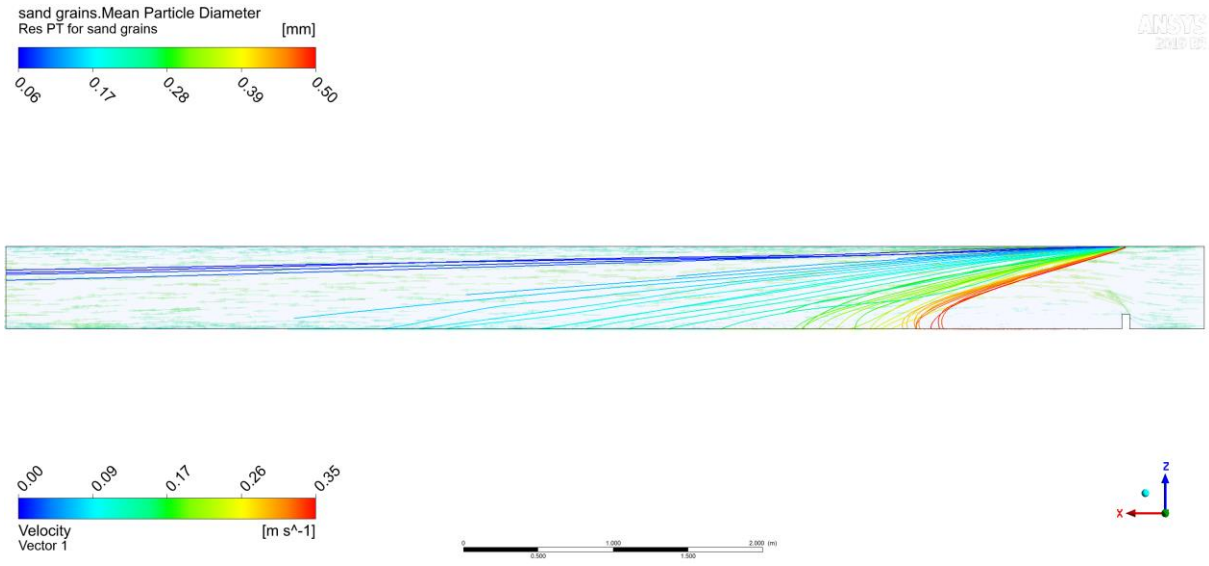

Figure 58: 1:20 scale of box flow with wall restriction, 0.15 m/s inlet velocity, longitudinal view

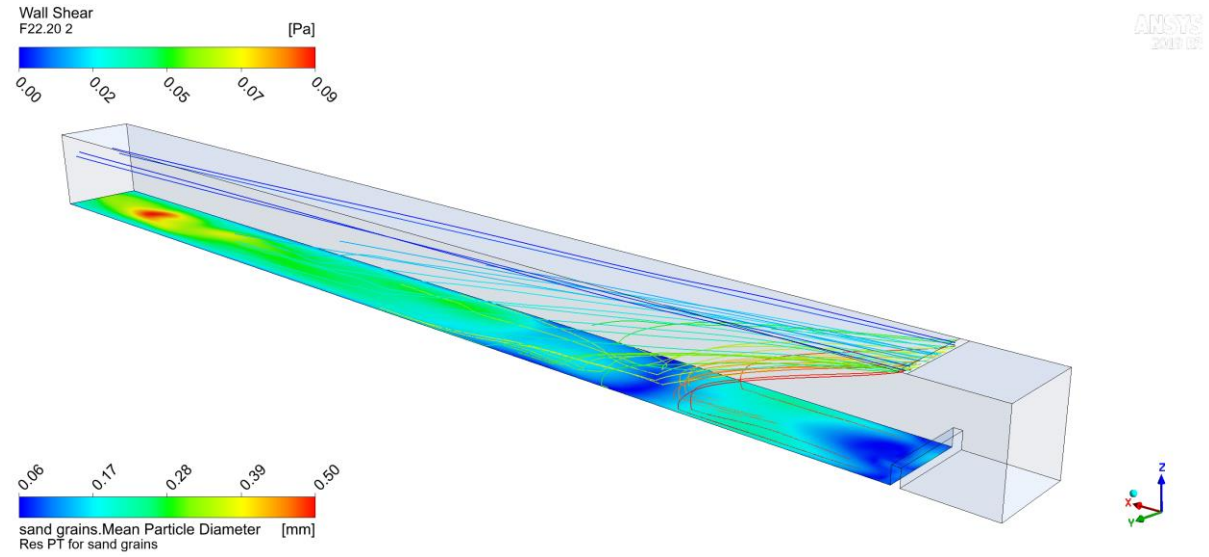

Figure 59: 1:20 scale of box flow with wall restriction, 0.15 m/s inlet velocity, wall shear stress, perspective view

- **Box flow with wall 1:20 velocity 0.64 m/s**

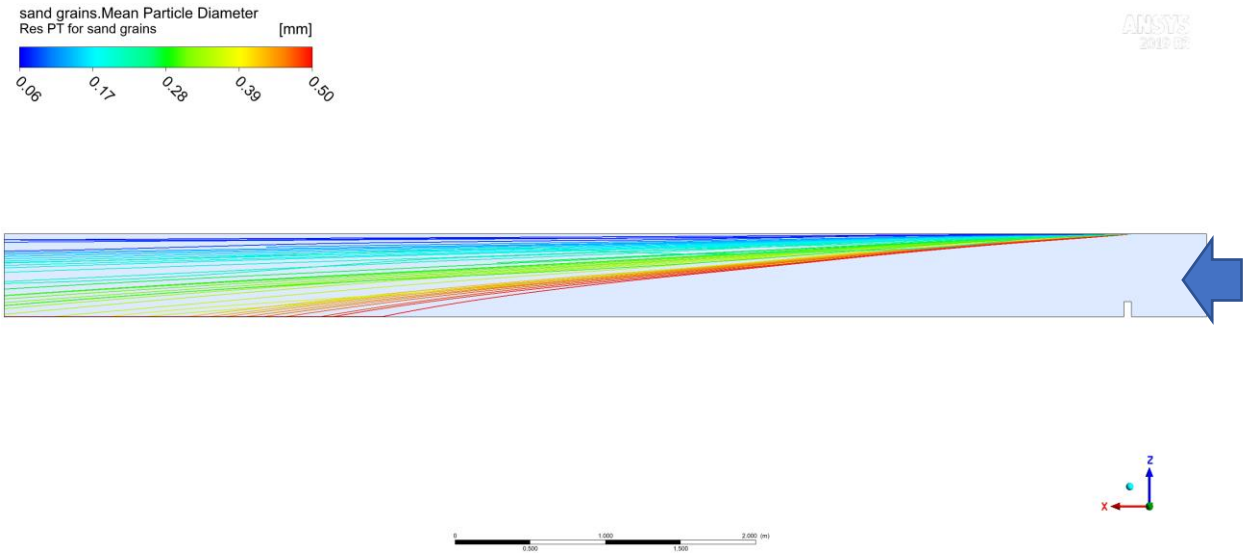

Figure 60: 1:20 scale of box flow with wall restriction, 0.64 m/s inlet velocity, longitudinal view

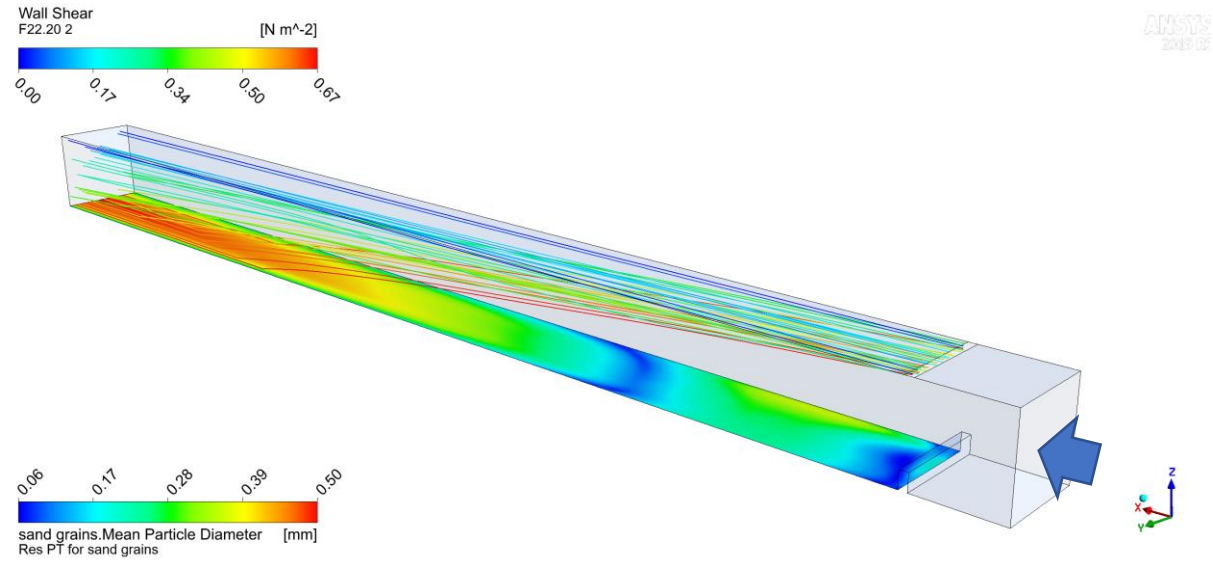

Figure 61: 1:20 scale of box flow with wall restriction, 0.64 m/s inlet velocity, wall shear stress perspective view

- **Box flow with wall scale 1:20 velocity 0.67 m/s – large grains**

These simulations in the systematic box flow approach are additionally done with larger grains than 1.0 mm, up to 30 mm diameter. The direct comparison of the box flow particle tracking simulation sustains the later used scaling approach of 1:1 particles in prototype velocity since the settling tracks of the same particles are independent of the geometry size.

Table 5: Data for idealized box flow simulations with wall

Scale	1:20	Geometry	Box with wall
		Particle injection	Above gate
Particles Diameter (1:20)	0.05-30 mm	Wall roughness	Smooth wall
Time	80s s	Software	CFX
Timestep	0.1 s	Inlet	Velocity
Particles Density	2650 kg/m³	Outlet	Pressure
Particle roughness	Non	Number of mesh elements	811,423
Particle Drag	Schiller-Naumann		
Turbulence Modelling	SST		

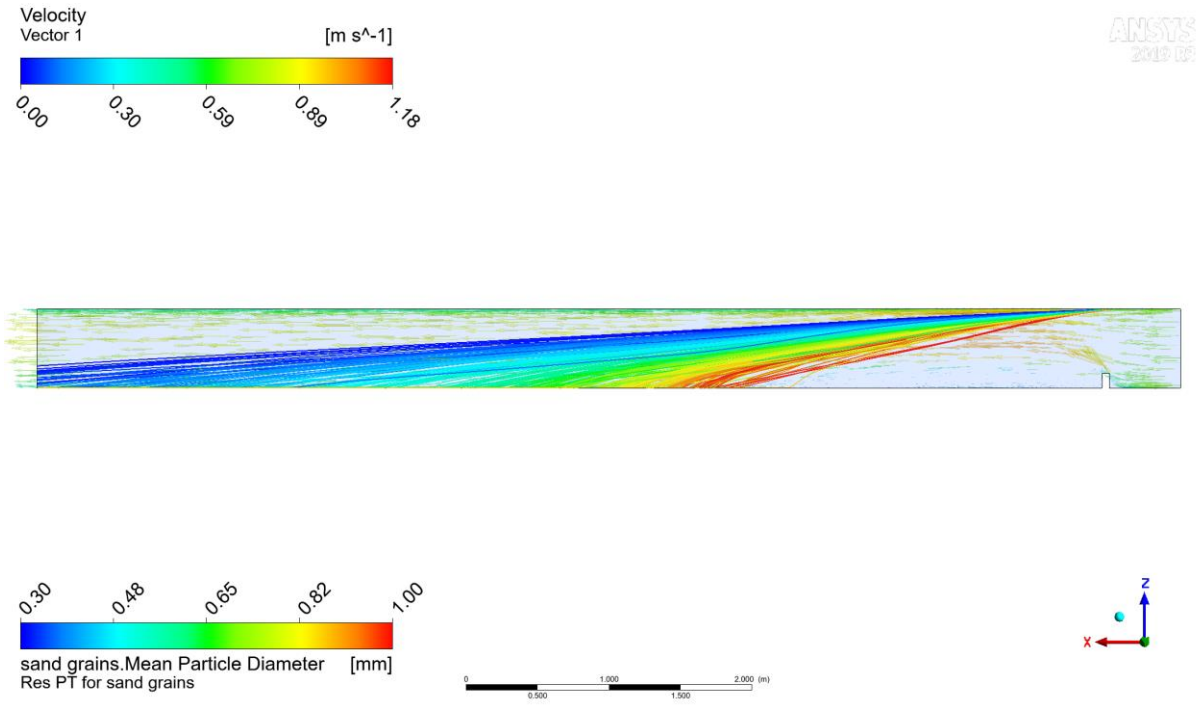

Figure 62: 3D CFD with particle tracking grains 0.3-1.0 mm, scale 1:20, 0.67 m/s inlet velocity, side view

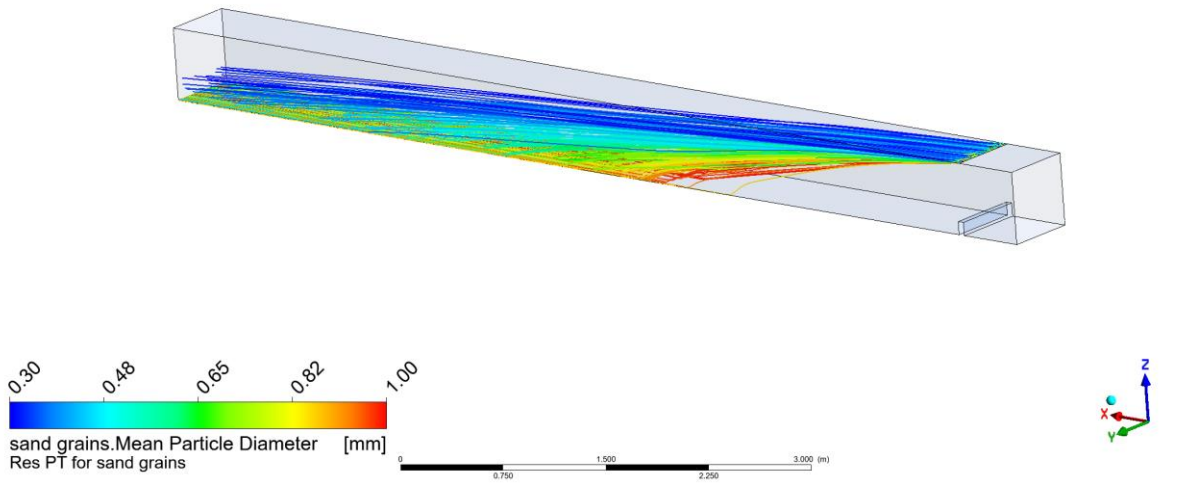

Figure 63: 3D CFD with particle tracking grains 0.3-1.0 mm, scale 1:20, 0.67 m/s inlet velocity, iso view

Figure 64 shows the settling tracks of 1.0 mm- 5.0 mm diameter grains. Figure 65 shows additionally the tracks for the bed load of these grains. One needs to notice that the calibration of the transportation on the ground with the tracking approach demands further research.

Figure 66 to Figure 71 show subsequently the particle behaviour of grains from 5.0 mm – 10.0 mm diameter, from 10.0 mm – 20.0 mm diameter and from 20.0 mm – 30.0 mm diameter. The results show increasingly steep gradients in the settling tracks.

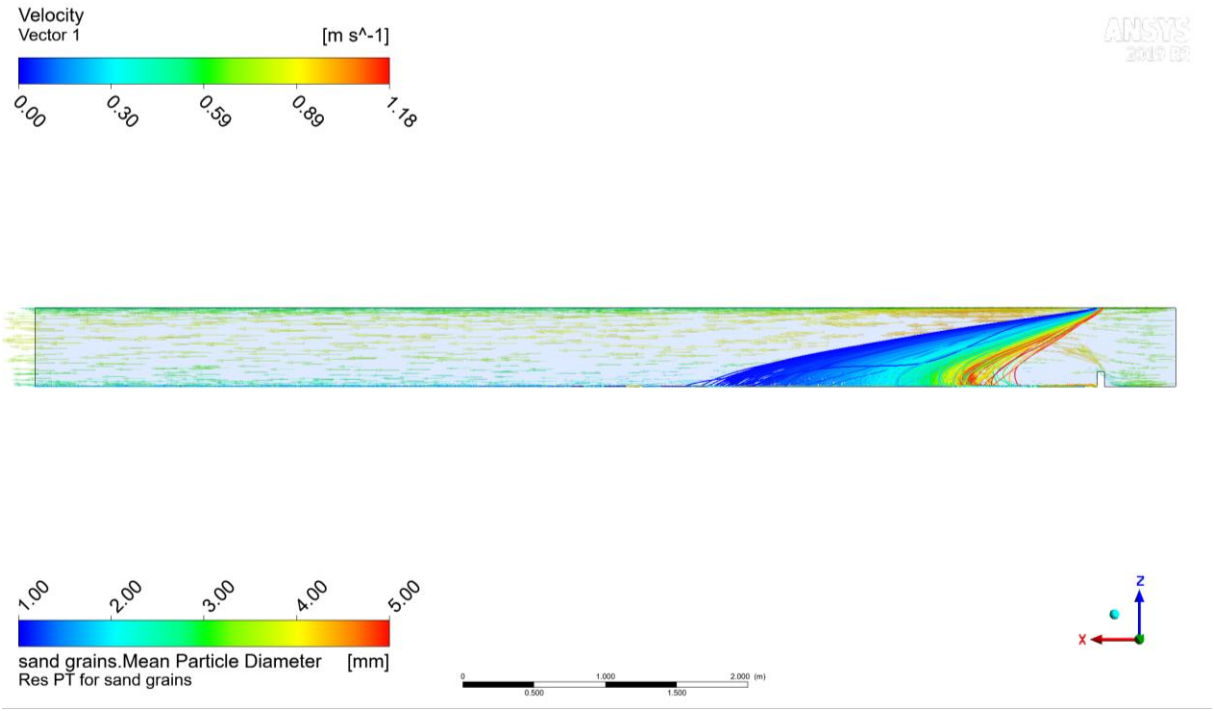

Figure 64: 3D CFD with particle tracking grains 1.0-5.0 mm, scale 1:20, 0.67 m/s inlet velocity, side view

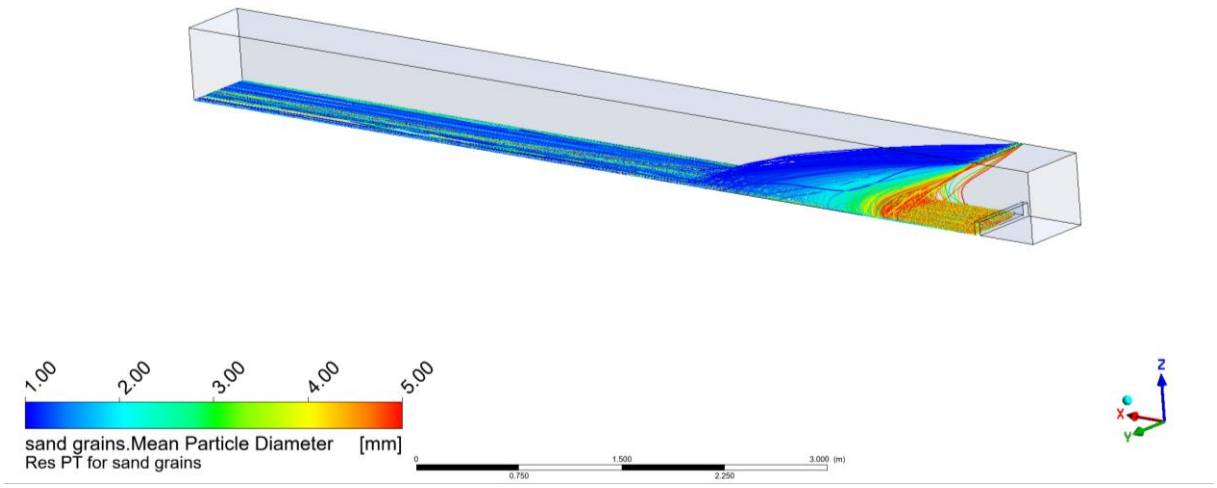

Figure 65: 3D CFD with particle tracking grains 1.0-5.0 mm, scale 1:20, 0.67 m/s inlet velocity, iso view

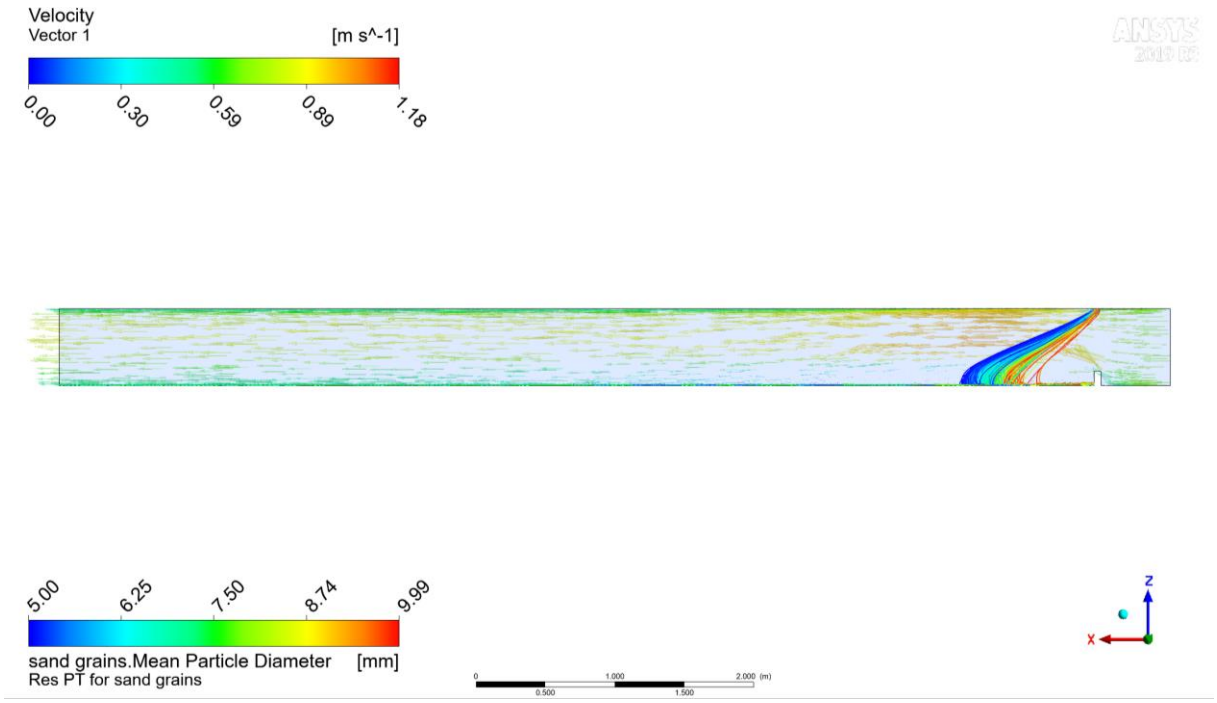

Figure 66: 3D CFD with particle tracking grains 5.0-10.0 mm, scale 1:20, 0.67 m/s inlet velocity, side view

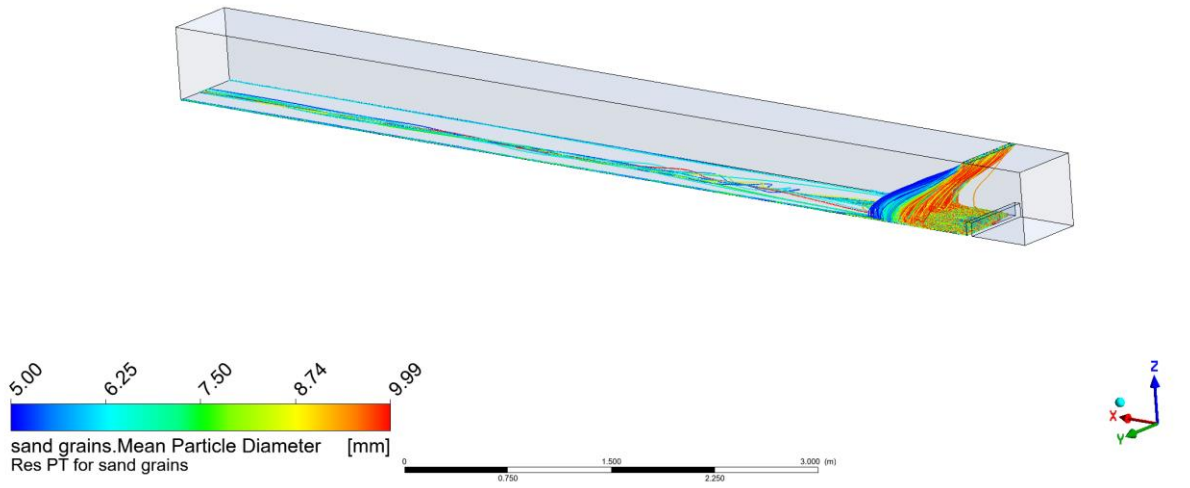

Figure 67: 3D CFD with particle tracking grains 5.0-10.0 mm, scale 1:20, 0.67 m/s inlet velocity, iso view

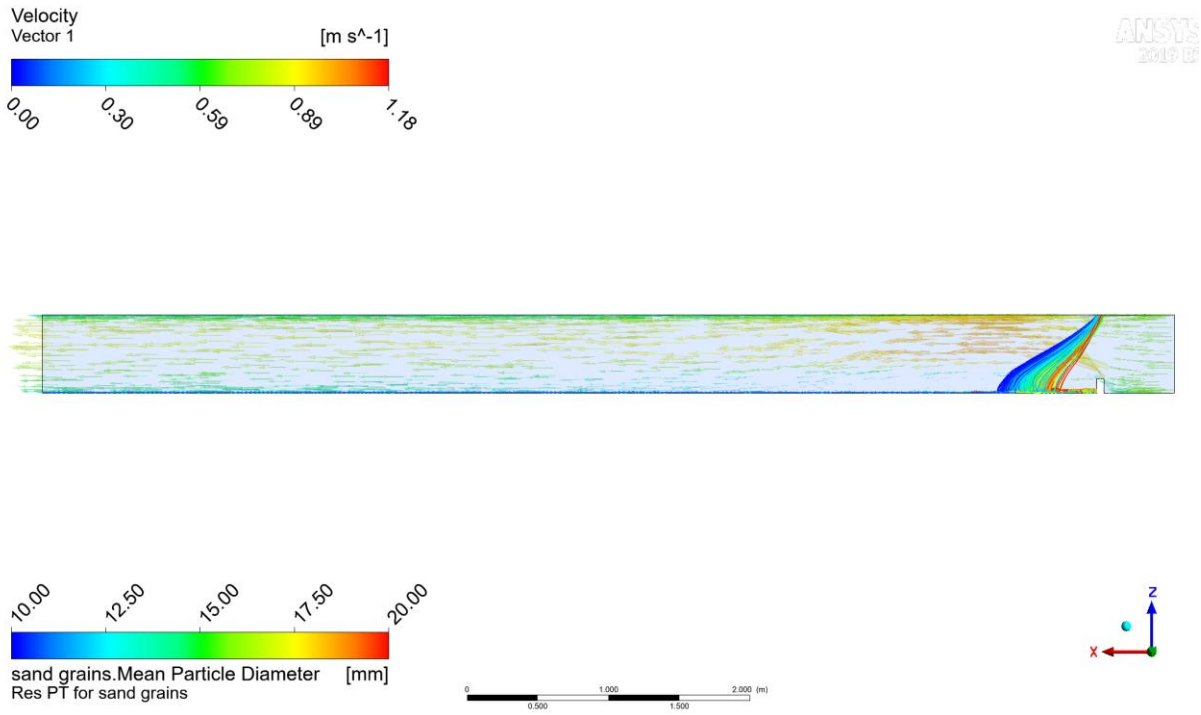

Figure 68: 3D CFD with particle tracking grains 10.0-20.0 mm, scale 1:20, 0.67 m/s inlet velocity, side view

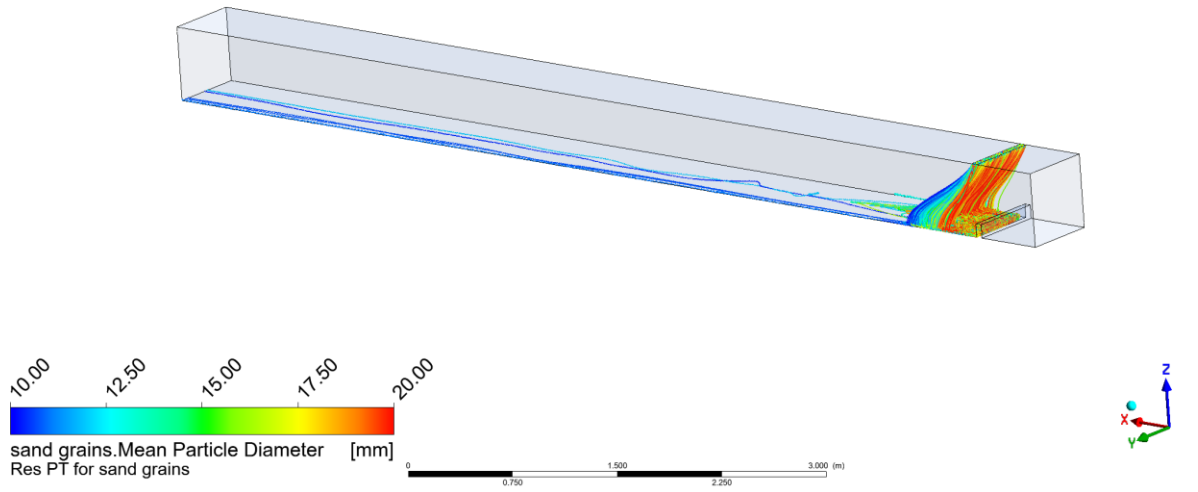

Figure 69: 3D CFD with particle tracking grains 10.0-20.0 mm, scale 1:20, 0.67 m/s inlet velocity, iso view

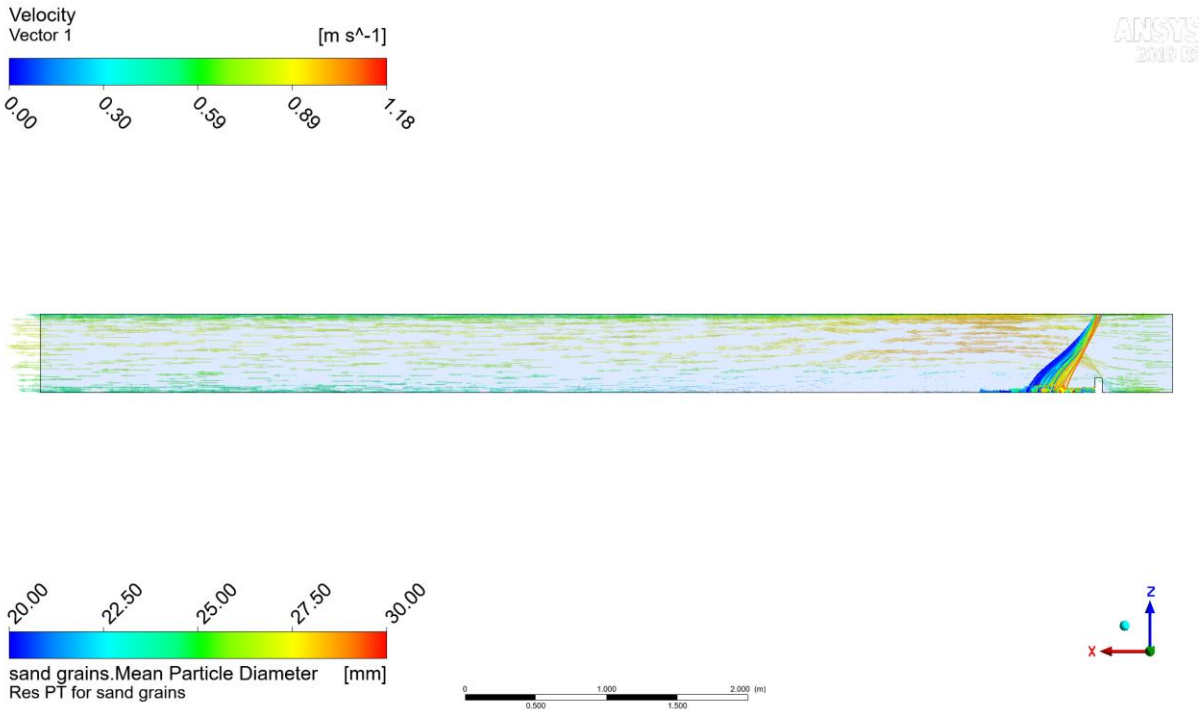

Figure 70: 3D CFD with particle tracking grains 20.0-30.0 mm, scale 1:20, 0.67 m/s inlet velocity, side view

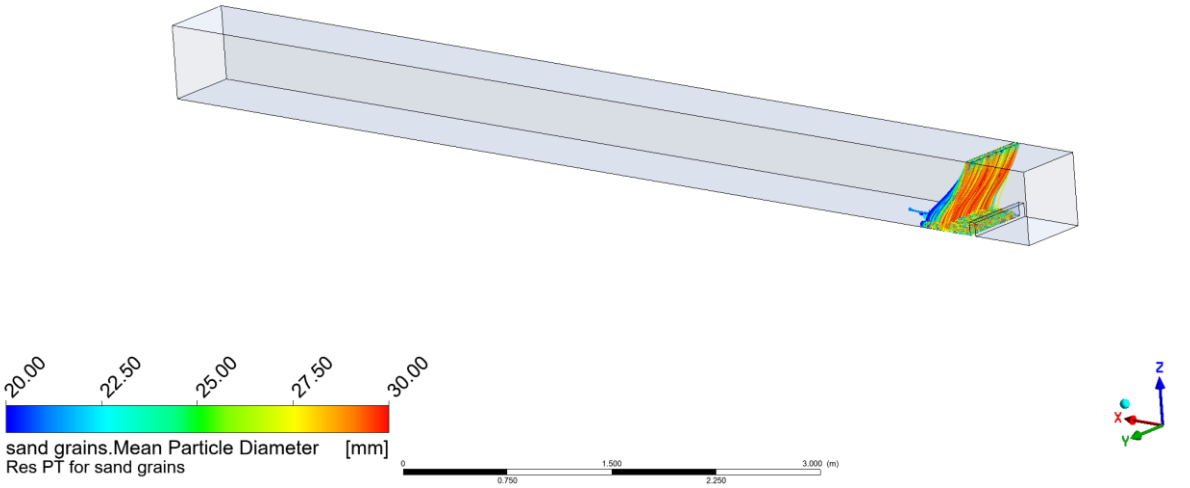

Figure 71: 3D CFD with particle tracking grains 20.0-30.0 mm, scale 1:20, 0.67 m/s inlet velocity, iso view

- **Box flow with wall scale 1:1 velocity 0.67 m/s – large grains**

This chapter describes respectively the simulations above but at prototype scale 1:1 for large grains.

Table 6: Data for idealized box flow simulations with wall

Scale	1:1	Geometry	Box with wall
		Particle injection	Above gate
Particles Diameter (1:20)	0.05-30 mm	Wall roughness	Smooth wall
Time	80s s	Software	CFX
Timestep	0.1 s	Inlet	Velocity
Particles Density	2650 kg/m³	Outlet	Pressure
Particle roughness	Non	Number of mesh elements	1,103,925
Particle Drag	Schiller-Naumann		
Turbulence Modelling	SST		

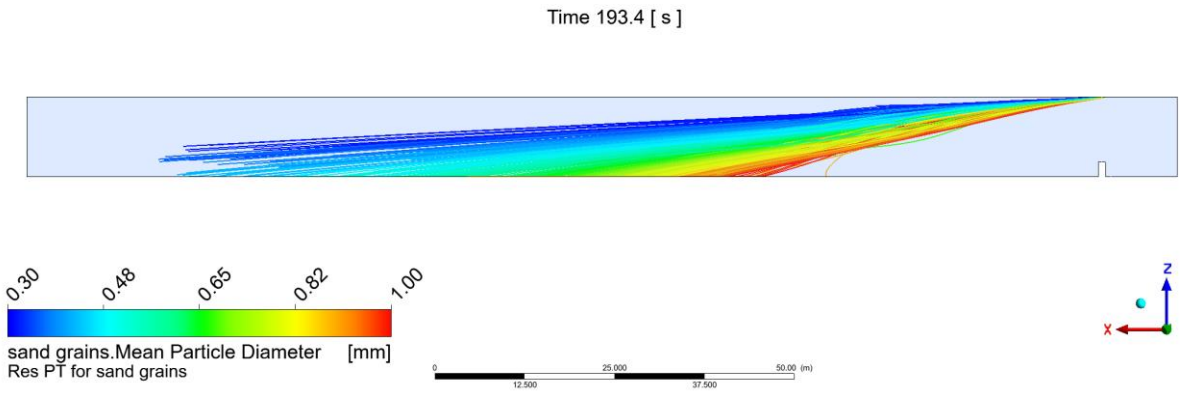

Figure 72: 3D CFD with particle tracking grains 0.3-1.0 mm, scale 1:1, 0.67 m/s inlet velocity, side view

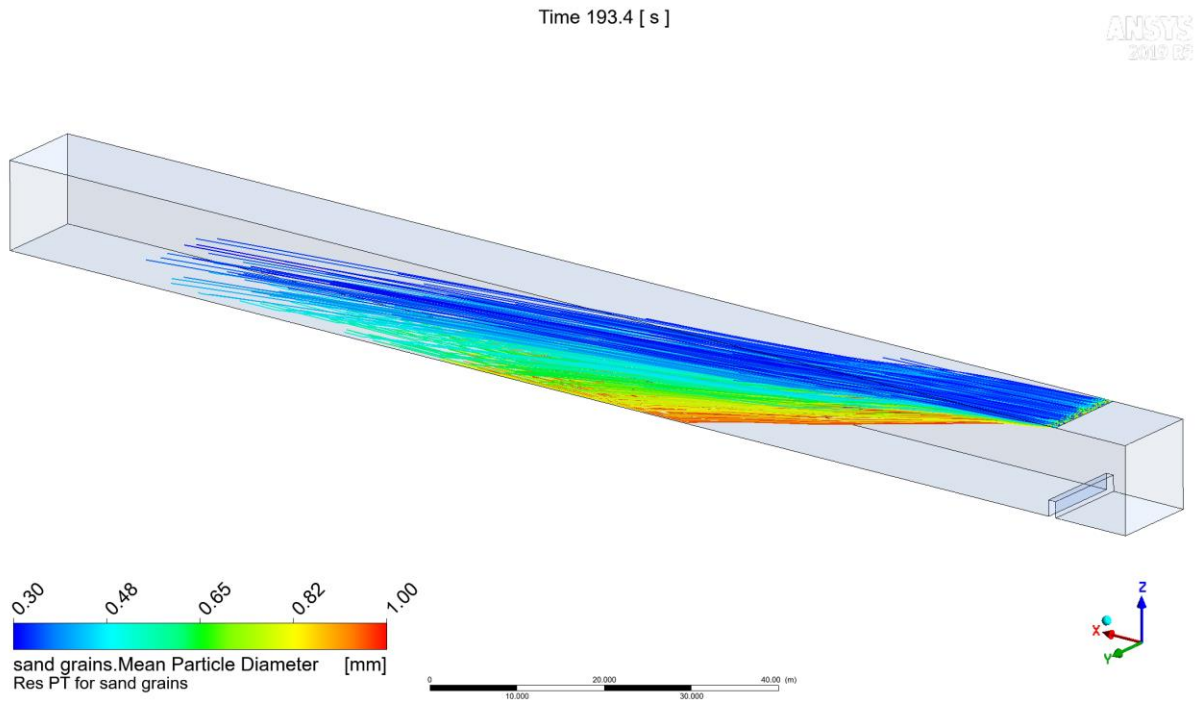

Figure 73: 3D CFD with particle tracking grains 0.3-1.0 mm, scale 1:1, 0.67 m/s inlet velocity, iso view

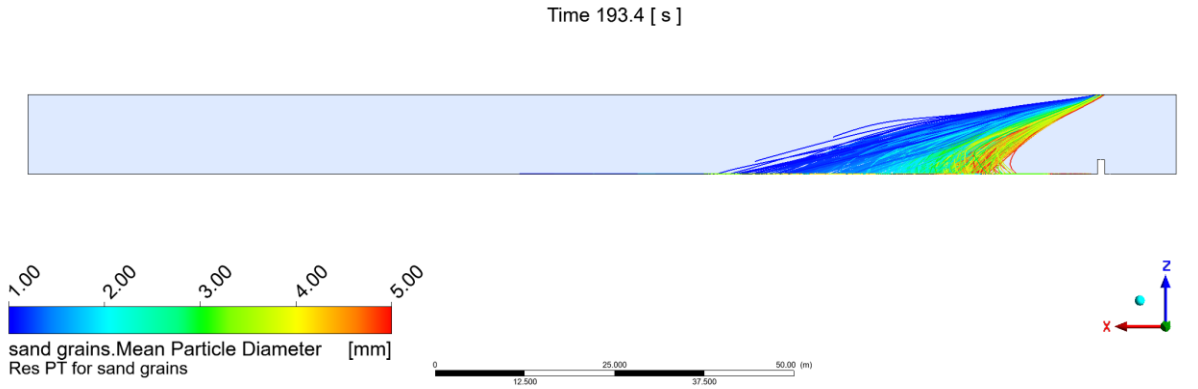

Figure 74: 3D CFD with particle tracking grains 1.0-5.0 mm, scale 1:1, 0.67 m/s inlet velocity, side view

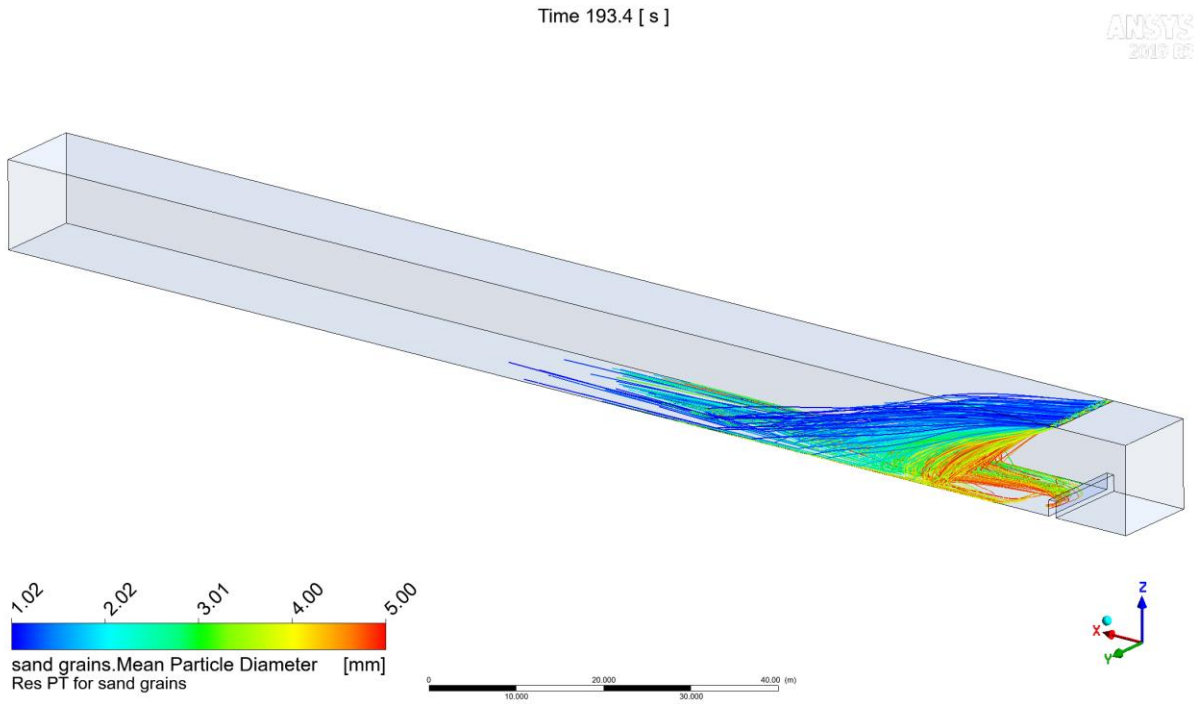

Figure 75: 3D CFD with particle tracking grains 1.0-5.0 mm, scale 1:1, 0.67 m/s inlet velocity, iso view

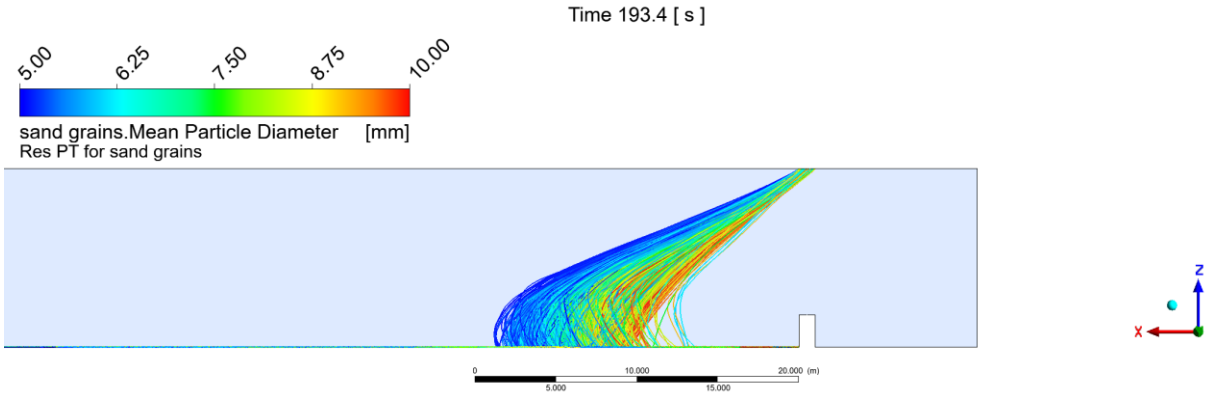

Figure 76: 3D CFD with particle tracking grains 5.0-10.0 mm, scale 1:1, 0.67 m/s inlet velocity, side view

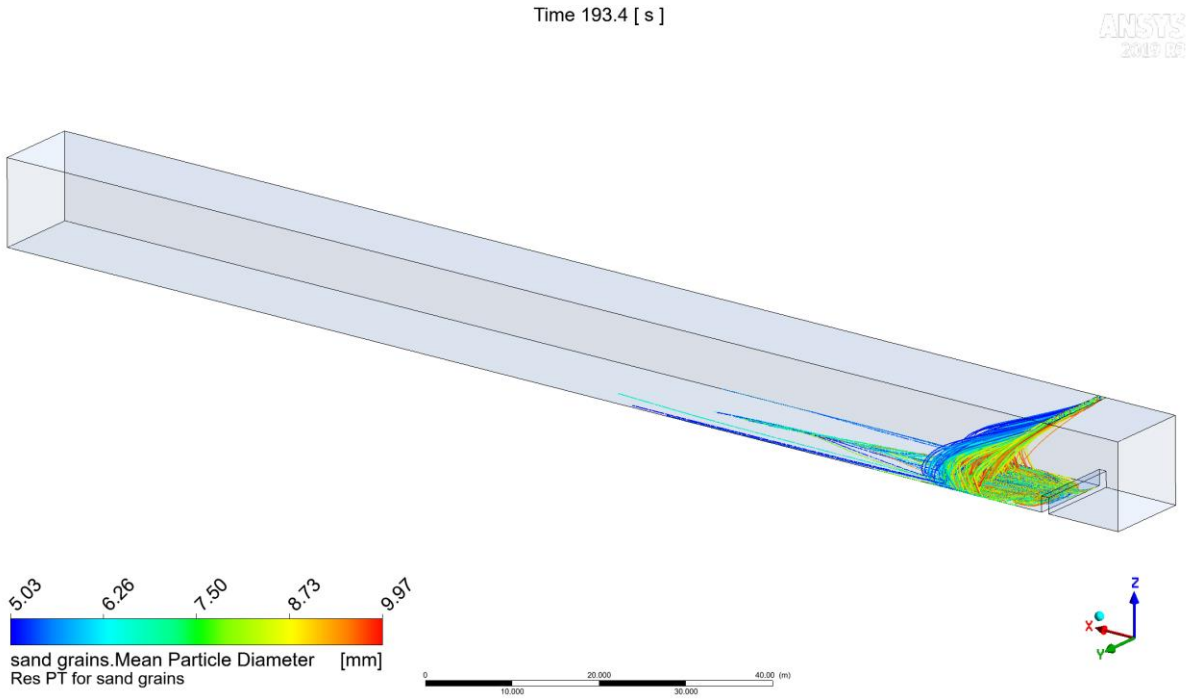

Figure 77: 3D CFD with particle tracking grains 5.0-10.0 mm, scale 1:1, 0.67 m/s inlet velocity, iso view

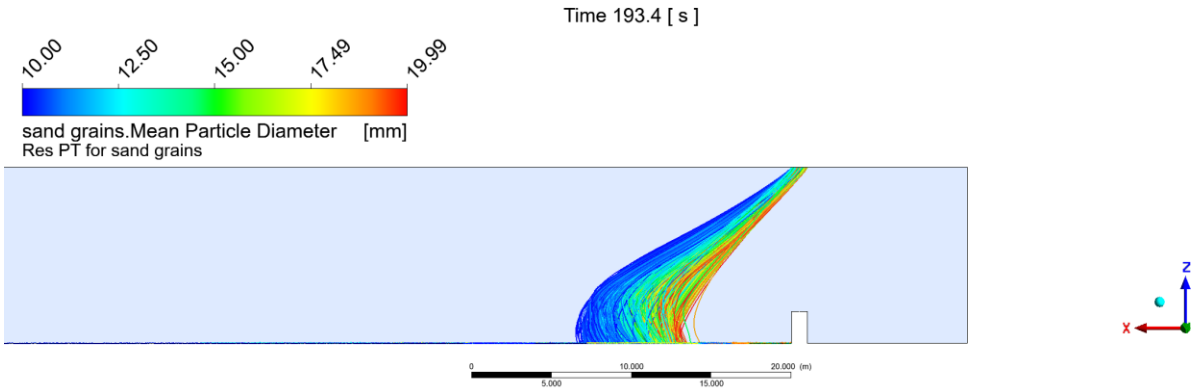

Figure 78: 3D CFD with particle tracking grains 10.0-20.0 mm, scale 1:1, 0.67 m/s inlet velocity, side view

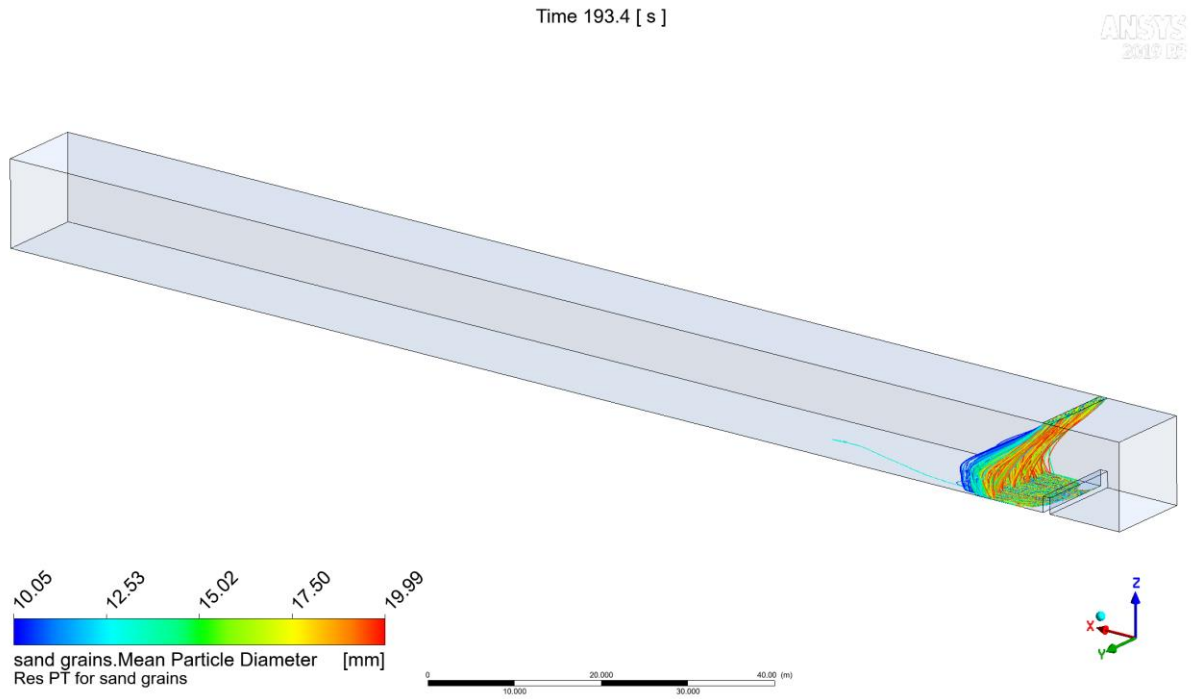

Figure 79: 3D CFD with particle tracking grains 10.0-20.0 mm, scale 1:1, 0.67 m/s inlet velocity, iso view

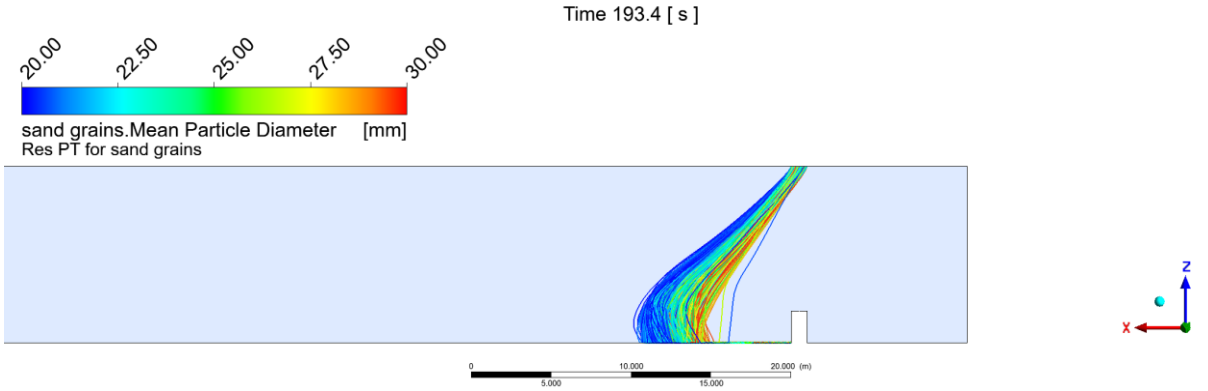

Figure 80: 3D CFD with particle tracking grains 20.0-30.0 mm, scale 1:1, 0.67 m/s inlet velocity, side view

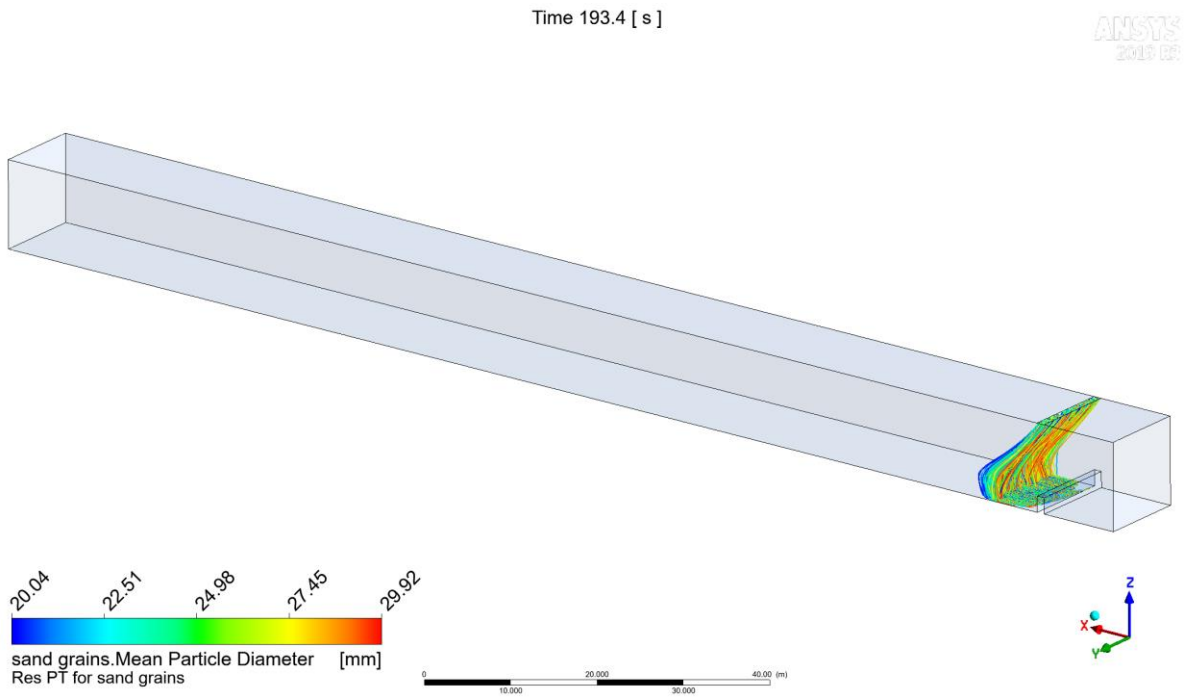

Figure 81: 3D CFD with particle tracking grains 20.0-30.0 mm, scale 1:1, 0.67 m/s inlet velocity, iso view

9.3 **3D CFD Simulations model 1:20**

This chapter describes particle tracking simulation with *Fluent.* A master thesis at NTNU was supported during the project (Naess 2020).

This chapter contains 1:20 model scale as in the model test in Trondheim.

In this chapter the simulations are numbered starting form Sim01. The specific properties used for the simulation are reported in a table.

9.3.1 **Particle tracking simulation 1:20 Sim01**

This simulation shows Froude scaled velocity and discharge for particle diameter of 0.5 mm.

Table 7: Data for simulation 01

Particles Diameter	0.5 mm	Wall roughness	0.1 mm
Time	80 s	Bottom roughness	0.1 mm
Timestep	0.1 s	Material	Acrylic Glass
Particles Mass	0.5 kg/s	Software	Fluent
Particles Density	2120 kg/m³		
Particle roughness	Non		
Particle Drag	sphere		
Turbulence Modelling	SAS		
Trap efficiency	100 %		

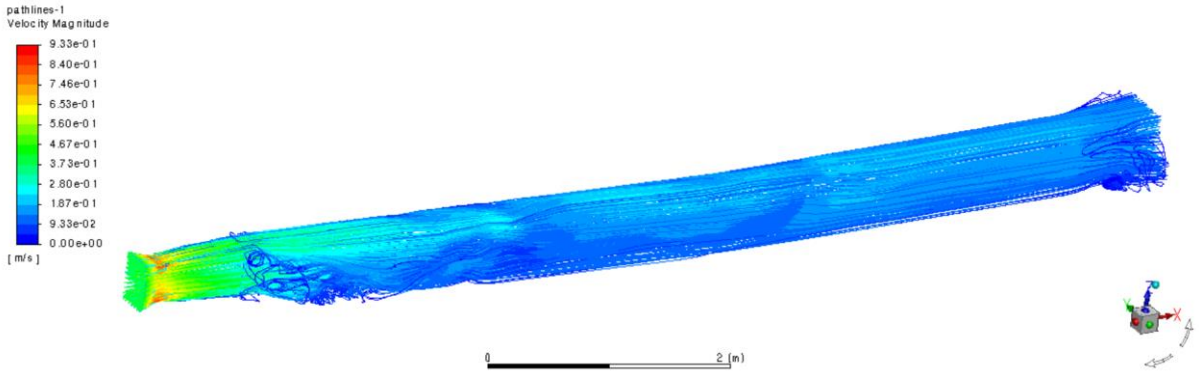

Figure 82: Result, velocity, Froude scaled full flow, 1:20 model test

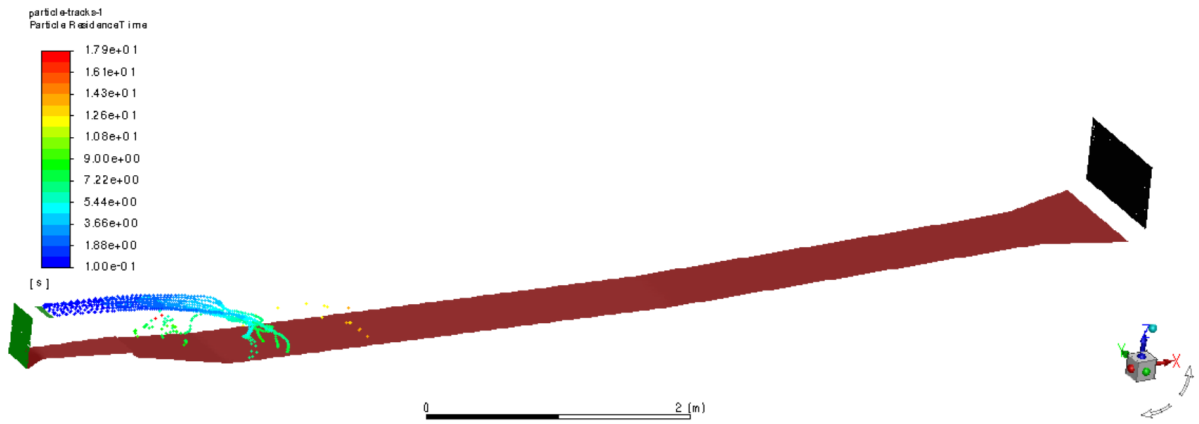

Figure 83: Result, 0.5 mm grains, Froude scaled full flow, 1:20 model test

9.3.2 **Particle tracking simulation 1:20 Sim_02**

This simulation shows Froude scaled velocity and discharge for particle diameter of 0.1 mm. Two trubulence models; SAS and k-eps are investigated.

Table 8: Data for simulation 2

Particles Diameter	0.1 mm	Wall roughness	0.1 mm
Time	80 s	Bottom roughness	0.1 mm
Timestep	0.1 s	Material	Acrylic Glass
Particles Mass	0.5 kg/s	Software	Fluent
Particles Density (80%)	2120 kg/m³		
Particle roughness	Non		
Particle Drag	sphere		
Turbulence Modelling	SAS, k-eps		
Trap efficiency	< 100 %		

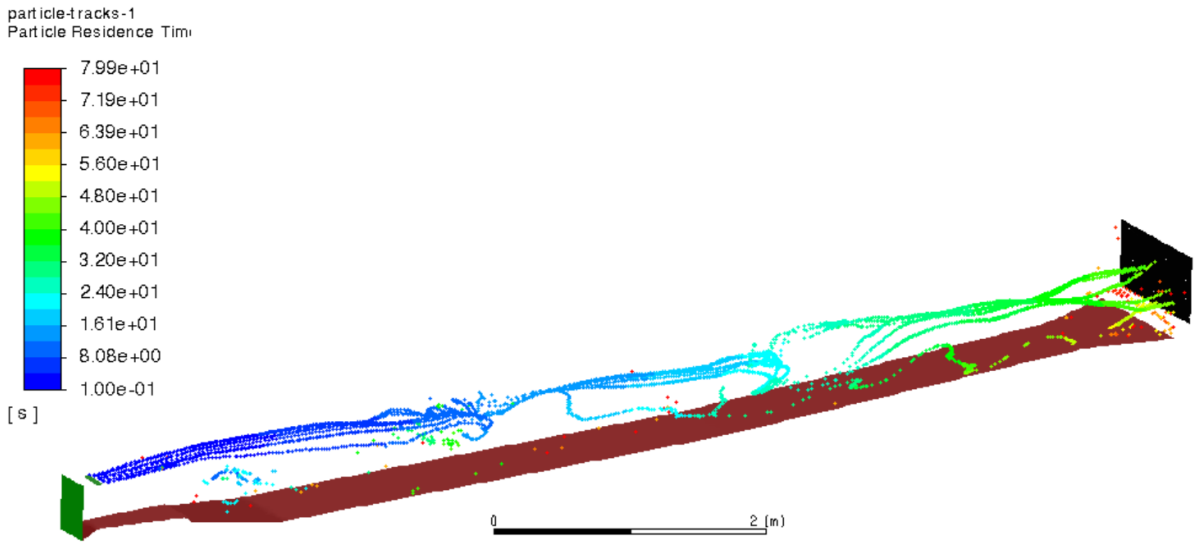

Figure 84: Result, 0.1 mm grains, Froude scaled full flow, 1:20 model test, SAS

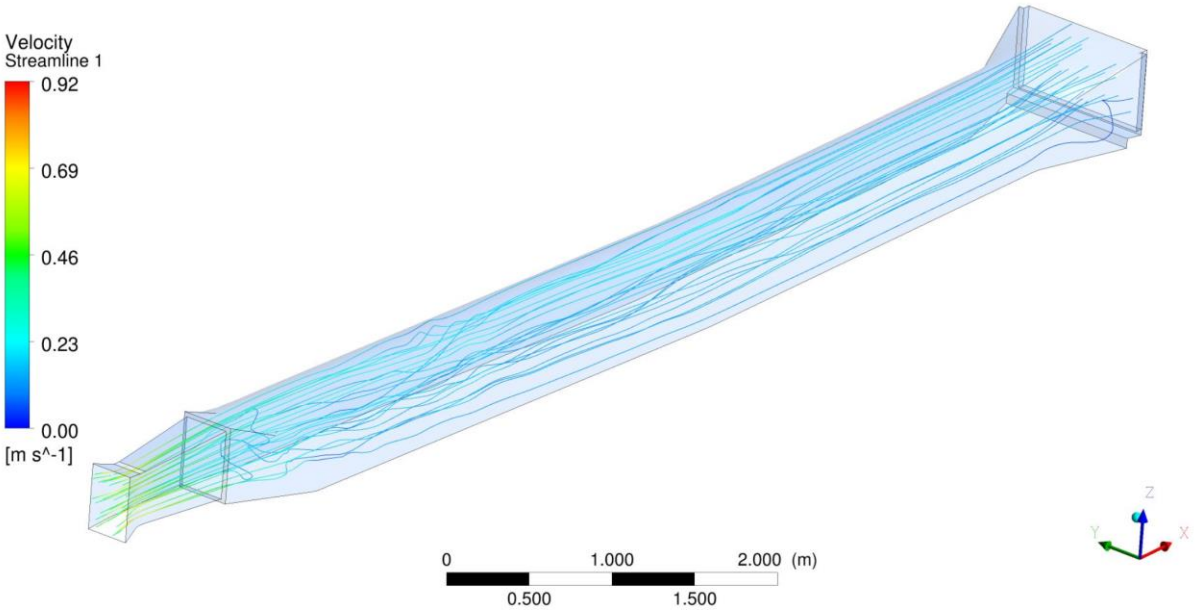

Figure 85: Streamlines 44.72 l/s, 1:20 model test, acrylic glass, SAS

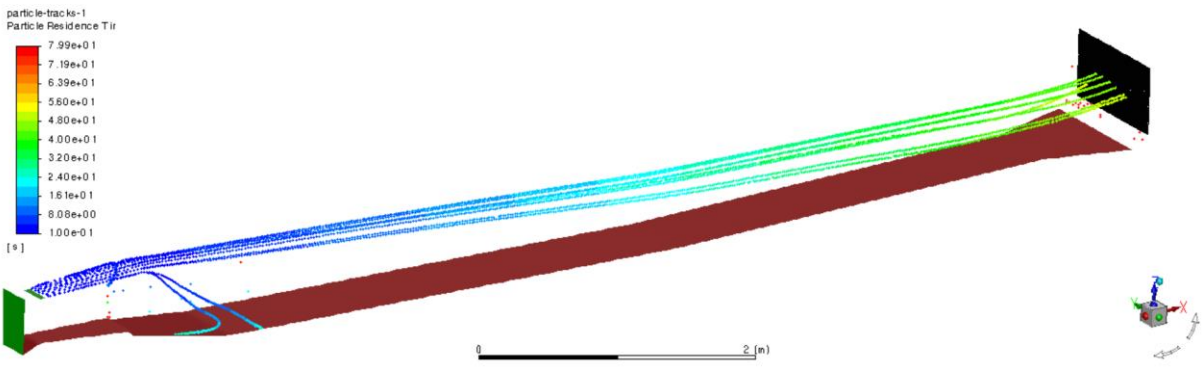

Figure 86: Result, 0.1 mm grains, Froude scaled full flow, 1:20 model test, k-eps

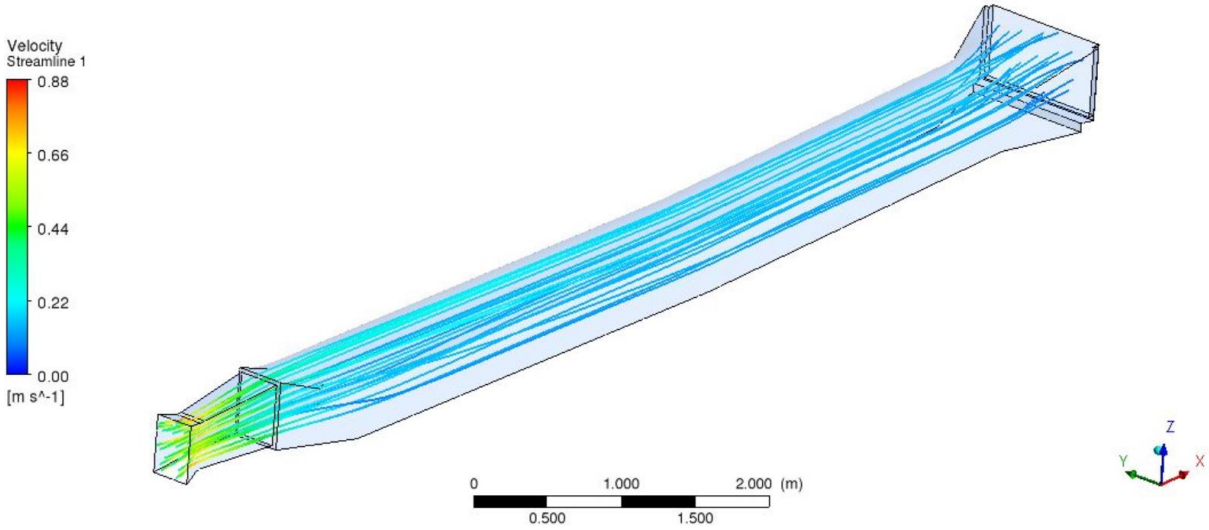

Figure 87: Streamlines 44.72 l/s, 1:20 model test, acrylic glass, k-eps

9.3.3 **Particle tracking simulation 1:20 Sim_07**

This simulation shows Froude scaled velocity and discharge for particle diameter of 0.3 mm

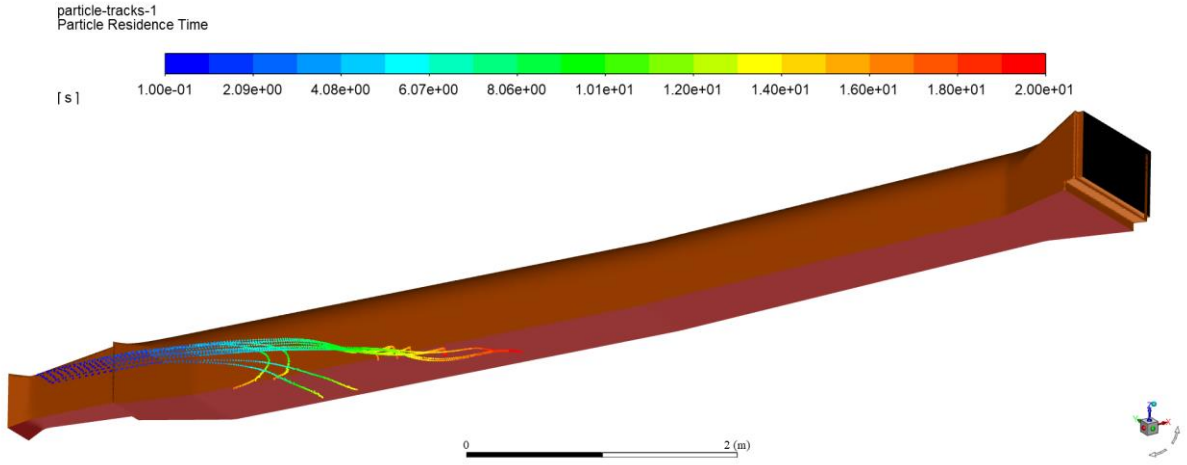

Figure 88: 1:20 model test, 0.3 mm grains - trap at bottom, iso view

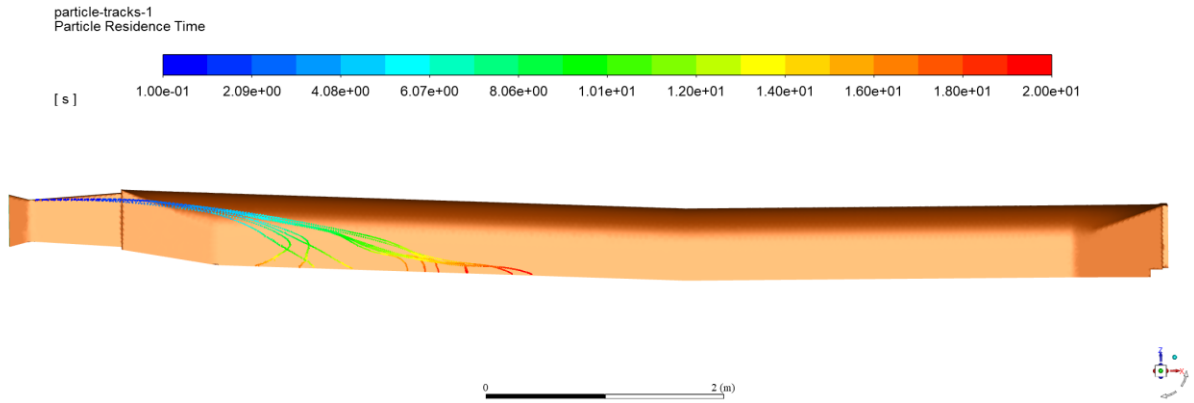

Figure 89: 1:20 model test, 0.3mm grains - trap at bottom, longitudinal view

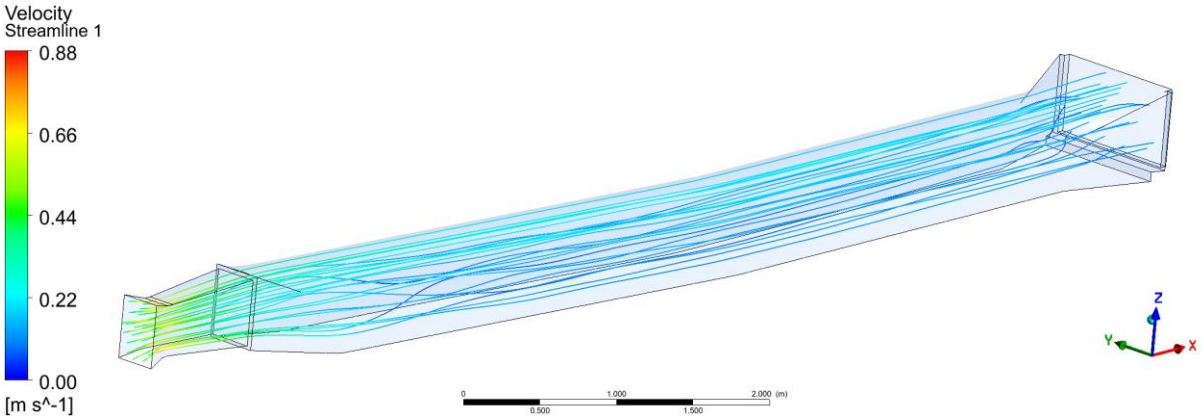

Figure 90: Streamlines 44.72 l/s, 1:20 model test, acrylic glass, k-eps

9.4 **3D CFD Simulations model 1:1**

This chapter contains 1:1 prototype simulation with *Fluent* to study the software's particle tracking properties.

9.4.1 **Particle tracking simulation 1:1 Sim_05a**

This simulation shows the result for a 1.0 mm sand grain influx and its trapping in the sand trap.

Table 9: Data for simulation 05a, rough mesh concrete

Scale	1:1	Geometry	full
Particles Diameter	1.0 mm	Particle injection	Above gate
Time	40 s	Wall roughness	300 mm
Timestep	0.2 s	Roughness constant	1.0
Particles Mass	1.0 kg/s	Bottom roughness	1.0 mm
Particles Density	2650 kg/m³	Material	Unlined Rock
Particle roughness	Non	Mesh	0.35 cm, no inflation
Particle Drag	sphere	Software	Fluent
Turbulence Modelling	SST-SAS	Discharge	80 m³/s
Trap efficiency	100%		

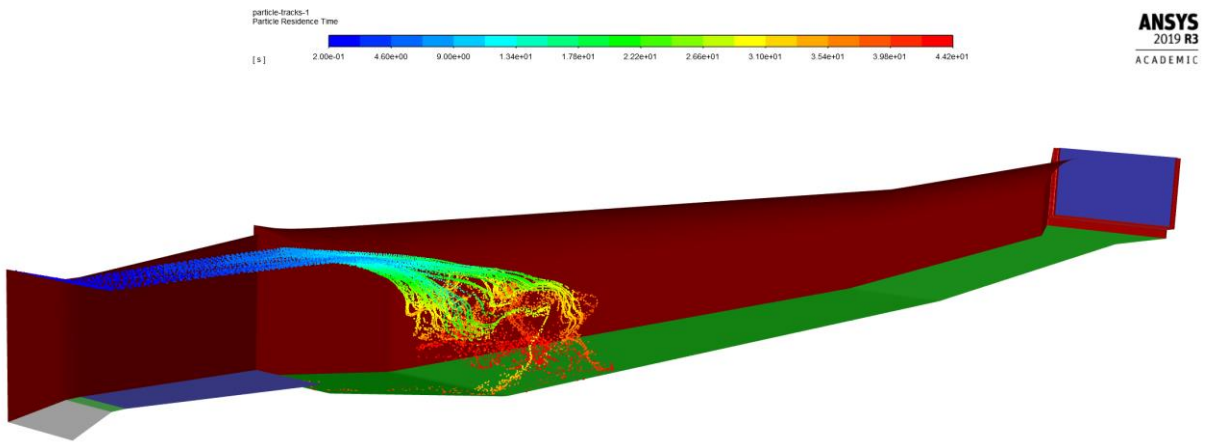

Figure 91: 1 mm sand particles, scale 1:1, 80 m³/s discharge

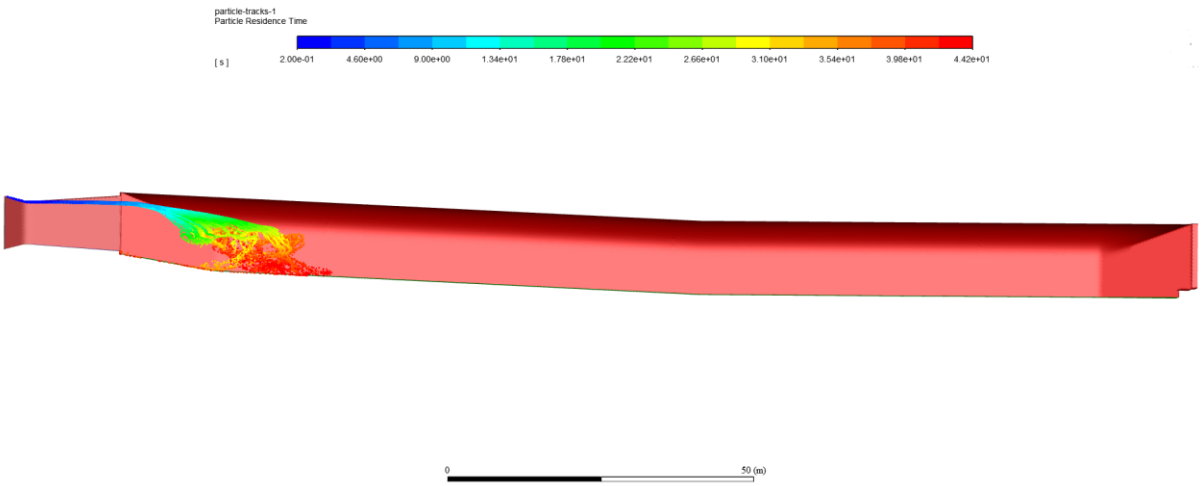

Figure 92: 1 mm sand particles, scale 1:1, 80 m³/s discharge, longitudinal view

9.4.2 **Particle tracking simulation 1:1 Sim_05b**

This simulation shows the result for a 1.0 mm sand grain influx and its trapping in the sand trap as continuation of Sim_05a. It can be seen that 1.0mm sand grains fall on the bottom and then be transported on the ground, which is also observed later in the model test and obviously happens in the prototype sand trap.

Table 10: Data for simulation 05a, fine mesh concrete

Scale	1:1	Geometry	full
Particles Diameter	1.0 mm	Particle injection	Above gate
Time	240 s	Wall roughness bottome	300 mm
Timestep	0.2 s	Roughness constant	1.0
Particles Mass	1.0 kg/s	Bottom roughness	1.0 mm
Particles Density	2650 kg/m³	Material	Unlined Rock
Particle roughness	Non	Mesh	0.35 cm, no inflation
Particle Drag	sphere	Software	Fluent
Turbulence Modelling	SST-SAS	Discharge	80 m³/s
Trap efficiency	100%		

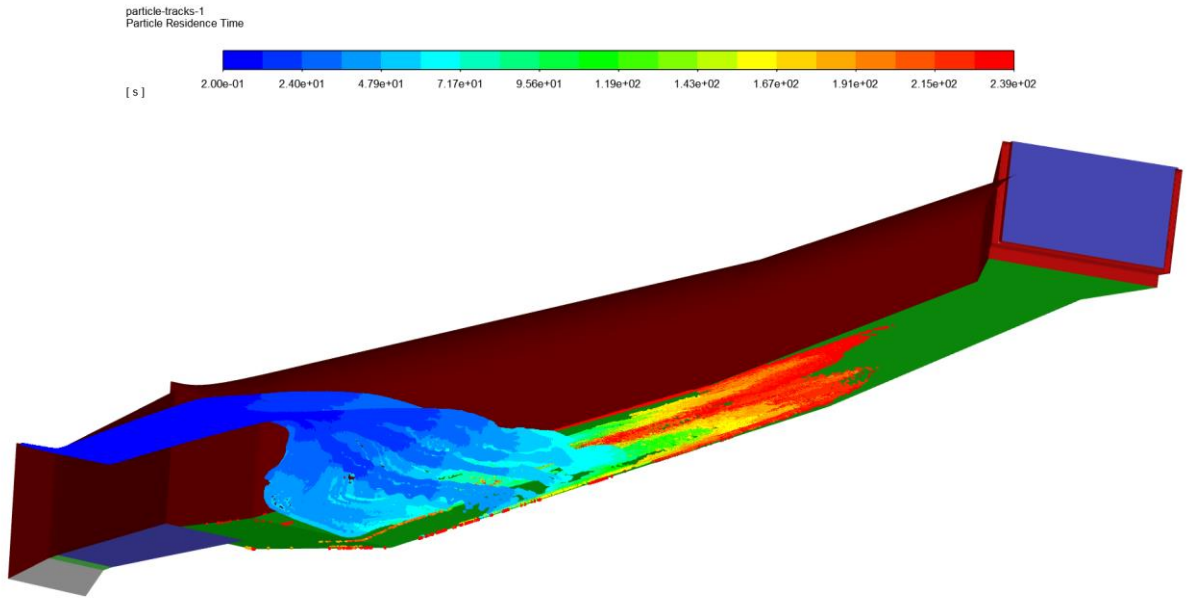

Figure 93: 1 mm sand particles, scale 1:1, 80 m³/s discharge, isometric view

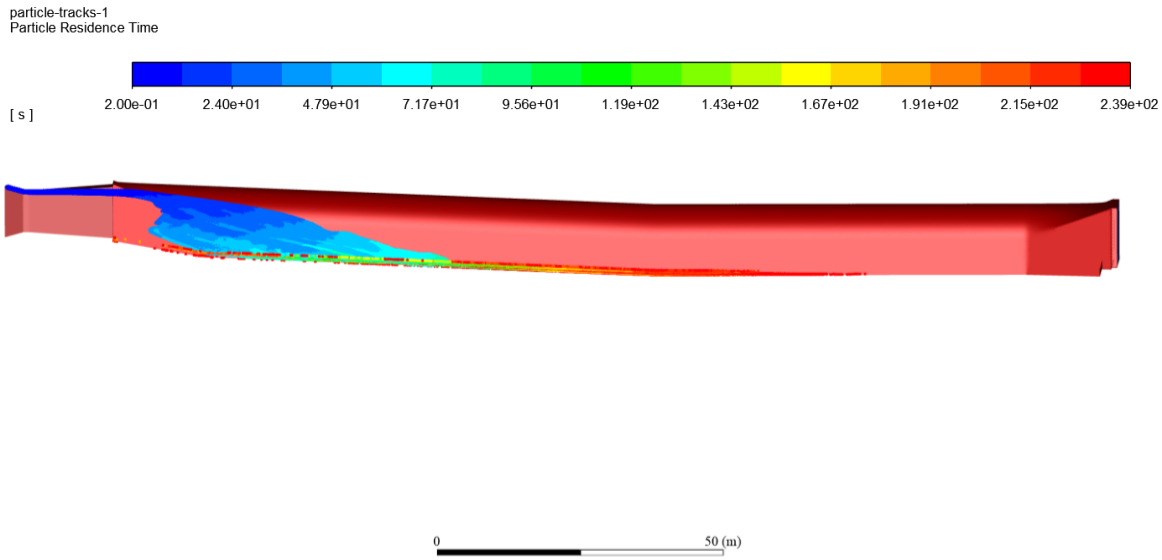

Figure 94: 1 mm sand particles, scale 1:1, 80 m³/s discharge, longitudinal view

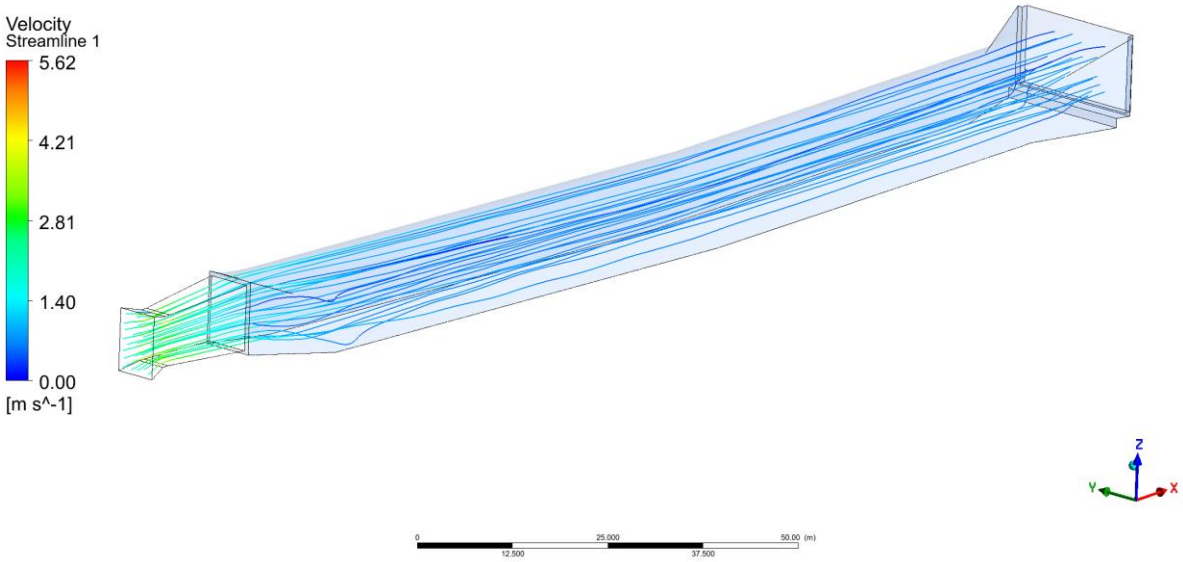

Figure 95: 1 mm sand particles, streamlines at final timestep, scale 1:1, 80 m³/s discharge, iso view

9.4.3 **Particle tracking simulation 1:1 Sim_06a**

This simulation shows the behaviour of particles with 0.3 mm diameter

Table 11: Data for simulation 06a, fine mesh concrete

Scale	1:1	Geometry	full
Particles Diameter	0.3 mm	Particle injection	Above inlet surface
Time	240 s	Wall roughness bottom	300 mm
Timestep	0.2 s	Roughness constant	1.0
Particles Mass	1.0 kg/s	Bottom roughness	1.0 mm
Particles Density	2650 kg/m³	Material	Unlined Rock
Particle roughness	with	Mesh	0.35 cm, no inflation, refinements concrete
Particle Drag	sphere	Software	Fluent
Turbulence Modelling	SST-SAS	Discharge	80 m³/s
Trap efficiency	<100%		

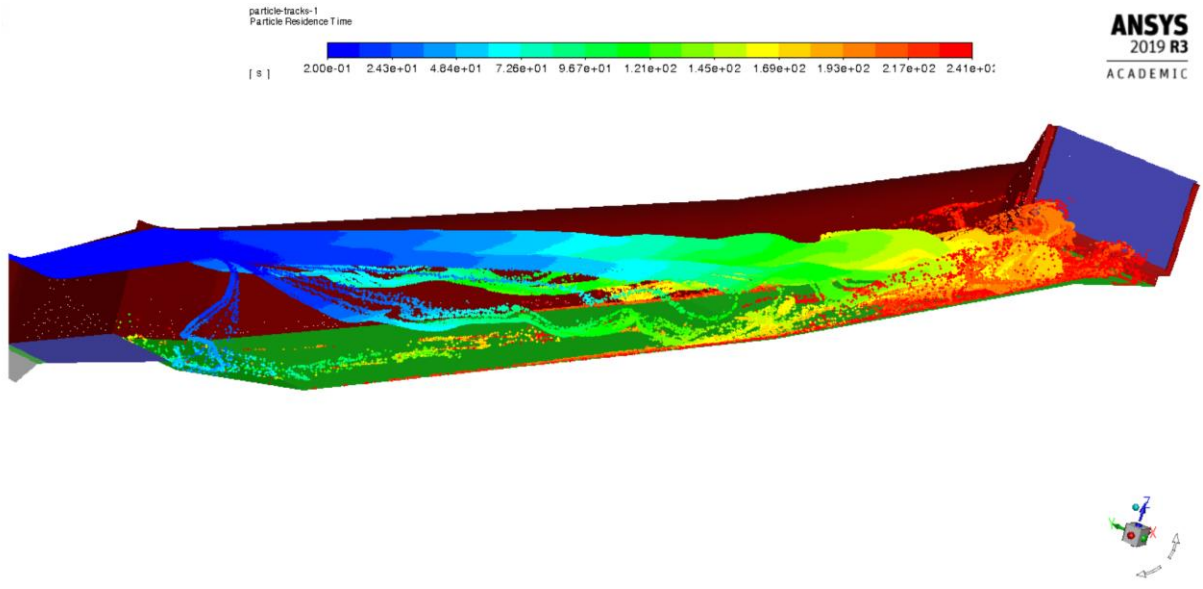

Figure 96: 0.3 mm sand particles, scale 1:1, 80 m³/s discharge, isometric view, outflow of particles

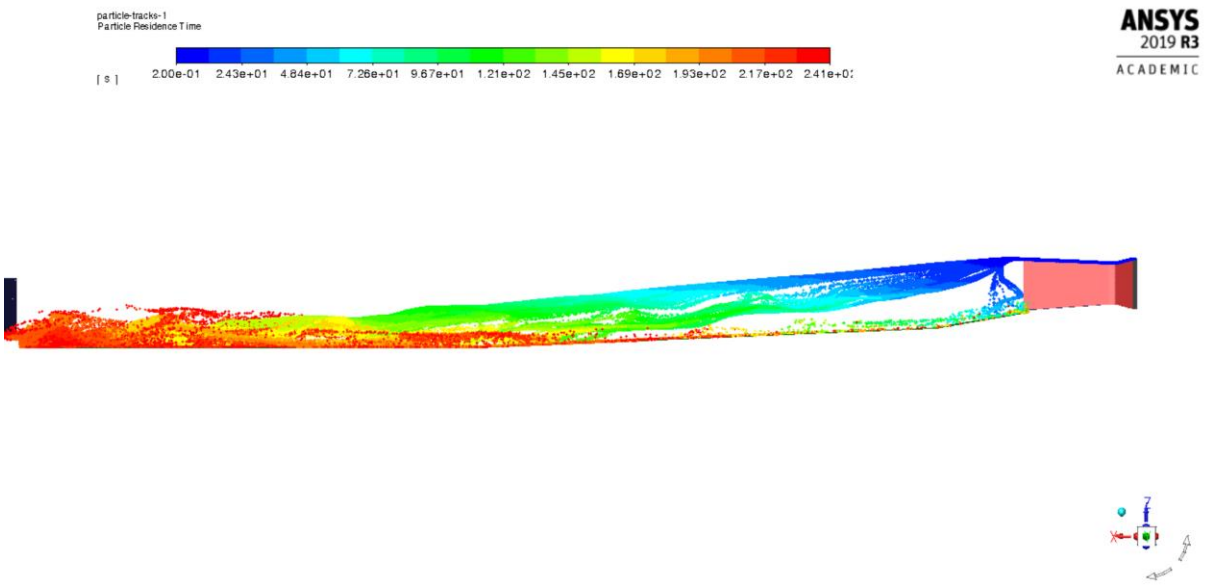

Figure 97: 0.3 mm sand particles, scale 1:1, 80 m³/s discharge, side view, outflow of particles

9.4.4 **With approach flow geometry scale 1:1 Sim_14**

Simulation with 0.3 mm to 1.0 mm sand grain with approach flow of Tonstad sand trap using the software *CFX.*

Table 12: Data for simulation 14

Scale	1:1	Geometry	full
Particles Diameter	0.3 mm -1.0 mm	Particle injection	Above inlet surface
Time	240 s	Wall roughness bottom	300 mm
Timestep	0.2 s		
Particles Mass	0.5 kg/s	Bottom roughness	1.0 mm
Particles Density	2650 kg/m³	Material	Unlined Rock
Particle roughness	no	Mesh	0.35 cm, no inflation, refinements concrete
Particle Drag	sphere	Approach flow	From MHT
Turbulence Modelling	SST	Software	CFX
Trap efficiency			

The simulation contains the effect of the approach geometry. The particles are inserted at the upper side of the gate. Figure 98 shows the effect of the backflow region after the gate where sediments are transported backwards on the bottom.

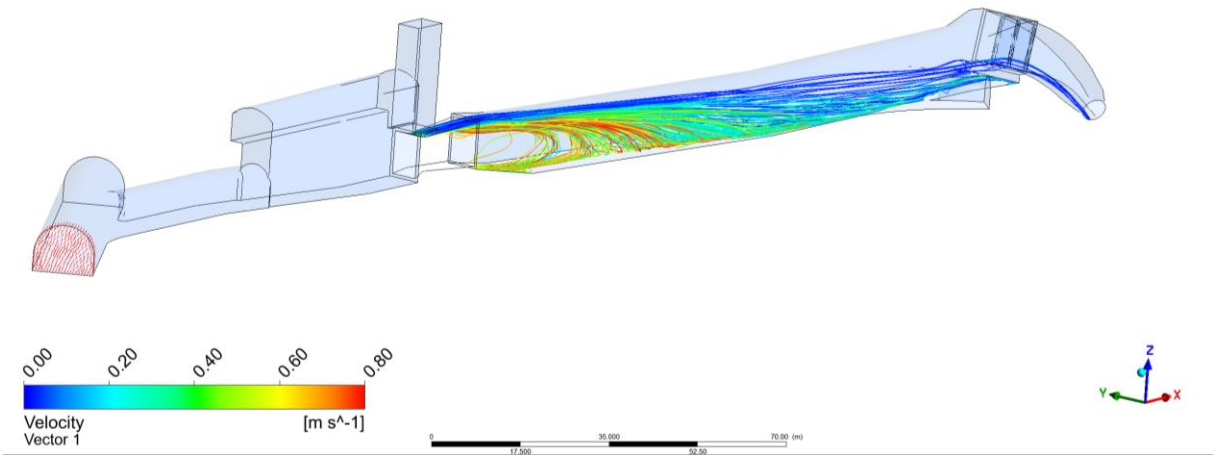

Figure 98: 0.3 mm – 1.0 mm sand particles, scale 1:1, 80 m³/s discharge, full view

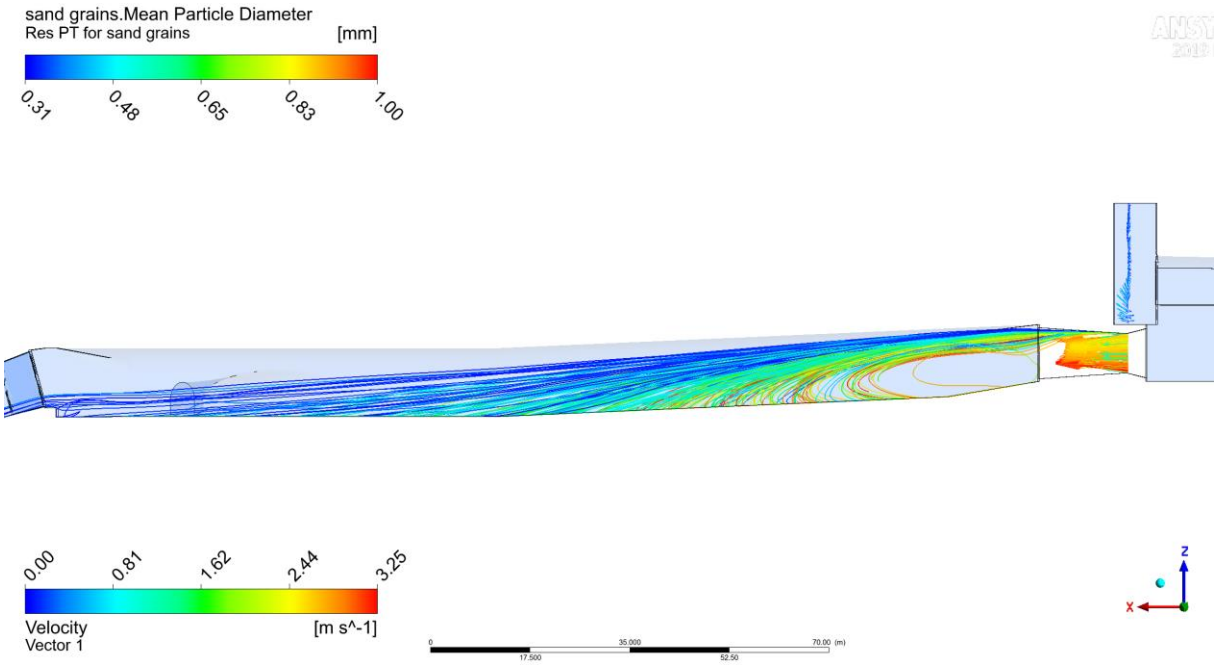

Figure 99: 0.3 mm – 1.0 mm sand particles, scale 1:1, 80 m³/s discharge, side view

Figure 100 shows additionally to the figures above the velocity distribution in the section where the gate is placed, the most restricted flow section of the investigated geometry.

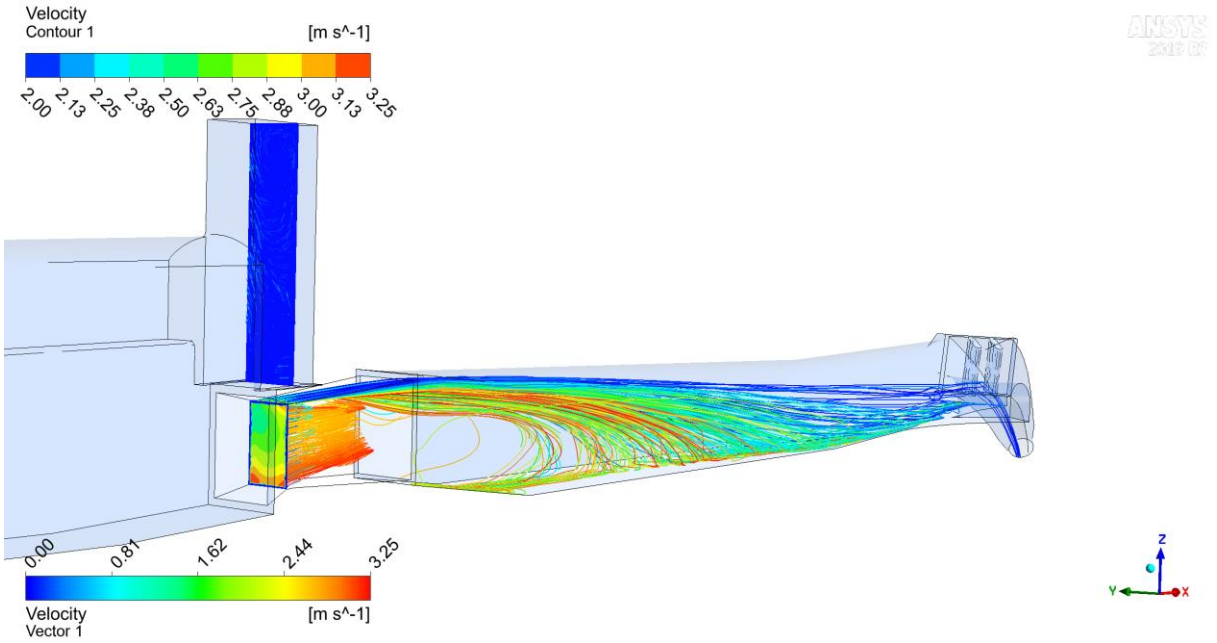

Figure 100: 0.3 mm – 1.0 mm sand particles, scale 1:1, 80 m³/s discharge, perspective view

9.4.5 **With approach flow geometry and sediment disposition scale 1:1 Sim_15**

Simulation with 0.3 mm to 1.0 mm sand grain with approach flow of Tonstad sand trap.

Table 13: Data for simulation 15

Scale	1:1	Geometry	full
Particles Diameter	0.3 mm -1.0 mm	Particle injection	Above inlet surface
Time	240 s	Wall roughness bottom, ks	300 mm
Timestep	0.2 s		
Particles Mass	0.5 kg/s	Bottom roughness, ks	1.0 mm
Particles Density	2650 kg/m³	Material	Unlined Rock
Particle roughness	no	Mesh	0.35 cm, no inflation, refinements concrete
Particle Drag	Schiller Naumann	Approach flow	included
Turbulence Modelling	SST	Software	CFX
Trap efficiency		Discharge	80 m³/s

Figure 101 and Figure 102 show the result of the simulation, larger particles fall down earlier and smaller particles up to about 0.6 mm are directly conveyed to the pressure shaft.

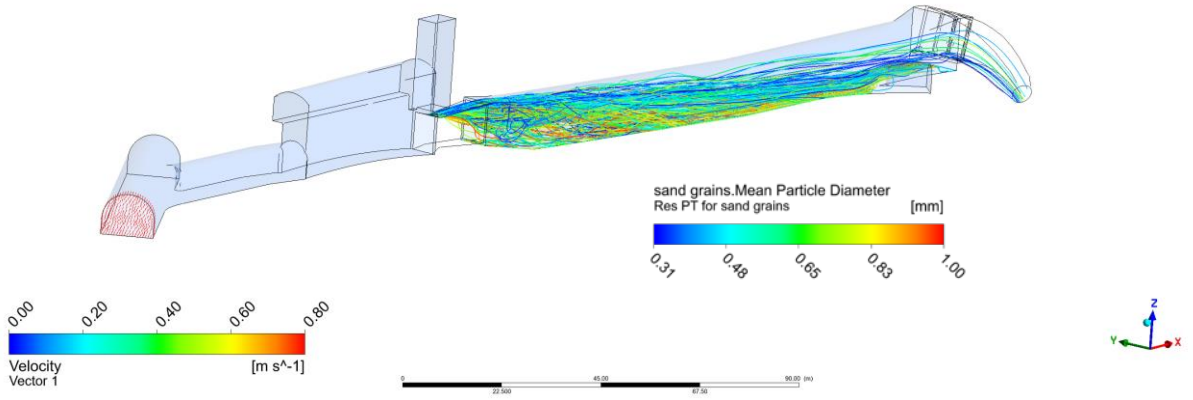

Figure 101: 0.3 mm – 1.0 mm sand particles, scale 1:1, 80 m³/s discharge, full view

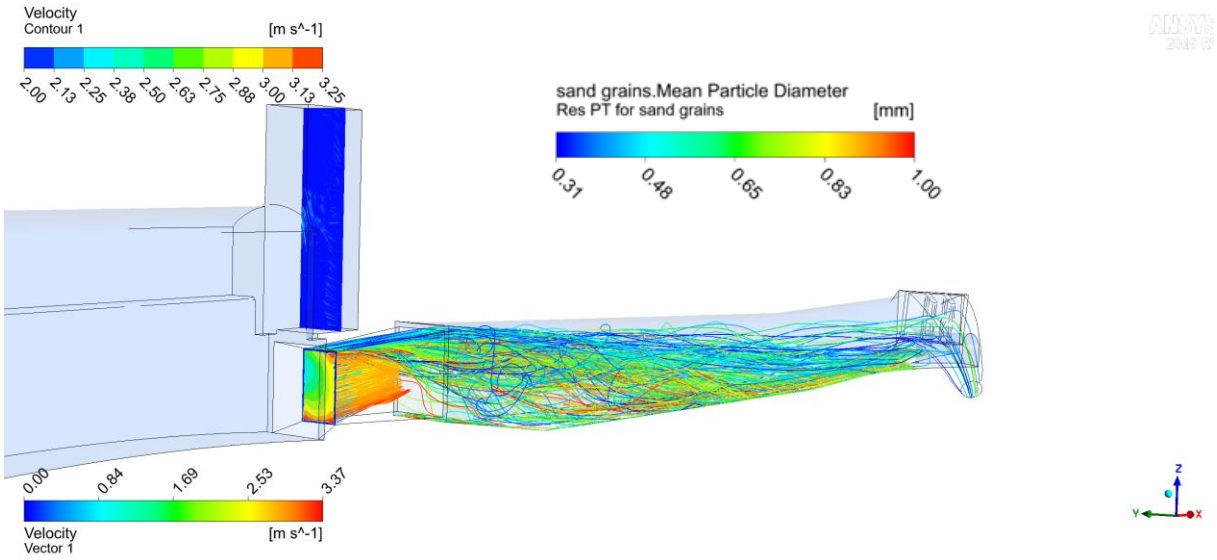

Figure 102: 0.3 mm – 1.0 mm sand particles, scale 1:1, 80 m³/s discharge, perspective view

9.4.6 **With approach flow geometry scale 1:1 Sim_16**

Simulation with 0.3 mm to 1.0 mm sand grain with approach flow of Tonstad sand trap. In contrast to sim_14 this case is simulated with the SAS SST turbulence model and a finer mesh.

Table 14: Data for simulation 16

Scale	1:1	Geometry	full
Particles Diameter	0.3 mm -1.0 mm	Particle injection	Above inlet surface
Time	240 s	Wall roughness bottom	300 mm
Timestep	0.2 s		
Particles Mass	0.5 kg/s	Bottom roughness	1.0 mm
Particles Density	2650 kg/m³	Material	Unlined Rock
Particle roughness	no	Mesh	0.35 cm, no inflation, refinements concrete
Particle Drag	sphere	Approach flow	From MHT
Turbulence Modelling	**SAS-SST**	Software	CFX
Mesh size	> 4 mio. elements		

Figure 103 and Figure 104 show for certain time points of a transient simulation, the bottom wall shear stress in the pressurized sand trap for the 80 m³/s discharge during a transient simulation. It shows the effect of the jet due to the gate restriction that creates local flow

accelerations acting until the rake with an amplitude on the bottom to transport up to fine gravel grains very far downstream of the sand trap. This can be confirmed by prototype observations. Also, this simulation shows the disadvantageous effect of the access tunnel, creating a vortex and local higher flow velocities.

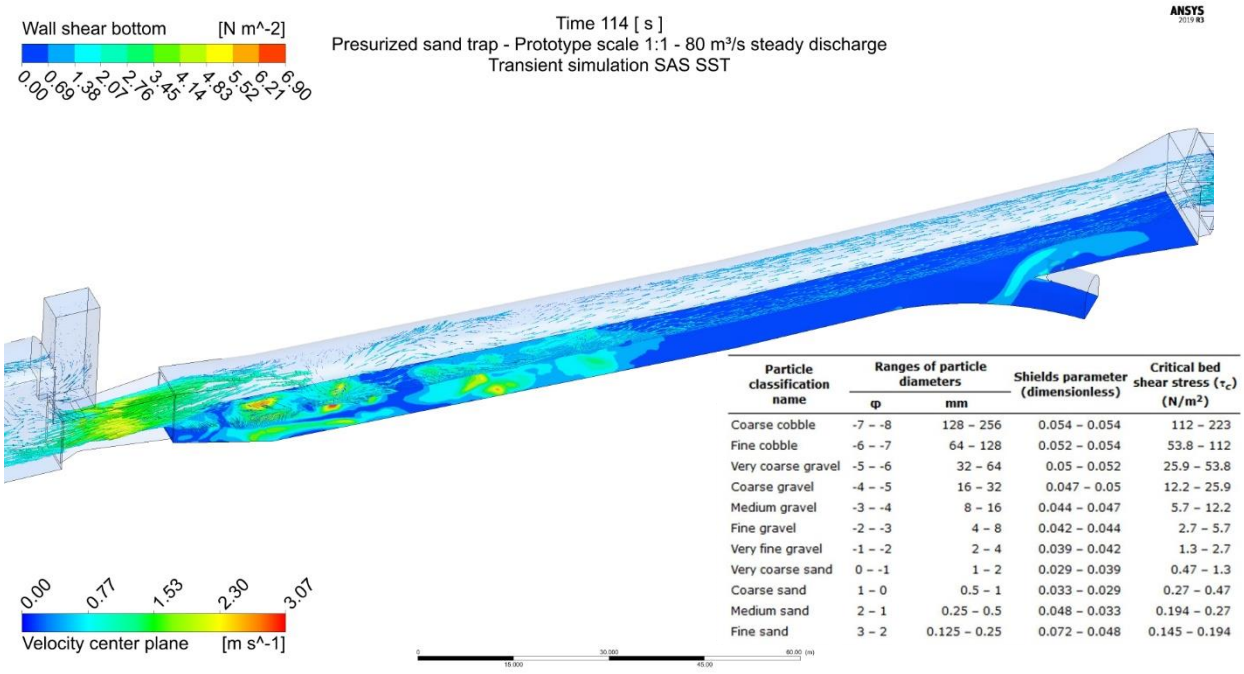

Particle classification name	Ranges of particle diameters		Shields parameter (dimensionless)	Critical bed shear stress (τ_c) (N/m^2)
	φ	mm		
Coarse cobble	-7 – -8	128 – 256	0.054 – 0.054	112 – 223
Fine cobble	-6 – -7	64 – 128	0.052 – 0.054	53.8 – 112
Very coarse gravel	-5 – -6	32 – 64	0.05 – 0.052	25.9 – 53.8
Coarse gravel	-4 – -5	16 – 32	0.047 – 0.05	12.2 – 25.9
Medium gravel	-3 – -4	8 – 16	0.044 – 0.047	5.7 – 12.2
Fine gravel	-2 – -3	4 – 8	0.042 – 0.044	2.7 – 5.7
Very fine gravel	-1 – -2	2 – 4	0.039 – 0.042	1.3 – 2.7
Very coarse sand	0 – -1	1 – 2	0.029 – 0.039	0.47 – 1.3
Coarse sand	1 – 0	0.5 – 1	0.033 – 0.029	0.27 – 0.47
Medium sand	2 – 1	0.25 – 0.5	0.048 – 0.033	0.194 – 0.27
Fine sand	3 – 2	0.125 – 0.25	0.072 – 0.048	0.145 – 0.194

Figure 103: Scale 1:1, 80 m³/s discharge, velocity vectors in center plane and bottom wall shear stress, time point 114 s

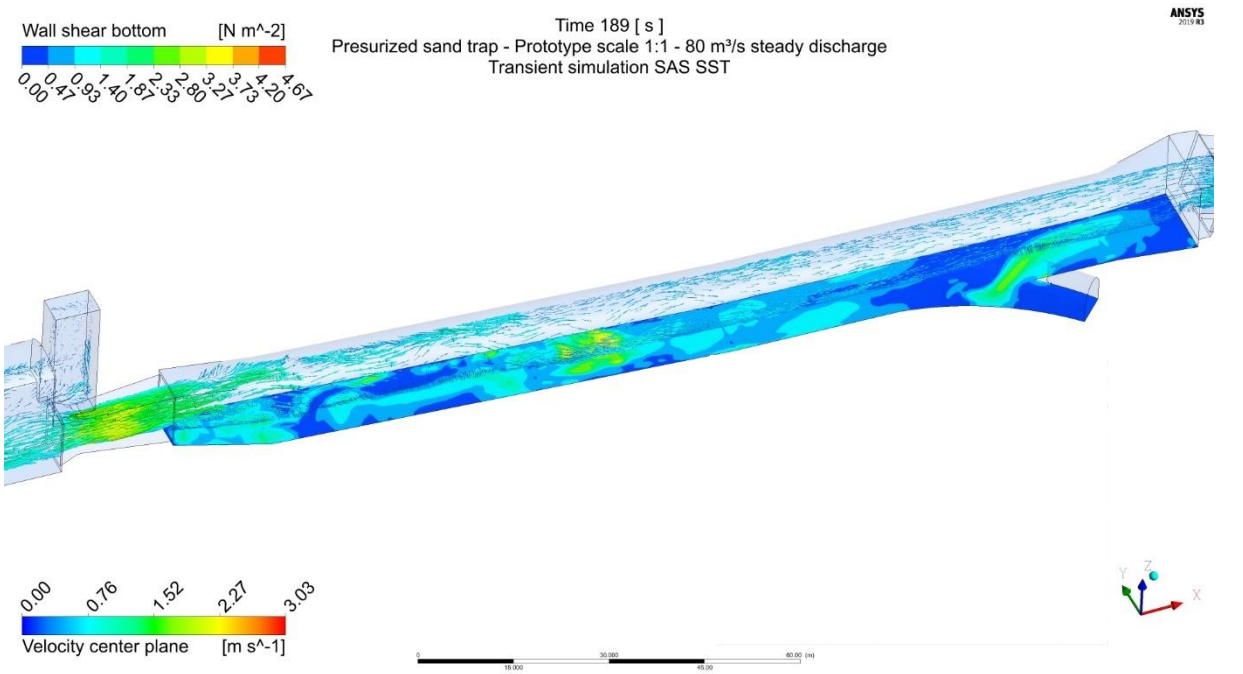

Figure 104: Scale 1:1, 80 m³/s discharge, velocity vectors in center plane and bottom wall shear stress, time point 189 s

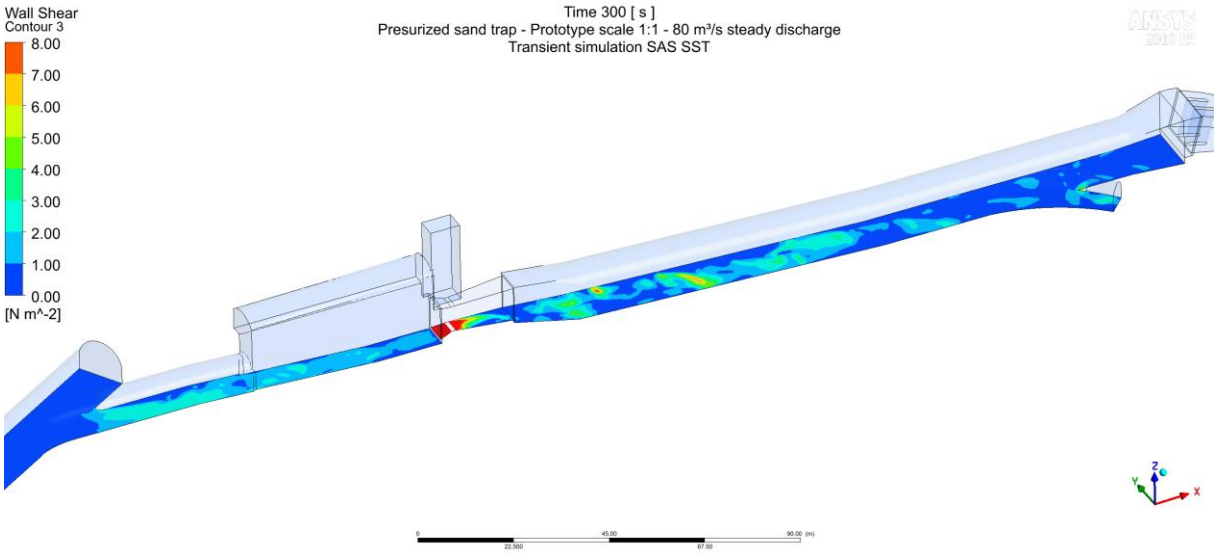

Figure 105: Scale 1:1, 80 m³/s discharge, bottom wall shear stress including the approach tunnel to the surge tank, time point 300 s

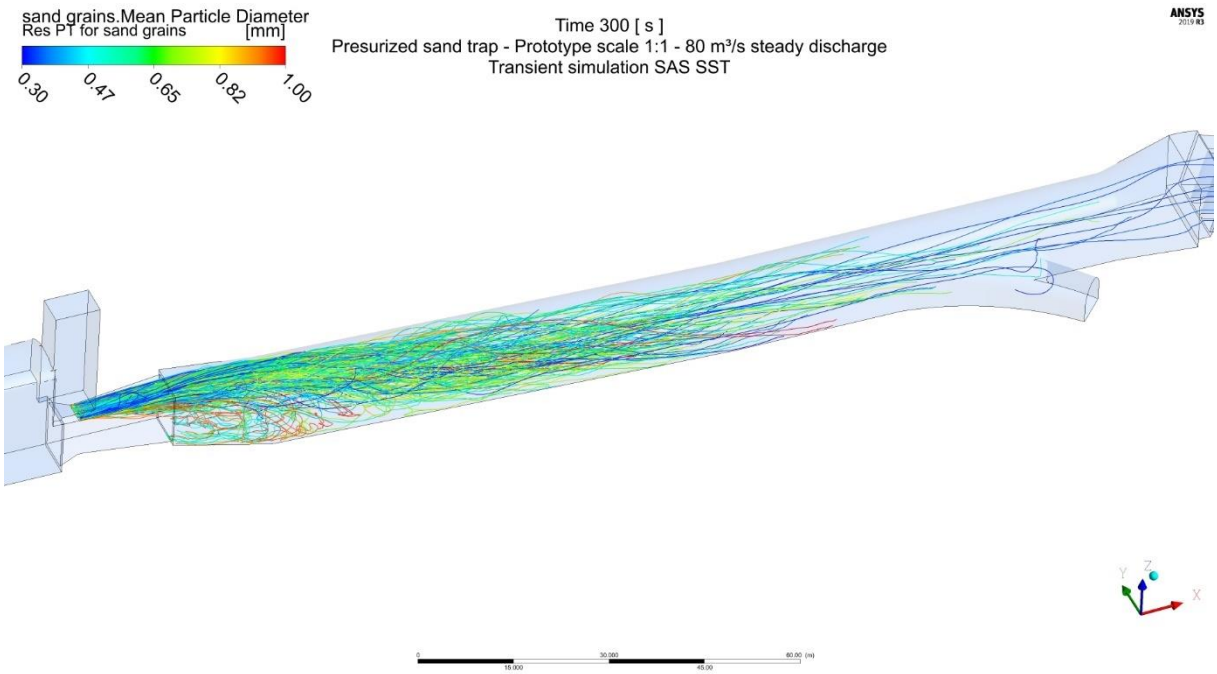

Figure 106: Scale 1:1, 80 m³/s discharge, particle tracking paths for sediment grains of 0.3 mm to 1.0 mm, time point 300 s

The figures below show that especially for small grains from 0.3mm to about 0.5mm no significant settling can be achieved.

The various plots in Figure 107 to Figure 112 show different specific particle diameter scales to identify the effect of particle diameter. However, the effect of the bottom transportation as later observed in the model test are a question of further research. In the numerical simulation this depends on the wall and particle friction.

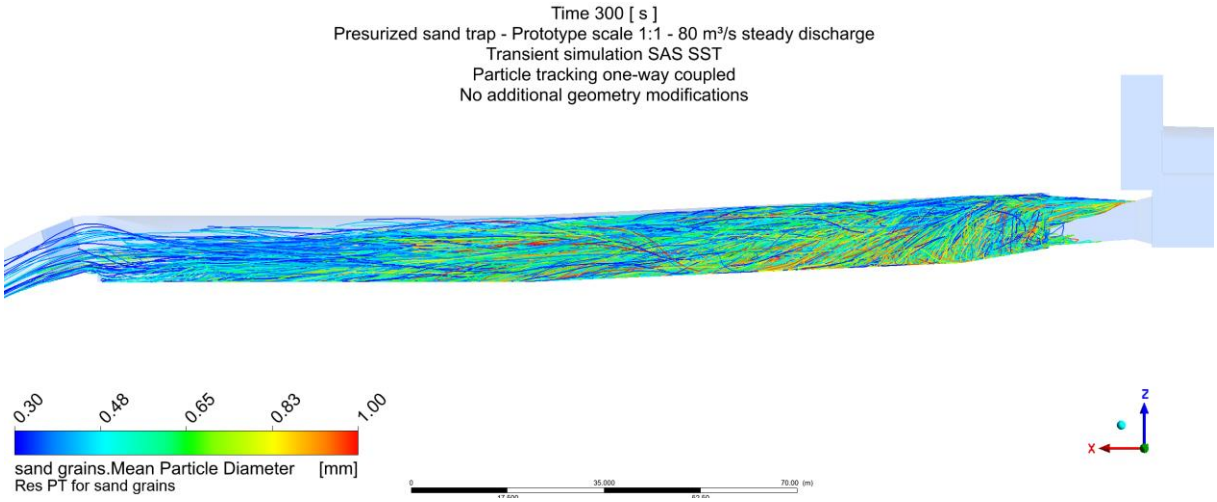

Figure 107: Scale 1:1, 80 m³/s discharge, particle tracking paths for sediment grains of 0.3 mm to 1.0 mm, time point 300 s, view y-axis

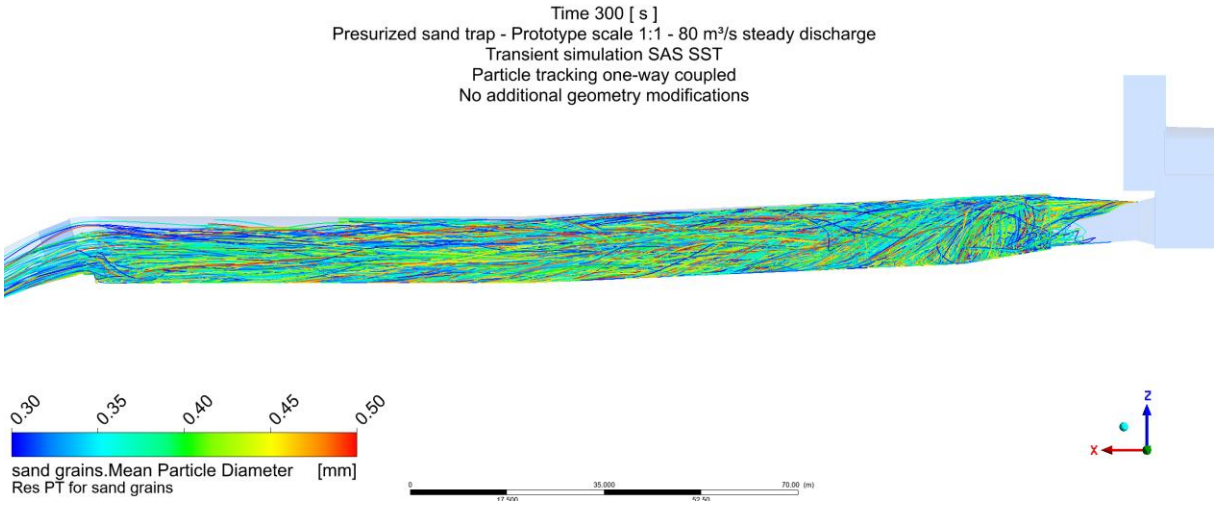

Figure 108: Scale 1:1, 80 m³/s discharge, particle tracking paths for sediment grains of 0.3 mm to 0.5 mm, time point 300 s, view y-axis

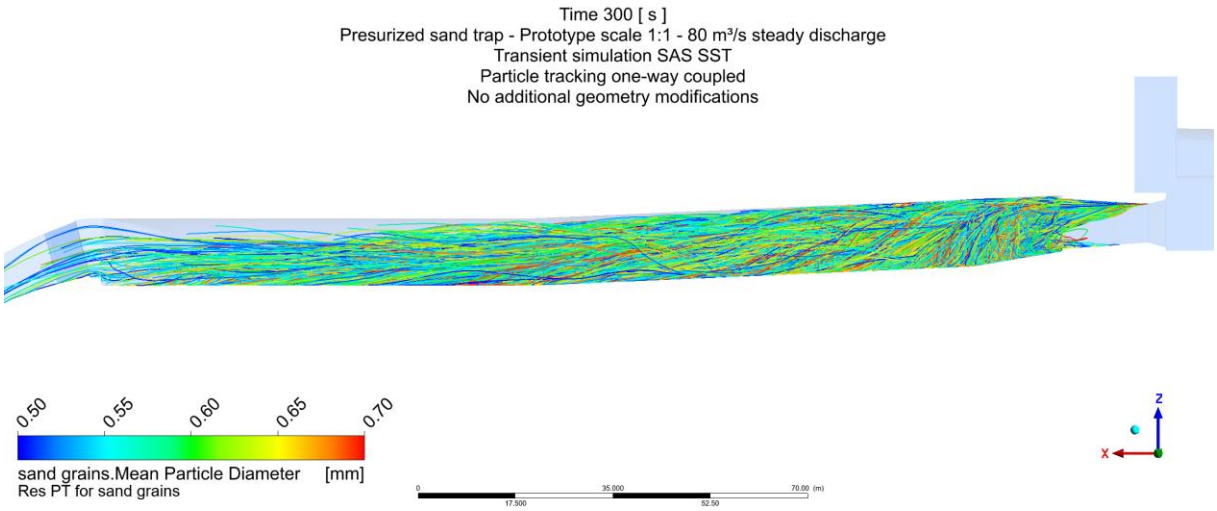

Figure 109: Scale 1:1, 80 m³/s discharge, particle tracking paths for sediment grains of 0.5 mm to 0.7 mm, time point 300 s, view y-axis

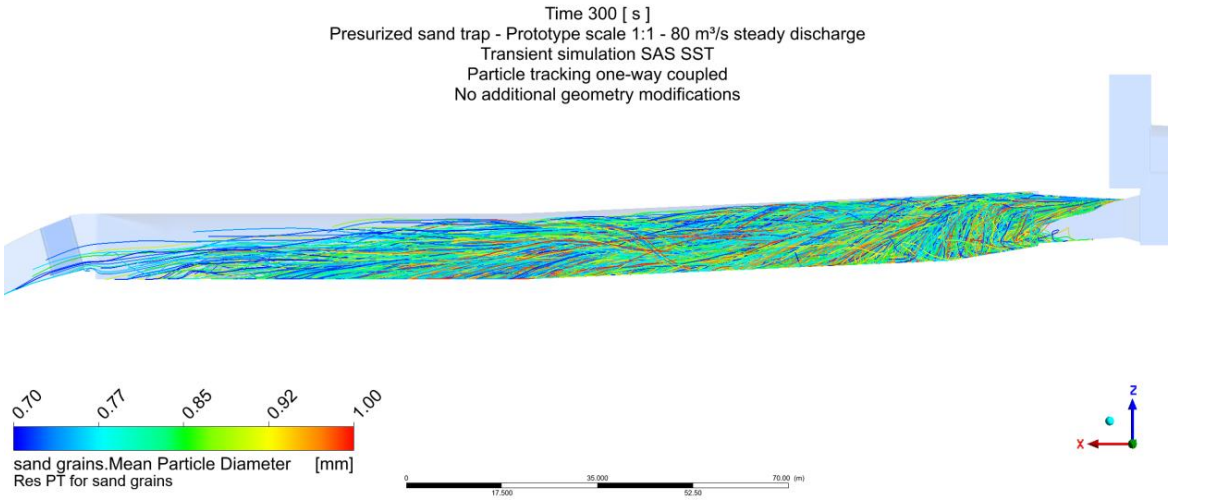

Figure 110: Scale 1:1, 80 m³/s discharge, particle tracking paths for sediment grains of 0.7 mm to 1.0 mm, time point 300 s, view y-axis

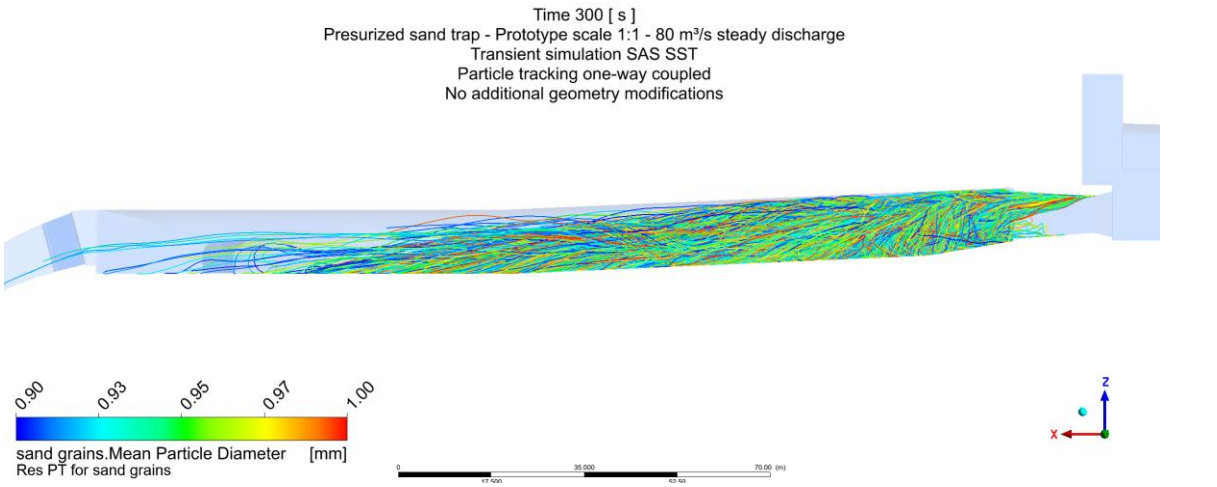

Figure 111: Scale 1:1, 80 m³/s discharge, particle tracking paths for sediment grains of 0.9 mm to 1.0 mm, time point 300 s, view y-axis

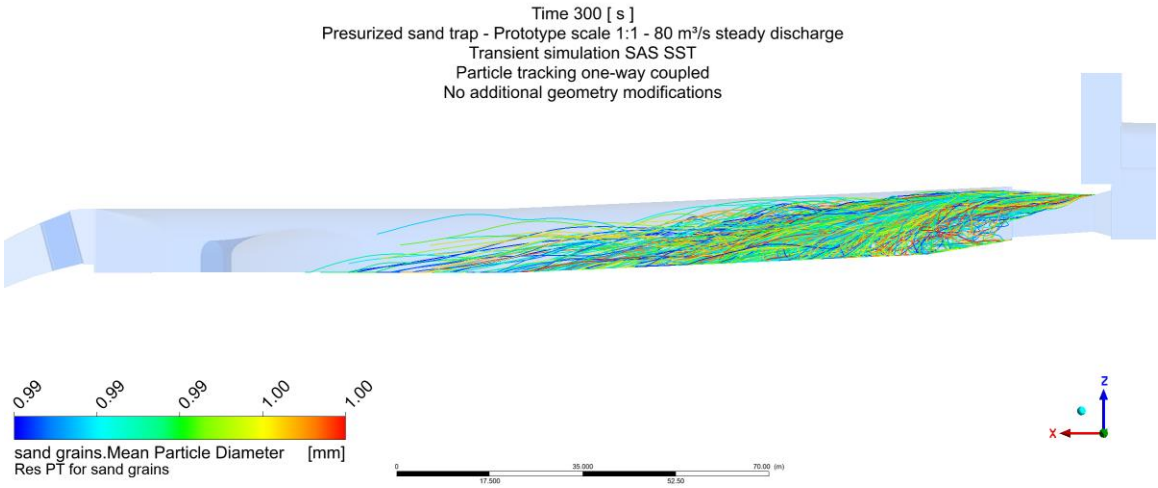

Figure 112: Scale 1:1, 80 m³/s discharge, particle tracking paths for sediment grains of 0.99 mm to 1.0 mm, time point 300 s, view y-axis

9.4.7 **Start-up unit No.5 with surge tank response Sim 26**

This simulation considers the start-up of unit no.5 and the transient flow effects in the surge tank and its effect on the sediment transportation in sand trap chamber.

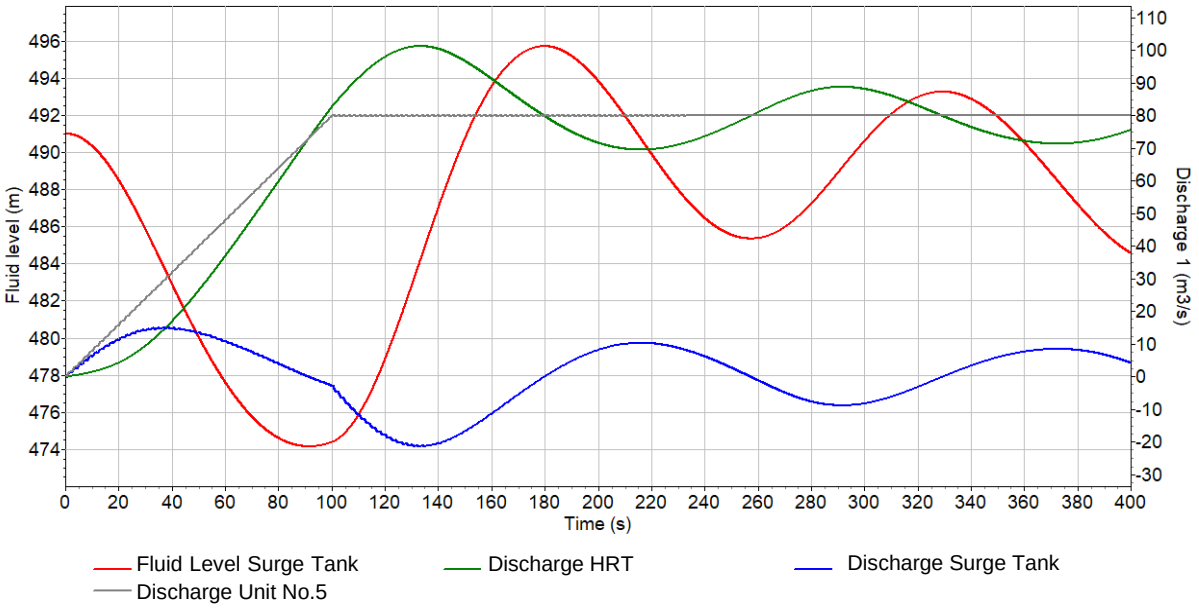

Figure 113: Result of 1D simulation, start-up Unit No.3 to 80 m³/s in 100 s at reservoir levels 491 m a.s.l., discharge (resp. velocity) from ST and Headrace flow as input for 3D CFD with particle tracking

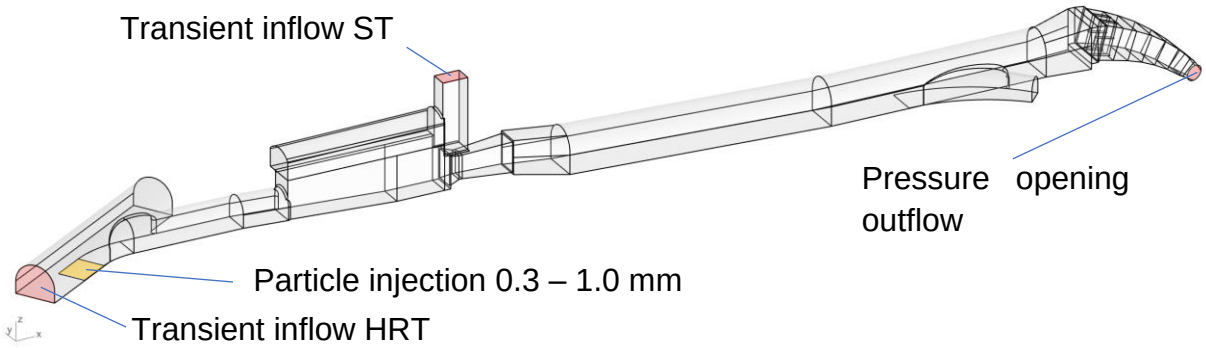

Figure 114: Boundary conditions for transient particle simulation

Figure 115 to Figure 118 show the transient case with water flow start-up and particle injection at unfavourable location above the gate section. The results show that there is no significance detectable and no need to extra take the surge tank oscillation into account to the particle behaviour in the sand trap.

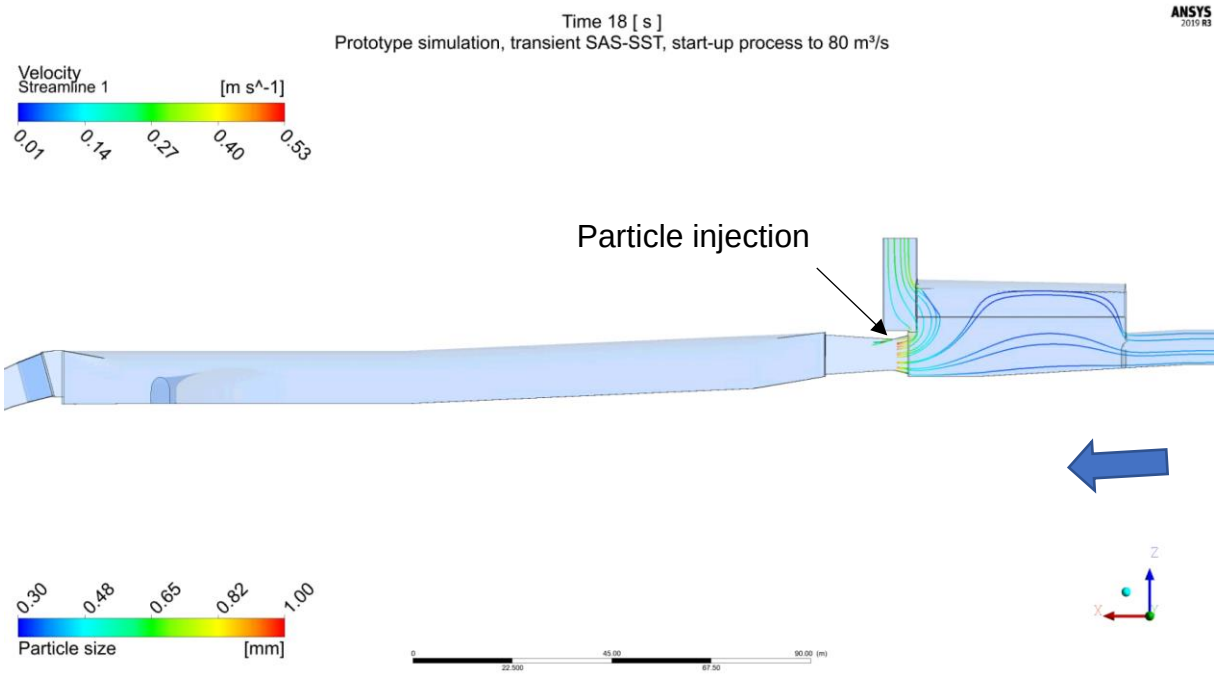

Figure 115: Start-up with inflow from surge tank and accelerating headrace tunnel, particle input from gate section, time 18s

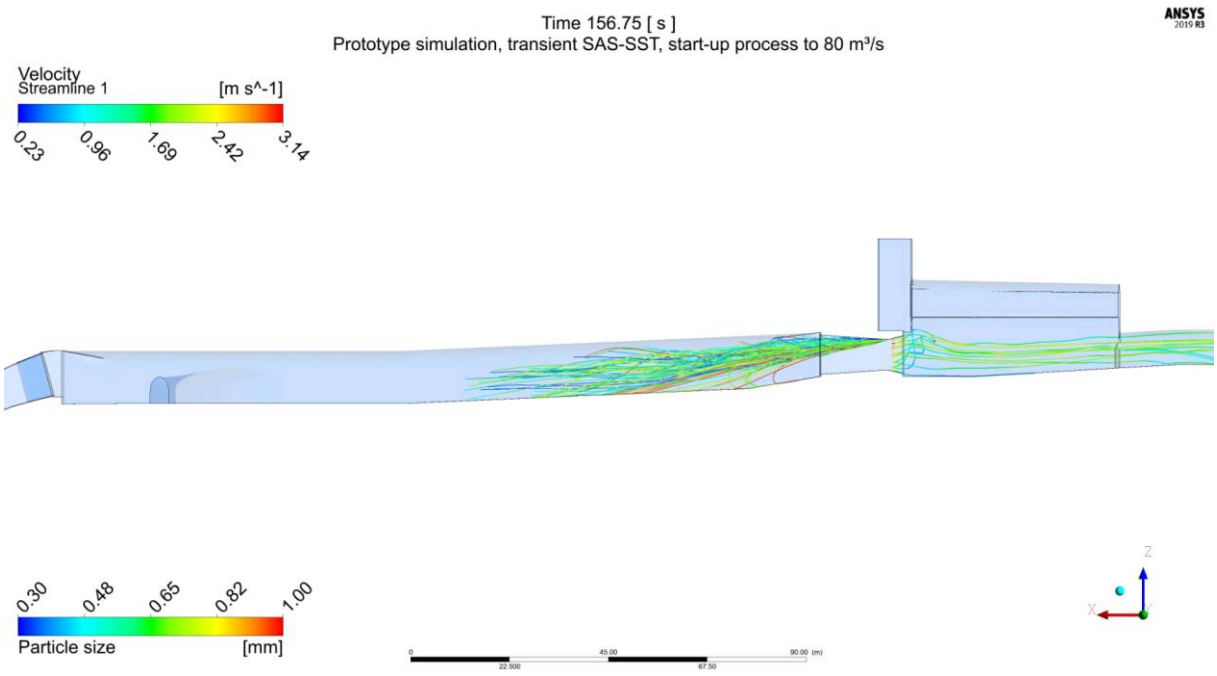

Figure 116: Start-up with inflow from surge tank and accelerating headrace tunnel, particle input from gate section, time 156.75s

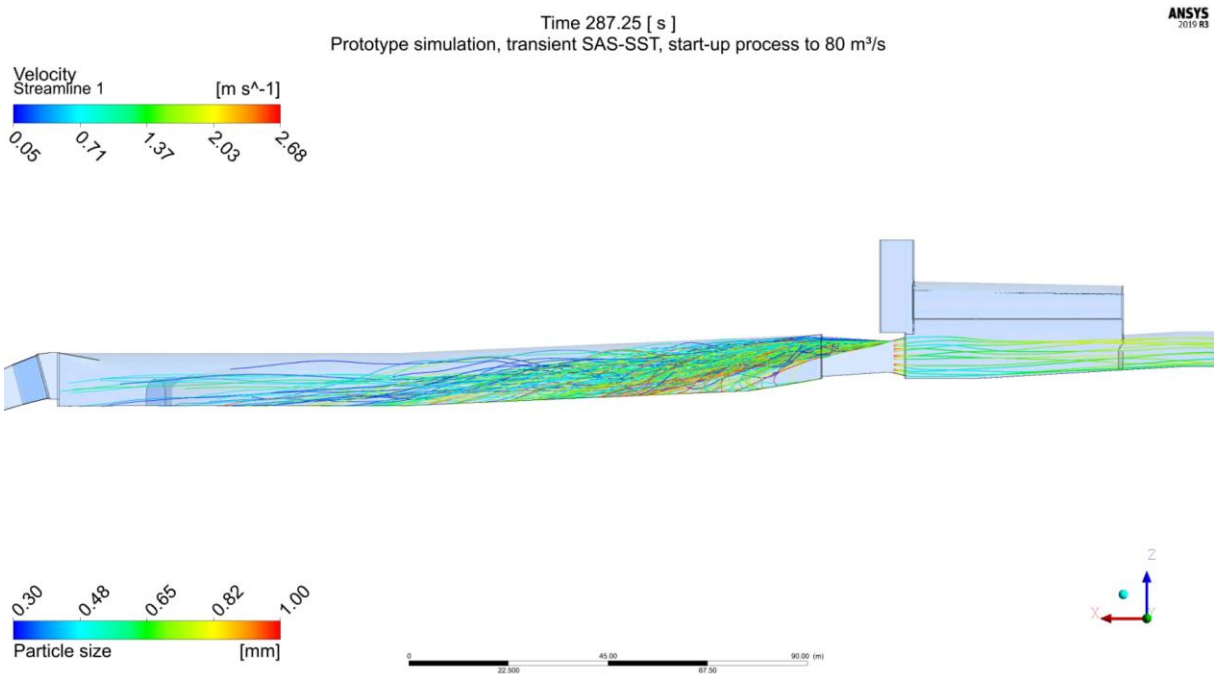

Figure 117: Start-up with inflow from surge tank and accelerating headrace tunnel, particle input from gate section, time 287.25s

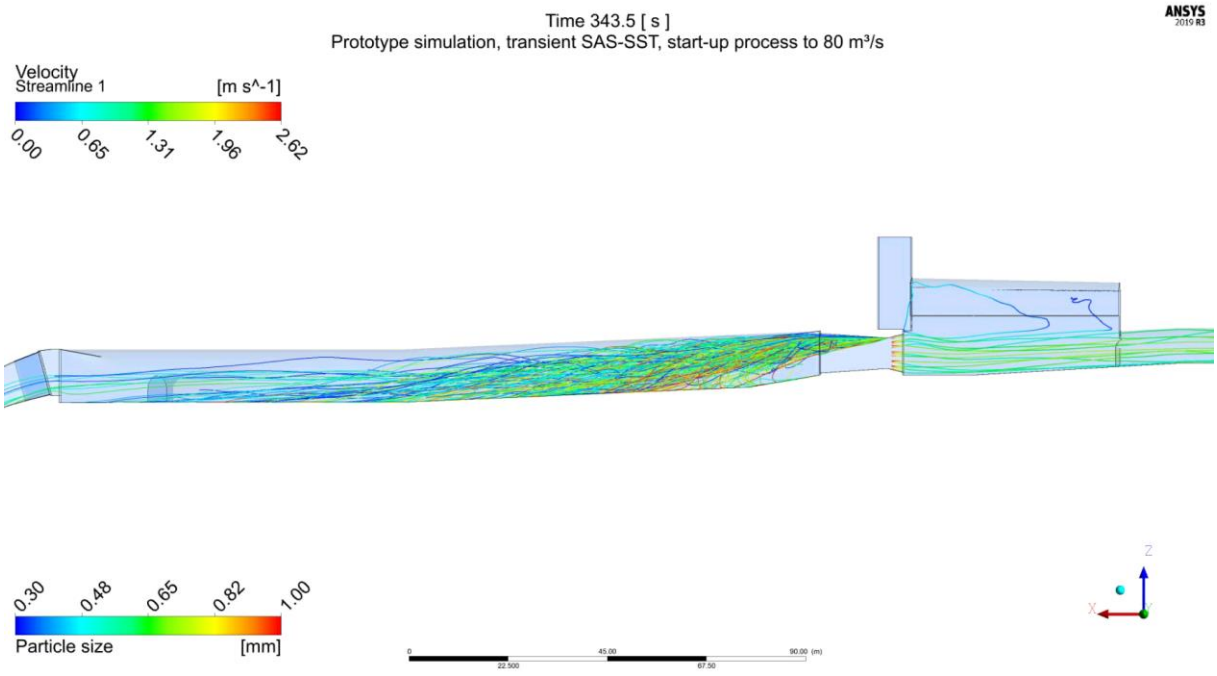

Figure 118: Start-up with inflow from surge tank and accelerating headrace tunnel, particle input from gate section, time 343.5

11. 3D CFD particle simulations – geometry for flume

This chapter describes the particle tracking simulation in the design geometry of the sand trap to be situated in the physical model test. The geometry is slightly idealized by removing the adit tunnel and the section widening upstream of the weir.

Table 15: Boundary conditions for particle flow simulations

Scale	1:20 and 1:1	Geometry	Tonstad plans
Particles Diameter (1:1)	0.25-1.0 mm	Particle injection	Above gate
Particles Diameter (1:20)	0.05-0.5 mm	Wall roughness	Smooth wall
Time (1:20 resp. 1:1)	80s resp. 300 s	Software	CFX
Timestep	0.1 resp. 0.2 s	Inlet	Velocity
Particles Density	2650 kg/m³	Outlet	Pressure
Particle roughness	Non	Particles	One-way coupled resp. fully coupled
Particle Drag	Schiller-Naumann		
Turbulence Modelling	SST		

11.1 Scale 1:1 particle tracking simulation Sim_19

Figure 119 and Figure 120 show the particle tracks for 0.3 mm to 1.0 mm grains in 1:1 scale sand trap chamber at 1.64 m/s inflow velocity, defining the design case for 80 m³/s.

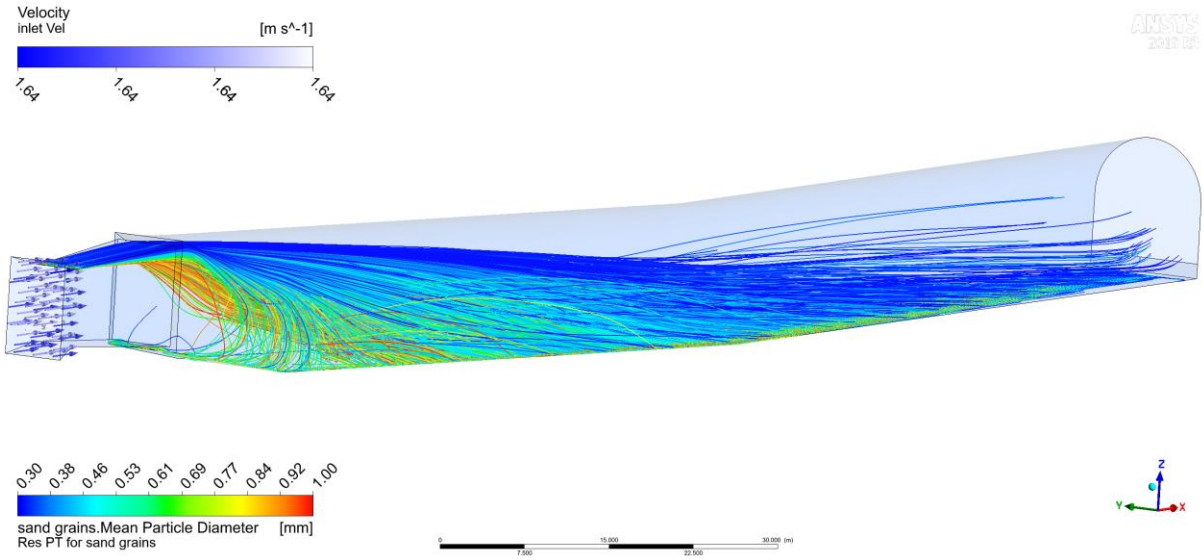

Figure 119: 3D CFD with particle tracking grains 0.3-1.0 mm, scale 1:1, 1.64 m/s inlet velocity, perspective view

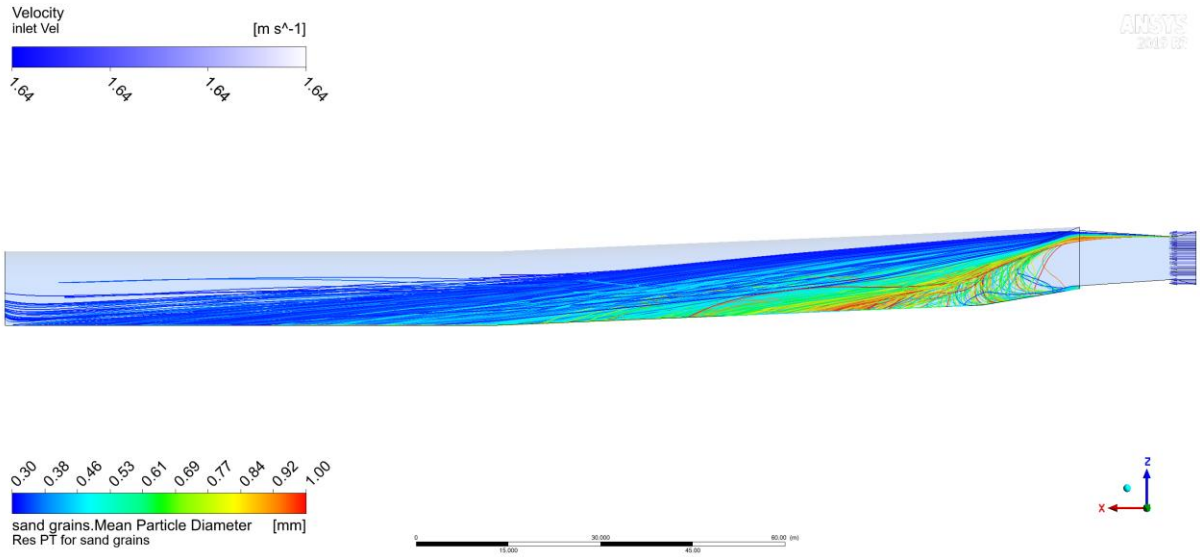

Figure 120: 3D CFD with particle tracking grains 0.3-1.0 mm, scale 1:1, 1.64 m/s inlet velocity, undisturbed inflow, side view

11.2 **Scale 1:36.67 particle tracking simulation Sim_20**

Figure 121 and Figure 122 show the particle tracks for 0.3 mm to 1.0 mm grains in 1:36.67 scale sand trap chamber at 1.64 m/s inflow velocity, defining the design case for 80 m³/s. The results reflect the applicability of the proposed prototype sediment feeding at prototype velocity.

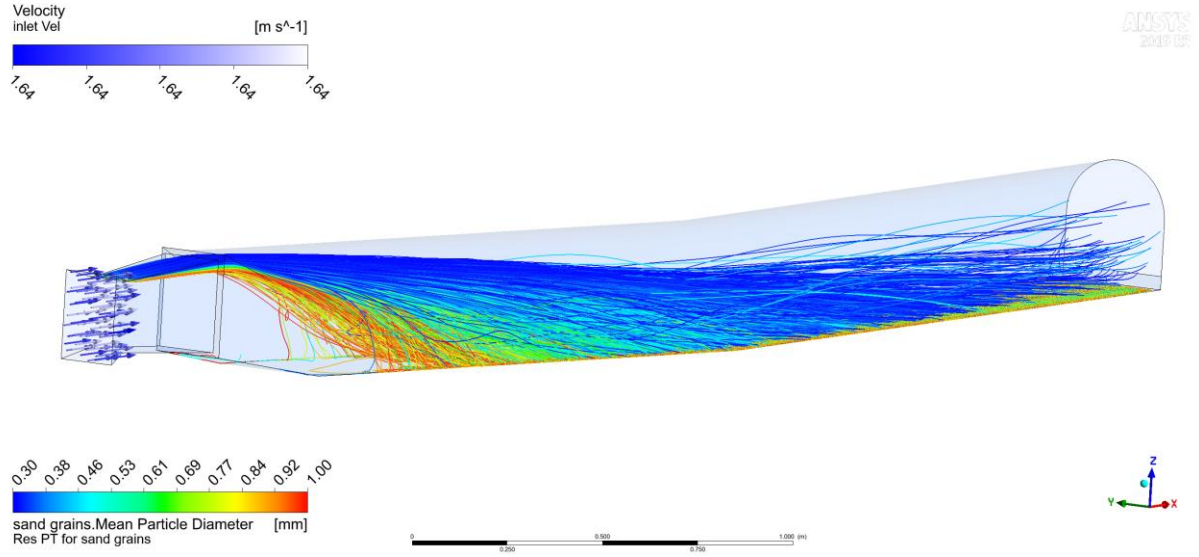

Figure 121: 3D CFD with particle tracking grains 0.3-1.0 mm, scale 1:36.67, 1.64 m/s inlet velocity, perspective view, one-way coupled

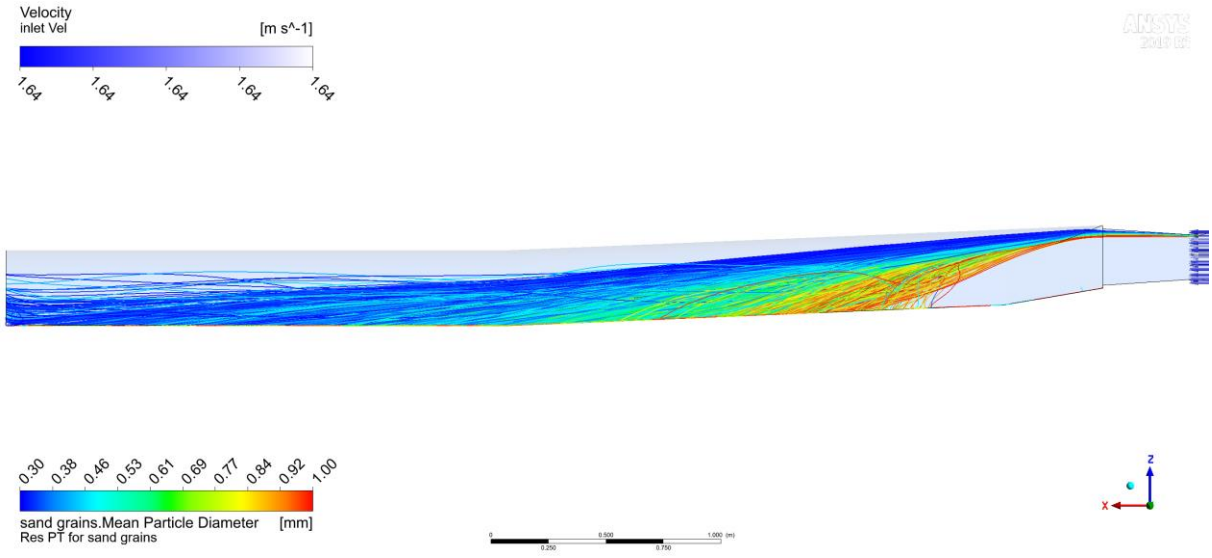

Figure 122: 3D CFD with particle tracking grains 0.3-1.0 mm, scale 1:36.67, 1.64 m/s inlet velocity, undisturbed inflow, side view

11.3 **Scale 1:36.67 particle tracking simulation, Sim_24**

Figure 123 shows the particle tracks for 0.3 mm to 1.0 mm grains in 1:36.67 scale sand trap chamber at 1.64 m/s inflow velocity as above but with fully coupled sediment tracking simulations. The costlier simulation shows more complex particle tracking patterns, but also confirms the scaling approach.

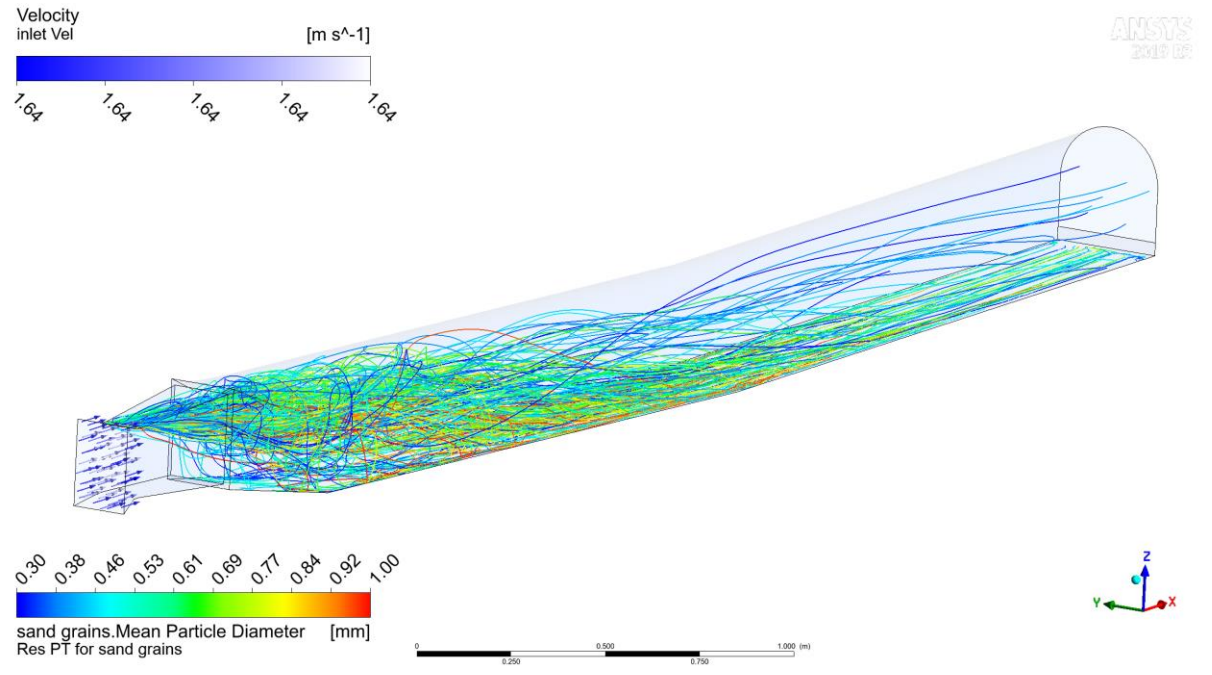

Figure 123: 3D CFD with particle tracking grains 0.3-1.0 mm, scale 1:36.67, 1.64 m/s inlet velocity, perspective view, fully coupled

11.4 **Scale 1:36.67 with approach flow – prototype discharge _Sim25**

This simulation of the 1:36.67 scaled geometry of the surge tank was done by imposing the prototype velocity representing 80 m³/s in the prototype and 0.0586 m³/s in the model scale. The simulation is transient with constant inflow discharge. The conclusion is, that similar wall shear values in the sand trap are calculated as for 1:1 scale simulation. Also, the wall shear peak pattern is moving along the bottom, meaning to accelerate the movement of sediments until the rake structure. The higher wall shear values in the approach tunnel may indicate that sediments are moved directly from the main tunnel to the sand trap. Since sand trap no. 3 is the first in flow direction of the headrace tunnel, this seems to be the reason why most sediments are found in the Sand trap no. 3 as a sediment trap prior to the main chamber.

Figure 124 to Figure 126 show the results of the transient simulation and the bottom shear stress development in particular.

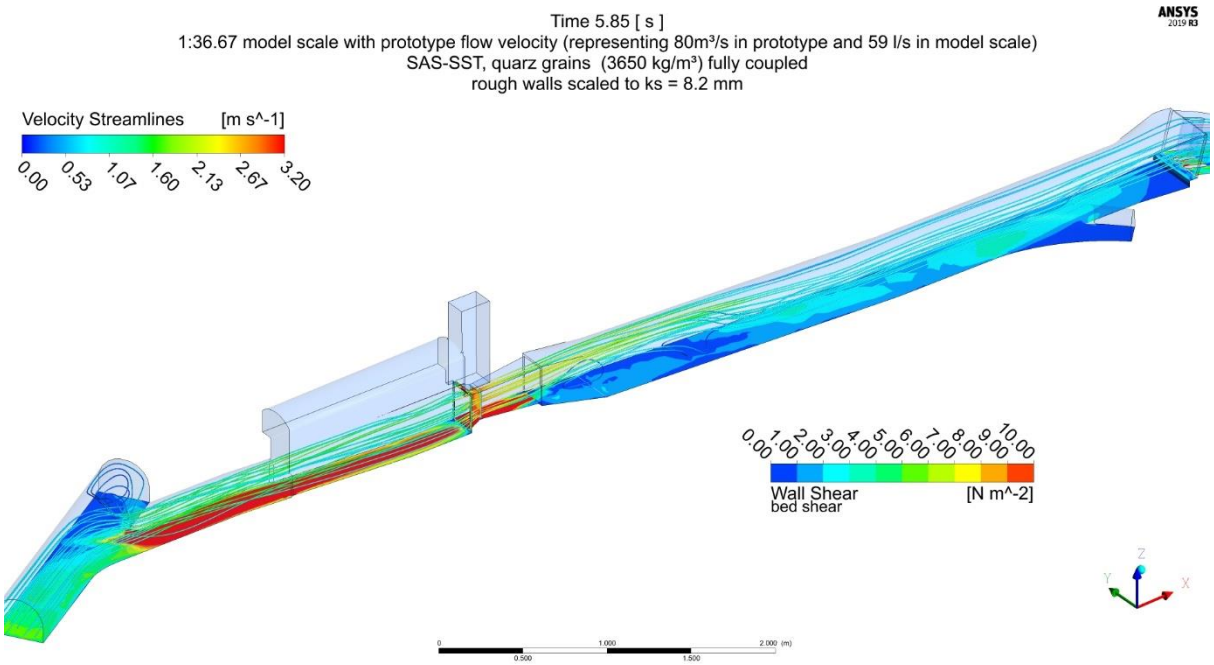

Figure 124: 3D CFD scale 1:36.67, prototype velocity, 3D view, bottom wall shear, time 5.85 s

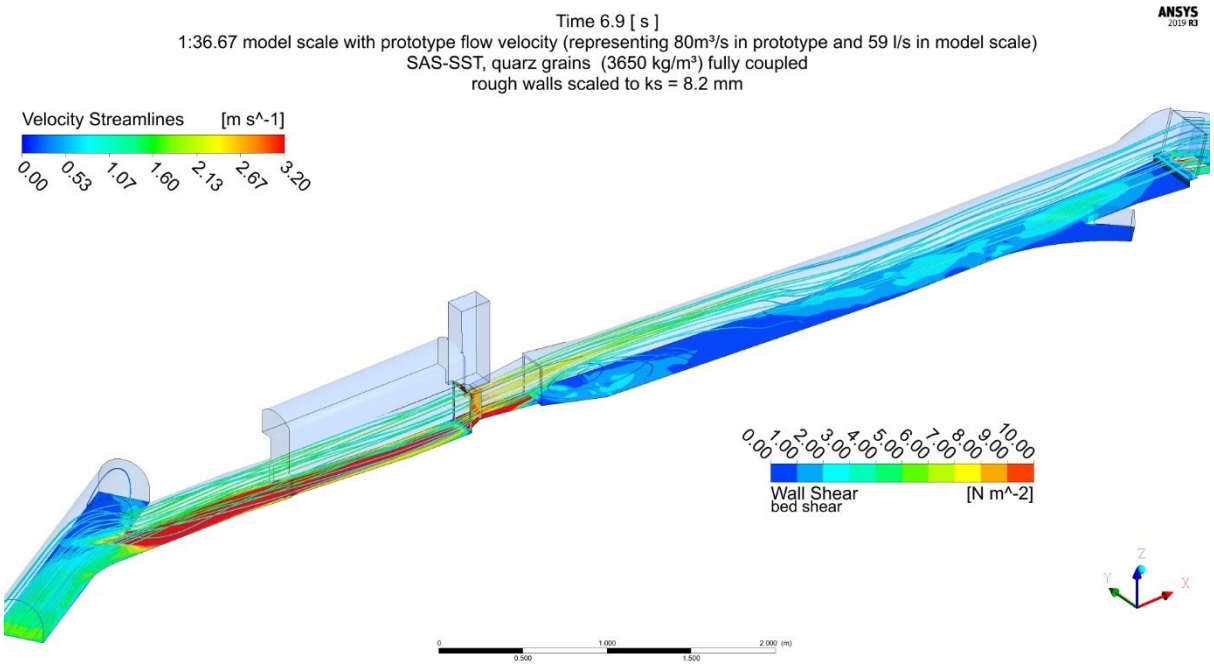

Figure 125: 3D CFD scale 1:36.67, prototype velocity, 3D view, bottom wall shear, time 6.9 s

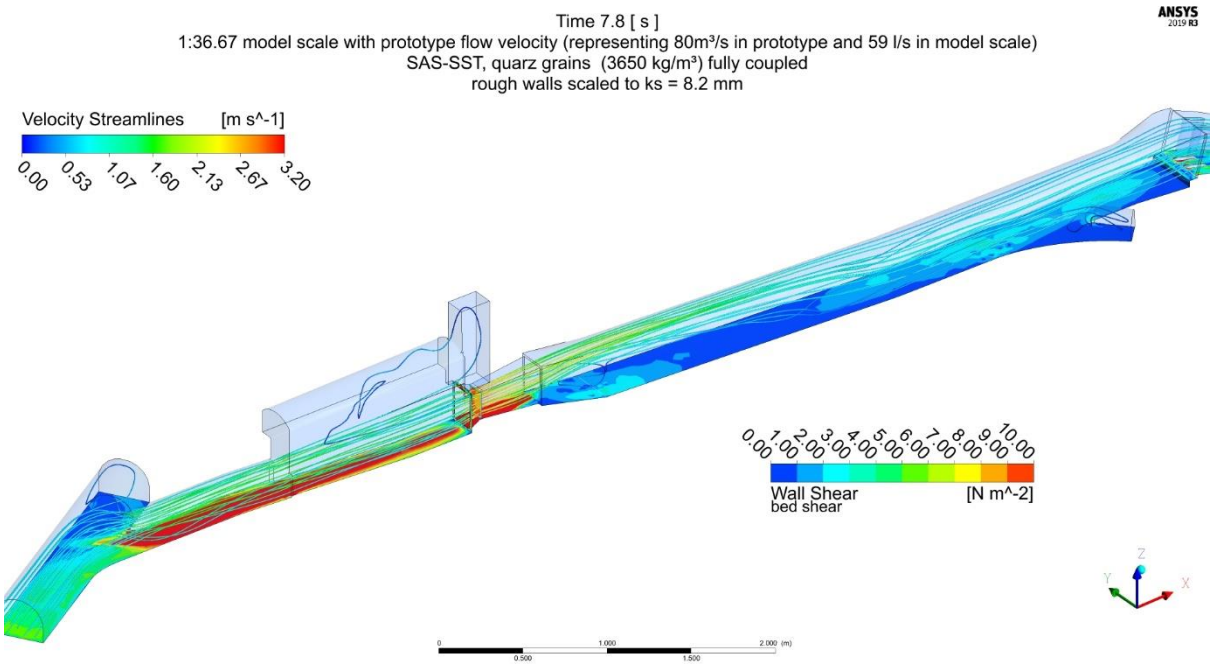

Figure 126: 3D CFD scale 1:36.67, prototype velocity, 3D view, bottom wall shear, time 7.8 s

Figure 127 shows additionally to the particle tracks the velocity isosurface of 1.0 m/s in the chamber, generating a predominant jet into the chamber.

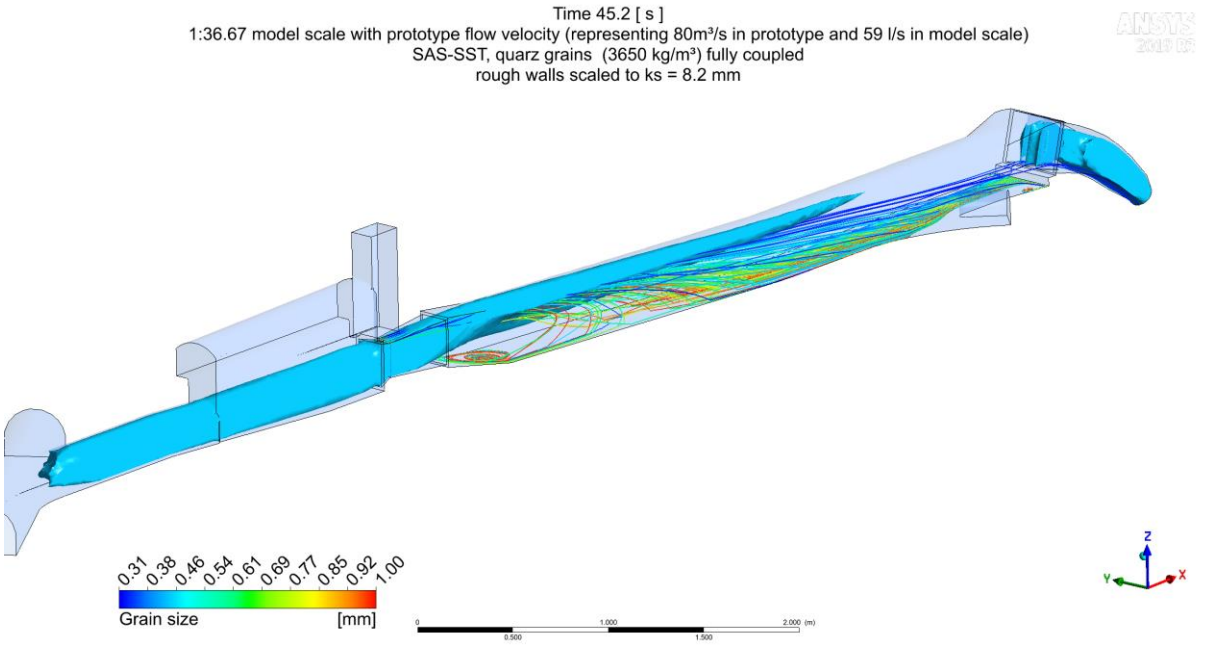

Figure 127: 3D CFD scale 1:36.67, prototype velocity, 3D view, isosurface velocity 1.0 m/s, particle tracking 0.3 mm – 1.0 mm

11.5 **Scale 1:36.67 with particle tracking, plexiglass roughness**

Table 16: Boundary conditions for particle flow simulations

Scale	1:36.67	Geometry	Tonstad plans
Particles Diameter	0.25-1.0 mm	Particle injection	Above gate
		Wall roughness	Plexiglass ks=0.1mm
Time (1:20 resp. 1:1)	80s resp. 300 s	Software	CFX
Timestep	0.05 -0.1	Inlet	Profile from approach flow
Particles Density	2650 kg/m³	Outlet	Pressure
Particle roughness	None	Particles	One-way coupled
Particle Drag	Schiller-Naumann		
Turbulence Modelling	SAS-SST		

Figure 128 shows the flow pattern for this simulation. A long prolonging jet with 1m/s near the bottom is visible. The results of the particle tracking indicate that this does not influence the particle settling behaviour.

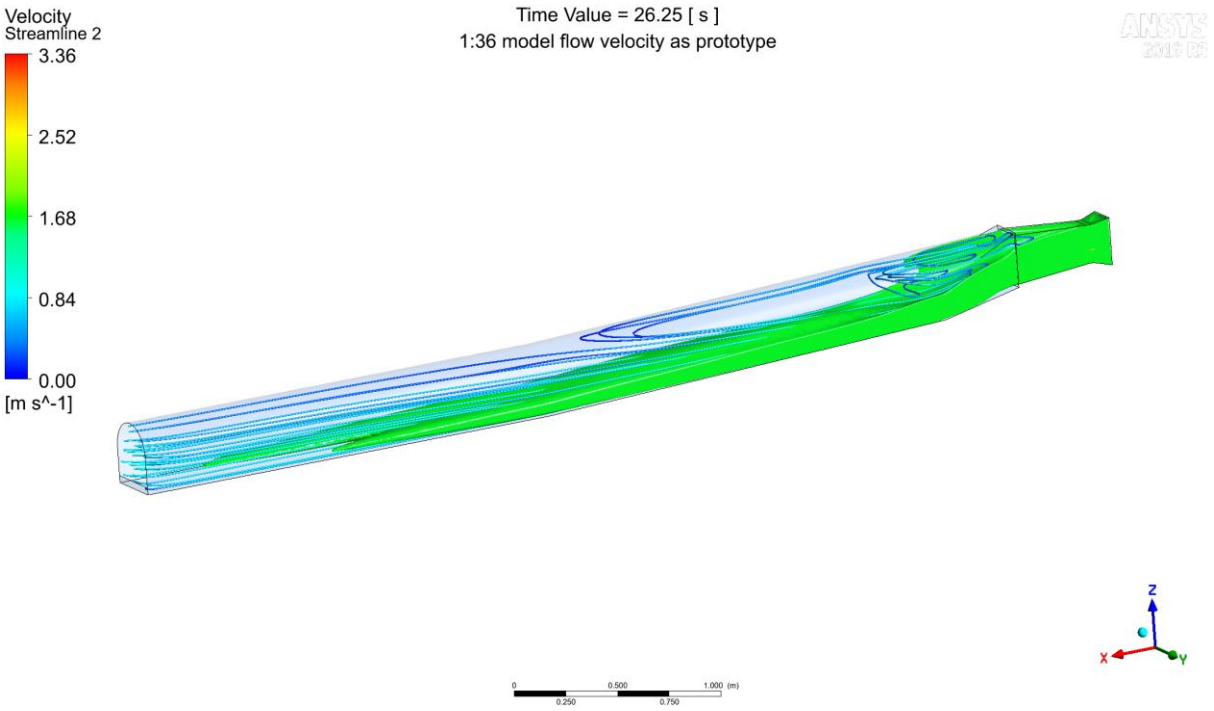

Figure 128: 3D CFD scale 1:36.67, streamlines velocity and 1 m/s velocity isosurface

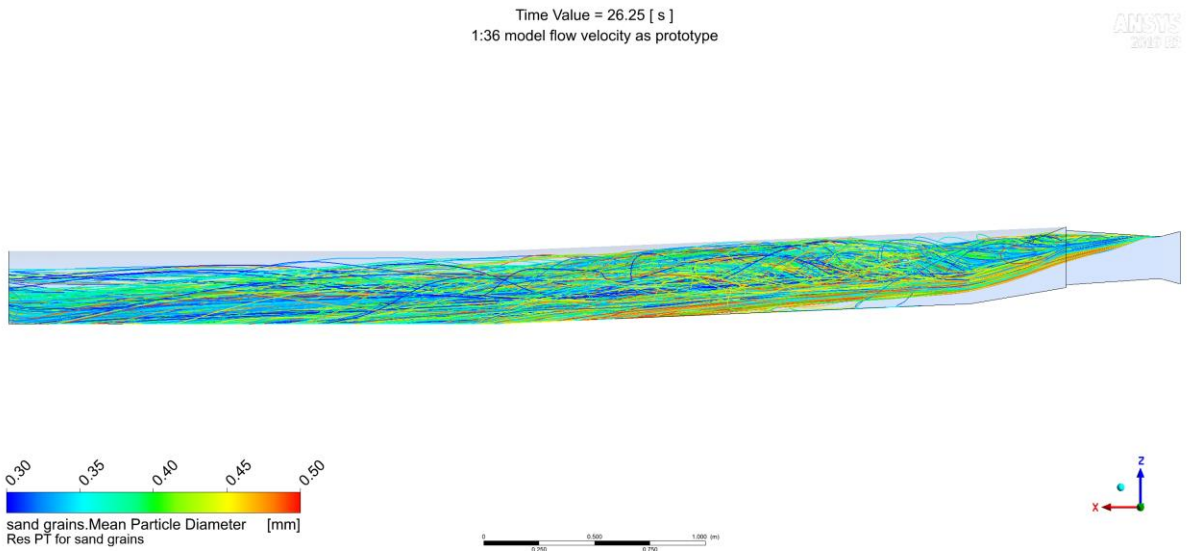

Figure 129: 3D CFD scale 1:36.67, prototype velocity, particles 0.3 - 1.0 mm, side view

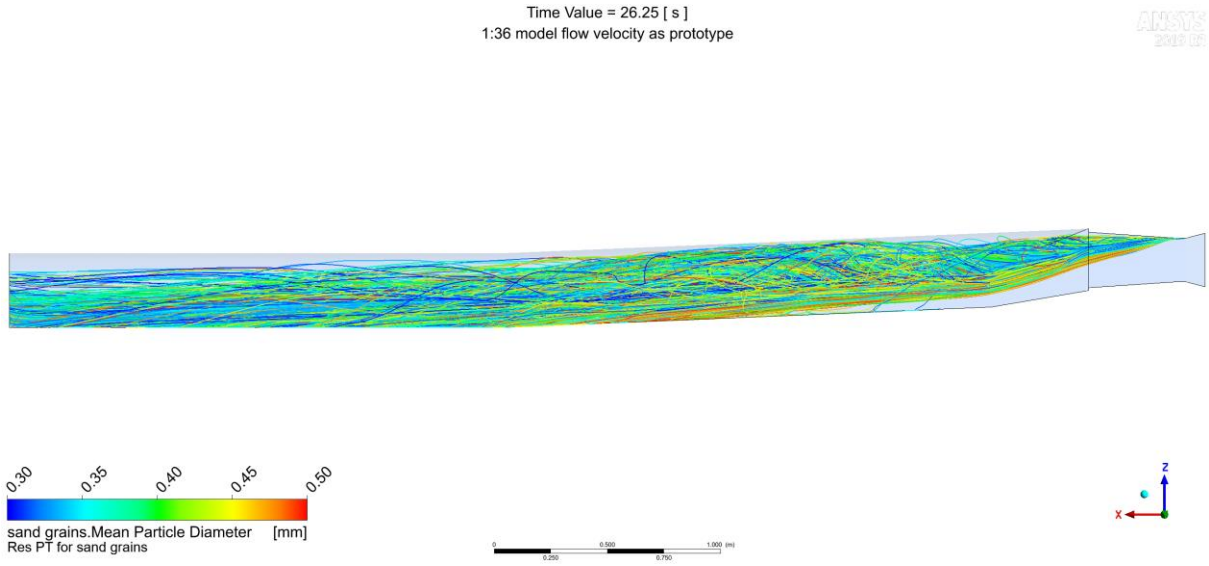

Figure 130: 3D CFD scale 1:36.67, prototype velocity, particles 0.3 - 0.5 mm, side view

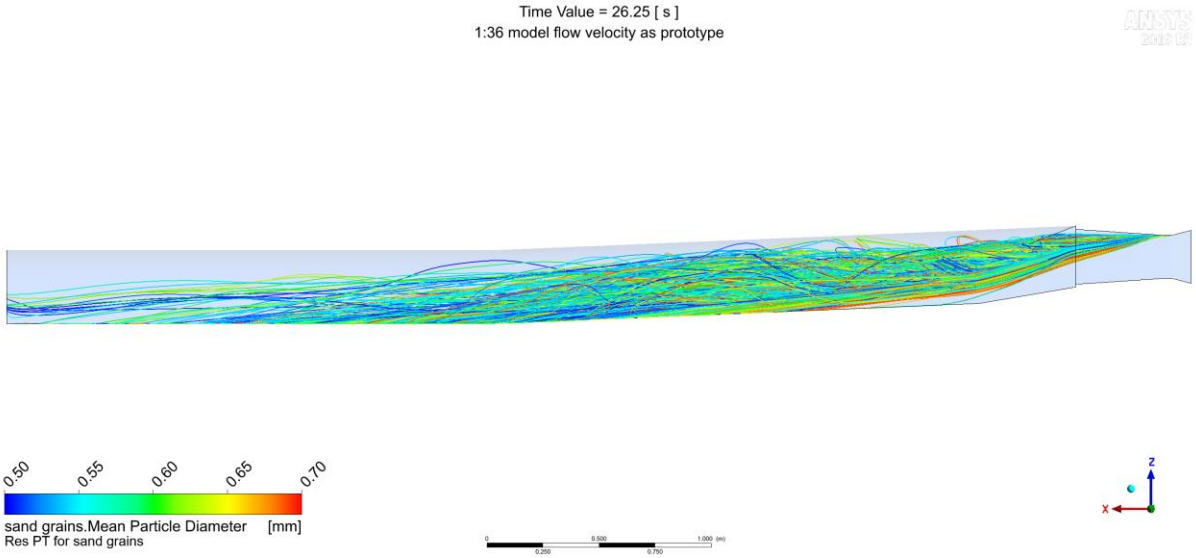

Figure 131: 3D CFD scale 1:36.67, prototype velocity, particles 0.5-0.7 mm, side view

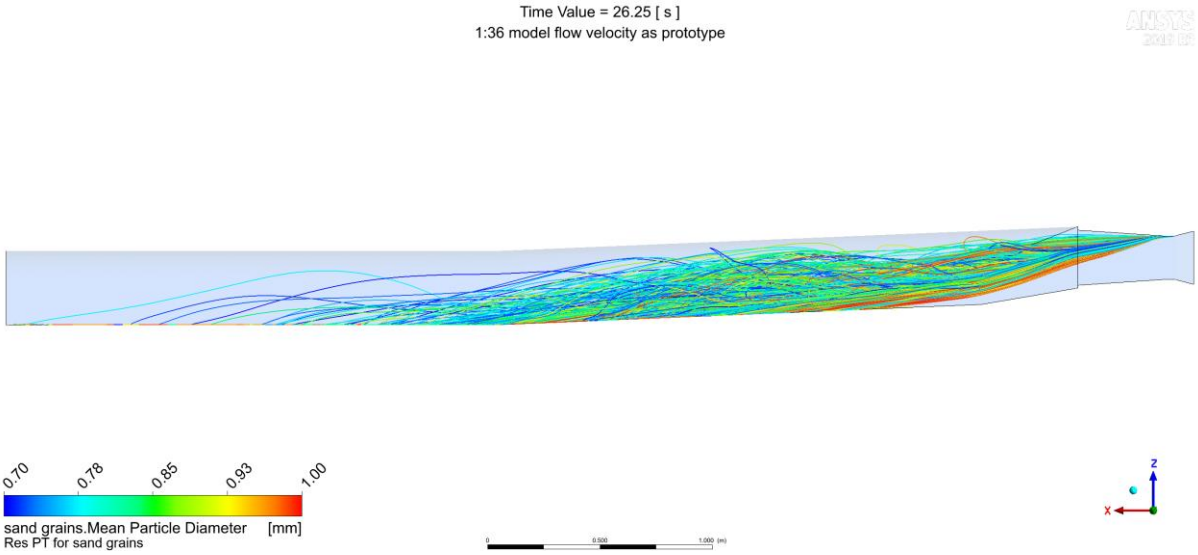

Figure 132: 3D CFD scale 1:36.67, prototype velocity, particles 0.7-1.0 mm, side view

12. Diffusor investigations 3D CFD

This chapter aims to describe the diffusor aspects and geometry adaption proposals.

12.1 Original design - present situation

Figure 133 shows the present flow situation for Q=80 m³/s in the centre-plane of the sand trap. The flow through the concrete diffusor (a) shows a very attached flow situation, while the transition to the unlined part with the rock diffusor (b) significantly shows a disturbed flow situation, what is believed to create the oscillations in the sand trap that is causing the far-distance transportation of the fine sediments.

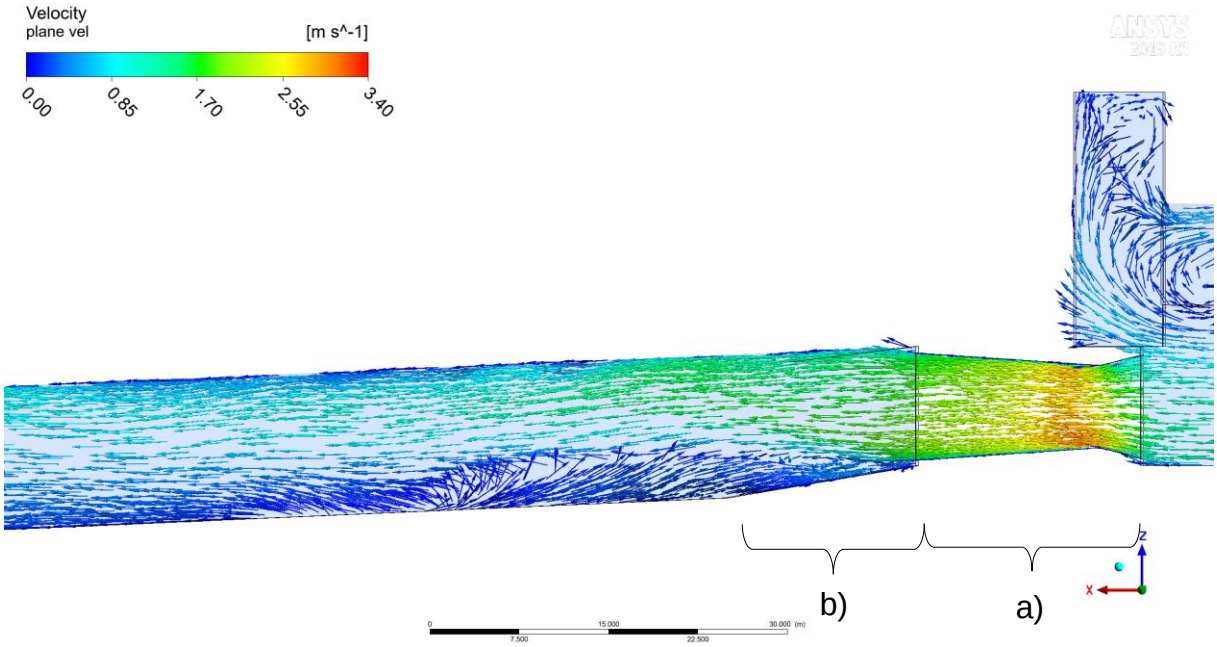

Figure 133: Centre-plane velocity vectors for 80 m³/s in prototype scale, certain time point

Figure 134 shows the influence of disturbance downstream of the diffusor, leading to inefficiency in the settling behaviour of fine sediments. In combination with Figure 133 the vectors indicate also a significant influence of the horizontal widening of the flow section.

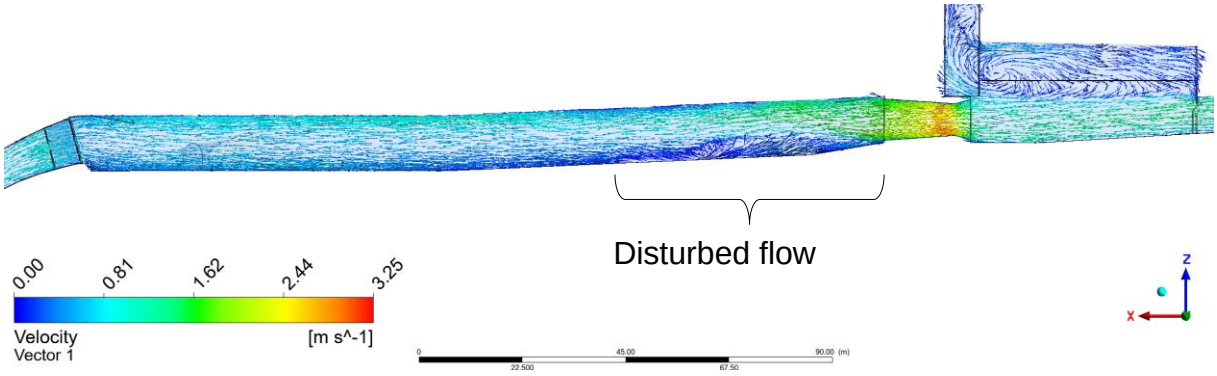

Figure 134: Centre-plane velocity vectors for 80 m³/s in prototype scale, certain time point

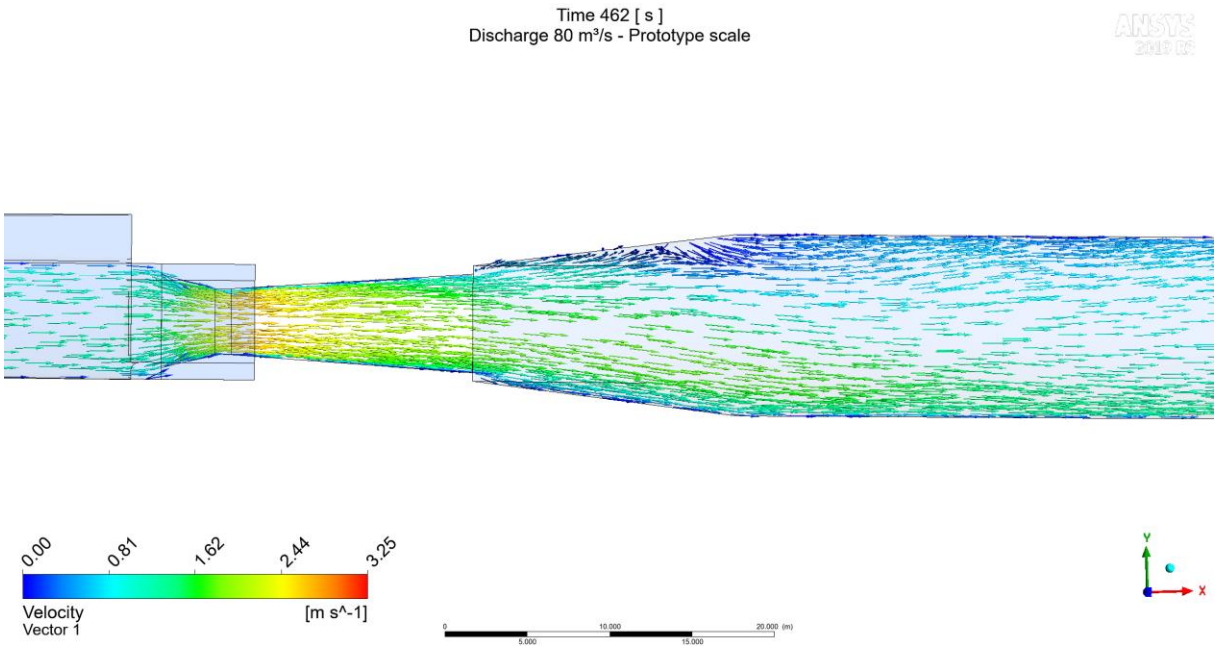

Figure 135: Horizontal centre-plane velocity vectors for 80 m³/s in prototype scale, time point 462 s

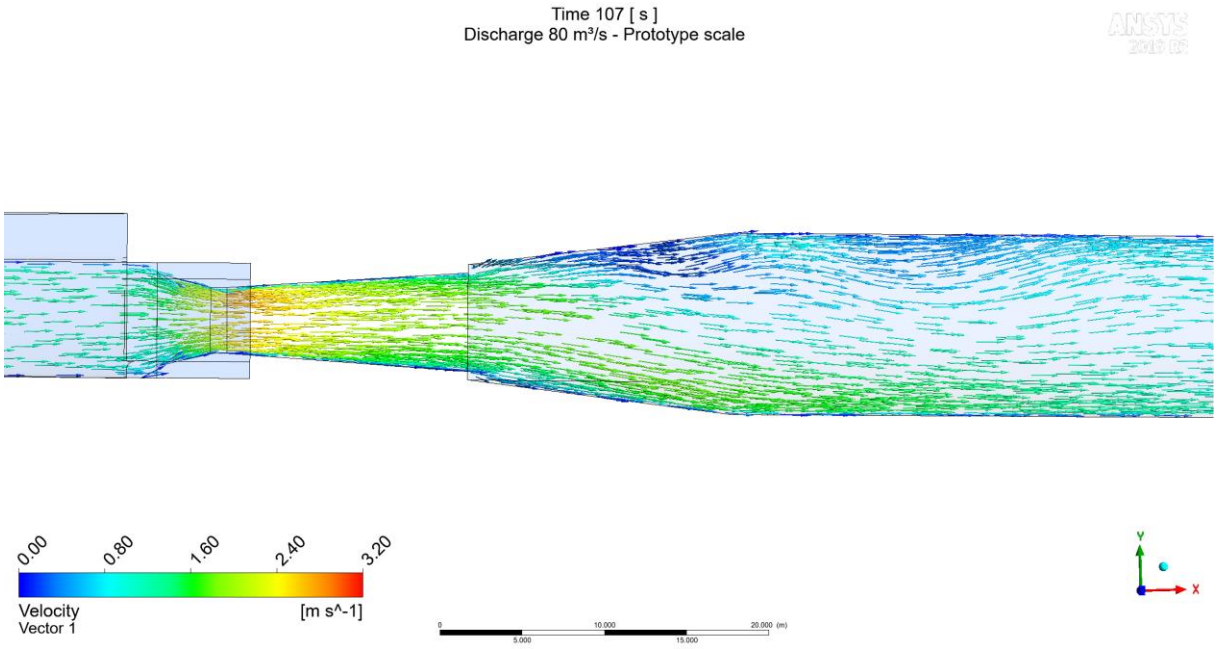

Figure 136: Horizontal centre-plane velocity vectors for 80 m³/s in prototype scale, time point 107 s

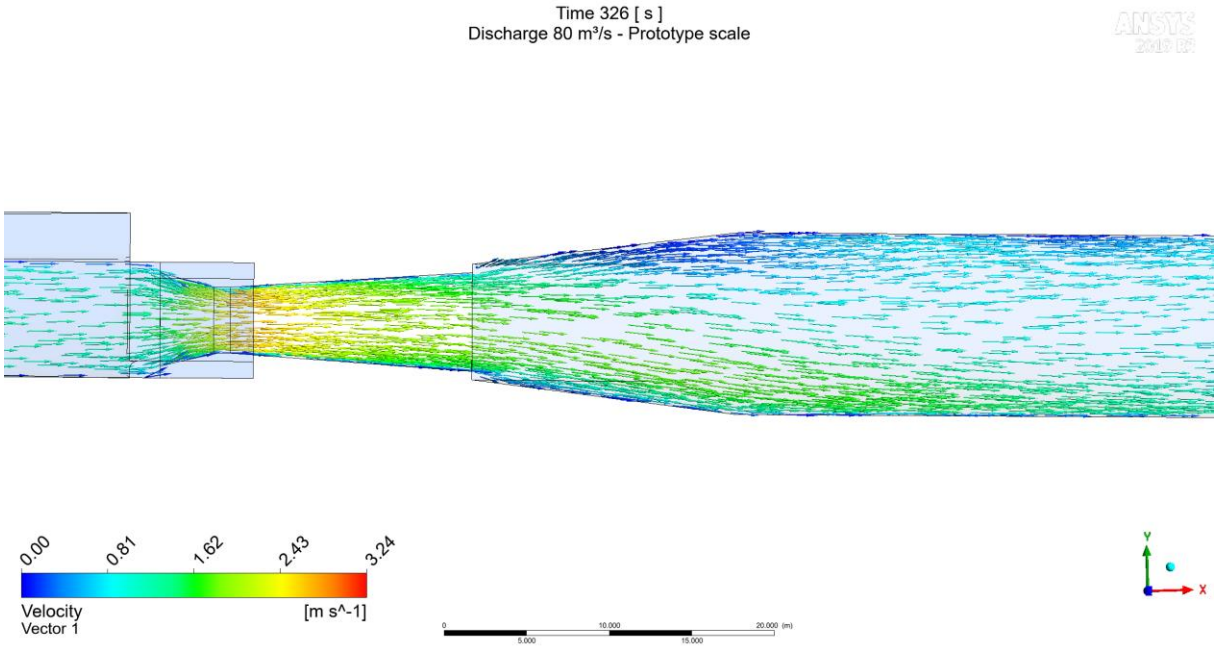

Figure 137: Horizontal centre-plane velocity vectors for 80 m³/s in prototype scale, time point 326 s

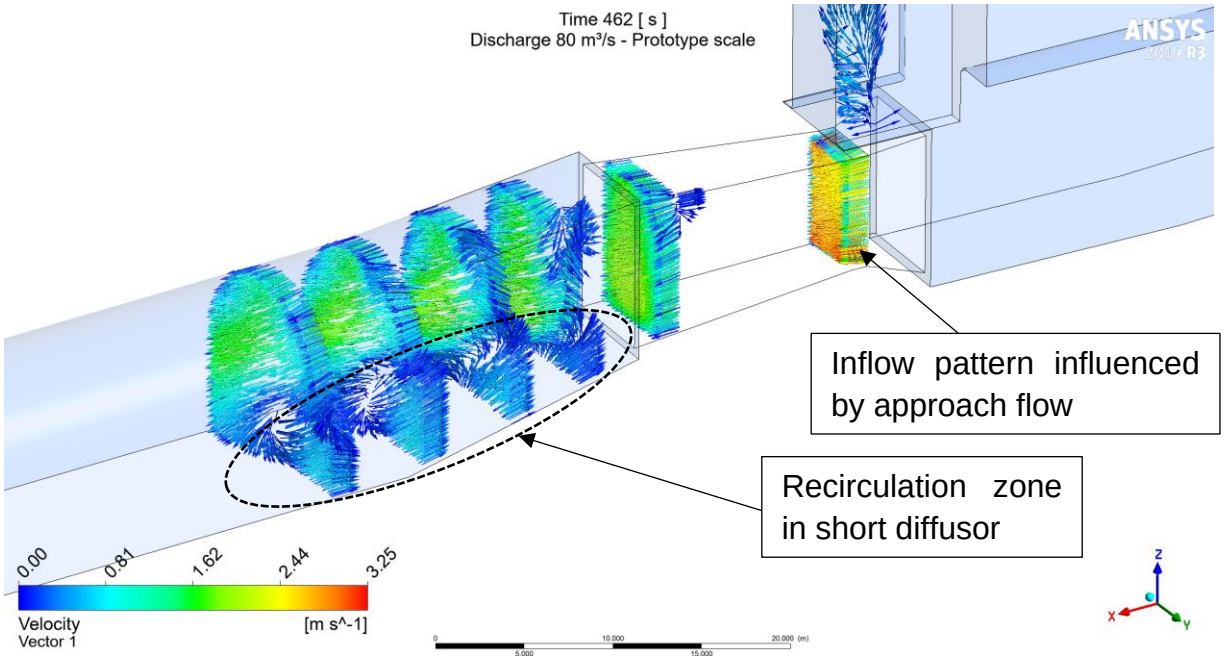

Figure 138: Velocity vectors for 80 m³/s in prototype scale in diffusor section, smooth wall boundary condition, time point 462 s

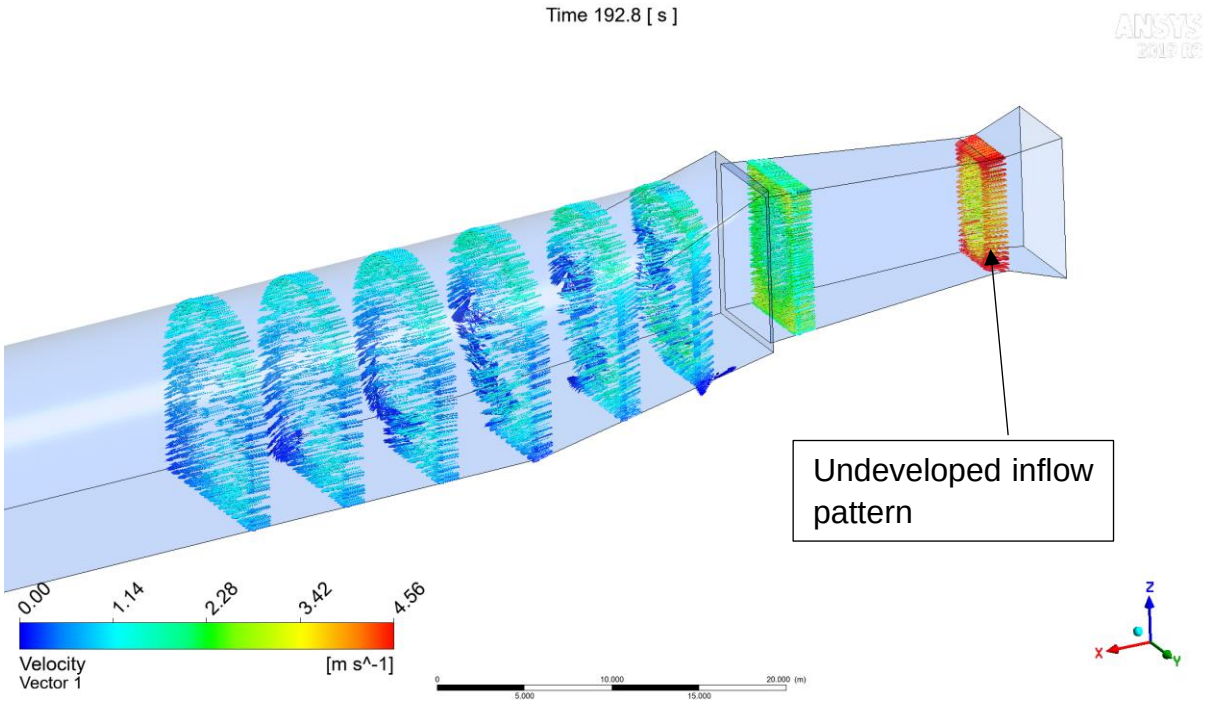

Figure 139: Velocity vectors for 80 m³/s in prototype scale in diffusor section, smooth wall, time point192.8 s, inlet velocity ideally imposed – no approach flow

Figure 140 and Figure 141 show the swirling flow strength indicator. The regions with high swirling flows are also suspected and observed as regions with high sediment lifting activity. In the physical model test the sediment lifting was made visible.

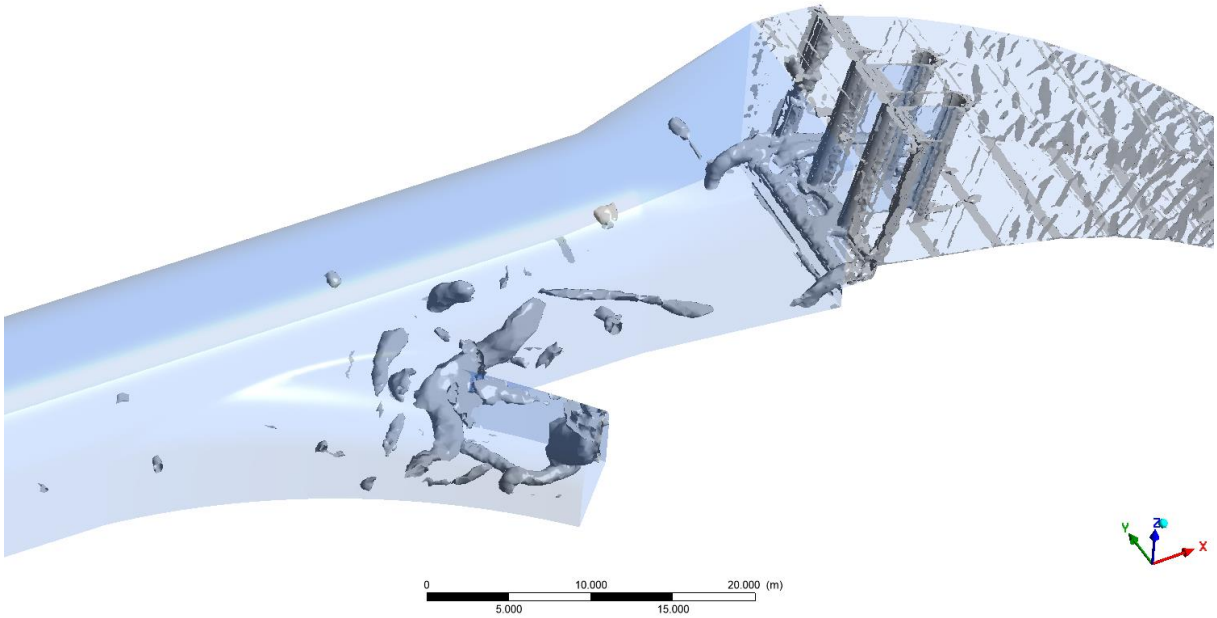

Figure 140: Swirling strength indicator 0.01 [1/s], discharge 80 m³/s, vortex flow at rakes and the access tunnel

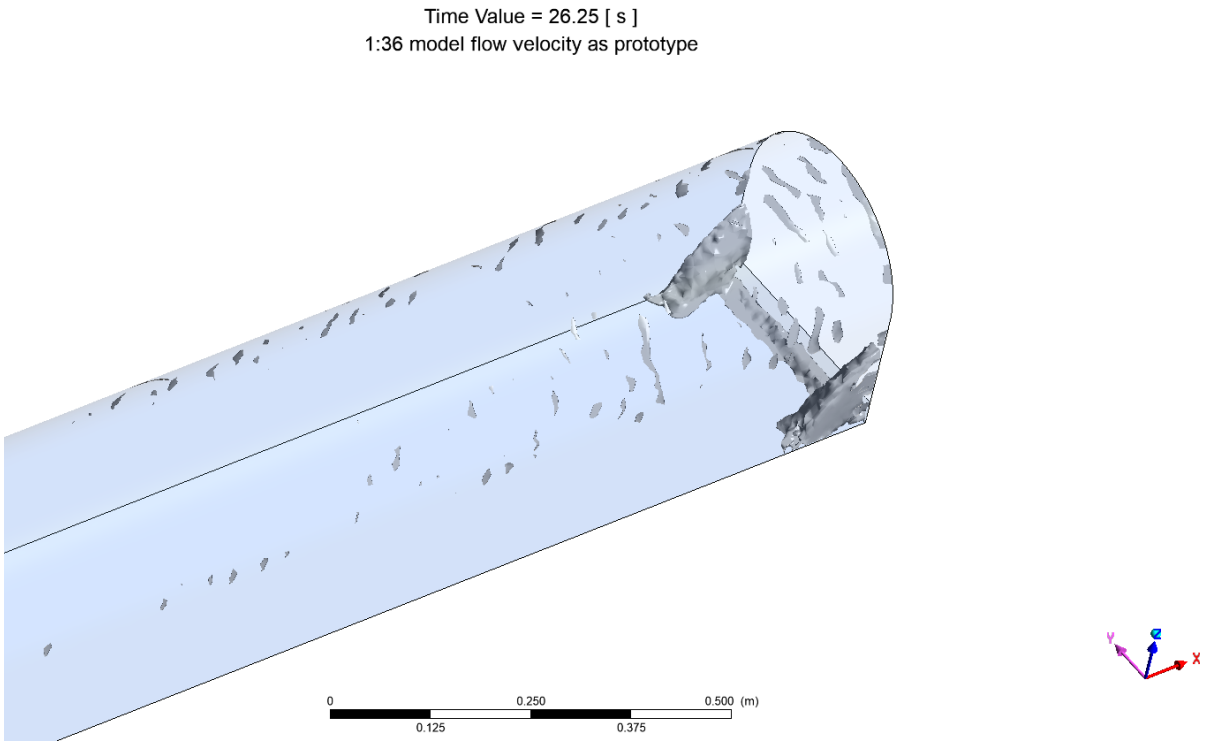

Figure 141: Swirling strength indicator 0.01 [1/s], discharge 0.059 m³/s, velocity equivalent to the prototype, vortex flow at the weir for the 1:36.6 model

12.2 **Wing profile rigid flow calmer**

This chapter shows the approach of placing wing profiles in the diffuser to distribute and improve the flow. The results show that no improvement was observed.

12.2.1 **Without approach flow**

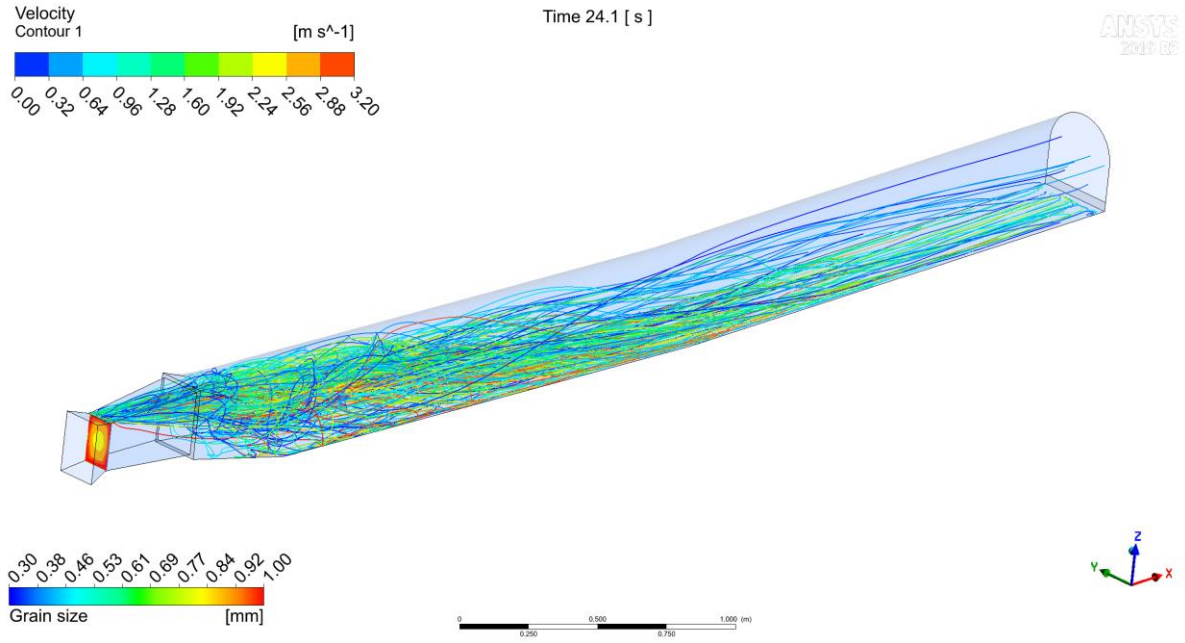

Figure 142: particle tracking without wing profiles, without approach flow, ideal rotational flow, scale 1:36.67

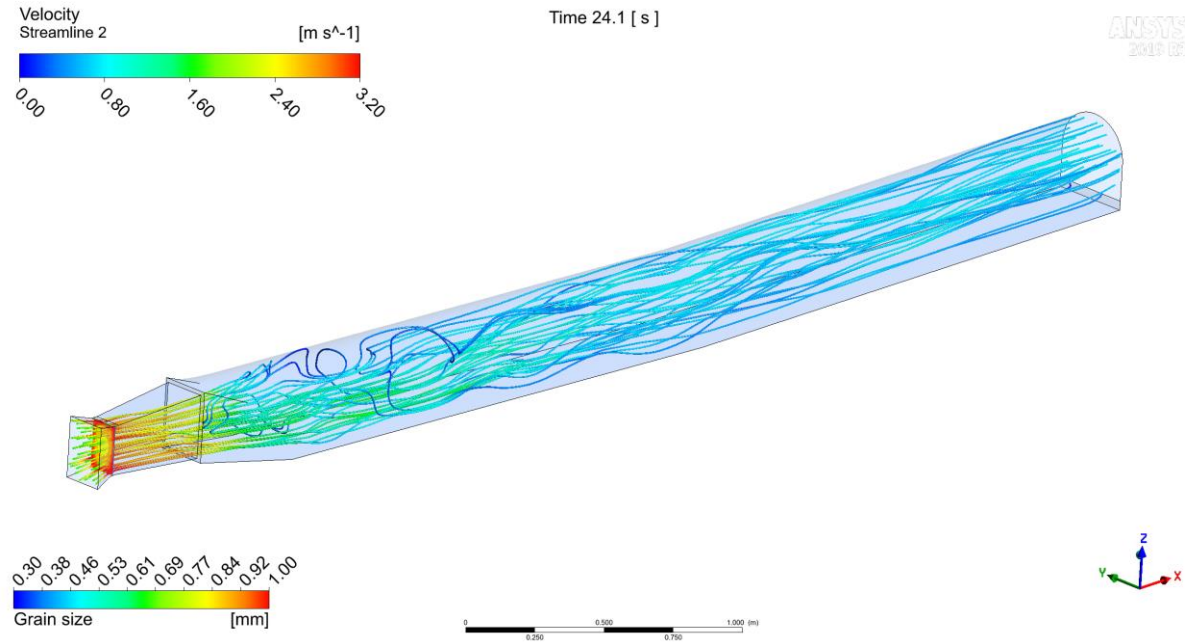

Figure 143: velocity streamlines without wing profiles, without approach flow, ideal rotational flow, scale 1:36.67

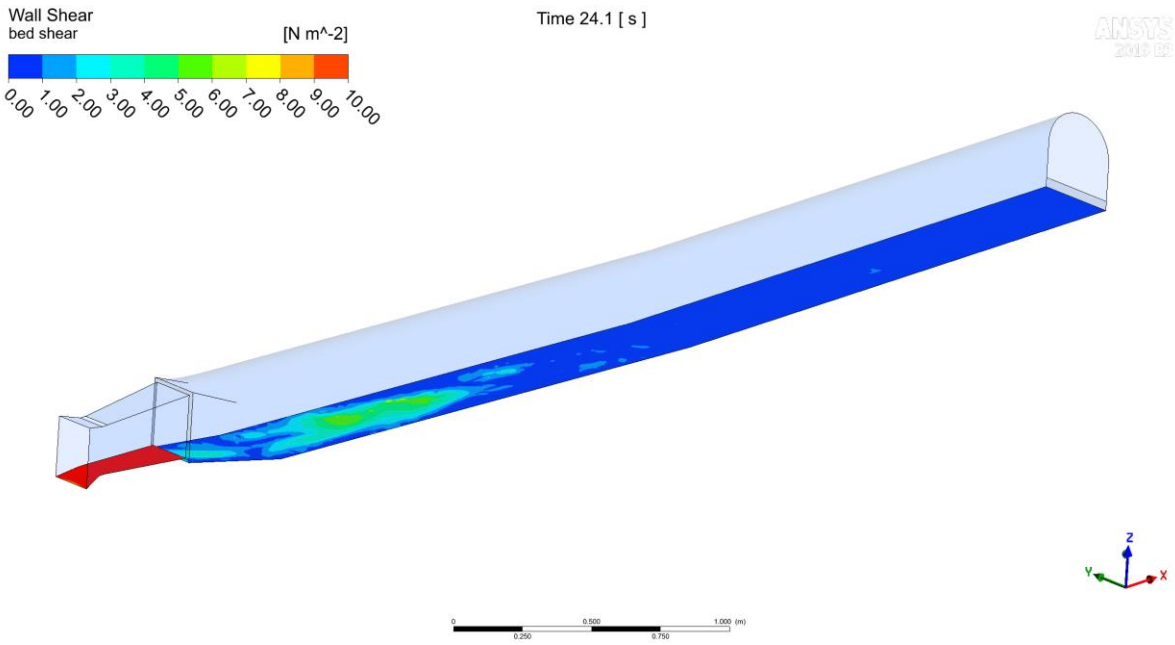

Figure 144: bed shear stress without wing profiles, without approach flow, ideal rotational flow, scale 1:36.67

12.2.2 **With approach flow**

The results below show the effect of the wings profiles with approach flow upstream the surge tank.

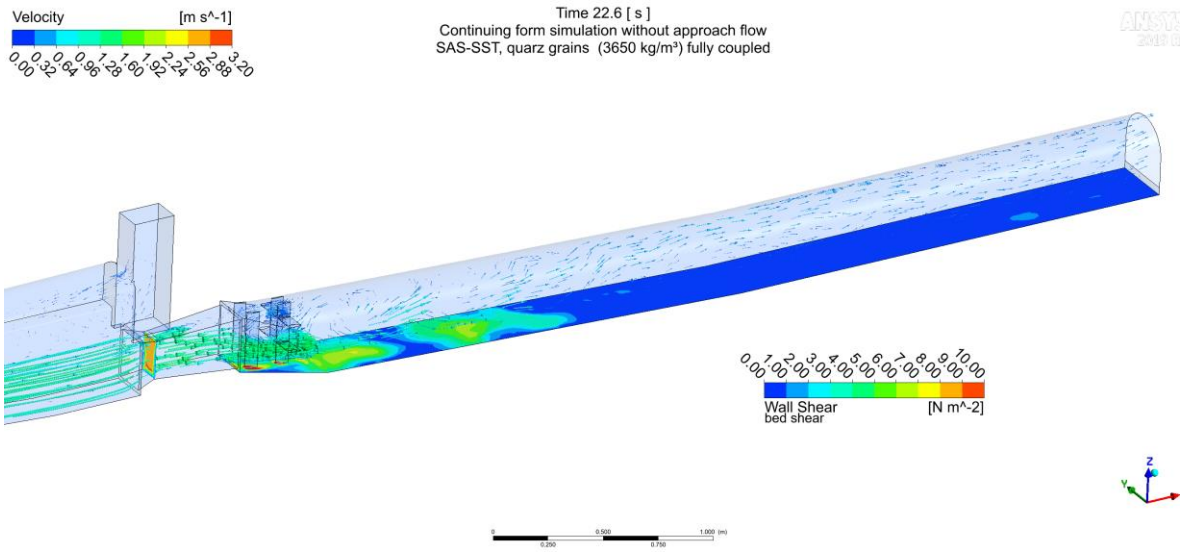

Figure 145: Velocity vectors and bed shear stress with wing profile flow straighteners, improved situation

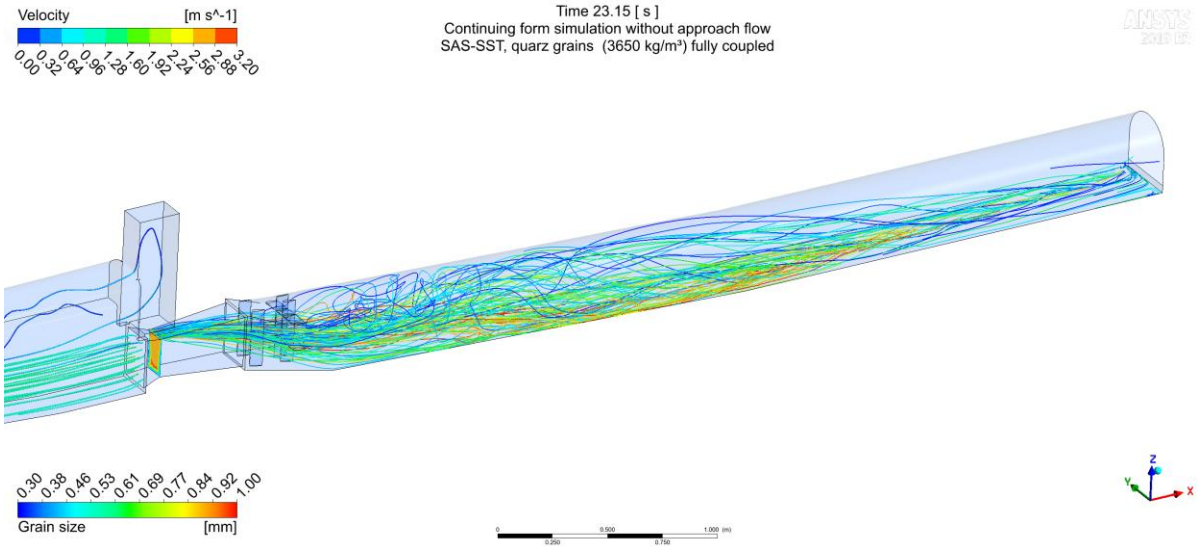

Figure 146: particle tracking with wing profile flow straighteners, improved situation

Figure 147: Velocity in centre plane

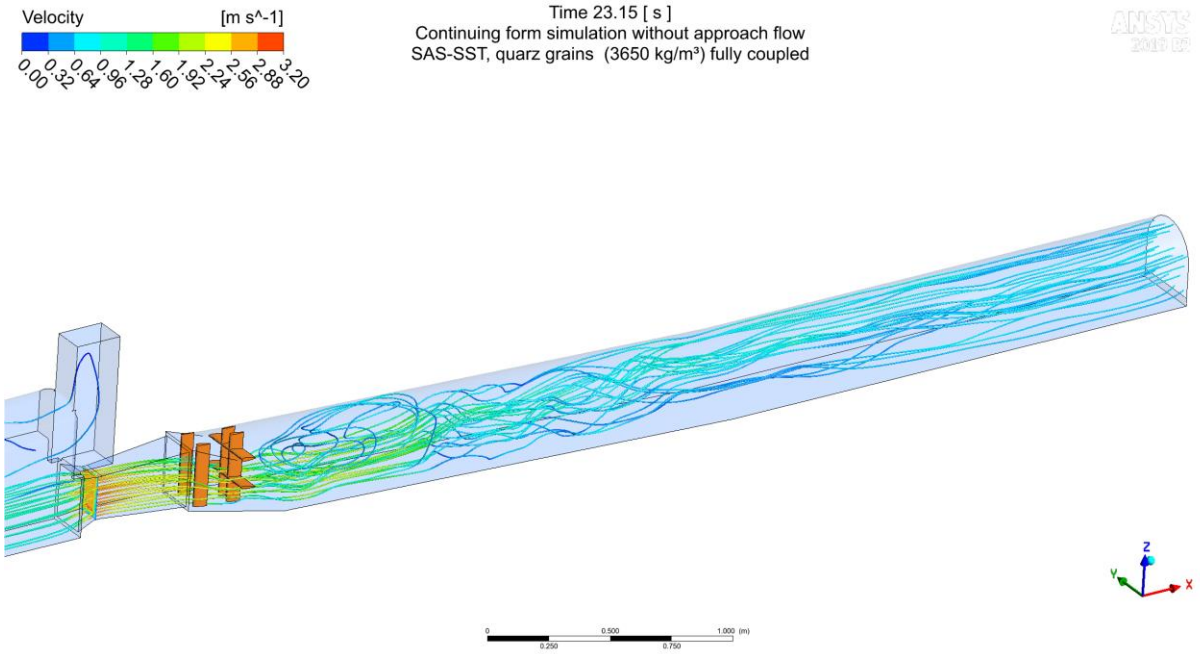

Figure 148: Streamline velocity

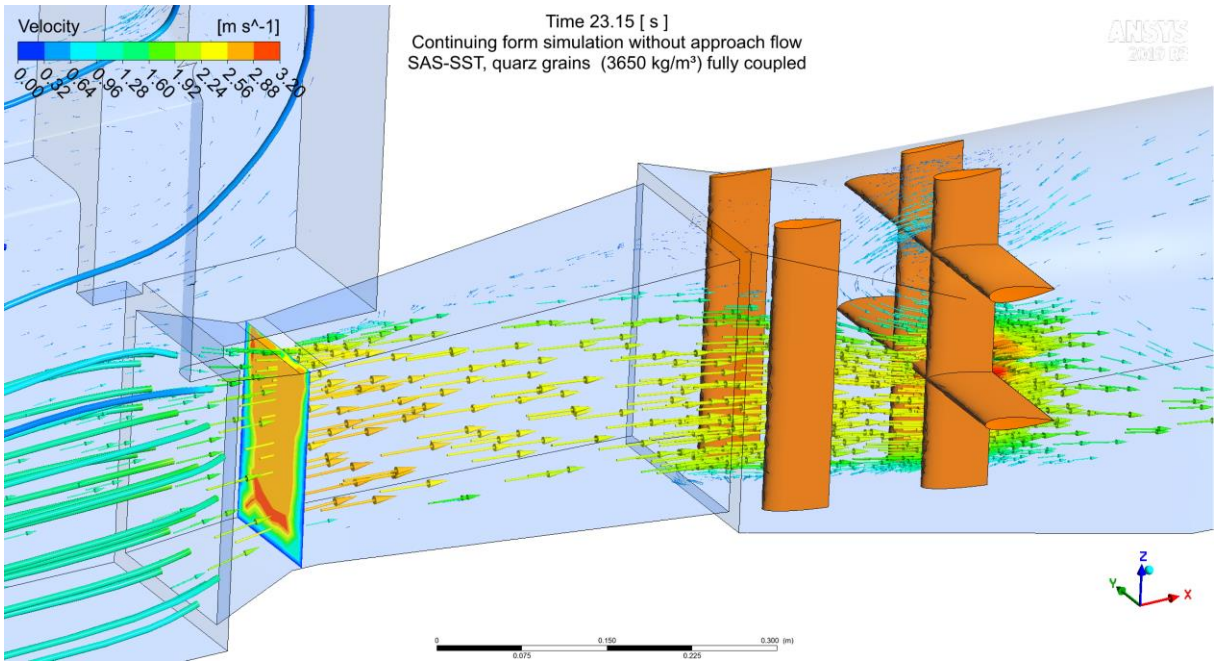

Figure 149: Velocity in vertical centre plane

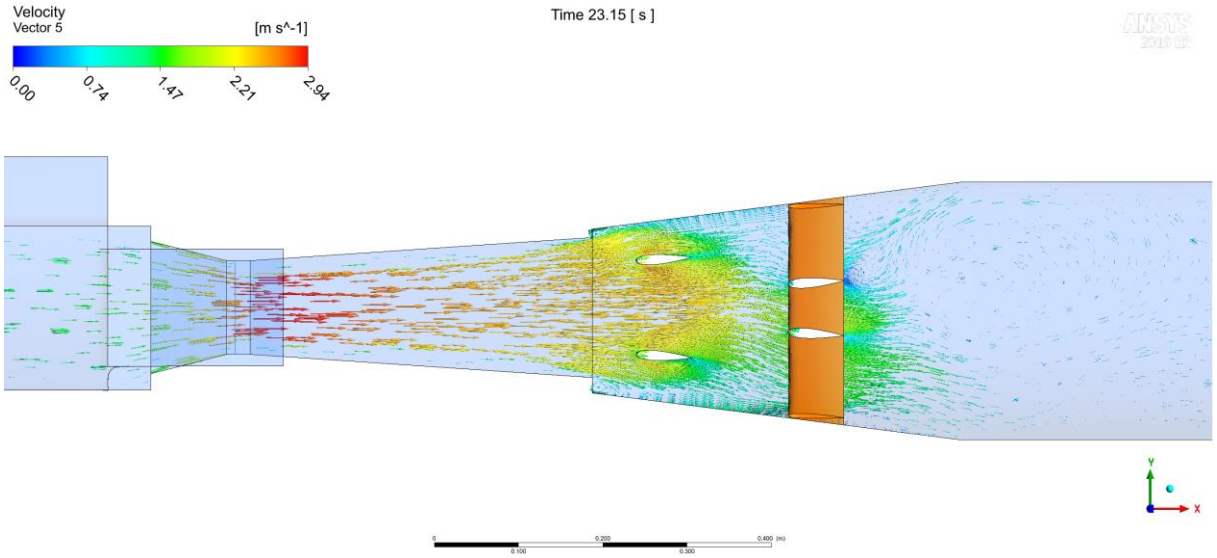

Figure 150: Velocity in horizontal centre plane

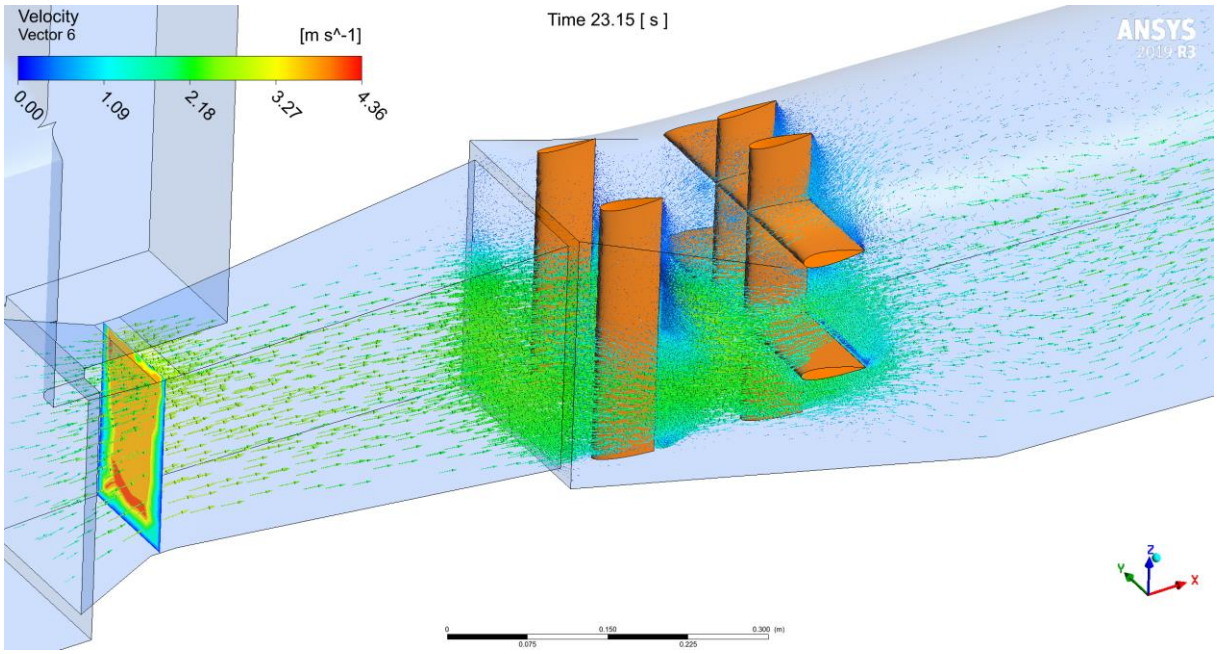

Figure 151: Velocity in horizontal 3d vectors

12.3 Ramp design variants for diffusor improvement

This chapter describes the attempt to improve the jet flow behaviour in the sand trap chamber by various ramp designs starting from bottom ramps to combined variants with side walls and calming pillars and calming rakes. The rakes were later also tested in the physical model test.

12.3.1 Ramp design 01 bottom inclination adaption

Figure 152 to Figure 154 show the ramp design for improving the diffusor at the bottom. An inclination of 6° was chosen to connect the ramp with the sand trap bottom.

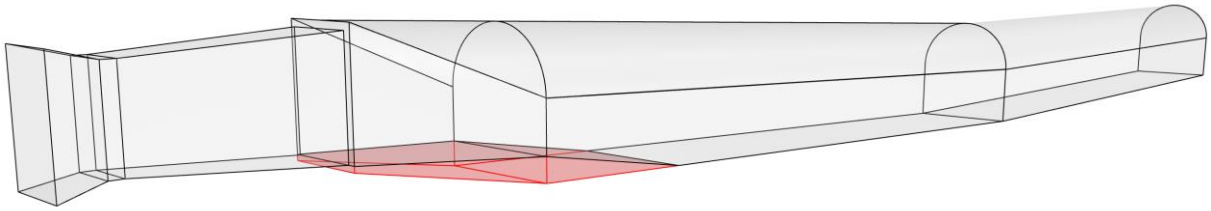

Figure 152: Ramp design approach with continued inclination in the diffusor and 6° angle in the constant sand trap section, 3D view

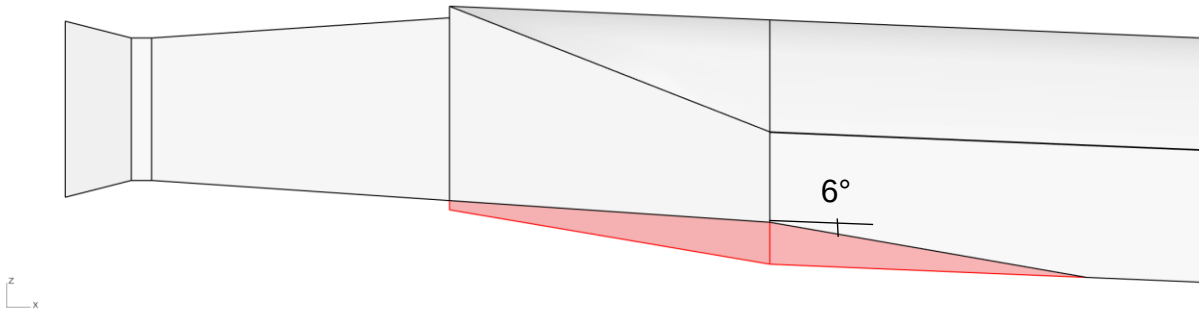

Figure 153: Ramp design approach with continued inclination in the diffusor and 6° angle in the constant sand trap section, side view, detail

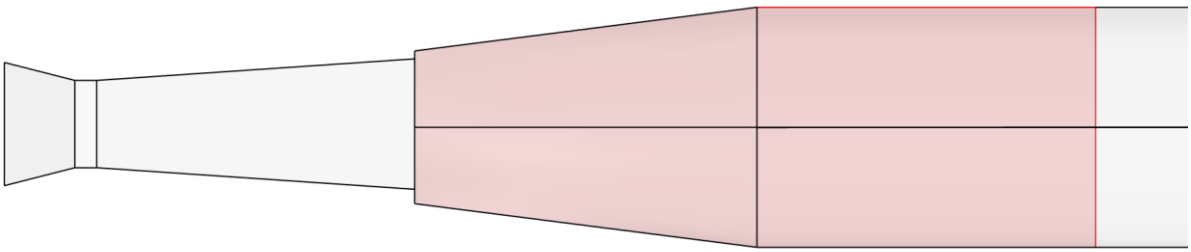

Figure 154: Ramp design approach with continued inclination in the diffusor and 6° angle in the constant sand trap section, plan view, detail

Figure 155 shows the flow vectors in the diffusor section downstream of the gate section including the effects of the upstream approach flow as boundary conditions. The complexity of the flow in the diffusor is visible.

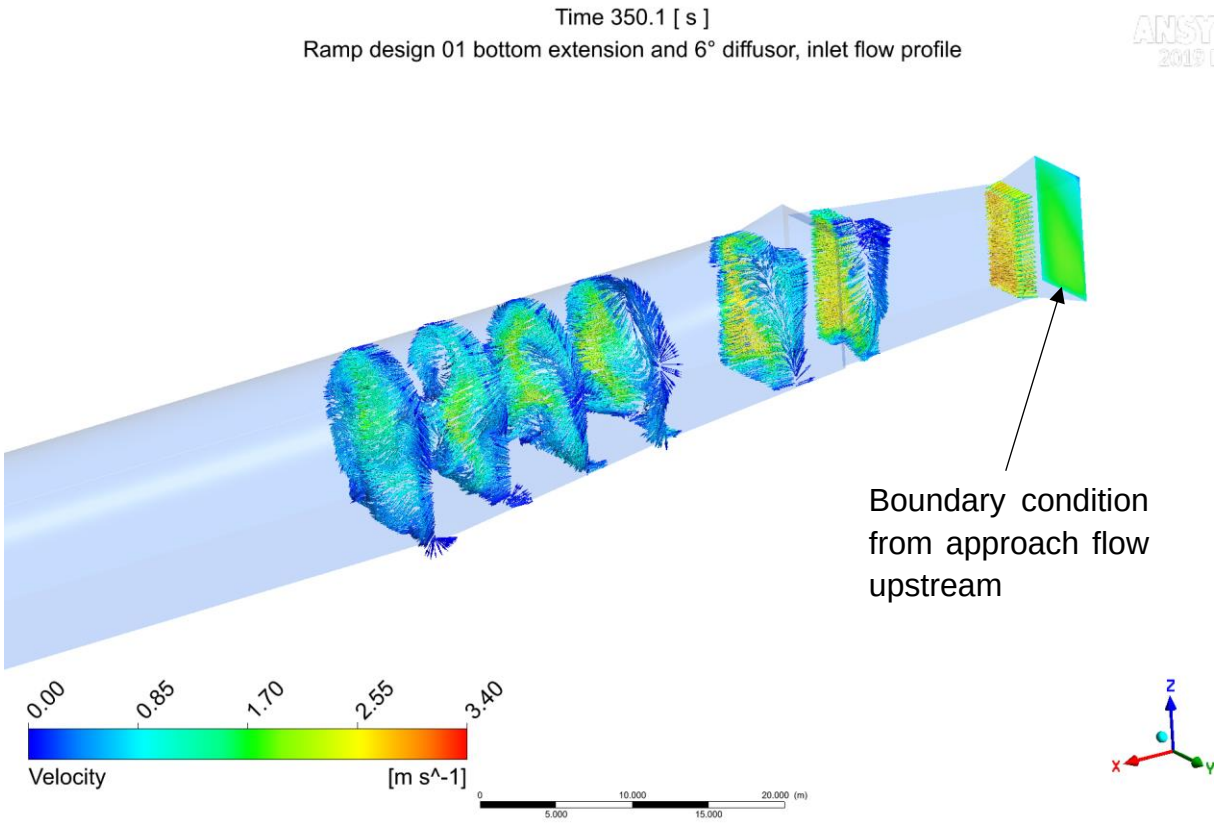

Figure 155: Ramp design 01 – flow pattern, results vectors

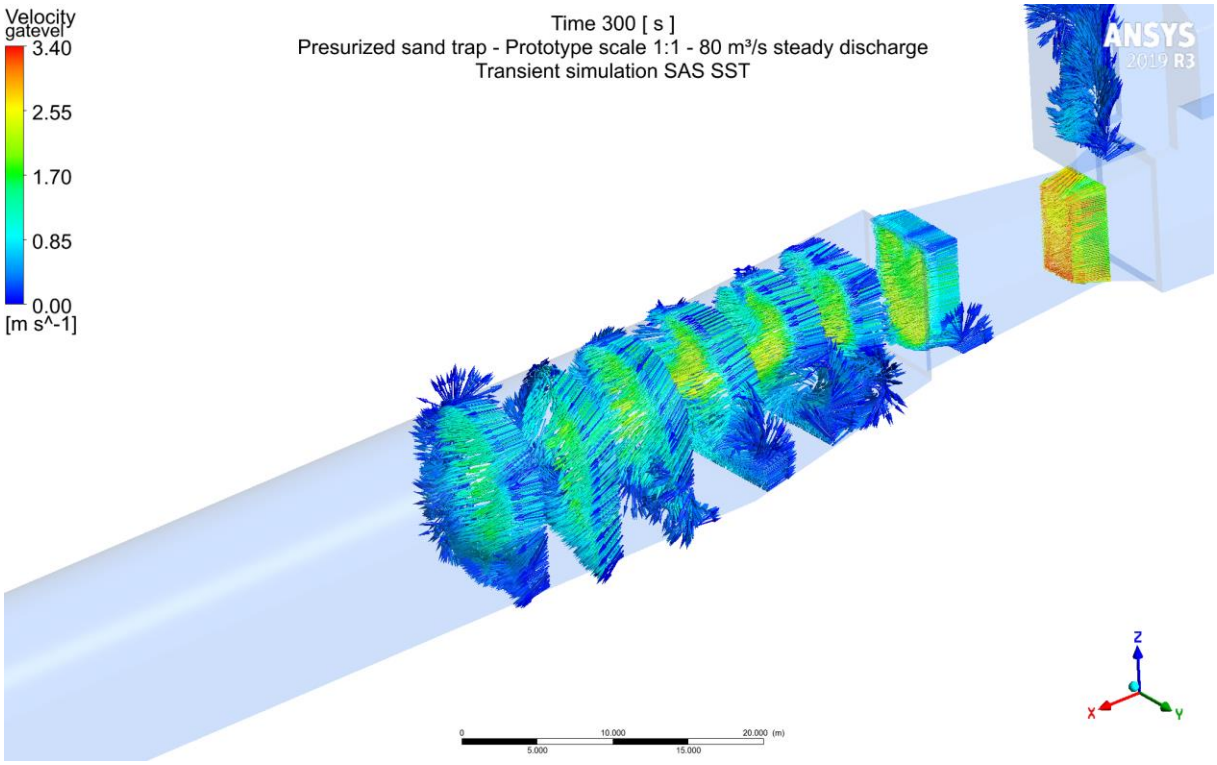

Figure 156: Plan design– flow pattern, results vectors, rough walls ks = 300m unlined rock

At the bottom of the start-up chamber in the surge tank sediment deposits are modelled to create an artificial “bump”. Simulations show, that this has an additional disturbing effect on the flow to the gate and thus on the jet entering the diffusor in the sand trap.

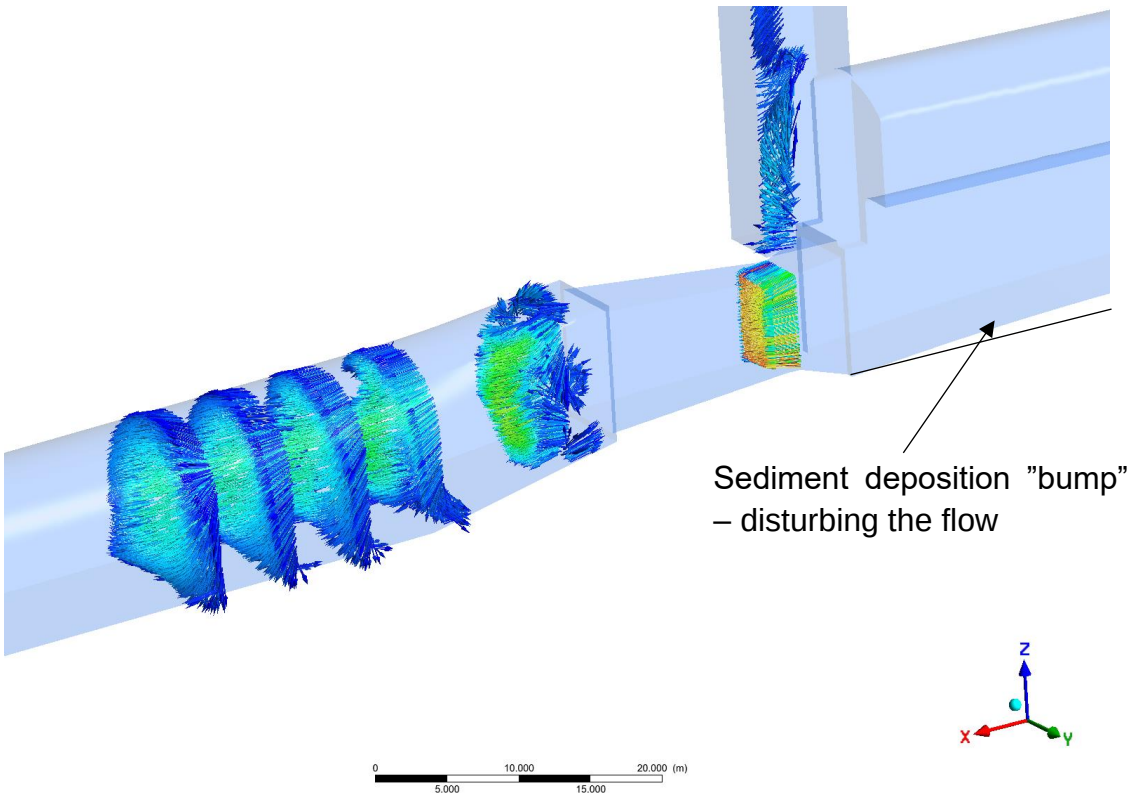

Figure 157: Present design, sediment deposit – flow pattern, results vectors, smooth walls

Figure 158 to Figure 162 show jet visualization via isosurface representation of 1 m/s in the diffusor section and the extend into the sand trap chamber.

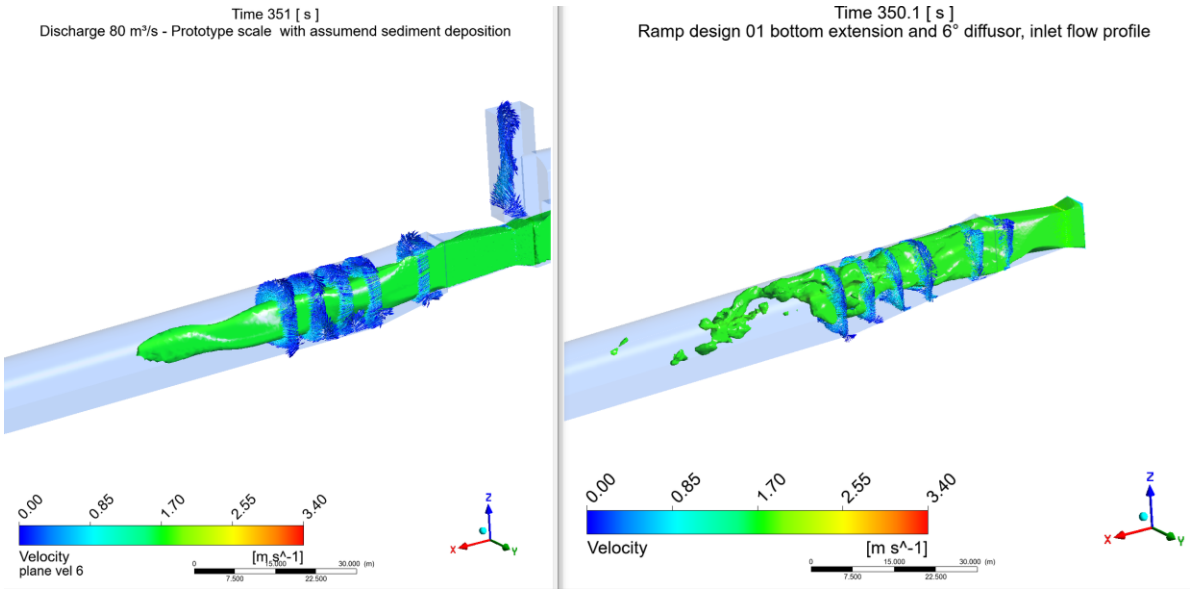

Figure 158: Comparison isosurface1 m/s (green), geometry with sediment deposition (left), ramp 01 design (right)

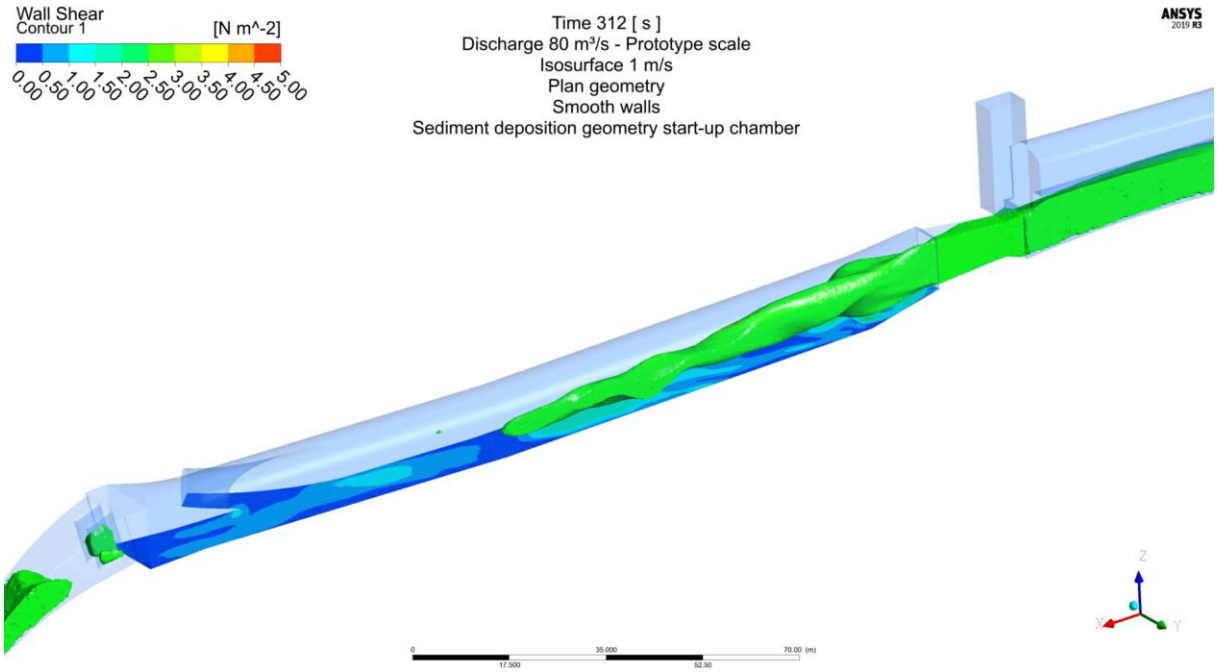

Figure 159: 1:1 scale, plan design smooth walls, 80m³/s time step with far reaching jet, isosurface u-velocity 1 m/s

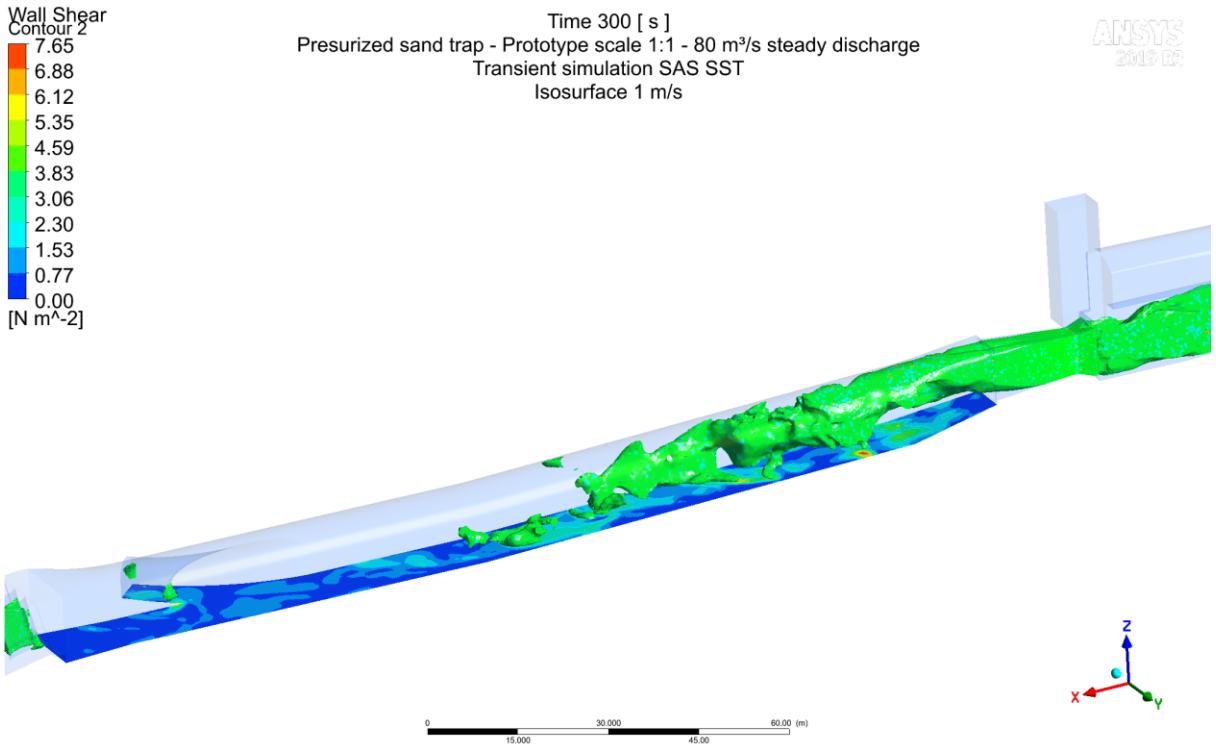

Figure 160: 1:1 scale, plan design rough walls ks=300 mm, 80m³/s time step with far reaching jet, isosurface u-velocity 1 m/s

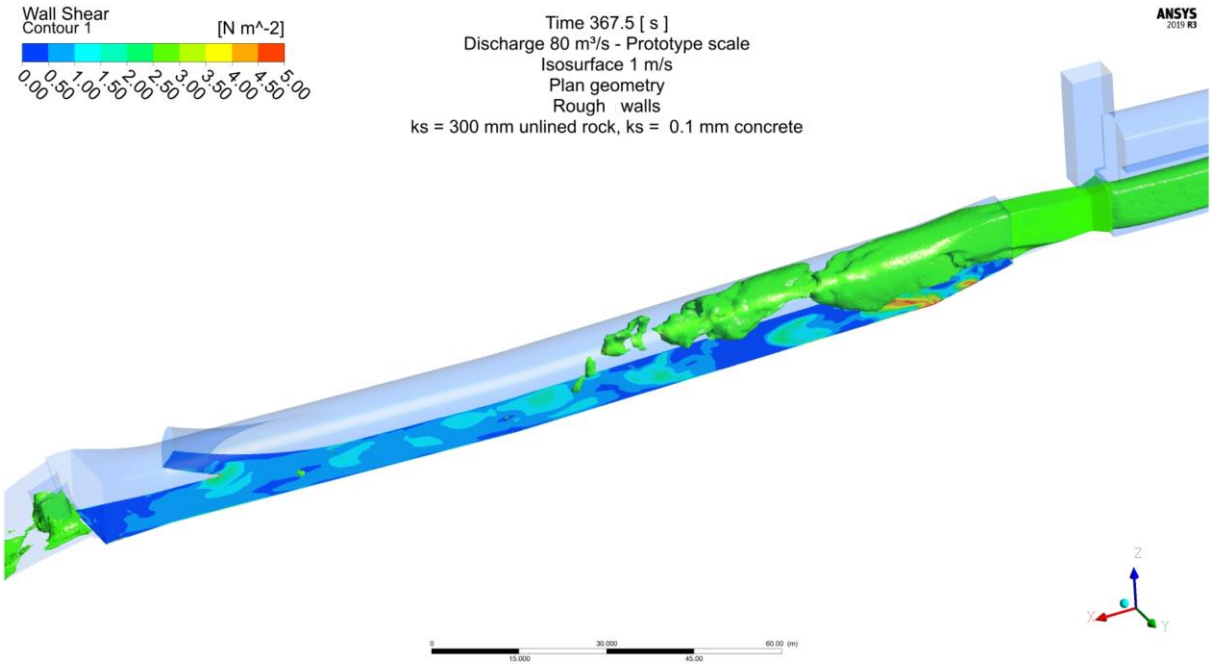

Figure 161: 1:1 scale – prototype geometry, rough walls, 80m³/s time step with far reaching jet, isosurface u-velocity 1 m/s

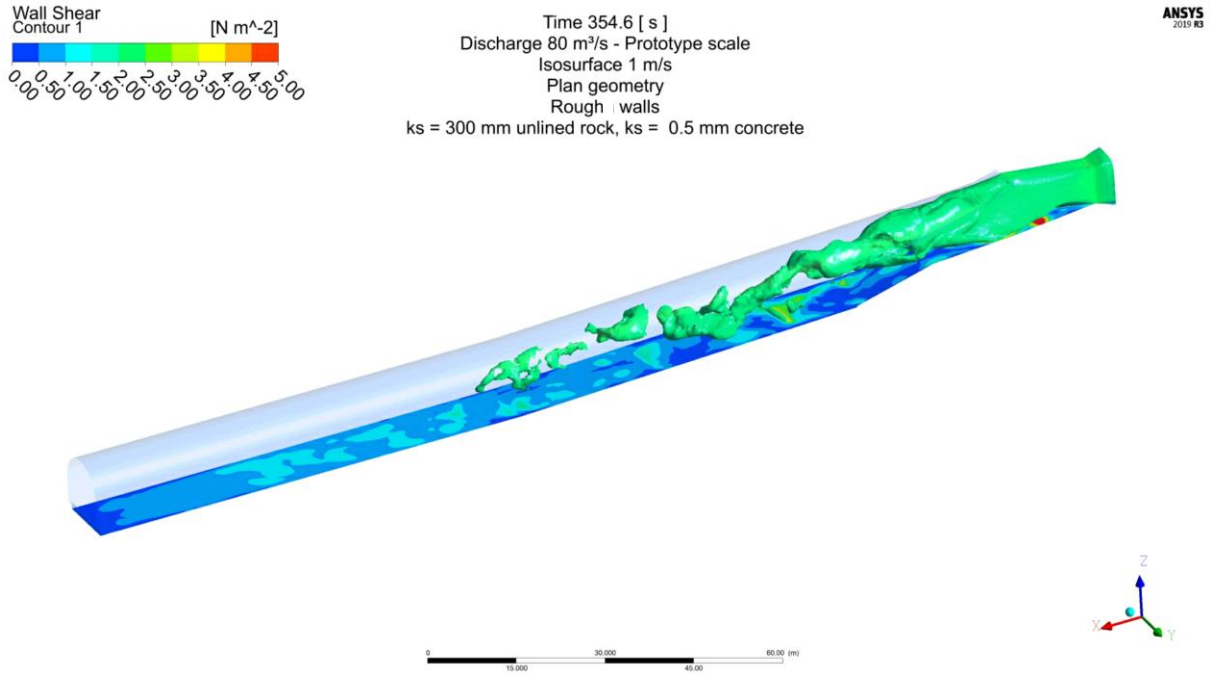

Figure 162: 1:1 scale – geometry as in flume, rough walls, 80m³/s time step with far reaching jet, isosurface 1 m/s, Ramp 02 design

12.3.2 **Ramp design 02 bottom and side walls adaption**

In addition to the ramp design 01 concrete sidewalls are placed and investigated in terms of 3D CFD simulations. An abrupt change from concrete to unlined walls remain. In these abrupt section changes swirl flows are detected in the model test lifting sediments. The following design approach aims to improve the diffusor jet flow. The unlined crown section is kept in place.

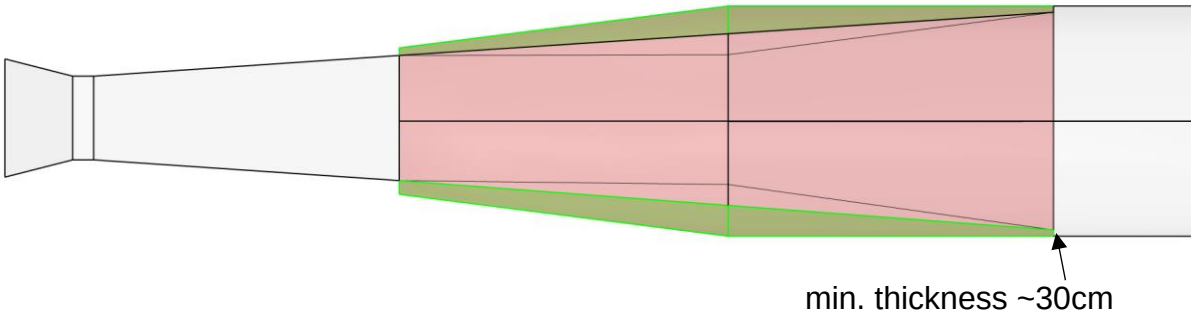

Figure 163: Side walls as diffusor extension in addition to bottom ramp, plan view

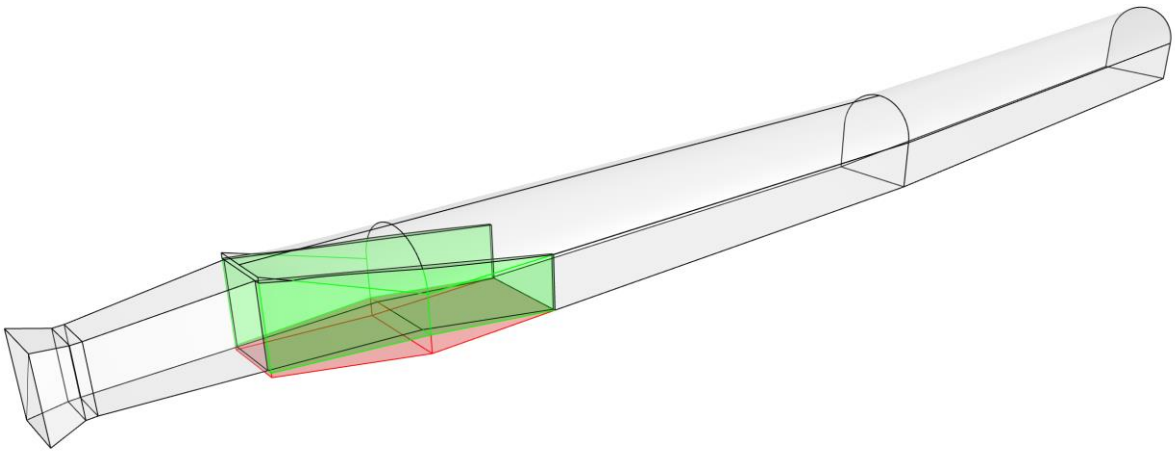

Figure 164: Side walls as diffusor extension in addition to bottom ramp,3D view

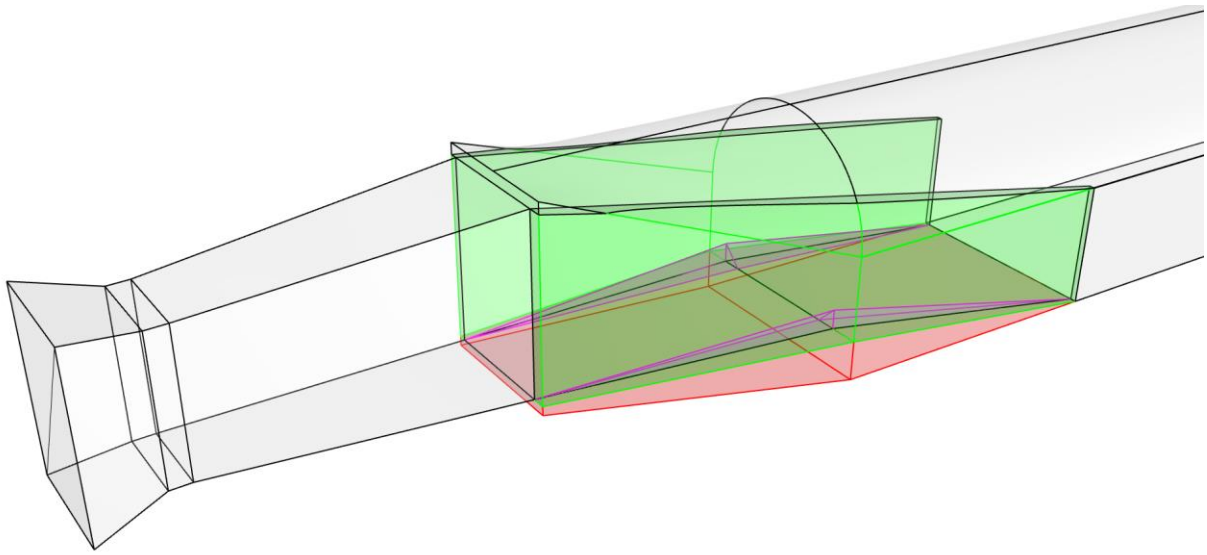

Figure 165: Side walls with chamfer as diffusor extension in addition to bottom ramp, 3D view

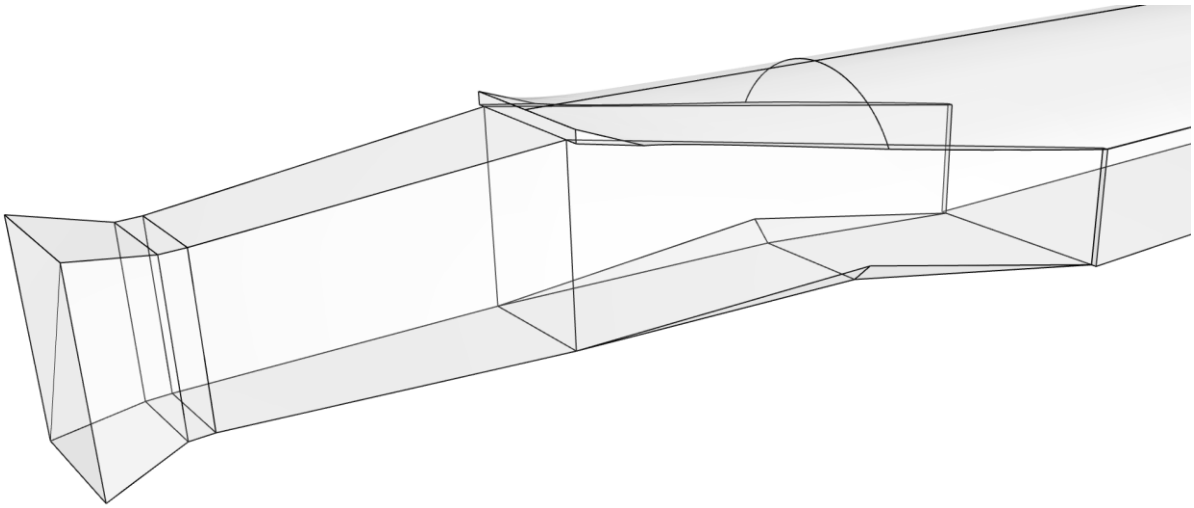

Figure 166: Side walls with chamfer as diffusor extension in addition to bottom ramp,3D view, water solid

Figure 167 shows the result of the design approach no.2. A slightly improved jet is generated, however not sufficiently enough to prevent backflow.

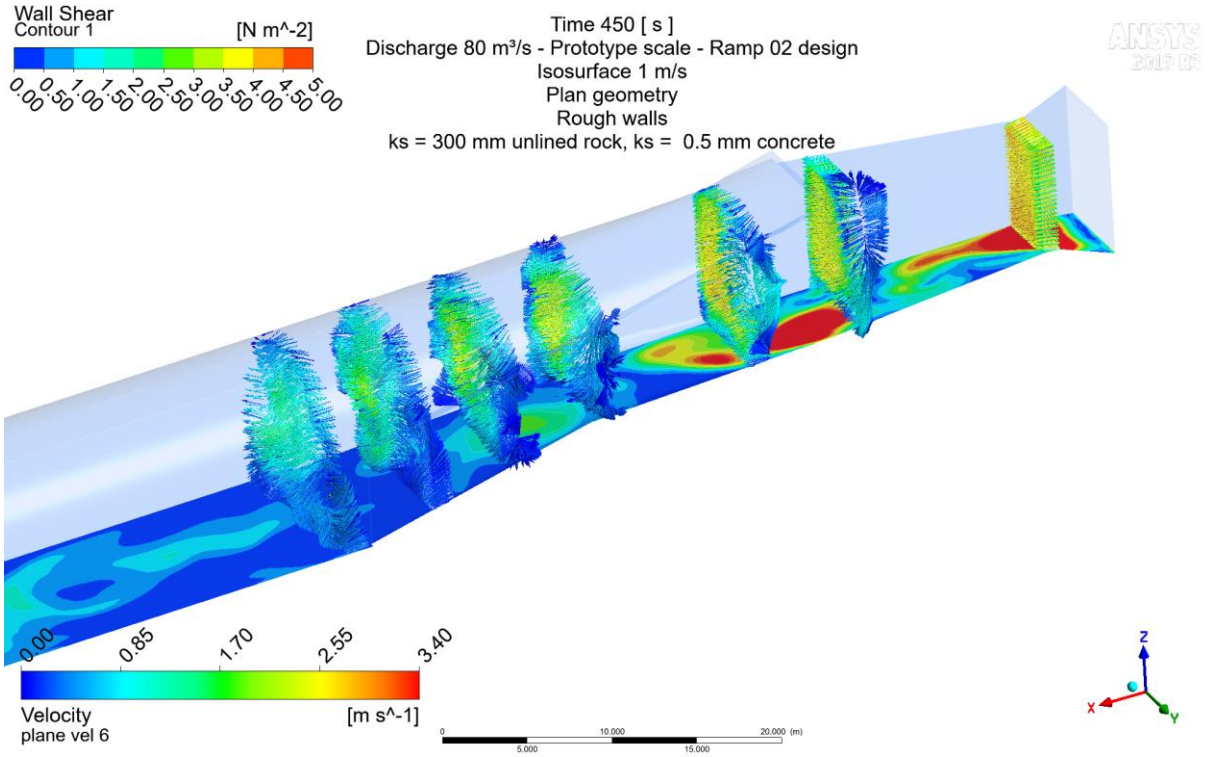

Figure 167: Side walls with chamfer as diffusor extension in addition to bottom ramp,3D view, results, vectors in diffusor section

12.3.2.1 Large grain simulation 1 mm grain roughness

The following simulation show an approach of utilizing large grain particle tracking simulation at the design 02 approach. Larger particles interact more with the bottom and are transported as bed load. Further research on that application of particle tracking 3D CFD is recommended.

Figure 286 shows the result after 156 s with 80 m³/s discharge with rough particles parameter: Sommerfeld Frank Roughness Length: 1 mm, Roughness Height: 1 mm, Roughness Height Std. 0.5 mm. The large particles from 20 mm to 30 mm are not transported to the section observed in the prototype.

Table 17: Boundary conditions for the particle flow simulation

Scale	1:1	Geometry	Tonstad plans
Particles Diameter (1:1)	20-30 mm	Particle injection	Above gate
		Wall roughness	300 mm unlined, 0.5 mm concrete
Time (1:20 resp. 1:1)	156 s	Software	CFX
Timestep	0.15 s	Inlet	Velocity
Particles Density	2650 kg/m³	Outlet	Pressure
Particle roughness	Non	Particles	One-way coupled
Particle Drag	Schiller-Naumann	Particle Roughness	Sommerfeld Frank
Turbulence Modelling	SAS SST	Roughness Length:	1 mm
		Roughness Height:	1 mm
		Height Std.	0.5 mm

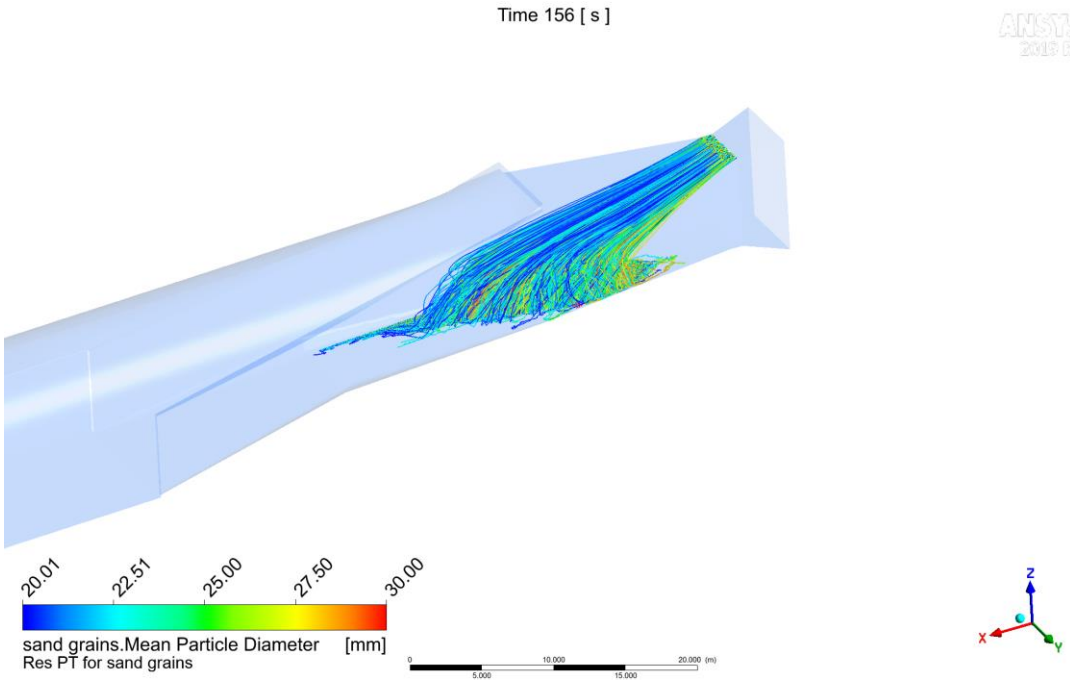

Figure 168: Side walls with chamfer as diffusor extension in addition to bottom ramp,3D view, large particles with particle roughness

12.3.2.2 Large grain simulation 0.5 mm grain roughness

Table 18: Boundary conditions for the particle flow simulation

Scale	1:1	Particle injection	Above gate
Particles Diameter (1:1)	20-30 mm	Wall roughness	300 mm unlined, 0.5 mm concrete
		Software	CFX
Time (1:20 resp. 1:1)	192 s	Inlet	Velocity
Timestep	0.15 s	Outlet	Pressure
Particles Density	2650 kg/m³	Particles	One-way coupled
Particle roughness	Non	Particle Roughness	Sommerfeld Frank
Particle Drag	Schiller-Naumann	Roughness Length:	0.5 mm
Turbulence Modelling	SAS SST	Roughness Height:	0.5 mm
Geometry	Tonstad plans	Height Std.	0.25 mm

Figure 169 shows the result of the simulation with the chosen parameters from Table 18. It fits to the observations inside the sand trap. The combination of 0.5 mm concrete roughness and 0.5 mm grain roughness is a promising approach for the simulation.

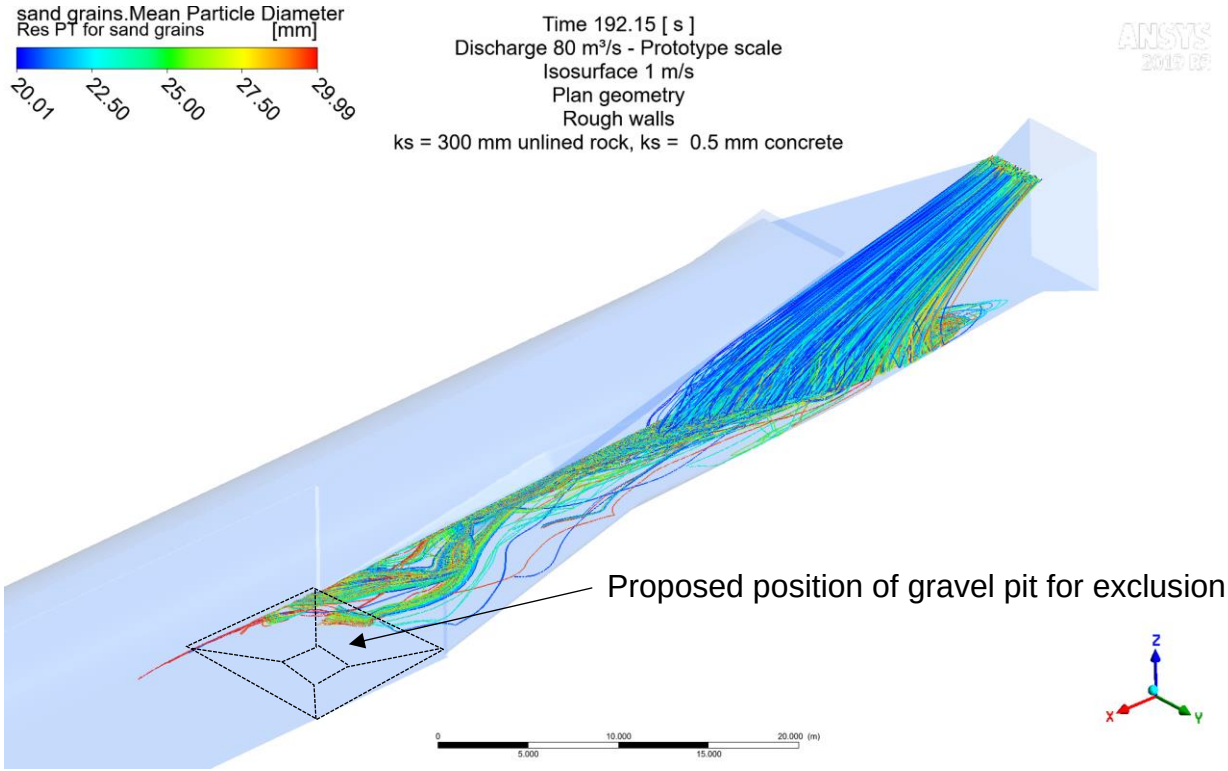

Figure 169: Side walls with chamfer as diffusor extension in addition to bottom ramp,3D view, large particles with particle roughness

12.3.3 **Ramp design 03- calming pillars**

In addition to Ramp 01 and ramp 02 design with side walls additionally round calming pillars are placed. The pillars have also an opening gap to be passable (Figure 170).

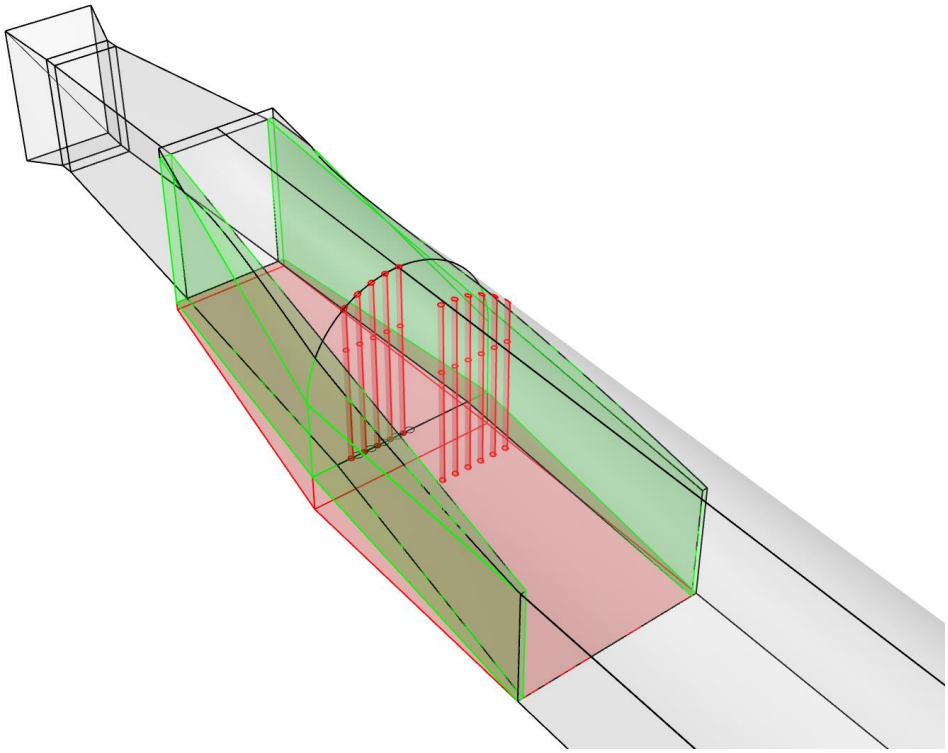

Figure 170: Ramp 01 & side walls & flow calming pillars with Di 0.3m, distance 0.5 m, passable positioning

Figure 171 shows the result of a transient simulation with isosurface velocity 1 m/s.

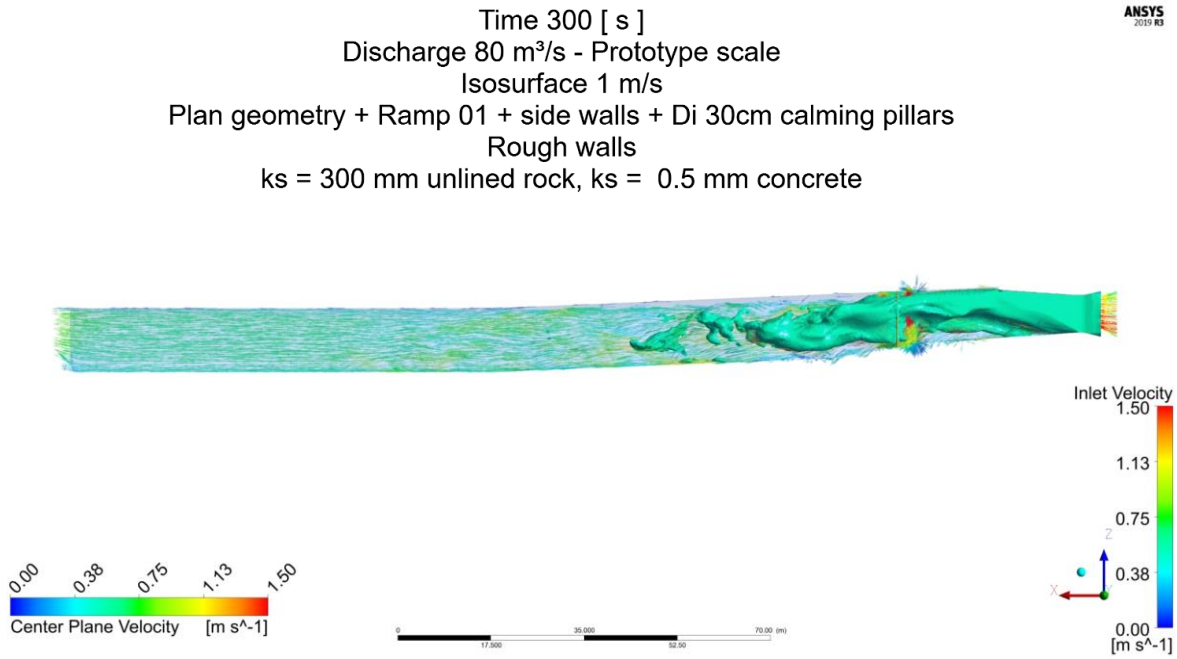

Figure 171: Ramp 01 & side walls & flow calming pillars with Di 0.3m, distance 0.5 m, passable positioning, side view, isosurface 1 m/s

Figure 172 shows a detail of the isosurface simulation with round pillars and ramp 01 and ramp 02 design. Figure 173 shows the plane velocities for the load case of 80 m³/s discharge.

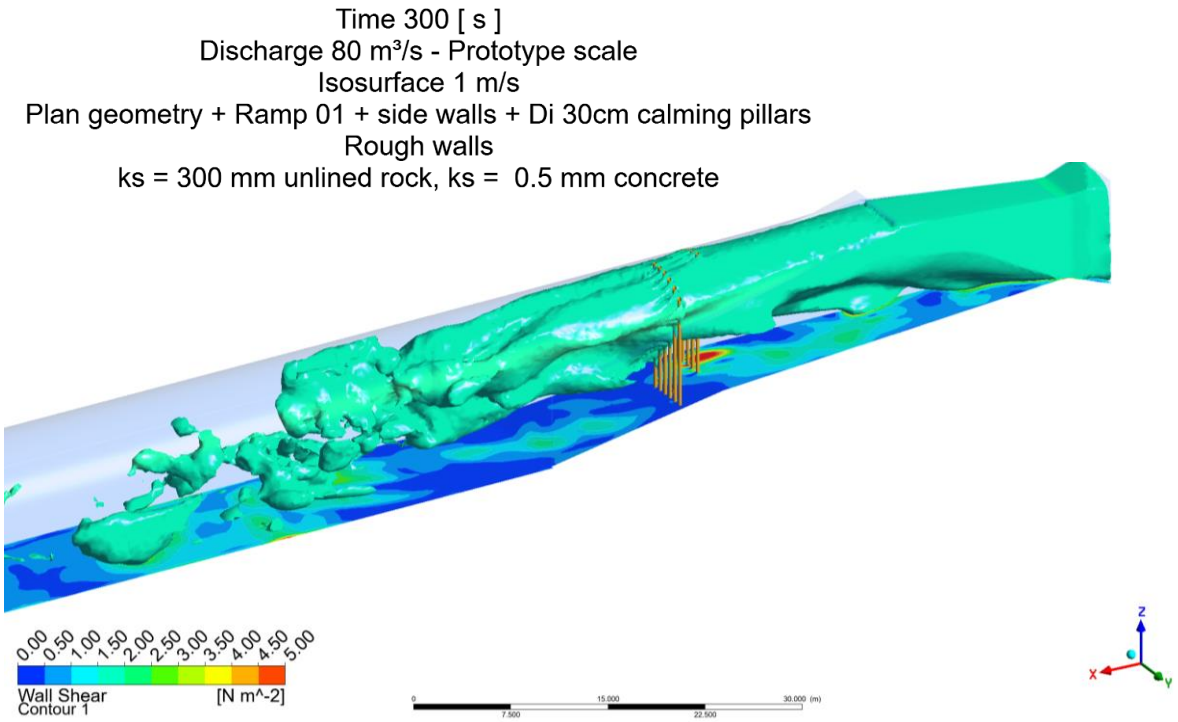

Figure 172: Ramp 01 & side walls & flow calming pillars with Di 0.3m, distance 0.5 m, passable positioning, 3D view, isosurface 1 m/s, bottom wall shear, detail

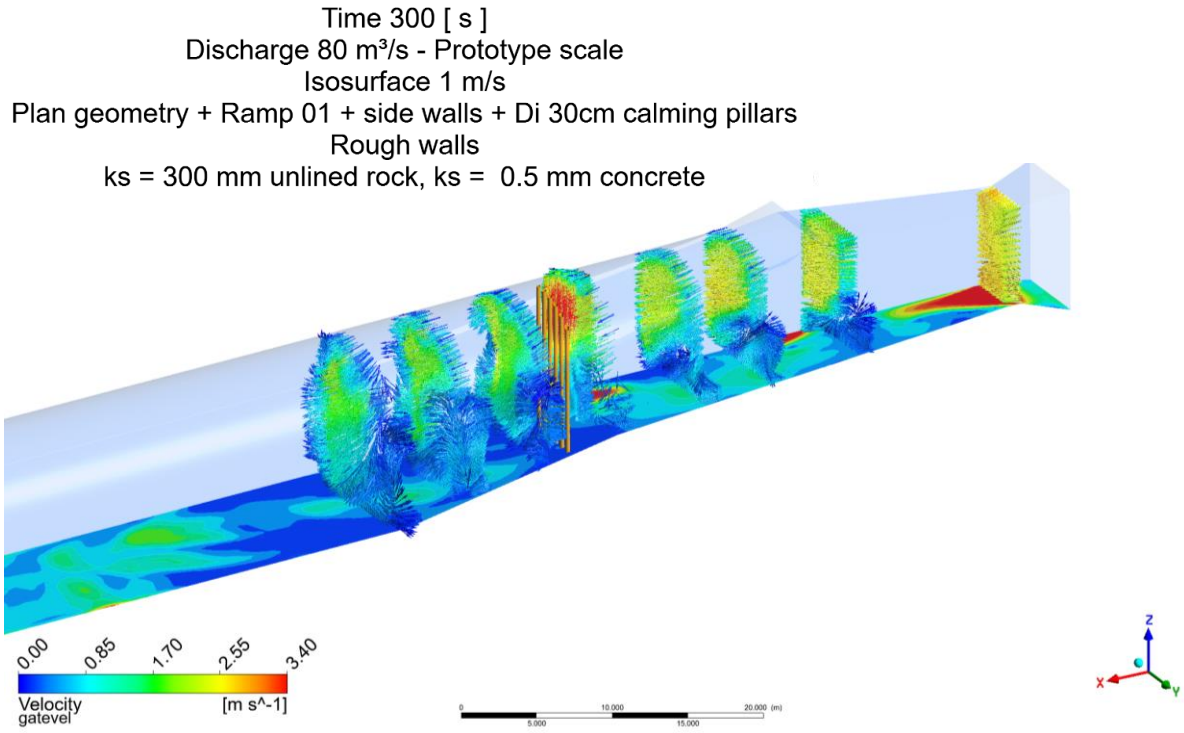

Figure 173: Ramp 01 & side walls & flow calming pillars with Di 0.3m, distance 0.5 m, passable positioning, 3D view, isosurface 1 m/s, bottom wall shear

Figure 174 compares the original design with the ramp 03 variant. It can be shown that a significant earlier dissipation of the jet is realized by the structure.

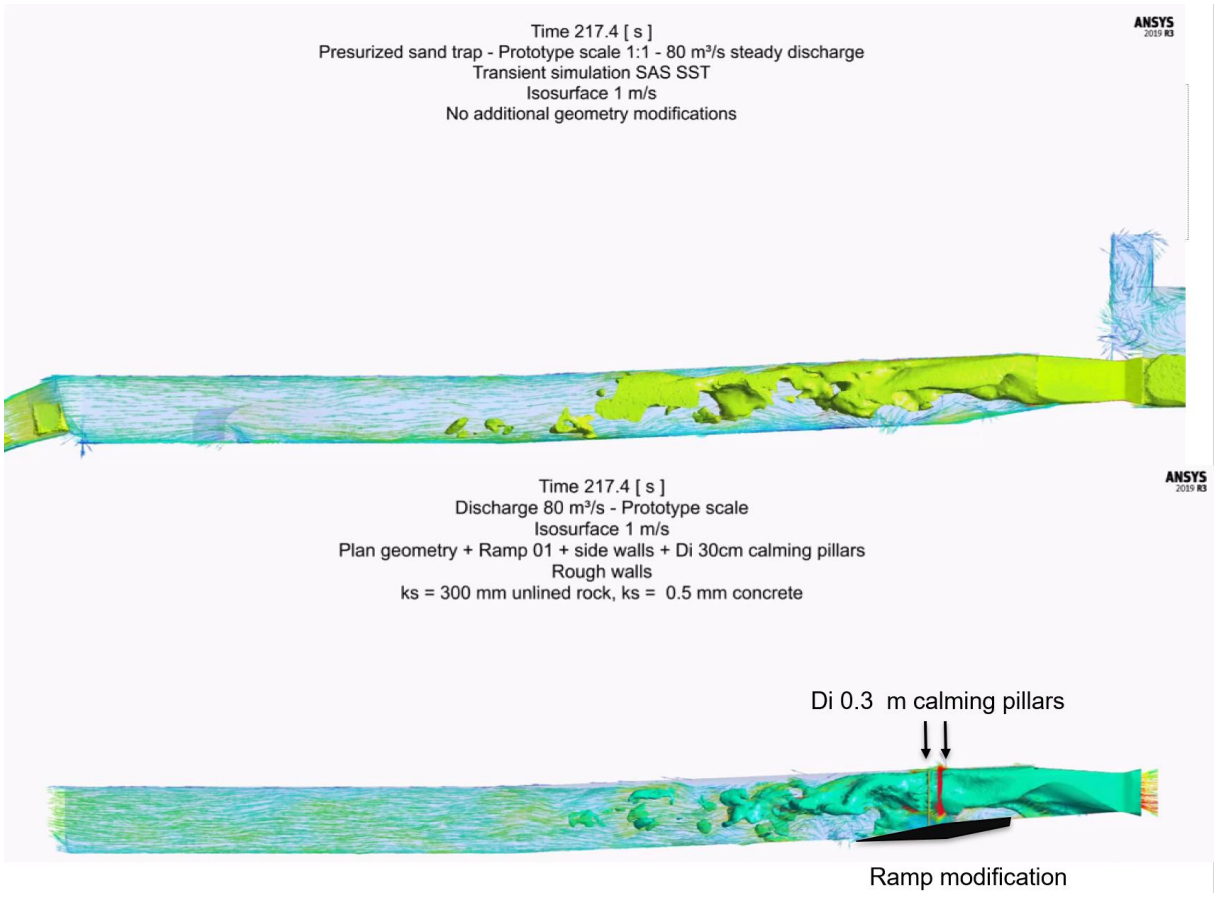

Figure 174: Comparison of Ramp design 03 and original design with 1 m/s isosurface

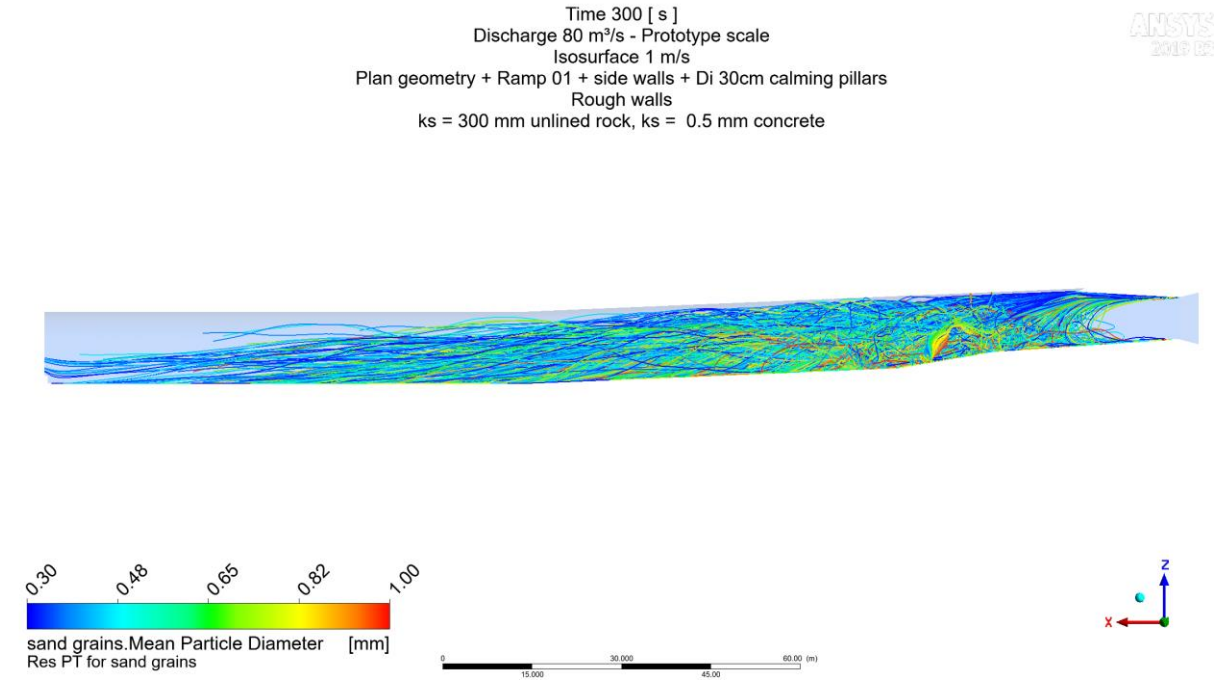

Figure 175: Ramp 01 & side walls & flow calming pillars with Di 0.3m, distance 0.5 m, passable positioning, side view, particle tracking 0.3 mm to 1.0 mm

Figure 176 shows that smaller particles are directly transported in suspended flow through the sand trap without settling.

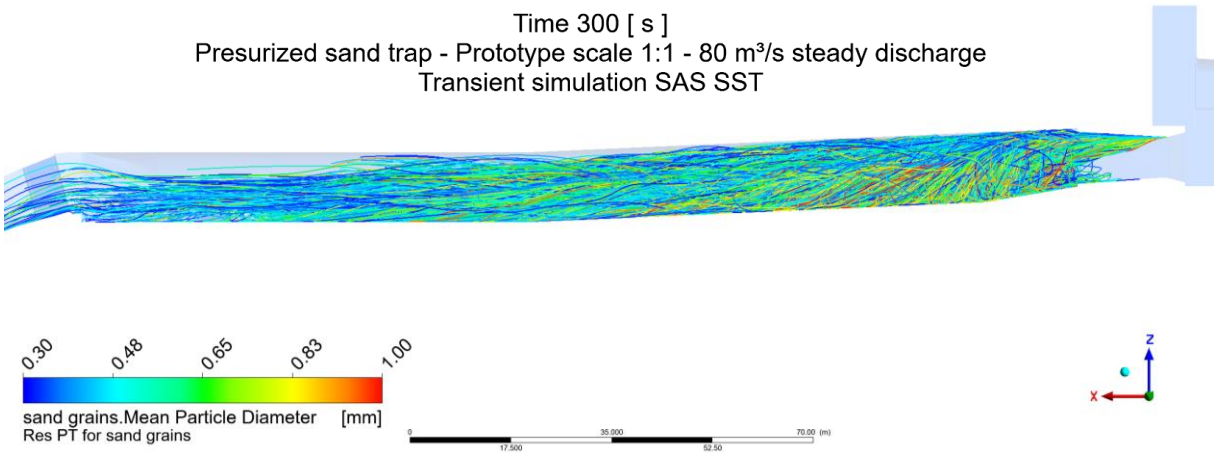

Figure 176: Original design, particle tracking 0.3 mm to 1.0 mm

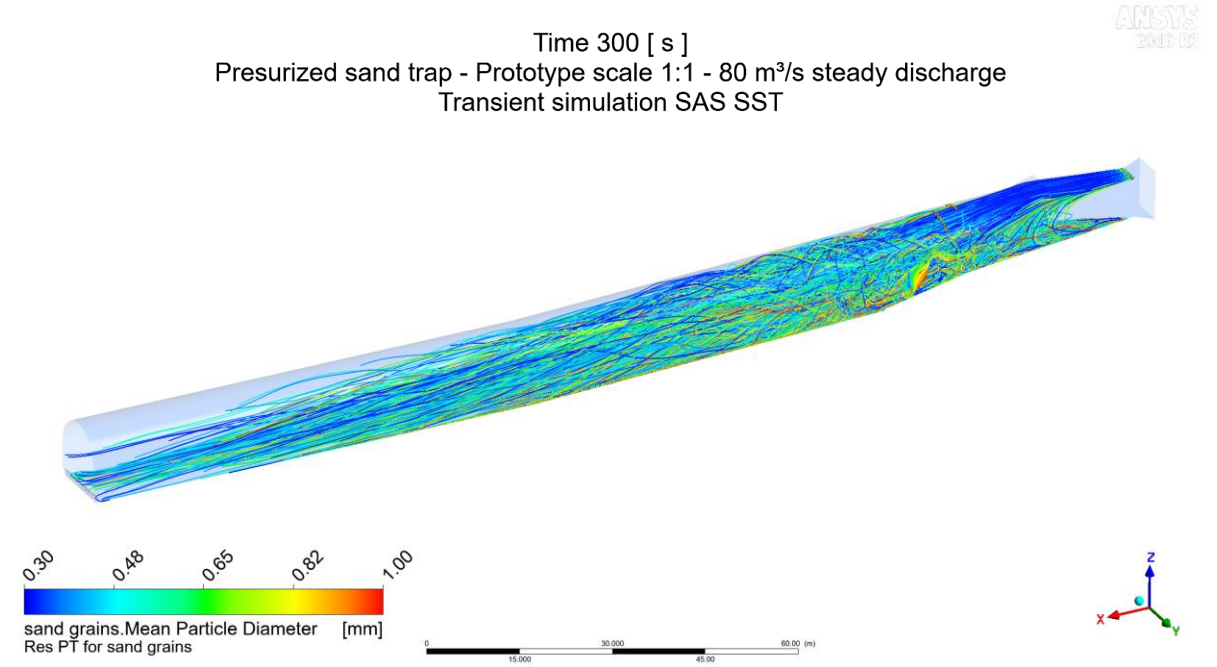

Figure 177: Ramp 01 & side walls & flow calming pillars with Di 0.3m, distance 0.5 m, passable positioning, 3D view, particle tracking 0.3 mm to 1.0 mm

Figure 178 shows the comparison of the original geometry and geometry with Di 0.3 m calming pillars with particle tracking simulation, it can be seen that only a very slight settling improvement can be noticed.

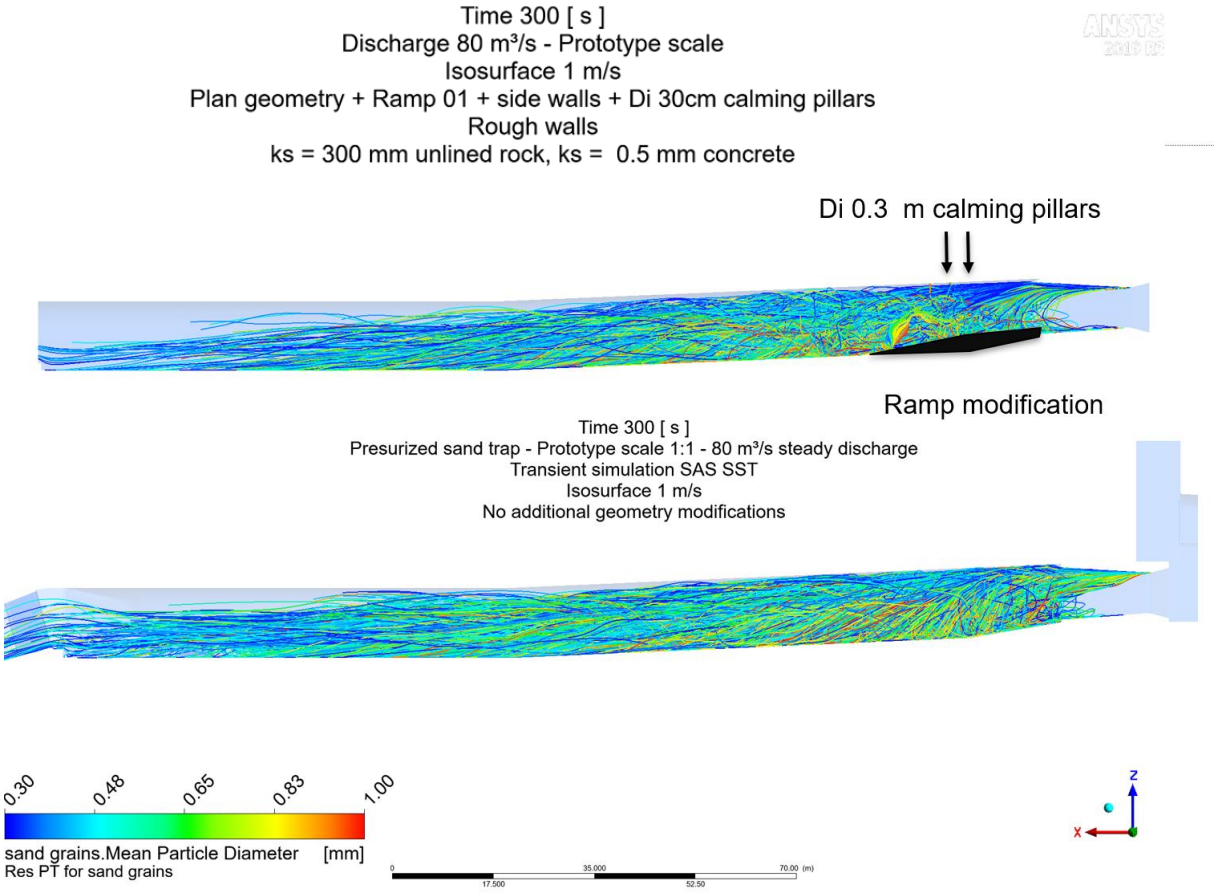

Figure 178: Comparison of original geometry and geometry with Di 0.3 m calming pillars by particle tracking simulation

12.3.4 **Ramp design 04; ramp, sidewalls and squared calming piles**

This geometry adaption proposal introduces quadratic passable calming pillars with dimensions of 20 cm / 20 cm. The calming piles are placed with an opening gap to allow walk and drive through in case of maintenance. The piles are placed in combination with design approach 01 and 02.

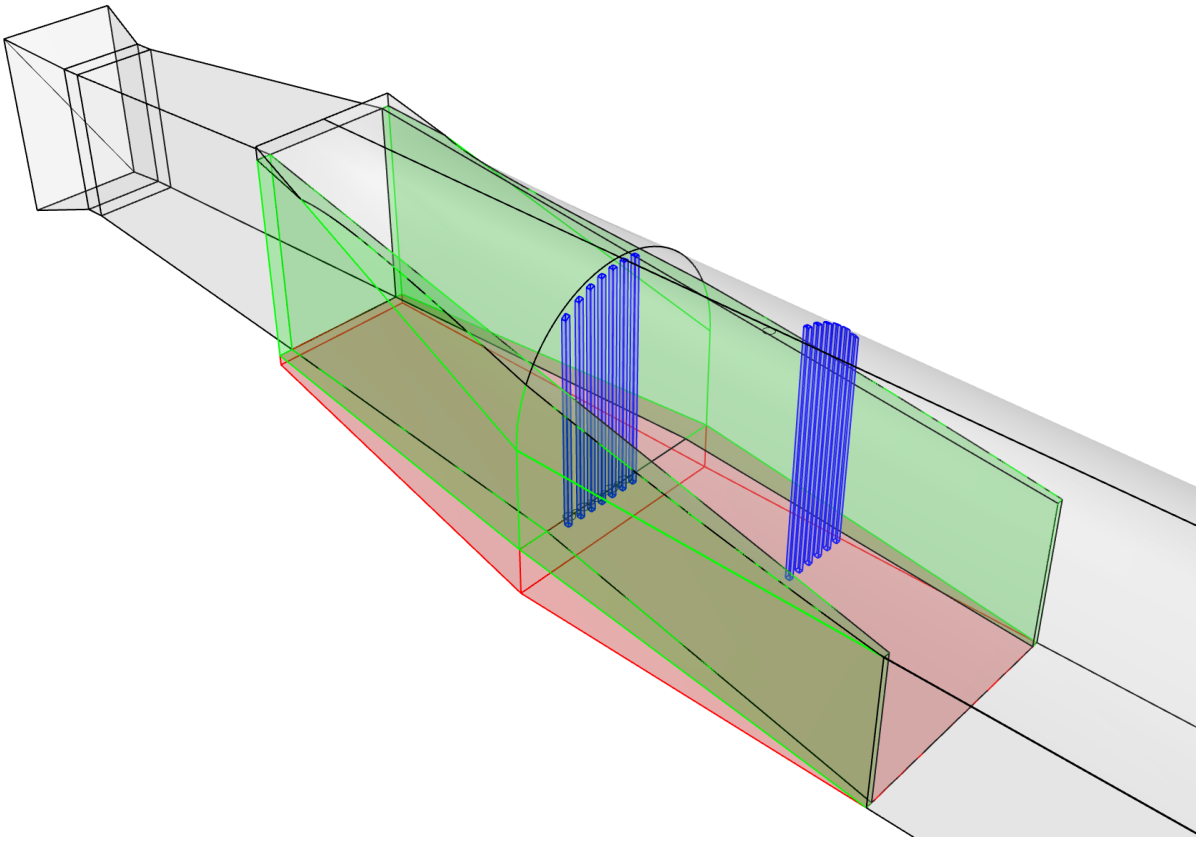

Figure 179: Side walls as diffusor extension in addition to bottom ramp plus squared calming piles with 20/20 cm distance 40 cm, 3D view

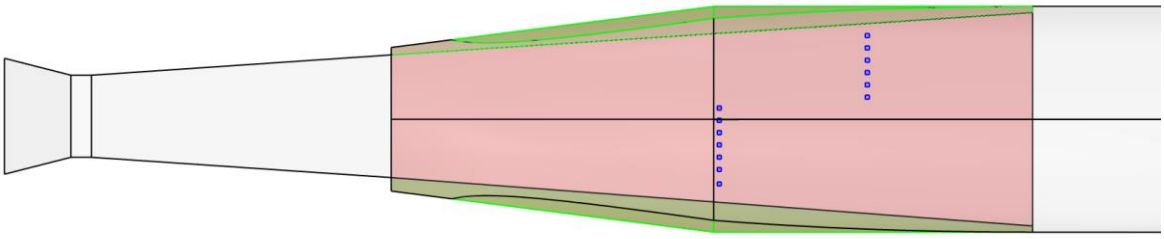

Figure 180: Side walls as diffusor extension in addition to bottom ramp plus squared calming piles with 20/20 cm, plan view

12.3.5 **Ramp design 05: double row calmers**

For the ramp design variant 05 the quadratic calmers are doubled by a distance of 40 cm.

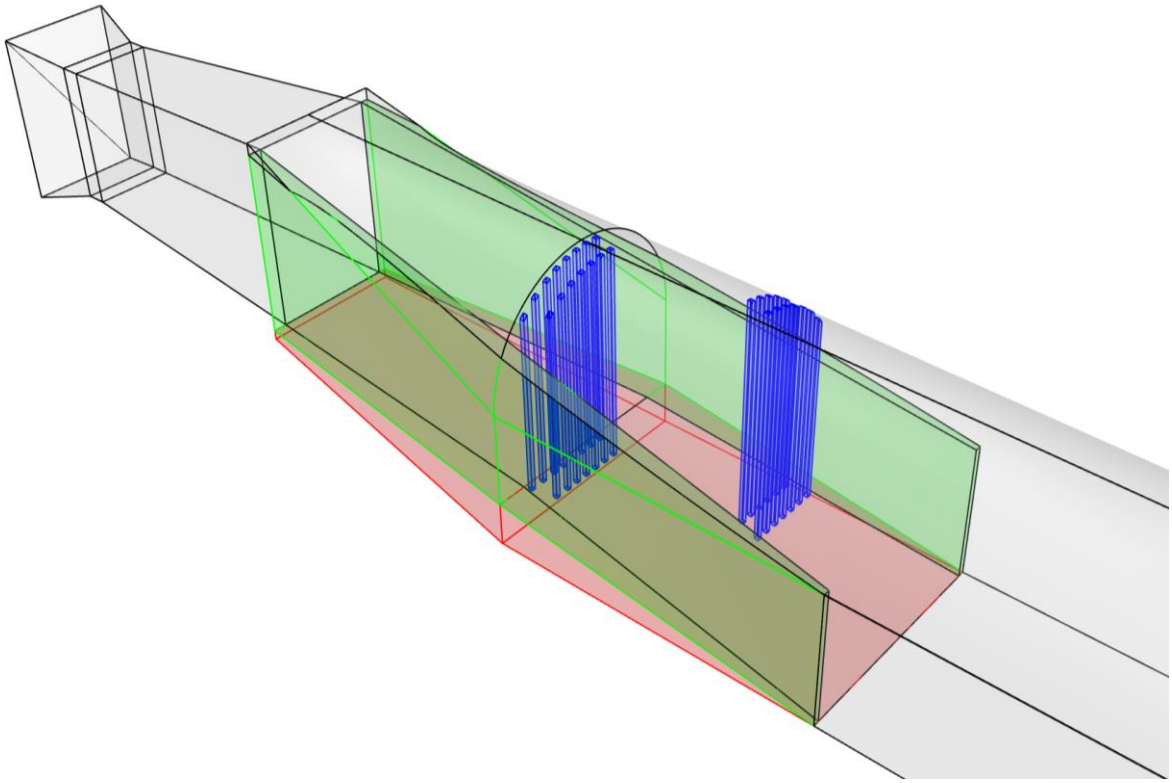

Figure 181: Side walls as diffusor extension in addition to bottom ramp plus double row squared calming piles with 20/20 cm distance 40 cm, 3D view

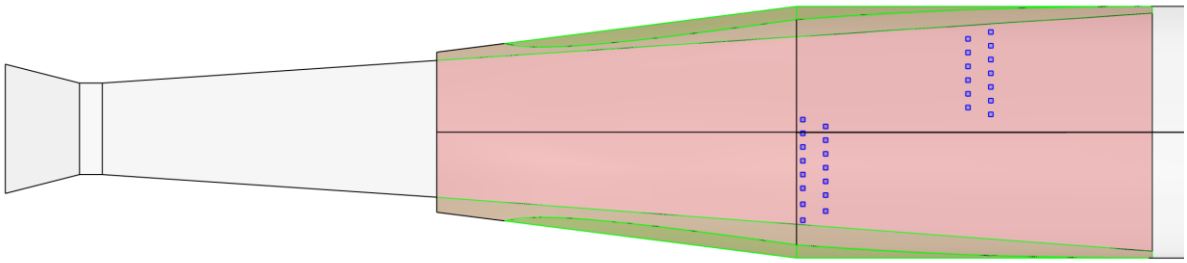

Figure 182: Side walls as diffusor extension in addition to bottom ramp plus double row squared calming piles with 20/20 cm distance 40 cm, plan view

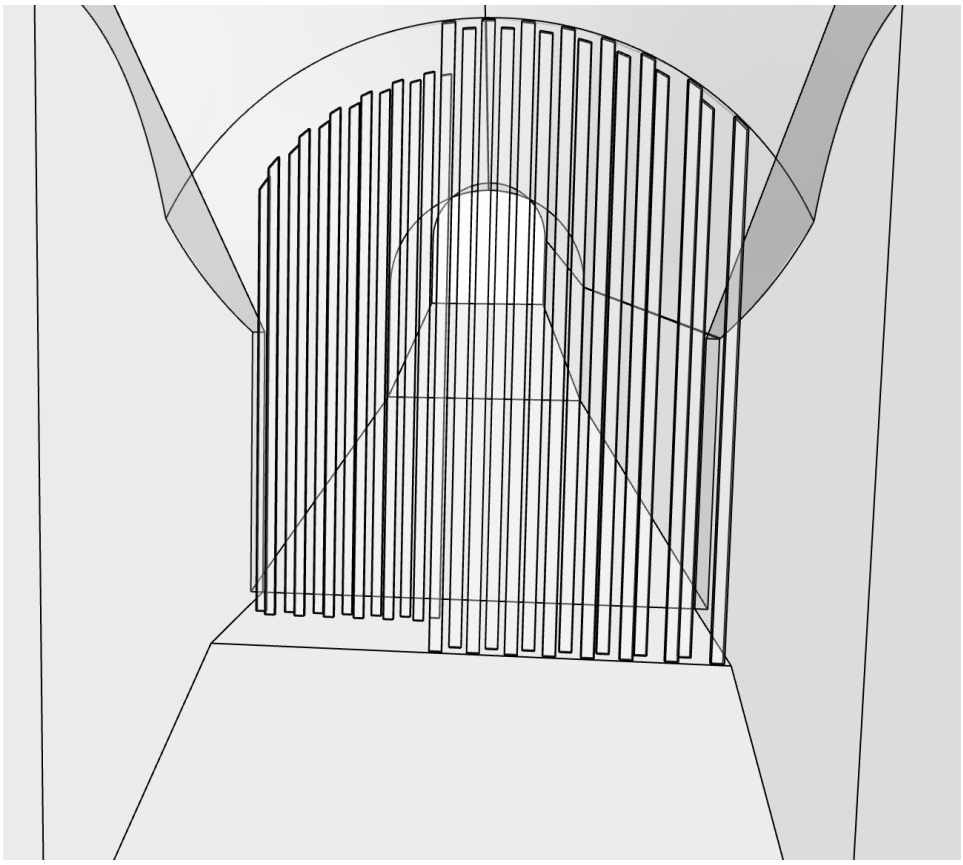

Figure 183: Side walls as diffusor extension in addition to bottom ramp plus double row squared calming piles with 20/20 cm distance 40 cm, view from inside

Figure 184 and Figure 185 show the comparison between the ramp design 02 (left) and ramp design 05 (right). Ramp design 05 with the double row flow calmers show a significantly improved flow dissipation and a shorter impact of higher velocities indicated by an isosurface of velocity 1.0 m/s.

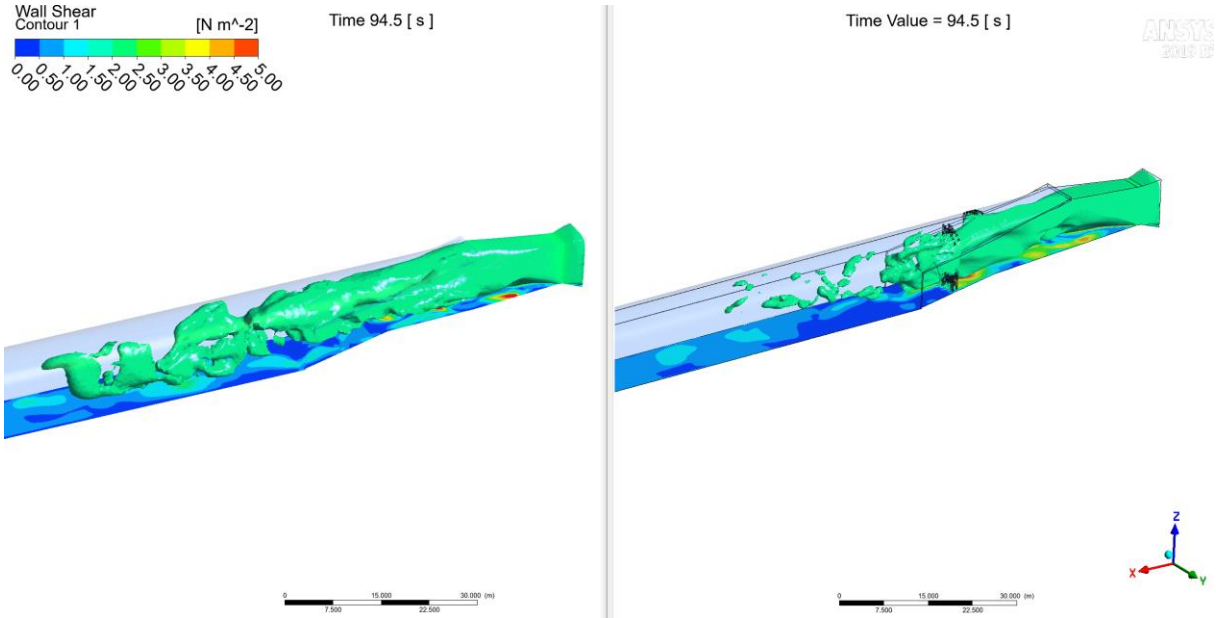

Figure 184: Comparison Ramp 02 (left) and Ramp 05 (right) at timepoint 94.5 s, constant discharge of 80 m³/s

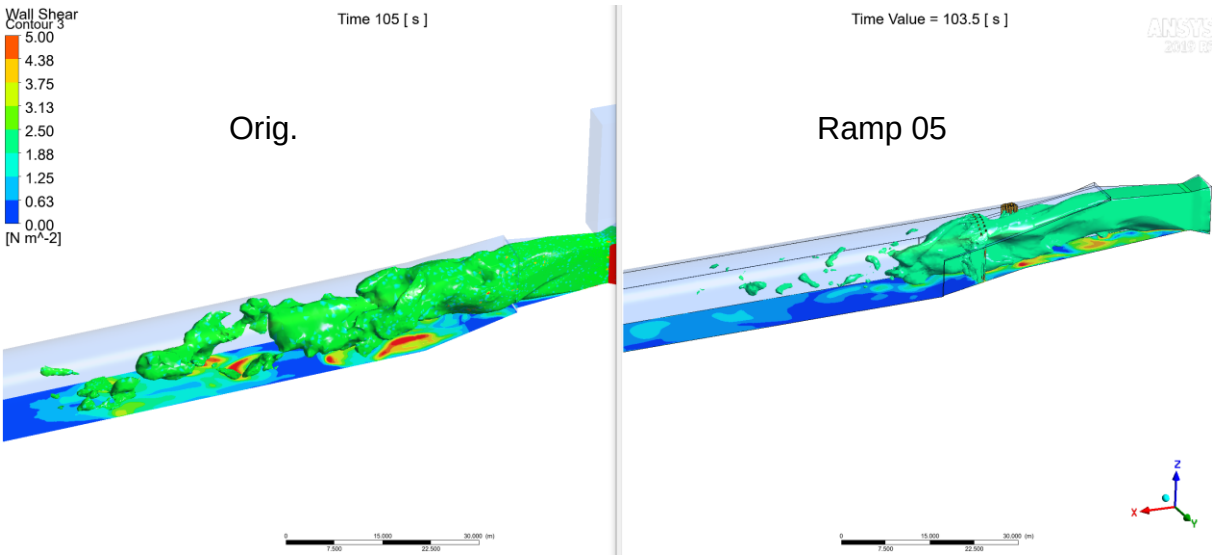

Figure 185: Comparison original design (left) and Ramp 05 (right) at timepoint 105 and 103.5 s, constant discharge of 80 m³/s

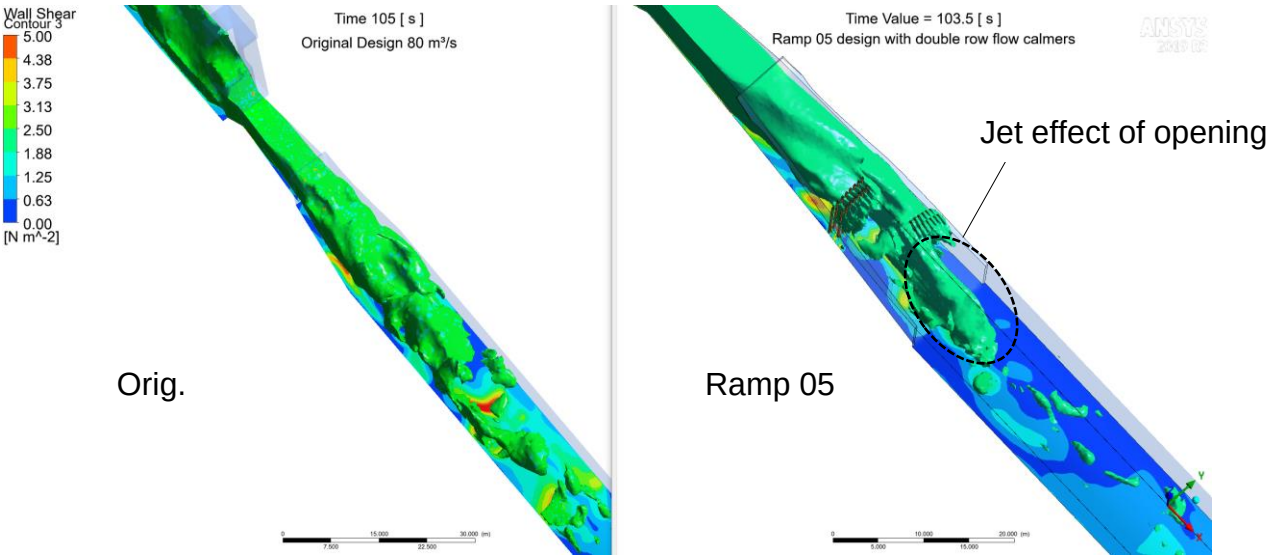

Figure 186: Comparison original design (left) and Ramp 05 (right) at timepoint 105 and 103.5 s, constant discharge of 80 m³/s

Particle tracking Ramp design 05

The figures below show different particle diameter distribution results for the transient simulation with 80 m³/s.

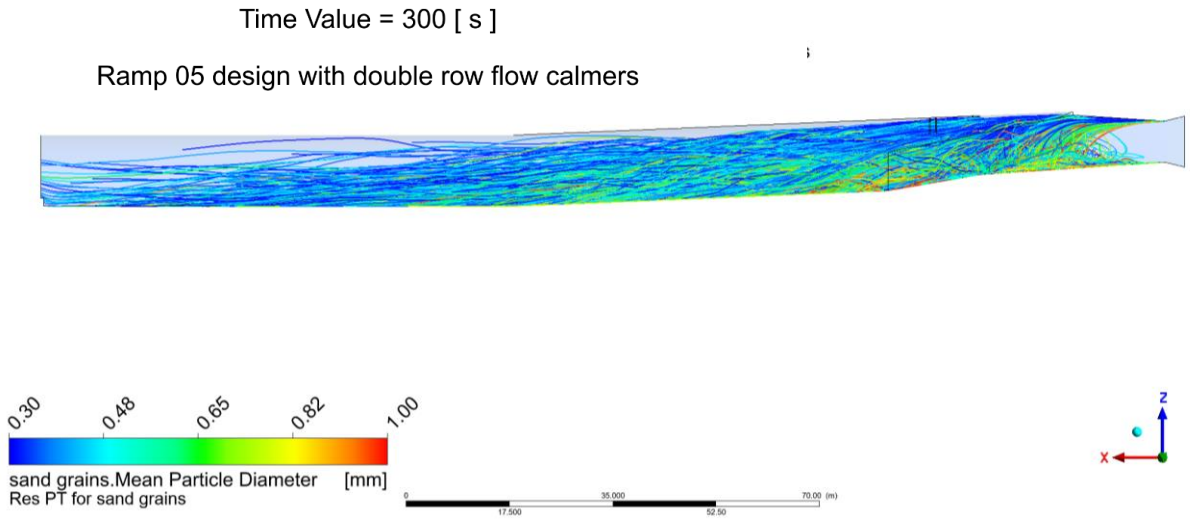

Figure 187: ramp design 07, particle tracking one-way coupled diameter 0.3 mm - 1.0 mm

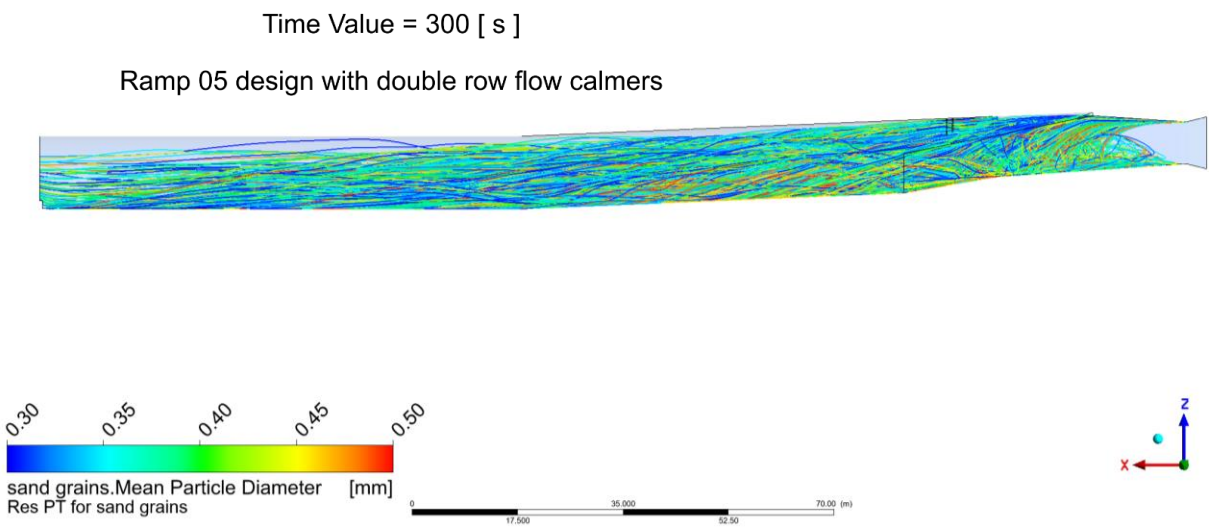

Figure 188: ramp design 07, particle tracking one-way coupled diameter 0.3 mm - 0.5 mm

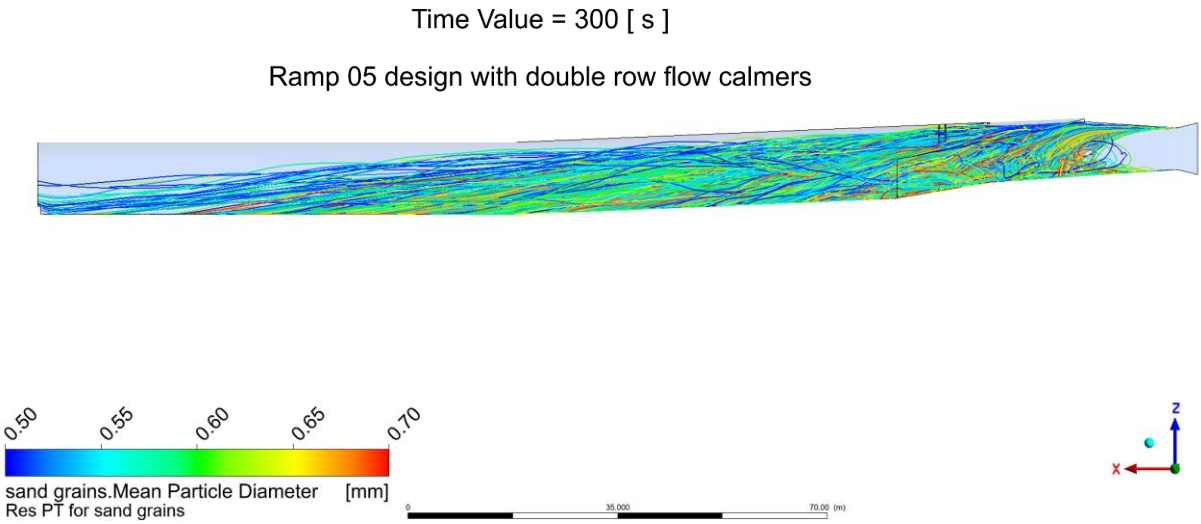

Figure 189: ramp design 07, particle tracking one-way coupled diameter 0.5 mm - 0.7 mm

Figure 190 and Figure 191 show the comparison of the particle tracking simulation with double row flow calmers and without. A slight improvement in the settling behaviour is visible and gives the basis for placing calming rakes in the model test setup.

In the physical model test it was later observed that re-suspending at the weir in combination with significant bed load transportation particles behaviour will not be improved by the calming rakes.

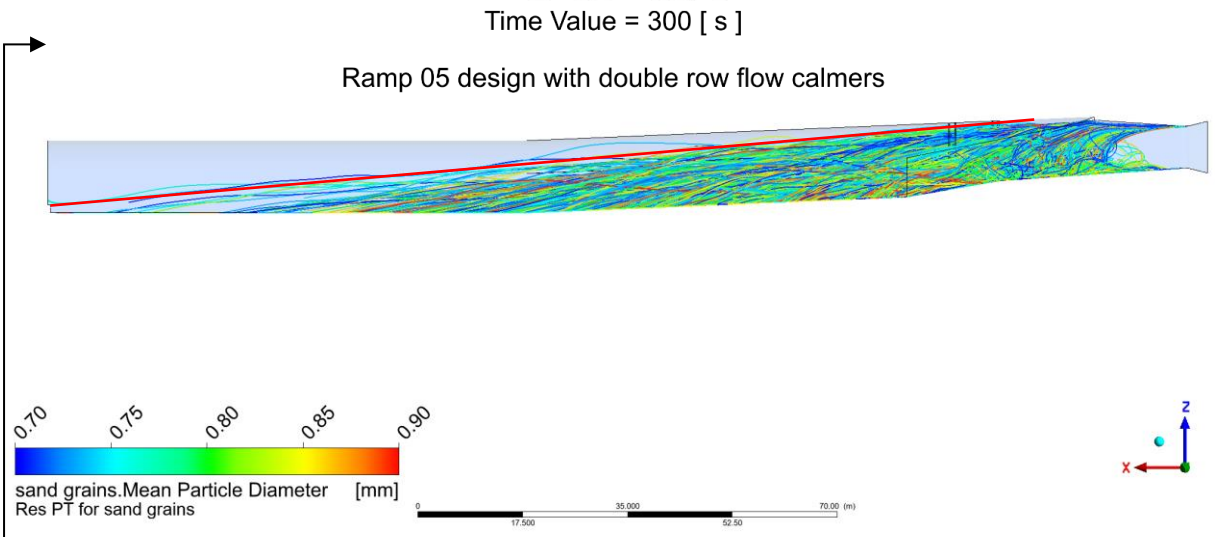

Figure 190: ramp design 05, particle tracking one-way coupled diameter 0.7 mm - 0.9 mm

comparison

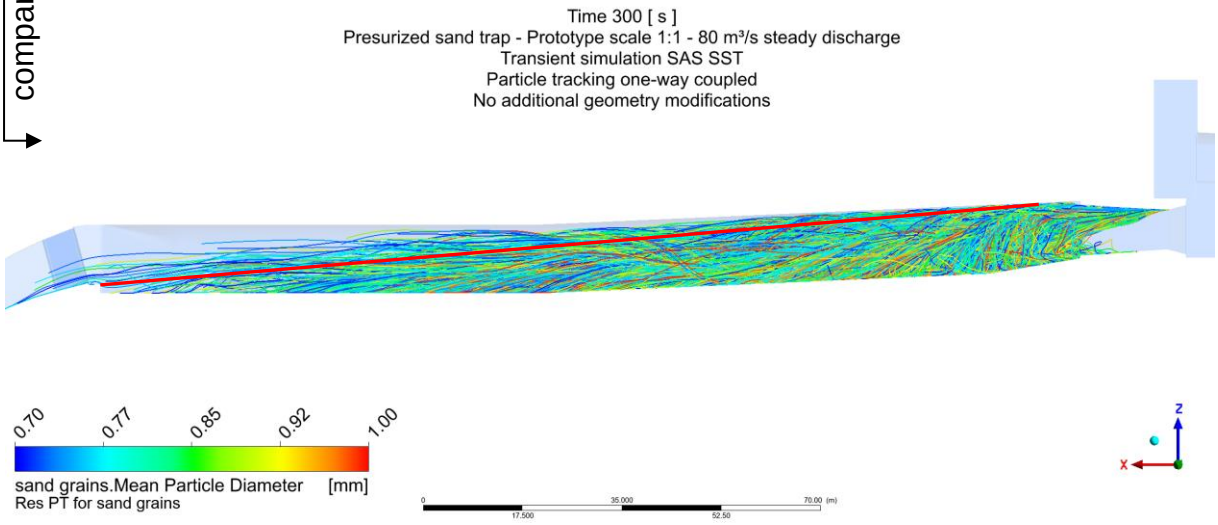

Figure 191: Scale 1:1, 80 m³/s discharge, particle tracking paths for sediment grains of 0.7 mm to 1.0 mm, time point 300 s, view y-axis – Comparison to **Figure 190**

The results below show particle tracking simulation outcome for different diameter ranges.

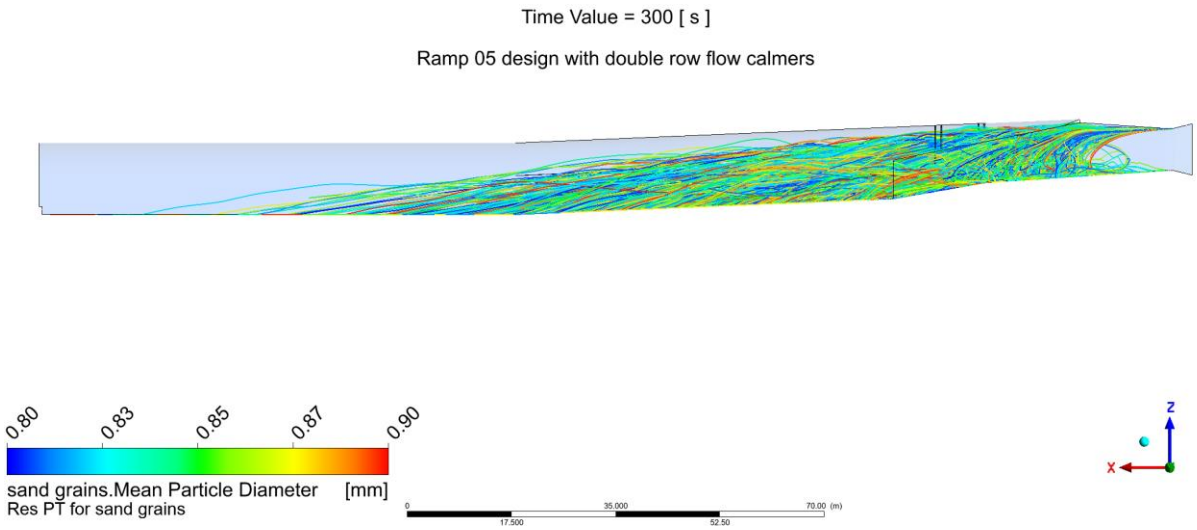

Figure 192: ramp design 07, particle tracking one-way coupled diameter 0.8 mm - 0.9 mm

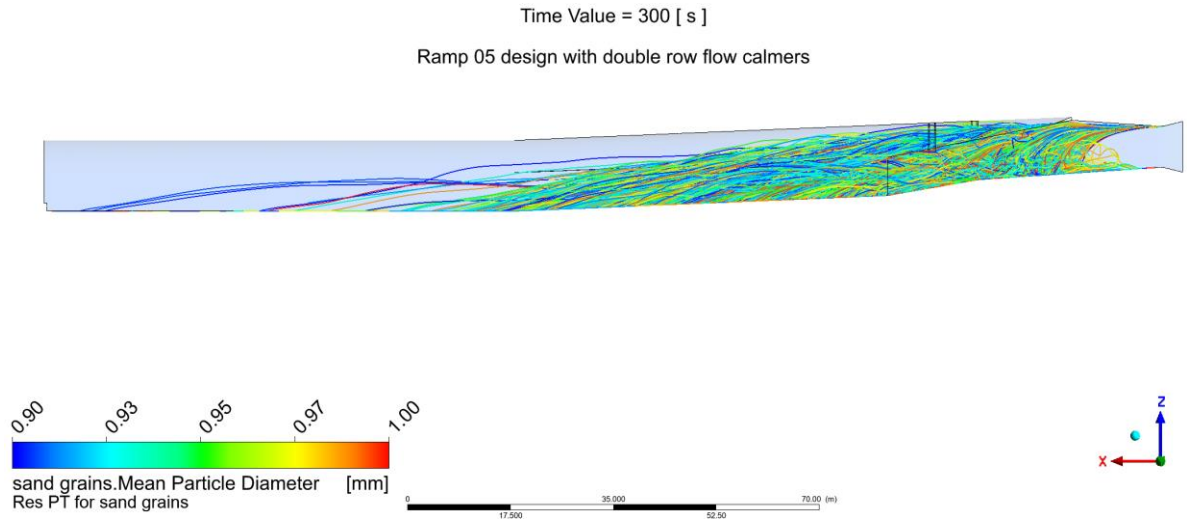

Figure 193: ramp design 07, particle tracking one-way coupled diameter 0.9 mm - 1.0 mm

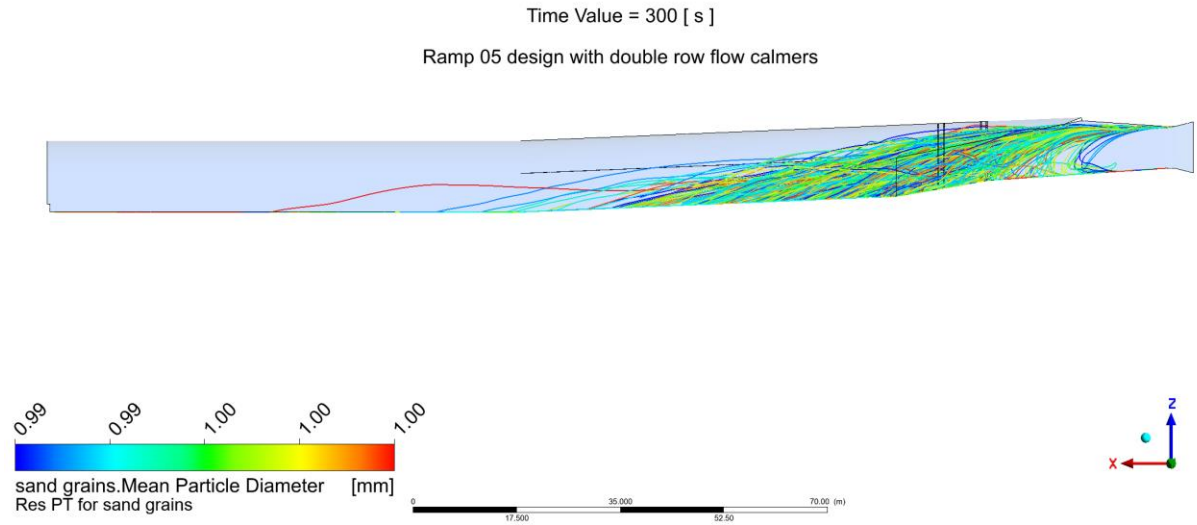

Figure 194: ramp design 07, particle tracking one-way coupled diameter 0.99 mm - 1.0 mm

12.3.6 **Ramp design 06: double row flow calmers**

The geometry in Figure 195 and Figure 196 describes flow a calmer geometry with double row 200/200 mm squared piles. No ramp adaption is included. The choice of the sides considers a possible connection to an extension chamber with a discharge of about 60 m³/s.

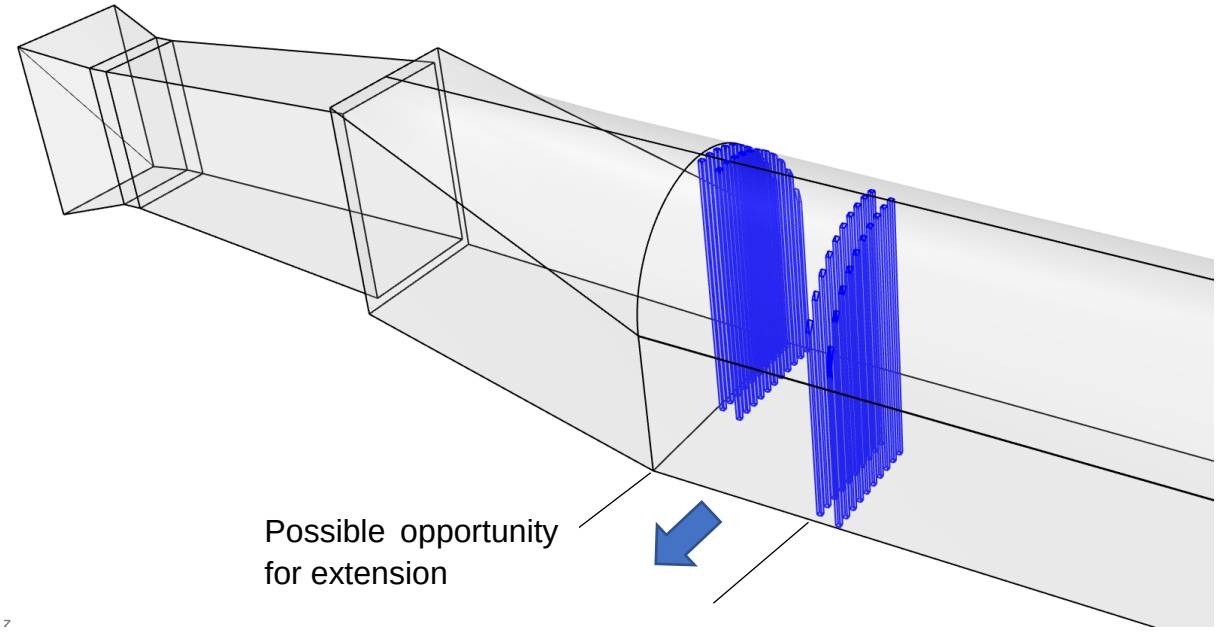

Figure 195: 200/200 mm double row flow calmers, no ramp modifications, 3D view

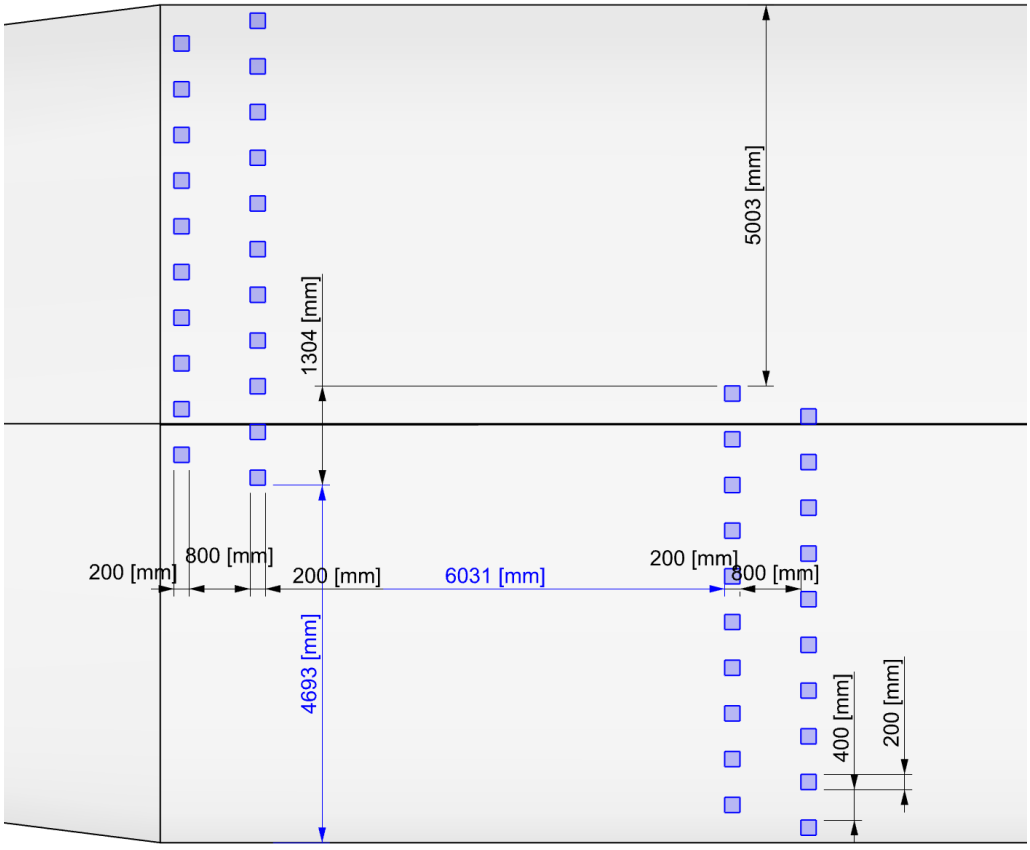

Figure 196: 200/200 mm double row flow calmers only, plan view

12.3.7 **Ramp design 07: double row flow calmers**

In difference of Ramp design 06 this variant offers 10.2 m distance between the calmers to allow the attachment of the extension chamber. No additional concrete structures investigated as ramp design 01 and 02 at the diffusor are proposed

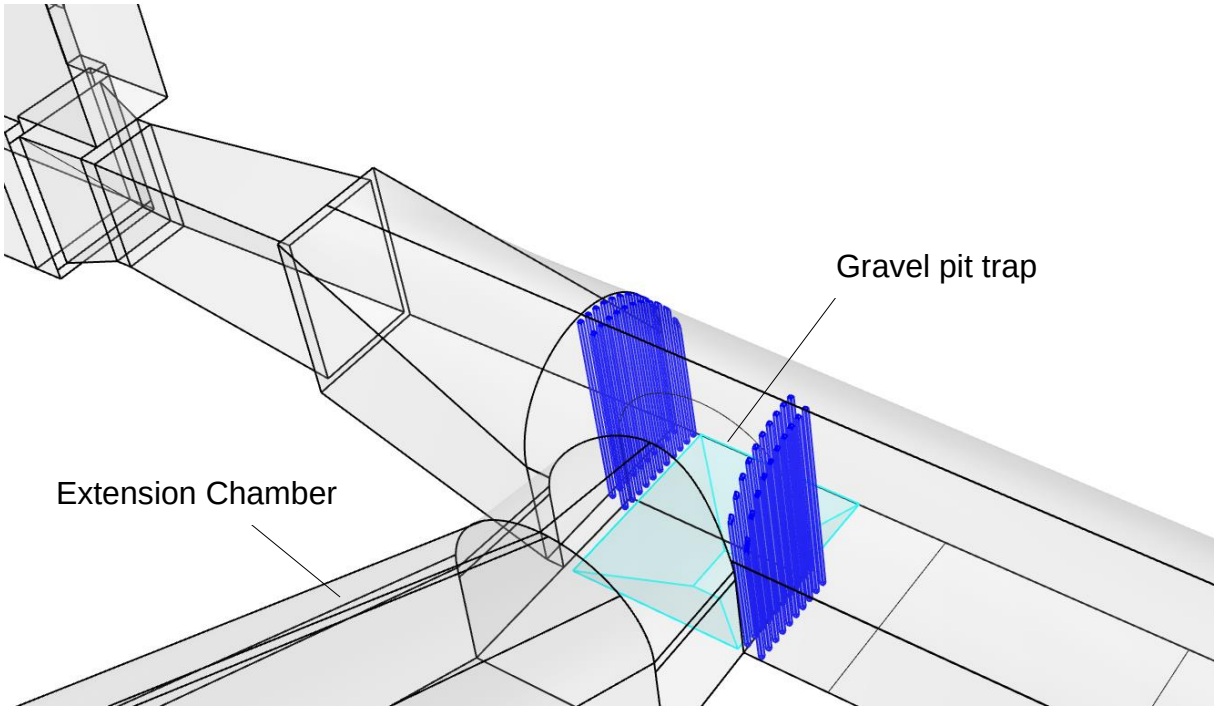

Figure 197: 200/200 mm double row flow calmers, no ramp modifications, 3D view

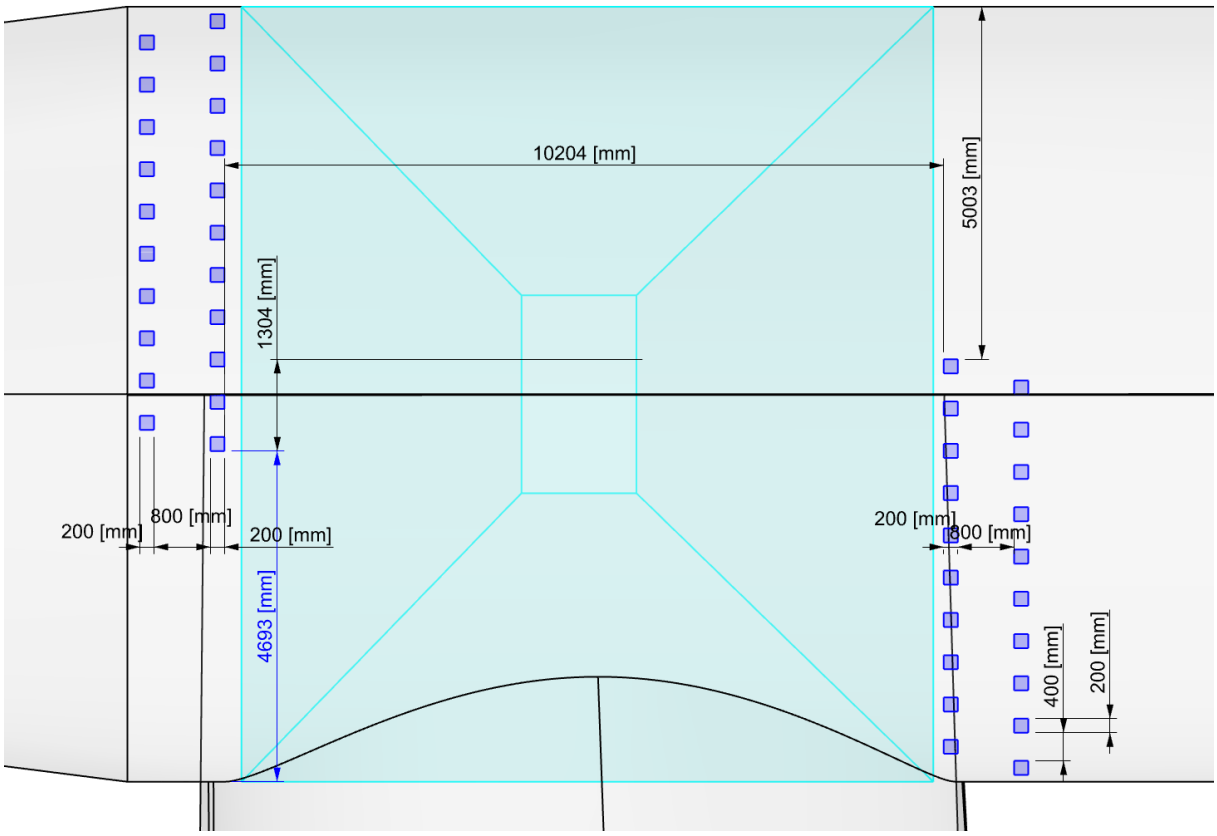

Figure 198: 200/200 mm double row flow calmers only, plan view variant B)

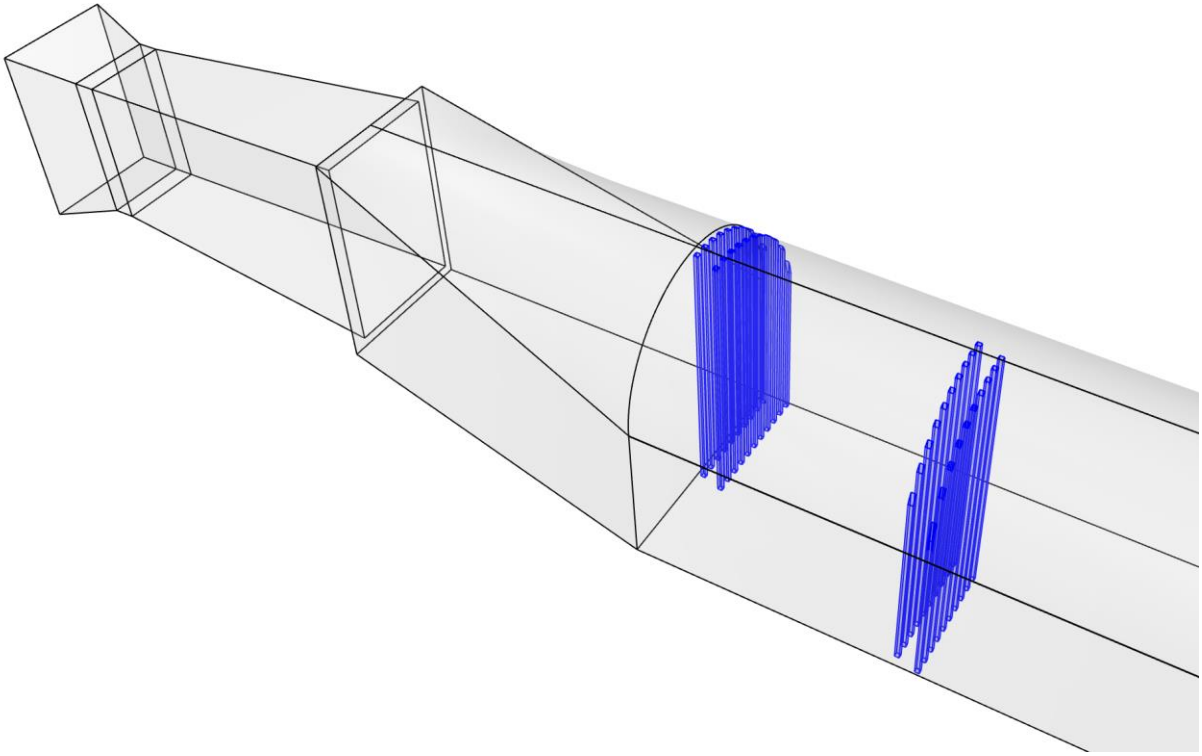

Figure 199: 200/200 mm double row flow calmers, no ramp modifications, for 3D simulation, 3D view

12.3.8 **3D CFD diffusor results comparison**

The figures below compare the ramp variants by isosurface velocity distribution

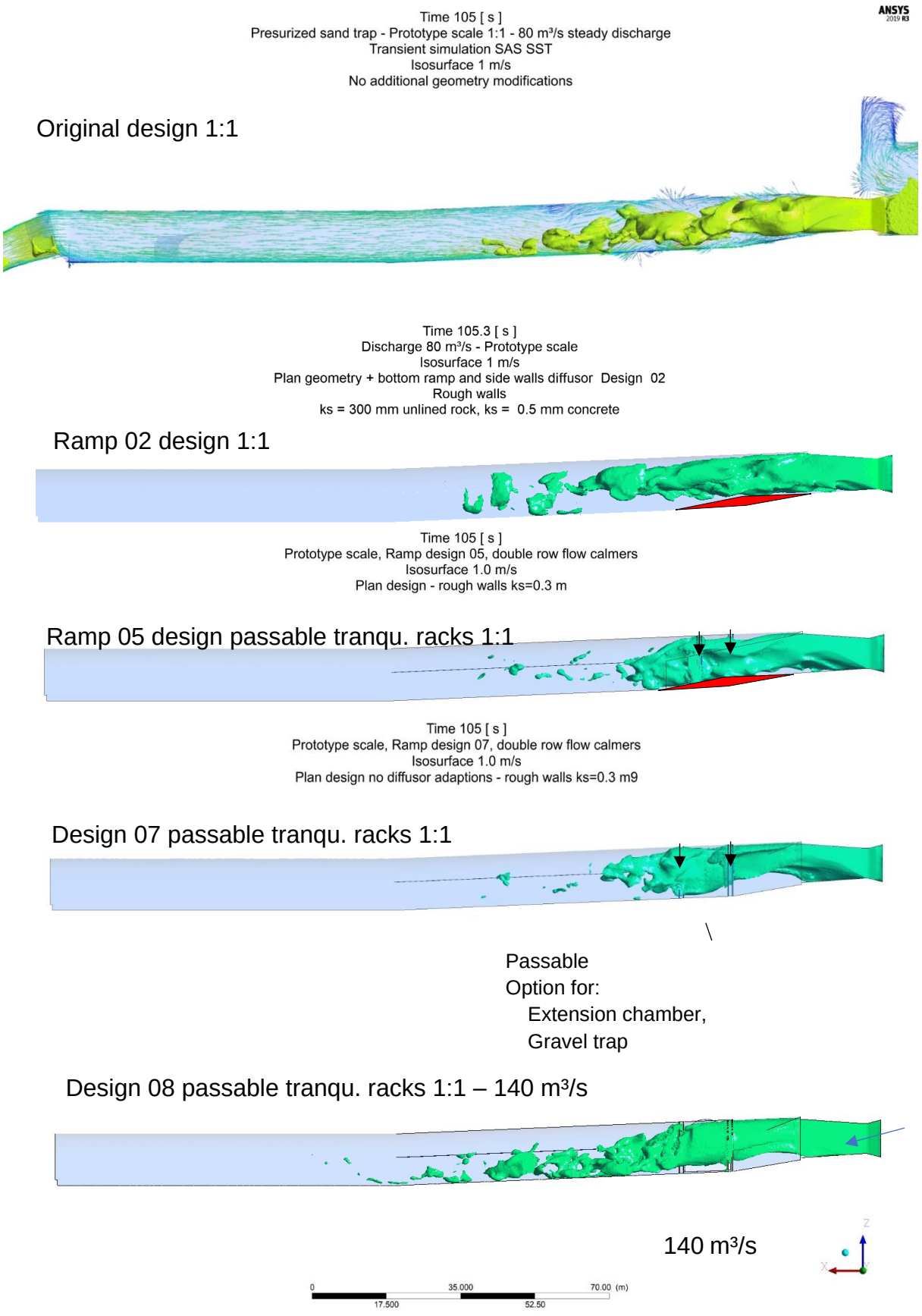

Figure 200: comparison of different design stages, isovolume 1 m/s

13. Surge tank extension and upgrade to with pump turbine

This chapter briefly investigates the possibility of adding the extension chamber directly to the sand trap chamber directly downstream of the diffusor. Previous investigations have shown that a discharge upgrade of about 25% in the pressure tunnel of Tonstad power plant is possible, which is about 60 m³/s. Further extrapolation of the upgrade aspect leads to the possible application of a reversible pump turbine as unit 6 Tonstad. Following this approach, Tonstad powerplant can be upgraded in power production and even allow negative grid regulation and significant pumping operation.

Therefore, an orthogonal attached chamber is proposed, allowing water flows in both direction; turbine flow and pump flow as well as hydraulic shortcut flow between unit 6 and unit 5. The design discharge of unit 5; 80 m³/s plus 60 m³/s for unit 6 = 140 m³/s design discharge in the headrace tunnel.

In the investigated approach the 140 m³/s need to pass the surge tank no.3 gate restriction. Further proposals for creating a direct connection from the extension chamber to the headrace tunnel can be very meaningful. The design of the proposal includes both a possible additional access tunnel and the further possibility to connect the extension chamber to the headrace tunnel.

13.1 3D CFD investigations

This chapter shows the results for the 3D CFD simulations for the attached expansion chamber.

60 m³/s to unit 6 – boundary condition 1

Figure 201 shows the streamlines for uniform inlet flow condition in turbine direction to unit 6 with double row flow rakes in the sand trap chamber no.3.

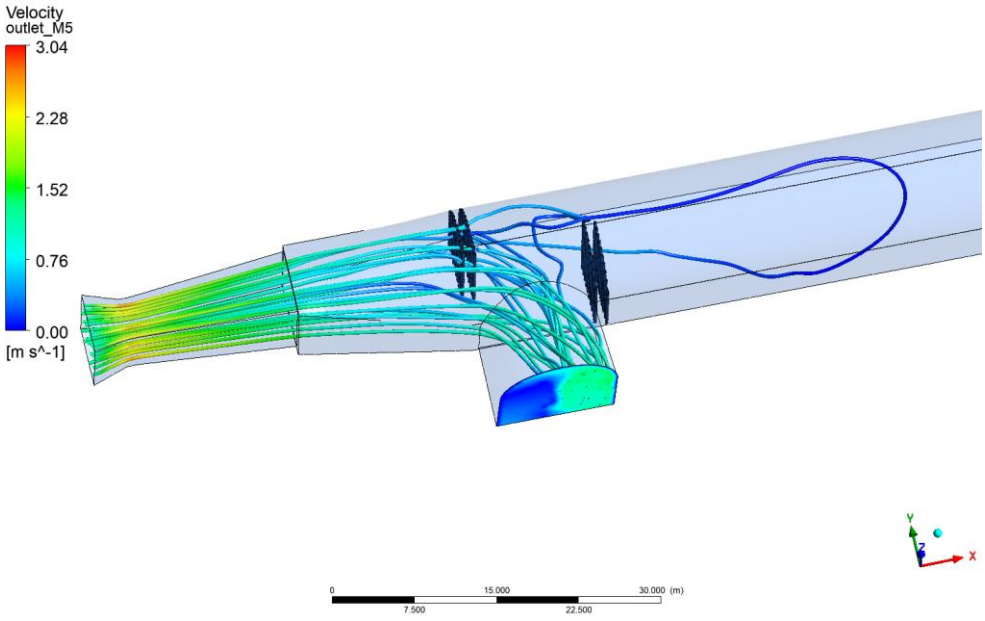

Figure 201: boundary condition 1, 60 m³/s outflow to unit 6

140 m³/s from the headrace tunnel inflow boundary condition

Figure 202 to Figure 204 show the boundary condition for 140 m³/s inflow to the sand trap. These simulations are undertaken to generate the boundary condition for 140 m³/s to be used as inlet condition for further simulations without the need to apply the approach flow directly.

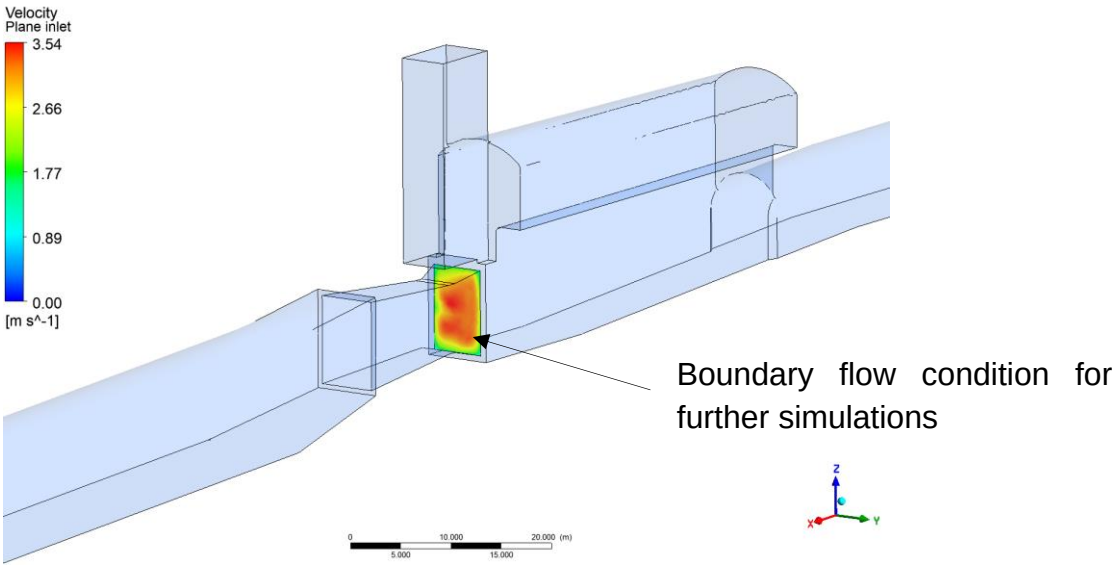

Figure 202: boundary condition 2, 140 m³/s inflow, simulation with approach flow geometry

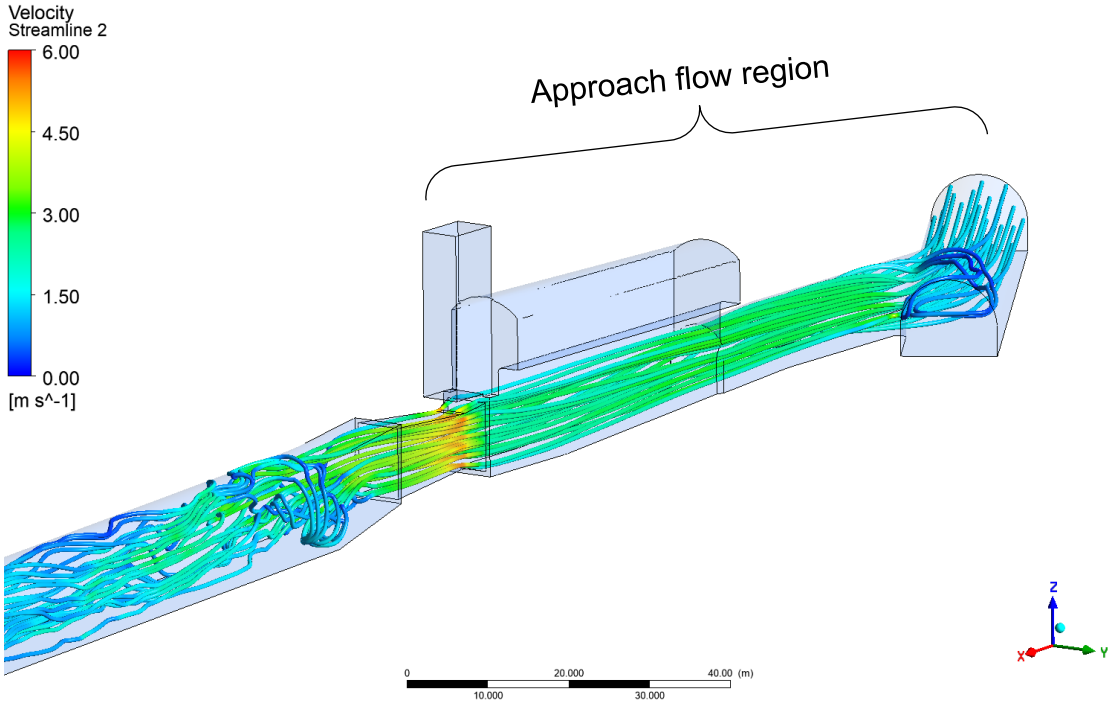

Figure 203: 140 m³/s inflow, simulation with approach flow geometry, streamlines

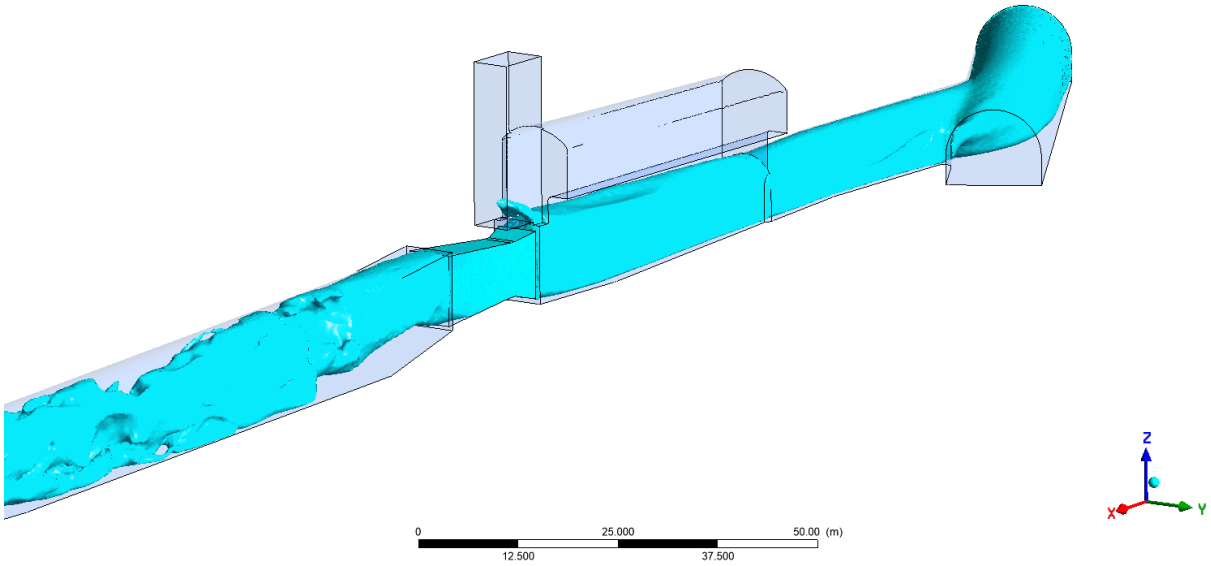

Figure 204: 140 m³/s inflow, simulation with approach flow geometry, 1 m/s isosurface

140 m³/s from headrace → 80 m³/s to unit 5, 60 m³/s to potential new unit

Figure 205 shows the result for the sand trap chamber of the inflow of 140 m³/s into the sand trap chamber with 60 m³/s diverted to unit 6 via the extension chamber. Isosurface flow velocity of 1 m/s and bottom wall shear is plotted. The geometry contains double flow rakes that are passable.

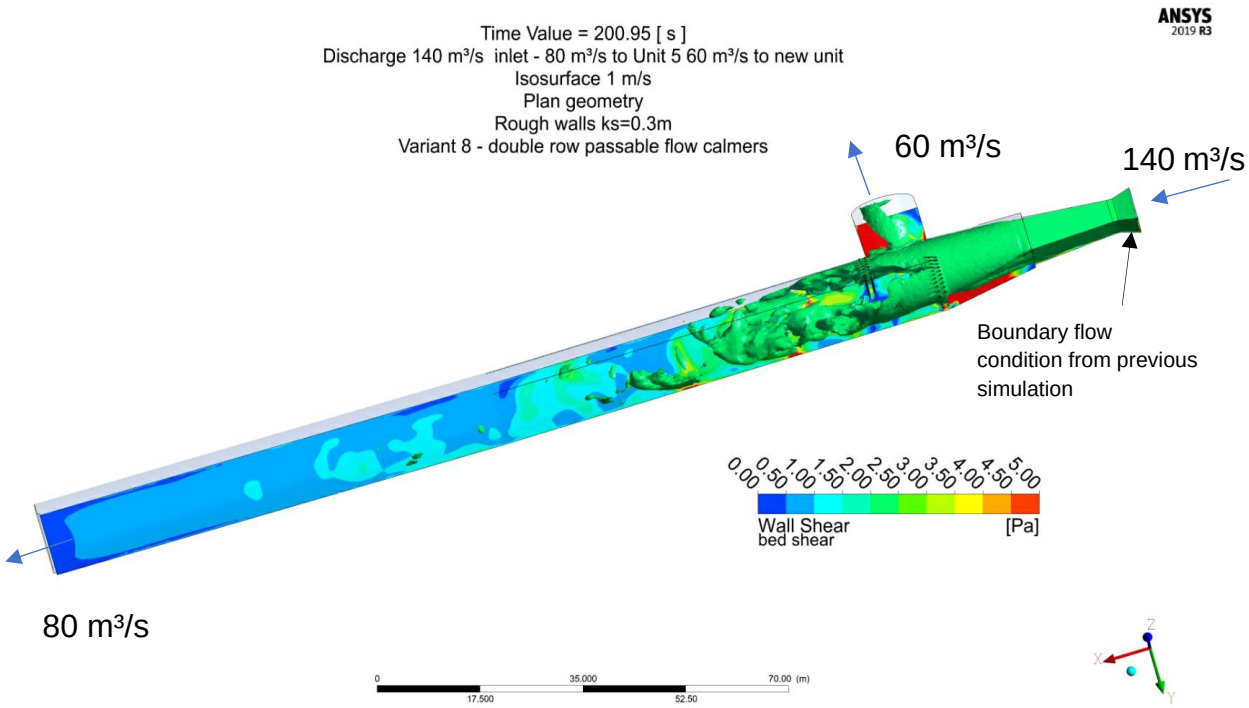

Figure 205: 140 m³/s from headrace, 80 m³/s to unit 5, 60 m³/s to new unit, isosurface 1m/s, bed shear stress

Figure 206 shows that the passable flow calmer works without bypassing the flow and thus the principal functionality of the passable rake design. However, in transient flow conditions the situation keeps very turbulent and complex.

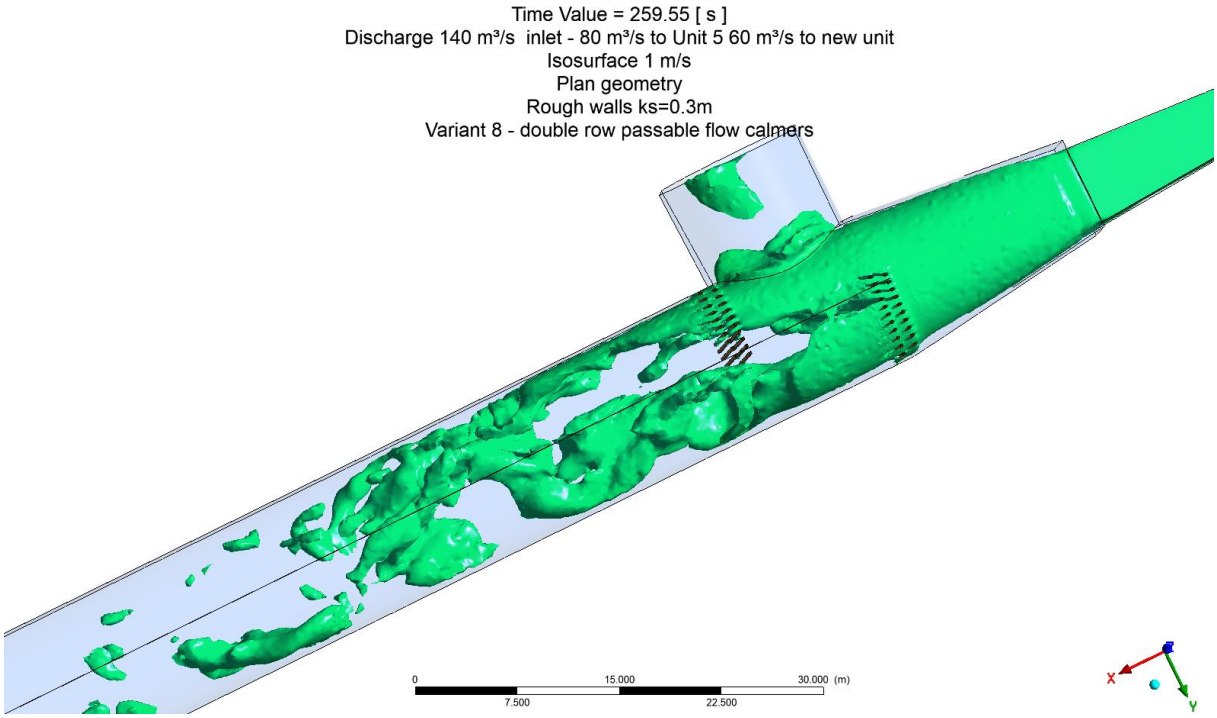

Figure 206: 140 m³/s from headrace, 80 m³/s to unit 5, 60 m³/s to new unit, isosurface 1m/s, detail

Figure 207 shows the particle tracking simulation for the situation as shown above. Obviously even larger particles are transported directly as suspended flow over the weir with having the flow calming rakes. Later in physical model test it was confirmed that with the rakes the sand trapping effect was even lower as without.

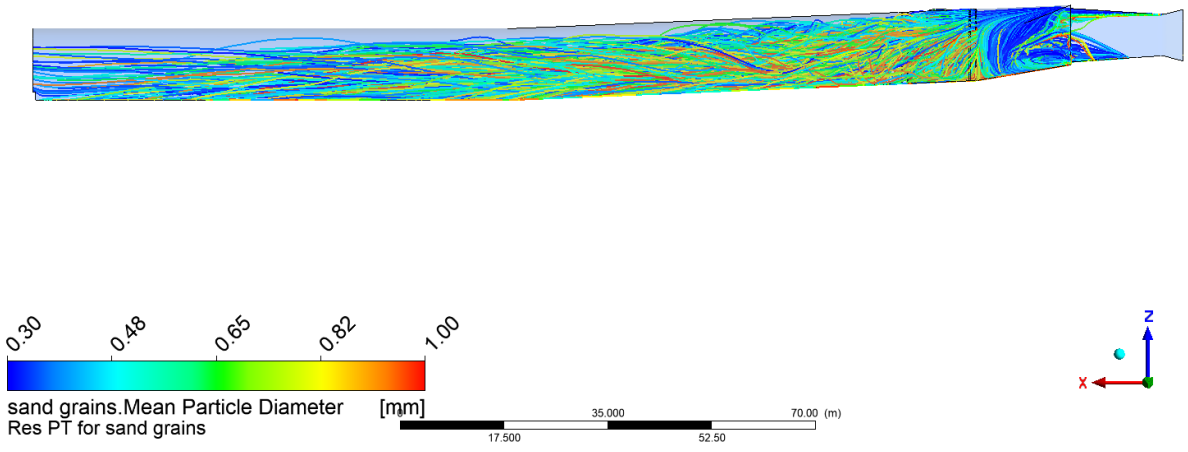

Figure 207: 140 m³/s from headrace, 80 m³/s to unit 5, 60 m³/s to new unit, sediment particle transportation

14. Model test in flume 1:36.67

The aim of the investigations is to improve the sedimentation process and the possibility to remove the these automatically. To sustain the hydraulic investigations the physical model test in scale 1:36.67 is a main part of the present report. Figure 208 shows the physical model test with its parts and the PIV systems installed. Arrows indicate the flow direction and the admission of sediment probes. The walls of the sand trap are represented as the glass walls of the flume. The flow is pressurized by constraining crown elements. The free surface is indicated in Figure 208.

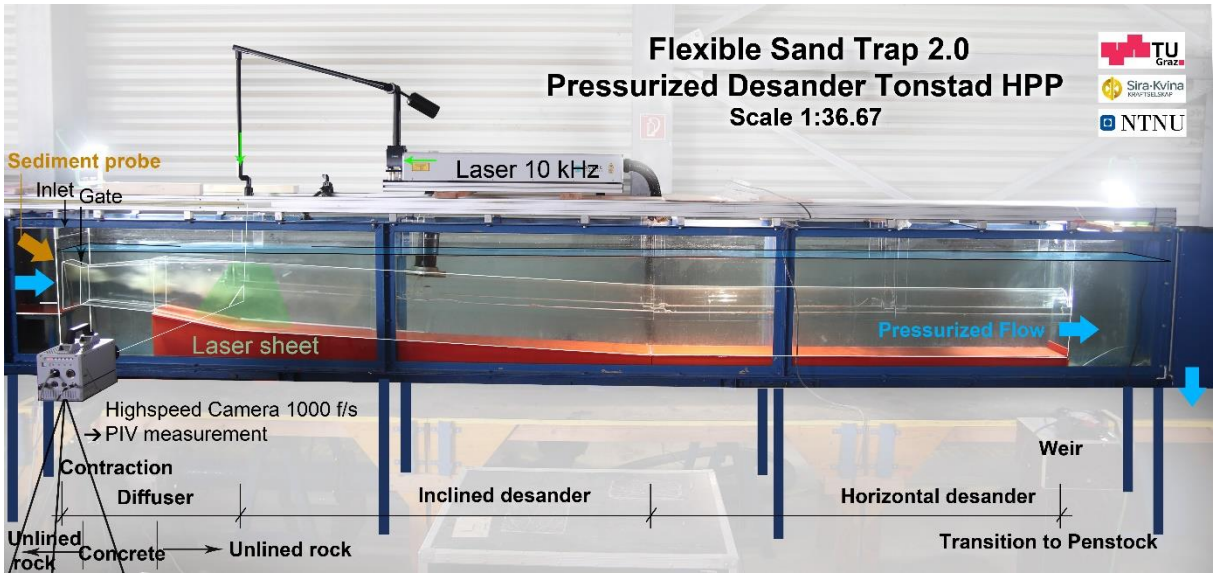

Figure 208: Model test of pressurized sand trap in the flume, scale 1:36.67, equipped for PIV measurements

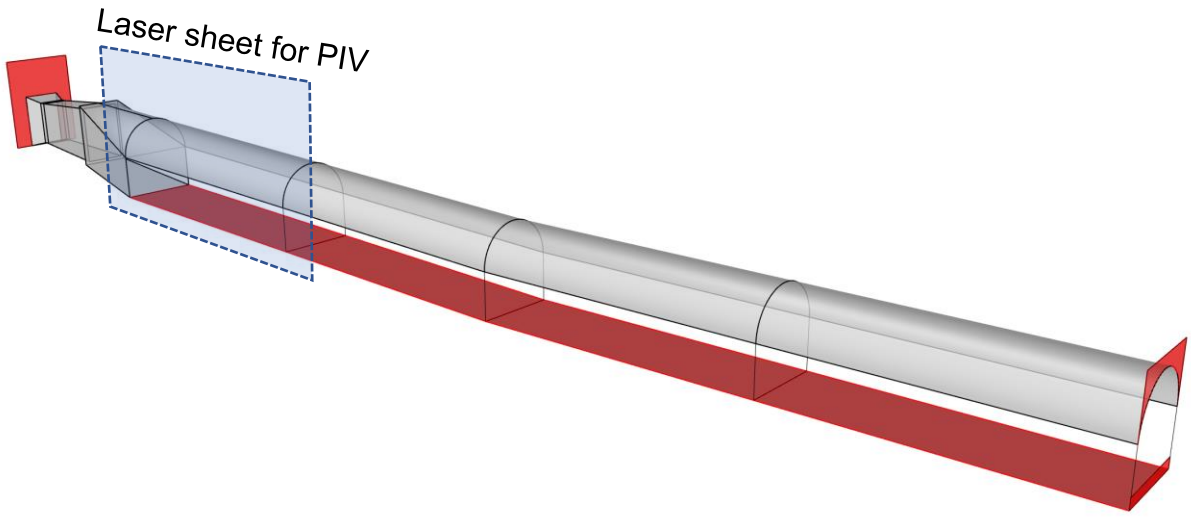

Figure 209: 3D design of the sand trap in the flume model test at TU Graz

Figure 210 shows the plexiglass diffusor for the model test and the wood mold.

Figure 210: 3D geometry realization in plexiglass 1:36.67

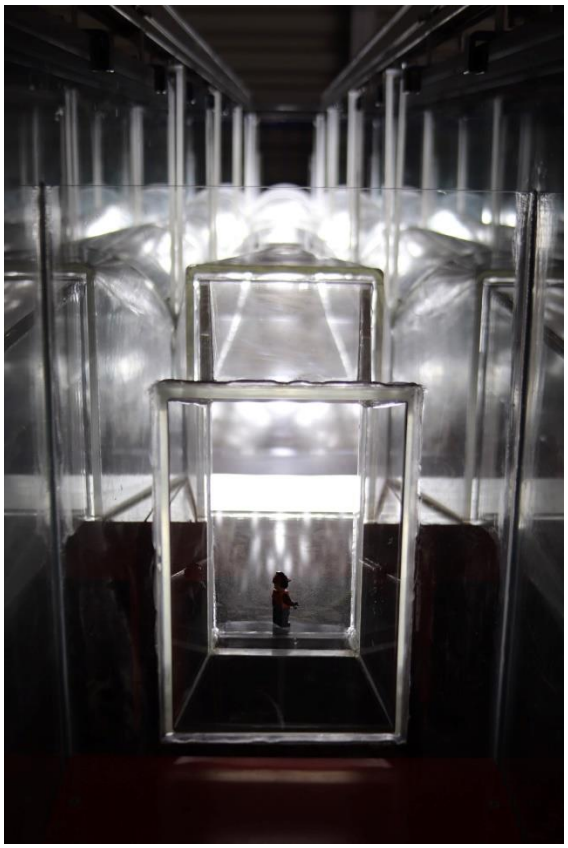

Figure 211: Plexi glass model 1:36.67 with Lego person as human scaling

14.1 **PIV measurements**

PIV measurements are undertaken to understand the turbulent flow pattern of the jet coming from the gate restriction entering the sand trap chamber. The measurements demanded high efforts for the equipment and the measurements. The full picture of the investigations is approached by the combination of investigation methods such as the model test with prototype sediments supported with PIV and 3D CFD simulations with particle tracking.

Figure 212 shows the measurement principle of the PIV.

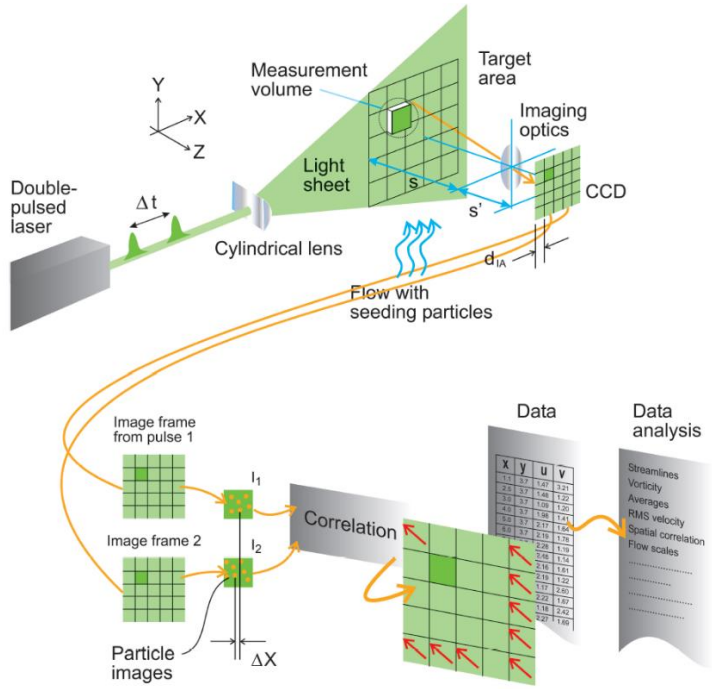

Figure 212: Principle of PIV (*Dantec Dynamics*)

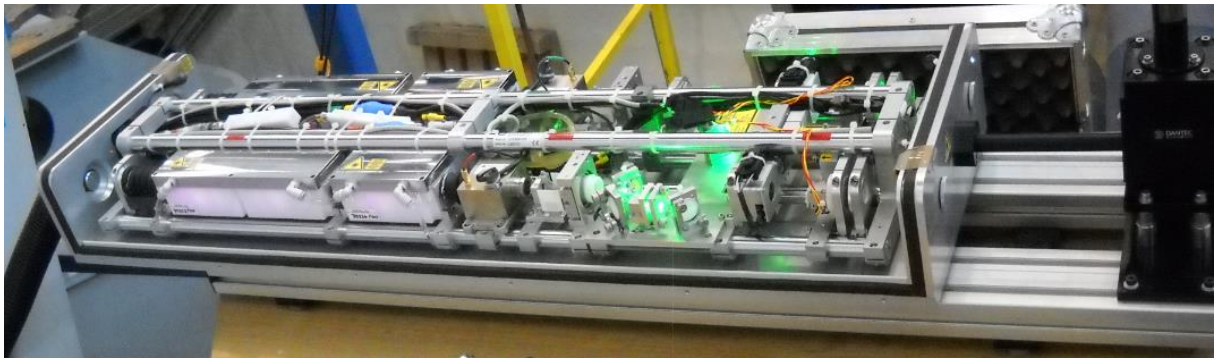

Figure 213: Double laser canon, class 4 laser

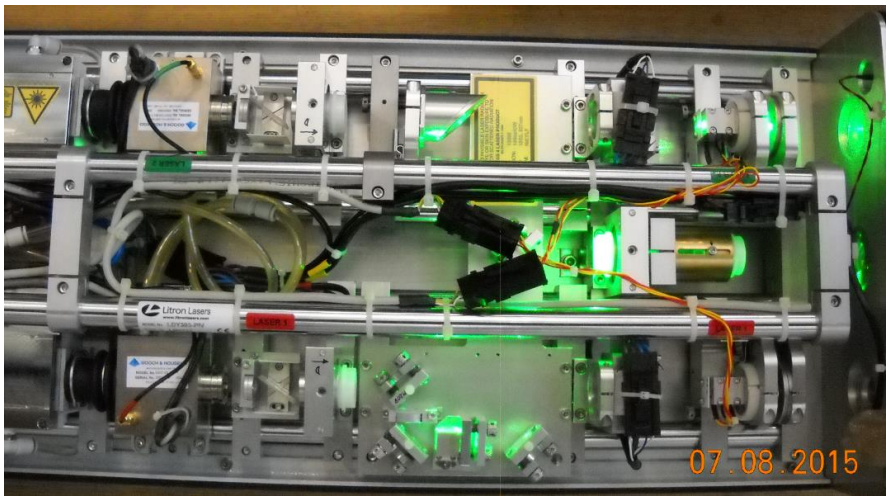

Figure 214: Double laser canon, class 4 laser, only left laser in operation

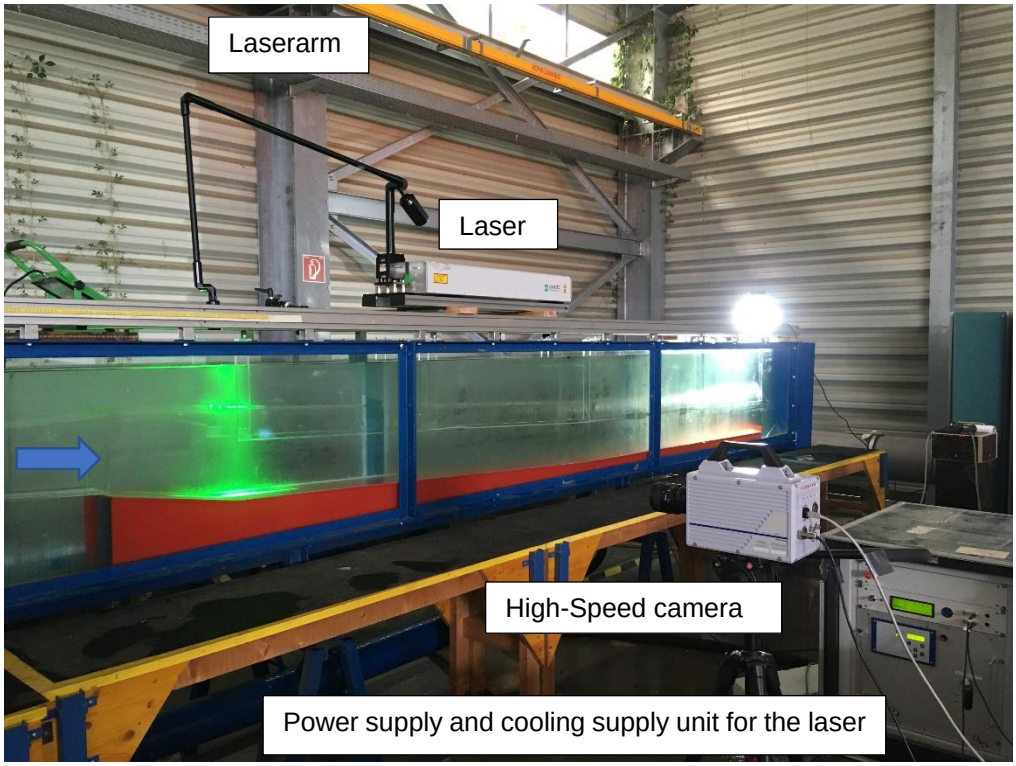

Figure 215: PIV equipment in operation

14.2 **PIV results**

Figure 216 shows the two investigated PIV positions; Pos. 1 at the end of the diffusor section and Pos. 2 in the center of the flat sand trap section upstream of the weir.

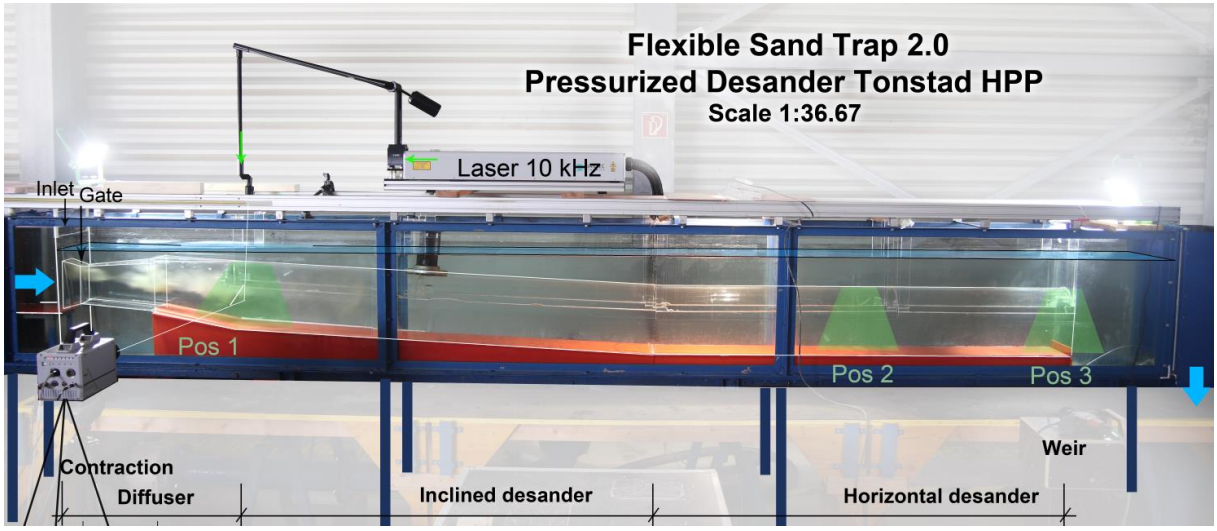

Figure 216: Pos 1, Pos 2, Pos 3 in flume with pressurized sand trap

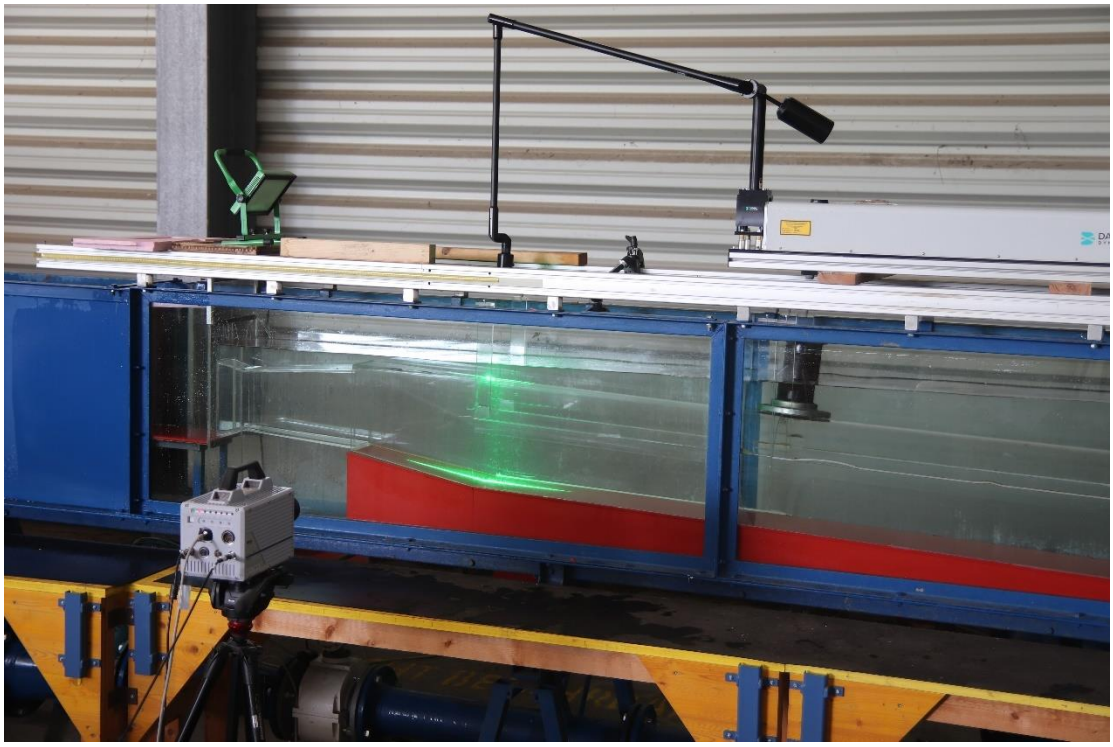

Figure 217: PIV Pos. 1

Figure 216 shows the defined Pos. 1, Pos. 2 and Pos. 3 to investigate the flow with the PIV system

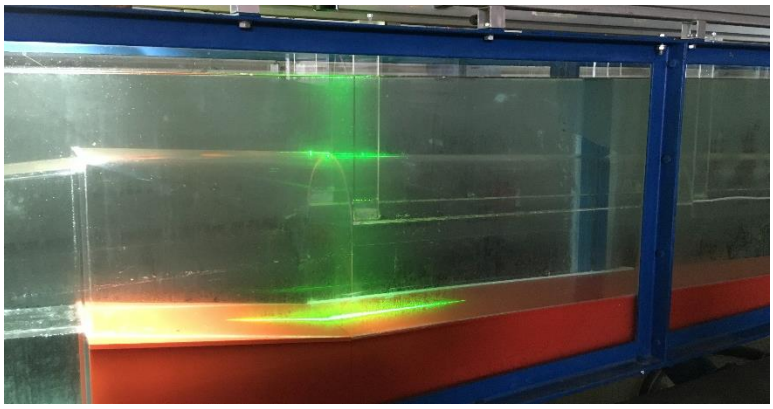

Figure 218: Pos 1, transition section

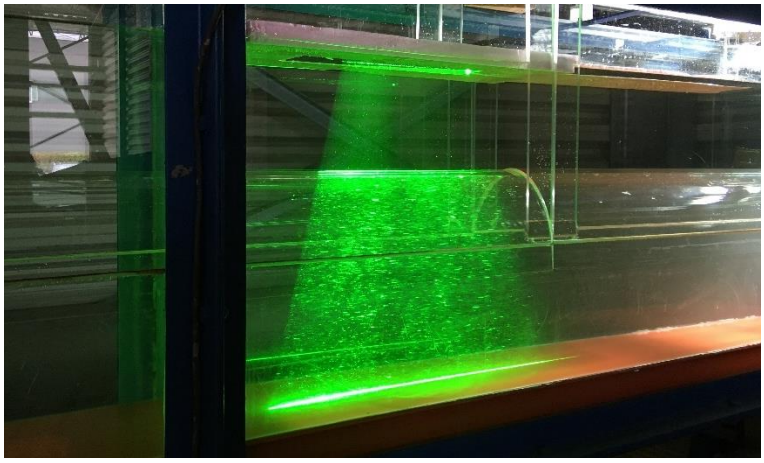

Figure 219: Pos 2, middle section of flat gallery part

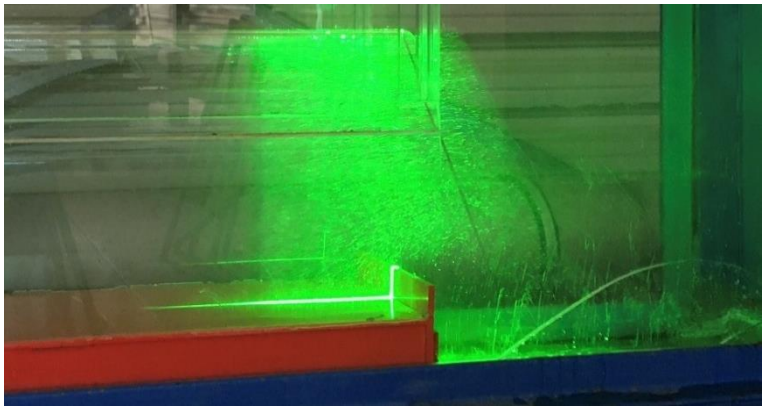

Figure 220: Pos. 3, weir section

Note: The measurements with PIV has encountered several challenges by the equipment. Thus, Pos.3 could not be fully investigated. However, since Pos. 1. and 2. are in very good correlation with the 3D CFD the PIV measurements are seen as a confirmation of 3D CFD.

Results from PIV measurements at the sand trap diffusor (Pos. 1) are showing that the jet from the gate restriction separating the flow section into an upper part and a recirculation zone at the bottom. Figure 221 shows that velocities in the jet, at the higher limit prototype discharge of 80 m^3/s (60 l/s in the model test), are reaching 2 m/s. In the lower part of the cross section is visible recirculation zone. Turbulences are lifting the sand from bed load into the jet zone to support movement further downstream in the sand trap. The flow restriction from the gate is creating a catapult effect for the sediments. Related to the Figure 133, physical model is confirming the results from the CFD simulations.

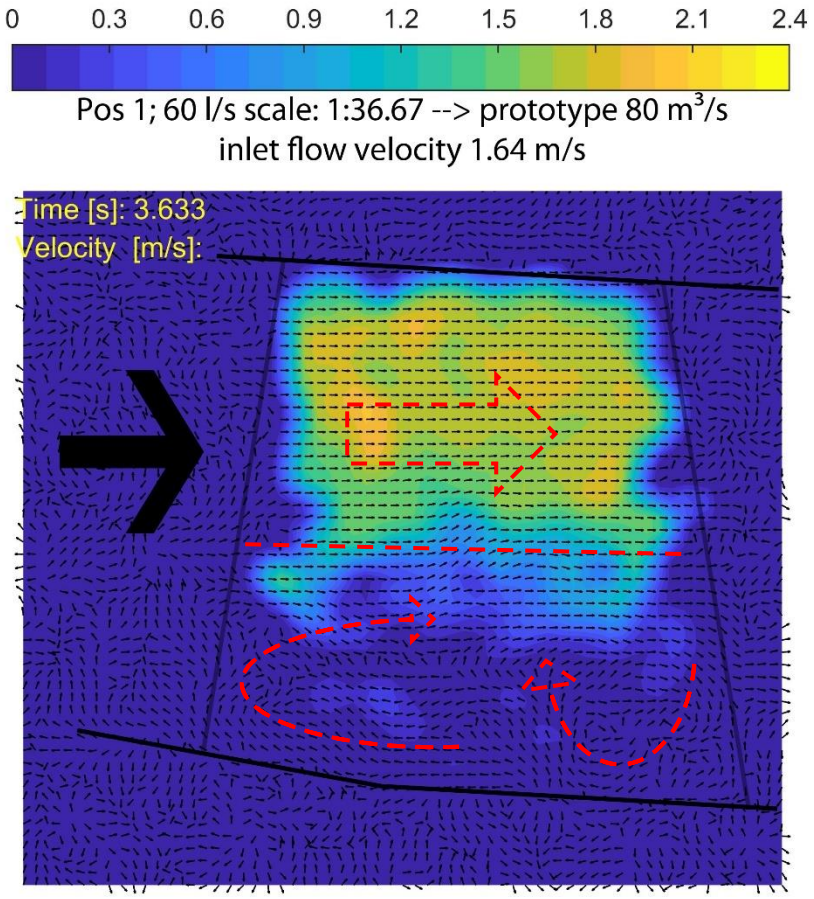

Figure 221: Flow velocity at the position 1, model discharge 60 l/s

At Pos. 2, as Figure 222 is indicating, the velocities are lower, reaching 1.3 m/s at the higher limit prototype discharge of 60 l/s (80 m^3/s in the prototype). In this section, the jet is not stable and is oscillating between the crown to the bottom of the cross section.

Tests with the lower limit discharge of 41 l/s (in prototype 55 m^3/s), are showing the same flow pattern and confirming the behaviour of the jet. Figure 223 shows that the velocities during the lower limit discharge are reaching 0.6 m/s.

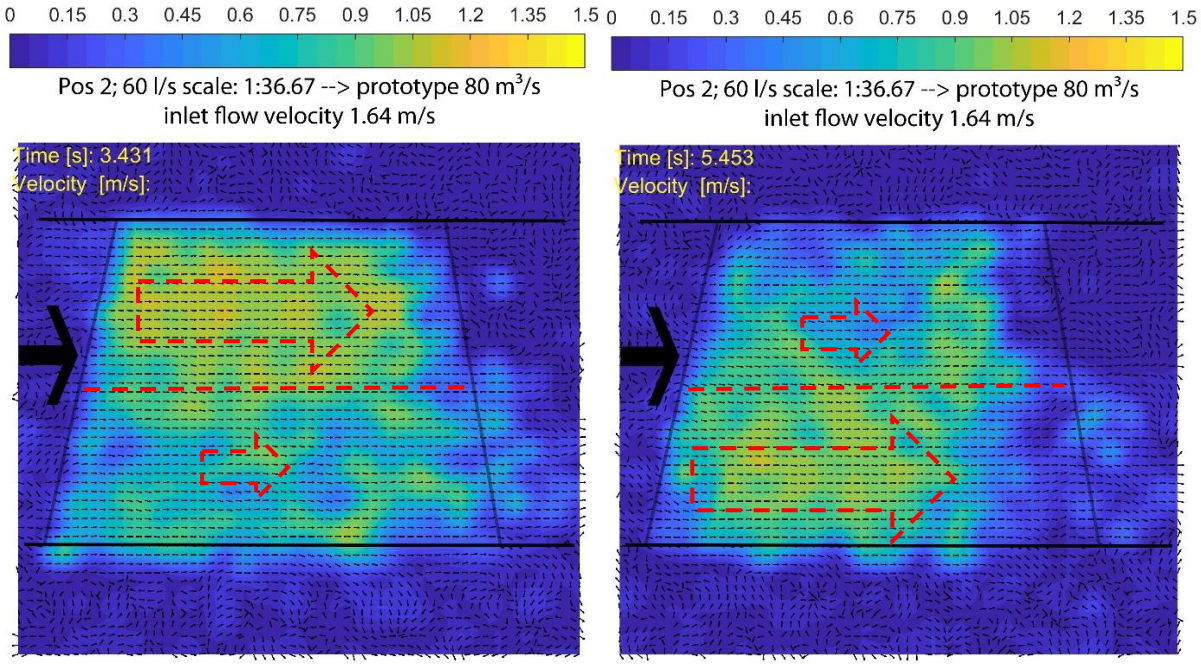

Figure 222: Flow velocity at the position 2, model discharge 60 l/s

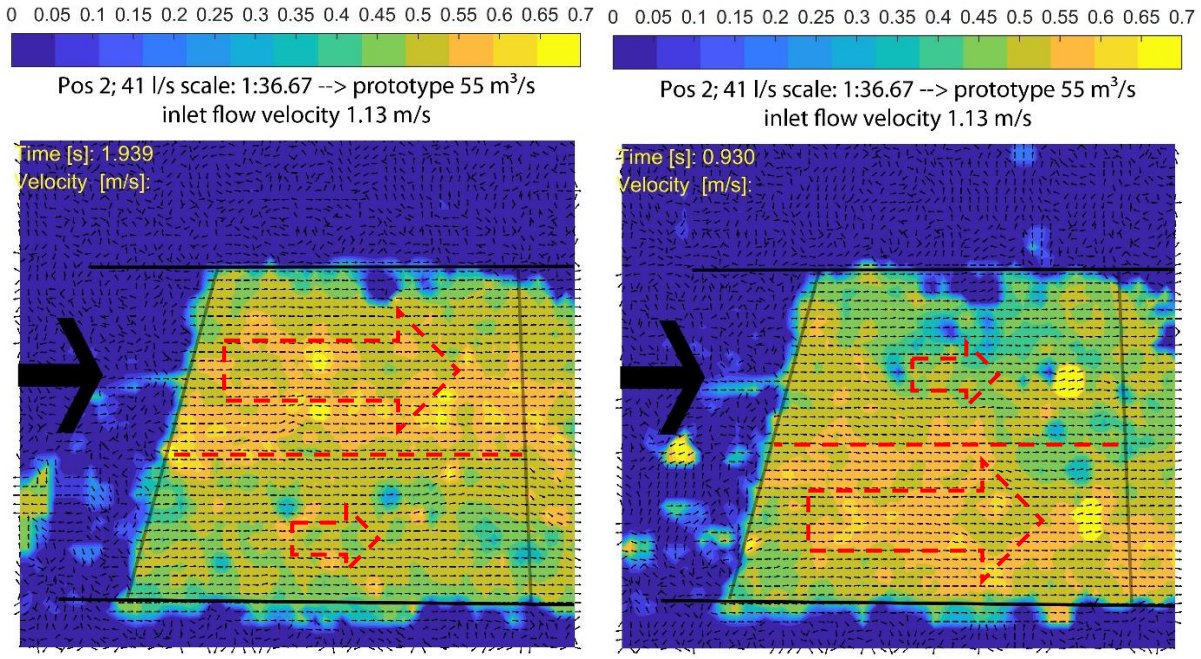

Figure 223: Flow velocity at the position 2, model discharge 41 l/s

The oscillation of the jet and this pattern throughout the whole length of the sand trap chamber is found as the reason for high flow and high shear forces on the bottom transporting and resuspending sediments that mitigate the trapping effect of the sand trap.

14.3 **Local loss in flume**

Due to reason of running the model test with 1:1 velocity also the local loss of the jet dissipation is equal to the prototype.

14.4 **Original plan design**

For the original plan design a local loss of 12 cm water column is measured.

With the hydraulic parameters:

- flow section in the sand trap of 120 m²
- discharge 80 m³/s
- flow velocity in the chamber of 0.67 m/s
- local loss of 0.12 m mwc

Local loss = $\zeta * v^2/2g$

ζ = 5.3 [-] … local loss factor of the restriction, without the friction loss of the unlined wall in the chamber

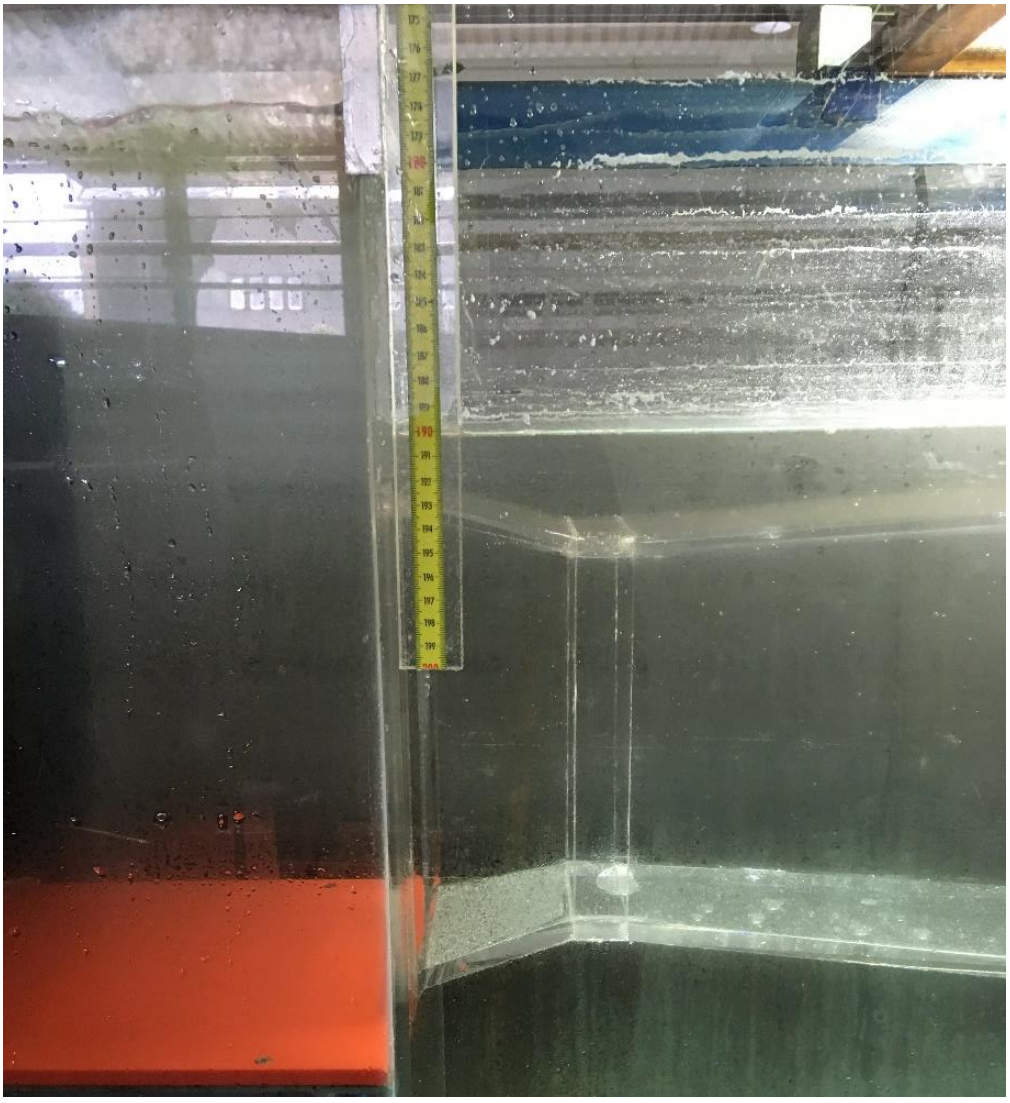

Figure 224: 12 cm head loss for 60 l/s, prototype velocity for 80 m³/s

14.5 Sand flow investigations

This chapter describes the investigation of the sand transport in the sand trap of Tonstad power plant and the investigations in the 1:36.67 scaled small-scale hydraulic model test.

14.5.1 Sand situation in the prototype

Figure 225 and Figure 226 show the situation in the prototype. Sediments are deposited unevenly in the chamber. Coarse and fine material in the rear part near the end of the diffusor and sand material at the weir. The concrete bottom appears clean from sediments in large portions. These aspects lead to the conclusion that especially sand is transported over the whole length of the sand trap.

Email Havrevoll O. 2020 06 29 referring to Figure 19: *The dotted lines are from 2020. They fit nicely in the pattern that was evident already in 2018. Also, I've included a line with a weighted average of the sediments from 2020. The coarse material amounted to 80 m³ and the fine material to 20 m³, so I added all the samples and made a new curve, but multiplied the mass of the coarse samples by 4. This is the thick black dot-dash-line.*

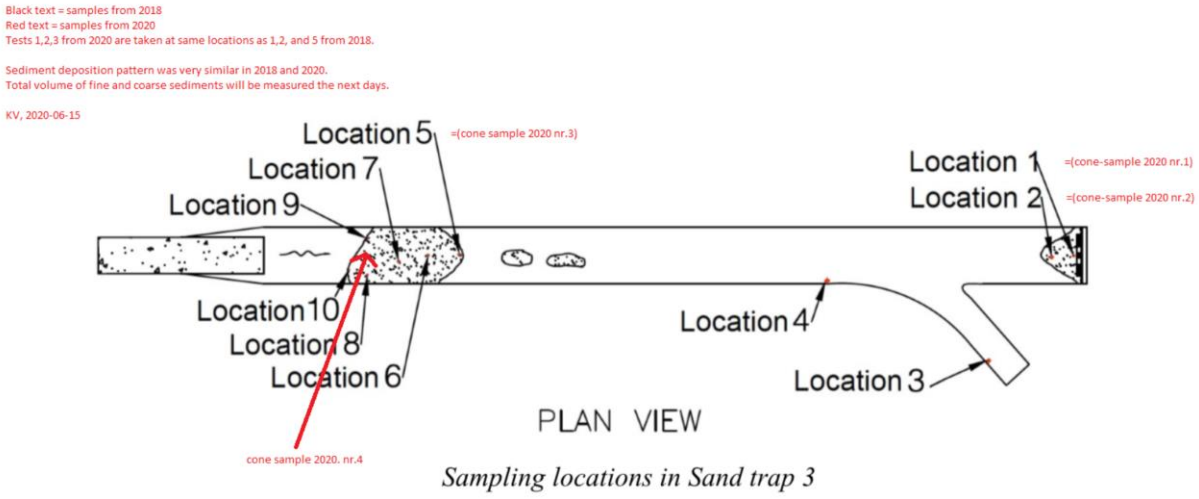

Figure 225: sediment specimen for the sieve curves, sediment deposits in prototype

Figure 226: sediment deposits in the prototype sand trap

14.5.2 **Sediment scaling**

The sediments are scaled 1:1, to achieve this, the flow velocities in the flume model are also kept at 1:1 magnitude as described in the chapter (8.4), boundary conditions. The sand grain distribution is 0.3 mm to 1.0 mm grain size of quartz with a raw density of 2650 kg/m³.

Figure 227 shows the sand grains applied in the model test for all test runs.

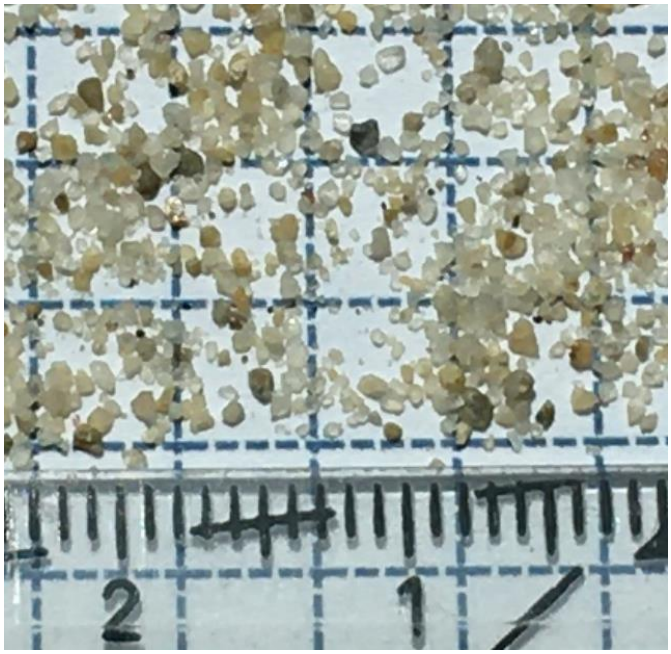

Figure 227: Sediment 0.3 – 1.0 mm quartz grains

14.5.3 **Model test discharges**

The sand flow investigations are basically utilized by three different discharges that are derived from a discharge plot from the power plant operation of Tonstad (Figure 228). These discharges are scaled to the 1:36.67 model test by velocity equality to prototype, using the scaling numbers as described in chapter 8.4.

A) Upper limit discharge: 80 m³/s / 1342 [-] → 59.6 l/s

B) Mean discharge: 65 m³/s / 1342 [-] → 48.4 l/s

C) Lower limit discharge: 55 m³/s / 1342 [-] → 41 l/s

In this report the values of 59.6 l/s and 48.4 l/s are equally meant by 60 l/s and 48 l/s. However, the IDM does have about 1% range of fluctuation.

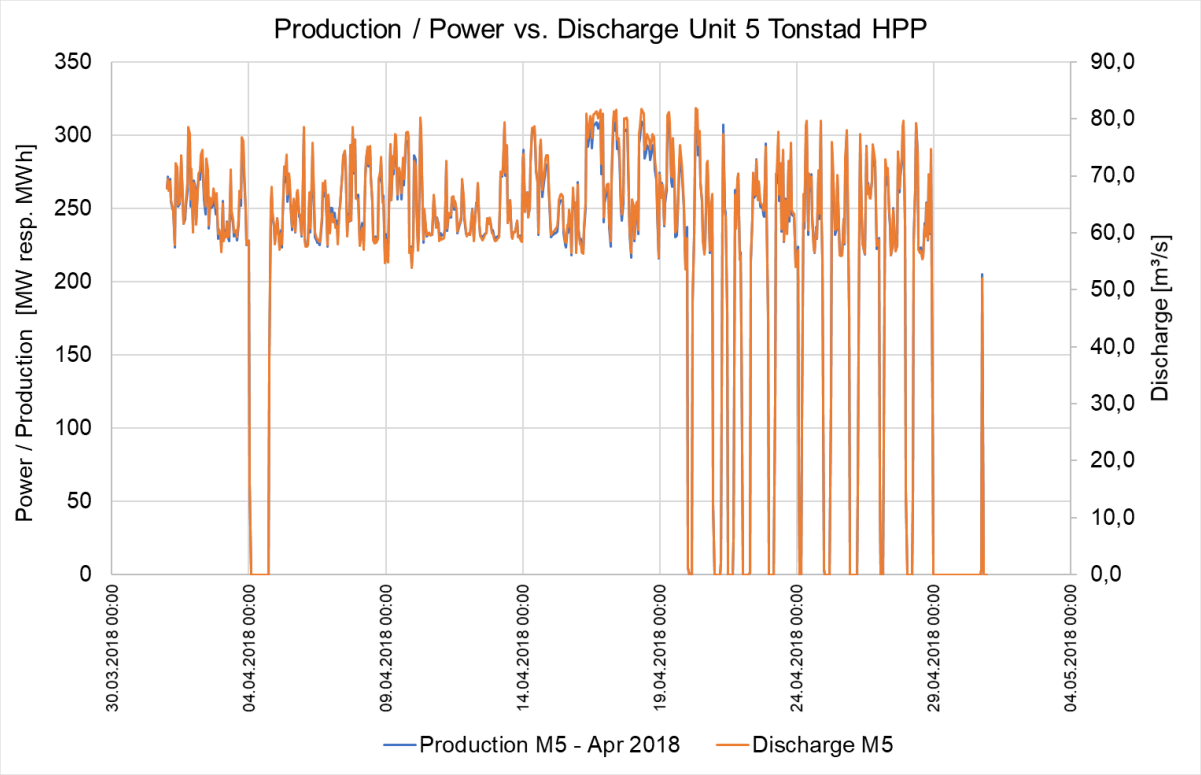

Figure 228: Observed Power output and assumed discharge of unit 5

14.5.3.1 Upper value of observed discharge; 59.6 l/s

This chapter shows the movement of 0.5 l of sand in the model test, it is shown that 100% of the probe is transported through the sand trap chamber and over the weir.

Table 19: Parameters of model run 59.6 l/s

Sand grain	0.3 mm – 1.0 mm	Prototype time scale: 36.67 sand emptying	180*36.67 = 6600 s → 1.8 h
Discharge	59.6 l/s	Water discharge prototype	80 m³/s
Time of flow	3 min =	Sand amount, model	0.5 l
		Sand amount, prototype	0.5 * 36.67^3= 24 655 l → 24.65 m³

The amount of 0.5 l of sand is flushed in 3 minutes, resp. 14.65 m³ is flushed in 1.8 h in the prototype. The sand is accumulating at the weir, fluctuating vortices lift the sediment in varying concentration over the weir.

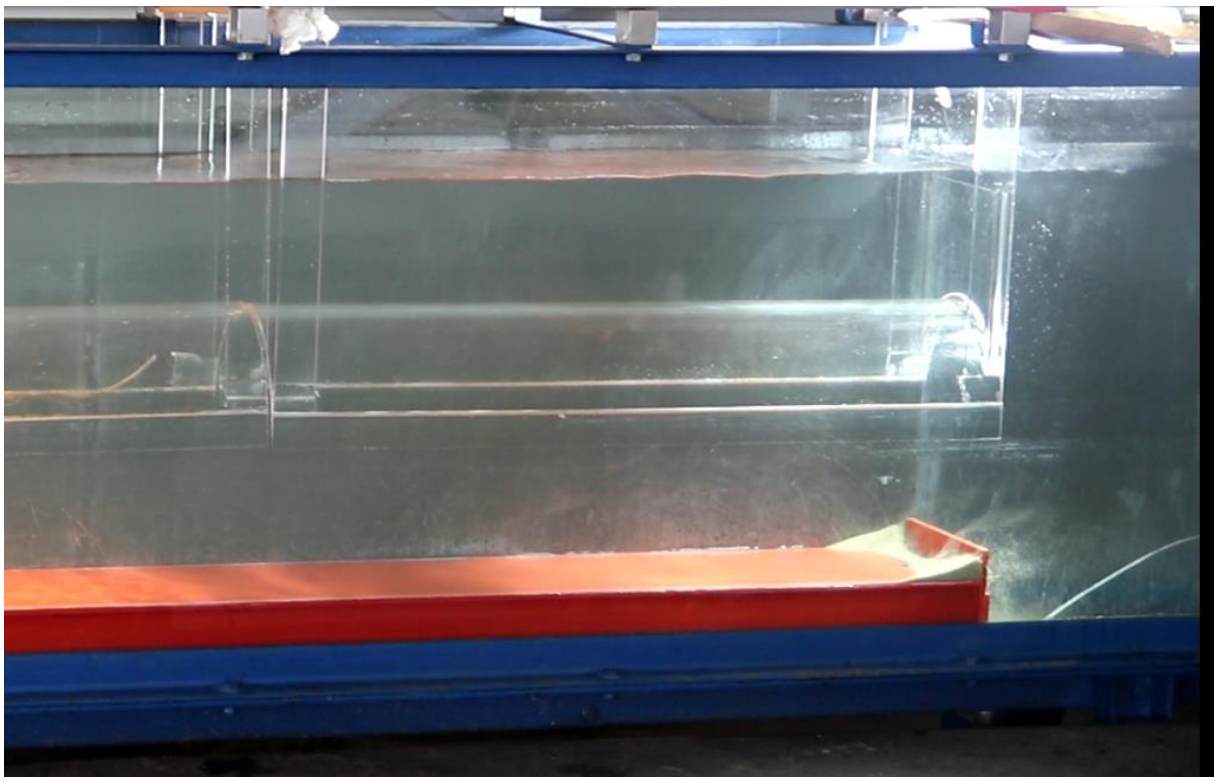

Figure 229: Discharge 59.6 l/s, sand inflow 0.5 L, sand overtopping weir downstream, snapshot

14.5.3.2 Mean value of observed discharge; 48 l/s

Also, for 48 l/s 100 % of the sand is flushed through and overtopping the weir.

Table 20: Parameters of model run 48 l/s

Sand grain	0.3 mm – 1.0 mm	Prototype time scale: 36.67 sand emptying	820*36.67 = 30,070 s → 8.35 h
Discharge	48 l/s	Water discharge prototype	65 m³/s
Time of flow	13 min 40 s = 820 s	Sand amount, model	0.5 l
		Sand amount, prototype	0.5 * 36.67^3= 24 655 l → 24.65 m³

➔ No difference between sand from above or from bottom inflow

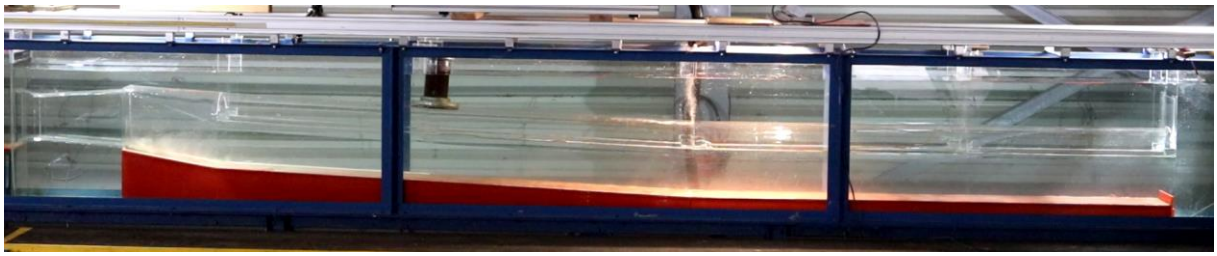

Figure 230: Discharge 48 L/s, sand inflow 0.5 L, sand storm in diffuser, snapshot 17s

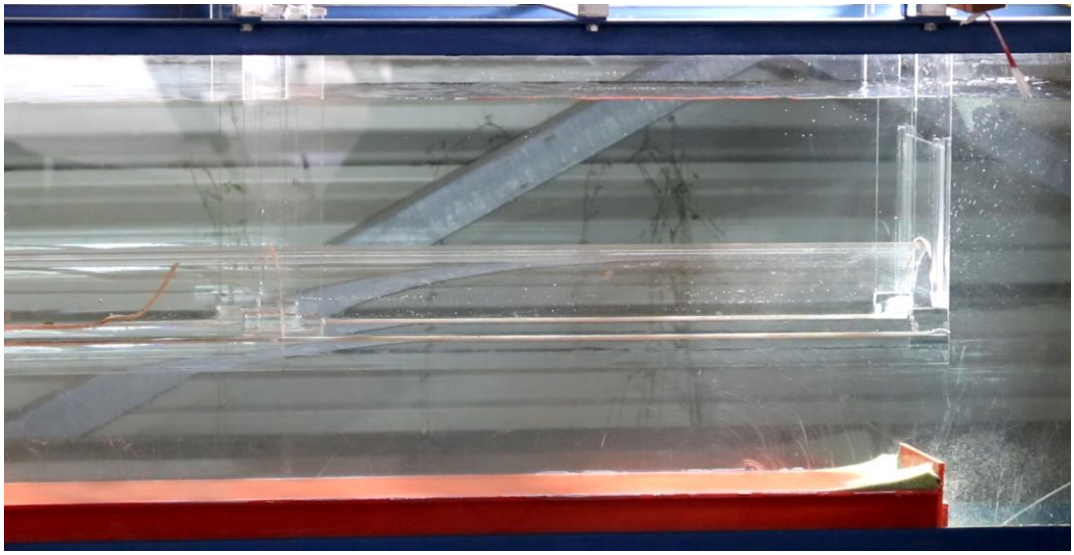

Figure 231: Discharge 48 L/s, sand inflow 0.5 L, sand overtopping weir downstream, snapshot 6 min 50 s

Fully emptying over time in about 8.35 h in prototype, about 25 m³. Sand density of 0.045 L_{sand}/L_{water}.

➔ Assumptions: A constant sand inflow is given in the prototype and the found amount is a fraction of the sand transported over time

14.5.3.3 Low value of observed discharge; 41 l/s

Also, for the lower bound of 41 l/s, representing 55 m³/s prototype flow, the sand is fully flushed through. However, the time span to flush the 0.5 l is significant longer as for the upper bound discharge of 60 l/s.

Table 21: parameters of model run 41 l/s

Sand grain	0.3 mm – 1.0 mm	Prototype time scale: 36.67 sand emptying	2160*36.67 = 79 207 s → 22 h
Discharge	41 l/s	Water discharge prototype	55 m³/s
Time of flow	36 min = 2160 s	Sand amount, model	0.5 l
		Sand amount, prototype	0.5 l * 36.67^3= 24 655 l → 24.65 m³

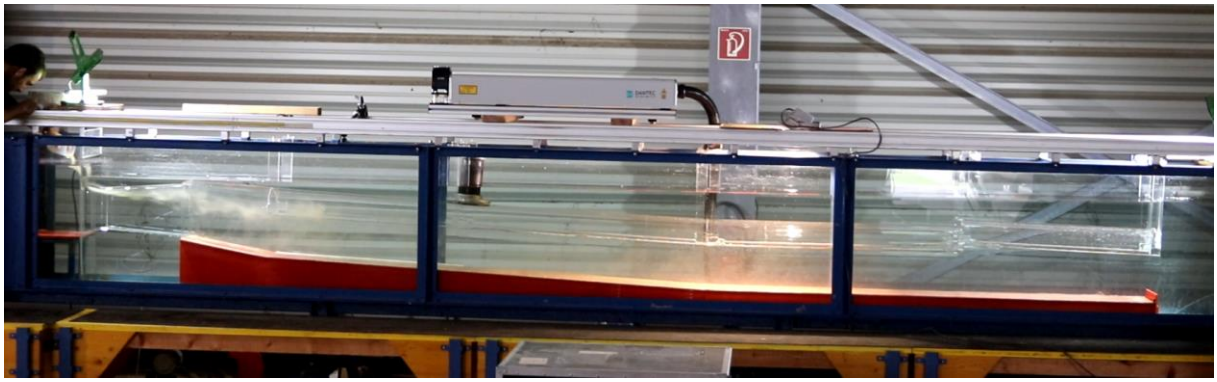

Figure 232: Discharge 41 L/s, sand inflow 0.5 L, sand from above, snapshot 21 s

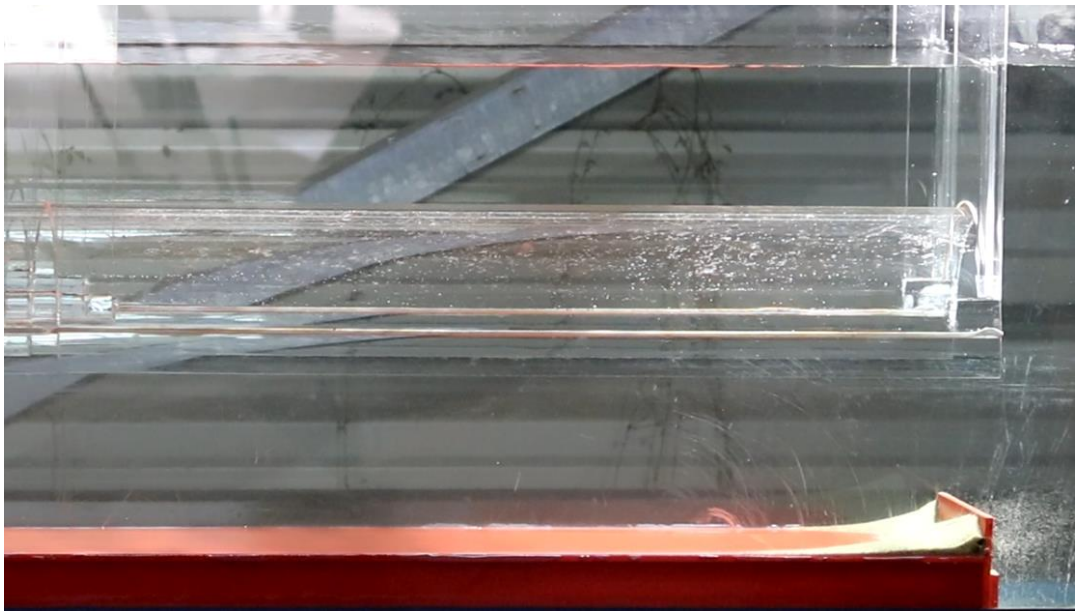

Figure 233: Discharge 41 L/s, sand inflow 0.5 L, sand overtopping weir downstream, snapshot

Figure 234 is from the model test and Figure 235 in the prototype. The discharge and the sediment concertation of the flow in the prototype is unknown. However, the pictures show very comparable results and sustain the model test approach with 1:1 scaled sediment and 1:1 Scaled flow velocities.

Figure 234: Discharge 41 L/s, sand inflow 0.5 L, sand overtopping weir downstream, snapshot

Fully emptying over time in about 22 h in prototype, about 25 m³. Sand density of 0.02 L_{sand}/L_{water}.

Figure 235: Sediments in the prototype at the bottom before the rake to the pressure shaft (picture: Sira Kvina)

14.5.4 Sand flow investigations with heightened weir

Investigations are made to check the effects of downstream weir heightening. Factor of 2 [-] (double) and 3 [-] (triple) are investigated.

14.5.5 Weir height test- double

To investigate the influence of the weir on the sand flushing, it is heighted by the factor of 2 [-] from to 3.5 cm to 7 cm resp. in prototype scale from 1.3 m to 2.6 m (Figure 236).

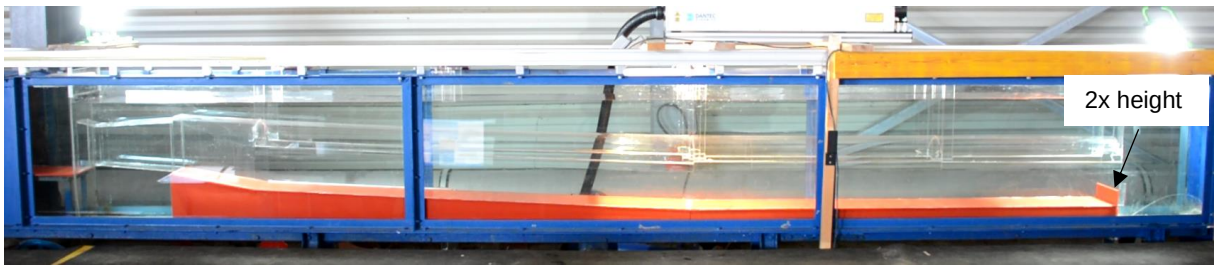

Figure 236: Geometry of double weir height

14.5.5.1 High value of observed discharge; 59.6 l/s – double weir height

The investigation shows that 100% of the sand probe is flushed, but it takes by the factor of 2.6 [-] longer as for the weir height 1.0 [-].

Table 22: Parameters of model run 59.6 l/s

Sand grain	0.3 mm – 1.0 mm	Prototype time scale: 36.67 sand emptying	460*36.67 = 16'868 s → **4.68 h** Time factor to 1.0 weir height: 4.68 / 1.8 = **2.6 [-]**
Discharge	59.6 l/s	Water discharge prototype	80 m³/s
Time of flow	7 min 40 s = **460 s**	Sand amount, model	0.5 l
		Sand amount, prototype	0.5 * 36.67^3= 24 655 l → 24.65 m³

Figure 237 shows the strong vortices at the wall corners upstream of the weir, that is very effectively lifting sediments over the weir.

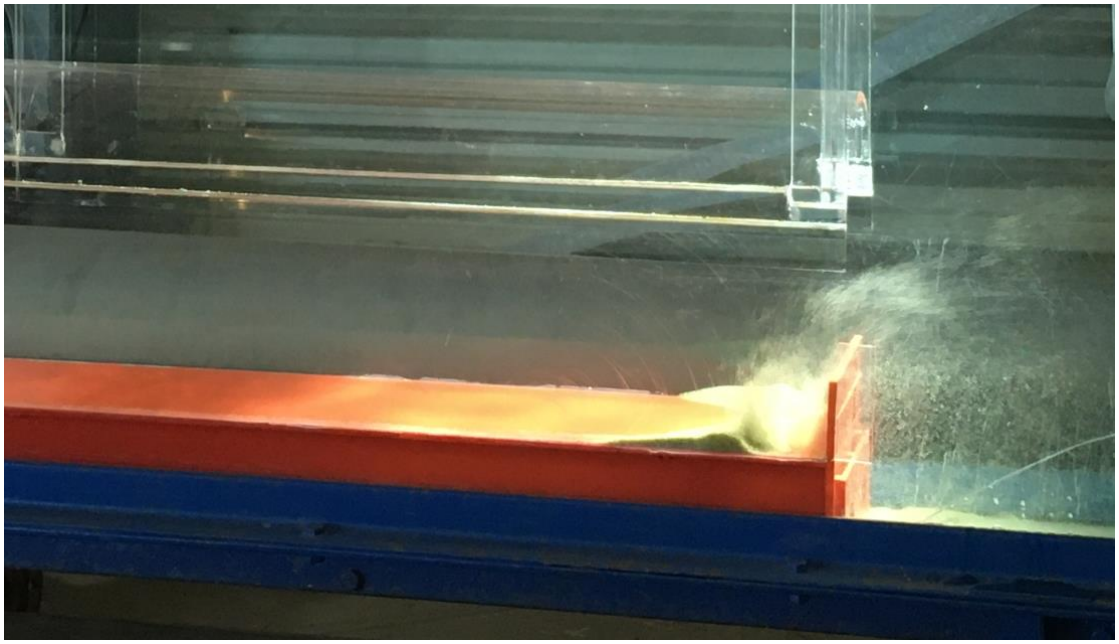

Figure 237: Discharge 59.6 L/s, weir height 2.0 [-], sand inflow 0.5 L, sand overtopping weir downstream, snapshot

14.5.5.2 Mean value of observed discharge; 48 l/s – double weir height

Table 23: parameters of model run 48 l/s

Sand grain	0.3 mm – 1.0 mm	Prototype time scale: 36.67 sand emptying	1200*36.67 = 55'005 s → 15.27 h Time factor to 1.0 weir height: 15.27 / 8.35 = **1.8 [-]**
Discharge	48 l/s	Water discharge prototype	65 m³/s
Time of flow	25 min = 1500 s	Sand amount, model	0.5 l
		Sand amount, prototype	0.5 * 36.67^3= 24 655 l → 24.65 m³

Figure 238 shows in a sequence the creation of the vortex flow that lifts very effectively sediments over the weir. The vortices occur in a certain frequency.

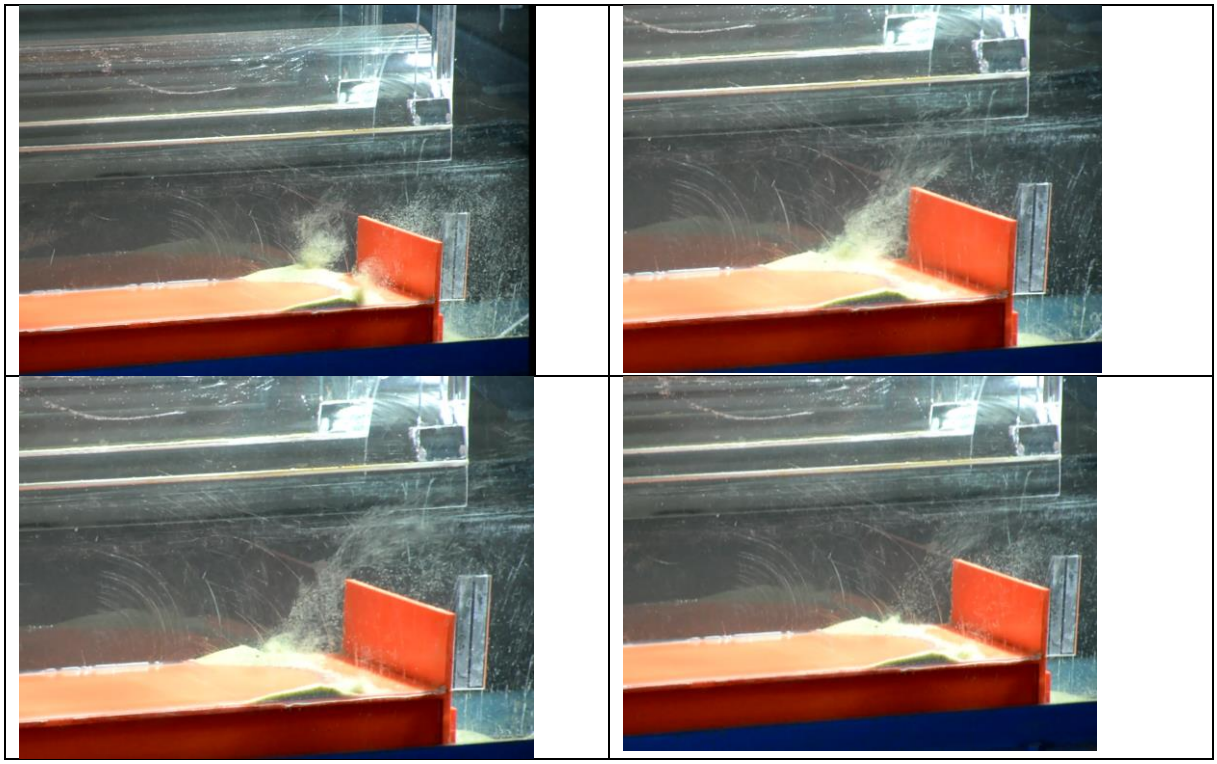

Figure 238: Sequence of flushing sand, creation of vortex flow

14.5.6 **Weir height test - triple**

To investigate the influence of the weir on the sand flushing, it is heighted by the factor of 3 [-] from to 3.5 cm to 10.5 cm resp. in prototype scale from 1.3 m to 3.9 m.

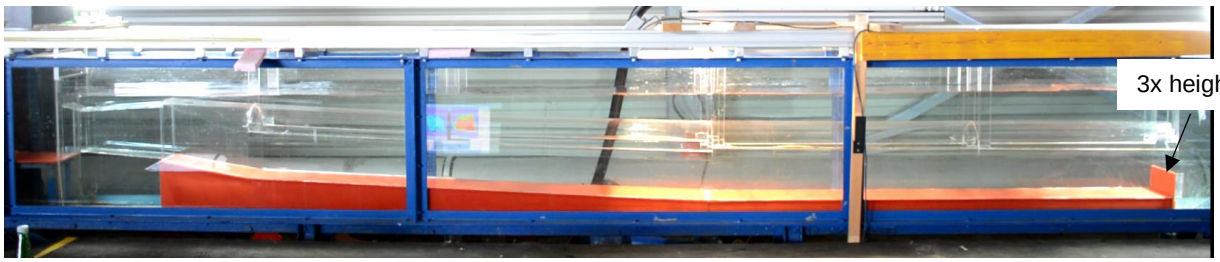

Figure 239: Geometry of triple weir height

14.5.6.1 High value of observed discharge; 59.6 l/s – triple weir height

Table 24: Parameters of model run 59.6 l/s

Sand grain	0.3 mm – 1.0 mm	Prototype time scale: 36.67 sand emptying	607*36.67 = 22'259 s → **6.18 h** Time factor to 1.0 weir height: 6.18 / 1.8 = **3.43 [-]**
Discharge	59.6 l/s	Water discharge prototype	80 m³/s
Time of flow	10 min 7 s = **607 s**	Sand amount, model	0.5 l
		Sand amount, prototype	0.5 * 36.67^3= 24 655 l → 24.65 m³

As for the single and double weir height the sand is 100% flushed at the discharge of 59.6 l/s.

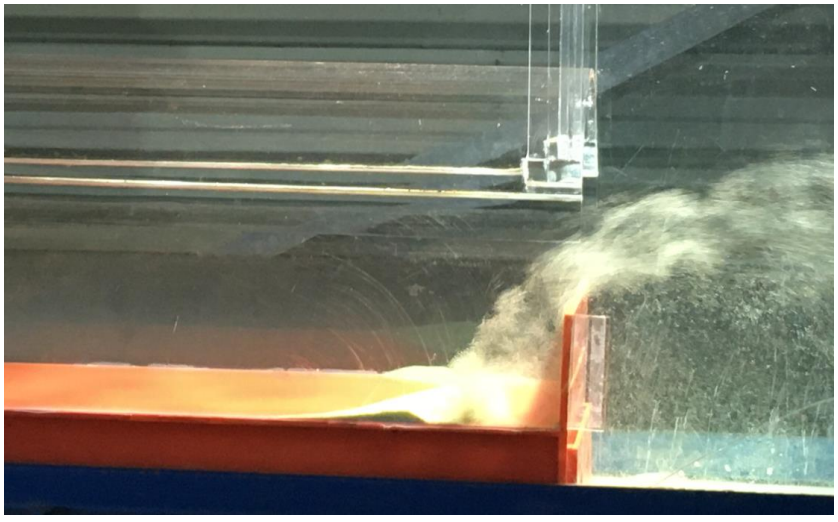

Figure 240: Discharge 59.6 L/s, weir height 3.0 [-], sand inflow 0.5 L, sand overtopping weir downstream, snapshot

14.5.6.2 Middle value of observed discharge; 48 l/s – triple weir height

Table 25: Parameters of model run 48 l/s

Sand grain	0.3 mm – 1.0 mm	Prototype time scale: 36.67 sand emptying	2100*36.67 = 77'007 s → **21.39 h** Time factor to 1.0 weir height: 21.39 / 8.35= **2.56 [-]**
Discharge	59.6 l/s	Water discharge prototype	80 m³/s
Time of flow	35 min = **2100 s**	Sand amount, model	0.5 l
		Sand amount, prototype	0.5 * 36.67^3= 24 655 l → 24.65 m³

Figure 241 shows the effect of the sediment lifting over the weir with vortex flows at starting from three points at the dune, the two wall corners and the center.

Figure 241: Discharge 48 L/s, weir height 3.0 [-], sand inflow 0.5 L, sand overtopping weir downstream, snapshot

14.5.7 **Weir heightening results and conclusion**

The downstream weir heightening does not prevent the flushing of sand, but increases the time. The highest rate of sand flushing is given close to the weir by the creation of vortex flow close to the side walls.

Four sand moving pathways are identified in the sand trap (Figure 242):

1: Bed load with resuspension
2: Dune moving
3: Direct weir overtopping
4: Vortex weir overtopping at side walls

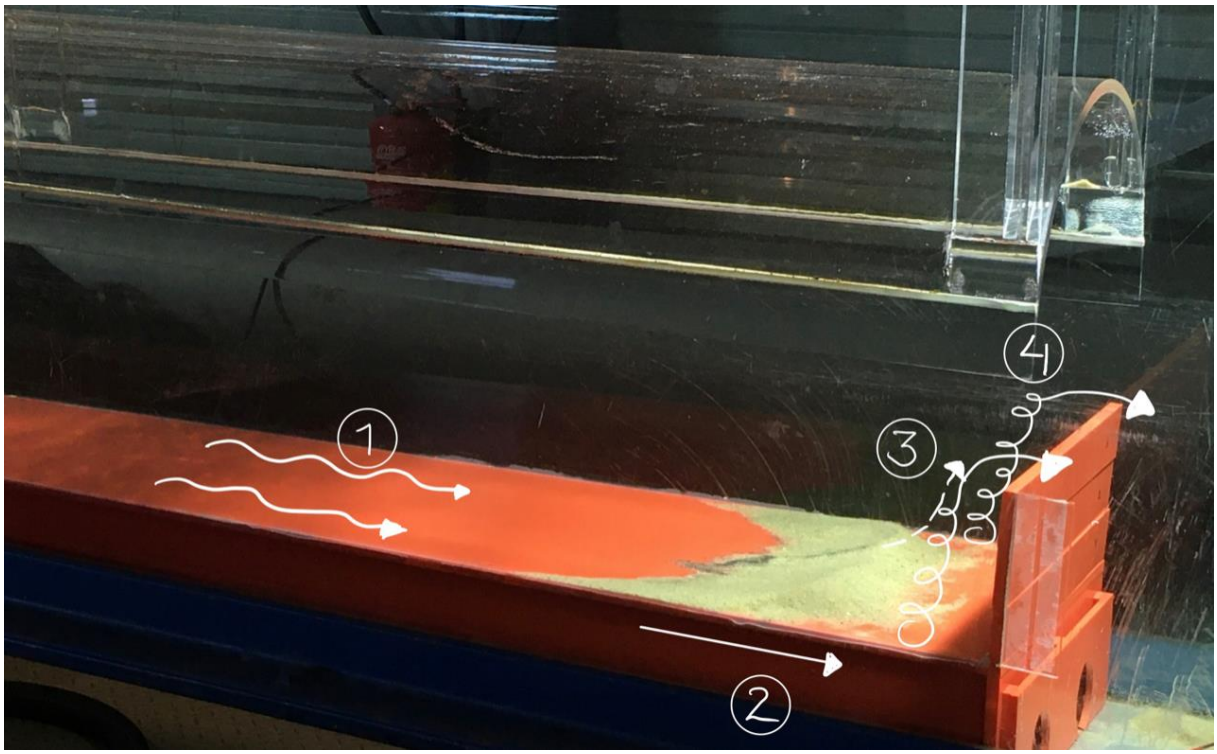

Figure 242: Discharge 48 L/s, weir height 3.0 [-], sand inflow 0.5 L, sand overtopping weir downstream, snapshot, description of sand moving paths

Sand moving path no. 3, the direct overtopping is dependent on the weir height. Since the dune moving (nr. 2) is relatively slow and the direct overtopping (Figure 243) is less dominant when heightening the weir, higher weirs increase the timespan to flush the sand.

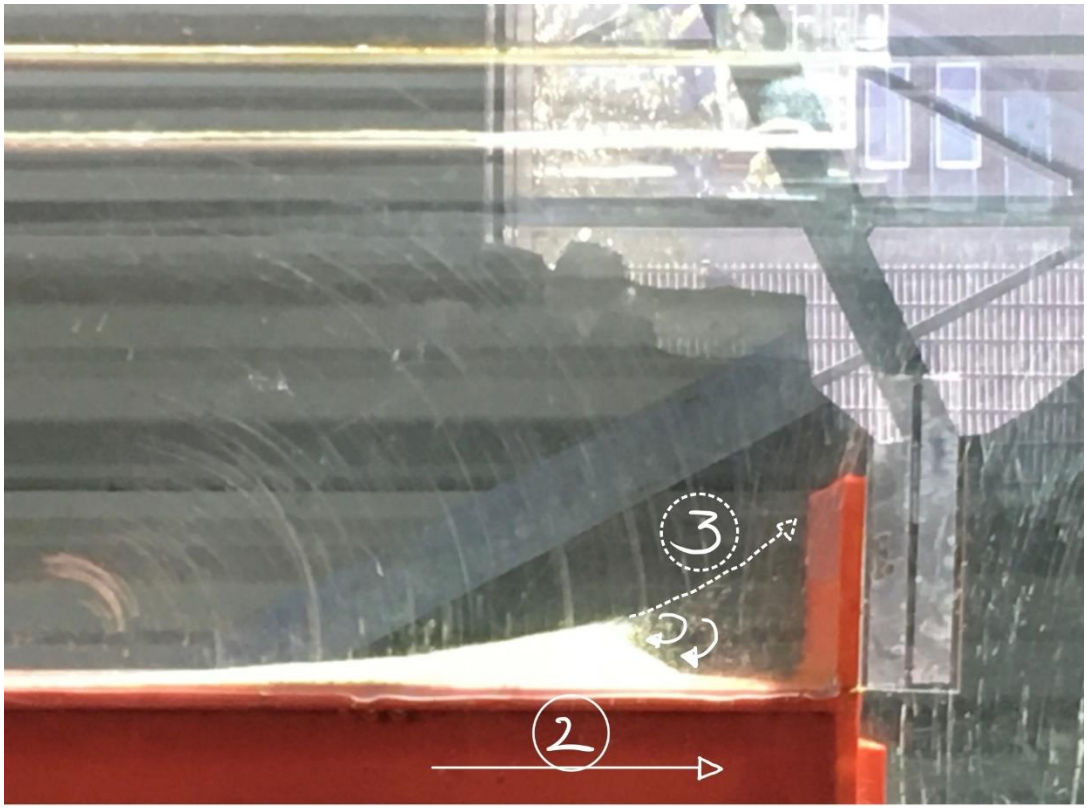

Figure 243: Discharge 48 L/s, weir height 2.0 [-], sand inflow 0.5 L, description of sand moving paths

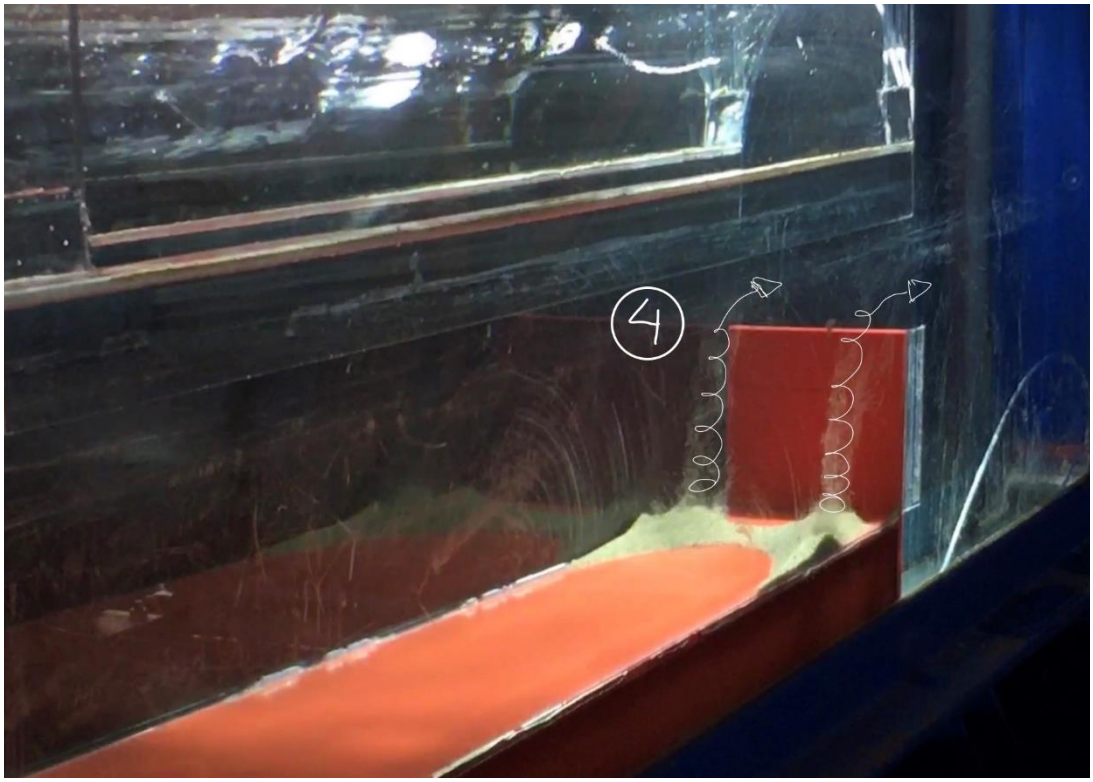

Figure 244: Discharge 48 L/s, weir height 3.0 [-], sand inflow 0.5 L, description of vortex moving path

Table 26 quantifies the time span of sand flushing of 25 m³/s (0.5 l in model scale).

Table 26: Results of weir heightening – time demand of flushing

Discharge	Weir height	Time prototype	Factor
59.6 l/s – 80 m³/s	1 x	1.8 h	1
	2 x	4.68 h	2.6
	3 x	6.18 h	3.43
48 l/s – 65 m³/s	1 x	8.35 h	1
	2 x	15.27 h	1.8
	3 x	21.39 h	2.5
41 l/s – 55 m³/s	1 x	22 h	
	2 x		
	3 x		

14.5.8 **Ribs at weir - sand flow investigations with**

A rib proposal is investigated in the model with the dimensions as shown in Figure 246. The rib geometry is 1 m width by 1 m gap, height is equivalent to the weir height.

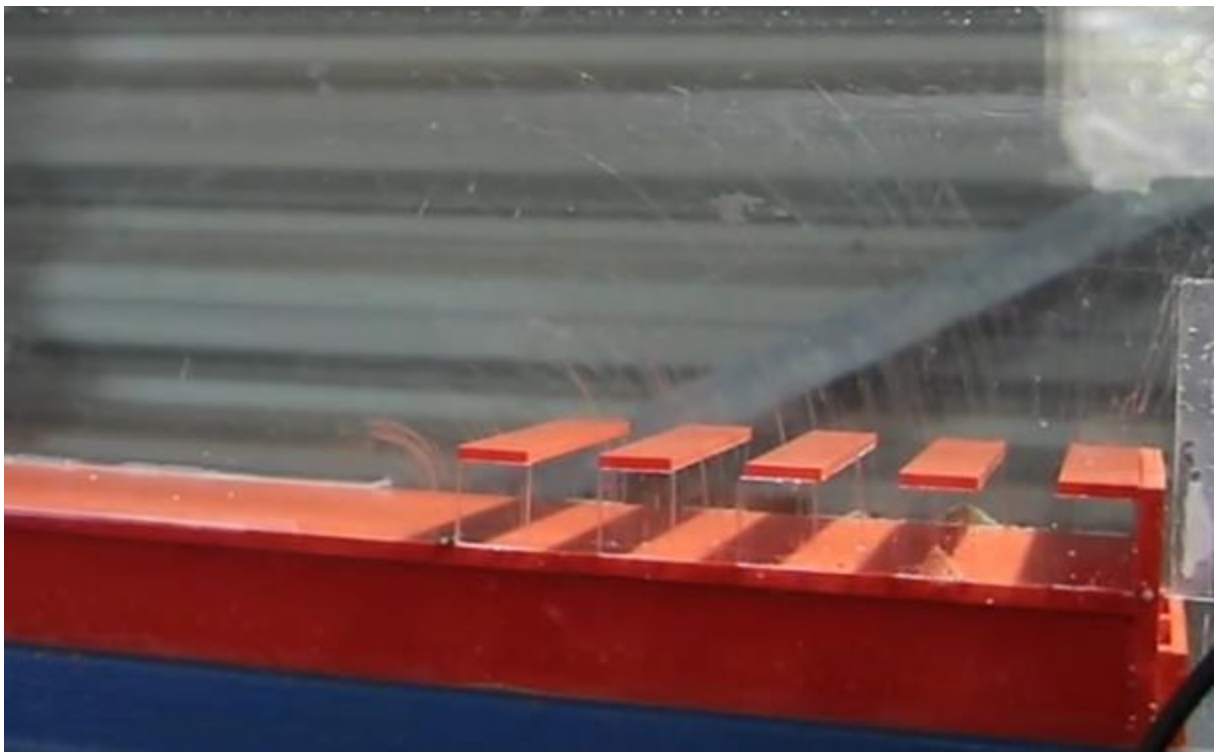

Figure 245: Ribs upstream of weir, H=1.3 m (prototype) weir height, B = 1 m, distance = 1 m, thickness 18.3 cm

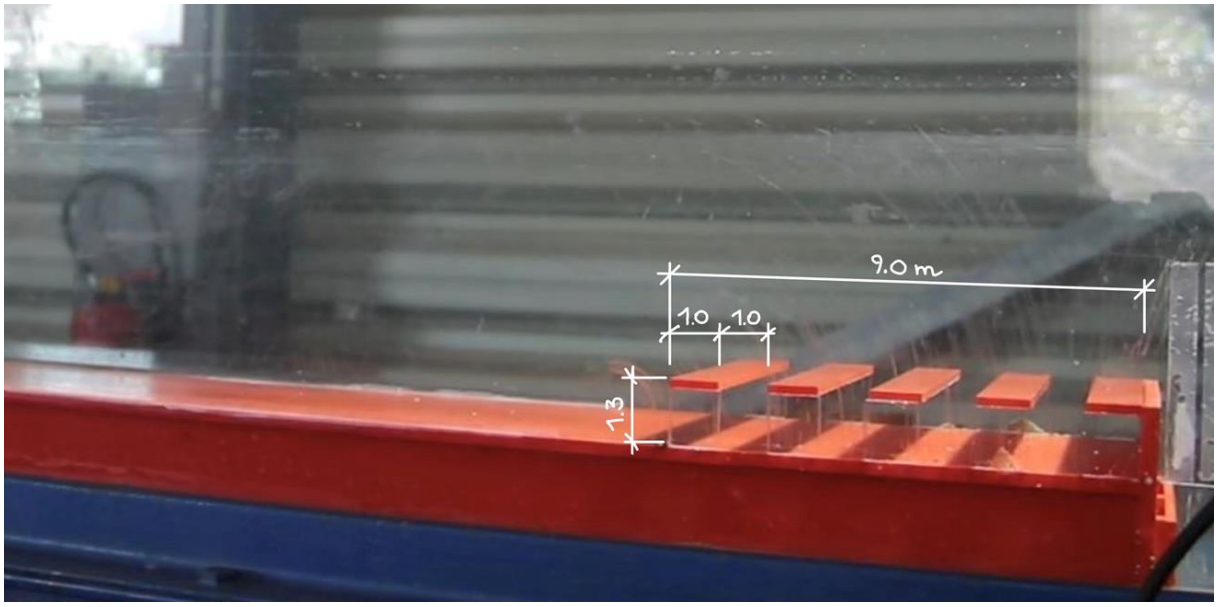

Figure 246: Ribs upstream of weir, H=1.3 m (prototype), dimensioning

14.5.8.1 59.6 l/s 5 ribs sand flushing

Sequence 01 – 12 show the sand transportation process in the sand trap at max. discharge of 59.6 l/s (80 m³/s). Within 250 sec. in the model test the sand of 0.5 l is 100% flushed, 2.54 h prototype scale.

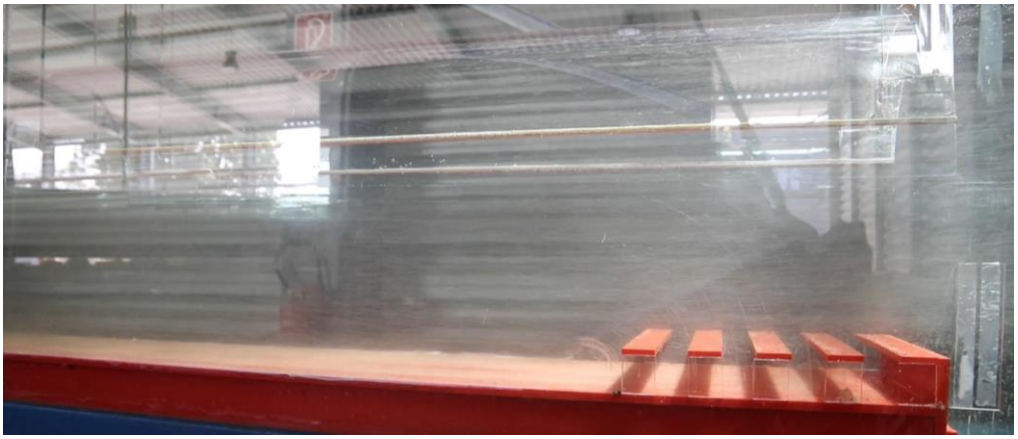

Figure 247: 59.6 l/s, sand transport – fine sand suspended load and bed load – 11 sec., sequence 01

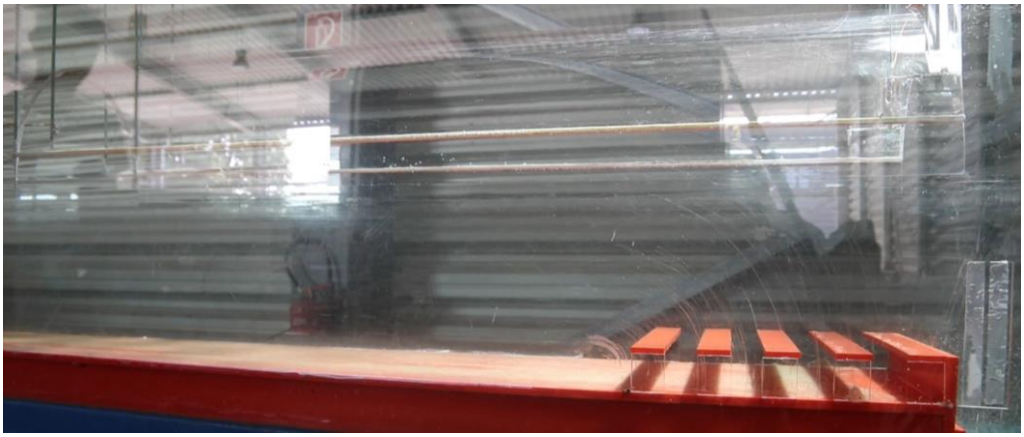

Figure 248: 59.6 l/s, sand transport as bed load – 15 sec., Sequence 02

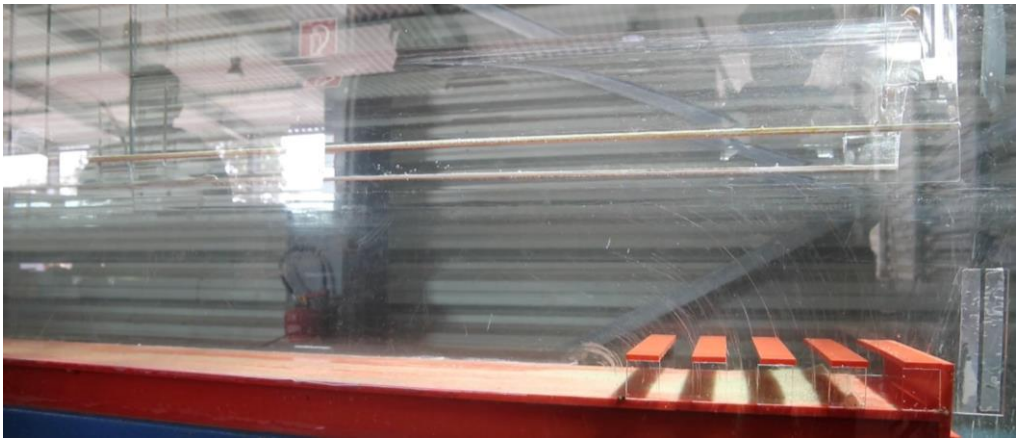

Figure 249: 59.6 l/s, sand transport as bed load, forming of a dune under rib No.2 -, 25 sec., Sequence 03

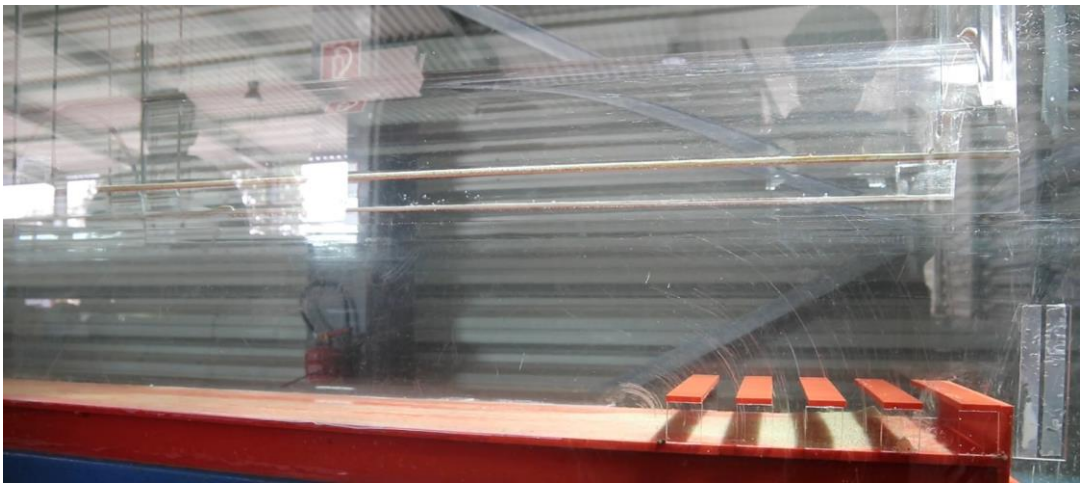

Figure 250: 59.6 l/s, sand transport as bed load, accumulating a dune under rib No.2 – 30 sec., Sequence 04

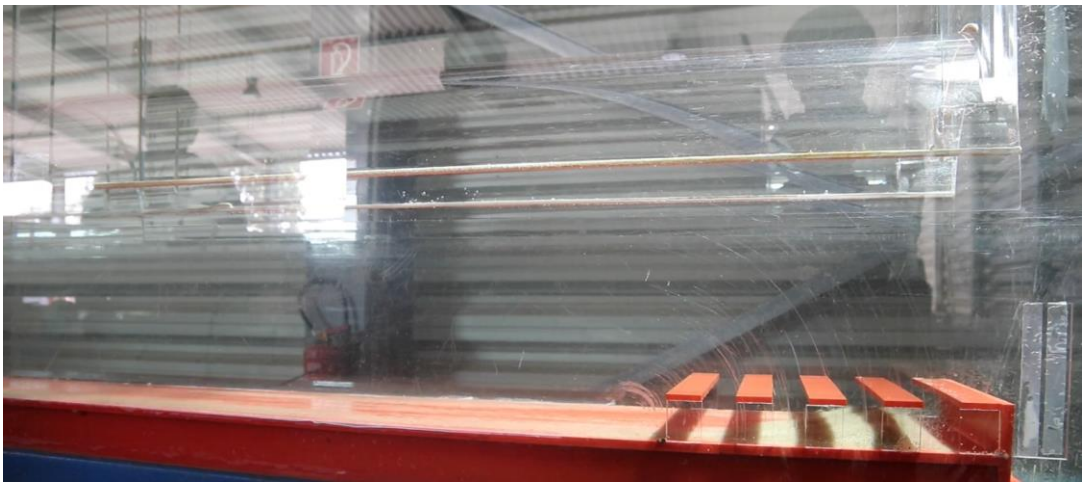

Figure 251: 59.6 l/s, sand transport as bed load, accumulating a dune under rib No.2 – 40 sec., Sequence 05

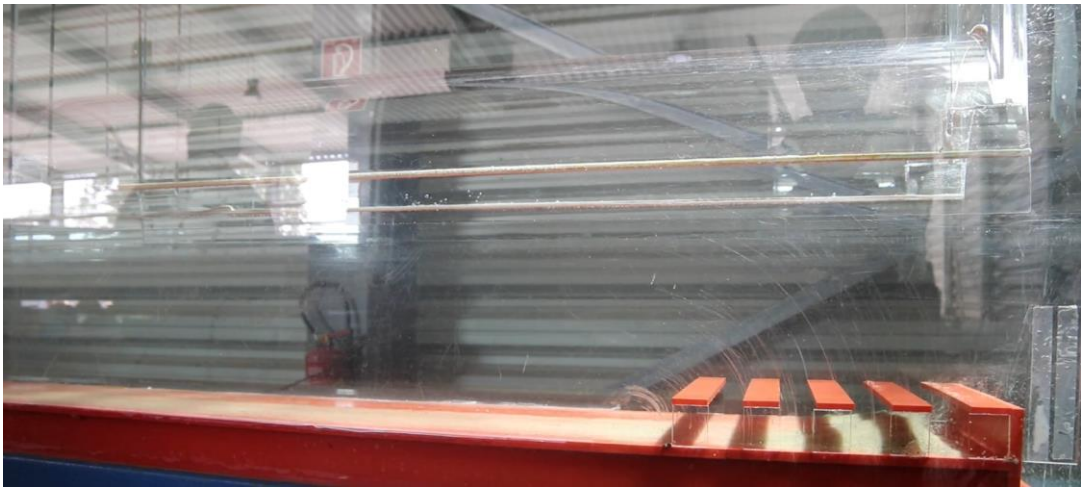

Figure 252: 59.6 l/s, sand transport as bed load, accumulating and moving the dune under rib No.2 further downstream – start of direct sand flushing over the weir- 50 sec., Sequence 06

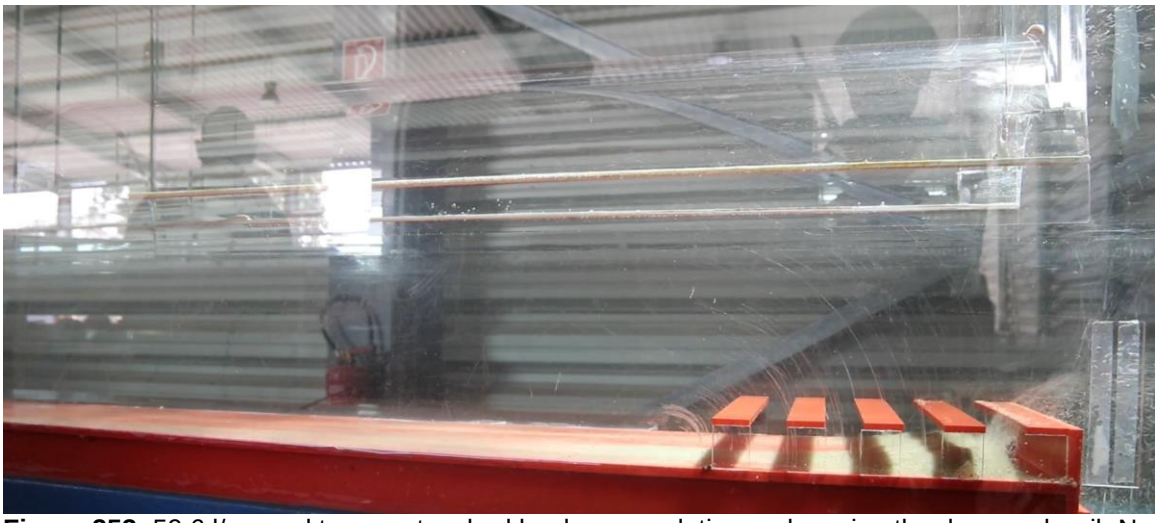

Figure 253: 59.6 l/s, sand transport as bed load, accumulating and moving the dune under rib No.2 further downstream – advancing of direct sand flushing over the weir- 70 sec., Sequence 07

Figure 254: 59.6 l/s, sand transport as bed load is finished, accumulating and moving the dune under rib No.2 further downstream – advancing of direct sand flushing over the weir- 85 sec., Sequence 08

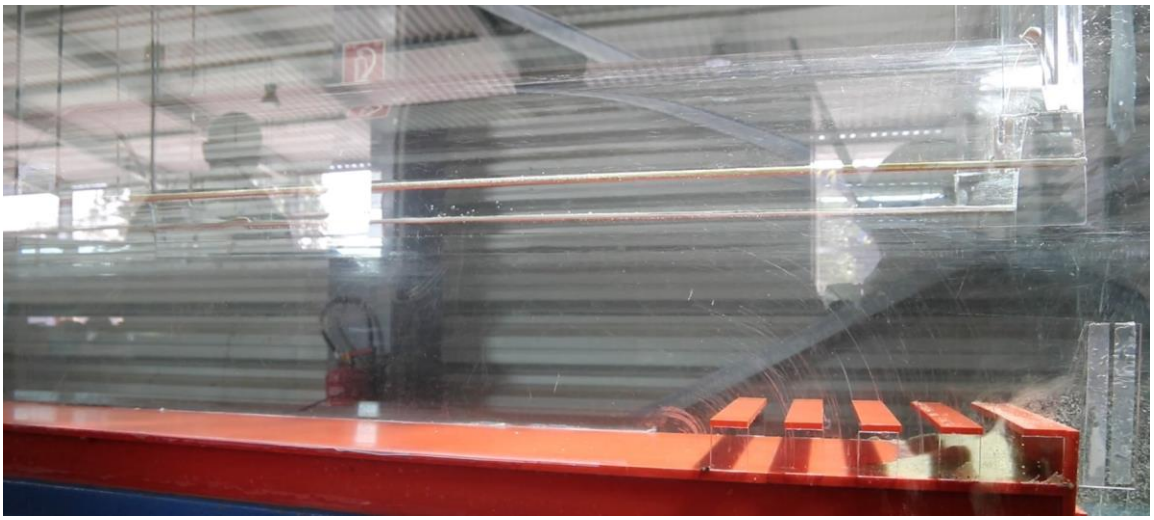

Figure 255: 59.6 l/s, sand transport moving the dune under rib No.1 – constant flushing of sand directly over the weir- 110 sec., Sequence 09

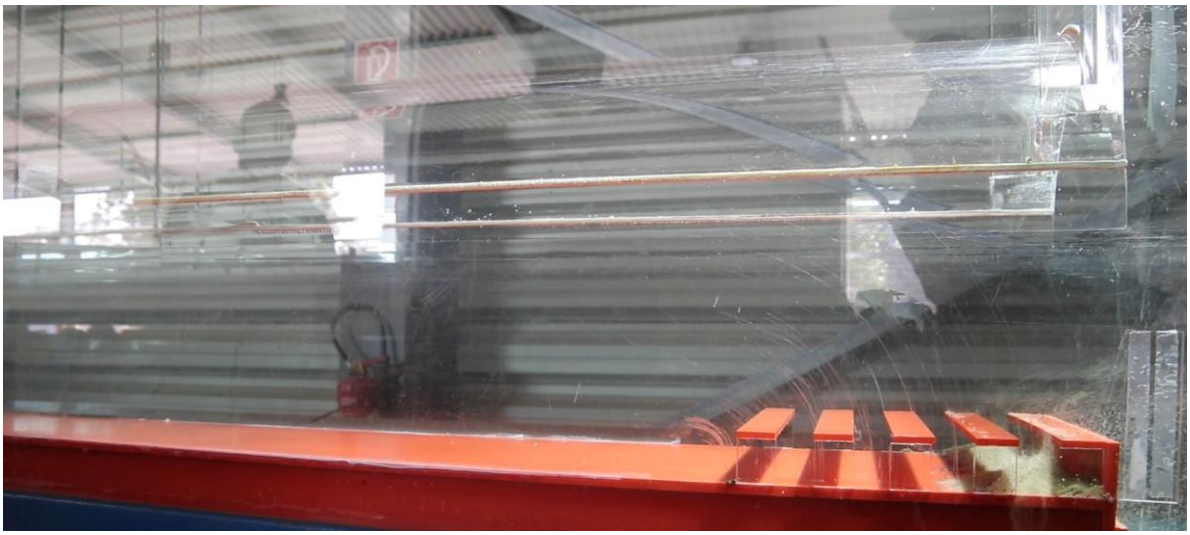

Figure 256: 59.6 l/s, sand transport moving the dune under rib No.1 – constant flushing of sand directly over the weir- 120 sec., Sequence 10

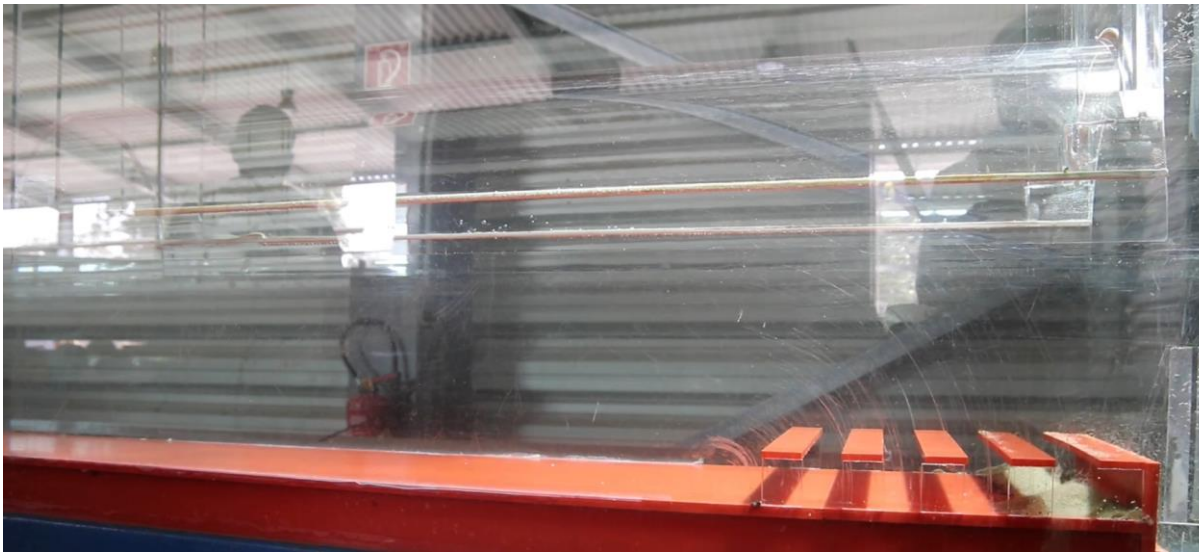

Figure 257: 59.6 l/s, sand transport moving the dune under rib No.1 – continued flushing of sand over the weir- 190 sec., Sequence 11

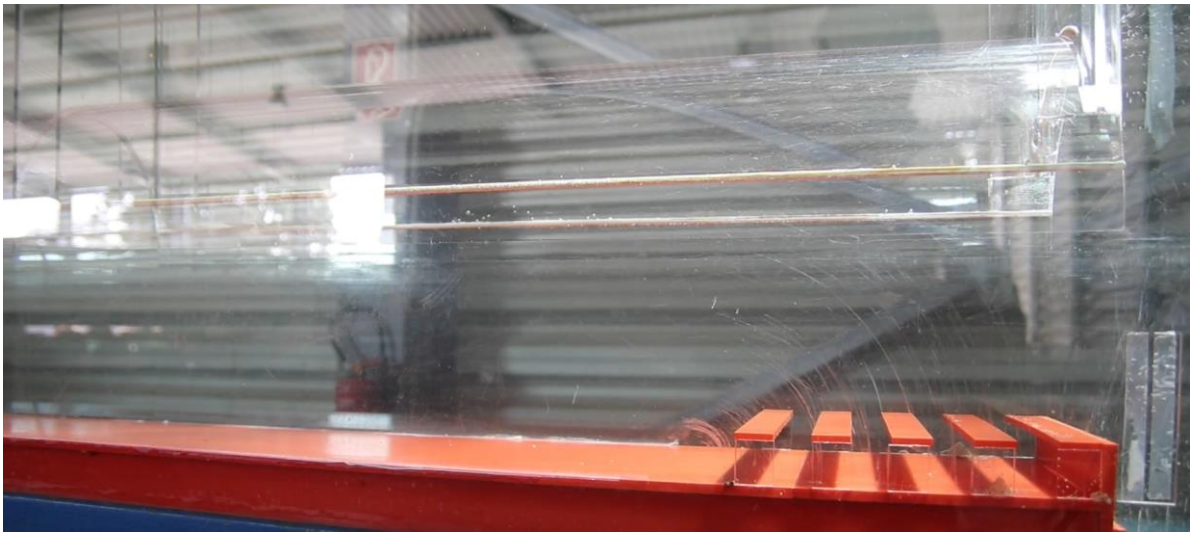

Figure 258: 59.6 l/s, sand transport moving the dune under rib No.1 – continued flushing of sand over the weir- 250 sec., Sequence 12

Figure 259: Flow visualization with sand transport under the ribs

Figure 260 shows the 3D CFD RANS simulation of the ribs in the sand trap geometry as it is investigated in the model test. It is visible that a significant flow is present under the ribs. The flow velocity is less as in the main section of the sand trap. The effect of this is that the sand dune is moving slower as without ribs. However, close to the weir as seen in Figure 259 the sand is effectively flushed over the weir.

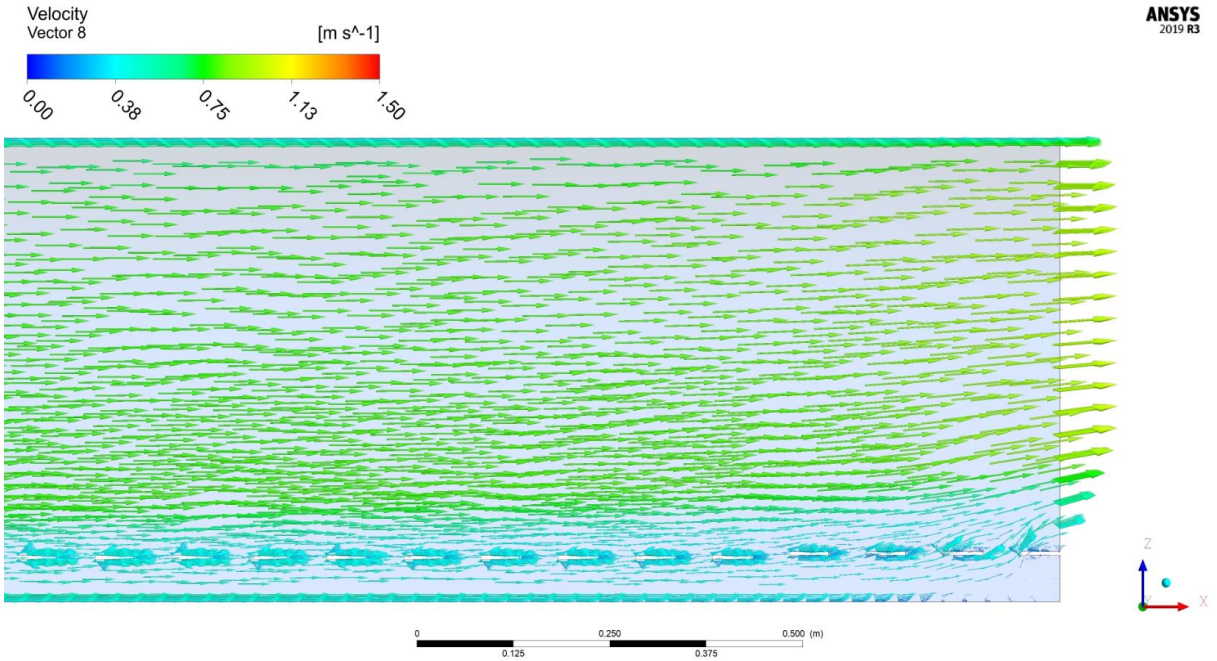

Figure 260: Flow visualization hydrodynamic 3D CFD simulation (1:20 scale) prototype discharge (equivalent to 80 m³/s and 59.6 l/s in 1:36.67 scale), time snapshot

14.5.9 **Ramp design with ribs to create sand trap compartments**

The previous model test runs have clearly shown that ribs alone cannot sufficiently trap the sand. Figure 261 shows the schematic sketch of the ramp to be put in the chamber in front of the weir to securely trap sediments. The ramp is the main element to be added to the concept of the ribs. The combination of the ramp and the ribs is shown to be a straightforward design concept to retrofit sand traps and also to allow automatic flushing. The ramp has an inclination of 8%, that was sufficiently proven by the model tests.

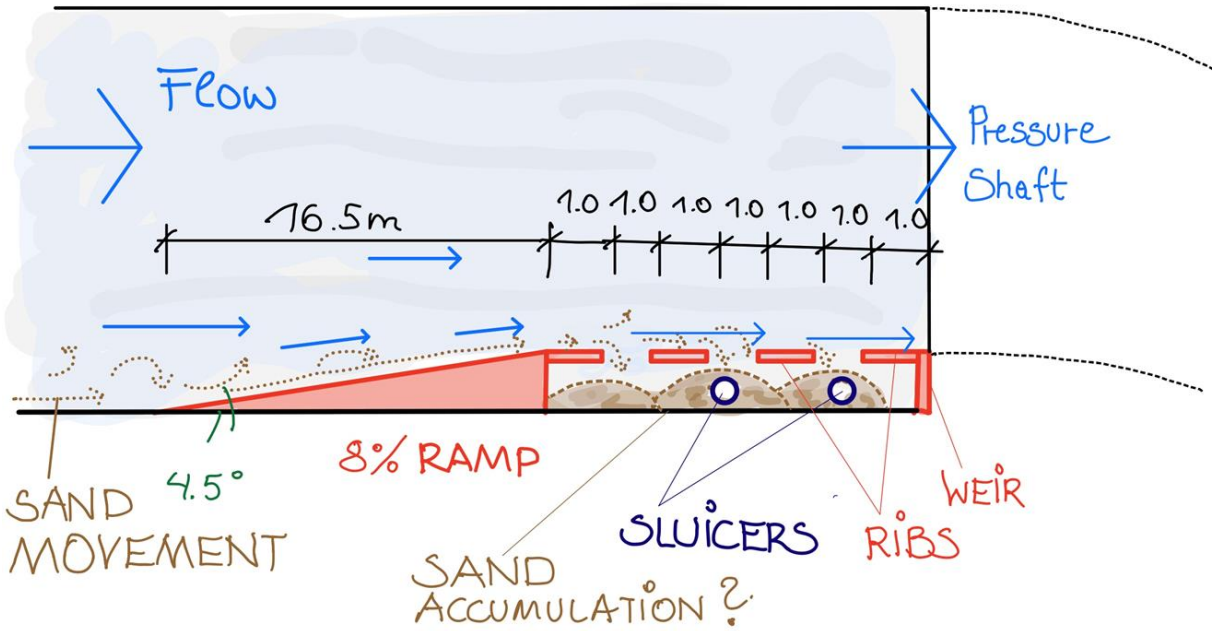

Figure 261: Test proposal for ribs design with ramp and sluicing pipes, schematic

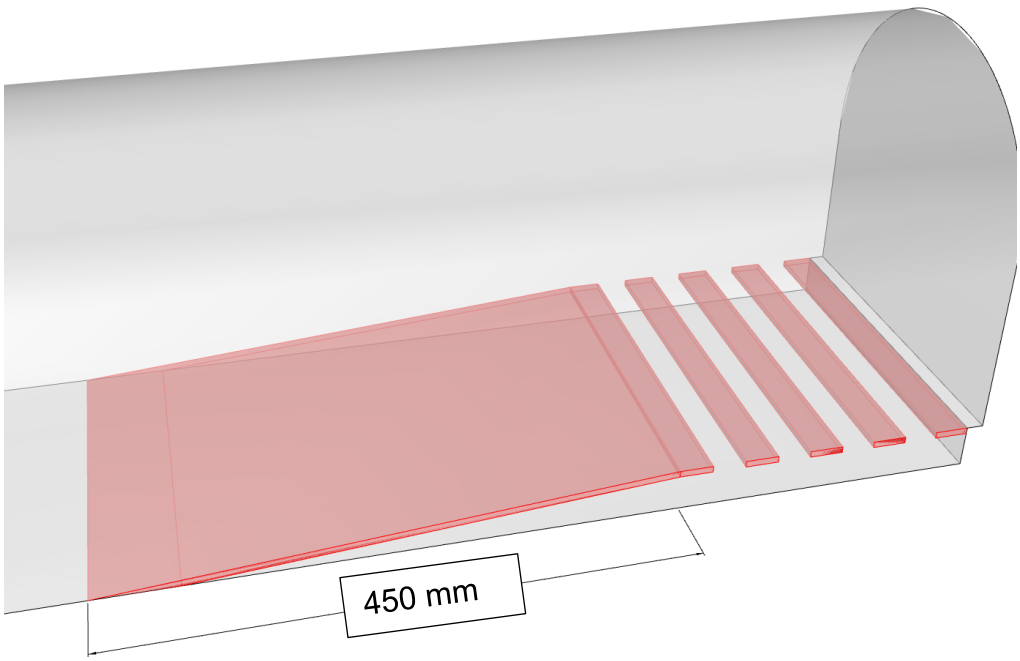

Figure 262: Test proposal for ribs design with ramp and sluicing pipes, 3D geometry, model scale

14.5.10 **Results of ribs with ramp 60l/s resp. 80 m³/s**

Sand can be efficiently trapped with the combination of the 4.5° (8%) ramp inside the chamber leading to compartments separated by ribs (Figure 263, Figure 264).

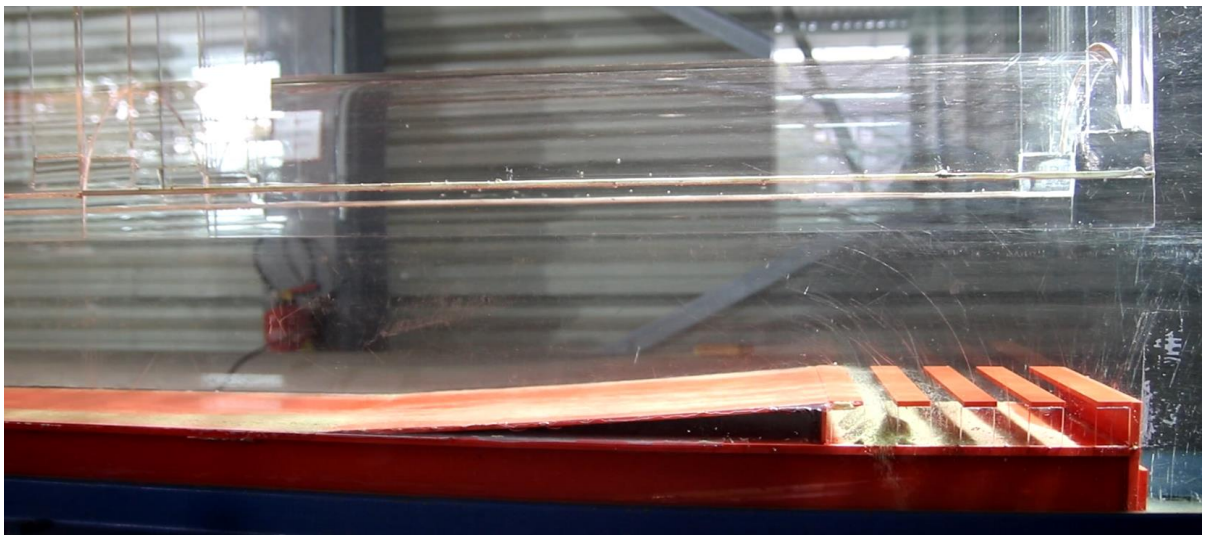

Figure 263: Result with 60 l/s resp. 80 m³/s for prototype with sand 0.3-1.0 mm

The model test shows that sand is safely trapped. Some rotational flow with sand particles between the ribs is visible. The model runs suggest to avoid steps in the rib geometry to minimized induced rotational flows.

Figure 264: Result with 60 l/s resp. 80 m³/s for prototype with sand 0.3-1.0 mm

14.5.11 **Methodology to measure the trapped sand**

A removable rib construction in the sand trap model test allows to collect and measure the trapped sand. The measurement is utilized volume related. The sediment input was constant material of 0.3 mm to 1.0 mm sand grain diameter. The input sand was always 500 ml, measured by the plastic cup in the pictures below.

Figure 265: Removable rib construction for sand collection

Figure 266: Left; sand input 500 ml, right; sand collected after the run

Figure 267: Left; sand input 500 ml, right; measured volume of collected trapped sand in relation to 500 ml input sand

14.5.12 **Results of ribs with ramp 48l/s resp. 65 m³/s**

Sand can be efficiently trapped with the combination of a 4.5° ramp inside the chamber also for the 48 l/s reference discharge (Figure 268, Figure 269).

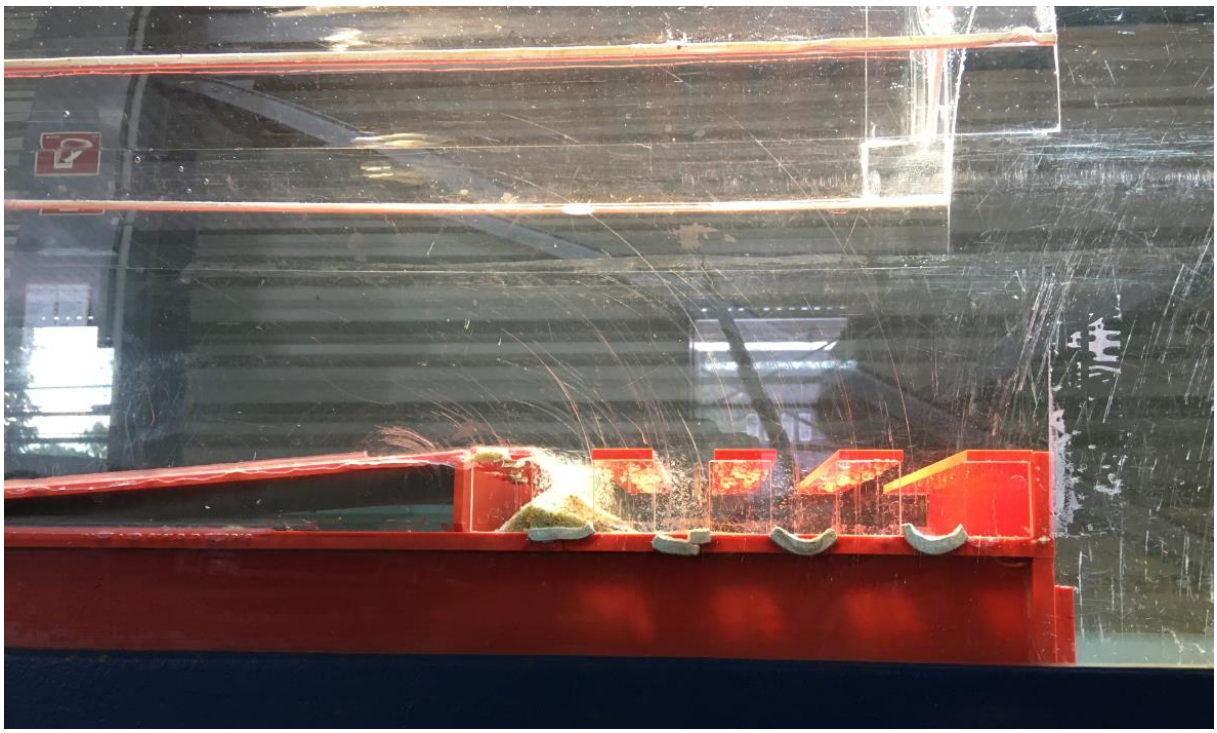

Figure 268: Result with 48 l/s resp. 65 m³/s for prototype with sand 0.3-1.0 mm, view compartments

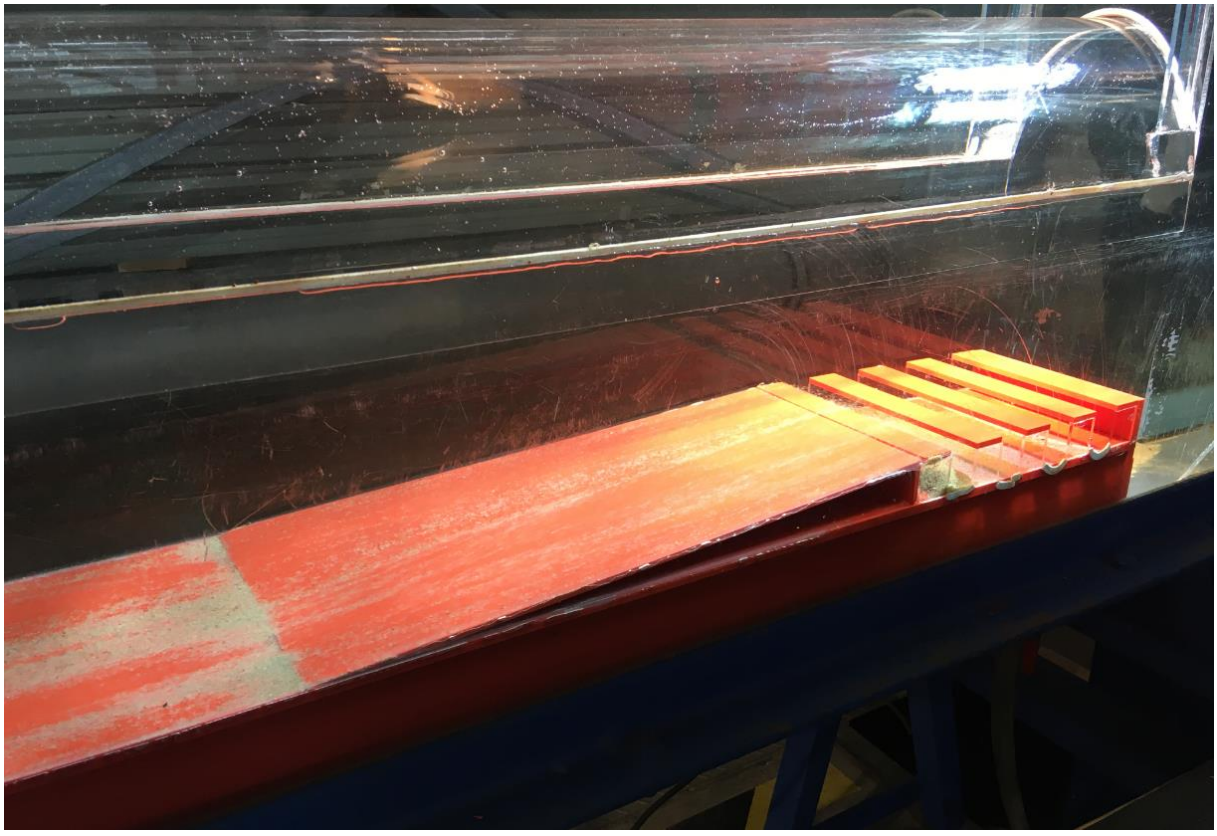

Figure 269: Result with 48 l/s resp. 65 m³/s for prototype with sand 0.3-1.0 mm, view ramp

14.5.13 **Suggestion for implementing with sluicing pipes**

Figure 270 shows the sketch of the rib design with ramp and sluicing pipes that are partially slotted in the section of the opening. The sluicing pipe transports the sediment upstream, thus the highest loaded compartment directly downstream of the weir can be very effectively sluiced. With a sluicing element the sediment in the chamber can be controlled. It is also proven, that the rib configuration is very safely trapping larger particles that have the potential to harm the turbine and other mechanical parts.

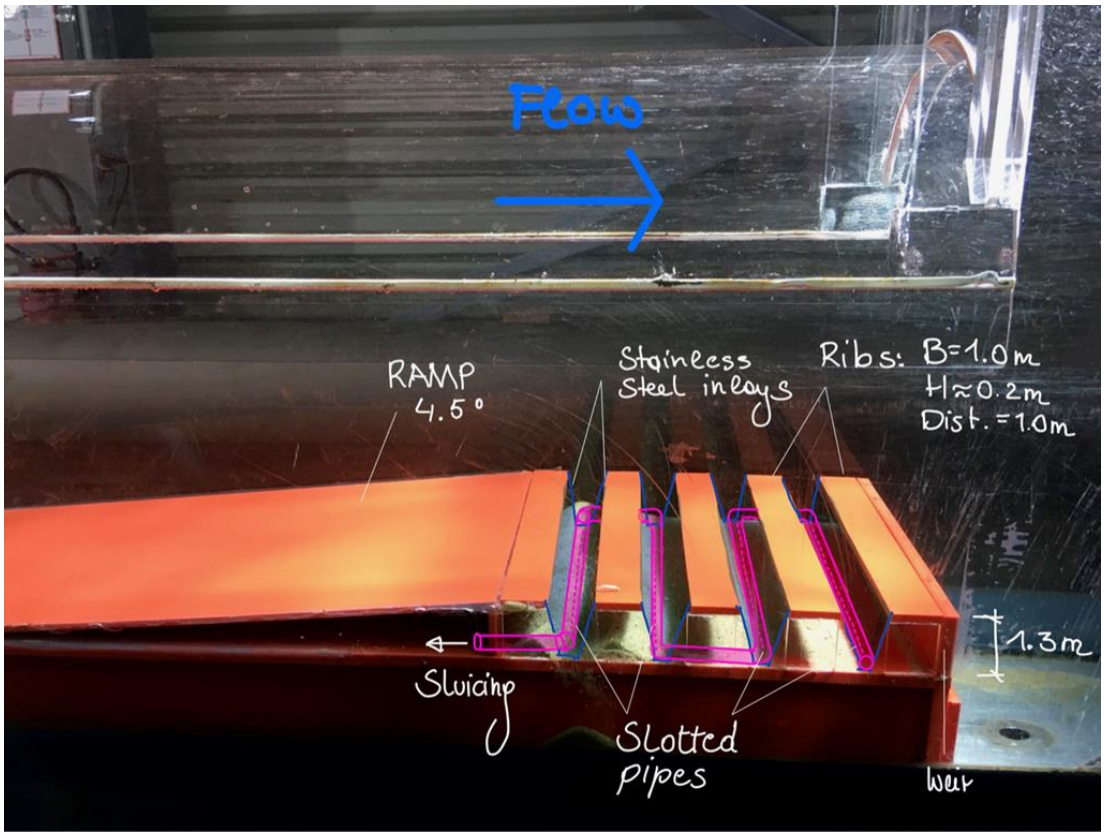

Figure 270: Suggestion of implementing slotted sluicing pipes together with the ribs

14.6 **Flow calmers design**

This chapter describes the geometry found and investigated for the proposal of flow calmers in the sand trap. As the research question proposed a passable design was the aim to be found and defined. The geometry to be investigated in the physical model test consists of rectangular obstacles in the prototype dimension of 20 cm / 40 cm. The distance between the single calmer obstacle is 40 cm. The flow calmers are placed in double rows, but centered to the gap of the upstream row. The distance between the rows is 600 mm. To allow passability and a possible connection to an extension chamber a distance of 10 m is chosen (Figure 271, Figure 272).

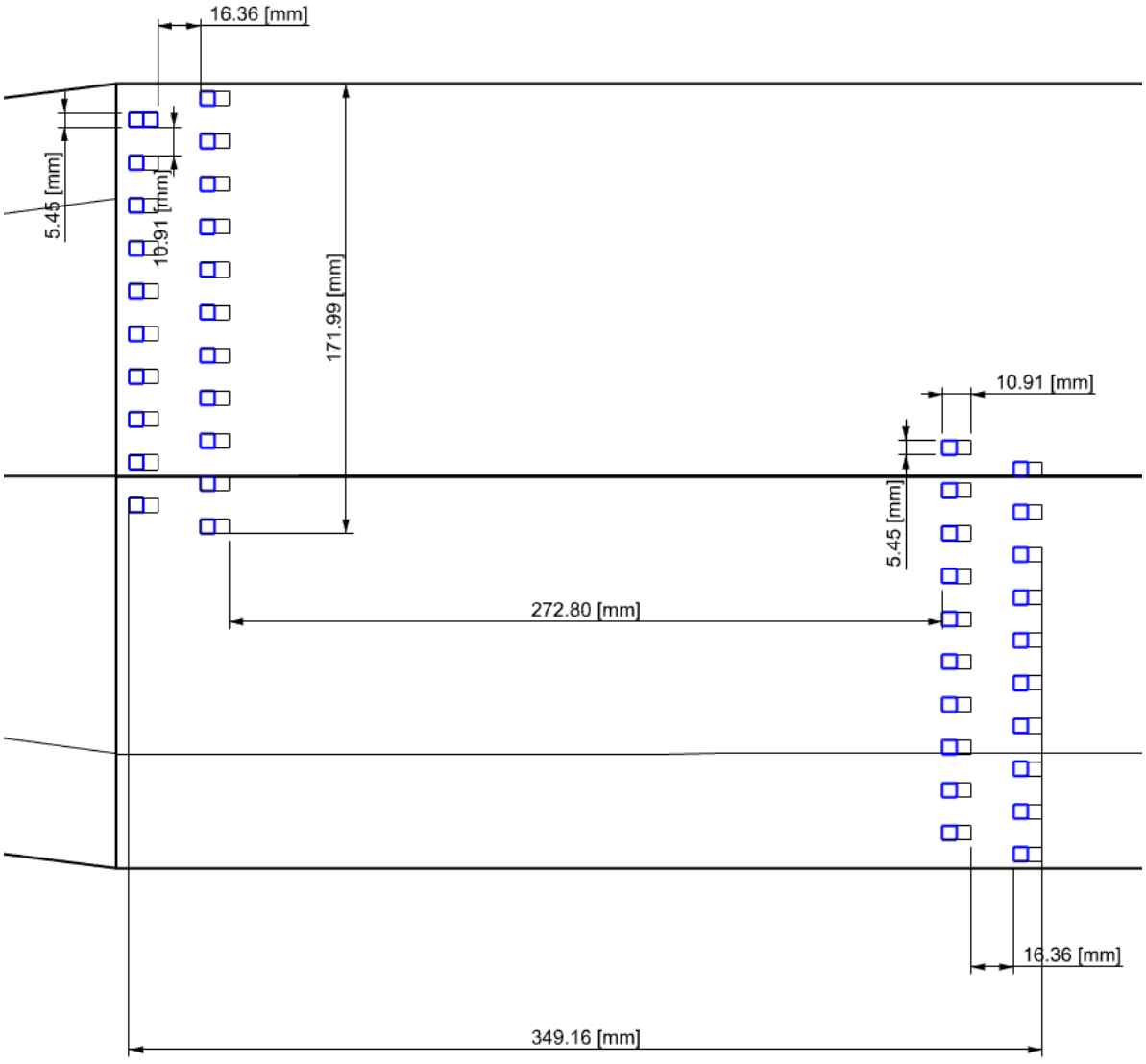

Figure 271: Flow calmer design, model test size 1:36.67

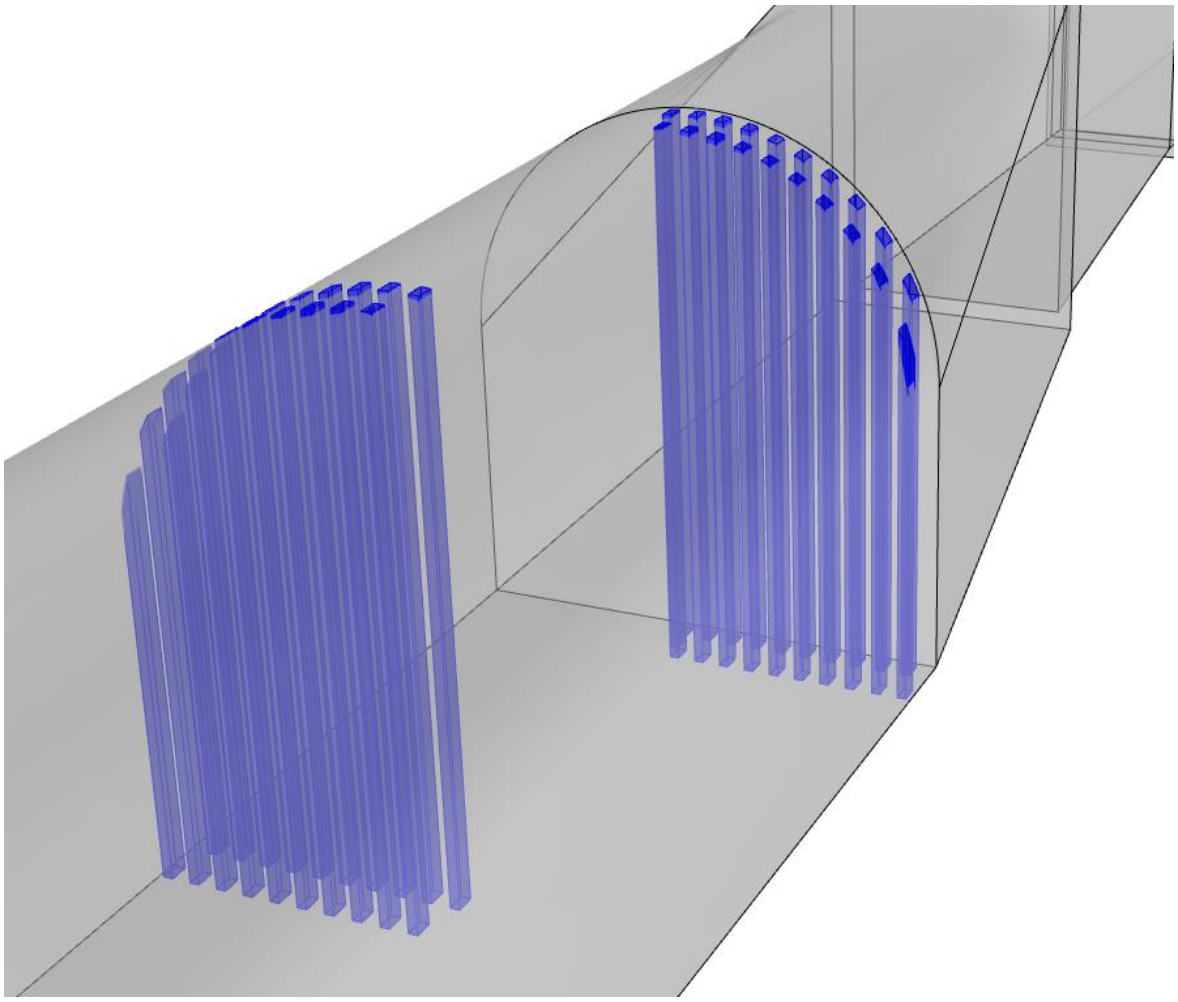

Figure 272: Flow calmer design, 3D geometry

14.6.1 **Model test placing flow calmers**

Figure 273 and Figure 274 show the placed flow calmers in the physical model test.

Figure 273: Flow calmer downstream direction

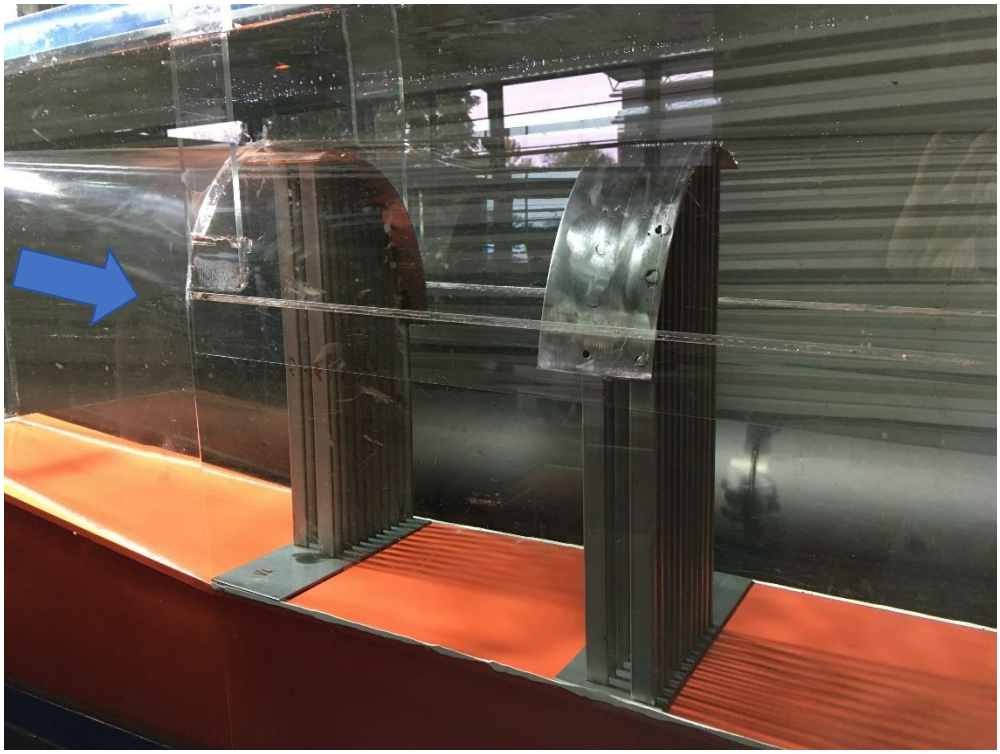

Figure 274: Flow calmer upstream direction

14.6.2 **Model test runs flow calmers**

Figure 275 shows the model test run with 59.6 l/s with sand. The image shows two strong vortices in the sudden section expansion from the concrete part to the unlined section. These vortices are capable of lifting sand up to 50% of height of the whole chamber. Suggesting from this observation generally such situations need to be structurally reduced in the design of sand traps.

In general, it was observed that the flow calmers do not improve the sediment situation, in fact, they even have a disadvantageous effect on the sediment situation in the sand trap. Thus, it can be clearly said that flow calmers are not recommended for the Tonstad sand trap.

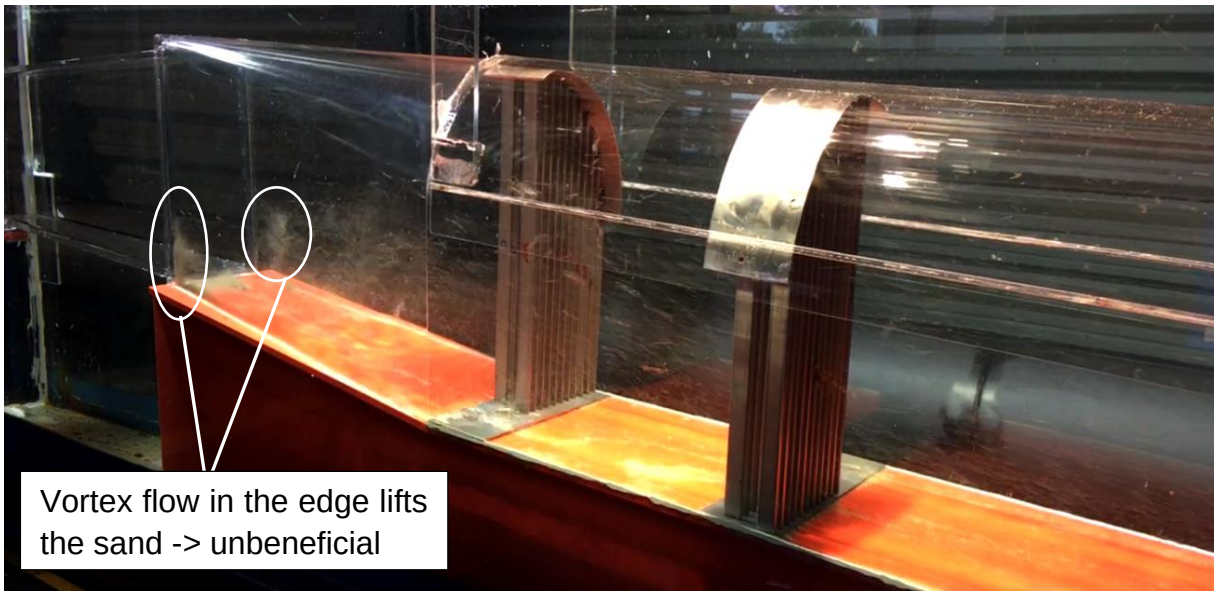

Figure 275: Flow calmer with sand and discharge of 59.6 l/s

Figure 276 shows the sand lifting zone in the expansion section of the diffusor and the resuspending of sand transported through the whole chamber, the latter aspect is even increased at higher sediment concentration in the flow.

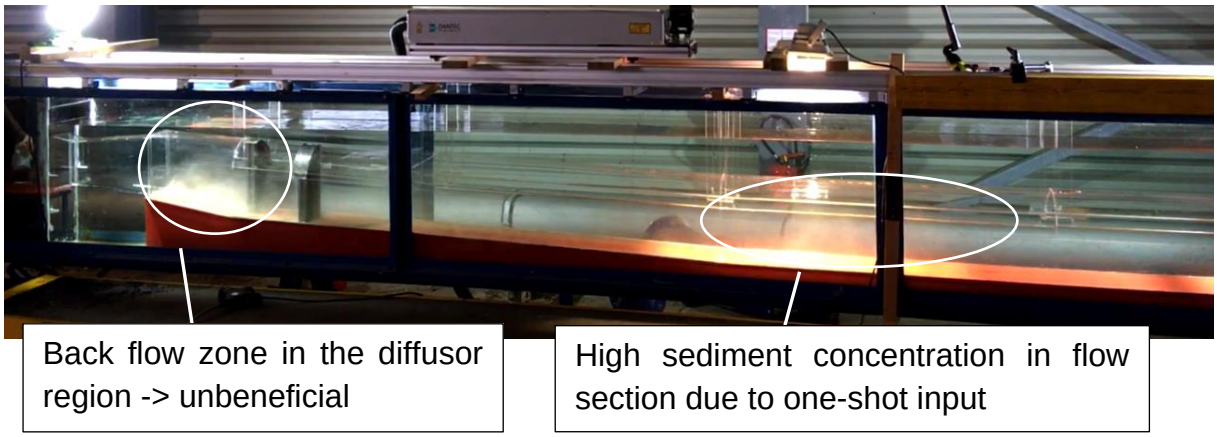

Figure 276: Flow calmer with sand and discharge of 59.6 l/s

14.7 **Results of sand trap investigations**

The investigations have shown that the sand settling cannot significantly improved by the flow calming device and thus not recommended for the Tonstad sand trap.

Table 27 and Table 28 show the efficiency of the sand trap ribs with 0.3-1.0 mm sand probe in comparison of the three characteristic discharges. Table 27 shows that the flow calmer does not have significant influence on the result and rather makes it even less effective for sand trapping.

Table 27: Efficiency of sand trap ribs, emphasis on rakes

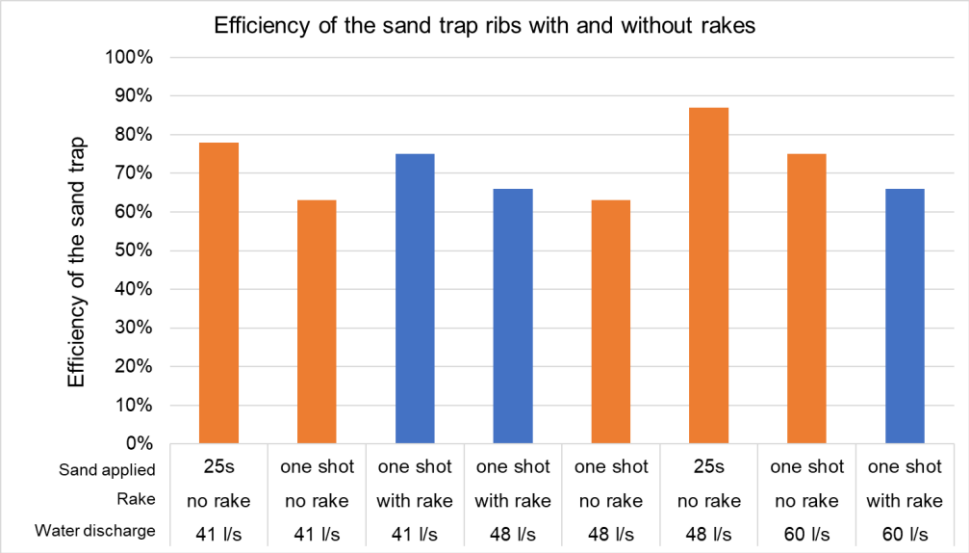

Table 28 shows the same result emphasizing on the time span the sediment probe of 500 ml was applied to the model test run; (i) in one shot or in (ii) 25 seconds. The results for this case show a significant correlation to the time span. The higher the inflow concentration the lower the efficiency. This aspect seems to be relevant for further research.

Table 28 Efficiency of sand trap ribs, emphasis on time sand input

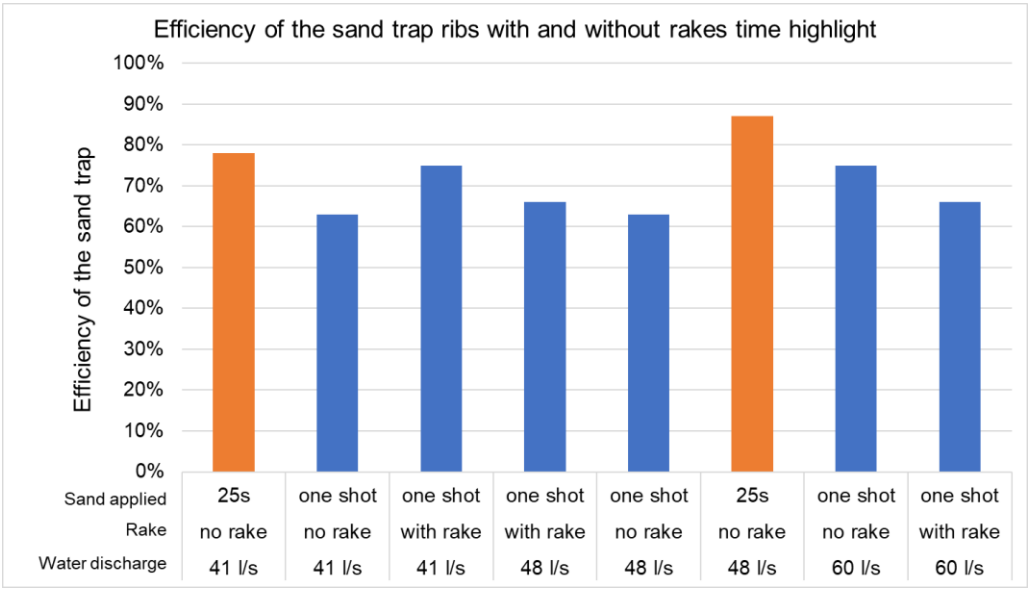

15. 1D numerical modelling with SIMSEN

This chapter describes the SIMSEN 1D numerical model that was set up for the project to widen the list of software Tonstad power plant is hydraulically modelled and also to include the extension chamber with preparing to add the possible pumped turbine unit no. 6.

15.1.1 **Abbreviations**

Quantity:	Unit:	Description:
A_v	m^2	Free surface cross-sectional area in the venting tank
A_r	m^2	Free surface cross-sectional area in the riser pipe
L_{hv}	s^2/m^2	Hydraulic inertia of the venting tank
Kd	-	Local loss, equivalent to ζ
P_p	MW	Pump input power
H_{BE}	m	Best efficiency head
Q_{BE}	m^3/s	Best efficiency discharge
nsp	m^3/s	Specific speed
NPSH	m	Net positive suction head of the pump
H_s	m	Static draft head with reference to tail water surface above runner centreline
H_a	m	Atmospheric pressure at the tailwater surface altitude
H_v	m	Vapor pressure head of water for highest expected temperature
H_f	m	Head loss in the pump suction line
RPT	-	Reversible pump-turbine

15.1.2 **SIMSEN system of Tonstad power plant**

Input parameters, regarding the hydraulic conduits, for SIMSEN model are based on calibrations done by Mauko (2020). With exception off the wave propagation speed which is calculated from length of the element end the time step, as follows from the SIMSEN User Guide. Brook intakes are modelled with a surge tank element, since this is also how they behave. Surge tank elements with inclined shaft are allowing to model brook intake shafts with non-constant inclination and non-constant cross section. This is important for tanking in consideration varying hydraulic inertia regarding to the water level in the brook intake. Function elements are used to describe change in the shaft

cross section and inclination due to varying water level. Parameters of all the pipes used in the 1D model are listed in the Table 29.

Table 29: Parameters of the hydraulic conduits used in the SIMSEN model

Pipe	Length	Nb roundup	Area	Hydraulic diameter	Zin	Zout	Friction loss coefficient λ
	[m]	[-]	[m2]	[m]	[m]	[m]	[-]
PiOusdal	2366.44	198	59.4	6.4	478	468	0.06
ShaftMidst	480	40	15	7.3	480.88	468	0.06
PiMidst	499.96	42	59.4	6.4	468	454.1	0.06
ShaftLila	57.15	5	10	6.0	461.413	455.09	0.06
PiLila1	2000	167	56.6	6.1	455.09	456.72	0.06
PiLila2	1196.11	100	56.6	6.1	456.72	457.7	0.06
ShaftRost	750	63	6	4.6	480	457.7	0.06
PiRost1	2300	192	56.6	6.1	457.7	454.29	0.06
PiRost2	2300	192	56.6	6.1	454.29	450.87	0.06
PiRost3	1253.46	105	56.6	6.1	450.87	449.01	0.06
PiHomst1	2300	192	50.9	5.9	459	456.22	0.06
PiHomst2	2300	192	50.9	5.9	456.22	453.44	0.06
PiHomst3	2300	192	50.9	5.9	453.44	450.67	0.06
PiHomst4	221	19	50.9	5.9	450.67	450.4	0.06
ShaftJos	59.03	5	8	5.3	454	450.4	0.06
PiJos	470	40	50.9	5.9	450.4	449.01	0.06
PiTr1	2167	181	95	8.3	449.01	444.79	0.06
PiTr2	2000	167	95	8.3	444.79	440.9	0.06
PiAsmund	1964.86	164	15	8.7	449.71	441.13	0.06
PiStiga1	1869.344	156	15	8.7	441.13	449.9	0.06
PiStiga2	1000	84	15	8.7	449.9	466.3	0.06
ShaftFore	1753.69	147	15	8.7	468.7	466.3	0.06
PiFore	1617	135	15	8.7	466.3	440.9	0.06
PiFoMa	1517	127	95	8.3	440.9	442.41	0.06
TS3							
PiTS12	93	8.0	95	8.3	442.408	442.5	0.06
PiTS3	100	9	95	8.3	442.408	440	0.06
PiTS1	40	4	62.292	6.9	442.5	442.5	0.06
PiTS2	41	4	62.292	6.9	442.5	442.5	0.06
Surge tanks							
Sandtrap11	104.615	9	100.87	10.6	442.5	436.75	0.041
Sandtrap12	104.62	9	130.02	12.0	436.75	434	0.041

Sandtrap 21	106.5	9	100.87	10.6	442.5	436.75	0.041
Sandtrap 22	106.5	9	130.02	12.0	436.75	434	0.041
Sandtrap 3	223	19	119.017	11.5	440	434	0.041
Penstock1	575	48	10.18	3.6	434	44.67	0.0074
Penstock2	575.5	48	10.18	3.6	434	44.67	0.0074
Penstock3	647.629	54	18.096	4.8	434	39	0.0074
PiT1	14.27	2	3.14	2.0	44.67	42.5	0.0074
PiT2	22.64	2	3.14	2.0	44.67	42.5	0.0074
PiDS1	62	6	59.8	8.2	30	37.25	0.05
PiT3	14.3	2	3.1	2.0	44.67	42.5	0.0074
PiT4	22.6	2	3.1	2.0	44.67	42.5	0.0074
PiDS2	54	5	59.8	8.2	30	37.25	0.05
PiT5	12	1	5.725553	2.7	39	39	0.0074
PiDS3	112	10	50	7.5	30	37.25	0.05
Tailrace1	67	6	100.9	5.2	37.25	37.25	0.05
Tailrace Tunnel	711	60	100.9	5.2	37.25	37.25	0.05
UPGRADE							
PiT6	12	1	4.294164	2.3382686	39	39	0.0074
Excentry	30	3	137	11.4	437.3	450	0.041
Penstock4	692.4835	58	33.21268	6.5028993	430	7.5	0.06
TailRPT	823	69	34.172	6.597819	7.5	37.25	0.05

Upper and lower chamber of the surge tank are modelled using the functions describing different cross-sectional area of the chambers and the shaft. Loss coefficient at the chamber entrance is calculated using CFD simulations, values are described in the chapter 15.2.

Mechanical mass connected to each turbine is simulating the inertia of the rotating mass of the turbine with shaft and rotating part of the generator during the island mode of operation. In case that turbine is supplying power to the grid, function element is set to increase the inertia of the mechanical mass to very high value, that way simulating the infinite inertia of the network.

Figure 277 shows the 1D-numerical representation of Tonstad power plant in SIMSEN. This includes also the approach of potential pump turbine unit no.6.

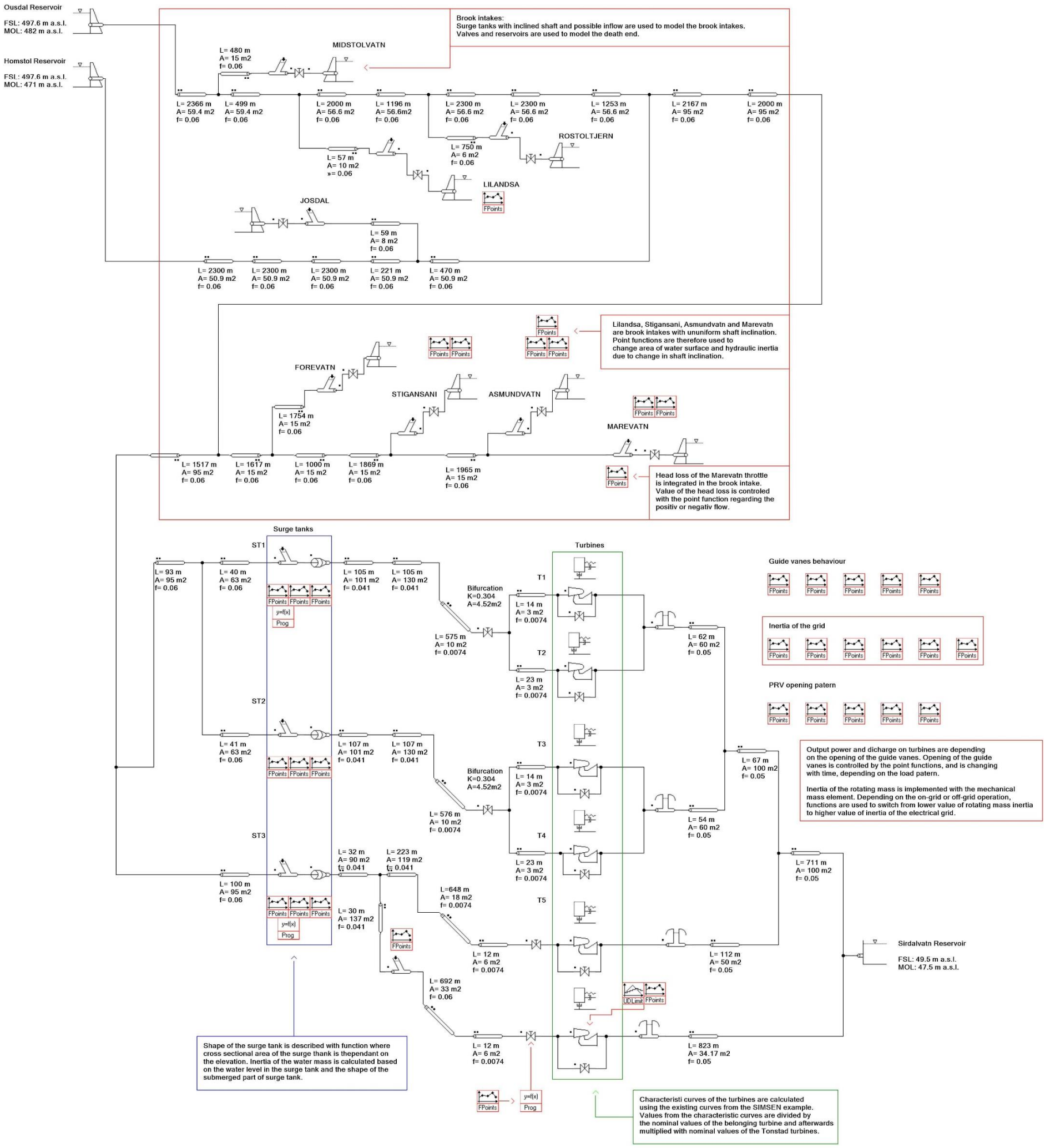

Figure 277: 1D-numerical SIMSEN scheme of Tonstad power plant with pump turbine extension

15.1.3 **Turbine characteristics**

The transient behaviour of hydraulic machines in SIMSEN is modelled using characteristic curves. Since characteristic curves of the Tonstad HPP are not available, they are calculated using the characteristic curves from the SIMSEN example. This is done so that characteristics from the SIMSEN example are divided by nominal values of the turbine to which they belong and then multiplied with nominal values of the Tonstad turbines. Since the example turbine from witch the characteristic curves are taken is a pump turbine, new characteristic curve does also have shape typical for the pump turbines, which can be seen at the Figure 278.

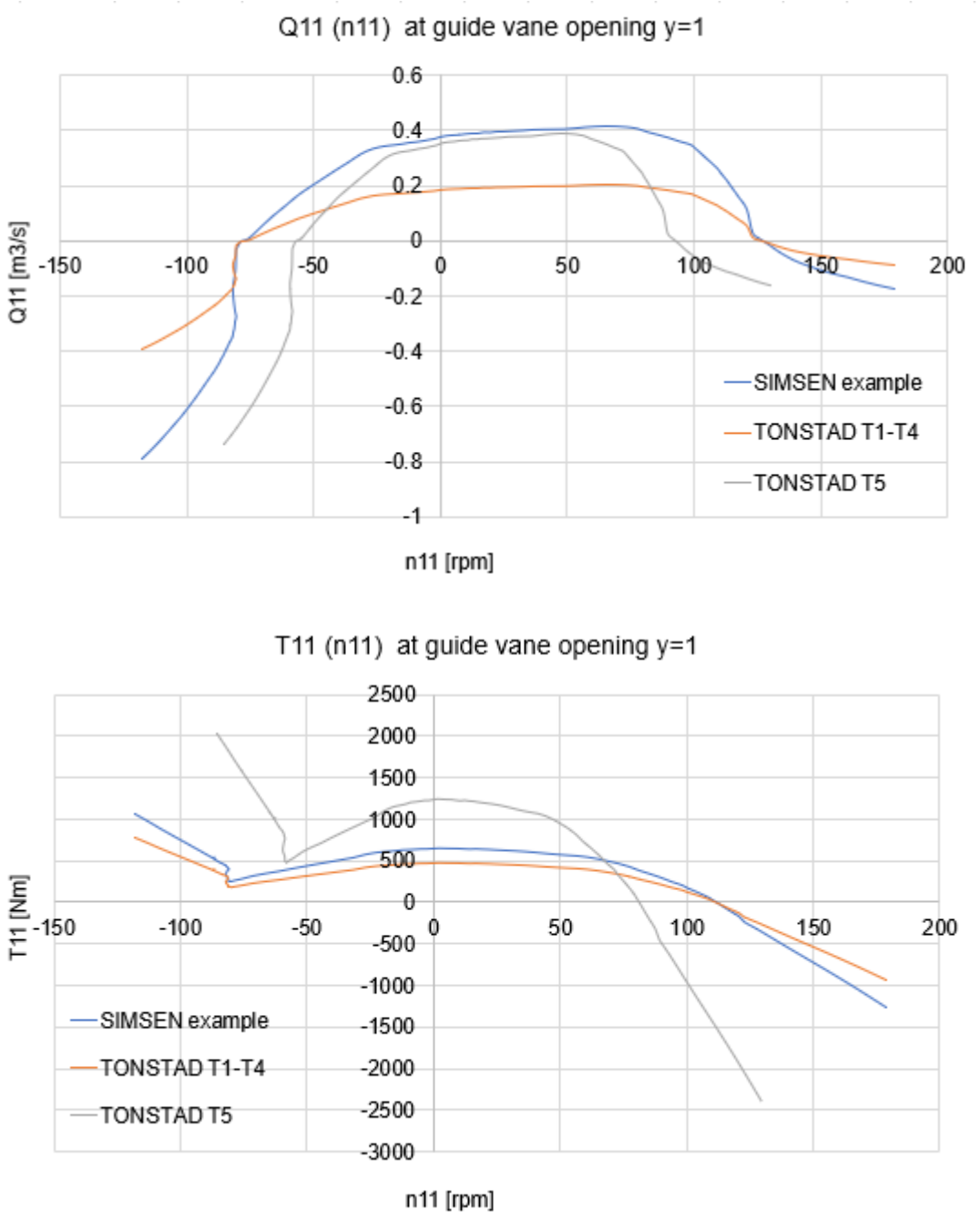

Figure 278: Turbine characteristic curves

15.1.4 **Throttle Marevatn**

In the brook intake pipe a throttle (Figure 279) is placed and model in terms of 1D-CFD.

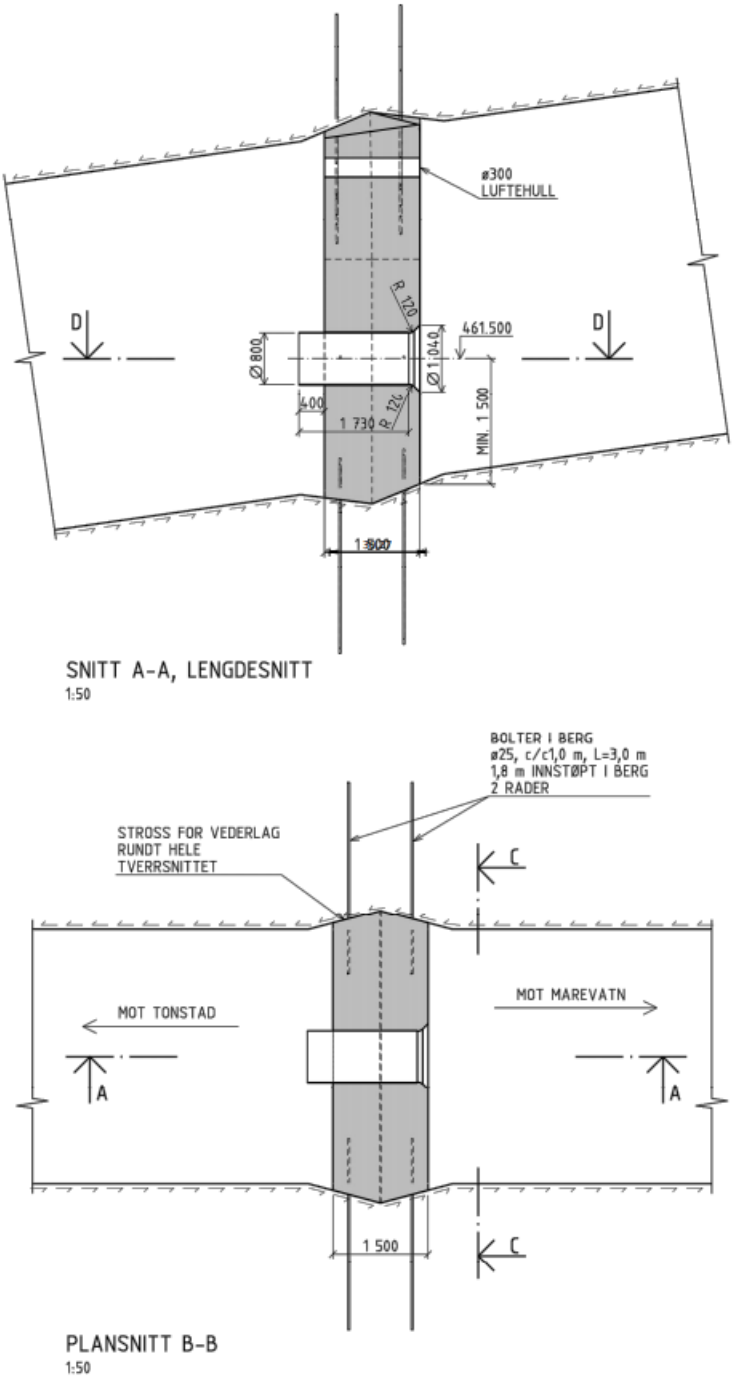

Figure 279: Section cut of Marevatn throttle

Local losses for positive flow and negative flow through the Marevatn throttle are sum of the three separate losses:

- pipe entry loss
- friction loss caused by the flow through the narrow section
- loss caused by sudden flow expansion that is calculated using Borda-Carnot equation.

				Borda-Carnot	Inlet	Friction				
	A1 [m^2]	A0 [m^2]	A2 [m^2]	ζloc1 [/]	ζloc2 [/]	λ [/]	L0 [m]	D0h [m]	ζfr [/]	ζ [/]
Negative flow:	19.64	0.50	19.64	0.9494	1.0000	0.0074	2.13	0.8	0.020	1.969
Positive flow:	19.64	0.50	19.64	0.9494	0.2000	0.0074	2.13	0.8	0.020	1.169

15.1.5 **Gate inlet of sand trap**

Local losses at the gate inlet of sand trap are sum of two separate losses, since it is assumed that friction is not causing significant loss in comparison with the expansion or constriction of the flow.

Because there are differences in the inlet structures of the sand traps No.1 and No.2 in comparison with sand trap No.3, different coefficients ζ´ were used to determine the local losses.

$$\zeta_{loc} \equiv \frac{\Delta p_{loc}}{(\rho w_0^2/2)} = \zeta' \left(1 - \frac{F_0}{F_1}\right)^{3/4}$$

Figure 280: Local loss at the entrance to the sand traps. (Idelchik, pg. 198)

In case of the santrap No.3 following graph from the Idelchik´s Handbook of Hydraulic Resistance is used.

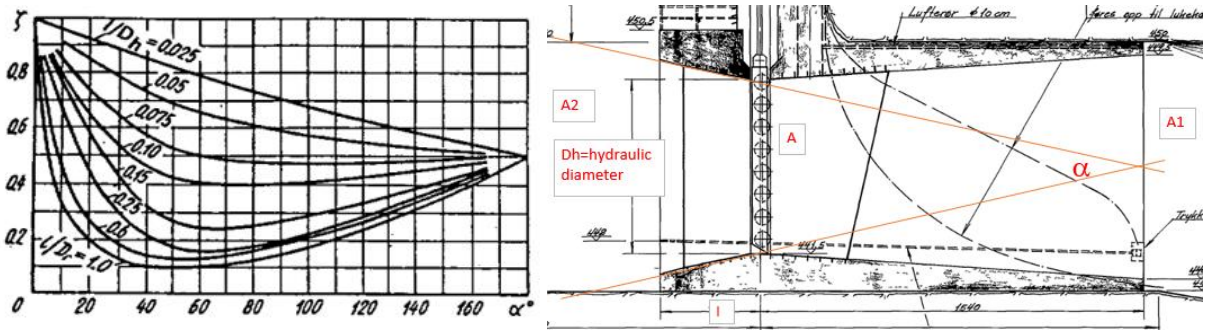

Figure 281: Local loss at the entrance in the sand trap No.3 gate inlet.

15.2 **Filling coefficient upper chamber**

The filling coefficient is found with Cdv = 8.0 and the exponent nv = 1.59. The values show some standard deviation, but due to the uneven water level in the surge tank and the transient filling in chamber it was found to be sufficiently correct. The values were defined in terms of 3d CFD simulations.

		Goal value	40,00		Formula
		Standard deviation	4,44	Q=Cdv(hcr-hcv)^{nv}	$Q=\mathbf{Cdv}(hcr-hcv)^{nv}$
					hcr… head riser
H1	H2		Cdv	nv	hcv… head vent or chamber
Average H Chamber	Average H Shaft	Difference delta H	8,00	1,5940	

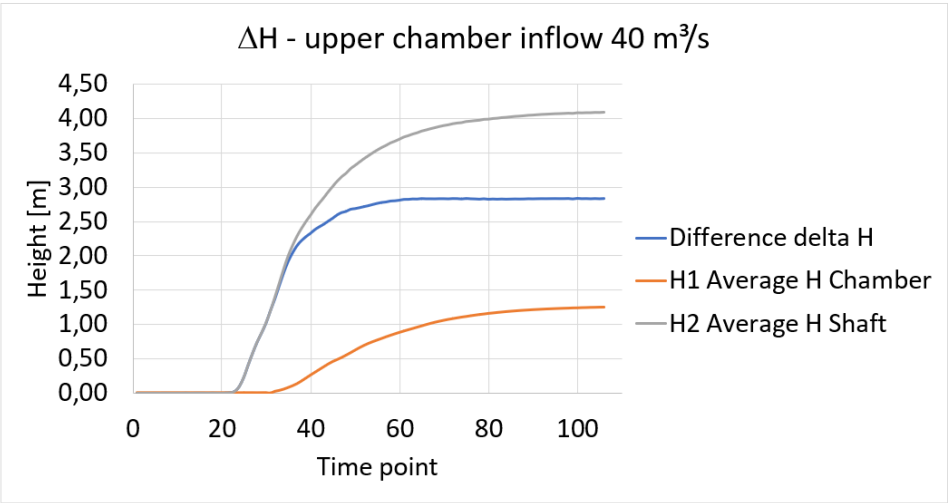

Figure 282: Filling coefficient for 40 m³/s

		Goal value	85,14		Formula
		Standard deviation	3,45		$Q=\mathbf{Cdv}(hcr-hcv)^{nv}$
					hcr… head riser
H1	H2		**Cdv**	**nv**	hcv… head vent or chamber
Average H Chamber	Average H Shaft	Difference delta H	**8,00**	**1,5940**	

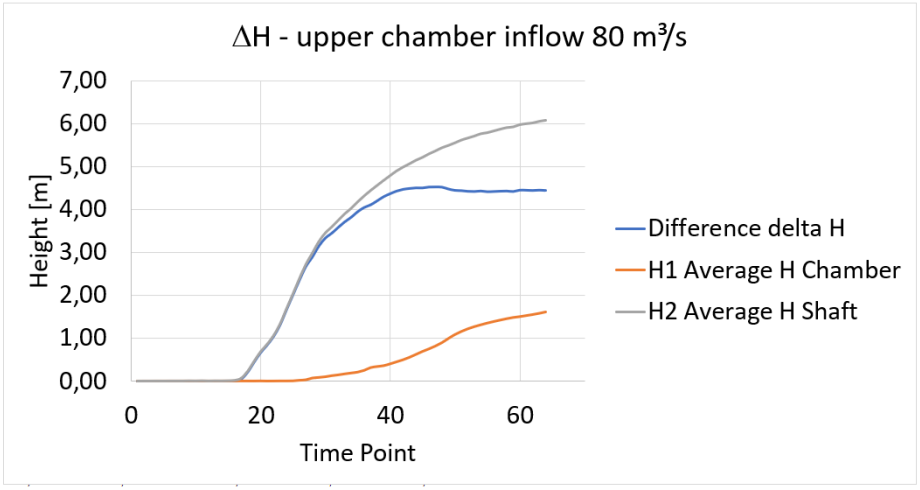

Figure 283: Filling coefficient for 80 m³/s

Figure 283 and Figure 284 show the geometry of the upper chamber of surge tank no.3 and the shaft section cut of surge tank no.1 and no.2.

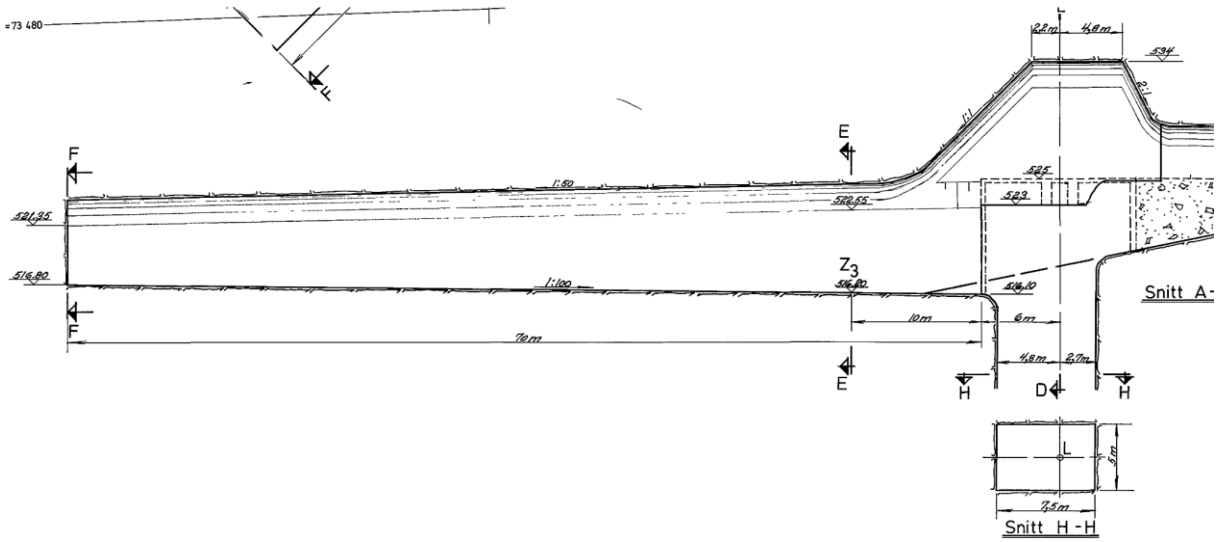

Figure 284: Upper chamber No.3 geometry

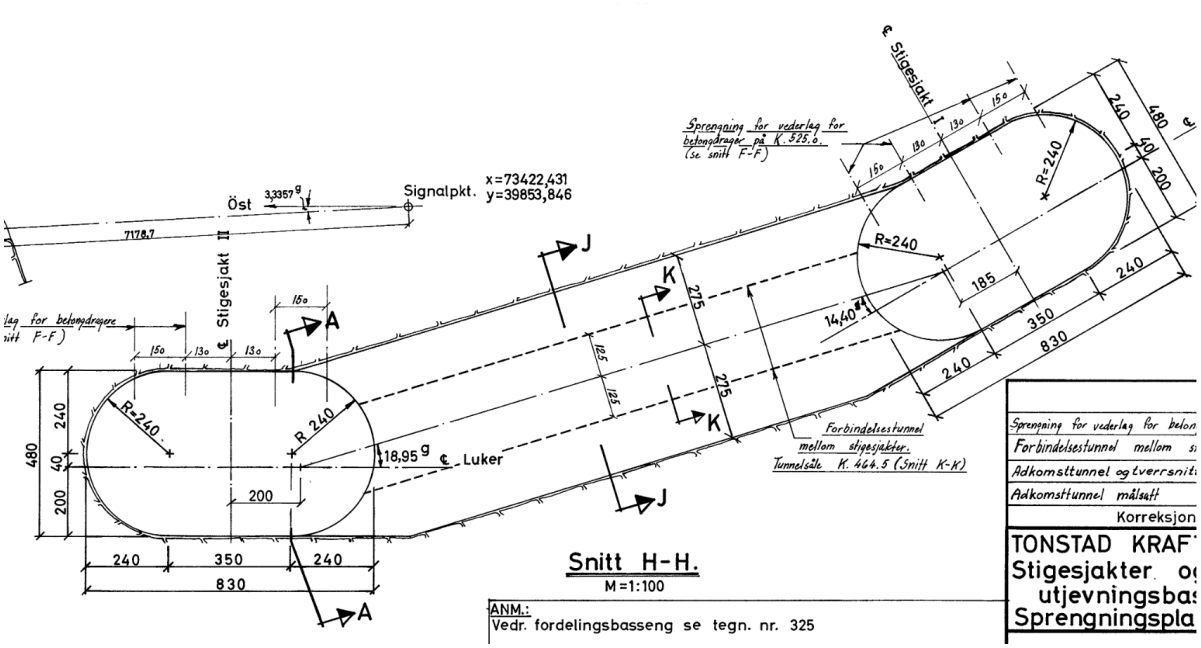

Figure 285: Shaft design of surge tanks No.1 and No.2

15.3 **Upper chamber restriction coefficient**

This chapter briefly describes the generation of the upper chamber filling coefficient. The 3d geometry is given in Figure 286.

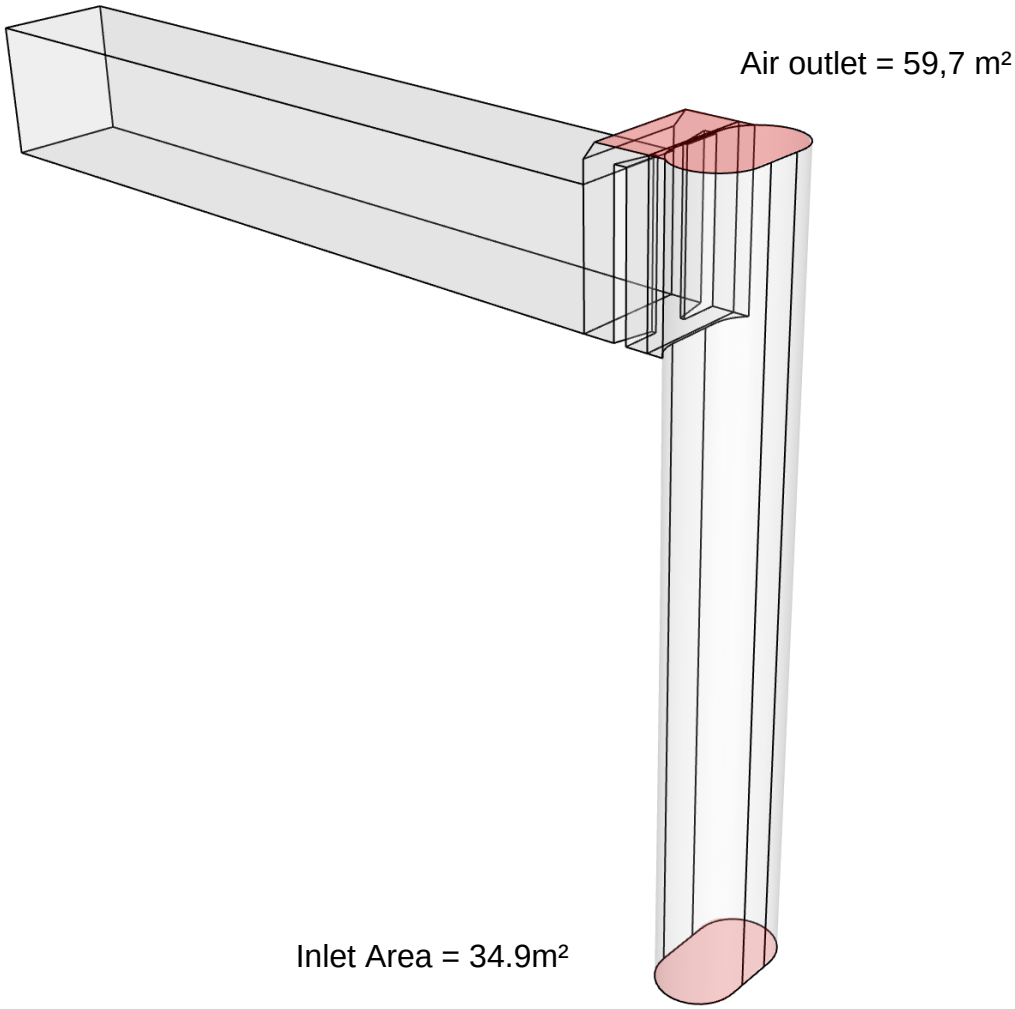

Figure 286: 3D geometry of upper chamber No.1 and No.2 with idealized chamber design for 3D CFD

Filling with 40 m³/s

The 3D CFD simulations were conducted by filling of 40 m³/s, the head loss can be used to unify the hydraulic filling parameter. Figure 287 to Figure 290 show the impact of the wall restrictions entering the upper chamber of the surge tank. These walls are placed in all three upper chamber entries.

Inlet velocity: 40 / 34.9 = 1.146 m/s

Air outlet velocity: 40 / 59.7 = 0.67 m/s

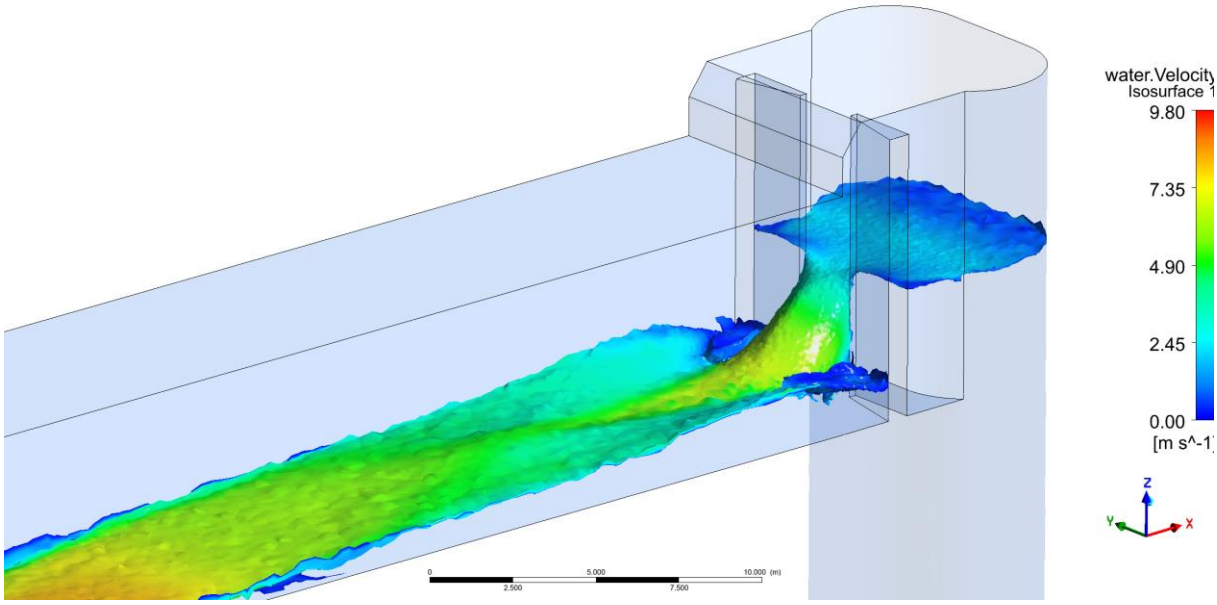

Figure 287: Filling with 40 m³/s into the upper chamber of Surge tank shaft No1 resp. No.2, iso view

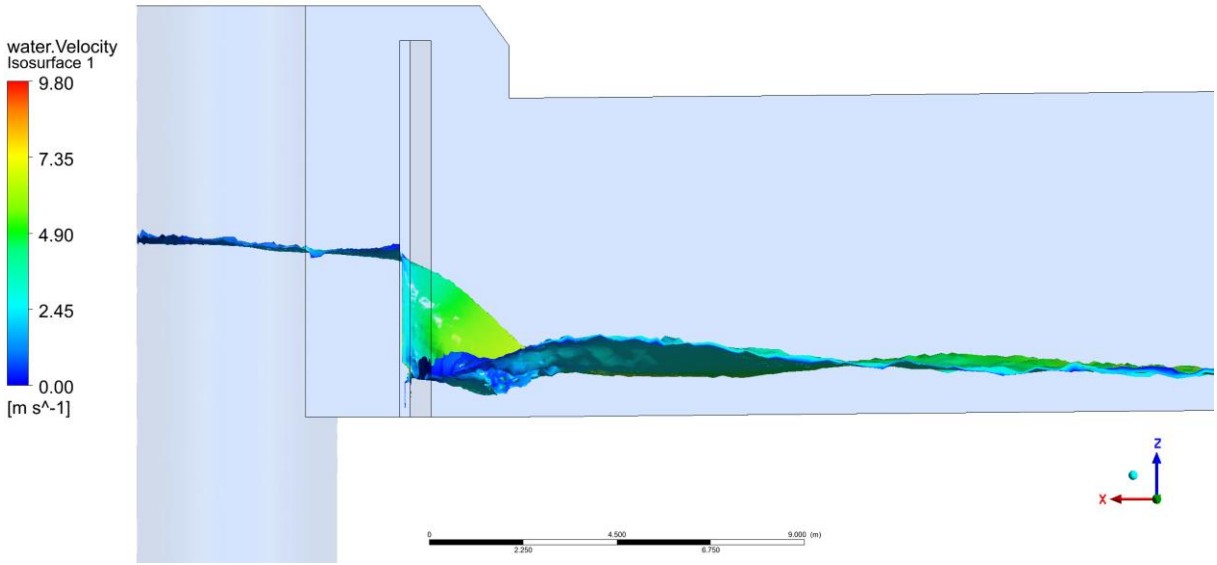

Figure 288: Filling with 40 m³/s into the upper chamber of Surge tank shaft No1 resp. No.2, side view

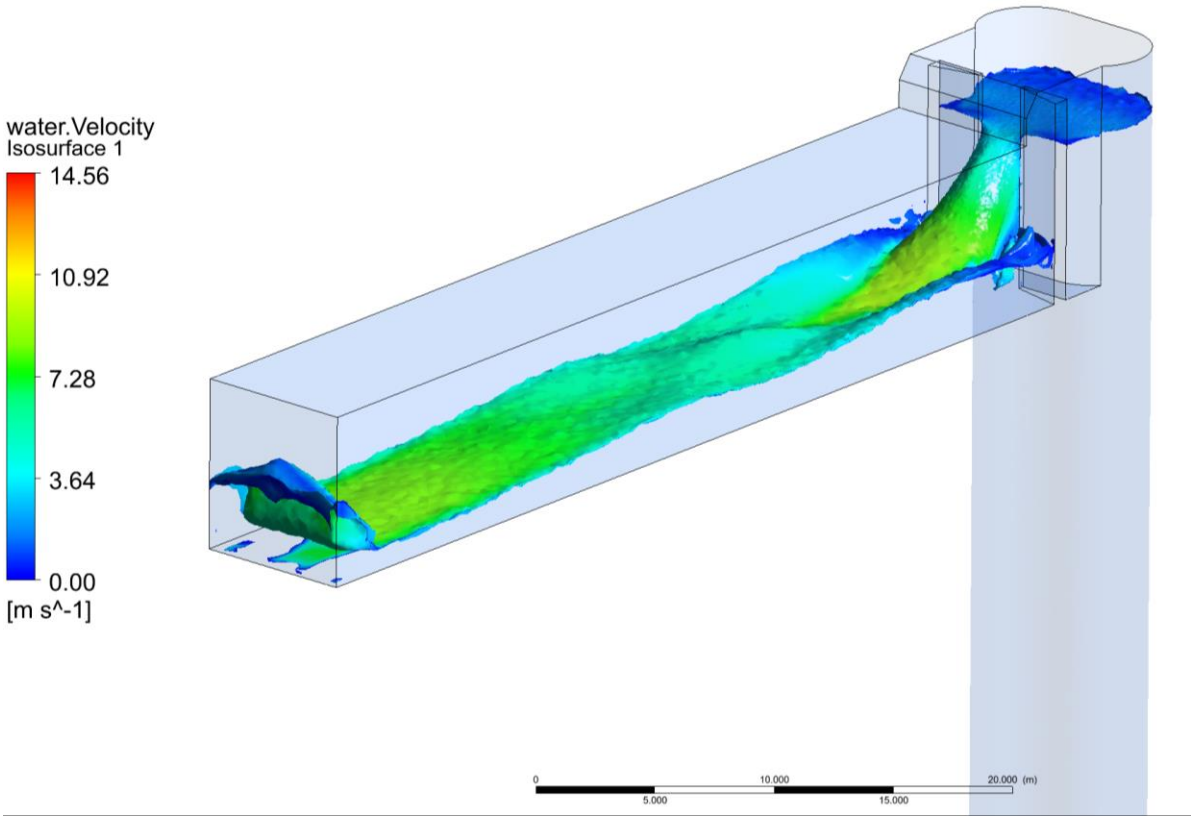

Figure 289: Filling with 40 m³/s into the upper chamber of Surge tank shaft No1 resp. No.2, iso view

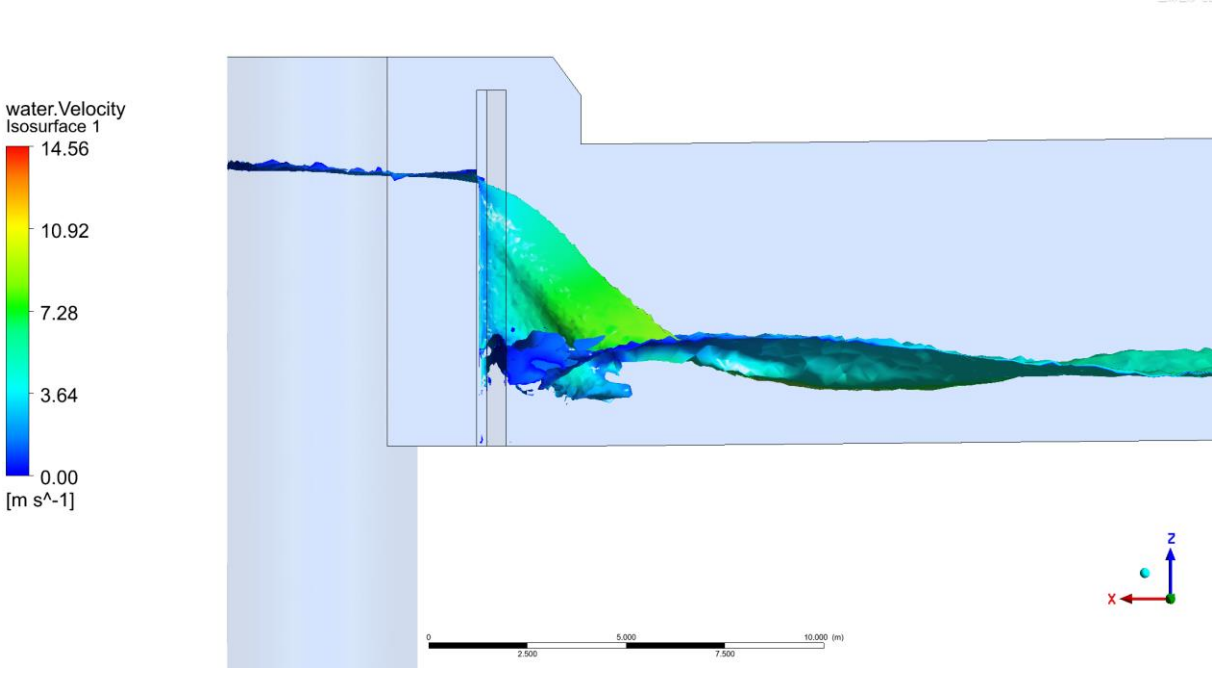

Figure 290: Filling with 80 m³/s into the upper chamber of Surge tank shaft No1 resp. No.2, side view

Figure 291 and Figure 292 the emptying of the upper chamber is represented. At a certain point the emptying capacity is not sufficient to follow the flow demand of the headrace tunnel, thus the outflow creates a significant water fall. Intruding also air bubbles into the conduit system.

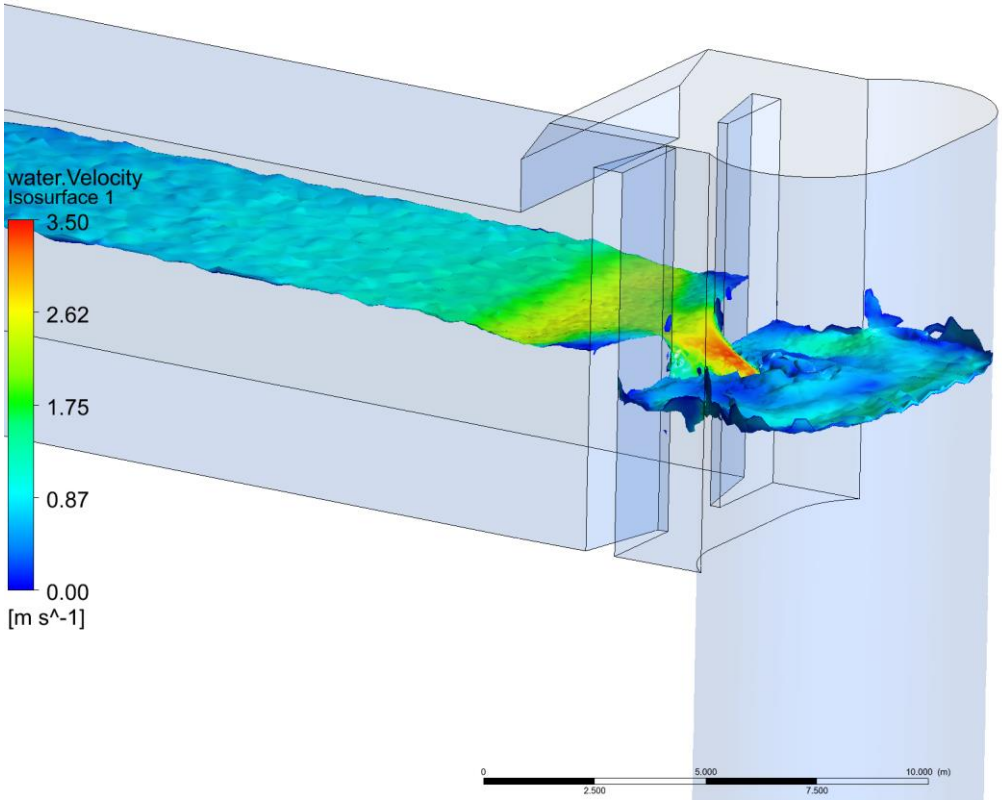

Figure 291: Emptying of 40 m³/s from the shaft of Surge tank shaft No1 resp. No.2, iso view

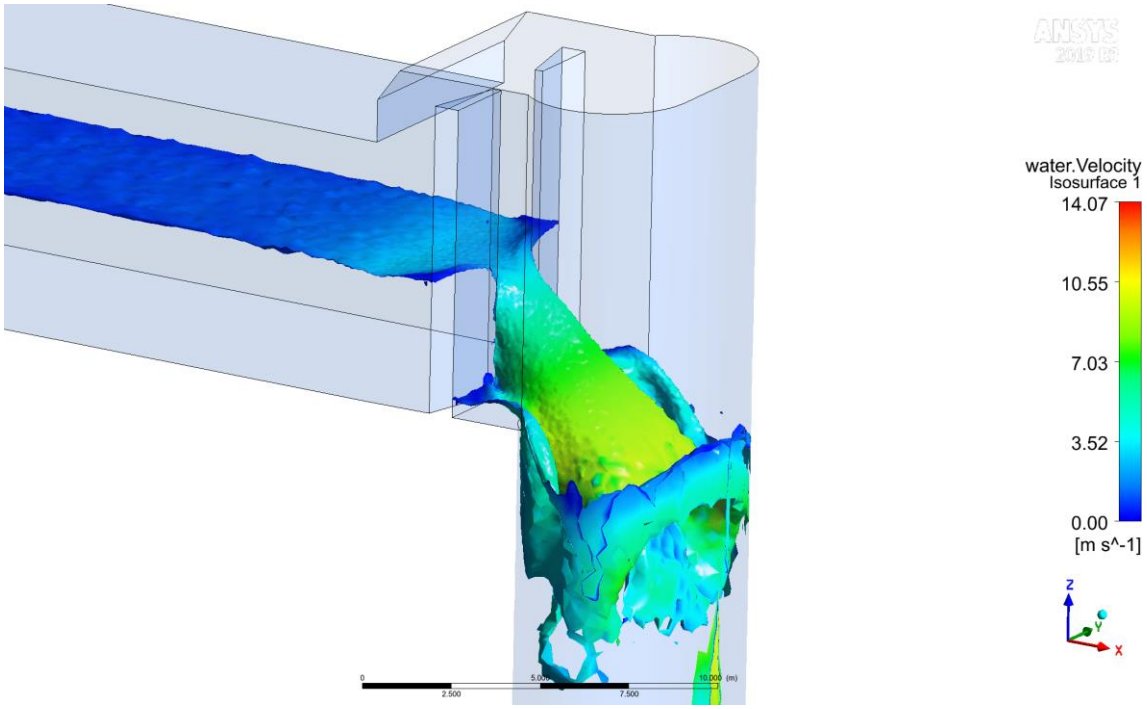

Figure 292: Emptying of 80 m³/s from the shaft of Surge tank shaft No1 resp. No.2, iso view

15.4 Upgrade with the reversible pump turbine

Beside the capacity increase, additional reversible unit will have significant influence on the flexibility of the power plant. Solution from Sterner (2018), with the semi-air cushion surge tank of the Unit No.6, connected as extension chamber to the sand trap of the Unit No.5 also allows operation of the power plant in the hydraulic short-circuit mode. Such setup is therefore used for 1D numerical simulations.

15.4.1 Reversible pump-turbine characteristics

Design procedure is following R.S. Stelzer and R. N. Walters (1977).

The pump turbine is designed with following design conditions:

Output: 236 MW

Head: 450 m

Turbine discharge: Q_t= 60 m^3/s

Pump-turbine operation range: 432.5 m to 450.1 m

Assumptions:

Pump BEP Head: 440 m

Turbine efficiency: η_t= 89%

Pump efficiency: η_p= 92%

Pump discharge: $Q_p = \frac{Pp*\eta p}{H_{BE}*\gamma} = 60.1\ m^3/s$

Pump rotational speed: $n = \frac{nsp*{H_{BE}}^{3/4}}{{Q_{BE}}^{1/2}} = 758.53\ r/min \quad \rightarrow \quad n = 750\ r/min$

Pump submergence: H_s = NPSH - H_a + H_v + H_f

H_s = 40 m

15.4.2 Hydraulic conduits of the RPT

Headrace tunnels are following to Mauko (2020) capable to conduct discharge for the additional unit, for this reason and because of their length no adaptations are made in this part. In the tailrace tunnels is noticed that higher discharge would cause significant increase of the head loss. Therefore, in 1D model is used additional tailrace tunnel for the Unit No.6. Since the additional tunnel will be executed in the same material as the existing one, using the similar excavation method, friction coefficient is assumed to be the same. Diameter of the tailrace tunnel is calculated assuming the same head loss as in the existing tunnel. Penstock No.4 is assumed to have the same inclination and the same head loss as the penstock No.3. Because of the deeper submergence of the RPT, penstock No.4 will be 692 m long. Because of the high rock quality, penstock No.4 is assumed to be built without lining. Diameter of the penstock is calculated assuming the same head loss as in the penstock No.3.

16. Semi-air cushion chamber

In previous investigations it was found that the Tonstad power scheme can be upgraded of 25% discharge flow in the headrace tunnel if lower chamber capacity of the surge tank is expanded (Richter, Vereide und Zenz, Upgrading of a Norwegian pressurized sand trap combined with an open air surge tank 2017), (Sterner 2018). Figure 293 and Figure 294 show the lower chamber extension.

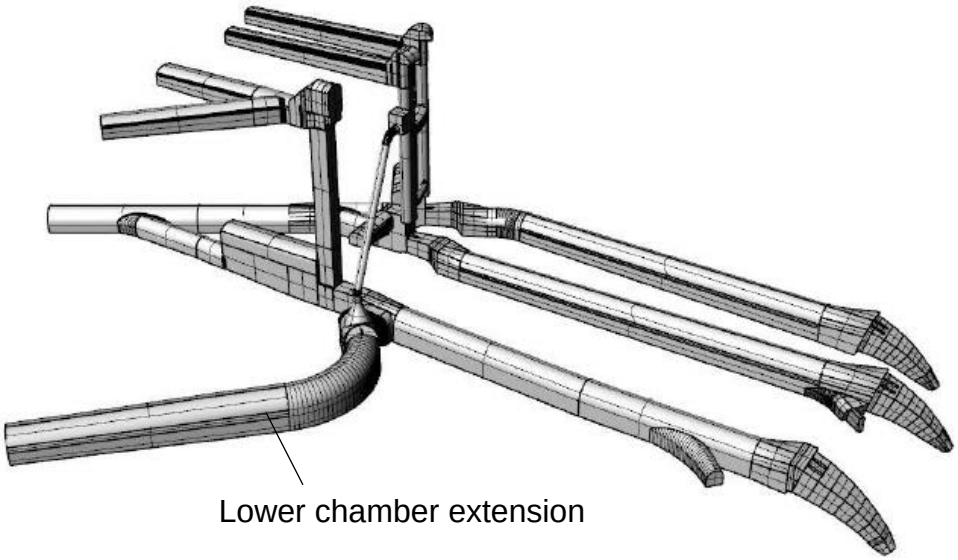

Figure 293: Geometry of the Surge Tank Tonstad with extension chamber (Sterner 2018)

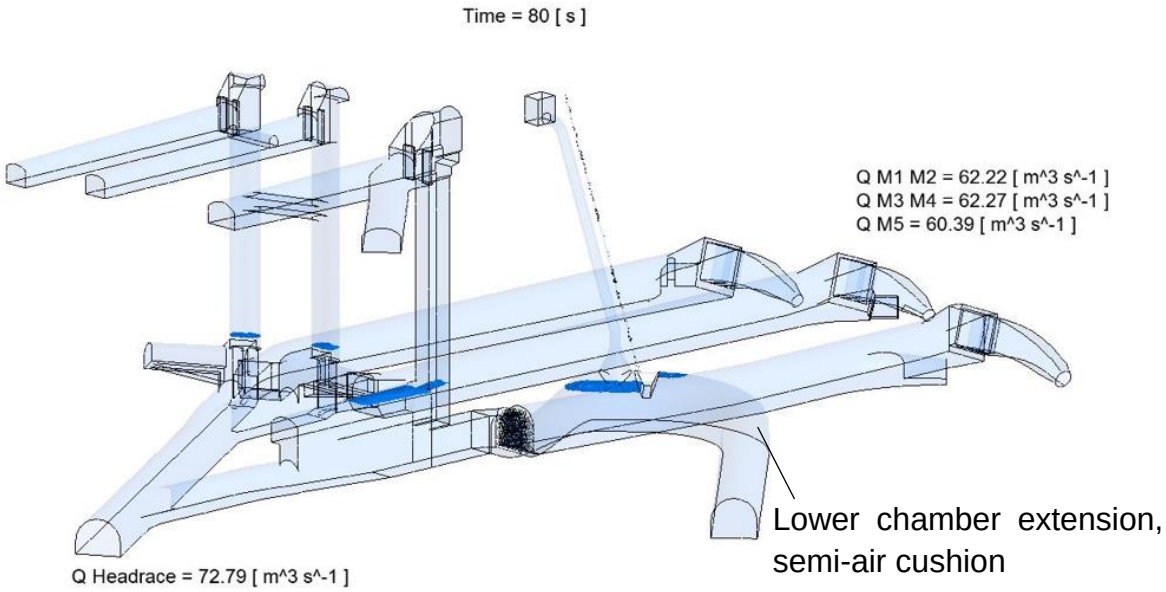

Figure 294: Timestep of differential effect in surge tank Tonstad with extension chamber, creating semi-air cushion (Sterner 2018)

For the present report the semi-air cushion approach was further investigated to improve the design principle and to check its ability for a potential Tonstad upgrade in discharge and flexibility.

Furthermore the principle is investigated to be a potential surge tank geometry for specific surge tank design purposes.

16.1 Semi-air cushion principle design

Figure 295 shows the principle layout of the semi-air cushion design as initial design for Tonstad upgrade. The crown throttle is the structural detail to create and separate the semi-air cushion, a temporary air cushion that is filled with water in relation to the air release via the aeration pipe. The aeration pipe is the throttling element that is decisive for the tuning of the semi-air cushion. This is mainly done by choosing the aeration pipe diameter and can be enhanced by manual adjustments somewhere at an accessible place of the aeration pipe (at top) to calibrate and fine-tune the loss. No automatic moving element is recommended to be installed in order to prevent unintended closing. The Temporary air cushion also equivalently represents the water volume as for an upper chamber since its filled under pressure, due the throttled air outflow. The substitution of the upper chamber filling demand depends on the specific design load case.

The semi-air cushion in Figure 295 separates between aeration pipe and water riser. The volumes were found in previous 1D numerical transient simulation applying a 25% discharge upgrade of Tonstad power plant. The water riser, together with the whole surge tank system fulfils the stability criterion. This riser allows under-pressure-free operation of the semi-air cushion. A minimal water level is important to be left, especially in the application of a flow-through semi-air cushion as discussed below for potential pump-turbine upgrade. Furthermore, in the approach the crown throttle level was defined in deeper level.

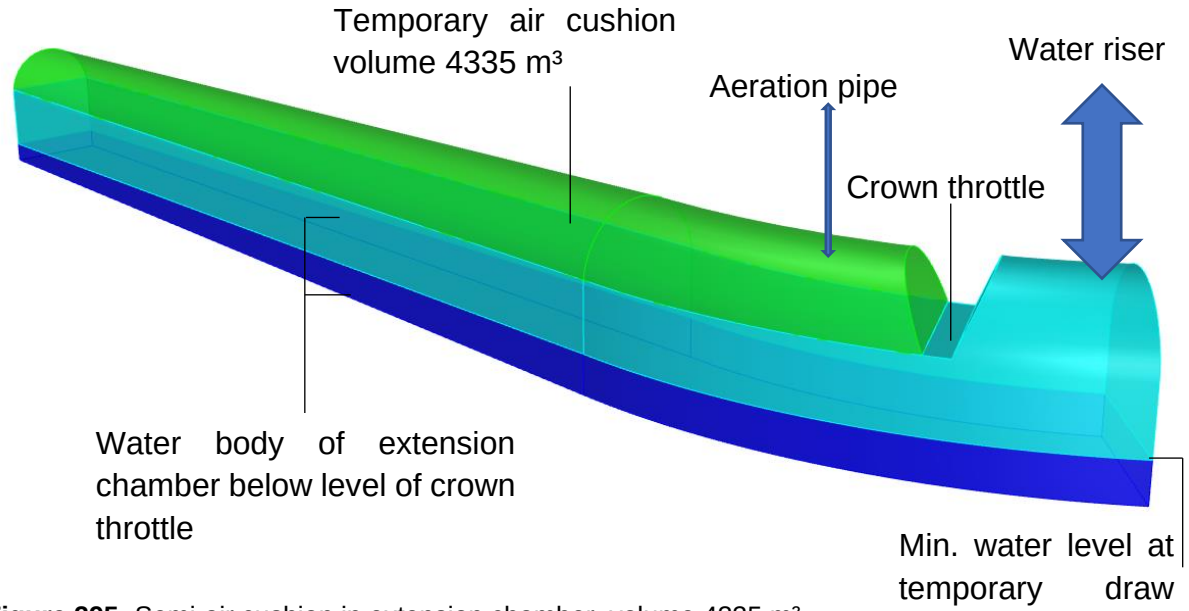

Figure 295: Semi-air cushion in extension chamber, volume 4335 m³

16.2 **Air pipe and water pipe geometry**

Figure 296 to Figure 303 shows the design approach with an air pipe of Di = 0.4 m and water riser with Di = 3.0 m for the semi-air cushion surge tank design. The extension chamber is attached downstream of the diffusor and showing the combination with potential calming rakes as investigated above, as shown, these rakes finally were found to be recommended due to inefficient sedimentation improvements.

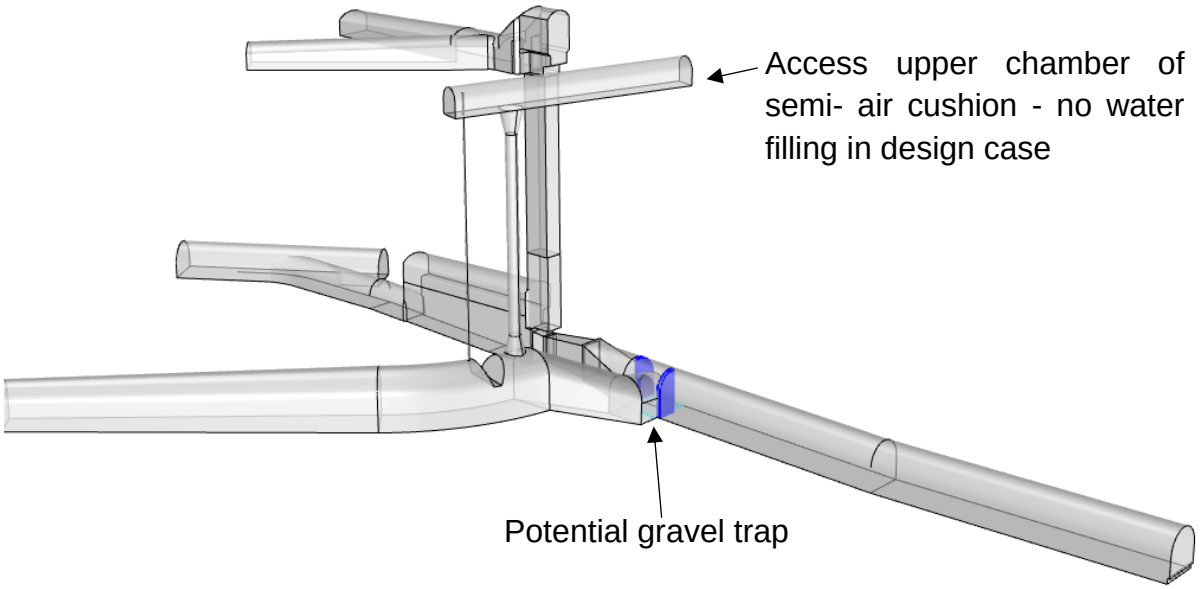

Figure 296: Semi-air cushion in extension chamber, upper chamber, air vent pipe, tranquilizing rake opportunity

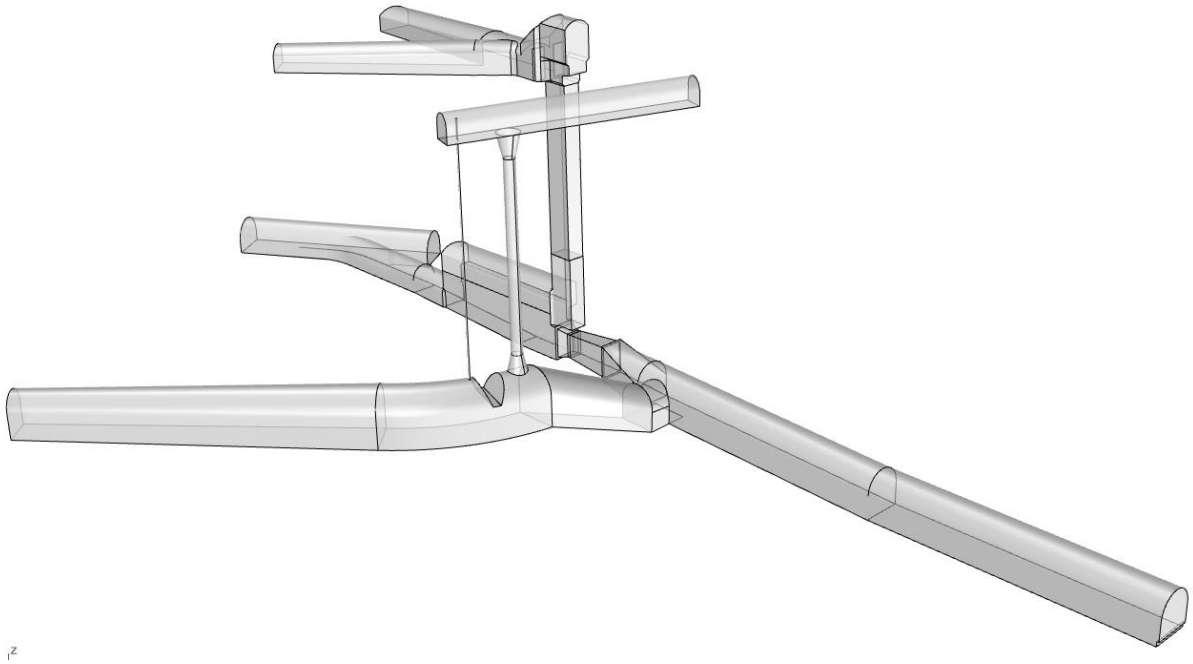

Figure 297: Semi-air cushion in extension chamber, upper chamber, air vent pipe

The potential gravel trap would consist of a point lowering downstream of the diffusor to collect gravel on a highly concentrated point to be sluiced by gravel sluicer.

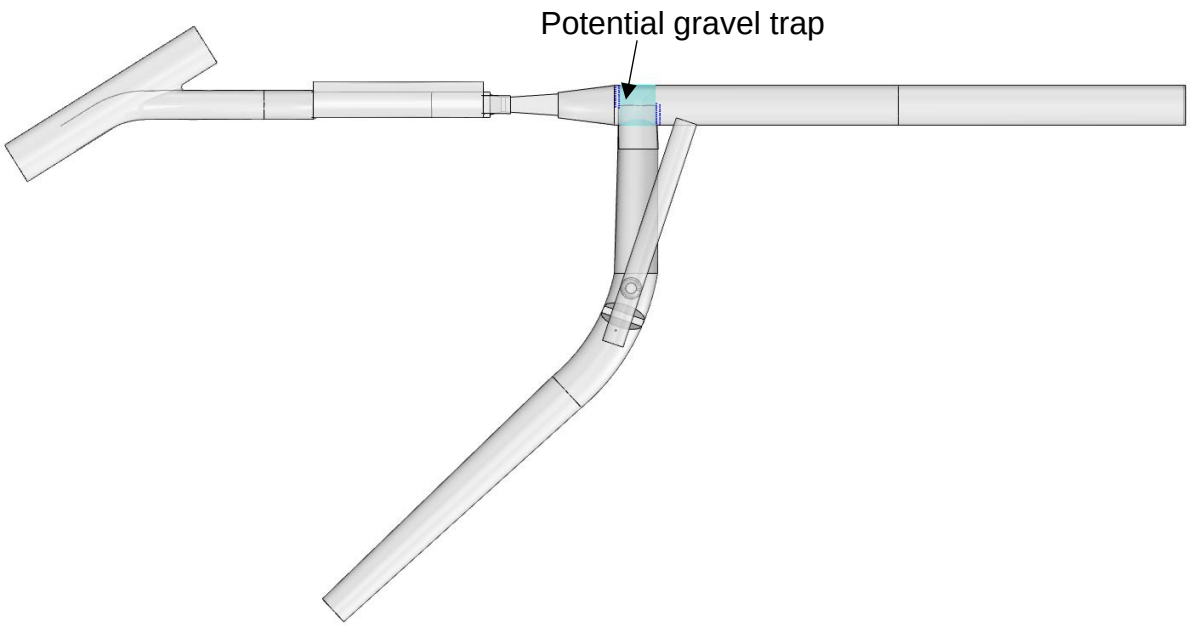

Figure 298: Semi-air cushion in extension chamber, plan view

Figure 299 shows the geometry levels of the semi-air cushion design proposal. The level of the access upper chamber invert is with 526.7m above the crown of the existing upper chambers of Tonstad power plant. Thus, this chamber is not intended to be filled with water. However, it contains volume for safety aspect.

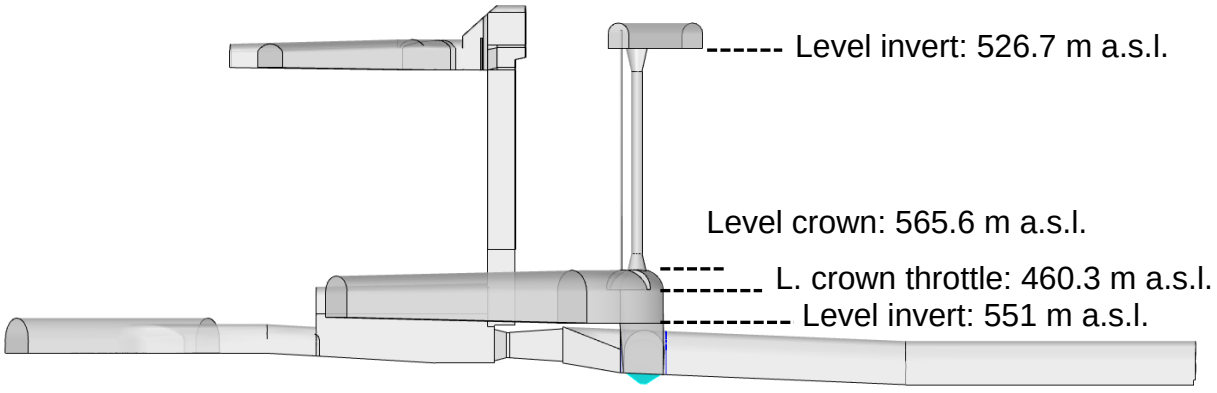

Figure 299: Semi-air cushion in extension chamber, side view with surge tank No.3

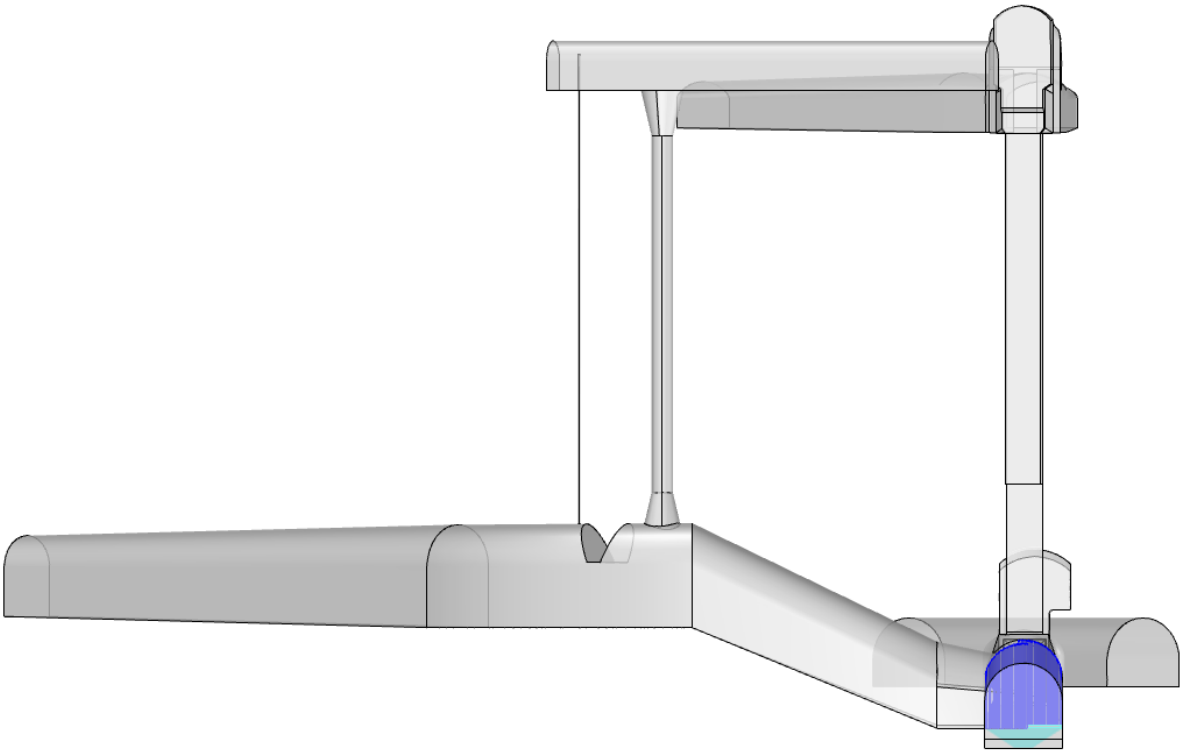

Figure 300: Semi-air cushion in extension chamber, front view with surge tank No.3

Figure 301 shows a detail proposal of aeration pipe inlet/outlet in the access upper chamber. The pipe mouth is lead further inside the access upper chamber with a significant higher level as the bottom. This allows to keep air flow only. Due to pressure gradient at the outlet flow with high velocities, freezing must not decrease the operational safety.

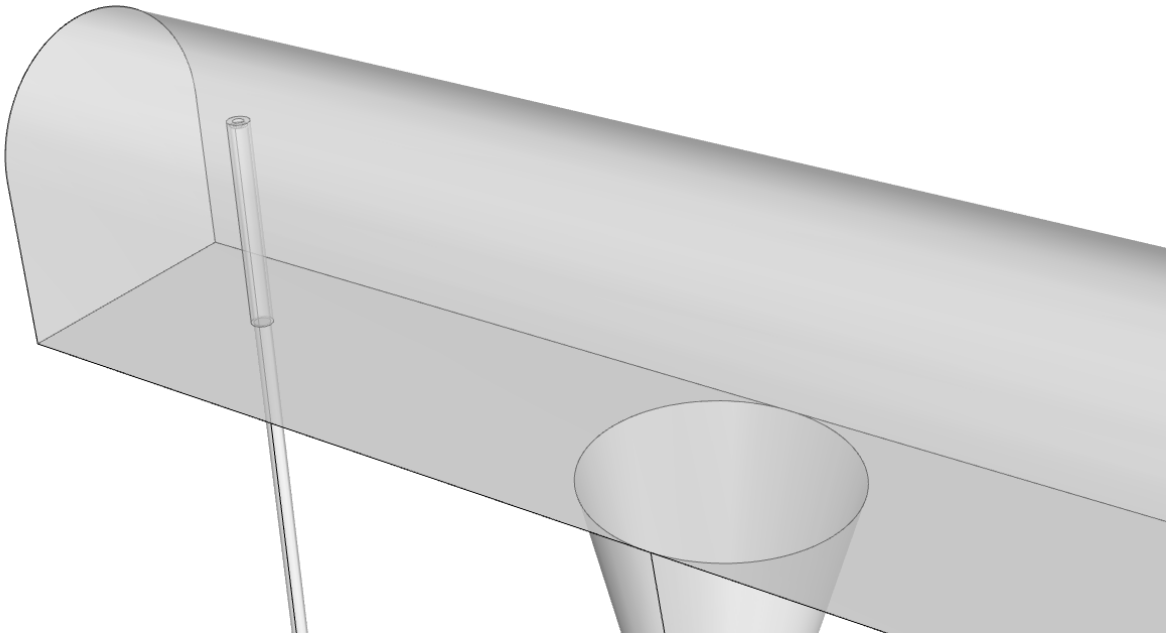

Figure 301: Semi-air cushion in extension chamber, detail air vent, shaft connection

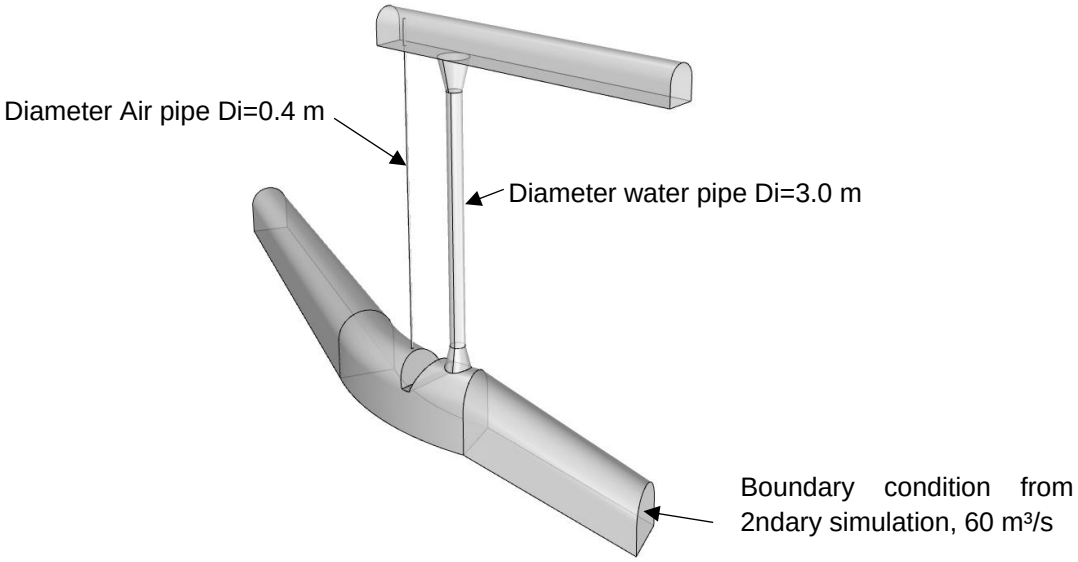

Figure 302: Semi-air cushion in extension chamber, geometry for 3D simulation

Figure 303 shows the free surface water level at lower crown throttle elevation in the 3D CFD simulation.

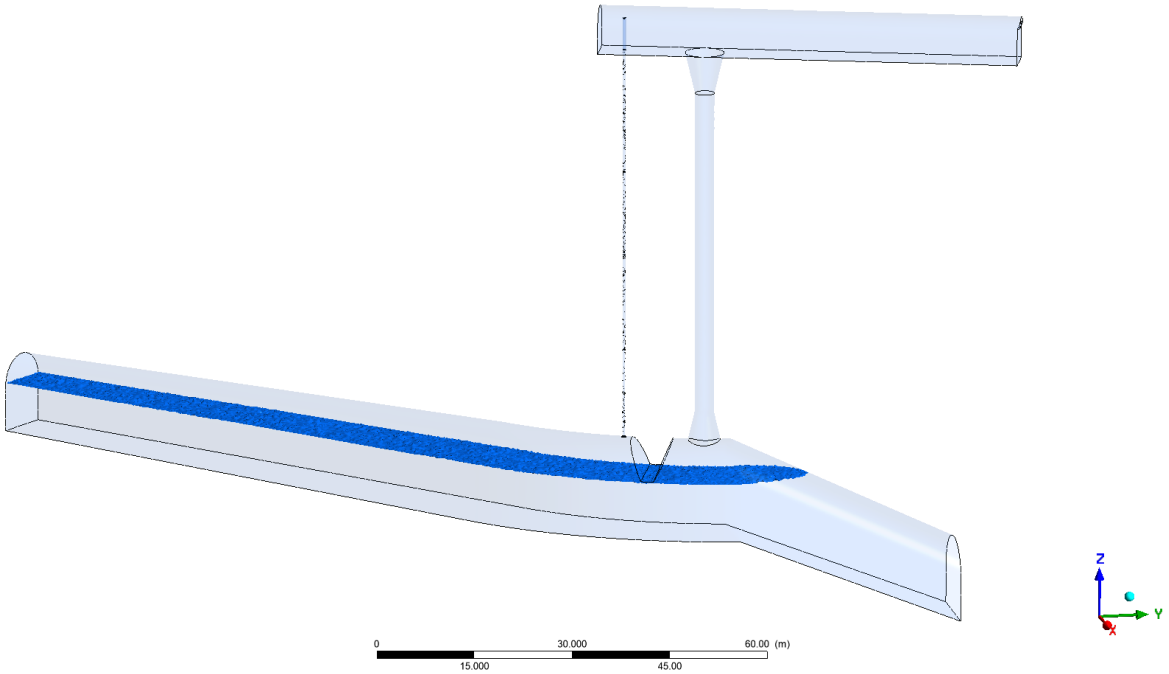

Figure 303: Semi-air cushion initial condition for simulation

16.3 **Semi-air cushion design in flow-through for pumped-turbine unit**

Several design iteration steps were investigated to propose the following design that allows a potential operation of a pumped storage unit to be connected to the existing Tonstad hydraulic power plant system.

The design as shown in Figure 304 additionally contains a sand trap design, that is to be covered by ribs according to the sand trap investigations above. The sand trap in this case is a longitudinal trench that can be equipped with a longitudinal sluicing device and the ribs creating the actual sand trap. Instead of a ramp the trench is a lowering of the bottom of the chamber.

The lower level of the crown throttle was found to be set at 456.3 m a.s.l. to best balance the up-surge flow of the mass oscillation in accordance with the existing surge tanks no. 1 to no. 3. Therefore, the crown throttle and the bottom of the semi-air cushion at this section are lowered to 447 m a.s.l.

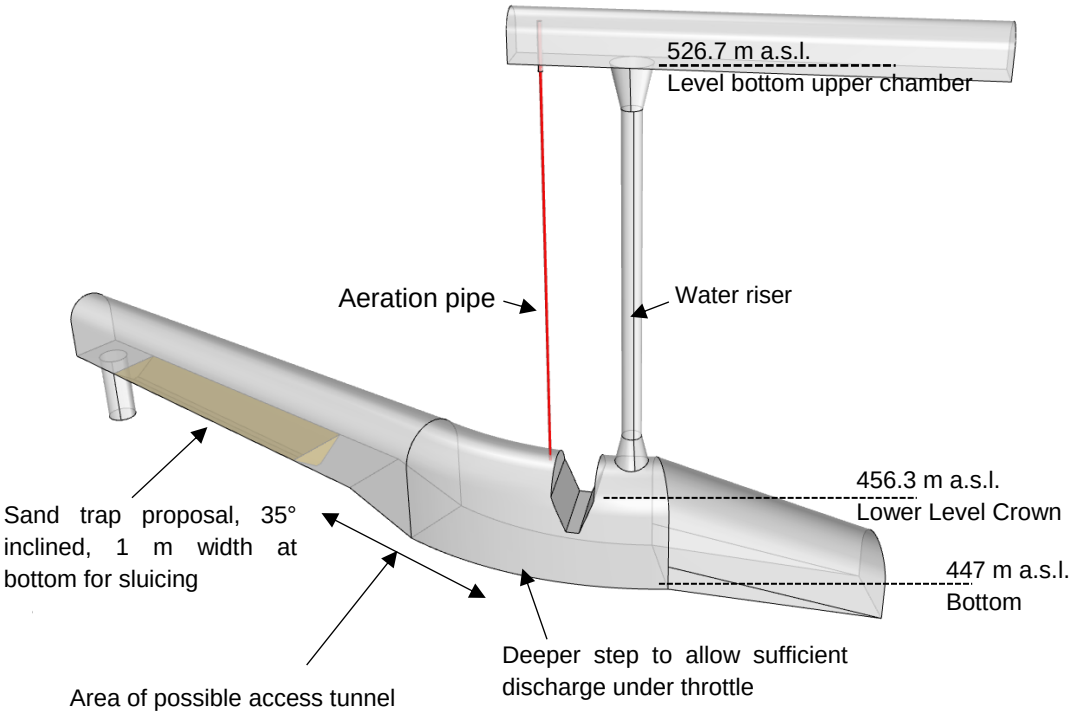

Figure 304: Flow-through semi-air cushion with sand trap proposal and deeper crown throttle.

16.4 **Time for semi-air cushion during oscillation**

Figure 305 shows the mass oscillation event of start-up and emergency shut-down of Tonstad power plant with 5 units plus unit 6 with in sum 25% higher discharge. The 1D-numerical simulation was done with a WANDA model built up for Tonstad power plant (Flextrap project 1.0). The model was adapted to allow simplified capturing the semi-air cushion effect regarding the mass oscillation. This simulation is needed to define the discharge and volume demand of the semi-air cushion water volume.

The filling time of the semi-air cushion water volume directly leads to the assumption of the aeration pipe diameter to be designed.

The simulation includes all surge tanks of Tonstad and shows an oscillation filling time of about 120 s.

The Semi-air cushion must be in accordance to the existing surge tank system of Tonstad in order to properly balance the discharge and pressure rates between the specific surge tanks no. 1 to no. 3.

The lower level of the crown throttle is decisive for best balancing the discharges between the existing surge tank and the potential new attached extension chamber. Once the water level reached the level of the crown throttle, the throttled outflow of the aeration shaft starts and throttles the upswing in the semi-air cushion surge tank.

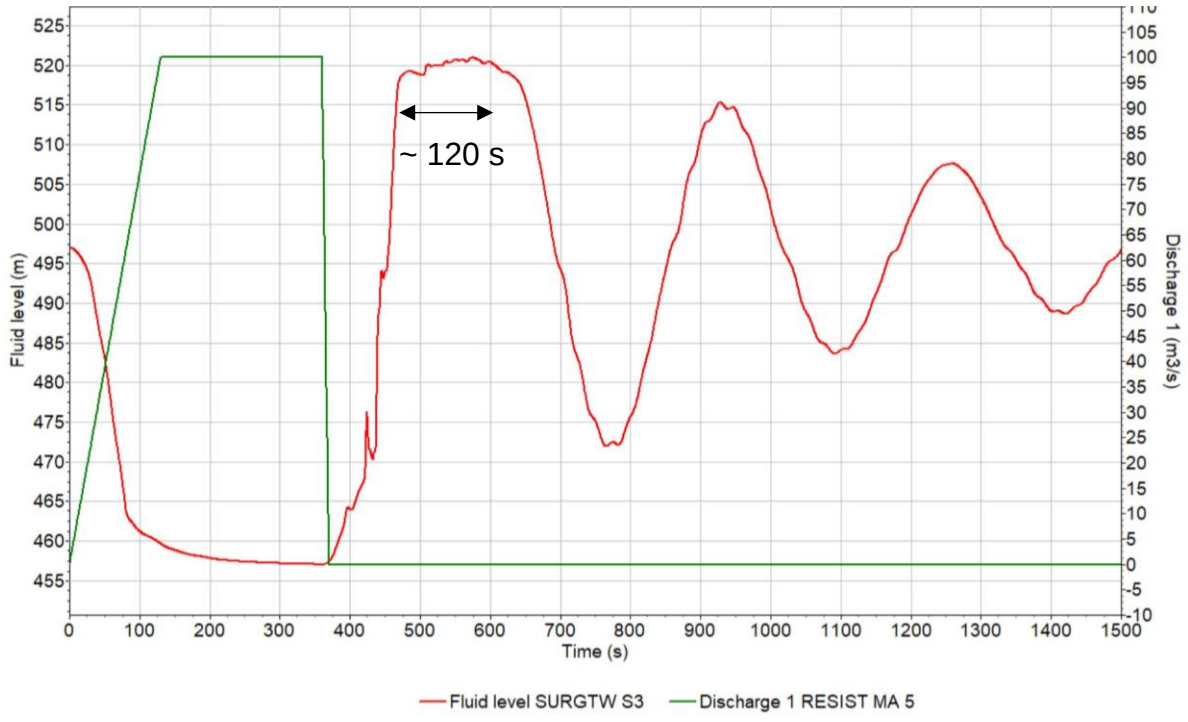

Figure 305: Mass oscillation with expansion chamber with 25% discharge upgrade – opening – shut down, capacity level 497 m a.s.l.

16.5 **Aeration pipe Design**

The aeration pipe defines the throttling effect of the air release at filling of the water volume behind the crown throttle. The air pipe is proposed to consist of a steel pipe.

16.5.1 **Air pipe Di = 0.5 m**

To allow 75 m³/s discharge an air pipe with Di = 0.5 m is applied. Figure 306 and Figure 307 show a possible design of an asymmetric air throttle inlet. Further, it was found to recommend a simple air pipe expansion from the pipe to the ambient chamber.

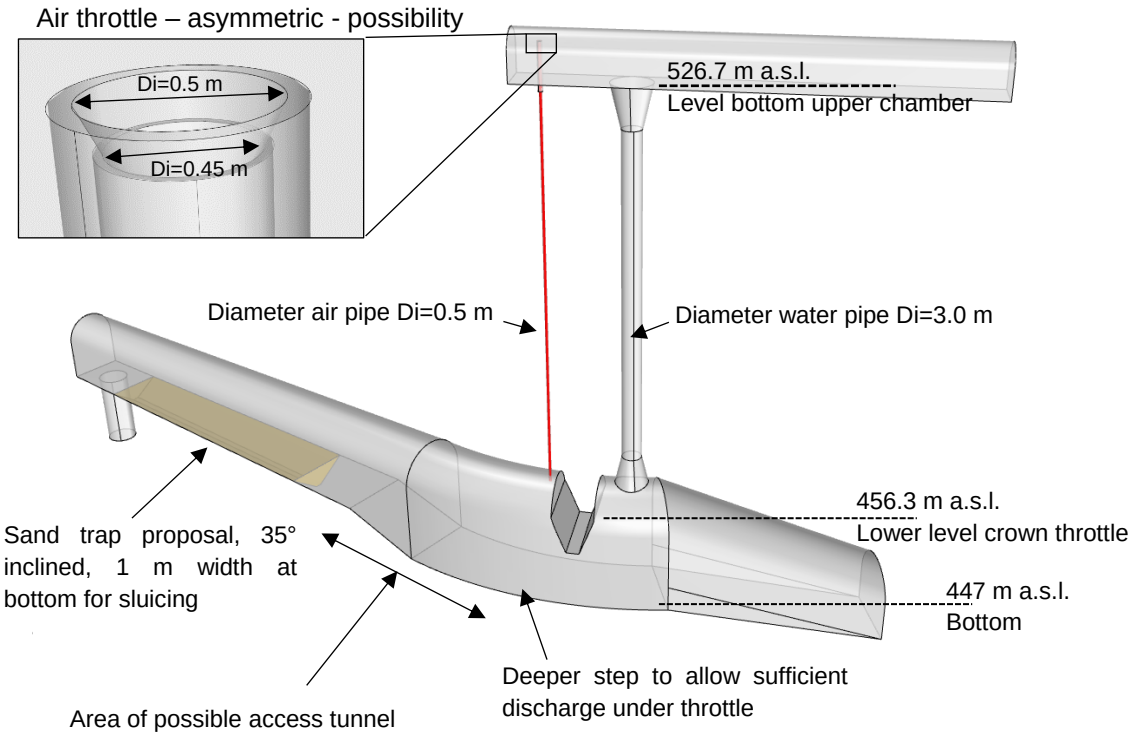

Figure 306: Semi-air cushion with sand trap proposal and deeper crown throttle, air pipe Di = 0.5 m for 75 m³/s discharge at 72 m head difference

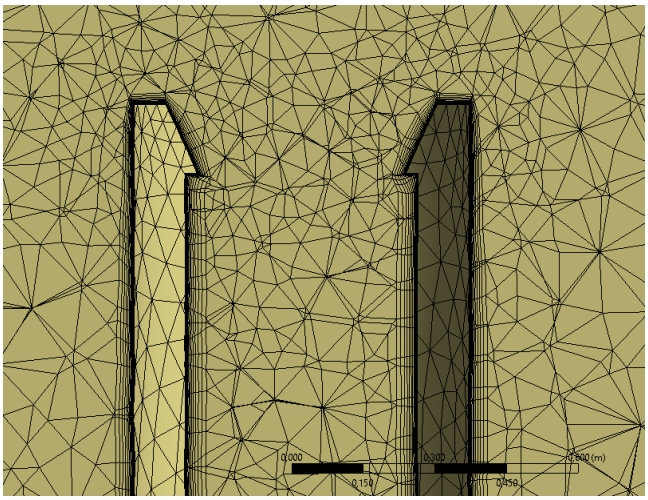

Figure 307: Meshing of air throttle with unstructured mesh and inflation layer

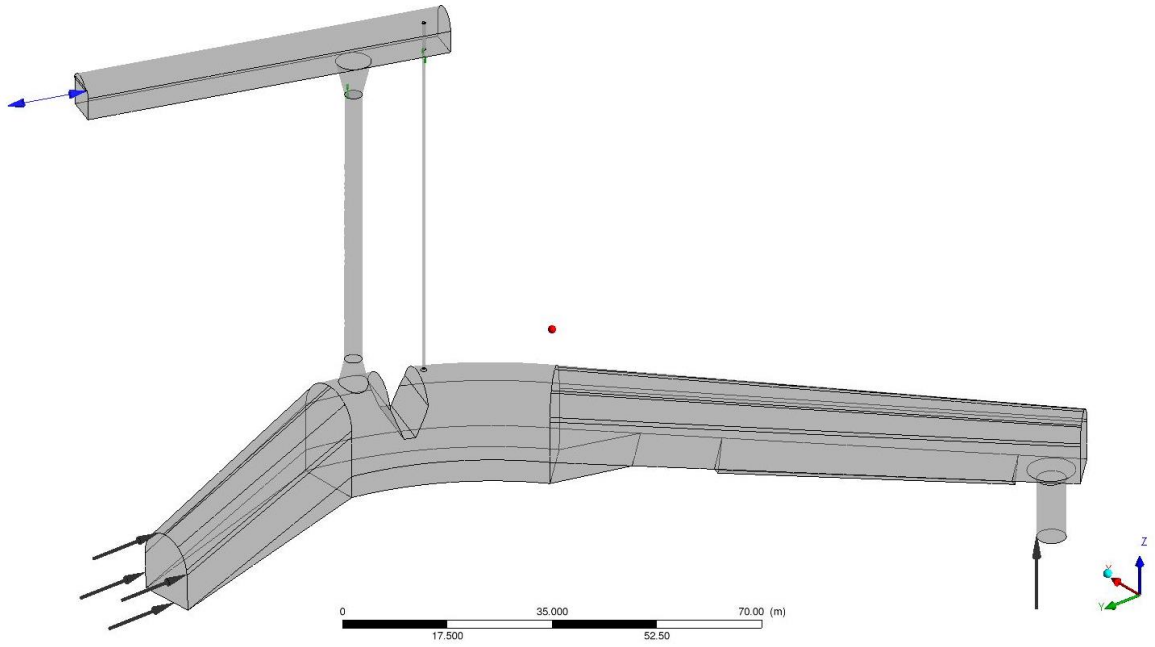

Figure 308: Boundary conditions setting for the 3d CFD simulation

Figure 309 shows the steady state operation of unit no. 6 with 60 m³/s. A steady flow with free surface is generated. The rest of Tonstad power plant is in this load case also in full operation. Thus, the 60 m³/s represent the additional 25% discharge at potential Tonstad upgrade. The ribs are not yet placed in this simulation. The free surface is still allowing pressurized flow through the sand trap chamber no. 3 of Tonstad power plant.

Further hydraulic investigations are recommended to check if the gate section of surge tank no. 3 is capable resp. adaptable of 140 m³/s.

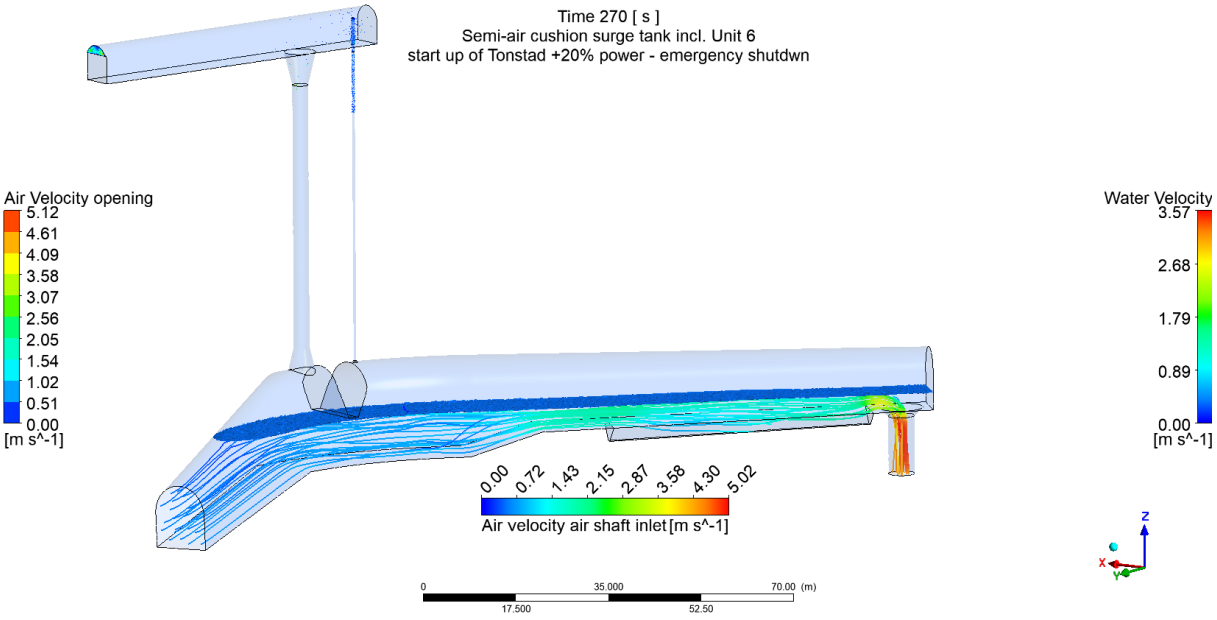

Figure 309: Steady state operation at full operation Tonstad with +25% discharge and 20% power upgrade via unit no. 6

Figure 310 shows the differential effect of the air throttling pipe; the water level in the water riser is representing the pressure upstream the crown throttle, that is in hydraulic connection to the water levels and pressure levels of the surge tanks no.1 and no. 2.

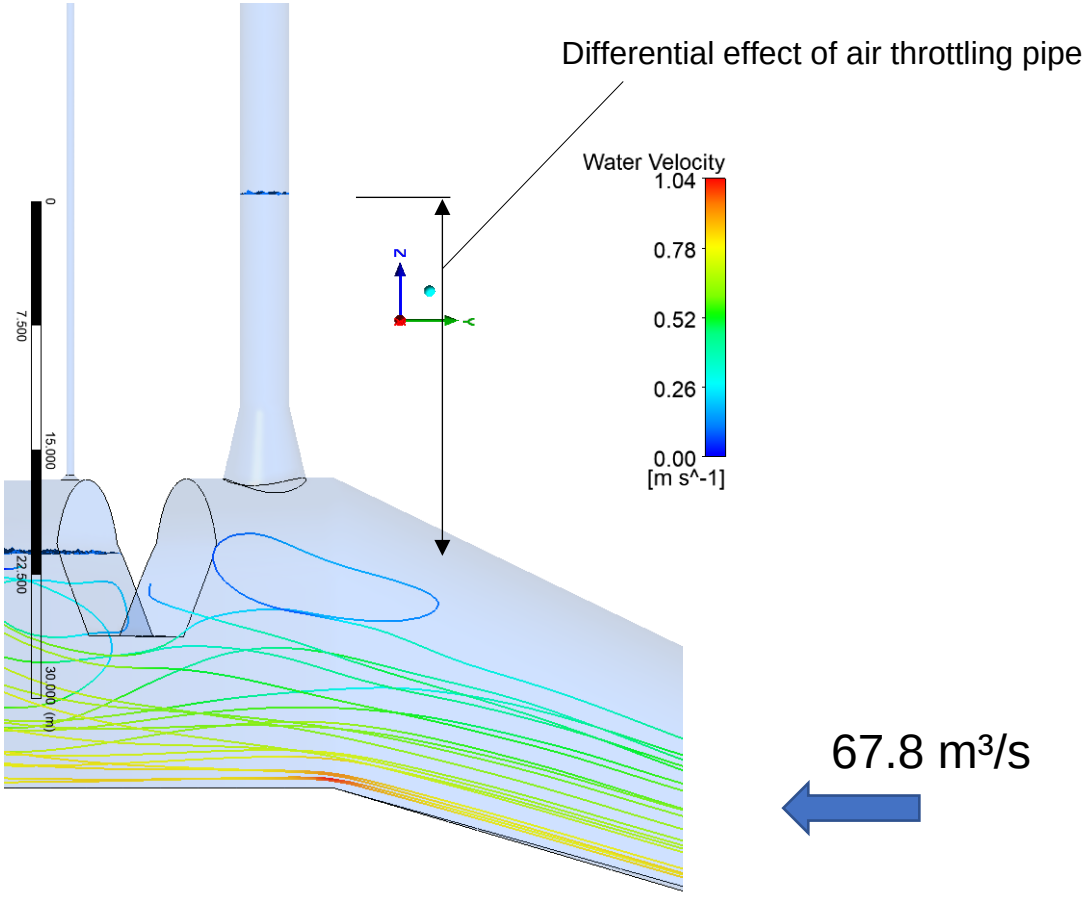

Figure 310: Upsurge in semi-air cushion with 67.8 m³/s inflow, head difference 21.5 m w.c, detail

Figure 311 shows the starting up-surge event in the semi-air cushion surge tank. The air flow has been accelerated to up to 480 m/s at the outlet of the aeration shaft, throttling the air cushion and creating the differential effect. The figure shows the certain time step of 472.25 s.

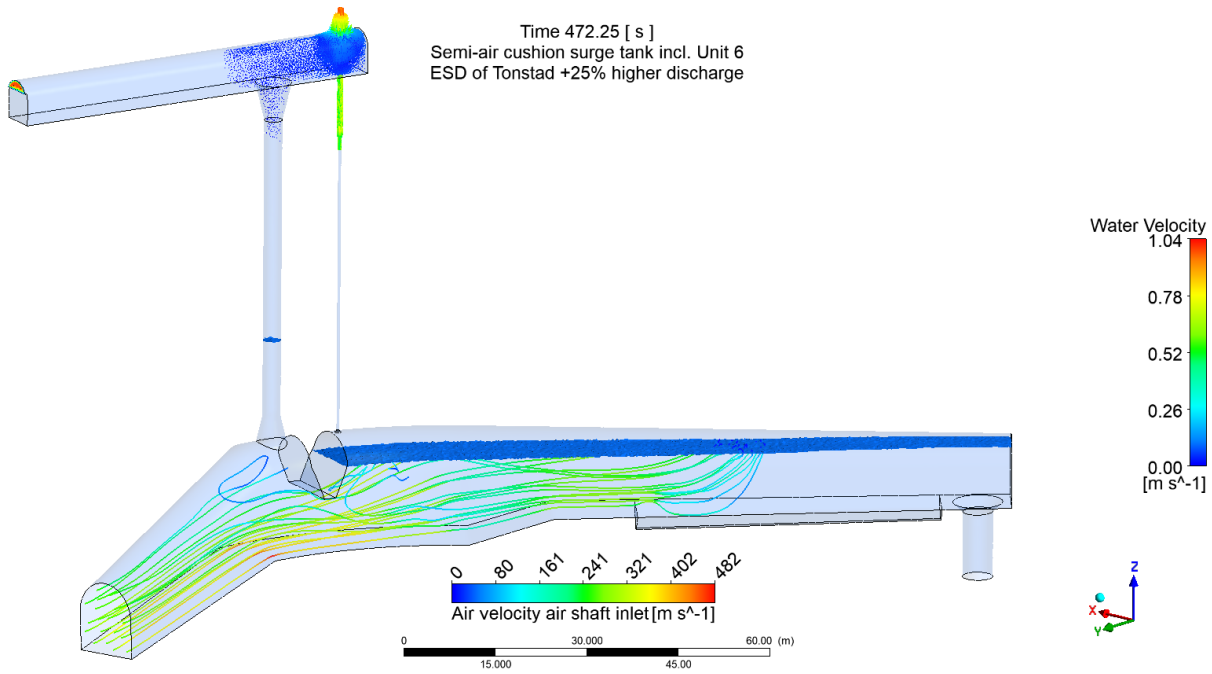

Figure 311: Upsurge in semi-air cushion with 67.8 m³/s inflow, head difference 21.5 m w.c. smooth pipe wall friction

Figure 312 and Figure 313 show the outlet detail of the aeration shaft entering into the upper chamber of the semi-air cushion with flow velocity.

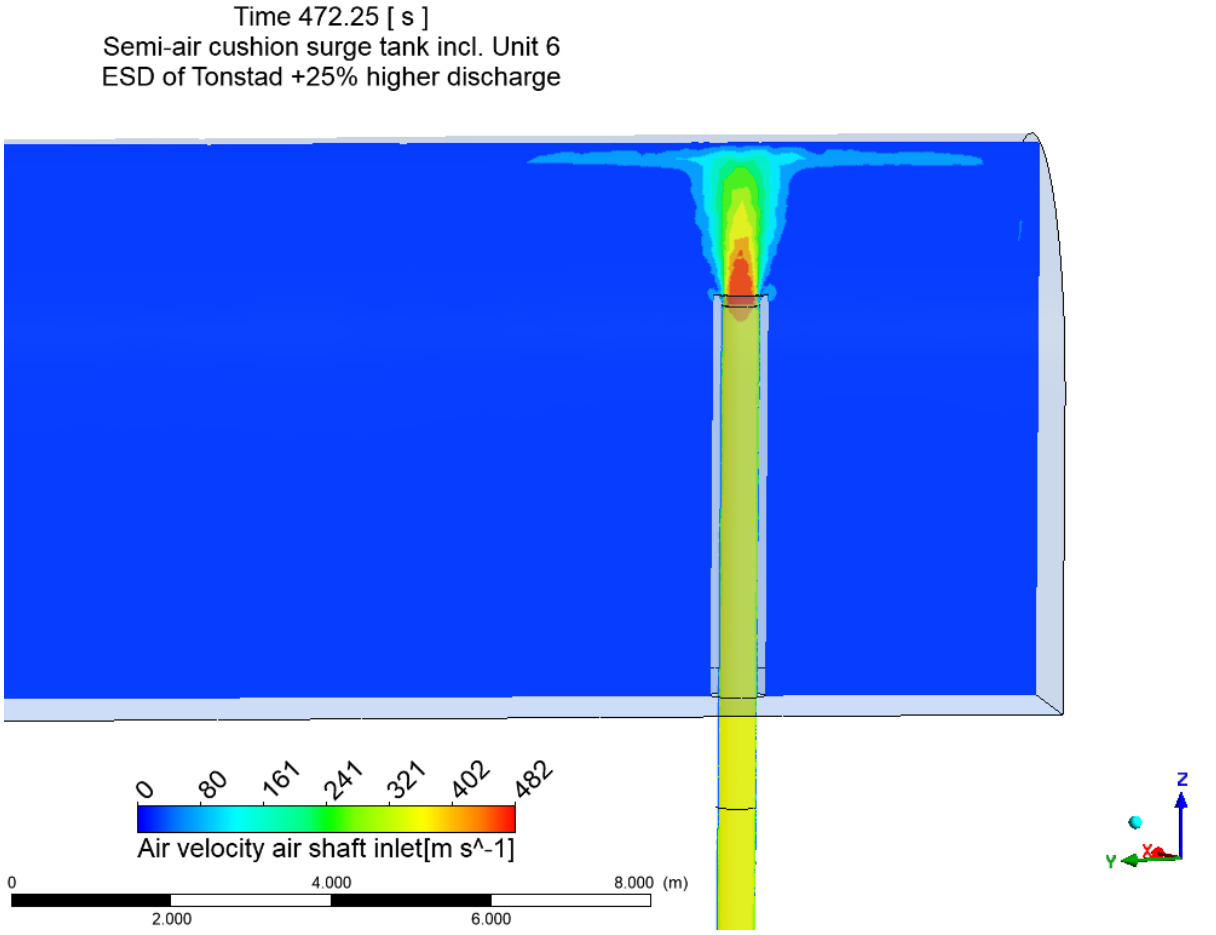

Figure 312: Upsurge in semi-air cushion with 67.8 m³/s inflow, air outlet, air velocity, average air velocity in shaft: 355 m/s

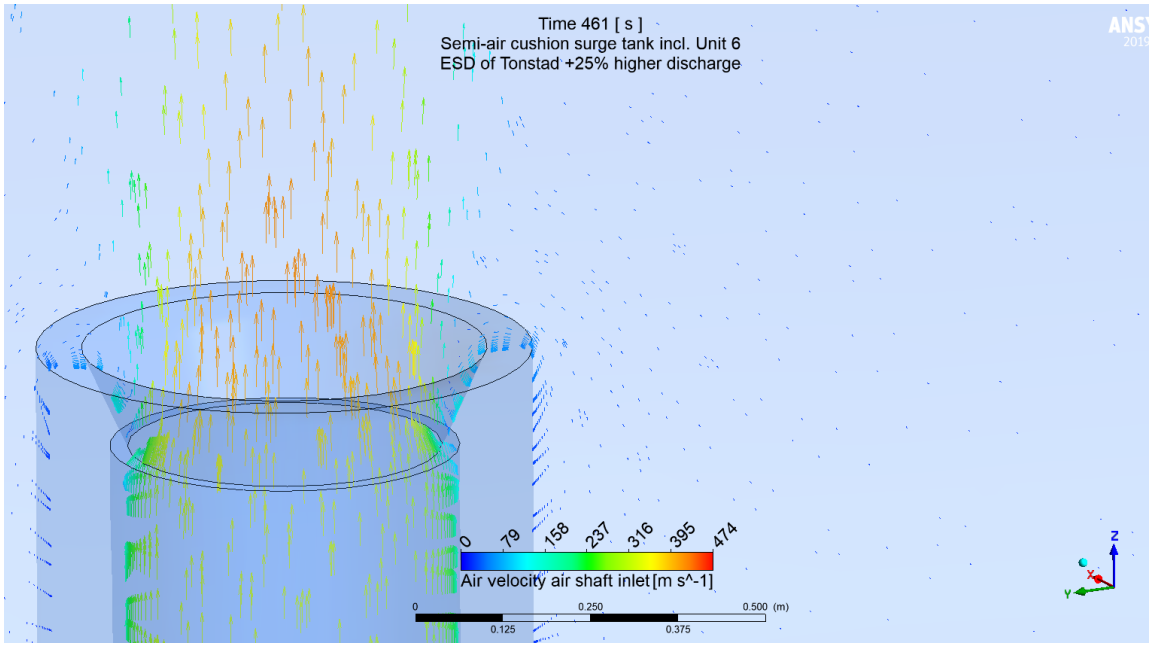

Figure 313: Upsurge in semi-air cushion with 67.8 m³/s inflow, air outlet, air velocity

Table 30 is how the air throttling pipe is calculated; by Darcy-Weisbach friction formula and the outflow loss by applying a specific local loss coefficient:

$$\Delta p = \lambda \cdot \frac{l}{d_H} \cdot \frac{\rho}{2} \cdot v^2 + \sum \zeta \cdot \frac{\rho}{2} \cdot v^2$$

Δp Pressure loss
λ friction factor
l length
d_H hydraulic diameter
ρ density of the fluid
v velocity
ζ local loss coefficient

The recalculation of the 67.8 m³/s discharge to a head loss of 21.5 m shows that the smooth wall has a loss of 17.76 m w. c. for 67.8 m³/s air discharge and the local loss with sharp edge of Di 0.45 m generates a ζ [-] of 1.66 [-].

Table 30: Air pipe loss, smooth wall di = 0.5 m recalculation of 3D CFD

Air Outflow UPSURGE

Tonstad airpipe loss friction loss														
Q [m³/s]	L [m]	D_i [m]	A [m²]	ks [mm]	T [C°]	v [m/s]	E kin	rho air	ν [m²/s]	Re [-]	C-W-1	C-W-1	λ	ΔP [Pa]	mwc
67.80	66	**0.50**	0.194	**0.000**	4	349.21	6215.48	1.15	1.36E-05	12,738,475	14.342	14.567	0.005	45253	4.44

Tonstad airpipe loss - water pipe - local loss outflow							
Q [m³/s]	D_i [m]	A [m²]	rho	v [m/s]	ζ	ΔP	mwc
67.8	**0.450**	0.159	1.15	426.30	**1.66**	1.74E+05	17.06

Sum of losses airpipe	mwc
	21.50

16.5.2 **Air pipe Di = 0.4 m**

The internal diameter of 0.4 m was found to be the design diameter for the proposed semi-air cushion solution (Table 31).

Table 31: Air pipe loss, steel wall di = 0.4 m

Air Outflow UPSURGE

Tonstad airpipe loss friction loss

Q [m³/s]	L [m]	D_i [m]	A [m²]	ks [mm]	T [C°]	v [m/s]	E kin	rho air	ν [m²/s]	Re [-]	C-W-1	C-W-1	λ	ΔP [Pa]	mwc
67.80	66	**0.40**	0.126	**0.100**	4	539.54	14836.81	1.15	1.36E-05	15,833,757	8.342	8.342	0.014	396871	38.93

Tonstad airpipe loss - water pipe - local loss outflow

Q [m³/s]	D_i [m]	A [m²]	rho	v [m/s]	ζ	ΔP	mwc
67.8	**0.400**	0.126	1.15	539.54	**1.66**	2.79E+05	27.33

Sum of losses airpipe	mwc
	66.26

16.5.3 **Air pipe geometry only**

A semi-air cushion design with only an air pipe design was checked and found not to be appropriate and recommended since the air throttling effect may create a cavity if pressures below atmospheric pressure is created during a transient event. This approach is not recommended.

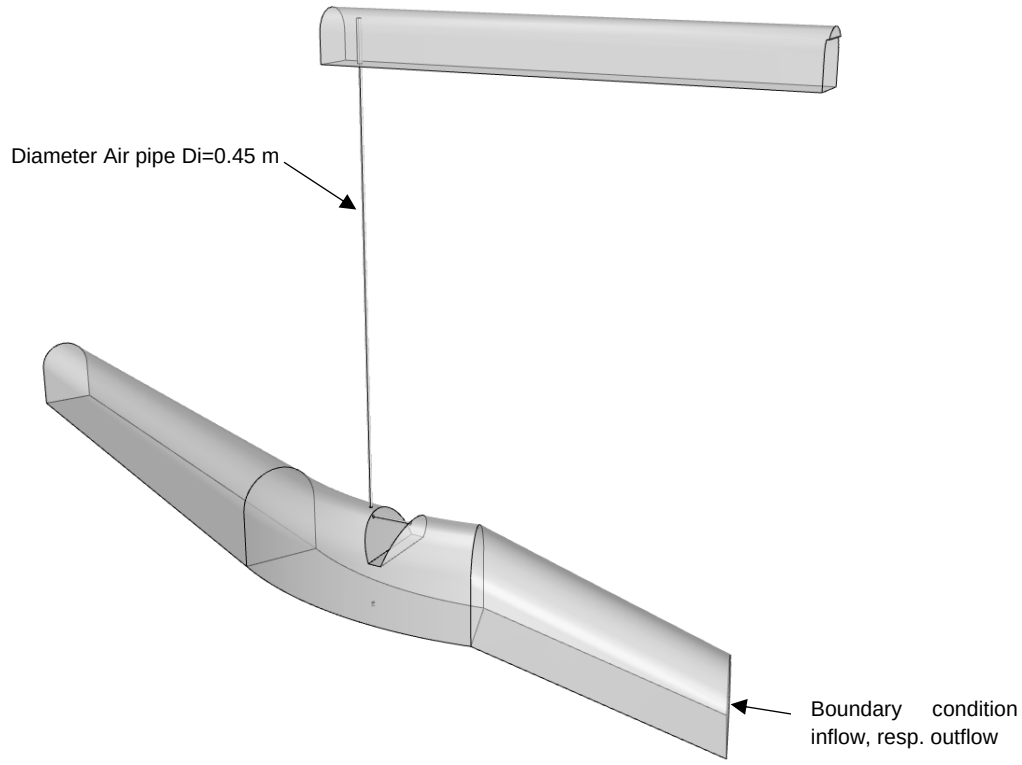

Figure 314: Semi-air cushion without water riser, only with aeration pipe, not recommended

16.6 **Tonstad extension semi-air cushion design proposal**

This chapter briefly summarizes the geometry proposal for the Tonstad semi-air cushion surge tank in the extension chamber in context to the existing surge tank geometry.

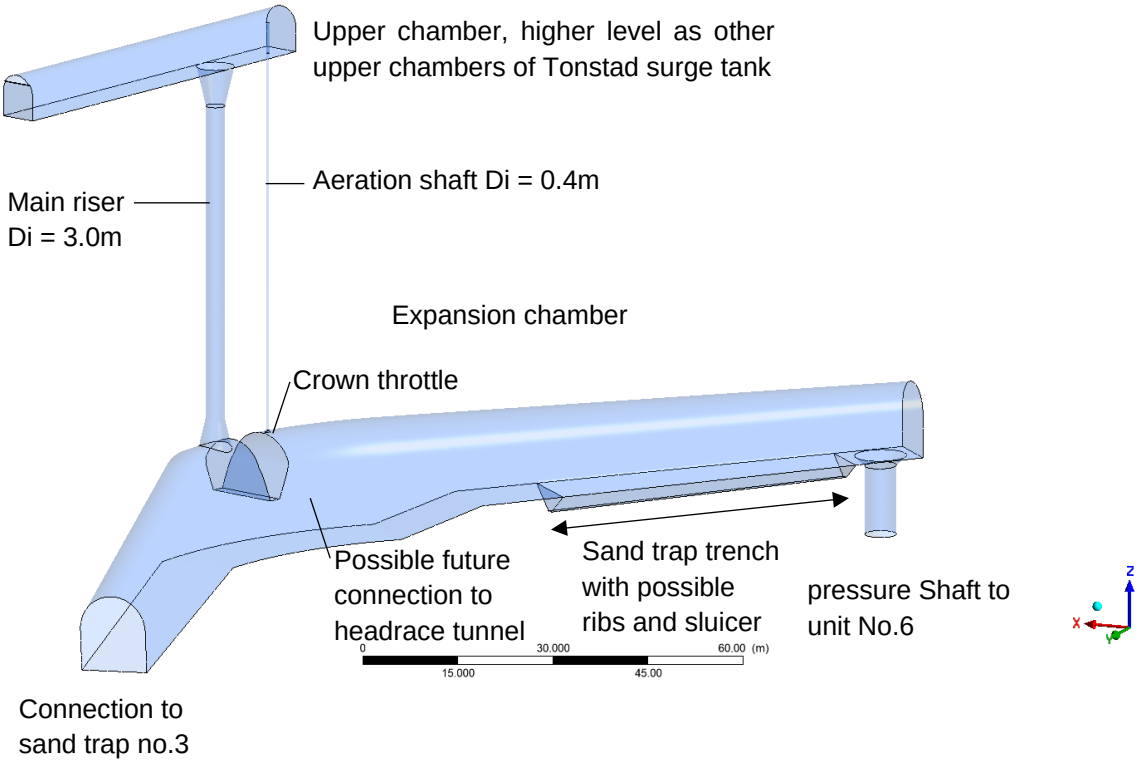

Figure 315: Geometry, final proposal extension chamber Tonstad with semi-air cushion

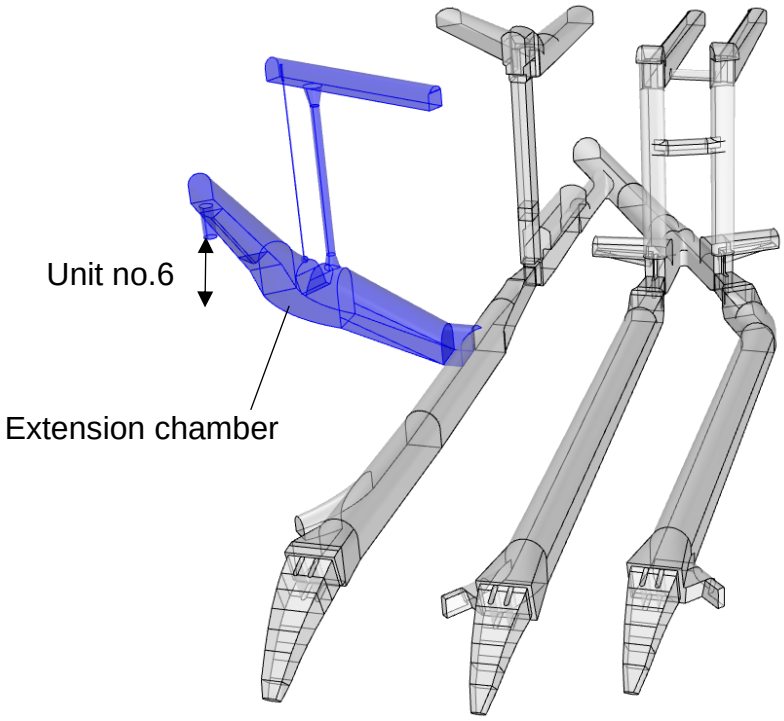

Figure 316: Geometry, final proposal extension chamber Tonstad with semi-air cushion at existing Tonstad system

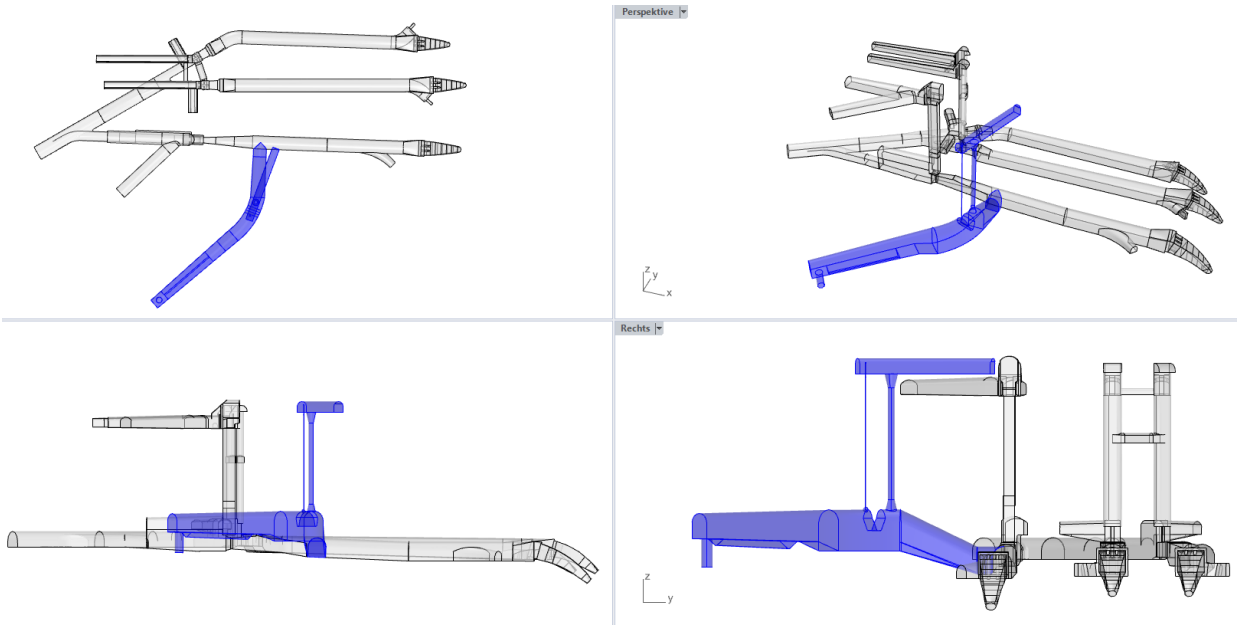

Figure 317: Geometry, final proposal extension chamber Tonstad with semi-air cushion at existing Tonstad system, views

Figure 318 shows the geometric levels of the extension chamber defining the hydraulic communication of the whole system. By defining the crown throttle level this is a design parameter to adjust the hydraulic behaviour of the extension system for optimized operation.

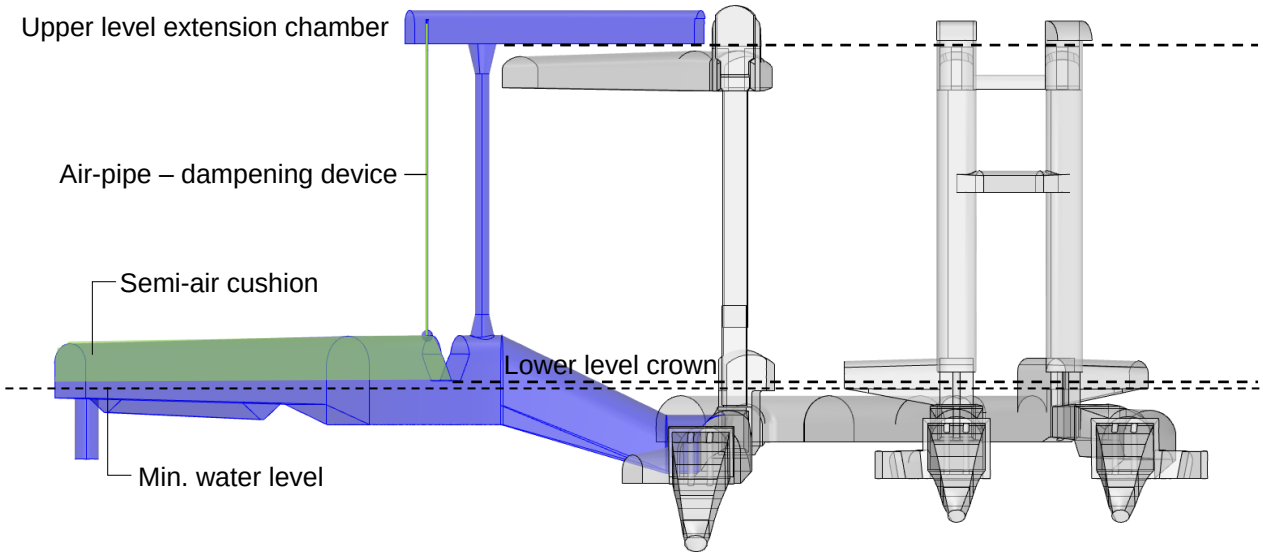

Figure 318: Geometric heights of the attached chamber compared to existing scheme

Figure 319 shows the pressurized discharge in the extension chamber and semi-air cushion for turbine mode operation at potential unit no.6.

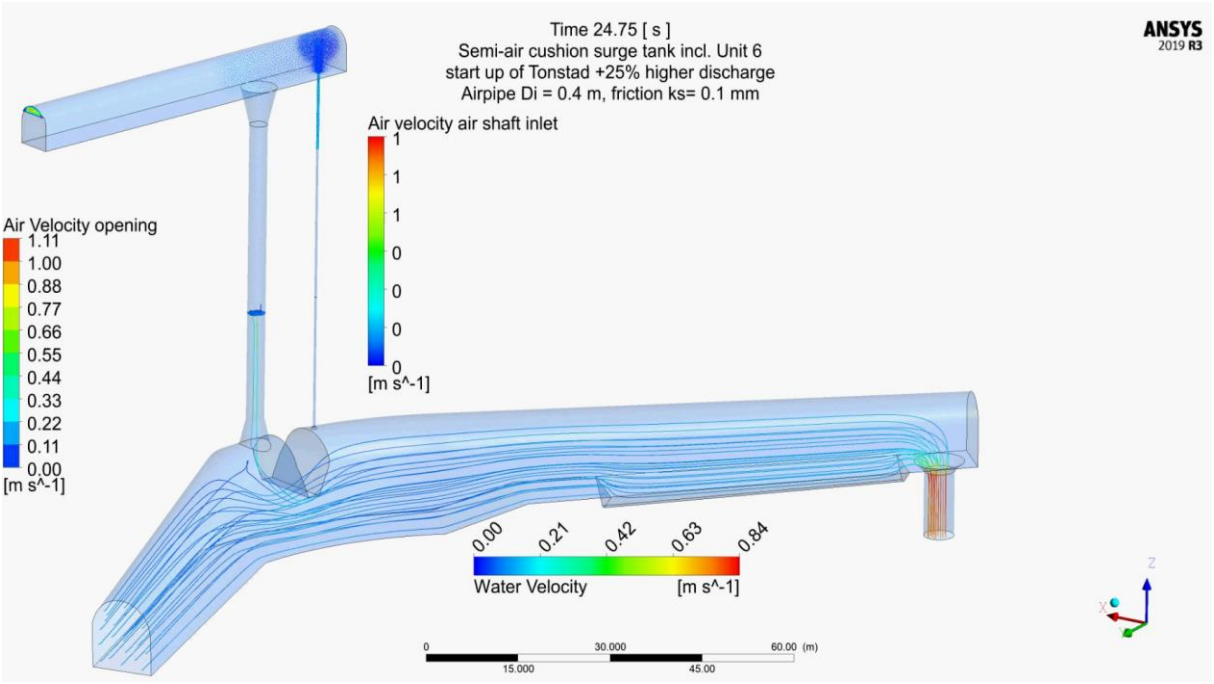

Figure 319: Result of transient simulation extension chamber

17. Summary and conclusions

17.1 Sand trap Tonstad

The investigations of the model test with sand have shown that the pressurized sand trap at Tonstad power plant is not a sand trap since sand is not trapped, the chamber dampens the sand transportation into the power plant, but does not stop it. Sand particles were finally flushed 100%. These findings fit with observations in the prototype.

A small-scale hydraulic model test was investigated in the flume at a scale of 1:36.67. In the physical model test sediment tests with sand in 1:1 prototype scale was undertaken. The 1:1 scaling approach of sand in the model test was an important finding during the investigations to improve sand trap model tests in general. This sediment scaling comes along with 1:1 flow velocity, resulting in scale 1:36.67 time scaling. The hydraulic model test was additional investigated in detail in terms of PIV measurements on two certain sections, supporting the results from 3D CFD with the jet and the oscillating nature of the jet created by the flow restriction of the gate section of the sand trap.

The pressurized sand trap flow investigations were detailly accompanied by 3D CFD simulation with particle tracking.

A local loss factor of $\zeta = 5.3$ [-] in relation to the velocity in the sand trap chamber flow section is measured in the physical test and suggested for 1D application.

To upgrade the chamber to a sand trap with automatic sluicing function a rip design with minimum four compartments is suggested, a ramp with inclination of 4.5° (8%) protects the compartments from high flow velocities and thus resuspension. Pressure transducers are recommended to monitoring the sand in the compartments.

The ramp with four compartments directly upstream of the weir can be a first prototype structure to be implemented in the prototype sand trap chamber.

A separation of gravel and sand is straightforward according also to findings in the prototype. Therefore, the sand trap with ramp and ribs, positioned in front of the weir is added by a gravel trap at end of the diffusor after the gate.

The influence of heightening of the weir was investigated by doubling and tripling it, it was found that this does not improve the sand trapping effect. Due to significant vortices, sand particles are suspended and transported over the weir into the pressure shaft.

Disadvantageous aspects of the existing prototype sand trap geometry are visible in the investigations:

- The geometry of the access tunnel, creating vortices and higher bottom wall stresses that act in favour to sediment transport and uneven flow conditions.
- Short length of the diffusor creating significant backflow region

- Sudden change of flow section from concrete to unlined section creating vortex flows that lift particles
- Particle catapulting effect of the flow restriction due to the gate section

With 3D CFD flow simulations several ramp designs were investigated to potentially improve the diffusor flow behaviour. It can be summarized that smaller diffusor angles can improve the jet flow in general. For Tonstad sand trap the effort compared to the positive effect on the flow or the local loss cannot be proven, due to its specific geometry. The abrupt diffusor enlargement creates a dominant backflow zone with particles being lifted in the highly turbulent zone which is unbeneficial for the settling behaviour. This effect also corresponds with the jet inclination from the inlet. Future sand trap designs demand for more detailed hydraulic investigations ahead of construction. The physical tests show that larger particles such as gravel is kept in place after the diffusor. Thus, this location is predestined for a grave trap with special gravel sluicer. Therefore, gravel is trapped in a gravel trap directly after the diffusor ramp. The sand was found to be trapped efficiently in ribs with compartments directly upstream of the weir. The rib design is: 1 m width by 1 m opening. The most important aspect for effective trapping is the placing of a ramp (inclination of 4.5° resp. 8%) that is shedding the compartments from flow disturbances. From these compartments sluicing pipes can deliver the trapped sediments out via the access tunnel, in order to allow automatic sluicing. The compartments were found to allow up to almost 90% trap efficiency for the 0.3 mm to 1.0 mm sand probes.

In the physical test the effect of heightening the weir was tested by doubling and tripling the weir height downstream. It was found that still 100% of the sediment probe is flushed. However, the time range is longer to flush the sediments. The main hydraulic effect that flushes the sediments are significant vortex flow at the wall edges of upstream of the weir that occur in certain frequency and are very effective in lifting sediments over the weir.

A main initial part of the investigations was to design flow calming rakes that are passable. These rakes were designed in terms of 3D CFD and investigated in the physical model test. However, the outcome is that the rakes do not beneficially improve the sand trapping effect. Thus, it is not recommended to install such rakes.

Tests with flushing the sediments, also gravel show that these larger particles that may seriously harm machine units can be efficiently trapped in ribs upstream of the weir.

Sluicing devices need to be equipped with sensors measuring the sediment filling degree. With these measures it is possible to tune the system for optimized sediment management.

Opening of the gate for filling still needs to be done with much care. However, an automatic sediment flushing opportunity may minimize the risk of large sediment movement due to the fact that the chamber has to be emptied less often.

Free surface flow events must be prevented in the sand trap chamber. If free surface flow is reached due to low water level in the surge tank, firstly the pressure tunnel upstream of the surge tank is creating free surface flow. Due to the lower level of the crown of the sand trap this chamber does not easily creates free surface flow, before that free surface is created upstream of the surge tank in the headrace tunnel system.

The physical tests have shown that air can be created by inlet vortices at the gate section. This effect needs to be further considered and checked for potential upgrading the plant via sand trap no.3. for the potential flow of 80 m³/s + 60 m³/s (25% discharge upgrade).

17.2 **Sand trap for pressurized flow in general**

An important outcome of the investigations is the finding and application of the prototype size particle scaling law on sand trap physical model tests. For this purpose, 1:1 sediment size feed the flow at 1:1 inlet velocity. The results in the physical model test are very comparable with the observations in the prototype sand trap. Systematic 3D CFD simulations with particle tracking were undertaken that sustain this approach, both with comparable wall shear stresses and with matching sediment settling paths.

Theses systematic simulations were undertaken in rectangular boxes to study the particle tracking behaviour with leas possible 3D geometry effects to focus on the main scaling parameters.

It can be concluded that ribs are very effective to create sand trap compartments, if placed in lowered bottom or combined with a ramp for upgrades. A longitudinal trench design may be straightforward to concentrate sediments in the centre for improved sluicing.

17.3 **Extension chamber with semi-air cushion surge tank**

The extension chamber that was previously found and suggested to allow a 25% discharge upgrade of Tonstad power plant was further investigated. It was additionally investigated with a potential pump turbine unit connection. The extension chamber is a significantly large water reservoir to act as a lower chamber for the whole Tonstad scheme. In order to best integrate this surge tank device a semi-air cushion approach was investigated and further improved. It consists of separate air, and water shafts and a crown throttle creating a cavity that is temporarily pressurized with air. 3D CFD simulations were undertaken to show its operability and to compare with design criterion. The hydraulic parts of the throttled aeration pipe are to be designed in accordance to the crown throttle and in accordance to the entire hydraulic system of the hydropower plant via 1D-numerical simulation. The semi-air cushion approach for Tonstad additionally acts as an upper chamber to improve the mass oscillation security for emergency shutdowns.

18. Outlook for further investigations

The sediment trap investigations have shown that the concentration of sediments has a significant impact on trap efficiency. A higher concentration leads to less efficiency, more particles are kept in suspension. Further research is suggested to determine the impact of sediment flow concentration and the corresponding trap efficiency.

18.1 Particle tracking simulations

Many simulations utilizing particle tracking for sediment modelling were undertaken and show very realistic results compared to common sand trap design. The software *CFX* and *Fluent* were compared for that purpose. CFX was found to be more convenient since a full range of particles can be observed.
An important open question for this tool is the capability of modelling the resuspension of sediments in the flow, how it was observed in the model test and is obviously happening in the prototype sand trap.

As another point for more detailed investigation proposals the particle behaviour on various walls and on the bottom is of interest, that also may lead to resuspension via local turbulence fluctuations, that might not be covered by the RANS approach.

18.2 Semi-air cushion surge tank

The semi-air cushion surge tank has several benefits for surge tank upgrades and may also be a promising concept for new large surge tank structures. Further investigations are seen very meaningful.

19. References

Daxnerová , J. *Hydraulic Scale Modelling of Flow Calming Structures for Hydropower Plants.* NTNU Trondheim, Master Thesis, 2019.

de Jong, R.J., H.W.R. Perdijk, D. Develay, J. Gautier, und J. Binquet. „Hydraulic Model Studies of Desilting Basins of a Hydro-electric Project.“ *Proceedings of 5th International Symposium on River Sedimentation* , Karlsruhe 1992.

Develay, D., J. Binque, E. Divatia, und C.R. Venkatesha. „Desilting Basin System of the Dul Hasti Hydroelectric Project.“ *Hydraulic Engineering, ASCE*, 1996: 122(10): 565-572.

Harb, G. *Numerical Modeling of Sediment Transport Processes in Alpine Reservoirs.* Dissertation, Graz University of Technology, 2013.

Mauko, G. *WaterHammer Simulation for Tonstad HPP upgrade.* Graz University of Technology, 2020 - ongoing.

Naess, Rakel. *CFD Simulations of Open and Closed Sand Trap Design for Tonstad Hydropower Plant.* Trondheim : Master thesis at NTNU, 2020.

Ortmanns, Ch. *Entsander von Wasserkraftanlagen.* Dissteration, ETH Zürich: VAW Mitteilungen 193; https://ethz.ch/content/dam/ethz/special-interest/baug/vaw/vaw-dam/documents/das-institut/mitteilungen/2000-2009/193.pdf, 2006.

Richter, W. *Surge Tank Design for Flexible Hydropower.* Dissertation: Graz University of Technology, 2020.

Richter, W., K. Vereide, und G. Zenz. „Upgrading of a Norwegian pressurized sand trap combined with an open air surge tank.“ *Geomechanics and Tunneling*, 2017: DOI: 10.1002/geot.201700027.

Richter, Wolfgang, Wolfgang Dobler, und Helmut Knoblauch. *Hydraulic and Numerical Modelling of an Asymmetric Orifice within a Surge Tank.* 4th International Symposium on Hydraulic Structures, Porto, 2012.

Ruetz, M. *Particel Image Velocimetry (PIV) Messungen am Modellversuch Wasserschloss Krespa (in German), Particel Image Velocimetry (PIV) Measurements at the surge tank Krespa.* Master Thesis, Graz University of Technology, 2014.

Schiller, L., und A. Naumann. „Über die grundlegende Berechnungen bei der Schwerkraftaufbereitung.“ *Zeitschrift des Vereines deutscher Ingenieure*, 1933: Leipzig.

Steinkjer, S. M. *Hydraulic Scale Modeling of Sediments for Pressurized Sand Trap .* NTNU Trondheim, Master Thesis, 2018.

Stelzer, R. S., und R. N. Walters. *Estimating Reversible Pump-Turbine Characteristics.* Engineering monograph, Denver: Office of Design and Construction Engineering and Research Center Denver, 1977.

Sterner, L. *3D CFD Simulations for Tonstad Surge Tanks Upgrade, Master Thesis, Graz University of Technology.* Graz, 2018.

U.S. Geological Survey. *Scientific Investigations Report 2008–5093.* 10. Jan 2013. https://pubs.usgs.gov/sir/2008/5093/table7.html (Zugriff am 21. 08 2019).

Urach, Th. *Modelluntersuchungen am Wasserschloss Krespa des PSKW Obervermuntwerk II (in German), Model Test investigations on the surge tank Krespa of the Obervermuntwerk II.* Master Thesis, Graz University of Technology, 2015.

Vereide, K., W. Richter, O. Havrevoll, L. Lia, und T. Jacobsen. „Upgrading of Sand Traps in Existing Hydropower Plants.“ *Proceedings of Hydro Congress.* Seville, 2017.

Wikipedia Reynoldsnumber. kein Datum. https://en.wikipedia.org/wiki/Reynolds_number (Zugriff am 02. 12 2020).

Zhou, H., G. Wang, C. Jia, und C. Li. „A Novel, Coupled CFD-DEM Model for the Flow Characteristics of Particles Inside a Pipe.“ *Water* (MDPI) 11 (2019).